

University of Bath



PHD

Acoustic emission and acousto-ultrasonics on aromatic polymer composites

Russell-Floyd, Richard S.

Award date:
1991

Awarding institution:
University of Bath

[Link to publication](#)

General rights

Copyright and moral rights for the publications made accessible in the public portal are retained by the authors and/or other copyright owners and it is a condition of accessing publications that users recognise and abide by the legal requirements associated with these rights.

- Users may download and print one copy of any publication from the public portal for the purpose of private study or research.
- You may not further distribute the material or use it for any profit-making activity or commercial gain
- You may freely distribute the URL identifying the publication in the public portal ?

Take down policy

If you believe that this document breaches copyright please contact us providing details, and we will remove access to the work immediately and investigate your claim.

Download date: 13. May. 2019

**Acoustic Emission and Acousto-Ultrasonics on Aromatic
Polymer Composites**

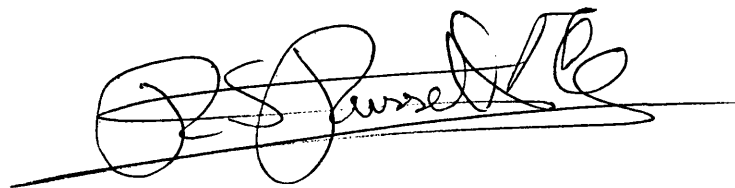
Submitted by Richard S Russell-Floyd
for the degree of PhD
of the University of Bath

1991

COPYRIGHT

Attention is drawn to the fact that copyright of this thesis rests with its author. This copy of the thesis has been supplied on condition that anyone who consults it is understood to recognise that its copyright rests with its author and that no quotation from the thesis and no information derived from it may be published without the prior written consent of the author.

This thesis may be made available for consultation within the University Library and may be photocopied or lent to other libraries for the purposes of consultation.

A handwritten signature in black ink, appearing to read 'R S Russell-Floyd', written over a horizontal line.

R Russell-Floyd

UMI Number: U034426

All rights reserved

INFORMATION TO ALL USERS

The quality of this reproduction is dependent upon the quality of the copy submitted.

In the unlikely event that the author did not send a complete manuscript and there are missing pages, these will be noted. Also, if material had to be removed, a note will indicate the deletion.



UMI U034426

Published by ProQuest LLC 2013. Copyright in the Dissertation held by the Author.
Microform Edition © ProQuest LLC.

All rights reserved. This work is protected against
unauthorized copying under Title 17, United States Code.



ProQuest LLC
789 East Eisenhower Parkway
P.O. Box 1346
Ann Arbor, MI 48106-1346

UNIVERSITY OF BATH
LIBRARY

25

5 JUN 1992

Ph.D.

5059812

Acknowledgements

I wish to extend my thanks, firstly to my supervisor, Mr. M.G. Phillips, senior lecturer at the School of Materials Science, University of Bath, for his advice, guidance and encouragement during the three years of research work and subsequent writing up. In addition, I wish to thank Mr. M. Mogushi for advice concerning acoustic emission hardware and software and Dr J. Nixon for carrying out most of the moulding of APC2 laminates at Bath, Dr. R. Moore and colleagues at ICI, Wilton for APC2 material, collaborative studies and funding.

Abstract

This investigation of acousto-ultrasonics (AU) has given an unbiased assessment of the technique based on statistical inference. The most important factors affecting AU have been systematically investigated. The optimisation of test conditions to achieve optimum sensitivity of AU to material characteristics has been considered. A quantitative method for this optimisation has been demonstrated for the two AU parameters, the Stress Wave Factor (SWF) and the root mean square (RMS) voltage. The limit of detectability of defects in a particular composite system has been determined. This has been carried out by a quantitative statistical method which takes account of the scatter in AU data, predominantly the result of coupling variability. This scatter has been quantified and shown to be the major obstacle to the use of AU to detect defects in aromatic polymer composite (APC2), a carbon fibre reinforced thermoplastic material.

The mechanical properties of APC2 have been determined in tensile and flexural tests, the results of which compare favourably with those in the literature. The methods of material fracture in this composite have been studied in a variety of methods of stressing, and this has helped to demonstrate the reasons for the high fracture toughness of APC2.

The acoustic emission response of APC2 has been recorded over a wide variety of loading regimes, specimen dimensions and lay-ups using amplitude distribution analysis. The acoustic emission (AE) is attributed predominantly to fibre failure processes, the matrix showing ductile behaviour which appears to generate little noise.

The technique of acoustic emission has been used for defect detection in APC2 with mixed results. The intrinsic variability of acoustic emission has been investigated and a systematic investigation of the possible causes of this variability has been carried out. One limitation of AE for this purpose appears to be coupling variability between AE sensors and specimen. It has been demonstrated that AE is highly sensitive to small

changes in specimen thickness and that it can distinguish between different modes of crack propagation in APC2 and in epoxy/carbon fibre composites. Good correlations have been determined between fracture toughness (G_c), fibre fractures and AE parameters in double cantilever beam tests, and between failure stresses and strains and AE parameters in four point bend tests.

A novel acoustic emission analysis package has been developed for MSDOS IBM compatible machines. This software includes dedicated graph plotting, quantification of acoustic emission amplitude distributions by a variety of statistical descriptive parameters, and conversion of data into a format compatible with any commercial spreadsheet software. This software was written in an effort to develop quantitative AE parameters usable for NDT.

CONTENTS

1. INTRODUCTION	1
1.1 An Overview Of The Thesis	1
1.2 Non-destructive Evaluation (NDE)	3
1.3 Ultrasonics And Acoustic Emission: The Fundamentals	5
1.3.1 Ringdown Counting	7
1.3.2 Event Counting	7
1.3.3 Rise Time, Decay Time and Event Duration	8
1.3.4 Acoustic Emission Energy	8
1.3.5 Amplitude Distribution Analysis	8
2. ACOUSTO-ULTRASONICS: AN INTRODUCTION AND LITERATURE REVIEW	10
2.1 The Basic Principles Of AU Testing	10
2.2 Methods Of Signal Processing: AU Parameters	12
2.3 Factors Affecting The Stress Wave Factor	14
2.4 A Review Of The Literature On Acousto-Ultrasonics	16
2.4.1 Assessment of Strength	19
2.4.2 Bonding	22
2.4.3 Assessment of Degradation	24
2.4.4 Locating the Position of Eventual Specimen Failure	26
2.4.5 Defect Detection	27
2.4.6 Studies of the Principles Behind AU Testing	29
2.5 AU Pulse Characteristics	32
2.6 Conclusions	35
3. ACOUSTO-ULTRASONICS: EXPERIMENTATION	37
3.1 A Study Of Experimental Conditions	37
3.1.1 The Problem and the Aims	37
3.1.2 The AETC AU206 Acousto-Ultrasonic Testing System	38
3.1.3 Performance Criteria	40
3.1.4 Material Investigated	40
3.1.5 Fixed Experimental Conditions	41
3.1.6 Experimental Variables	42
3.2 Optimisation Of Instrument Settings	48
3.2.1 Preliminary Experiments	49
3.2.2 Selection of 'SWF difference' as a Sensitivity Parameter	52
3.2.3 Analysis of Variation and Covariation	53
3.2.3.1 <i>Analysis of variance of SWF</i>	54
3.2.3.2 <i>Analysis of variance of DSWF</i>	55
3.3 An Investigation Of Quasi RMS Voltage	56

3.4 An Investigation Of The Use of High Gains	59
3.4.1 SWF Measurements with an Air Gap Between Transducers	59
3.4.2 The Effect of the AU206 Amplifier on Received AU Pulses	60
3.4.3 The Effect of Received AU Pulse Shape on SWF Readings	62
3.4.4 Conclusions with Respect to the Use of High Gains	63
3.5 A Study Of Defect Detection In APC2 By Means Of Acousto-Ultrasonics	64
3.5.1 Scanning of APC2 Plates with 'Moulded-in' Defects	65
3.5.2 Impact Damage in Plates	67
3.5.2.1 <i>UD plates</i>	67
3.5.2.2 <i>Cross-ply plates</i>	68
3.5.3 Influence of Damage in Strip Specimens	69
3.5.3.1 <i>Variability due to coupling</i>	70
3.5.3.2 <i>Comparison of impacted, holed and crushed samples with non-defective samples</i>	71
3.5.4 Determination of the Minimum Size of Through Thickness Hole Detectable in APC2 by AU	72
3.6 Discussion Of AU Results	74
3.7 Conclusions	87
3.8 Further work	89
4. AROMATIC POLYMER COMPOSITES	91
4.1 Introduction	91
4.1.1 The Matrix - Victrex PEEK	93
4.1.2 The Reinforcing Carbon Fibres	94
4.1.3 The PEEK/Carbon Fibre Interface	95
4.1.4 Crystallisation	96
4.1.5 Mechanical Properties	98
4.1.6 Toughness	100
4.1.7 Moulding	102
4.1.8 Conclusions	104
4.2 APC2 Moulding And Specimen Preparation	105
4.3 Mechanical Testing of APC2	107
4.3.1 Tensile Testing	108
4.3.2 SEN Fracture Toughness Testing	108
4.3.3 Flexural Testing	108
4.4 Microstructural Investigations Of APC2	109
4.4.1 SEM of Fracture Surfaces	109
4.4.2 Fibre/Plies/Matrix Distribution	111
4.4.3 Fibre Damage Monitoring in APC	112
4.5 Discussion/Conclusions	114

5.	ACOUSTIC EMISSION	116
5.1	Introduction	116
5.1.1	A Brief Review of the Literature	117
5.2	Acoustic Emission Systems Used	118
5.2.1	Acoustic Emission Detection	119
5.2.1.1	<i>Transducers</i>	119
5.2.1.2	<i>Preamplifiers</i>	120
5.2.1.3	<i>Coupling</i>	120
5.3	Signal Processing And Data Storage	121
5.3.1	Marandy MR1004 System	121
5.3.2	AETC 203 System	123
5.4	RFPLOTS And RFGGRAPH AE Analysis Software	124
5.5	Factors Affecting AE Testing	126
5.5.1	The Effect of Coupling Variation On AE	126
5.5.2	AE Transducers	128
5.5.3	The Effect of Distance From Event Source on the Received Event Characteristics	130
5.5.4	Attenuation	131
6.	ACOUSTIC EMISSION TESTING OF APC2	134
6.1	Preliminary Investigations/Standardisation Of Test Conditions	134
6.2	Three Point Bend Testing	135
6.2.1	0° Plates	137
6.2.1.1	<i>Standard plates</i>	137
6.2.1.2	<i>Comparison of defective 0° laminates with non-defective</i>	138
6.2.1.2.1	<i>Numeric AE parameters</i>	138
6.2.1.2.2	<i>Graphical methods of comparison</i>	141
6.2.2	90° Plates	142
6.2.3	0°/90° Cross-ply	143
6.2.4	Narrow Plates	144
6.3	Carbon Fibre Epoxy And Unreinforced PEEK	144
6.4	Double Torsion Testing	145
6.5	Tensile Tests	147
6.6	Four Point Flexure	149
6.6.1	Comparison of Four with Three Point Loading	150
6.7	Interrupted Loading Cycles	152
6.8	Discussion/Conclusions	152

7.	ACOUSTIC EMISSION AND CRACK LENGTH MONITORING OF DCB APC2 AND FIBERITE/CARBON FIBRE COMPOSITES	157
7.1	Introduction	157
7.1.1	Preliminary Investigations	157
7.1.2	Objectives	160
7.2	Experimental	160
7.2.1	Specimen preparation	160
7.2.2	Testing procedure	161
7.3	Results	163
7.3.1	Ensuring Reproducibility of Coupling	163
7.3.2	Acoustic Emission and Crack Growth Behaviour	163
7.3.2.1	<i>Acoustic emission with simultaneous crack length monitoring</i>	164
7.3.2.2	<i>Tabulation of crack growth and AE data</i>	166
7.3.2.3	<i>Correlation of G_c/fibre breaks and AE events</i>	168
7.3.2.4	<i>AE amplitude distribution and crack growth</i>	170
7.3.2.4.1	<i>Effect of crosshead speed</i>	171
7.3.2.4.2	<i>Comparison of PEEK/carbon with Fiberite/carbon DCBs</i>	173
7.3.2.4.3	<i>Comparison of interlaminar with intralaminar crack propagation</i>	174
7.3.2.5	<i>The effect of crack front to transducer distance</i>	174
7.3.2.6	<i>Unstable crack propagation</i>	176
7.3.3	SEM of DCB Fracture Surfaces	177
7.3.3.1	<i>APC2 interlaminar</i>	178
7.3.3.2	<i>APC2 interlaminar high crosshead speed</i>	178
7.3.3.3	<i>APC2 intralaminar</i>	179
7.3.3.4	<i>Fiberite/carbon interlaminar</i>	180
7.3.3.5	<i>Fiberite/carbon intralaminar</i>	180
7.4	Discussion/Conclusions	181
8.	CORRELATION OF ACOUSTIC EMISSION, ACOUSTO-ULTRASONICS AND MECHANICAL PROPERTIES OF APC2	184
8.1	Introduction	184
8.1.1	The problem	184
8.1.2	Aims	186
8.2	Experimental	186
8.2.1	Acousto-Ultrasonic Measurements SWF and RMS Voltage Measurements	187
8.2.2	Monitoring the Quality of the Coupling	187

8.2.3 Flexural Testing and AE Monitoring	188
8.3 Results	192
8.3.1 Correlating AU parameters with Four Point Flexural Properties	192
8.3.2 Monitoring Coupling Quality	193
8.3.3 Comparison of the Acoustic Emissions from Two Systems on the Same Specimen	194
8.3.4 Correlation of AE with Mechanical Properties	195
8.4 Discussion/Conclusions	197
9. FINAL DISCUSSION	200
10. FINAL CONCLUSIONS	207
10.1 Aromatic Polymer Composite 2	207
10.2 Acousto-Ultrasonics	207
10.3 Acoustic Emission	208
10.4 Cross-Correlation Of AU, AE And Mechanical Properties	209
10.5 AE Study Of Fracture In The Fibre Direction Of UD Composites	210
11. SUGGESTIONS FOR FURTHER WORK	211
REFERENCES	212
FIGURES AND TABLES	229
Chapter 1 (Figures and Tables)	230
Chapter 2 (Figures and Tables)	231
Chapter 3 (Figures and Tables)	241
Chapter 4 (Figures and Tables)	280
Chapter 5 (Figures and Tables)	296
Chapter 6 (Figures and Tables)	308
Chapter 7 (Figures and Tables)	338
Chapter 8 (Figures and Tables)	368
APPENDICES	381
Appendix 1: The Fundamentals Of Ultrasonics	381
A1.1 The Physical Principles of Ultrasonics	381
A1.1.1 Ultrasonic waves at boundaries	383
A1.1.2 The decibel notation	385
A1.1.3 Resonance	386
A1.2 Attenuation	386
A1.2.1 Geometric attenuation	387

A1.2.2 Absorption	388
A1.2.3 Scattering	389
A1.2.4 Dispersion	390
A1.3 Transducers	390
Figures for Appendix 1	393
Appendix 2: Statistical Techniques	396
A2.1 Snedecor's F Test	396
A2.2 Descriptive Measures of an Amplitude Distribution Histogram	396
A2.2.1 Moments for grouped data	397
A2.2.2 Skewness	397
A2.2.3 Kurtosis	399
Appendix 3: The Marandy MR1004 Acoustic Emission System (A Manual For RFPLOTS And RFGGRAPH - Acoustic Emission Analysis Software)	400

Chapter 1

INTRODUCTION

1.1 An Overview Of The Thesis

The main aims of this project fall into two areas: The evaluation (and possible further development) of the technique of acousto-ultrasonics as a means of non-destructive evaluation (NDE), and the study of the structure, properties and acoustic emission of APC, with a view to the development of acoustic emission as a means of non-destructively evaluating APC components. The investigations of the two NDE techniques, although conducted largely independently, shared the same application material, similar coupling problems and were applied to similar material defects. In both cases, there was an initial period of preliminary investigation and optimisation of the techniques, followed by acceptance of standard test conditions then application to APC2 material evaluation.

Acousto-ultrasonics (AU), was originally developed by A Vary (NASA/Lewis, USA) (1,2,3,4), and is still in its infancy. It involves the propagation through a material of ultrasonic stress pulses which mimic the characteristics of true acoustic emission (AE) events. Acoustic emission (AE) types of signal processing and analysis are then used to characterise (quantify) the received (attenuated) pseudo AE events and to derive the Stress Wave Factor (SWF) which has been claimed to be highly sensitive to variations in composite material properties, and thus to be a suitable NDE parameter.

Chapter 1 is an introduction to the general area of non-destructive evaluation, acoustic emission and ultrasonics (a more detailed background of the principles of ultrasonics is given in the appendices).

Chapter 2 presents the principles and background of acousto-ultrasonics including a critical review of the literature.

Chapter 3 deals with acousto-ultrasonics experimentation. Firstly an investigation into the effect of various experimental conditions on the AU SWF parameter is described. This is followed by an optimisation of instrument settings using the statistical analysis of variation and co-variation. The final section describes attempts to use AU to detect a variety of defects in APC2 laminates.

Chapter 4 looks specifically at carbon fibre reinforced PEEK. A short review of the early literature is followed by an account of the mechanical property determinations carried out and observations of the fracture surfaces made during the project.

Chapter 5 deals with the general aspects of acoustic emission, including a brief introduction to the fundamentals and literature of acoustic emission amplitude distribution analysis testing of composite materials. Descriptions of the acoustic emission systems used and software developed in the program are given. Experimental investigations into the effects of test conditions on the acoustic emission output of APC2 are described.

Chapter 6 gives an account of the results of applying AE monitoring to the detection of defects in APC2 laminates, in particular, defects introduced during moulding. Results are based on tensile and flexural stressing.

Chapter 7 describes collaborative work with ICI on the monitoring of fracture processes in APC2, using the Bath AE system interfaced to the ICI crack extension monitoring system. Slow cracking in carbon fibre reinforced PEEK and epoxy specimens was investigated using double cantilever beam (DCB) specimens.

Chapter 8 draws the various elements of the research together describing an investigation into the cross correlation between acoustic emission, acousto-ultrasonic and mechanical property parameters of APC2 specimens.

The final chapters present an overall discussion, conclusions and suggestions for further work. The appendices include definitions of statistical tests and parameters used and computer programs written during the project, including the acoustic emission analysis software developed by the author which is in general use by research groups at the School of Materials Science, University of Bath.

1.2 Non-destructive Evaluation (NDE)

Composite materials, in particular fibre reinforced polymer composites, are replacing more conventional materials in increasing quantities and in an increasing diversity of engineering applications. This particularly applies to lightweight, high strength and high stiffness composites (high specific strength and specific modulus) now being used in various high technology primary structures, for example in the aeronautical industry. In such critical applications it is essential that these composite structures fulfil their design requirements, in other words, that they do not fail. The high cost of these advanced materials and the inability to recover scrap further contributes to the importance of non failure. Suitable means of non-destructive evaluation (NDE) are therefore of the utmost importance. Unfortunately, fibre reinforced composites present many problems for NDE owing to their heterogeneous nature, their susceptibility to fabrication errors and the uncertainty of the effects of individual flaws and flaw populations on structural integrity. Composites may fail in ways quite unrelated to any introduced flaws. They may be notch insensitive and may show interaction of various failure modes such as fibre fracture, matrix cracking, fibre/matrix debonding and delamination (5,6).

Ideally, an object is subjected to non-destructive inspection (NDI) to ascertain the presence and nature of imperfections. If no imperfections are found, the object is fit for service. Any imperfections detected are considered with respect to specifications such as design criteria, mechanical failure theory, regulatory standards or the like. An object containing imperfections which are deemed insignificant with respect to possible failure is passed fit for service. Those failing to conform to specifications are rejected, possibly

repaired and re-inspected, or destructively tested to determine the cause of the imperfection to allow correction of the cause of the defect.

There are a wide variety of types and sources of defects found in composites. NDE processes are required to assess the importance of these defects throughout the life of composite components (5). During fabrication, porosity and degree of cure must be monitored, during service certification, such defects as ply misalignment and poor fibre distribution should be monitored. In service, damage assessment must be conducted (hydrothermal degradation, impact damage, fatigue, static overstressing and corrosion and chemical attack). NDE also has an important role to play in development and materials/component testing.

There are a variety of NDE/NDI techniques which show some applicability to composite materials. These include:

1. Ultrasonics (immersion and contact)
2. Acoustic emission
3. Visual/Optical (including holographics)
4. Sonics (resonance and coin tap)
5. Penetrants (dye and radio opaque liquids)
6. Dielectric (capacitance)
7. Electromagnetic waves (eddy currents and microwaves)
8. Thermal (thermographic)
9. Radiography and radiometry (x-ray and neutron)

The methods most commonly used for composites at the present are ultrasonics (7,8) in particular C-scanning (9). In this technique laminates are typically placed into a water bath over which a single 5 to 10 MHz focussed transducer is scanned. The amplitude of the echo, corresponding to the part of the received ultrasonic pulse which has travelled through the specimen and reflected off the bottom of the tank, is monitored. Scans are

typically mapped as dark and light areas corresponding to amplitudes falling above and below a preset threshold. This technique has shown particular applicability to the detection of delaminations and internal surfaces in composites (9,10). B-scanning is another pulse-echo ultrasonic technique used for locating defects, by measuring time of flight of an echo from surfaces such as internal flaws.

Most of the previously mentioned techniques are largely qualitative, yielding information only about the presence and type of flaw. The probability of the imperfections causing premature failure is best addressed by theoretical mechanics methods such as fracture mechanics (6). At the outset of this project, acoustic emission and the related hybrid technique of acoustic emission and ultrasonics, namely, acousto-ultrasonics, showed most promise as genuine NDE methods capable of quantitative evaluation of the salient properties of advanced fibre reinforced composite materials, in particular, strength and stiffness. Ultimately it is the aim of these NDE techniques to yield some simple accept/reject criterion for composite structures, to establish both the integrity of the material and the response of a structure made of that material (9). In addition, these techniques promise to be of significant use for the research and development of new composites such as APC2.

1.3 Ultrasonics And Acoustic Emission: The Fundamentals

Both the techniques of acoustic emission and acousto-ultrasonics are based on the propagation and detection of stress waves within materials. These stress waves (mechanical vibrations) are high frequency sound waves termed ultrasonic waves because their frequencies lie above those audible to the human ear (20-20,000 Hz). Any consideration of AE and AU should therefore begin with a brief examination of the principles behind the production, propagation and detection of ultrasonic elastic waves. This has been given as appendix 1, which covers the basic principles behind the different types of ultrasonic waves, wave velocities, reflection and mode conversion, and in particular, attenuation in solids.

Acoustic emission as formally defined by ASTM is 'the class of phenomena where transient elastic waves are generated by the rapid release of energy from localised sources within a material, or the transient elastic waves so generated'.

Acoustic emission events are usually monitored with a piezoelectric (PZT) transducer coupled (often with a viscous fluid couplant) to the surface of the item under stress. The electrical signal from the transducer is passed through a preamplifier (typically 40 - 80 dB gain) and often a high pass filter to cut off low frequency noise below around 100 kHz, before being analysed. AE activity is typically categorised into continuous and burst types, the latter being applicable to composite materials where discrete micromechanical events such as fibre fractures are the dominant source of acoustic emission, rather than more continuous deformation processes such as dislocation movement in metals.

In broad terms, acoustic emission events are of the form shown in figure 1.1, having a short rise time to maximum amplitude followed by a near exponential decay down to the background noise level. This idealised signal can be represented by

$$V = V_0 e^{-Bt} \sin \omega t \quad \dots 1.1$$

where V = output voltage of transducer,
 V_0 = initial signal amplitude,
 B = decay constant,
 t = time,
 ω = angular frequency.

Various characteristics of AE pulses (which are essentially damped sinusoids) can be analysed. The various parameters monitored from AE events and displayed in figure 1.1 are used in acoustic emission testing, however simple event and ringdown counting are the most common.

1.3.1 Ringdown Counting

Each event produces multiple threshold crossings (ringdowns) due to the oscillating particle motion of sound waves. The number of ringdown counts recorded is a complex function of various factors: frequency response of the structure and sensor, the signal amplitude, coupling efficiency, sensor sensitivity, attenuation and damping characteristics of the structure, amplifier gain and threshold.

When the time taken for the signal to decay down to the background noise level is long relative to the period of oscillation, the number of ringdowns N from a single event is given by the relation (11)

$$N = \frac{\omega}{2\pi B} \ln \frac{V_o}{V_t} \quad \dots 1.2$$

where V_t = threshold voltage,
 V_o = initial signal amplitude,
 B = decay constant,
 ω = angular frequency.

The higher the amplitude of the event, the more threshold crossings it produces. Simple acoustic emission monitoring systems count these ringdowns. More sophisticated devices monitor the rate of generation of ringdowns. A root-mean-square meter can be used to monitor the mean pulse amplitude, giving a guide to the amount of energy being dissipated by the stressed article.

1.3.2 Event Counting

More sophisticated acoustic emission systems count individual AE events by sensing an initial threshold crossing and a rise time. Consecutive events are distinguished by a fixed 'dead time'. This method of analysis has the disadvantages of the 'dead time' limiting the rate at which events can be recorded, and the fact that event amplitude is not monitored.

1.3.3 Rise Time, Decay Time and Event Duration

The rise time is the period between the first threshold crossing of the signal during an AE event and the peak amplitude. The decay time is the period from peak amplitude to the last signal oscillation which exceeds threshold. The event duration is the summation of rise time and decay time. It is the time between the first and last ringdown above threshold of an event.

1.3.4 Acoustic Emission Energy

The electrical energy of a received AE event is proportional to the area under the voltage/time curve

$$U = \frac{1}{R} \int_0^x V^2 dt \quad \dots 1.3$$

where V = voltage,
 R = resistance of the measuring circuit,

Various methods are available for determining relative measures of AE energy. None give the absolute energy quantity. Digitisation of the signal and integration of the waveform is the most direct. An approximation of the rate of AE energy production is given by the root-mean-square voltage. Relatively simple apparatus can be used to monitor it. However one disadvantage is the relatively slow response time of rms meters compared to the duration of most AE events making V_{rms} indicative of average energy.

1.3.5 Amplitude Distribution Analysis

This analysis method counts events (as in normal event counting) however the amplitude of each event is also recorded. Almost exclusively, a log amplifier is utilised to cope with the typical 4 orders of magnitude range in event amplitudes. A multi-channel memory records the numbers of events within specified ranges of amplitude, thus allowing the production of event amplitude distributions.

If a cumulative amplitude distribution is plotted with a logarithmic scale, then the slope of the resulting graph line is termed the b slope and sometimes used as a single numerical parameter to describe the amplitude spectrum. Alternative parameters, for example, the mean, variance, skewness and kurtosis, derived by taking moments around the distribution's mean (see appendix 2), can also be used.

Event and ringdown counting have been applied to various quality assurance and in service life assurance testing (12), however they give no information as to the specific character of source 'events' which produce AE stress waves.

Acoustic emission frequency spectrum analysis has also been conducted however it is likely to be of limited use in practice due to the dominating effects of specimen and transducer resonances (13,14). Event source location can be achieved by using multiple transducers and measuring event arrival time. Event counting, the amplitude of events and to a lesser extent ringdown counting are the principal AE parameters used in this research project.

Chapter 2

ACOUSTO-ULTRASONICS: AN INTRODUCTION AND LITERATURE REVIEW

Acousto-ultrasonics (AU) combines the technologies of acoustic emission and ultrasonics to allow, it is claimed (1,2,3,15,16,17,18,19,20,21), the characterisation of composite material properties, in particular, strength, by truly non-destructive means. Simulated stress waves are used to quantify the condition of material, in particular composite material, with respect to defect states, damage conditions and variations of mechanical properties. A constant repeated broadband ultrasonic pulse is injected into a material and then detected at some distance away by a lower frequency transducer. The received pulse is then quantified by means of the types of signal processing used in acoustic emission. This yields a numerical AU parameter, the Stress Wave Factor, which is claimed to be applicable to the evaluation of both discrete defects (7,22,23), and more importantly for composites, to the integrated effect of minor defects and diffuse populations of sub-critical flaws (1,4,7,15). It is claimed that this will infer sensitivity of AU to strength, fatigue life, stiffness, toughness and dynamic response (2,4,7,8,15,21,22,24,25,26,27,28,29,30,31).

AU was developed in the late 1970's by NASA/Lewis Research Centre in conjunction with Acoustic Emission Technology Corporation (AETC, Sacramento, California). AETC was, at least until 1987, the only company to produce a commercial AU system, the AET model 206 AU, and it is the aim of this research project to determine whether AU in general (and the model 206 AU in detail) is a valid and useful method of NDE of composites, in particular APC.

2.1 The Basic Principles Of AU Testing

Figure 2.1 shows diagrammatically the principles of AU testing. A broadband ultrasonic transducer (0.1 to up to 5 MHz) is coupled to the surface of a component (almost

exclusively a thin plate-like structure) at normal incidence using a coupling medium such as a viscous liquid or compliant rubber sheet. A repeating pulsed oscillator generates an electrical input signal, either short spike or square wave burst (of selected frequency and duration) at regular intervals into the emitter transducer. This introduces an ultrasonic stress pulse which mimics the characteristics of true acoustic emission pulses produced spontaneously when a material is stressed. The introduced pulses are essentially longitudinal ultrasonic waves (longitudinal wave transducers being used) spreading out through the thickness of the component until they meet interfaces such as free boundaries. The divergence of the introduced pulse will yield non normal incidence at the component surfaces, oblique angle reflections and hence propagation of the pulse laterally along the thickness of the plate. The pulses will undergo multiple reverberations (reflections), mode conversions and attenuation and scattering prior to being detected and received by a second transducer usually coupled to the same surface as the emitter, at some fixed distance from the emitter (typically 25 mm - 100 mm ⁽¹⁵⁾). The receiving transducer must typically be an acoustic emission sensor of high sensitivity. This is necessary because of the large attenuation coefficients of composite materials.

The received pulses are amplified through a preamplifier (typically 40 dB) and filtered through band pass filters before being analysed. The analysis (signal processing) is usually accomplished by virtue of conventional acoustic emission methods, the original and the most common of which in AU, is to count ringdowns, oscillations of the received signal above a preset threshold.

The received ultrasonic stress waves which go to make up the received pulse envelope should largely be from waves which have propagated through the material directly between the emitter and receiver transducers, though reflections at specimen boundaries will introduce some echos into the AU waveform from outside this region. The received pulse, and any AU parameter which quantifies it, should be largely representative of the condition of the material immediately between the emitter and receiver transducers.

Thus, for the assessment of larger areas of composite plates, the AU probes must be repeatedly moved and recoupled over the surface. As with conventional ultrasonic testing, the test specimen must be scanned.

2.2 Methods Of Signal Processing: AU Parameters

The characterisation and quantification of acousto-ultrasonic pulses, exhibiting complex combinations of echos of various amplitudes and durations (32), yields a numerical AU parameter, which should characterise the degree of modulation of the AU pulse after its propagation through the test material. A typical received AU pulse, recorded from AU testing of a 16-ply 0/90 APC2 laminate is included as figure 2.2. The different methods of quantifying these pulses will now be considered.

The Stress Wave Factor (SWF) was the original acousto-ultrasonic parameter, defined by Vary (2), and the most widely used. It has been the primary subject of investigation in the work included within this thesis. With reference to figures 2.1 and 2.3 the SWF is defined as follows: AU pulses are generated at a repetition rate of $1/p$, the number of threshold crossings (ringdowns) above a preset threshold C are accumulated over a time period T and the SWF is defined as:

$$\text{SWF} = C \cdot T \cdot 1/p. \quad \dots 2.1$$

A time gate is normally used to select a chosen part of the pulse envelope over which to count ringdowns. The SWF is a ringdown count of each pulse, summed over the number of pulses generated during the counting time period. It is a dimensionless number. Since each pulse is essentially identical to the next (16), assuming that the pulsing rate is sufficiently low to prevent overlapping of subsequent pulses (each pulse rings down before the next arrives), a less complicated parameter would be the number of ringdowns per pulse, an AU parameter occasionally quoted by other researchers (33).

Other parameters have also been used to characterise the received pulse. Rodgers (15) and Green (8) have used the root-mean-square (RMS) voltage of the signal as a measure of the energy content of the received AU pulse, termed the signal level. The relative energy of the acousto-ultrasonic signal can be defined in the time domain as:

$$E_{\text{time}} = (V_{\text{rms}})^2 = 1/T \int_{t_1}^{t_2} V^2 dt \quad \dots 2.2$$

where T is a time period t_1 to t_2

t is time

V is time varying voltage.

More recent work by a few authors has involved somewhat more sophisticated signal processing in the frequency domain. An analogous expression to 2.2 can be written in the frequency rather than the time domain as

$$E_{\text{freq}} = (S_{\text{rms}})^2 = 1/F \int_{f_1}^{f_2} S^2 df \quad \dots 2.3$$

where F is a frequency interval f_1 to f_2

f is frequency

S is a function of frequency.

Any waveform can be represented in sinusoidal form by a fourier series as the sum of a given number of oscillations unlimited in time and contained in a frequency band of given width. Govada et al (34), Kautz (26,35), Duke et al (36) and Talreja et al (37,38,39) have digitised the captured AU wave forms and used fast fourier transform algorithms to determine the frequency spectra, from which AU parameters have been determined. Talreja (37,39,40) defined several shape and scaling parameters to describe the frequency spectrum, by considering it to be a plane figure that is closed on the frequency axis. Various moments of the frequency spectrum about the amplitude axis were then determined by a method analogous to that used later for determining moments of an amplitude distribution histogram (see appendix 2). Parameters, including the area under

the power spectral density curve and centroid, skewness and kurtosis of the frequency spectrum, have been proposed as alternative AU parameters (23,39). Kautz has used the RMS of the power spectrum of the AU pulse partitioned in the frequency and time domains (35).

Vary also quotes peak voltage of the pulse as a possible AU parameter which is analogous to amplitude sorting of acoustic emission. Peak amplitude has been used by Mittelman et al (41).

Williams and Lampert used a modification of Vary's SWF in which, before summation, each ringdown was given a weighting proportional to its peak voltage (20).

Some authors have acquired the practice of presenting AU readings normalised against the maximum value found for a material and experimental test configuration (2,39,42,43,44). This practice tends to make it difficult to compare data from different sources, in particular for SWF data, because the underlying ringdown count per pulse becomes impossible to determine by the reader.

2.3 Factors Affecting The Stress Wave Factor

Vary et al reports that his SWF is a measure of the signal strength (4,7,18). Theoretically, defective material found between the transducers will scatter and attenuate the ultrasonic pulse more than will good quality, non-defective material, thus producing fewer ringdowns and a lower SWF. For material without major defects the SWF is claimed to be sensitive to the efficiency of strain energy transfer, areas of high SWF would exhibit improved stress wave energy transfer, lower probability of stress concentration and failure (4,7,8,18,45). Hence low values of SWF should correlate with sites of probable weakness and hence probable specimen failure.

The SWF is a dimensionless number. It is proposed to be a comparative measure of material quality, but it depends on many factors:

1. Coupling between transducers and specimen
 - a) contact pressure,
 - b) type of couplant.
2. Emitted ultrasonic pulse
 - a) emitter transducer (type),
 - b) pulse excitation characteristics
 - (i) energy (for 'pulse' type excitation)
 - (ii) frequency and duration (for 'burst' type excitation)
 - c) trigger rate (pulses/sec).
3. Received signal and processing
 - a) AE transducer (type),
 - b) gain (dB),
 - c) counting rate (s^{-1}),
 - d) threshold (v),
 - e) gate width (microseconds).
4. Inter-transducer separation.

These factors with the exception of the types of transducer used have been investigated within this research project.

Assuming that all these factors are kept constant, any variation in SWF should be a reflection of material under investigation according to Vary et al (1,2,3,4,5,7,18,21,42), Williams et al (13,20,46), Green and Rogers (8,15,16,22), and Henneke et al (17,47) these being the authors of most work published by the start of this project. The literature reports correlations of the SWF with various characteristics of several composite materials, some basing work on the AETC AU206 acousto-ultrasonic testing system.

2.4 A Review Of The Literature On Acousto-Ultrasonics

There are a few general remarks to be made about the literature available on acousto-ultrasonics, before considering it in more detail. Almost all work has originated from the USA. Many of the published papers on acousto-ultrasonics have been straightforward descriptions of how the AU technique, and in particular the original SWF, has been correlated with various material characteristics (1,2,3,4,8,10,15,16,17,18,19,20). More recently there has been more work investigating the fundamentals of the technique such as wave propagation modes and scattering and attenuation in composites (13,26,35,48,49,50). In addition, there have been papers which have reviewed and promoted the technique, mainly by authors such as Vary, Green and Rodgers (15,16,22). More recently there has been a shift towards the use of more complex acousto-ultrasonic parameters other than Vary's original SWF, based around the frequency spectra of the received AU pulse, indicating perhaps that the original SWF is not wholly satisfactory for material characterisation.

The story of acousto-ultrasonics starts in 1976 with the work by Egle and Brown on the development of artificial acoustic emission sources for the investigation of the frequency spectra of acoustic emission events (14,51). An electric spark, laser beam and piezoelectric generator were all found to be suitable for producing pseudo-acoustic emission events, though the latter source was considered most useful because of its simplicity and convenience, ease of control of the wave form and the type of stress pulses generated (longitudinal and/or shear). It can be assumed that the extent to which these simulated acoustic emission events will be modulated is dependent on the condition of the material through which they propagate. If parameters are defined which characterise these modulated 'simulated' events, then any change in the condition of the material will be reflected by a change in these AU parameters. Further, the ability of the material to transmit stress away from sites of stress concentration will at least partly contribute to high failure strength. Good quality material which can delocalise stress by

good stress wave transmission will, it is argued ⁽¹⁾, show greater strength than poor quality material which does not.

Vary ^(1,2) bases the fundamental principle of acousto-ultrasonics on the following hypothesis. At the onset of fracture in a material, spontaneous stress waves will promote rapid crack growth unless their energy is dissipated in other ways. The rapid and efficient transmission of stress wave energy away from crack nucleation sites is desirable if the energy cannot be absorbed locally without cracking. By introducing artificial stress waves into a material and monitoring how they are modulated and thus how good the material is at transmitting these stress waves, the ability of the material to delocalise stress away from local flaws (stress concentration sites) can be determined.

Acousto-ultrasonics was originally developed for the non-destructive examination of composites, in particular, components involving fibre reinforced laminated sheet. In these materials, failure is often not associated with single overt defects, as is the case for most homogeneous materials, but with the cumulative net effect of damage and distributed flaws ^(9,15,18,43). One of the alleged advantages of AU is its ability to assess the integrated effects of minor defects and diffuse populations of sub critical flaws ^(4,15). Other salient advantages claimed ^(1,15,18,21,36) include, from a practical point of view, single surface access for probe attachment and the ability to cope with the high attenuation coefficients typical of composites and their marked anisotropy. In addition, AU has ability to propagate investigative stress waves in directions of principal applied stresses (parallel to fibres within the plane of the plate) and even in curved laminates because of the waveguiding effects of laminate surfaces ⁽⁷⁾. The technique is claimed to be applicable to the NDE of various complex bonded structures in which adverse geometric factors preclude the use of conventional ultrasonic techniques ^(15,18).

In broader terms, acousto-ultrasonics may be considered to be simply an ultrasonic attenuation technique and can be likened to conventional pulse - echo ultrasonic testing,

but using alternative (AE) methods of signal processing. However, AU is distinctive in its use of relatively long duration pulses which undergo multiple reflections before reception and its use of acoustic emission methods of signal processing. This leads to a single numerical parameter which is claimed to possess the ability to rate materials according to strength (1).

In general the presence of defects or flaws in material will be expected to cause increased attenuation. The variety of defects in composites include porosity, microcracks, delaminations, poor bonding (between plies and between fibres and matrix), variations in cure state, variations in fibre volume fraction and fibre alignment. The question which should be addressed is to what extent the variations in material structure which infer variations in mechanical properties, will affect the attenuation and modulation of AU pulses and to what extent the Stress Wave Factor monitors them, and is sensitive to them.

Vary and Bowles first applied acousto-ultrasonics to the assessment of strength in graphite fibre/polyimide unidirectional composite laminates (1,2). Since that time, acousto-ultrasonics has been applied to a fairly wide variety of materials (usually composite on a micro or macro scale). Kautz has applied the acousto-ultrasonic technique to several composite materials. To sections of graphite fibre/epoxy and graphite fibre/kevlar fibre/epoxy hybrid filament wound cylinders (26,27) and graphite fibre/epoxy and unreinforced pure epoxy plates (35). Henrique applied AU to wood fibre hardboards (43), Mittelman et al to human bone (41), Phani and Bose to jute/glass fibre reinforced polyester (24), Govada and Duke to metal matrix composites (10), Williams et al to double-braided nylon rope (29) and Srivastava and Prakash to glass/polyesters (30). The material properties or characteristics investigated with AU include strength (1,2,24,25), stiffness (37,40,47), bond strength (15,18,33,52,53), impact damage (8,20,54) and fatigue life/damage (34,37,38,40,47).

The first use of AU investigated the effect of void content on strength of 2.3 mm thick 12-ply unidirectional Hercules AS graphite fibre/PMR-15 polyimide plates (1,2,7). The SWF was used and was measured by using a 2.25 MHz emitter, receiver resonant at 0.5 MHz and water as couplant. The SWF was reported to have a positive correlation with cure pressure as shown in figure 2.4. Laminates were prepared at different cure pressures ranging from 50 to 800 psi and consequently the measured laminate void content varied from 0 - 5.2 % and fibre volume fraction from 0.607 - 0.655. This, in turn, caused significant variations in the interlaminar shear strength (ILSS). Velocity, through thickness attenuation and SWF measurements were made on the laminates and the different parameters compared. The most significant conclusion from this was that plates which exhibited lower overall SWF measurements also showed a lower mean and greater variation in through thickness attenuation from point to point across the plate (measured by a twin probe immersion method). Variation of attenuation and SWF measurements appeared to be the result of scattering attenuation due to varying concentrations and sizes of voids, these voids causing reduced ILSS. A similar effect has been reported by Rogers (15). In this case RMS voltage decreased with increasing porosity in 2 mm thick UD graphite/epoxy laminates as shown in figure 2.5. In this figure each point is the mean of 30 readings across a laminate, but no measure of scatter is given, an omission common in the literature on acousto-ultrasonics.

2.4.1 Assessment of Strength

An early piece of work by Vary and Lark showing that the SWF has a positive correlation with σ_{UTS} (and $(\sigma_{UTS})^2/E_{elastic}$) in 8-ply graphite/epoxy (4) as shown in figure 2.6 has been widely reported by reviewers of the technique. However it should be noted that the variation of specimen strengths stemmed from the different lay-ups of specimens, namely 0° , 10° , 90° , $0^\circ/\pm 45^\circ/0^\circ$ and $\pm 45^\circ$. The greater the alignment of the reinforcing fibres in the principal axis of subsequent tensile testing, the higher the SWF and not surprisingly, the strength, which showed more than an order of magnitude variation. Similar trends are reported in glass/epoxies (7).

SWF has been reported to vary systematically with interlaminar shear strength (measured by short beam shear tests) for graphite/polyimide and glass/polyester composites (1,2,3,4,7). In addition, ultrasonic modulus (density multiplied by the square of the wave speed, ρv^2) varied in a similar manner with ILSS (2). The SWF is also reported to be sensitive to strength variations associated with fibre-resin bonding, voids and fibre-resin ratios in the same type of composite (2,7). Green reviewed work on AU (16,22), concluding that the SWF was a sensitive indicator of composite strength variation and could predict potential failure locations in composite laminates.

Kautz investigated AU as well as ultrasonic velocity in 3.02 and 3.34 cm thick segments of Kevlar/graphite epoxy filament wound cylinders (27). Kautz defined alternative stress wave factors. He determined the energy content of the signal over each of the four 250 kHz frequency bands in the range 0 - 1.0 MHz by determining the root mean square voltage integrated over the sweep time. These energies were correlated with the ILSS. It was found that only the 0.5-0.75 MHz frequency range produced a correlation with ILSS as is shown in figure 2.7. It should be noted that the ILSS values were claimed to vary from 400 and 1400 MN/m². These strengths are impossibly large for a resin composite, in addition to representing a large variation from nominally identical material. Also, the scatter in the data would indicate that this stress wave factor can only predict ILSS within about $\pm 25\%$. Kautz also found a good positive correlation between through thickness velocity and density. This is somewhat unexpected considering the fundamental proportionality of ultrasonic wave velocity to $\sqrt{E/\rho}$.

In his next publication, Kautz reports an optimum frequency range for AU testing, (0.6-1.0 MHz) (26). Frequencies above this range were deemed unsuitable owing to excessive attenuation of the injected pulse. Further to this, longitudinal waves with fewest reflections before reception were considered least ambiguous for AU testing, giving the first 20 microseconds of the received pulse as the portion most sensitive to variations in ILSS of sections of graphite/epoxy filament wound pipes.

An interesting comparison of two AU parameters was made by dos Reis ⁽⁴³⁾. He recorded Kautz's SWF ⁽²⁷⁾, the square of the amplified transducer output voltage integrated over the time of sweep, and the redefined SWF of Govada et al ⁽⁵⁵⁾, namely the root mean square of the power spectral density. Each was correlated after normalisation with the peel strength of 6 mm rubber sheet bonded in vulcanisation to 2 mm steel plate. Both parameters gave very similar results and positive correlation coefficients with peel strengths (varied by deliberately introducing defects). It therefore appears that there is little essential difference between the various definitions of the stress wave factor. All methods measure signal strength, but by slightly different means.

The AU206 system was used with the transducers in the through transmission configuration on 26 mm cubes of gypsum, a porous brittle solid ⁽³¹⁾. A positive correlation between the normalised SWF (E) and compressive failure strength (σ) was claimed from the data shown in figure 2.8. Careful examination shows that the normalised SWF values decrease from 1.00 to 0.91 for an approximate halving of the failure strength, yet Vary ⁽¹⁸⁾ and Henneke et al ^(17,55) have reported that SWF values are only reproducible to approximately $\pm 10\%$. It would therefore appear unlikely that the correlation is of any real significance.

Asok De, Phani and Kumar reported good correlation between the SWF and three point flexural strength (modulus of rupture, MOR) of 3.5 mm diameter MgO-Al₂O₃-SiO₂ glass ceramics ⁽⁵⁶⁾. In contrast to the work of most authors the SWF was, in this case, shown to vary inversely with strength, a lower SWF indicating greater strength. This was concluded to be due to ultrasonic scattering loss by the crystallites in the glass ceramic. Initiation and growth of numerous small crystallites (higher MOR) reportedly produced increase scattering, whilst larger crystals (lower MOR) decreased scattering. This explanation cannot be verified because frequencies, wavelengths and wave speeds were not reported.

Using various position, shape and scaling parameters to describe the frequency spectral distribution of the received AU pulse (basically taking moments of the frequency distribution), Talreja investigated the effect of fibre alignment, impact damage and modulus variations in several composite systems. One of these parameters, the zeroth moment of the power spectral density, which is the area under the power spectrum curve and apparently equivalent to the analog RMS voltage of the signal ⁽⁴⁵⁾, showed good correlation with Vary's SWF ⁽³⁸⁾ and several material variables. These were elastic modulus variations resulting from property measurements at angles to the principal fibre direction in a unidirectional composite ⁽³⁹⁾, and with laminate stiffness reductions due to tension/tension fatigue damage in graphite/epoxies ⁽³⁸⁾.

Mittelman et al applied AU in the through transmission mode to 1 cm long, 1 cm diameter cylinders of human bone ⁽⁴¹⁾, finding a positive correlation (linear correlation coefficient of 0.68) between peak amplitude and bone density, but apparently no correlation with Vary's SWF.

2.4.2 Bonding

AU has been applied to the NDT of various bonded structures. According to Rodgers ⁽¹⁵⁾ disbonding of a metal skin from a variety of honeycomb core materials can be characterised by an AU signal increase in areas of poor bonding. This was considered to result from the signal mode converting into Lamb waves in the metal skin, rather than being dissipated into the honeycomb substrate which occurs when bonding is adequate. This appears to contradict the work by Vary et al ⁽¹⁸⁾ on the evaluation of diffusion bond quality between a metal honeycomb and porous wire form substrate. In this instance, the authors reported an increase in the signal strength (SWF) with *improved* bond quality. They concluded that poor bonding between honeycomb and porous wire form substrate resulted in lower energy transmission and hence lower values of the SWF.

Brahma and Murthy ⁽⁵²⁾ using the SWF claimed 'good sensitivity' of AU to bond quality of sintered copper-lead strips used for plain bearings when using the through transmission mode (emitter and receiver on opposite faces of a plate). This conclusion was based on the results of 12 specimens, half good and half defective. Specimens were chosen for their defectiveness by visual examination: the 'bad' bond quality between copper and lead was obviously quite severe. Apparently, little if any, consideration was given to the scatter in SWF measurements which was considerable according to the limited data reported in this paper. The configuration of AU testing (both transducers on the same surface) was found to be less than adequate for the NDE of copper-lead bond quality, a through thickness probe configuration was needed which showed a reduced AU signal for poor bonded areas.

Srivastava and Prakash reported a positive correlation between the SWF and breaking strength of single lap joints between GRP and GRP, and CFRP and CFRP substrates. The bond line was Araldite two pack epoxy adhesive ⁽⁵³⁾. The correlation is shown in figure 2.9. Although confidence levels for the regression lines to the data are given, the values of the stress wave factor are quoted as the maxima for each sample, but the number of readings per sample and the scatter in the data recorded are not quoted. In addition, a pulse rate of 1000 pulses/second and sampling time interval of 1/8 sec were reportedly used, yet the SWF data in figure 2.9 do not increase in integer multiples of 125 as one would expect.

Williams et al have claimed a linear correlation between the SWF and the bond strength of adhesively bonded automotive glass fibre composite single lap joints (SMC substrates and urethane adhesive) ⁽³³⁾. SWF measurements were made with the AU206 and reported as an average number of ringdowns for a single pulse. Bond strengths were varied by the introduction of major defects produced by under curing and the use of mould release agents at the bond lines. This induced a reduction of up to 90% in normal bond strength as may be seen in figure 2.10, where the SWF is plotted against bond

fracture strength. The reported reproducibility of SWF measurements is no better than $\pm 10\%$, and it should be noted that in figure 2.10 the number of ringdowns per pulse decreased by a maximum of only 25% for a decrease in strength of 90%, a decrease only slightly greater than the expected scatter in the data. The correlation between the SWF and bond strength would appear, therefore, not to be statistically significant, and this in spite of the fairly major defects used to reduce specimen bond strength.

2.4.3 Assessment of Degradation

Another of the advantages claimed of AU is the ability to assess degradation in composite materials, for example from moisture absorption (24,25), cyclic fatigue (37,40,47) and impact damage (8,20,47,54). Srivastava and Prakash (30) found a positive linear correlation between the SWF and 3 point flexural fatigue life of a 5 mm thick 0/90 E glass/epoxy laminate. SWF has been correlated with the residual strength of impact-damaged carbon fibre/epoxy composites (8,20,47), apparently due to the detected effects of intrinsic flaw populations.

AU has been applied to assessment of fatigue induced degradation in composites by Govada et al (34). Fatigue damage development was monitored in $[0,\pm 45]_s$, $[0,90]_s$ and $[0,90,\pm 45]_s$, graphite/epoxy laminate coupons subjected to tension-tension fatigue (loading ratio 0.1 and σ_{\max} 70% of UTS). Their chosen AU parameters were based on taking moments of the frequency spectrum (scale, shape and location parameters). The root mean square of the power spectral density was found to decrease with decreasing stiffness due to cyclic fatigue (34). The fatigue damage was reportedly primarily matrix crazing and fibre breakage distributed throughout the volume of the material subjected to fatigue. Although it was noted that there was scatter in the AU data, no measure of this was given, so the ultimate sensitivity of the AU parameters to fatigue damage cannot be assessed from this reference.

Dos Reis and McFarland have used the AU206 for the NDE of rope, in this case, 1.59 cm diameter steel wire rope with a resin binder (28,43). The pulse mode of excitation was used on different rope samples subjected to different numbers of tension/tension fatigue cycles, the results of which are shown in figure 2.11. There is an apparent decrease in the SWF with an increasing number of fatigue cycles. Fatigue damage included a maximum of 47 obviously broken wires. According to the experimental conditions (instrument setting) namely pulse rate (1/p) of 250 pulses per second and an accumulation time (T) of 0.25 seconds, the SWF values should be approximately integer multiples of 62.5 which they clearly are not. There appears to be an anomaly here. In addition, no measure of experimental scatter is given.

Dos Reis has applied the AU206 to the non-destructive examination of 8.1 mm thick wood fibre hardboards with different compositions subjected to cyclic soak tests (43,57). SWF measurements were made at the end of each soaking cycle and then plotted against the percentage calliper swell (the increase in board thickness due to swelling as a percentage of the original thickness) as is shown in figure 2.12 (43). The trend of decreasing SWF with increasing calliper swell would be expected considering the very large increases in board thickness recorded (up to 90%) and thus consequential decreases in modulus. The small number of samples tested and the lack of any estimation of experimental scatter must reduce the usefulness of this data. In addition, the effect of hydrothermal degradation on surface finish and hence AU coupling has not been considered. Hydrothermal attack is likely to degenerate the surface properties, surface finish and flatness (58), which is likely to impart a decrease in coupling efficiency and thus an apparent decrease in the SWF during subsequent testing. This factor has not been mentioned by dos Reis (43) or Phani and Bose (25).

Phani and Bose (25) also investigated hydrothermal aging with acousto-ultrasonics. They correlated 3 point flexural strength with the SWF (normalised) measured on 2.4 mm

thick CSM E glass/polyester laminates subjected to hydrothermal aging at temperatures up to 100°C.

Water immersion caused a large decrease in failure strength from 230 to 90 MN/m² which resulted in a decrease of the SWF reportedly due to hydrolytic attack of the fibres (swelling of the matrix (osmosis) and matrix plasticisation). Similar trends were determined for the hydrothermal aging of jute/glass hybrid laminates (24), and E and N glass/epoxy rods (44).

Williams and Lampert (20) investigated both through thickness attenuation and their modified SWF with respect to repeated drop weight impacts in 10-ply unidirectional graphite/epoxy, using the FC500 emitter/AC 375 receiver transducer combination used by the AU 206 acousto-ultrasonic system. Their modified SWF (each ringdown was given a weighting proportional to its peak voltage before summation), is plotted against through thickness attenuation in figure 2.13.

Clearly, increasing numbers of impacts (each approximately 2.5 J) causes a decrease in the SWF and an increase in the attenuation. However one should note that the SWF dropped by only 2, from 31 after 10 drop weight impacts, and 4 after 40 impacts. Such small reductions in the SWF, which are unlikely to exceed normal experimental scatter (not quoted in this reference), after such major damage, must indicate that the technique is an unrealistic method of impact damage detection.

2.4.4 Locating the Position of Eventual Specimen Failure

It has been claimed that AU is able to locate the position of eventual failure in composite coupons containing no overt defects, when they are subsequently tested to destruction in tension. In experiments conducted on 8-ply AS carbon fibre/PR-288 epoxies SWF measurements made at 15 regular intervals along the gauge length of tensile test pieces have been reported not only to rate the specimens correctly according to strength but also

to locate the loci of eventual failure ⁽⁴⁾. The minimum value of the SWF identified the point of eventual failure. Similar results have been reported for a $[0,90_3]_s$ E-glass/epoxy (9,47,55,59).

2.4.5 Defect Detection

Any defect or discontinuity present in the material under investigation leads to the attenuation of stress waves and thus the reduction of stress wave energy transmission ⁽²⁵⁾. Against this background, AU has been applied to the detection of a variety of different types of defect, in addition to sites of impact damage already mentioned.

Madhav and Nachlas ⁽²³⁾ applied the AU technique to the comparison of various types of defect introduced into different quadrants of a 12" square 6-ply unidirectional graphite/epoxy plate, using the square root of the zeroth moment of the frequency spectrum (after Talreja ^(37,39,40)) as the AU parameter. The three defects, a one inch crack, a one inch square delamination and a mixture of the two, were claimed to be distinguishable from good non-defective material. However, no mention was made of the reproducibility of AU measurements, apart from a concluding remark that 'minor modifications of the experimental apparatus will assure the repeatability of the AU response'.

Talreja also investigated graphite/epoxy filament wound specimens, one prepared under normal autoclaving conditions, one without autoclaving and hence porous, and one with chopped pieces of Teflon mixed with the epoxy matrix ^(37,39). None of the AU parameters could reliably distinguish the defective specimens from the good quality specimen using the conventional disposition of AU transducers on the same face of the specimen. Only in the through transmission mode (transducers on opposite faces) could the RMS value make a valid distinction. Of the various parameters studied by Talreja, the RMS value, which showed greatest sensitivity to material variation, also showed

greatest scatter, up to 35% of the mean. Scatter bars were included in the reporting of data in this instance.

Williams et al applied the AU 206 to double braided 0.64 cm diameter nylon rope ⁽²⁹⁾. Pulse mode SWF measurements were made on defective and non-defective rope samples loaded in tension at intervals from 0.2 to 4.5 kN. The transducers were clamped using a large fixed coupling pressure to the outside circumference of the rope. No couplant was used. The flat transducer faces were therefore dry coupled to the curved surface of the rope. The results of this exercise are shown in figure 2.14. Perhaps the most significant point to be made is that no single SWF value at a single load level can be used to distinguish all the types of rope samples considered. To explain the load/SWF plots in figure 2.14, it was proposed that there are two competing mechanisms for stress wave conduction in the ropes. Firstly, transducer to rope contact area: high loads cause a decreased compliance of the rope, lower surface area of transducer to rope contact and hence a reduced stress wave conductivity and lower SWF. Secondly, rope compaction: higher tensile loads compact the fibres in the rope causing improved stress wave transmission and higher SWF values. Furthermore, it was proposed that an increase in the volume of material under test reduces the SWF by increasing the available volume into which the injected ultrasonic energy can spread and be lost. This was the explanation given for defective rope with a reduced cross sectional area giving increased SWF readings, all other factors being constant.

Hemann et al ⁽⁶⁰⁾ used the RMS voltage in the 10-15 microsecond time portion, 0 - 1.285 MHz frequency portion of the AU signal for correlation with the transverse crack density, produced by preloading 0°/90° and woven fabric carbon fibre reinforced PMR-15 polyimide. The RMS voltage (the mean of 5 or 7 measurements per specimen) is plotted against crack density in figure 2.15. The decrease in RMS voltage with increasing crack density is quite evident. However it should be noted that for a fixed crack density there can be a considerable range of RMS values associated with it. The

scatter in readings produced by repeated coupling and recoupling of the transducers, which is not apparently considered in this paper, would further diminish the feasibility of this technique for crack counting. The decrease in RMS or any other measurement of AU pulse energy with increasing crack density is explained by ultrasonic theory: cracking reduces the local stiffness of the material, and cracks act as inhomogeneities for ultrasound scattering. Kinra and Dayal demonstrated a six fold increase in the attenuation of flexural Lamb waves for an increase in the number of transverse cracks between source and receiver from 0 to 14 in a $[0/90_4]_s$ graphite/epoxy ⁽⁶¹⁾. They concluded that in this case stiffness was the fundamental factor affecting attenuation, cracking causing a decrease in stiffness. The wave speed was also found to be appreciably affected by damage (cracking).

2.4.6 Studies of the Principles Behind AU Testing

In addition to the literature describing application of AU to the NDT of materials, there have more recently been investigations into various facets of acousto-ultrasonics, aimed at understanding the principles behind the technique. Included in this are such areas as attenuation, the frequencies of the AU pulses used and wave propagation.

Kinra and Dayal ⁽⁶¹⁾ investigated the effect of damage (transverse cracks) on both the wave speed and attenuation of Lamb waves propagating in thin $0^\circ/90^\circ$ graphite fibre/epoxy laminates. At 500 kHz, the attenuation was found to increase considerably and the wave speed diminish with increasing densities of transverse cracks.

The frequency range of incident pulses and the distance between transducers are two important factors in acousto-ultrasonics which have been given little consideration in the literature until recently, according to Pilarski et al ⁽⁴⁹⁾. Earlier AU research involved transducers close together, with essentially longitudinal wave propagation and few reverberations of the pulse before reception at the receiver. Later work has involved transducers at a greater distance, which allows Lamb waves to develop, assuming that

wavelengths are commensurate with the plate thickness ⁽⁴⁹⁾. Rayleigh (surface) wave propagation can only occur when the plate thickness is much greater than the wavelength. The high frequencies required for this are too highly attenuated by the highly absorbent polymer matrices and scattering inhomogeneous fibre structure in fibre reinforced plastics, and this precludes their use in AU testing. This is unfortunate since a variation of Rayleigh wavelength would allow the depth of penetration of the interrogating ultrasonic energy, and thus the depth of the material investigated, to be controlled.

The sensitivity of AU to the presence of defects in composites is at least partly dependent on the phenomenon of ultrasonic wave scattering, an area considered by Roberts et al ⁽⁶²⁾. Roberts et al based their investigations on 16-ply UD carbon fibre reinforced epoxy in the 10 MHz frequency range. They stated that scattering, which occurs as a result of material inhomogeneity, will be weak either if the microstructural inhomogeneities in density and/or elastic properties are sufficiently small (weak scattering) or if all the characteristic dimensions of the internal structure are sufficiently small (long wavelength scattering). The latter condition has particular significance to most composite materials in which areas of non uniform fibre distribution are found. These, in addition to areas of porosity, impact damage and cracks, can act as scattering sites which contribute to modulation of an ultrasonic AU signal. Roberts et al found that attenuation due to scattering was greatest at 90° to UD fibres owing to the greater inhomogeneity of the internal structure in this direction.

Govada and Duke ⁽¹⁰⁾, investigating the SWF and attenuation in boron carbide/titanium and alumina fibre/aluminium metal matrix composites, have shown areas of lowest SWF to coincide with areas of highest attenuation. Increasing stress was found to increase attenuation.

Application of AU to 0.25 cm thick graphite/epoxy and neat epoxy sheets led Kautz to conclude that AU energy propagates in two modes in a composite; a more rapid mode through the fibres and a slower mode through the matrix. The latter is subject to greater attenuation at higher frequencies ⁽³⁵⁾. These conclusions might have been partly predicted considering the approximate two orders of magnitude increment in modulus from epoxy resin to carbon fibres. Talreja ⁽³⁹⁾ noted that the frequencies of AU stress waves are largely maintained at all angles relative to fibres in UD composites. The work of Ono and De Spain ⁽¹⁹⁾ led to similar conclusions to those of Kautz and Talreja. They studied wave propagation, peak amplitude attenuation and velocity in the AU testing of 0.65 mm 0/±45 graphite fibre reinforced epoxy sheets with and without a honeycomb core. They concluded that AU energy propagates in two general forms, high frequency waves (1 to 2 MHz) travelling at speeds of 6000-7000 m/s, and low frequency waves (below 500 kHz) travelling at 1500-2000 m/s. They noted that porosity in the composites could be detected by increased attenuation (peak amplitude) of the AU pulse. Discrimination was best when looking at the high frequency waves (as would be expected for small inhomogeneous inclusions such as porosity). However these were much more sensitive to transducer coupling and required a high degree of sensitivity to detection, so that extraneous noise could be a problem. Low frequency wave velocity was also found to decrease with porosity.

From its inception acousto-ultrasonics has involved the introduction of longitudinal waves via transducers at normal incidence to the surface of a specimen. However, it has been suggested that non-normal incidence would be preferable since it would allow the type of incident wave to be controlled, by variation of angle of incidence and frequency. For example, incident shear waves have been claimed to give improved sensitivity to interfacial weakness determination in Al-epoxy adhesively bonded structures ⁽⁴⁹⁾.

The effect of specimen resonances on acousto-ultrasonic testing has been investigated by Williams et al using a 10.16 mm thick aluminium block ⁽¹³⁾. The spectral content of the

received wave form was found to be dominated by the natural frequency response of the test piece when the input frequency was at or spanned the resonant frequency of the test piece. In addition, resonance effects caused node and antinode lines to exist on the surface of a specimen. These lines correspond to peaks and troughs at specific frequencies in the received transducer output. In general, more lines occur per unit area at higher frequencies. From this it may be seen that transducer location will further affect the frequency spectrum contained within the received wave form.

2.5 AU Pulse Characteristics

In this section consideration will be given to the way in which the acousto-ultrasonic pulses propagate through material, and the possible factors which influence the characteristics of the received signal, which, via signal processing, yields the SWF.

The two electrical excitation pulses available using the AU206 which stimulate the emitter transducer are shown in figure 2.16. The pulse mode generates a single short duration negative high voltage input spike which excites the predominant resonant responses of the transmitter sensor ⁽¹⁵⁾. The burst mode delivers a gated sine wave of continuously adjustable frequency (100 - 1500 kHz) and duration (8 - 90 microseconds) of much lower amplitude, approximately 10 V.

The source of the AU pulse is the electrical excitation signal. Between this source and the final reception of the pulse at the receiving transducer, the signal has undergone considerable change as is shown in figure 2.2 (see earlier) where typical received pulses are presented for APC2 in the pulse mode. Modulation of the signal occurs as a result of the characteristics of the emitter and receiver transducers, coupling between both transducers and the specimen and by the material.

Although the emitter transducer emits predominantly longitudinal waves, a certain shear component must also be present. In addition, the beam from the transducer is conical

(beam spreading occurs). Hence, the injected waves strike the free boundaries of the specimen both normally and at angles. Non normal reflections at laminate boundaries will disseminate the energy into shear components ⁽¹⁾. Over the longer inter-transducer distances used, the interaction of longitudinal and shear waves in relatively thin laminates would be expected to produce Lamb waves ^(45,50,63,64). This is significant because it infers that dispersion of the incident AU pulse will occur as a result of the frequency dependence of the speed of Lamb waves. Both theoretical and experimental investigations of AU wave propagation have, more recently, been reported.

AU wave propagation has been reported to be by Lamb waves in thin UD graphite/epoxy (for any angle of incidence, not just normal) ⁽⁶⁵⁾. Moon and Jerina report 6 mm Lamb wave lengths in 3 mm thick unidirectional graphite epoxy of similar density and elastic modulus to APC2 using the FC 500 emitter transducer and inter-transducer separation of 86 mm ⁽⁵⁰⁾. They also noted that dispersion and attenuation of the Lamb waves were all found to be increased in directions perpendicular as opposed to parallel to fibres. This obviously helps to explain the decreased value of SWF perpendicular to the fibres in APC2. There are two common methods of generating Lamb waves, non normal incidence using a wedge between longitudinal transducer and specimen, and normal perturbations from a transducer coupled directly to the surface of the test piece ⁽⁶⁵⁾. The latter is the accepted method of generating AU pulses.

Although Lamb wave propagation of AU signals is often cited, according to Williams et al ^(46,66) there is good agreement between experimentally determined voltage amplitudes and arrival times of AU pulses and theoretical predictions based on simple longitudinal wave propagation theory. Attempts at theoretical considerations of AU stress wave propagation have been based either on simple ray theory and plate surface reflections, or Lamb wave propagation. They have assumed the material to be effectively homogeneous and have ignored reflections from plate edges. As a result, longer time signals, random

fluctuations, including coupling variations, and material heterogeneity are beyond the scope of such theories, which are therefore somewhat lacking.

Surface wave propagation is likely to have been of little significance in AU testing of APC2. Taking the centre frequency of the FC 500 emitter transducer as 500 kHz and an approximate nominal maximum wave speed recorded of 6500 m/s in the principal fibre direction, then wavelengths of the order of 10 mm will result. For this wavelength and a laminate thickness in general no greater than 2.5 mm, it is clear that surface wave propagation will have been of little significance.

Observation of received AU pulse shapes indicates several important points. Firstly, the pulse is considerably more complex than the idealised damped sinusoid (short rise time and exponential decay down to the background noise) reported by Vary ⁽¹⁾. Peak amplitude of the pulse can lie more than 15 to 20 oscillations after the start of the pulse. Various peaks and troughs in the time domain exist in the pulse envelope and more than one frequency component is present, at least partly associated with different time portions of the signal. Oscillations are basically centred around the 375 kHz resonant frequency of the receiver transducer, however, the initial part of the pulse appears to be centred at a higher frequency. This higher frequency component propagates by either a shorter route, or more likely, higher speed than the main lower frequency component. Other authors have also reported two frequency ranges of AU energy propagation, the higher frequencies being more highly attenuated as would be expected ^(35,54).

Some of the factors cited by the literature as contributing to the characteristics of the received pulse include the following ^(2,4,7,35): constructive and destructive interference between individual wavefronts, angle of incidence of individual wavefronts, mode conversions, wave velocity, attenuation, bandpass properties of the material, and the density, tensile modulus and Poisson's ratio of the material.

Peaks and troughs in the received AU pulse will be a result of the arrival of waves which have followed different propagation paths according to Kautz ⁽³⁵⁾. Layered interfaces along a ray path can lead to multiple arrival times for propagating waves, interference between which can further complicate the waveform ⁽⁶⁷⁾, the laminates in composites acting as waveguides ⁽³⁵⁾. The ringing of both emitter and receiver transducers will also contribute to the long duration of received AU pulses.

When an ultrasonic wave propagates through a damaged composite, the interaction between the stress wave and the damage can affect the wave in two principal ways. Firstly, damage will in general reduce the stiffness, and since wave speed is directly proportional to the square root of elastic modulus, damage will reduce the wave speed. Secondly, the attenuation will increase because the crack - wave interaction will cause incoherent scattering of waves. In extremely heterogeneous media in which ultrasound suffers from strong and densely packed scatterings (voids, fibres, delaminations), acoustic energy will not be coherently transported across a body ⁽⁶⁸⁾.

It has been suggested ⁽³⁶⁾ that since the stresses in a composite are triaxial, unloading as a result of crack propagation (the growth of damage) would result in a complex combination of stress wave modes. It is therefore important that the artificial AE pulses used in AU also have complex combinations of wave modes, so as suitably to interrogate the material with respect to dynamic response to stress. The rate of load transfer in materials is characterised by the speed of sound propagation ⁽³⁶⁾.

2.6 Conclusions

Some general conclusions may be drawn from the literature which has been reviewed. Acousto-ultrasonics has been applied to a wide variety of materials and material characteristics. More recently varied ways of performing AU testing have been explored, for example, with higher frequency transducers, different methods of signal processing

and different AU parameters. However, the following test conditions have been most widely used, and apparently most successfully applied:

1. Investigation of fibre reinforced plastic composite materials in the form of thin plates with simple reinforcement lay-ups (unidirectional and cross-ply), most often with carbon fibre reinforcement.
2. AU pulses introduced by using a broadband emitter (approximately 0.1-2.0 MHz) at normal incidence, and with a lower frequency resonant receiver transducer (approximately 300 - 800 kHz).
3. Use of the AETC AU206 acousto-ultrasonic testing system.
4. Use of Vary's original Stress Wave Factor.

These areas of investigation have been the basis of the studies conducted in this thesis.

The various claims about the success of AU as a means of NDE require independent investigation. No work has been conducted on AU applied to thermoplastics or fibre reinforced thermoplastics such as APC. There has been no systematic study of the various factors which affect acousto-ultrasonic testing, and no investigation into how to optimise test conditions for sensitivity to material defects. It appears to be the rule rather than the exception, that estimates of experimental scatter are ignored when considering the ability of AU to detect changes in material condition.

The question which remains is whether acousto-ultrasonics has anything more to offer than conventional ultrasonic testing as a means of NDT. Certainly AU is, to some extent, an ultrasonic attenuation technique. It is perhaps significant that some investigations of AU also involved ultrasonic measurements of velocity or attenuation using conventional time-of-flight or pulse-echo methods, respectively (2,10).

Chapter 3

ACOUSTO-ULTRASONICS: EXPERIMENTATION

3.1 A Study Of Experimental Conditions

3.1.1 The Problem and the Aims

Acousto-ultrasonics is a comparative testing technique, the SWF having no absolute significance. A large array of experimental variables affect the results obtained with the technique. These factors include the choice of AU parameter used to monitor material quality, instrumentation settings and test conditions. Valid comparison of data can only be accomplished by maintaining all these constant. In addition, many of these factors affect both sensitivity and reproducibility of data.

At the outset of this work, almost all of the literature available concentrated on the use of Vary's Stress Wave Factor, usually on thin composite plates and with the pulse mode of excitation. This broad area was therefore chosen for primary investigation. In further justification the following points should be noted:

1. Only APC2 laminates up to 2.5 mm thick were of interest,
2. the 'burst' mode of pulse excitation which uses a low energy `long` burst of ultrasound is applicable to thicker plates,
3. Vary reports that the RMS level is proportional to the total number of ringdown counts per pulse (1,18) and results presented later in this study reinforce this.

Initial experimentation with the AU 206 acousto-ultrasonic testing system rapidly indicated that without some sort of systematic investigation into experimental conditions and the range of instrument settings, highly variable readings would result. These readings revealed little about composite plate structures except where major and obvious flaws were present. A systematic investigation of the acousto-ultrasonic technique, applied to a single material and using a single commercial testing system, had not been

carried out according to the literature. It was the aim of this work to complete such an investigation.

3.1.2 The AETC AU206 Acousto-Ultrasonic Testing System

In the early to mid 1980's Acoustic Emission Technology Corporation, Sacramento, California developed and started to market the first commercial acousto-ultrasonic testing system. This unit is intended as a fully developed and usable NDT system. It should be noted that a not insignificant number of other researchers have made use of this same system with at least some success (8,24,25,28,29,30,31,33,43,53,57,59).

The AU 206 is a self contained mains/battery operated instrument containing a pulser controlling module, a pulse reception/analysing module, a CRT display, a 3¹/₂ digit LED display and two probes/sensors.

The emitter transducer, which introduces the source AU pulse into the material, is an AETC FC500 broadband longitudinal wave ultrasonic transducer, nominally resonant at 500 kHz but with a flat sensitivity of -85 dB (relative to 1V/ μ Bar) over frequencies 0.1 to 3.0 MHz. It is 24.8 mm in diameter, 65.4 grammes in mass and has an epoxy wear plate. The pulse receiving/detection transducer is an AETC AC-375 acoustic emission resonant transducer with an approximate sensitivity of -65 dB (relative to 1V/ μ Bar), centre frequency 375 kHz, 22.1 mm in diameter, mass 24.0 grammes, also with an epoxy wear plate. An AETC model 140 40 dB preamplifier with integral 0.1 - 1.0 MHz band pass filters, preamplifies the output from the AC-375 before its input into the AU206 signal processing module.

The pulser controller module incorporates several controls for varying the characteristics of the emitter transducer excitation signal. It is switchable between two modes of operation, the pulse mode, which produces a sharp input spike of short duration and fixed frequency content variable in voltage amplitude as -50, -150 or -250 volts via the

pulse energy control, and the burst mode, which produces bursts of a fixed amplitude of 10 volts, but frequency variable from 100 kHz to 1.5 MHz ranging from 8 to 90 microseconds duration. Both are infinitely variable via separate uncalibrated potentiometer controls. The pulse trigger rate control allows pulsing rates of 0.25, 0.5, 1.0 or 2.0 kHz.

The signal processing module also contains a multitude of controls. A gain control accommodates variations in amplification in 1 dB steps over a 60 dB range. Total amplification, including the preamplifier, is within the range 40-100 dB. The threshold magnitude is adjustable from 0.25 to 6.2 volts and operates in one of two modes: 'fixed' or 'auto'. In the 'auto' mode, the threshold is set to a value relative to the background noise level. As the noise level increases or decreases, so does the effective threshold. This facility is claimed to remove the effects of noise on the SWF ⁽⁶⁹⁾, however in non-noisy environments it can be dispensed with and the 'fixed' mode used.

A ringdown counting time period controller is variable from $1/8$ to 8 seconds. The combination of this variable and pulser repetition rate will govern the number of pulses over which the displayed SWF is accumulated. A gate width control allows variation of the duration of the received pulse over which ringdowns are counted and is infinitely variable from 35 to 350 microseconds. The gate sweep is triggered by the emitter pulse trigger and so each sweep must include the transit time duration of the AU pulse between emitter and receiver transducers.

There is in addition, a scale and mode control for the $3\frac{1}{2}$ digit LED display, selectable to display the threshold, quasi-RMS voltage or the SWF, the latter subject to order of magnitude scaling factors from 1 to 10^4 .

The quasi-RMS or 'signal level' is an alternative AU parameter calculated by the AU206. It is a voltage which approximates the root-mean-square (RMS) value of the amplified

signal and is defined as $0.7 \times$ the AE signal peak level ⁽⁶⁹⁾ over a 0.5 sec response time. It is independent of the threshold and gate width.

The remaining controls to mention are the controls for the oscilloscope display of fixed 4.0 volt FULL SCALE DEFLECTION upon which are displayed the received AU pulses. The display is always triggered by the emitted pulse trigger and has a time base of 6.25, 12.5, 31.2 or 62.5 microseconds/division.

3.1.3 Performance Criteria

It is a prerequisite to any AU non-destructive testing that the chosen parameter combines adequate repeatability with adequate sensitivity. An AU parameter which seeks to rate material quality must, in the simplest sense, be capable of distinguishing good quality material from bad (adequate sensitivity). This can only be accomplished by either a scanning process across a single specimen (location of defective areas within good) or by repeat readings before and after introduction of defects. The parameter must, therefore, be reproducible, all other factors being constant. It is clear that the attainable sensitivity will be profoundly influenced by the repeatability of measurements.

It was therefore necessary first to select the most important factors which required analysis and investigate their effect on AU variability. Subsequently, it was required to optimise these factors, as far as possible, to give maximum sensitivity for the composite laminates and defects of interest.

3.1.4 Material Investigated

The SWF will be influenced by lateral and through thickness dimensions, in addition to the internal structure of a laminate under investigation. After a preliminary investigation of the effect of laminate thickness, dimensional effects were eliminated by use of a single sample for the investigation and optimisation of experimental variables. This

sample was a 20-ply UD laminate of Hercules AS4 carbon fibre reinforced PEEK (APC2) moulded by the manufacturers, ICI. The fibre volume fraction was 0.62, laminate thickness 2.5 mm, length parallel to fibres 500 mm and perpendicular to fibres 200 mm. This sample was C-scanned by ICI, Wilton, before use to ensure uniform good quality.

The test laminate was placed horizontally on a rigid foam backing of low acoustic impedance to ensure no coupling with, and therefore no leakage of ultrasonic waves out of the specimen and into or out of the supporting bench. Both transducers were placed onto the top surface and measurements were performed in two directions such that bulk stress wave propagation between transducers was directed parallel and perpendicular to the reinforcing fibres. The objective was to achieve the clearest possible distinction between these two directions, which in a UD composite material clearly represent extremes of property variation.

3.1.5 Fixed Experimental Conditions

Unless otherwise stated, all acousto-ultrasonic data has been recorded by using the following fixed conditions. The AU 206 system, including the FC500 broadband emitter transducer and AC-375 resonant receiver transducer, band passed 0.125-1.0 MHz with the pulse mode of excitation (short duration, high voltage spike).

The possible effects of specimen dimensions, transducer type and transducer location noted by Williams et al ⁽¹³⁾ and edge effects noted by Green and Rodgers ⁽⁸⁾ have, where possible, been removed by keeping all such factors constant when comparing values of the SWF.

3.1.6 Experimental Variables

It was first essential to ensure that the AU206 and transducer gave stable and reproducible readings from one day to the next. Accordingly, the transducers were bonded to the surface of a 16-ply APC2 plate with a silicone adhesive in order to achieve a fixed coupling condition. The AU206 was then activated from cold and both the SWF and quasi-RMS monitored continuously for a 24 hour period. This process was repeated a further four times, giving the results displayed in figure 3.1. In all cases both SWF and RMS decreased during warm up, achieving equilibrium after 8 hours. As a result of this, a standard 10 hour warm up period was always used before taking any AU measurements.

In early 1985, during the investigation of the effects of instrumentation on acousto-ultrasonic parameters, SWF and RMS voltage readings were recorded using the AU206 system at a specific location on a specific 20-ply UD APC2 plate. Late in 1986, towards the end of the investigation into AU, and after the AU206 hardware had been checked for correct functioning by the suppliers, these measurements were repeated on the same plate. Over all instrument setting ranges, the readings recorded were, within experimental scatter, identical.

The SWF, according to its definition (equation 2.1), should vary directly with the pulser repetition rate and ringdown cumulative time. Verification of this with respect to the AU 206 would allow these two experimental factors to be dropped from the investigation. Accordingly, emitter and receiver transducers were bonded to the surface of a 16-ply 0°/90° laminate in order to give constant coupling. The SWF was monitored over all available combinations of pulser repetition rate (0.25, 0.5, 1.0 and 2.0 kHz) and sampling time interval ($1/8$, $1/4$, $1/2$, 1, 4, 8 seconds). In figure 3.2 SWF is plotted as a function of cumulation time for each level of pulser repetition rate. Observation of the received pulse on a separate oscilloscope showed a small decrease in the overall pulse magnitude towards higher repetition rates, however the number of ringdown counts per pulse

remained constant at 41 over all levels of sampling time and repetition rate. In addition, each subsequent received AU pulse was found to be nominally identical to the next, all other factors being constant. Within limits, the instrumentation does perform according to specification and the pulse repetition rate and cumulation time may be considered as simple scaling factors of the SWF.

However, the pulse rate was not chosen purely arbitrarily, but according to the following considerations. An upper limit of the usable pulse rate is set by the requirement that each pulse rings down before the next arrives (no pulse overlap). It was found by experimentation that 1000 pulses per second, giving a 1000 microseconds allowable decay time per pulse, was the maximum available repetition rate at which no pulse overlap occurred in any of the samples investigated. Further, Henneke et al reports that lower pulse rates give greater stability of the recorded SWF ⁽⁵⁹⁾. As a consequence, a pulse rate of 1000 pps was used throughout the investigation of experimental conditions. Combining this with a sampling time of $\frac{1}{8}$ seconds, SWF measurements represent the number of ringdowns from 125 pulses. These conditions have been successfully used by other researchers ⁽⁵³⁾. In the work by Phani et al ^(25,31) several combinations of pulse rate and sampling time were used. The following parameters were investigated next.

1. Effect of couplant,
 - a) water (with wetting agent)
 - b) AET supplied SC6 couplant
 - c) petroleum jelly
 - d) methylated spirits
2. Directionality of transducers,
 - a) emitter
 - b) receiver
3. Effect of contact force on SWF,
 - a) on emitter transducer

b) on receiver transducer

4. Inter-transducer spacing (for a UD APC plate),

a) parallel to fibres

b) perpendicular to fibres.

The quality and reproducibility of the coupling between the transducer and test piece is particularly important for AU, since it is a scanning technique, such that the transducers must be repeatedly repositioned between readings. There is no internal calibration, as is provided in the back-surface echo in conventional ultrasonic testing for example. The possibility of error due to coupling variation is therefore considerable. Various factors such as the type of couplant must be considered; whether liquid, viscous liquid or compliant solid. For liquid couplants, important considerations are the ability to wet the surfaces, the thickness of coupling layer and the contact pressure (which will control coupling layer thickness and the degree of true solid/solid contact). There are obviously a vast range of possible coupling media and so a preliminary selection was required. The use of a compliant rubber layer was deemed inappropriate given the reported problems of reproducibility (54). Total submersion of specimen and transducer in a water bath would clearly be ideal but was inappropriate because of the types of transducers used and the complexity of the system. Direct coupling with viscous liquid couplants was the obvious choice by virtue of its widespread use in ultrasonics and acoustic emission (11,30,59,63,67,70,71,72).

Of the four couplants listed above, petroleum jelly proved to be the easiest to use and gave the most reproducible results for direct contact coupling of transducer to specimen. The formation of bubbles at the emitter sensor when water was used, and rapid evaporation of the methylated spirits led to a decay in measured SWF with time. This inapplicability of water as a couplant contradicts the work by Vary (1). The SC6 couplant (the proprietary couplant supplied with the equipment) showed similar reproducibility to petroleum jelly but proved very difficult to remove from the specimen once applied. As

a consequence, petroleum jelly was used for all further work. A variety of couplants have been used according to the literature. Many authors have used viscous liquids including petroleum jelly (15,19,20,30,30,33,41,43,53,59). Thin (1 mm - 2 mm) silicone rubber pads have also been used (18,35,43), but Kautz reports that this can introduce interference patterns into the received AU waveform as a result of multiple reflections within the pads (35). Furthermore, Mitchell reports that dry coupling techniques are notoriously sensitive to the force that is exerted on the pulser and/or sensor (54). Williams et al report results on nylon rope without any coupling mediums (29). Sundaresan and Henneke report that most AU work uses a viscous liquid couplant (45).

In addition to investigating various types of coupling media, alternative transducer mounting/loading jigs were fabricated and tested for their effect on coupling reproducibility. These included metal spring and foam rubber spring loading of transducers onto the test plate and non-contact coupling with a 0.01 mm to 3 mm layer of water as couplant (semi-water immersion of the transducers). None of the investigated methods gave any improvement in coupling reproducibility over the petroleum jelly, dead weight loading method using a simple fixture to maintain exact intertransducer separation. Consequently, this method was retained for all further investigations.

The effect of contact pressure on the SWF was investigated by independently varying the contact pressures of emitter and then receiver transducers using laboratory weights. Repeated couplings onto a horizontal test surface were made for each load/transducer combination using petroleum jelly couplant. Both magnitude and reproducibility of the SWF were influenced by the contact pressure, as shown in figure 3.3 For both transducers there is an increase in the SWF with increasing contact pressure, the rate of increase decreasing rapidly with pressure. The error bars represent 95% confidence limits (\pm two standard deviations).

The relative contributions of each transducer to the variability of the SWF are emphasised in figure 3.4 where coefficients of variation are plotted against contact pressure. As may be seen, the AE transducer (receiver) contributes considerably more to variability than does the emitter transducer. It was concluded that a constant contact pressure must be applied and this was achieved by applying a ten Newton weight to each transducer. The increase in SWF with contact pressure to a maximum has been reported by Henneke and Lemascon ⁽¹⁷⁾ who suggest a minimum contact force of 2 lbs (approximately 9 N) per transducer to ensure reproducibility.

The increase in SWF with contact pressure would be expected considering the following factors. Two nominally flat surfaces will only be in intimate contact over a fraction of the surface as a result of microscopic asperities. An increase in contact pressure increases the genuine surface area of contact hence improving stress wave transmission from transducer to specimen and vice-versa. In the presence of a viscous couplant, an increased pressure will ensure better and more reproducible dispersion of the couplant onto the microscopically uneven surfaces, thus increasing the SWF in magnitude and reproducibility.

The AE transducer showed no directionality as expected, but the emitter transducer produced a minimum in SWF within an approximate 5° arc directly opposite the connector plug.

Figure 3.5a shows the effect of inter-transducer separation on SWF measured both parallel and perpendicular to the carbon fibres in a 20-ply UD APC2 plate. Each point is the mean of ten repeat measurements at the same location, and error bars are, again, 95% confidence limits. Owing to the greater attenuation effects of the resin and the fibre/resin interfaces experienced by the stress waves when propagating at right angles to the fibres, the SWF decreases more rapidly with inter-transducer separation when measured perpendicular to the carbon fibres. The effective Young's modulus (E) measured parallel

to fibres is approximately 150 GN/m^2 , compared to 10 GN/m^2 perpendicular. It would therefore be predicted that the SWF was lower at right angles to the fibres. This is in accordance with the measured attenuation coefficients and longitudinal wave speeds (see later) and with the results of other workers (4,15,37,40,42). The apparent increase in the SWF measured parallel to fibres with *increasing* distance between transducers is surprising, however it should be noted that this is not always the case (see later). For other test conditions, the SWF does show a steady decline with inter-transducer separation. Even so, figure 3.5a is difficult to explain. Clearly it must be a limited effect over shorter inter-transducer distances, the signal eventually attenuating at large distances. This effect may be related to a transition between types of wave propagation, from longitudinal and shear wave modes to plate waves occurring over the distance range of 50 mm to 125 mm. Dispersion and the multiplication of echos over greater distances may also possibly account for this. Dispersion may cause an elongation of the AU pulse envelope as different frequencies propagate at different speeds. This elongation may cause an increase in the number of ringdowns within the envelope, which will cause an increase in the SWF with distance. Alternatively, this phenomenon could be explained by the specimen resonance effects noted by Williams et al (13) which cause peaks and troughs in transducer output as a result of proximity or distance to node and anti-node lines (respectively).

The effect of inter-transducer separation on the distinction between SWF measured parallel to fibres and that measured perpendicular to fibres, is shown in figure 3.5b. Student's t value for the pair comparison between means of 5 repeat readings made in each of the two directions is plotted as a function of inter-transducer distance. The markedly different attenuation coefficients in the two orientations mean that the maximum inter-transducer separation gives the greatest distinction between SWF parallel and SWF perpendicular to fibres. However, at a 99% confidence interval, the distinction between orientations is statistically valid at all separations for these instrument settings.

A constant inter-transducer separation was used in subsequent work. This was achieved by the construction of a simple jig to maintain a distance of 85 mm between centres, unless otherwise stated. This value was a compromise between the need to maximise the distinction between 0° and 90°, and the need to maintain an adequate absolute value of SWF in the latter. Too low a SWF in the 90° direction for good quality laminates would make it impossible to detect any reductions caused by defects. This value lies within the 25 mm - 100 mm inspection area between probes reported by Rogers (15). A further limitation on inter-transducer separation is the need to ensure sufficient space between probes to allow the introduction of defects without their affecting the coupling by virtue of surface deformation or damage.

3.2 Optimisation Of Instrument Settings

The number and range of instrument settings available with the AU 206 equipment are considerable. The most important are listed in table 3.1, which indicates the ranges available, the symbols used to describe them and the setting levels investigated. Pulser repetition rate and ringdown cumulation time have already been dealt with.

Unfortunately, no information was forthcoming, whether from the manufacturers, the agents supplying the AET model 206 AU or from the literature, to help in the optimisation of the instrument settings for sensitivity and reproducibility on a given material. In fact, as a result of the multitude of experimental variables, it is a notable disadvantage of AU that optimisation of test conditions is a necessary precursor to any particular material/structural investigation.

A systematic investigation of the four main instrument variables, namely pulse energy of the emitter, and threshold, gain and gate width of the signal processing equipment was undertaken. The objectives were, firstly, to assess the influence of these variables on both the magnitude and reproducibility of the SWF, and secondly, to optimise them for the detection of the chosen structural characteristic of the test laminate, namely the difference between fibre and transverse directions.

The values of the variables selected for this investigation were not chosen arbitrarily. For the given material type and specimen dimensions, gains much beyond 80 dB caused total saturation of the amplifier. A study of the amplifier response (see later) showed it to be linear up to 5.2 volts, above which the signal was clipped. A practical upper threshold limit of 4.0 volts was therefore set. A study of the received pulse shape showed that it rang down within 260 microseconds and so only additional background noise could be admitted by using gate widths greater than this value.

Table 3.1 shows the chosen levels of the variables investigated in a 7x5x4x3x2 experimental grid which with 5 replications (repeat recouplings of the transducers to the specimen surface) of each would have constituted 4200 separate measurements. However, some of these levels were suppressed as a result of preliminary work.

3.2.1 Preliminary Experiments

Values of SWF were plotted as a function of threshold, or of gate width, other settings being held constant.

Firstly, the effect of gate width was investigated. Figures 3.6a and 3.6b show SWF as a function of gate width, for 0° and 90° orientations respectively, at constant gain (60 dB) and pulse energy (level 1, -250 volts). Three graph lines are plotted on each figure.

These represent the SWF measured by using thresholds of 0.25, 0.65 and 2.0 volts. The variability of SWF at a given combination of settings is shown by the error bars, which indicate ± 2 standard deviations about the mean. For both orientations there is the expected near linear relationship at low gate widths, where the number of ringdowns is directly proportional to the gate width. However a continuing increase in gate width will encompass the tail of a pulse, where no further threshold crossings will be encountered. The curve will therefore decrease in gradient, as may be seen for the 2.0 volt threshold level in figures 3.6a and 3.6b.

At the minimum gate width of 33 microseconds, the SWF approaches the minimum value of 1 ringdown per pulse, a SWF of 125. This minimum is a result of inadequate screening within the AU206 between the pulsing and receiving modules. It allows the voltage spike, which excites the emitter transducer, to be 'detected' by the receiving module as a single ringdown as the gate sweep commences (see later).

A simple model may be proposed for the SWF/gate width behaviour. Since the receiving transducer is resonant at frequency 375 kHz, each 8 microsecond increase in gate width may be expected to admit a further three ringdowns beyond the effective minimum of 1. This results in an increase of the SWF by 375 if each ringdown exceeds the threshold. Hence the upper bound limit will be given by:

$$\text{SWF} = (G \cdot f_r + 1) \cdot t \cdot 1/p \quad \dots 3.1$$

- where
- G = gate width (microseconds)
 - f_r = transducer resonant frequency (Hz)
 - t = sampling time (seconds)
 - $1/p$ = pulse rate (Hz)

This proposed linear variation is shown in figures 3.6a and 3.6b as the line XY. For measurements in the fibre direction at shorter gate widths the relationship holds true, the first 40-50 ringdowns of each pulse crossing the threshold at all values of threshold in figure 3.6a. Thereafter, the SWF increases less rapidly with gate width. In the transverse direction, the mean number of ringdowns per pulse rises at a slower rate, as would be expected in view of the increased attenuation. The approximate time delay between pulse emission and reception for the 85 mm inter-transducer separation was determined from an oscilloscope to be 13 microseconds and 38 microseconds for the 0° and 90° orientations respectively. Since the gate sweep commences at the instant of pulse emission, it becomes apparent that in the 90° orientation equation 3.1 will overestimate the SWF by at least 250. The fact that SWF values may slightly exceed the upper bound

limit in the 0° orientation during the early part of the received pulse (up to 15 ringdowns) is evidence that higher frequency oscillations may be present, and that they show greater significance in the early part of the AU pulse. The tail of an AU pulse is likely to include ringdowns caused by echoes from regions outside the volume between the transducers. Thus, shorter gate widths may arguably be expected to improve AU sensitivity to variations in the quality of the material between the transducers.

At constant gate width (250 microseconds) and pulse energy (level 1, maximum) the SWF was measured as a function of threshold for each of the four gain settings, first parallel to fibres (figure 3.7a) then perpendicular to fibres (figure 3.7b). At 80 dB it will be seen that the SWF is almost independent of threshold up to the practical limit of 4 volts. The recorded SWF of approximately 10000 represents 80 ringdowns from each of the 125 pulses counted. At the transducer resonant frequency of 375 kHz this represents a pulse duration of 210 microseconds, which with the allowance of the previously mentioned transit time between transducers, fills the gate. Evidently therefore, at this pulse energy and gate width, only the last few ringdowns fall below 4 volts, so that there is a very slow decline in the SWF with increasing threshold. By the same argument, a modest attenuation within the sample will not alter the SWF. Further, the SWF recorded parallel and perpendicular to the fibres is the same within experimental error, thus confirming this insensitivity to material variation.

At lower gains, the SWF shows an exponential type decline with increasing threshold, as would be expected from the idealised AE or AU pulse shape. Considering both orientations, the 60 dB gain level gives the widest usable range of SWF values.

The next stage in the investigation was to explore the effect of pulse energy. This was conducted at constant gain (60 dB) and gate width (250 microseconds) over the range of practical thresholds for the 0° and 90° orientations, shown in figure 3.8. Obviously, an increased pulse energy produces an increased SWF. In addition however, there is a

tendency for the uncontrolled experimental error to decrease slightly towards higher energies at this level of gain. The proportional error therefore decreases markedly towards higher energies. This implies that the highest excitation energy should be used whilst ensuring non overloading of the amplifier.

The effect of threshold on the sensitivity of the SWF to fibre orientation is clearly shown in figure 3.9. Figure 3.9a presents a comparison of SWF values in the 0° and 90° orientations over the practical range of threshold settings. The distinction clearly improves towards higher threshold levels. This is emphasised in figure 3.9b where, at each threshold setting, a pair comparison of SWF values for the two orientations has been made, and the significance of the difference between means determined by Student's 't' test. For the sample sizes concerned (eight degrees of freedom) the difference becomes statistically significant at the 99.9% confidence level only when the threshold level exceeds 0.8 V.

3.2.2 Selection of 'SWF difference' as a Sensitivity Parameter

In general, the SWF measured in the fibre direction is greater than that in the perpendicular direction. This is due to the wave guide effect of the fibres and higher effective modulus in the former case, and greater attenuation in the latter. The sensitivity of AU to a material variable can be considered to be the difference in the measured SWF for a standard or non-defective piece of material compared to say a defective piece. The greater the difference, the more sensitive the system.

The most well defined material variable available was the difference in properties between the fibre direction and that perpendicular to it (transverse direction) in a unidirectional APC2 plate. Therefore, this variable, namely the arithmetic difference between SWF measured parallel to and perpendicular to the fibres, was used as a measure of sensitivity. This was termed the 'SWF difference' (DSWF). The problem was

then to determine the combination of instrument settings which optimised DSWF with respect to magnitude and variability.

3.2.3 Analysis of Variation and Covariation

This method of statistical analysis divides the total variance of the dependent variable in a set of data into components associated with the sources of the variability, and allows the relative importance of these contributions to be assessed (73).

The total variance is defined as the mean square deviation of the experimental values from the grand average. This total variance is divided into components associated with known sources of variation, namely the experimental factors, and interactions between these factors, so that their relative importance may be assessed. In addition, a residual variance estimate is found by subtraction. This is the variance unaccounted for by the experimental factors and can therefore be described as the 'experimental error' or uncontrolled scatter in the data. The variance estimates, determined both for the individual factors and interactions between them, are compared with the residual variance estimate using 'Snedecor's F-test'. This test determines which variance estimates exceed the residual at a chosen confidence level, and therefore, which are significant.

Most of the many thousands of calculations required to produce the final table of analysis of variation and covariation (table 3.2) were conducted on a BBC B microcomputer using three software routines developed by the author. The first program created data files on disc into which the 3360 data points were recorded. The second then called up the appropriate files, carried out the required calculations and recorded the results to disc. The third formatted the data and produced a hard copy of the analysis of variation and covariation (ANOVA) tables. The standard format of these tables is as follows: columns 1 to 5 are respectively, the source of the variance estimate, the sum of squares ($\sum(x-\text{mean})^2$), degrees of freedom (N-1), variance estimate (sum of squares

divided by the degrees of freedom) and finally, the F ratio with respect to the residual variance.

3.2.3.1 Analysis of variance of SWF

The first analysis of variation and covariation carried out was for the SWF as the dependent variable, investigating all 5 experimental variables. See table 3.1 for the symbols used. The ANOVA table for the SWF is included as table 3.2. It was encouraging to note that the residual variance (attributable to the intrinsic scatter in the SWF data), although of significant magnitude, was greatly outweighed by the contributions of the experimental factors.

Interpretation of the ANOVA table must, as a rule, start with the highest order interactions and work towards the individual experimental factors. It is not statistically valid to F-test a lower order interaction when a higher order interaction has proved significant (73). For significance at the 5% confidence level, the required value of the 'F ratio' is approximately 2 (and approximately 3 at the 1% confidence level) for the number of degrees of freedom concerned in the following tables. There are highly significant fourth order interactions between the combinations of variables TOEG and TQEG (using symbols defined in table 3.1). In addition, it is clearly evident from their estimates of variance, that all the experimental factors have highly significant effects on the magnitude of the SWF and that gain (G) has the greatest variance, and hence effect, of all.

Consequently a breakdown analysis for individual levels of G was conducted, although various 3rd order interactions still existed. This meant that further breakdown would have been required to simplify the analysis to manageable proportions. However there appeared to be little advantage in doing this, since the final and absolute variance attributable to the individual experimental factors was not of primary consequence to the investigation.

Apart from the obvious trends of increasing gain, gate width and energy and decreasing threshold causing increases of the SWF, it has been clearly demonstrated that the individual experimental factors do not exhibit simple effects on the SWF, but show complex interactions to high orders.

3.2.3.2 Analysis of variance of DSWF

To reiterate the point, the sensitivity of acousto-ultrasonics to a material variable can be measured by the difference in the SWF between a standard or non-defective piece of material and a defective piece. The greater this difference, the more sensitive the system. As mentioned earlier, the largest and best defined material variable available was the fibre direction in a unidirectional APC plate. Thus, the difference between SWF measured at 0° and 90° to the fibres, DSWF, was used as a measure of sensitivity. It was made the dependent variable in a further analysis of variation and covariation.

By converting the separate SWF measurements to DSWF, the original population reduced by half. The ANOVA table for this four factor problem of DSWF is shown in table 3.3. According to the rule that the variance of the sum or difference of two independent random variables is equal to the sum of their variances, the residual variance of DSWF is approximately twice that of the SWF. The third level interaction TGE is significant, although small in comparison with the second order interactions TG and GE. As previously stated, however, it is not valid to perform the F-test on the second order interactions when a third order interaction has proved significant.

It was therefore necessary to perform a breakdown analysis of variance, and, since G appeared in all significant interactions, besides having the largest individual variance estimate by far, this analysis was carried out for the other variables at each level of G. This demonstrated that, as the instrument gain increased, there was a decrease in the significance of the effects of the other experimental factors (which may be inferred, but not determined because of interactions) and their first order interactions. Most

importantly, at the maximum gain of 80 dB, DSWF became unaffected by the gate width.

T (threshold) and E (energy) were demonstrated to be the most significant variables and to interact. Therefore, it was appropriate to plot graphs of DSWF as a function of T for each value of G and E, rather than carry out further breakdown analyses. This is done in figures 3.10a - 3.10d. Each plotted point is the summed value of DSWF over the four levels of gate width (Q) and five replications. Means may thus be determined by division by 20. From these graphs it is finally possible to find maxima in DSWF which can give optimum instrument settings. It appears that increasing gain shifts the maxima of DSWF to higher threshold values, though for the 50 dB to 60 dB range it has little effect on the peak height. The four areas where the SWF is most sensitive to the key material property of fibre orientation are listed below.

	Gain	Energy	Threshold
1.	60 dB	E(1)	1.8 V - 4.0 V
2.	60 dB	E(2)	1.2 V - 2.0 V
3.	60 dB	E(3)	0.8 V - 1.7 V
4.	50 dB	E(1)	0.7 V - 1.4 V

The first of these combinations shows the greatest range of suitable threshold values and was therefore chosen as the primary combination of settings for further work. It should be noted that gate width apparently has little effect on DSWF within the limits tested, and this allowed some flexibility in deciding how much of the pulse was to be gated and how many ringdowns per pulse would be counted.

3.3 An Investigation Of Quasi RMS Voltage

In addition to the SWF, the AU206 is capable of determining an alternative AU parameter, namely, the quasi-RMS voltage, also termed the signal level. The AE module of the AU206 utilises a rectifier/peak detector to convert the analog AE signal from the

receiver transducer/amplifier into a DC voltage which is weighted to provide signal RMS when the input is a sine wave. This DC voltage is an approximation of the RMS value, being 0.7 x the AE signal peak level over a response/decay time of 0.5 seconds.

Throughout the investigation of SWF (described earlier), and in parallel to it, the quasi-RMS voltage (RMSV) was also monitored and investigated. Work on this alternative AU parameter was included because of the unpromising results from the SWF in response to 'moulded-in' defects in APC2, as described later. However, it is more logical to describe the work at this point.

Of the instrument variables pertinent to the investigation of SWF, those which are based in the time domain, namely gate width and sampling time, may be disregarded with respect to RMSV, having no effect on the magnitude of this parameter. This is because of the fixed response time of 0.5 seconds of the RMS voltmeter in the AU206. In addition, RMSV is not subject to a threshold, hence background noise cannot be excluded from the signal. It is not possible to select, either in the voltage or time domains, the portion of the received pulse which contributes to the magnitude of the RMSV AU parameter.

The effect of pulser repetition rate on RMSV is demonstrated in figure 3.11. This graph demonstrates that with an increasing number of pulses per second, the RMSV increases but at a decreasing rate. The explanation of this stems from the long response time of the voltmeter which gives an averaged measure of the signal level over 0.5 seconds. This time will include portions during which pulses arrive and portions containing the 'dead time' between pulses. It is clearly advantageous to use the highest pulser repetition rate (which does not cause consecutive pulse overlap). This will ensure that the greatest proportion of the 0.5 second response time includes received pulses and not the dead periods between pulses, during which residual background noise is the only contributor to the signal level.

The effect on RMSV of the instrument variables gain and pulse energy are demonstrated in figures 3.12 and 3.13. In figure 3.12 RMSV is plotted against gain for the two orientations of the transducers with respect to fibre direction in the 20-ply UD APC2 plate used for the investigation of SWF. Error bars are $\pm 95\%$ confidence limits. In figure 3.13 RMSV is plotted as a function of pulse energy. As would be expected, gain and energy increase RMSV and for levels of gain of 60 dB and below, the RMSV parallel to fibres is always greater than perpendicular. However at 80 dB gain the converse is true. The explanation of this phenomenon is unclear.

To investigate whether interactions between gain (G), pulse energy (E) and orientation (O) were occurring, an ANOVA with RMSV as the dependent variable was carried out. The results of this showed that second order interactions occurred between all variables.

Next, by an analogous process to that used for the optimisation of the SWF, a sensitivity parameter for RMSV was defined as the arithmetic difference between the RMSV measured parallel to fibres and that measured perpendicular to fibres, DRMSV. A second ANOVA was then carried out using DRMSV as the dependent variable. This led to the effect of pulse energy and gain being elucidated by plotting out summed values of DRMSV. The effect of pulse energy on DRMSV is demonstrated by figure 3.14, where values of DRMSV summed over 5 replicate readings and four levels of gain are plotted against pulse energy. Clearly, the maximum pulse energy gives the greatest sensitivity. A similar plot for gain against DRMSV summed over 5 replicate readings and 3 levels of energy (figure 3.15), demonstrated that 60 dB gain and 80 dB gave optimum values. These settings were therefore used in the subsequent application of AU to defect detection in APC2.

It is important to note that the significance of the differences between means of 5 repeat readings of RMSV measured parallel and perpendicular to fibres is markedly less than that for SWF. Values of Student's t for optimised test conditions are around 7 for RMSV

and 15 for SWF. The sensitivity of the SWF to the difference in material properties associated with fibre orientation is therefore better than the sensitivity of RMSV. Both AU parameters, SWF and RMSV were used for the subsequent application of AU to the detection of defects in APC2.

3.4 An Investigation Of The Use of High Gains

The investigation and optimisation of instrument settings indicated that intermediate gain and threshold settings produced the greatest sensitivity of the SWF. This appeared to be in contradiction to the work of Bhatt and Hogg ^(74,75,76) who also investigated the SWF with the AU206 instrumentation. They concluded that highly reproducible SWF readings, which were sensitive to defects, could be achieved by using very high gains and thresholds.

3.4.1 SWF Measurements with an Air Gap Between Transducers

Bhatt and Hogg ^(74,75,76) reported that the relationship between SWF and threshold shown in figure 3.16 occurred when a 10 cm air gap existed between the transducers. The data in this graph were insensitive to orientation and separation of the transducers. Within the plateau region (II) highly reproducible SWF measurements were recorded. Similar results were recorded using the equipment at Bath.

The explanation of this SWF/threshold graph was determined by observation of the received AU pulse using a separate oscilloscope (with external triggering from the emitter module of the AU 206).

The four regions in figure 3.16 can be described as follows:

1. Background noise (largely electrical).
2. Plateau region where 1 'rogue ringdown' per pulse is recorded.
3. Cut off threshold where the 'rogue ringdown' is excluded.
4. Region where threshold excludes everything.

At 100 dB gain the background noise is considerably amplified requiring a minimum threshold level of around 2.0 volts to exclude it. Within the threshold range of 2.0-5.0 volts (region II) the SWF remains constant at 1000. At a pulse repetition rate of 2 kHz and sampling time 0.5 seconds, this SWF is the result of one ringdown per AU pulse.

This single ringdown is the result of an electrical spike at the instant of emitter transducer excitation which is received by the receiver module. This 'rogue ringdown' is not a result of AU pulse propagation between transducers, but of electrical leakage of the output pulse from the emitter module of the AU 206 to the receiver module. This occurs either within the instrument itself or is due to insufficient screening of the emitter or receiver cable, connectors or preamplifier.

This excitation pulse, used to energise the emitter transducer, is an electrical discharge spike from a charged capacitor of -150 V magnitude (E2) with an effective duration of 6 microseconds. The magnitude of this received rogue ringdown at different gains was recorded from the external oscilloscope and is shown in table 3.4. It lies well above the normal level of background noise in the system and is clearly dependent on gain. This explains why the plateau (region II in figure 3.16) for the 'air gap' experiment is also gain dependent.

Bhatt and Hogg reported that any combination of gain, material between the transducers and disposition of transducers will produce a similar SWF/threshold graph to that shown in figure 3.16.

3.4.2 The Effect of the AU206 Amplifier on Received AU Pulses

The amplifier within the AU206 instrument has a maximum output capacity, above which the signal is not linearly amplified. This has a marked effect on the characteristics of the received AU signal particularly at high gains and small inter-transducer separations, for example in the through transmission mode. This effect is clearly

demonstrated in figure 3.17. At low to intermediate gains or intermediate to large inter-transducer separations, the typical received AU pulse is of the form shown in figure 3.17a. At high gains and/or small inter-transducer separation, the same injected AU pulse would appear as shown in figure 3.17a (multiple ringdowns of identical amplitude).

To elucidate this effect, the output of the internal amplifier of the AU206 was investigated. Keeping all other factors constant, three parameters were monitored over the available range of gains. The ringdown count of each pulse (essentially the SWF), peak voltage (amplitude) and RMS voltage of the received AU pulse are all plotted as a function of gain in figure 3.18. Data from two repeat couplings are presented in each case.

Below its upper limit of 5.3 volts, the amplifier has a linear response, as would be expected. However, beyond this the amplified signal increases only slightly more for further increments of gain setting. Consequently, the SWF exhibits an initial near linear increase with gain until the peak amplitude of the pulse exceeds the 'clipping' voltage. Beyond this the SWF rapidly achieves a fixed value, a 'plateau', at which each ringdown exceeds the threshold and no further rise in SWF occurs. The RMS voltage achieves its plateau region at a higher gain when all ringdowns become clipped. This corresponds to the approximate 5.3 volts maximum output voltage of the amplifier, which is higher than the threshold set for the ringdown counter, hence explaining the different gains at which the corresponding plateau regions commence.

The AU206 has an oscilloscope on which the received pulse is displayed. The oscilloscope has a fixed +4 volt to -4 volt full scale display. Consequently, this 'clipping' is not visible to the operator without a separate oscilloscope. The received pulse amplitude was therefore presumably destined to lie approximately within the range 0 to 4 volts.

3.4.3 The Effect of Received AU Pulse Shape on SWF Readings

Bhatt and Hogg produced graphs of SWF versus threshold for through transmission AU testing of APC2 and polyester resin of the form shown in figure 3.19. The plateau region (constant SWF over a range of thresholds) was deemed to be the region of instrument settings within which SWF readings should be made for composite material investigation. These graphs of SWF versus threshold were reproduced at Bath, using identical conditions as far as possible.

Material:	40-ply UD APC2	Sample time:	0.5 seconds
Pulse energy:	E2	Gain:	40 dB and 100 dB
Pulse rate:	2000 pps	Gate width:	Open (350 microseconds)

Figure 3.20 shows the graphs of SWF versus threshold for APC2, at 40 and 100 dB gain, made at Bath. Oscilloscope traces of the pulses at the two gains are included as figures 3.21a and 3.21b.

At 100 dB gain every ringdown exceeds the maximum output voltage of the AU206 amplifier, hence the very wide plateau region of 0 - 5.5 V. When the threshold voltage reaches this level, there is a sharp cut off to a SWF of zero which indicates that all ringdowns are of a similar amplitude (clipped). At a pulse rate of 2 kHz and a gate width of 350 microseconds there is no division between successive pulses. The true wave packet shape (a damped sinusoid) has been converted, by exceeding the maximum amplifier output, into a square wave packet. Any major change in the recorded SWF, under these conditions, would have to be an effective change in the mean frequency of the received pulse.

At 40 dB the AU wave pulse can be divided into two portions. The first 5-6 ringdowns are clipped and produce the main plateau in the SWF/threshold graph. The remaining ringdowns are un-clipped.

To check the results previously stated, the transducers were removed and recoupled (with new double sided tape as couplant) to check for effects of coupling. Similar SWF/threshold graphs and associated oscilloscope photographs were produced under the following instrument settings:

Material:	40-ply UD APC2	Sample time:	0.5 seconds
Pulse energy:	E1	Gain:	40 dB and 100 dB
Pulse rate:	1000 pps	Gate width:	Open (350 microseconds)

In accordance with the method of data presentation of Bhatt and Hogg ^(74,75,76), the graphs are plotted on log scales in figure 3.22. Complementary photographs of the pulse shapes at each gain setting are again included (as figures 3.23a and 3.23b). The trends are the same as for the combination of instrument settings used by Bhatt and Hogg.

3.4.4 Conclusions with Respect to the Use of High Gains

When inter-transducer separation is small (for example in the through thickness AU testing of thin laminates used by Bhatt and Hogg) and intermediate to high gains are used, most of the ringdowns of the pulse will be of such magnitude as to be 'clipped'. Hence the received pulse essentially becomes a square shaped wave packet which is highly insensitive to changes of attenuation of the signal (see figure 3.17b).

SWF readings made at high gains and high thresholds are reproducible and relatively unaffected by coupling variation. These conclusions agree with those of Bhatt and Hogg ^(74,75,76), but it must be argued that under these conditions the SWF becomes relatively insensitive to the material under investigation.

Use of the plateau region of the SWF/threshold graph at high gains ensures that the SWF is made up of only ringdowns which have saturated the amplifier. Any true variation in the amplitude of such ringdowns within the material under investigation will have no effect on its received (and processed) amplitude. High gain/high threshold SWF readings

will only be altered by a change either in the mean frequency or the duration of the received pulse if there is no pulse overlap.

From the AU pulse shapes occasionally included in the literature (2,3,4,20,42), use of high gains with corresponding clipped signals does not appear to be widespread.

It should be pointed out that if gain/threshold settings are chosen which ensure that all ringdowns are counted, then the SWF will become sensitive only to changes in the total number of ringdowns, not in their magnitude. A change in the SWF would result either from a change in the frequency of the signal or an increase in the number of ringdowns caused by auxiliary reflections of the AU pulse from, for example, delaminations, large voids or cracks. In general, the peak heights of the ringdowns contained within the received AU pulse span a large range of voltages, such that it is common for a few of the highest amplitude ringdowns to exceed the maximum output voltage of the amplifier. Since these high amplitude ringdowns are significantly above threshold, their clipping has no effect on the recorded SWF.

3.5 A Study Of Defect Detection In APC2 By Means Of Acousto-Ultrasonics

An extensive study of the factors affecting the absolute value of the AU parameters, SWF and RMS voltage has been carried out, followed by their optimisation with respect to reproducibility and sensitivity to a composite material variable, namely fibre orientation. Having done so, it was deemed appropriate to apply the acousto-ultrasonic technique to defect detection in APC2 laminates.

A study was therefore initiated to determine what types of defect AU could detect. Primary significance was given to data gathered by using the optimised test conditions for SWF. However various combinations of pulse energy, gain, threshold and gate width spanning the available ranges were used and RMS voltage and burst mode were subsequently included.

The material investigated was 16 or 20-ply UD or balanced 16 cross-ply APC2 moulded at Bath, details of which are included later. One of the main advantages claimed for AU is its ability to interrogate material and structures in the direction of maximum stress (3,15,42), which in composite materials is the principal fibre direction. In consequence, laminates were primarily tested parallel to fibres in UD laminates, although measurements perpendicular to fibres were recorded where applicable.

The basis of this investigation was to compare statistically the means of at least 5 repeat readings (recouplings of the transducers) between good quality laminates and those containing defects and between laminates before and after the introduction of defects. These deliberately introduced defects were generated either during lay-up and moulding, termed 'moulded-in' defects, or after moulding by drop weight impact, crushing or drilling. They were always positioned at the centre of the plate. By maintaining specimen dimensions, defect and transducer locations constant between defective/non-defective comparisons, any statistically significant differences in the means of repeat readings could be attributed solely to the effects of the defects. Statistical significance was tested by using a simple small sample Student t test, the normality of SWF data having been proved earlier.

All non-defective laminates were individually C-scanned at the Wilton laboratories of ICI before testing to ensure their quality.

3.5.1 Scanning of APC2 Plates with 'Moulded-in' Defects

Standard quality (non-defective) unidirectional 16-ply UD plates 150 mm x 100 mm x 2 mm were as a basis for comparison. Further plates were produced with defects located centrally in plan and through the thickness. Three types of defect were produced, in the following manner:

1. A 30 mm cut was made perpendicular to the fibres in each of the two centre plies.

2. A 30 mm square piece of aluminium foil was placed between the centre plies, which, based on the fact that PEEK shows poor adhesion to aluminium, represents a delamination,.
3. A 30 mm square section was cut from each of the centre two plies.

Standard and defective plates of identical size were AU tested in pairs. Subsequently, they were tested to destruction in three point flexure with associated monitoring of acoustic emission to allow comparison of these two NDE techniques.

AU SWF measurements were taken at 9 positions sampling the direction perpendicular to the fibres and at 9 positions sampling parallel to the fibres, yielding low resolution scans of the plates in two dimensions. 5 repeat readings were taken at each location and the mean value was taken to represent the SWF at a point midway between the two transducers. Thus, nine representative values of SWF were mapped onto a plan view of the plate, as illustrated in figures 3.24 and 3.25. Subsequent mechanical testing demonstrated the 'plies removed' defect to be the most severe and therefore this has been included as figure 3.24b parallel to fibres and figure 3.25b perpendicular to fibres. Complementary scans of a typical non-defective plate are included as figures 3.24a and 3.25a. In order to rule out any of the possible geometric effects noted in the literature (8,13), comparisons between SWF readings at similar locations were made between readings carried out on a good quality plate and defective.

At a 95 per cent confidence level, an average difference in SWF readings in excess of 29 parallel to fibres and 80 perpendicular to fibres is needed before any difference is significant. It therefore appears that the AU 206 system is insufficiently sensitive to detect 'moulded-in' defects.

In comparison, ultrasonic C-scanning showed the area of missing plies as a possible delamination. Mechanical testing indicated, though not conclusively, that the defective

plates were weaker in 3 point flexure than good plates. Associated acoustic emission monitoring gave some indications that defective plates gave both larger numbers of emissions to failure, more emissions at lower stress and sometimes a lower stress threshold below which the APC2 material did not emit.

3.5.2 Impact Damage in Plates

3.5.2.1 UD plates

A preliminary investigation of the sensitivity of AU to impact damage was carried out. Firstly, a 16-ply UD APC2 laminate plate was moulded and C-scanned to ensure that no overt defects were present. Five 150 mm x 25 mm samples were then cut from this plate. Mean values of SWF and RMS voltage were determined from 5 replicate readings at two combinations of instrument settings. Reading were recorded from three samples in the virgin condition and from two samples after the infliction of impact damage. The impact damage was produced by a domed 1 kg weight falling from a height of 500 mm onto the centre, giving an impact energy of 4.9 J. The impact was repeated ten times at the same location, causing permanent distortion of the specimens (visible from front and back surfaces) and some longitudinal cracking.

The means and standard deviations of grouped data from all good quality laminates (15 readings) and all defective laminates (10 readings) at the appropriate instrument settings are presented in columns 3 and 4 in table 3.5. The last column of this table presents Student's t values for pair comparisons of means of defective and non-defective plates. Student's t must exceed 2.81 for significance at the 1% level. It is apparent that although mean SWF and RMS voltage readings decrease with the introduction of impact damage in these UD laminates, as would be expected, and in accordance with the literature (8), the scatter in the data is too great for the differences in the SWF to be significant. The RMS voltage difference is however significant at the 1% level. The RMS voltage appears therefore to be more sensitive to impact damage than the SWF. The impact

damage is very severe, however, and a simple visual examination was more than adequate to locate the damage.

3.5.2.2 Cross-ply plates

A 16-ply 0/90 cross-ply plate 180 mm x 70 mm was prepared and tested as moulded, using the previously described format of five repeat readings. The instrumentation settings used were firstly, those already optimised and secondly, various other combinations to ensure coverage of the available ranges. The time of flight of the AU pulse was also monitored.

The laminate was then subjected to ten 4.9 J drop weight impacts at the same location producing a small but visible indentation on the front face. A subsequent C-scan, included as figure 3.26, clearly shows the extent of the damage, covering an area of approximately 100 mm². It has been shown elsewhere that at this energy level, impact produces a conical damage zone through the thickness of the plate ⁽⁷⁷⁾.

AU measurements were then made on the damaged plate, with the same combination of instrument settings as previously. The means and sample standard deviations (in brackets) of AU measurements before and after impacting are presented in columns 6 and 7 of table 3.6. Columns 1 to 5 show the instrument settings, and column 8 the Student's t value obtained from the pair comparison of the corresponding means. Only RMS voltage shows a significant difference (at the 1% level) after impacting, and surprisingly this difference results from an increase after impacting. In fact, the means of all data presented in table 3.6 increased after impacting. This is in apparent antithesis to the results recorded from UD material. The time of flight of the AU pulse of 13.75 microseconds (a wave speed of approximately 6200 m/s) showed no detectable difference after infliction of impact damage.

The severity of defects so far investigated appeared to have been insufficient to be detected by the SWF. An even more severe level of damage was therefore introduced into a cross-ply laminate. Two 16-ply 0/90 cross-ply plates 180 mm x 70 mm were prepared. One was tested as moulded, the other was subject to a single 5.7 J drop weight impact and then bent in four point flexure until top ply failure occurred. This plate was then AU tested and readings compared to those from the non-defective plate. Table 3.7 presents the means and sample standard deviations (in brackets) for the SWF and RMS voltage for each plate and the Student's t value for the pair comparison between plates. Clearly there is a highly significant decrease in RMS voltage and SWF as a result of this severe damage.

3.5.3 Influence of Damage in Strip Specimens

The ability of acousto-ultrasonics to distinguish between defective and non-defective 16-ply UD 16 mm wide by 180 mm long APC2 strip specimens was investigated.

AU measurements of SWF and RMS voltage were recorded by using combinations of instrument settings in both the 'pulse' and 'burst' modes of pulser excitation. In the 'burst mode', the maximum excitation frequency available (1.5 MHz) and minimum duration (9 microseconds) were used. Results from two combinations of pulse mode quasi-RMS voltage (RMSV), three combinations of pulse SWF, and one burst mode RMS and SWF are presented.

Five repeat AU readings were made longitudinally over the central portion of each of 48 nominally identical non-defective specimens. The average of these 5 readings was taken to represent the appropriate AU parameter for that specimen in the undamaged condition.

Three sets of five specimens were selected at random from the 48 non-defective specimens and subjected to deliberate damage at the mid point according to the following regime:

1. A single drop weight impact using a 0.825 kg domed weight falling through 870 mm, giving an impact energy of 7.0 J. This caused back face damage in the form of 2 cracks parallel to the fibres, 15 mm long and 5 mm apart.
2. Specimens were crushed between 10 mm diameter steel rollers perpendicular to the axis of the specimen under a load of 20 kN, producing a 2.3 mm wide indentation on both sides and across the full width of the specimen.
3. A 3 mm diameter hole was drilled at the centre of the specimens using a high speed steel twist drill rotating at 400 RPM.

The damaged specimens were AU tested again, five replicate SWF and RMSV values being measured in the central portion, spanning the defect.

3.5.3.1 Variability due to coupling

In order to determine the level of scatter in the results caused by coupling variability, 30 repeat AU readings were made for each of the seven combinations of instrument settings at one position on one specimen. The transducers were removed and re-coupled between each measurement. The mean, standard deviation, coefficient of variation and 95% confidence limits are presented for each AU parameter/instrument setting combination in table 3.8. It is interesting to note that with respect to repeat coupling, use of the 'auto' threshold increases the coefficient of variation for optimised pulse mode SWF measurements. The 'auto' threshold automatically increases the threshold to maintain a constant distance above the instantaneous background noise. Since the differences between all values recorded with and without the auto threshold facility were very small, the background noise was clearly not contributing significantly to the recorded AU signal.

3.5.3.2 Comparison of impacted, holed and crushed samples with non-defective samples

The mean values (with standard deviations in brackets) for the three groups of five samples before and after introduction of damage are presented in table 3.9. The grand mean and the coefficient of variation of all 48 samples in the undamaged state is included at the base of each column.

Using a Student's 't' test, the mean AU values from the groups of 5 samples were compared before and after introduction of defects. The results of these comparisons are shown in the upper half of table 3.10. Taking the 1% level as critical for a test of significance, 't' must exceed 3.36 for 8 degrees of freedom. Clearly, AU cannot reliably distinguish between samples before and after introduction of damage.

In the lower half of table 3.10 are the 't' values for comparisons between 5 defective samples and the total population of 48 non-defective. The critical value of 't' is 2.68 at the 1% level for 51 degrees of freedom. It appears that AU can reliably detect a 3 mm hole by decreases of pulse mode SWF and RMS voltage and drop weight impact damage by an increase in pulse mode RMS.

There is a discrepancy between the results of comparison of 5 pre-damage with 5 post-damage samples and the comparison of 5 post-damage with 48 non-defective samples. This discrepancy stems in part from differences between the mean values of groups of 5 pre-damage samples and the grand averages of all 48 non-defective samples. A more refined, single-sample comparison was conducted. In this, the arithmetic difference between SWF and RMSV values before and after defect introduction are determined for individual specimens. The mean difference of the five specimens was then tested for its significance of departure from zero using a Student's t test, the results of which are shown in table 3.11.

Since no value of 't' exceeds 4.6, which is its critical value at the 1% level for this number of samples, it must be concluded that AU could not reliably detect any of the defects in APC2 strip specimens.

3.5.4 Determination of the Minimum Size of Through Thickness Hole Detectable in APC2 by AU

As a result of the less than promising application of AU to the detection of moulded-in defects, impact damage and defects in strip specimens, it was decided to determine the minimum size of through thickness hole detectable in an APC2 plate using AU.

The plate selected was 20-ply UD APC2, nominally 290 mm x 220 mm. Sets of 10 repeat AU measurements were recorded with transducers aligned, first parallel and then perpendicular to the principal fibre axis, at a position near to the centre of the plate. The material condition was termed 'virgin' at this stage. Optimised instrument settings were used, and in addition, burst mode SWF and RMSV measurements were recorded, the burst frequency tuned to give a maximum output (resonance) and minimum duration.

Next, a 2 mm hole was drilled at the position mid-way between the location of the transducers. 5 more repeat readings were recorded in the two transducer orientations. This process was then repeated with the hole enlarged by increments up to 12.5 mm.

The mean and sample standard deviations of the replicate readings in each condition of the plate, namely virgin and with the specified hole diameter are presented in table 3.12a for measurements made parallel to fibres and table 3.12b for the perpendicular direction. Tables 3.13a and 3.13b give the values of Student's t for pair comparisons between corresponding mean AU values for drilled and undrilled material.

With consideration of the severity of the defect, it is considered that a 0.1% significance level ('highly significant') is appropriate for statistical proof of the detection of the

defect. At this significance level, and for the number of degrees of freedom applicable, Student's t must exceed 4.3 for significance. It is seen that optimised pulse mode SWF and RMSV can detect a minimum through thickness hole size of 4 mm. However burst mode RMSV is capable of detecting a minimum 2 mm hole, though only for measurements in the principal fibre direction. In fact, both AU parameters monitored and both pulse excitation modes showed significantly improved sensitivity to drill holes when measurements are made in the principal fibre direction. This would seem logical considering the likely waveguiding effects of the reinforcing fibres and the more significant decrease in 0° properties as a result of this type of defect.

SWF data recorded at the high gain of 80 dB have been included in this defect investigation to demonstrate that the saturation of the AU 206 amplifier, which causes clipping of the received AU pulse, reduces the sensitivity of the system to the presence of defects. A 6 mm hole for measurements in the fibre direction and a 12.5 mm hole for measurements in the direction perpendicular to fibres were the minimum detected defect sizes using high gains.

It is interesting to note that the greatest sensitivity of AU to through thickness holes is achieved by using RMSV and the burst mode of pulse excitation and not the SWF and pulse mode of operation usually reported in the literature. The reproducibility of these parameters, as measured by the coefficients of variation, plays an essential part in the sensitivity to defects. Comparing measurements made at the same gain of 60 dB, optimised pulse mode SWF and RMSV measurements exhibit coefficients of variation of around 5-6%, compared to 9-10% for burst mode RMSV and up to 15% for burst mode SWF. The sensitivity of burst mode RMSV therefore originates from a more rapid decline of RMSV with increasing hole size, which more than compensates for the reduced reproducibility of this parameter.

Coupling variation may be removed from the investigation of increased defect size on AU parameters by maintaining fixed coupling and then introducing and increasing the defect size. This has been accomplished by bonding the transducers in place onto the APC2 plate using a silicone adhesive. Figures 3.27a and 3.27b present normalised plots of SWF and RMSV as a function of increasing hole size for this fixed coupling condition in the two transducer orientations. The data were normalised by division by the initial virgin material reading in order to plot the different AU parameters on the same graph for comparison. It is clear that even small through thickness holes do cause a noticeable decrease in the magnitudes of AU parameters. This proves that it is the unfortunate uncontrolled variability of AU measurements which often precludes its successful application to defect detection.

3.6 Discussion Of AU Results

The acousto-ultrasonic technique has been investigated and applied to the non-destructive examination of carbon fibre reinforced PEEK (APC2). Many of the factors affecting the magnitude and reproducibility of the SWF and RMS voltage (AU parameters), have been investigated and optimised for one characteristic of one laminate (APC2). Following this, the technique has been applied to the identification of a variety of defects and found to be somewhat lacking. The results of this research project will now be discussed in more detail and with reference to the literature.

The AU206 instrument has been shown to require a considerable warm up period during which the measured SWF and RMS voltage values decline. After this period (approximately eight hours) the instrument appears quite stable, successive AU pulses are found to be identical, and the pulser repetition rate and sampling time interval act as simple scaling factors of the SWF. Hence, the division of any SWF value by the product of the sampling time and number of pulses per second, will yield the number of ringdowns per pulse which is the fundamental significance of this parameter.

Increasing coupling contact pressure, achieved by dead weight loading between AU transducers and specimen whilst using a viscous liquid couplant, was found to cause an increase in the SWF. A minimum load on each transducer of approximately 8 N was required for maximum reproducibility of coupling. This value is close to the 2 lbs per transducer reported by Henneke et al ⁽¹⁷⁾. This would be predicted by increasing the true surface/surface contact between transducer wear plate and specimen surface with increasing load, giving improved stress wave energy transmission across the interface. In addition, it is clear that a minimum contact load is needed to produce the lateral flow of a viscous fluid and removal of any enclosed air within an acceptable time period. This is necessary to produce a uniform reproducible coupling layer, which in turn improves reproducibility. SWF variation is found to be greater for the receiving transducer coupling than the emitter.

Of the plethora of instrument settings available with the AU206, four main variables have been identified as having the most significant effect on the magnitude, reproducibility and sensitivity to material characteristics of the SWF and RMS voltage. These are the instrument gain, gate width, threshold and pulse energy. Furthermore, these instrument settings show complex interactions, and in general, no simple rules have been found for achieving optimisation in different circumstances. The effects of these variables may be explained by their effects on the characteristics of the received AU pulse and on what portion of the pulse contributes to the magnitude of the SWF. The pulse energy and gain affect the magnitude and shape of the pulse which is processed. The threshold determines the portion of the pulse in the voltage domain which contributes to the SWF, and the gate width in the time domain.

A method of instrumentation setting optimisation has been suggested. This process may be broken down into three parts. Firstly, the selection of a parameter which represents the sensitivity of AU to a material characteristic. Secondly, the systematic variation of each of the instrument variables to produce an experimental grid. And finally the

analysis of variation and covariation of the sensitivity parameter to determine conditions for its maximisation. The sensitivity parameter selected was DSWF, the arithmetic difference between the SWF measured parallel to fibres and that measured perpendicular to fibres. The corresponding parameter DRMSV, was defined for the alternative AU parameter, RMS voltage. The necessity for optimisation of test conditions before AU can be expected to show sensitivity to material characteristics is also reported by Henneke et al (55). Furthermore, this is likely to be necessary for each material/structure/system combination.

Once conditions had been optimised, the SWF was found to show very good sensitivity to fibre orientation. However, the residual intrinsic variability in repeat readings produced a minimum coefficient of variation of 5%. This minimum is commensurate with that reported by Vary (18) and Henneke (17). This degree of scatter is considerable and was achieved even when great care was taken to reduce variation to a minimum. This scatter is considered to be largely associated with the uncertain quality of coupling and represents a significant limitation of the technique.

The investigation of the use of high gains and thresholds has highlighted some important limitations of the AU206 instrument. A maximum output amplitude of the internal amplifier of 5.3 volts causes higher amplitude ringdowns to be 'clipped'. The large range of amplitudes of ringdowns in a typical received pulse (particularly in the through thickness configuration of transducers) makes it very difficult to avoid some 'clipping' whilst maintaining a sufficiently high SWF which has sufficient resolution for material characterisation. The fixed 4 volt vertical scale on the oscilloscope of the AU206, used for observing pulses, compounds this problem by not showing the operator this 'clipping'. The 'clipping' of ringdowns which would always lie well above threshold, even in the presence of defects, will of course have no effect on the sensitivity or reproducibility of the SWF, though its effect on RMS voltage is less clear. The use of high gains can therefore yield meaningless SWF values owing to saturation of the

amplifier. It is clearly essential to monitor the received AU pulse shape during testing, preferably on a separate oscilloscope.

The application of AU to 'moulded-in' defects was totally unsuccessful. No statistically significant difference was found between mean SWF measurements made on these defective and non-defective APC2 plates. However, the defects had little effect on the mechanical properties of the plates and C-scans and acoustic emission testing had difficulty in identifying the defects. The ability of the PEEK matrix to flow during pressing and so 'heal' the defects, plus the general toughness of the composite and ductility of the PEEK, appears to confer considerable tolerance of the deleterious effects of defects. Such defects might be expected to be quite severe in other fibre reinforced epoxy composites.

In comparison to 'moulded-in' defects, two highly severe types of defect were detectable by both SWF and RMS voltage parameters. These were impact damage followed by flexure until outer ply failure occurred, and large through thickness holes of 4 mm and greater diameter. A large grey area between these two extremes exists in which statistically significant differences were much harder, and in the case of the SWF, impossible to find.

The results of applying AU to impact damage in UD and cross-ply APC2 laminates yielded mixed results. In general, the SWF proved insensitive to multiple impact damage, damage which has been shown by C-scan to produce extensive internal cracking in a cone shaped zone extending out from the front face point of impact (77). RMS voltage, however, appeared to be just capable of detecting such damage. Green has also found RMS voltage to be better at impact damage location than SWF (8). With reference to the ability of RMS voltage to detect the presence of repeated impact damage in APC2, this composite is very tough, as previously noted. It exhibits G_{1C} and K_{1C} values up to an order of magnitude greater than those of epoxy/carbon fibre composites

(78), apparently as a result of the ductility of the matrix and good adhesion to the fibres (see later). In light of this, it may be considered that the sensitivity of RMS voltage to ten 4.9 J drop weight impacts in a tough composite is comparable to the sensitivity to a single 15 J impact in a less tough graphite/epoxy composite shown by Talreja (39). Green (8) also reported detection of impact damage in quasi-isotropic 48-ply graphite epoxy by a reduction in the RMS voltage. However, no data are given as to the reproducibility of the RMS readings or of the drop weight impact energy. Williams and Lampert presented data on repeated drop weight impacts of around 2.5 J on 1.3 mm 10-ply Hercules AS/epoxy (20). Careful examination of these data indicates that between 10 and 40 impacts would be needed to generate a statistically significant decrease in the SWF, using the same tests of significance employed here.

It may be argued that the insensitivity of SWF to the various defects may have been the result of a misguided selection of instrument settings which rendered the system insensitive to such defects. In order to counter this argument, a variety of non optimised instrument setting combinations, spanning the available ranges, were also included in the investigation of defects. This was extended to include the burst mode of emitter transducer excitation which proved fruitful in improved detectability of through thickness holes, when measurements were made parallel to fibres. This improvement came about by a more rapid decline in the RMS voltage and SWF with increasing hole size but also an increase in the coefficient of variation of repeat readings, so indicating an apparent antithesis between sensitivity and reproducibility under some conditions. The type of excitation pulse used in AU appears to have a significant effect on the ability of AU to detect defects. Pulse rise time, fall time and duration all affect the waveform injected into the specimen (79), as does excitation pulse amplitude. The received pulse shape showed various changes with the different pulse energies available on the AU206. Pulse energy did not merely act as an amplitude scaling factor.

After optimisation, the SWF and RMS was certainly sensitive to fibre orientation, a very significant material characteristic. Increased stress wave energy propagation parallel to fibres compared to perpendicular to fibres has been noted by Vary (in 8-ply graphite/epoxy and glass/epoxy) (7). Dispersion has been found to be greater perpendicular rather than parallel to fibres in composites (50). Because of the great variation of elastic modulus and strength with fibre orientation, it may be argued that this proves the ability of AU to detect strength and modulus variations. Alternative test conditions may be needed however, for sensitivity to different defects whilst maintaining fibre alignment constant. The requirement to carry out extensive experimentation and optimisation for every type of defect or material characteristic for each material/structure/system combination over a multitude of experimental factors must surely limit the prospects of widespread use of AU.

More emphasis has been given to SWF and RMS voltage readings made parallel to fibres than perpendicular to fibres. This stems from one of the proposed advantages of AU, namely that the technique can and should interrogate material in the primary axis of loading in which highest stresses will be orientated (36). AU was found to be more sensitive to through thickness holes when measurements were made parallel to fibres than when made perpendicular to fibres in a unidirectional APC2 plate.

In general, the results of this investigation of AU indicate that the technique has little to offer for the non-destructive testing of APC2. The technique can only just detect multiple impact damage which is clearly detectable with the naked eye, C-scanning and AE. It could not detect impact, drilled hole and crush damage in strip specimens and had a limit of detectability of 2 mm - 4 mm hole size in large plates. AU was found to be largely insensitive to variations in mechanical properties of strip specimens (see later), though it is sensitive to fibre alignment.

When considering the results included in this thesis and the conclusions drawn, it is important to consider them with respect to results in the literature, which on the basis of conclusions drawn by the respective authors, are generally very positive and supportive of the AU technique. This discrepancy requires consideration. The actual AU measurements presented in this thesis, their accuracy and reproducibility are similar to those of the literature. SWF and RMS voltage measurements are reproducible to approximately $\pm 10\%$, the AU206 acousto-ultrasonic test equipment including transducers are identical to those widely used elsewhere (8,24,25,28,29,30,31,33,43,53,57,59,75,76). Specimen types, dimensions and types of defect are also similar. The main reason for the discrepancy, suggested by this author, is the difference in analysis of the data. Throughout the work at Bath, the sensitivity of AU to the material under investigation has been based on statistical significance tests, which take into account not just the means of AU measurements, but their uncontrolled scatter. In the literature, this is almost universally not the case, and it is very common for the variability of AU data to be completely ignored, in spite of its magnitude, and hence significance.

The reasons for the apparent lack of success in applying the AU206 acousto-ultrasonic testing system may be considered.

1. The acousto-ultrasonic approach may simply be unsuitable as a means of NDT or at least unsuitable for the particular carbon fibre reinforced PEEK composite in question. AU may be applicable to the more brittle epoxy and other thermoset composites, and not to composites with tougher, more ductile thermoplastic matrices. AU is certainly sensitive to some material characteristics in APC2. SWF and RMS voltage measurements are different for different orientations with respect to fibres in unidirectional APC2, and to gross artificial flaws such as through thickness holes and some major impact damage/ply failure. It is not therefore a question of whether AU is

sensitive to material characteristics in APC2, but of whether the sensitivity is sufficient to exceed the masking effect of variability caused predominantly by coupling.

2. The lack of success in the application of AU to NDE in APC2 may not be an intrinsic inability of the technique, but may be attributable to the main AU parameter used, namely Vary's Stress Wave Factor, the basis of the AU206 system. This parameter appears to have been chosen, at least in part, for its ease of determination with simple equipment. The inclusion of pulser repetition rate and sampling time in the definition of Vary's SWF appears to stem more from ease of processing than from any absolute significance with respect to sensitivity to material.

An AU parameter must quantify the effect of damage on the AU pulse in composite materials. When an AU pulse propagates through a damaged composite, the interaction between the wave and the damage can cause two things. Firstly, damage will in general reduce the stiffness, and, since wave speed is proportional to $E^{1/2}$, damage will reduce wave speed. Secondly, attenuation will increase as a result of incoherent scattering and reflection at crack surfaces. This explanation would account for a decrease in the AU206 SWF; an increased transit time reducing the ringdowns within the time window which starts at the instant of pulse emission into the material, and attenuation reducing the magnitude of the ringdowns, hence placing more below the threshold. In addition, the AU pulse frequency must be considered. In simple terms, a decrease in the mean frequency of the received pulse will give fewer ringdowns in a given gate sweep and hence a smaller SWF. Since it is the higher frequency component of an ultrasonic pulse that is most greatly attenuated by the small (relative to the wavelength) defects and inhomogeneities in composites, it becomes evident that damage will reduce the SWF as a result of a frequency shift. The central moment of the power spectrum density (in addition to the skewness and kurtosis) used by Talreja ⁽³⁹⁾ may monitor any frequency shift better than Vary's SWF.

The SWF is also affected by the received pulse shape in the time domain. The received pulse is made up of various echos, waves which have propagated by various paths, interacting with each other and all contributing to a very complex pulse envelope. Pulse shape is significantly affected by coupling variation. There is certainly no simple explanation for the various complex received pulse shapes which can be achieved from nominally similar material.

The SWF was originally reported by Vary to be a measure of the efficiency of stress wave energy transmission, such that good quality material with a more perfect structure would transmit this energy more efficiently than poor quality. Thus a lower SWF should correspond to poorer quality material. This is not necessarily the case. For example, in testing of bond quality, good bonding between material layers has been associated both with high and low SWF. For certain instrumentation and test condition combinations, it may be argued that the presence of a defect such as a delamination may cause greater numbers of echos/reflections from the internal surfaces, producing more ringdowns, possibly of lower amplitude. If the threshold is set moderately low or the gain set high, the increased numbers of ringdowns could all exceed threshold and thus cause an increased SWF. This is perhaps an over-simplification, but it is clear that a simple ringdown count will only partly characterise an AU pulse.

Both SWF and RMS voltage are dependent on a multitude of instrument variables which require extensive investigation and optimisation before any sensitivity to material variables can be achieved. Both are excessively sensitive to coupling variation. The RMS voltage has appeared more sensitive to the presence of defects.

The main AU parameters used in the literature are Vary's SWF, RMS voltage, moments of the frequency spectrum (zeroth moment, kurtosis and skewness), peak amplitude and a ringdown count of a pulse but with each ringdown given a weighting proportional to its peak voltage. The first three of these parameters account for almost all of the published

data. Of the moments of the frequency spectrum, the zeroth moment, found to be most sensitive to material variation, is in fact equivalent to the analog RMS voltage ⁽⁴⁵⁾. Consequently, it is evident that as yet, the two parameters investigated in this thesis are the most widely accepted AU parameters.

The increasing interest of the long standing researchers into other AU parameters ^(20,27,35,37,40,60) would appear to reinforce the conclusion that the original SWF is not a particularly useful parameter. Kautz compared Vary's SWF with other parameters and found it incapable of rating composites with respect to ILSS, whereas other parameters were able to (ie the RMS of the power spectrum density).

3. The frequency response of the equipment, in particular the transducers, may have been unsuitable for use with the APC2 laminates and defects investigated. The principle of AU is to use a higher frequency emitter and lower frequency receiver ⁽¹⁷⁾. The receiver transducer is often a resonant AE sensor because of the high sensitivity required to overcome the high attenuation of the test material. A resonant sensor would also seem useful if a ringdown count is used as the AU parameter because of the 'ringing' of non damped transducers. Without such high sensitivity and 'ringing', a sufficiently high ringdown count for a sufficient resolution to defects may be difficult to achieve. Thus, in defining the SWF, the sensing equipment must be selected for the logistics of measuring this parameter, rather than for optimum sensitivity to such factors as attenuation. The frequency range of AU used in this work was essentially set by the AU206 system which is supplied with a broadband emitter (0.1 - 2.0 MHz) and 375 kHz resonant receiver and the 0.1 - 1.0 MHz frequency response specification of the instrument ⁽⁶⁹⁾. The hypothesis behind the use of this frequency range appears to be the fact that most composite materials show very high attenuation at frequencies much above 0.75 to 1.0 MHz. An upper limit on the usable frequency range is set by the necessity to recover sufficient of the injected signal to be able to suitably analyse it. The most common frequency range of sensors in acoustic emission is 100 - 300 kHz ⁽⁴⁾ and

probably explains, in part, the selection of the AC375 receiver transducer used in the AU206 system.

The high attenuation coefficients of composites sets the upper limit of AU in the literature to between about 1 and 2 MHz (1,3,8,27). Vary (1) has suggested that for plate thicknesses around 2 mm, frequencies much below 0.1 MHz would not produce wave interactions appropriate to fibre reinforced plastic specimen microstructure. According to Vary, the ultrasonic wavelength must be of the same order of magnitude as plate thickness. Williams and Lampert have used the FC500/AC375 transducer combination on 1.3 mm graphite/epoxy (20). Vary used a 500 kHz receiver transducer for 1 mm - 1.3 mm thick graphite/epoxy (4) and suggests that the incident AU pulse should be broadband (0.1 - 2.0 MHz) and introduced at normal incidence (7). Rogers reports typical frequencies of AU processing as 100-400 kHz (15). Emitter and receiver centre frequencies as low as 75 kHz and 60 kHz respectively have been used, though in this case for fairly thick sections of wood (80).

Partitioning of the AU signal in the frequency domain by either switch selectable band pass filters or FFT on digitised pulses has been suggested by Kautz (26,27) as the best method of achieving optimisation of test conditions in the frequency domain.

Attenuation is frequency dependent. In general, higher frequencies are more highly attenuated, and hence the use of transducers of higher resonant frequencies, broader band receiver transducers or high pass filters may improve sensitivity. Since AU is at least in part an attenuation process, working at higher frequencies would be advantageous. High attenuation due to scattering requires the ultrasonic wavelength to be commensurate with the size of the wave scattering inhomogeneities, such as microcracks, fibre deficient areas and delaminations. Most of the inhomogeneities/defects in APC2 are small (of the order of fractions of a millimetre) in comparison to the likely wavelength of injected AU stress waves (of the order of millimetres). Therefore, any decrease in AU wavelength,

perhaps by working at much higher frequencies, may be an advantage. Interestingly, more recently, various workers and, in particular, those using AU parameters different from Vary's SWF, have used matched broadband sensors as emitter and receiver, working at frequencies up to 5 MHz (23,34,37,39,40).

4. AU may simply be insensitive to the types of defect investigated or they may simply not be severe enough to affect the mechanical properties of the APC2 laminates significantly. This would be the result of the high toughness of the composite, the ductility of the matrix, and the excellent adhesion between fibres and PEEK. AU may be primarily sensitive to strength and/or modulus. Much of the investigation of defect detection by AU in this thesis has been associated with single overt defects, such as drilled holes. This is clearly of importance, but it may be argued that since it is often difficult to correlate failure in composites with a single flaw, the sensitivity of AU to strength variation has not been investigated. However, as will be shown later, no correlation was found between AU and the normal variation of mechanical properties of a large population of nominally identical APC2 specimens.

5. Transducer disposition seems unlikely to be the cause of the lack of success. The inter-transducer separation distance is well within the range used by other authors for same surface transducer positions (15). In spite of the fact that a few authors have made use of AU in the through transmission mode (31,37,41,74,75), there appears to be little purpose in doing so for most testing: the technique becomes almost identical to conventional through thickness C-scanning, accurate alignment of transducers is a problem and the theoretical basis of AU, namely the measurement of stress wave interaction with microstructure in the principal direction of applied stress is usually negated using this arrangement. The advantage of only single surface access would also be lost. Kinra and Dayal (61) have shown this arrangement to produce no effect on wave speed and only a small effect on attenuation when looking for transverse ply cracks in 0/90 composites. However, Williams and Lee have reported good correlation between

through thickness attenuation and strength as a percentage of UTS in polyester reinforced glass (attenuation around 2.0 MHz decreases with increasing tensile strength) (32). Through thickness attenuation has also been demonstrated to be sensitive to small changes in cure temperature and pressure of carbon fibre reinforced epoxies, to correlate with void volume fraction, flexural fatigue life and to locate overt defects such as notches and holes (32)

6. The intrinsic scatter in AU measurements, and in particular the uncertain quality of coupling is, in the opinion of this author, too great and largely masks the effects of any material variation. Coupling is reported to be of great importance to AU (1,8,54). Vary acknowledges that for reproducibility of SWF transducer positioning, coupling mode and pressure must be carefully controlled (7). Green reports that RMS voltage is highly sensitive to both coupling characteristics and contact pressure (8). Noiret and Roget noted that both AE and AU have sometimes shown a lack of reliability (81). The claimed SWF reproducibility of $\pm 10\%$ (17,18), the best achieved in the work at Bath, is in fact likely to be a lower limit. Vary and Bowles have published SWF data subject to a $\pm 20\%$ and $\pm 28\%$ variability (1).

Unfortunately, there does not seem to be any easy method of significantly improving coupling reproducibility. The basic method of coupling adopted in this study is widely used elsewhere (15,19,20,30,30,33,41,43,53,59). It probably represents the highest level of consistency attainable, yet is highly laborious and impractical for large scale components/structures. It is reassuring to note that in the paper by Leaird and Kingdom (79) suggesting possible calibration standards (with particular reference to the AU206), Vaseline couplant and a simple 1 kg mass on each transducer was an ideal standard coupling condition.

A further contribution to variability may be associated with inexact positioning of transducers, a factor likely to be exaggerated when small defects lie between the

transducers. Electrical or mechanical noise is not considered to be of much significance to AU, proof being the lack of any significant reduction of the coefficient of variation of repeat measurements when using the auto threshold facility.

The various claims by researchers that AU is a powerful NDE tool have so far not lead to the application of the technique outside the laboratory ⁽⁵⁴⁾. It is suggested by this author that uncontrolled variation in readings due to coupling is a prime cause of this lack of applicability.

7. The selection of test conditions including the instrument settings may have been completely misguided, so making the AU206 system largely insensitive to APC2 material characteristics/defects. However, the inclusion of combinations of instrument settings spanning the available ranges must, at least in part, answer this possible criticism.

8. There is no in situ calibration available for AU testing, a fundamental weakness of the technique. The optimised test conditions which have been determined cannot easily be compared with the conditions of other authors. This is because all important test conditions are very rarely quoted in the literature, and in any case the material under test is likely significantly to alter the optimum test conditions. The specificity of AU measurements to the particular test equipment/material/instrumentation settings combination makes comparison of data from different sources largely impossible.

3.7 Conclusions

The most important conclusion to be drawn from this study of acousto-ultrasonics is that the technique shows little promise of becoming a useful means of non-destructive testing of aromatic polymer composites. Detailed conclusions, in brief, include the following:

1. The most important instrument settings have been optimised to obtain the best available reproducibility and sensitivity in the measurement of SWF and RMS voltage for one characteristic of one laminate.
2. Appreciable scatter in SWF measurements remains, even after optimisation. This scatter is largely due to variability of coupling and yields a minimum coefficient of variation of approximately 5% for SWF.
3. Instrument settings show complex interactions in their influence on SWF and RMS voltage, and no simple rules have been found to obtain optimisation in different circumstances.
4. A constant coupling load of at least 8 N per transducer is recommended for reproducibility of coupling.
5. The AU206 shows certain limitations/deficiencies. Firstly, insufficient screening allows the emitter transducer excitation pulse to 'leak' over to the signal processing module and thus to be recorded as a 'rogue' ringdown. Secondly, the amplifier has a maximum output voltage of 5.3 volts above which ringdowns are 'clipped'.
6. The use of high gain settings can yield meaningless SWF values, owing to saturation of the amplifier. Signal shape should invariably be monitored during measurements.
7. Both the SWF and RMS voltage are sensitive to fibre orientation in APC2.
8. Because of the substantial level of uncontrolled scatter, it is important that any differences between AU measurements should be established by a statistical test of means and standard deviations, such as Student's t test.
9. The SWF is incapable of detecting most of the defects investigated. These include 'moulded-in' defects, repeated 4.5 J drop weight impact damage, and crushing damage in strip specimens.
10. The RMS voltage appears more capable of detecting impact damage than the SWF, although it still appears to lack sufficient sensitivity and/or reproducibility for more general application.

11. The limit of sensitivity (minimum size of defect) to a single through thickness hole in 20-ply UD APC2 of SWF and RMS voltage is between 2 mm and 4 mm.

3.8 Further work

The first question to be answered when considering further work in the field of acousto-ultrasonics is whether it is worthwhile carrying out any further work. The results presented in this thesis are somewhat negative in comparison to those of other workers, but the large quantity of published data must indicate that there is a genuine use and need for AU, and that the technique does show some promise of development into a valid means of NDE. For this to occur, there must be considerable improvement in the reproducibility and/or sensitivity of the AU parameters used. The following areas of interest are therefore suggested:

1. Improved reproducibility of coupling.
2. Investigation of other methods of signal processing (development of alternative, more sensitive and reproducible AU parameters). Partitioning of the signal in both the time and frequency domains, a modified SWF over the early part of the AU signal for example. Vary has suggested the magnitude or areas of peaks of the frequency spectrum ⁽⁷⁾.
3. The use of higher frequencies and shorter wavelengths by use of matched broadband transducers with, for example, high pass filtering.
4. A similar optimisation and application of AU as that included in this thesis but to a conventional thermosetting matrix, carbon fibre reinforced composite.

With reference to improving coupling, other methods of ultrasonic wave generation and detection may be considered. For example Sarrafzadeh et al ⁽⁸²⁾ have suggested that a pulsed laser would be a suitable source, though reproducibility of surface absorption characteristics can be a problem. Dry coupling ultrasonic transducers, which are essentially conventional transducers designed around a low impedance compliant front face ⁽⁸³⁾, may offer improvements over more typical viscous liquid coupling transducers.

Irrigated probes may be another alternative. Resorting to submergence of an article into a water bath and the use of focused transducers would certainly aid coupling reproducibility but would negate one of the primary premises for the use of AU: easy and simple application to a variety of structures.

The use of alternative AU parameters is an obvious area of further work. The trend of more recent publications is to move into digitisation of received AU pulses and fast Fourier transformations to allow more involved analysis of the signal than the simple ringdown counting of Vary's SWF. Any of the signal characteristics analysed in acoustic emission testing may be proposed. For example, rise time, decay time and pulse duration. Partitioning of the received AU pulse in both the time and frequency domains warrants investigation. The use by several authors of AU parameters based around the characterisation (moments) of the frequency spectrum may be worth considering.

However, since the most sensitive of these parameters so far investigated is essentially identical to the RMS voltage used in this thesis, it may not be such a useful area of further work. In addition, Vary reports that peaks in the frequency spectrum are a function of material thickness, transducer and the instantaneous bandpass characteristics of the system ⁽⁷⁾. Hence, any AU parameter based around the frequency spectrum will be highly specific to a particular testing system and specimen type and geometry.

Chapter 4

AROMATIC POLYMER COMPOSITES

In 1982, ICI introduced Aromatic Polymer Composite 2 (APC2), a thermoplastic polyetheretherketone (PEEK) matrix reinforced with 62% by volume of continuous Hercules AS4 carbon fibres. Aimed at high performance applications such as aerospace, there was an obvious need for extensive characterisation of material properties and behaviour under stress, and suitable methods of non-destructive examination.

The aims of this investigation of APC2 may be summarised as follows:

1. To characterise the basic mechanical properties of APC2, in particular, material moulded at Bath.
2. To investigate the behaviour of APC2 under stress, including fracture.
3. To investigate the sensitivity of APC2 to defects.

The investigation of APC2 was carried out in parallel with, and to complement, the development of NDT methods for this material.

4.1 Introduction

Until recently, high performance applications of fibre composite materials had used thermosetting plastics reinforced with high loadings of stiff, long fibres, for example carbon, Kevlar or glass. In comparison, thermoplastics, which offer great versatility in processing, environmental resistance and toughness, had only been reinforced with low loadings of short fibres in much less critical applications.

According to Cogswell and Hopprich ⁽⁸⁴⁾ there have been two main reasons why high performance thermoplastic matrix composites have not been developed until recently, firstly, the inability of many thermoplastic resins to combine adequate stiffness at high temperature with sufficient resistance to chemical attack, and secondly, the high

viscosity of thermoplastic polymer melts which made thorough wetting of fibres possible only by laborious high pressure 'film stacking' technology.

In 1981, ICI introduced a range of polyetheretherketone (PEEK) resins under the trade name *Victrix* which were claimed to solve the aforementioned resin deficiencies (85). In 1982 ICI, UK commercialized their continuous process for production of pre-preg tape (APC1), 0.1 mm thick containing 52% by volume of Courtaulds XA-S-12K carbon fibres fully wetted with polyetheretherketone matrix. APC2 was introduced later. It contained 62% by volume of Hercules AS4 carbon fibres, giving improved fibre dominated properties (uniaxial strength/stiffness) with a wider processing window and claimed improvement in reproducibility of toughness (86).

This material is reported to show many improvements over current thermosetting resin composites and appears to have solved the problems which limited the success of the earlier 'high performance' thermoplastic composites (the amorphous polysulphones (87)) (88,89,90,91). These improvements are:

1. Almost indefinite shelf life of the pre-preg, no special storage requirements and consistent matrix chemistry (88,92).
2. Improved environmental resistance (in particular in warm wet conditions) (84,87,88,89,91,93). Low moisture absorption (84,91,94,95).
3. Improved damage tolerance, greater toughness and improved resistance to delamination (88,90,91,93,96,97,98).
4. Cheaper fabrication costs (multiple stage and rapid moulding based on conventional metal working automated technologies) (87,88,99,100).
5. Repairability (remoulding) (88,90,92).
6. Scrap recovery (by conversion of scrap into a high grade injection moulding compound) (90,92,101,102).
7. Fire resistance and negligible smoke generation (87,92,103)

8. Improvement of some matrix dominated mechanical properties (78,88,91,104,105).

It is in improved fracture toughness over thermosetting resin carbon fibre reinforced plastics that APC appears most promising. In service (implying the ability to withstand damage, ageing and hostile environment) mechanical properties, fall into two groups: fibre dominated and matrix dominated properties (88). The stiffness and strength of carbon fibre composites will be dictated by the properties of a single lamina and by the lay-up used (96). The matrix will make little contribution to these properties as lay-ups will be designed so that there are reinforcing fibres in the directions of maximum applied stresses. Essentially the matrix only transfers the stress to the fibres. In the case of toughness however, which relates to energy absorbing processes, the matrix and its interactions with the fibres will have a much stronger influence. This is particularly the case where delamination and transverse failure mechanisms are involved. Thus, it would be expected that tough resin systems would contribute to increased composite toughness.

4.1.1 The Matrix - Victrex PEEK

Victrex PEEK, $(\text{C}_6\text{H}_4\text{-O-C}_6\text{H}_4\text{-O-C}_6\text{H}_4\text{-CO})_n$, (molecular structure shown in figure 4.1) is an aromatic polyether. It has considerable crystalline character (up to 48% crystallinity) with a two-phase crystal/amorphous structure (89,92,98,106). The quoted melting temperature varies between 332°C (95,106) and 343°C (100) and it has a glass transition temperature (T_g) at 143°C (95,106). Amorphous PEEK crystallises readily at 177°C (95), but most rapidly at 230°C (99). The thermal properties of PEEK are analogous to those of polyethylene terephthalate (PET), another thermoplastic resin used for composites (106). Fully crystalline PEEK has a density of 1.32 g/cm³. Elastic modulus is 3.5-4.4 GN/m² and yield stress 100 MN/m² (87,89), both similar to those of epoxies. Being a thermoplastic, it can be repeatedly heated re-shaped and cooled and its semi-crystallinity confers good solvent resistance. Other closely related thermoplastics such as amorphous polysulphone have failed to achieve similar success in composites owing to their inherently poor solvent resistance (87).

Two main grades of PEEK resin have been used in composites. In earlier composite preparation by film stacking, a grade similar to that used for wire covering and injection moulding was employed. This grade required crystallisation at 220°C to develop optimum crystallinity (106), achieved by slow cooling after moulding or subsequent annealing. The grade used in APC pre-preg is chemically identical, but has been 'tailored' for rapid moulding to give a reproducibly high degree of crystallinity of around 35% when cooled rapidly (between 10°C/min and 600°C/min) from the melt to between 20 and 200°C, giving a spherulite size of approximately 2 microns (89).

In the composite, PEEK consists of small crystalline spherulites interspersed with amorphous regions, tie molecules joining the crystalline regions. PEEK crystals within the spherulites are in the form of stacks of lamellae which grow laterally outwards along the radial direction of the spherulites (see figure 4.2). The spherulites therefore represent the growth pattern of much smaller underlying crystals (107,108,109). The thickness of the spherulites is typically between 3 and 5 nm and increases with temperature of crystallisation. Their lateral dimensions are set by the inter-fibre spacing, namely 1-10 microns, 2 microns being apparently typical (84).

4.1.2 The Reinforcing Carbon Fibres

APC1 contains 54% by volume (62% by weight) of Courtaulds XA-S-12K, high strain, type I carbon fibres, nominal tensile strength 3620 MN/m², modulus, 220-248 GN/m² and failure strain 1.5%

APC2 contains 145 g/cm³ areal weight and 62% fibre volume of Hercules AS4 fibres of density 1.8 g/cm³, modulus of the order 235 GN/m², strength 3600 MN/m², strain to failure of 1.5% and average diameter 7 microns (100,104). Various other carbon fibres (normally in lower proportions) have been used with PEEK, both in APC pre-preg and via film stacking. The type of surface preparation given to the fibres (sizing) is a closely

guarded secret, probably being central to the success of APC (95). Current commercial treatments are often chemical or electrolytic oxidising processes (110).

Fibre packing in APC is reportedly uniform random (89), although as demonstrated in figure 4.3, some areas do show localised regular close packing. The thickness of the resin phase between fibres is of the same order as the fibres (10 microns).

4.1.3 The PEEK/Carbon Fibre Interface

The wetting and adhesion of PEEK to carbon fibres in APC is reportedly excellent (89,96,111,112,113,114). This has been demonstrated by the good transverse and shear properties, by microstructural examination of fracture surfaces and low void content. Void contents of less than 0.5% and typically 0.1% are claimed (100), apparently as a result of good wetting out of fibres during production of the pre-preg. Further credence to the claims of good fibre/matrix bond strength is given by assertions that fibre debonding and pull-out do not generally occur (89) with failure almost invariably occurring at some distance away from the interface (98).

Nucleation of PEEK crystals occurs both in the bulk matrix and at or near the carbon fibres, the relative importance of each depending, in part, on the rate of cooling (107,108). Interfacial bond strength is thought to be a result of trans-crystallinity from fibres to matrix, the fibres acting as heterogeneous nucleation sites (88,89), particularly in regions where two fibres are in close proximity (84,98). The surface of the particular type of carbon fibre used in APC must therefore be particularly important. Hartness reports that type II Courtaulds XA-S fibres act as inferior nucleating sites compared to type I fibres for PEEK (91). Harris (110) has investigated this area, and reports that the shear strength of various kinds of CFRP generally decrease as the degree of graphitisation of the carbon fibres increases, apparently as a result of the smoother surface of carbonised fibres (such as high strength or type II fibres). During pyrolysis of fibres, the loss of material causes surface roughness which is gradually eradicated during the higher temperature

graphitisation treatment. Diffusion assists the development of increased perfection of the crystallites. Chemically active groups contributing to the normally high surface energy of the carbon fibres are fewer the higher the carbonising temperature and are largely removed during graphitising treatments.

4.1.4 Crystallisation

The control and optimisation of the crystallinity of PEEK in APC2 is essential to the optimisation of its properties ⁽¹¹⁵⁾, in particular, its interlaminar fracture toughness. Unreinforced PEEK exhibits increased tensile and shear strength and strain to failure with increased crystallinity, but reduced fracture toughness and fracture energy ⁽¹¹⁵⁾. Springer and Berglund ⁽¹¹⁵⁾ reported a decrease in K_{1C} from 4.5 to 3 ksi $\sqrt{\text{in}}$ and G_{1C} from 11 to 7 lbf/in for APC2 for crystallinities from 0 to 33%. Blundell et al ^(107,108,109) have extensively investigated this.

The crystalline structure of PEEK depends on the thermal history, rate of cooling from the melt, annealing temperature, moulding pressure, the type and site of nucleation ^(89,116), in addition to the mobility of the molecule ⁽⁹¹⁾.

The overall crystallisation process consists of nucleation, followed by growth of the radial lamellar crystals which make up the spherulites. The process terminates when the growing spherulites impinge on each other or surrounding fibres, such that all the matrix space is enclosed within the boundaries of the spherulites. The lamellar thickness, lateral size of the spherulites, and overall crystallinity all increase with crystallisation temperature and, to a lesser extent, with the time spent at that temperature ⁽¹⁰⁷⁾. The crystallisation temperature during the moulding of APC is in turn affected by the cooling rate from the melt. In addition, increased pressure during cooling tends to allow spherulites to nucleate at higher temperatures ⁽¹¹⁶⁾.

During slow cooling, crystallization occurs at higher temperatures and the nucleation density of spherulites close to or on the fibres is higher. This is clearly shown in the

microstructures prepared by Cogswell (89). Under these conditions, PEEK crystals showed marked orientation relative to fibres (107), apparently as a result of a preferential growth at 90° to the fibres. This crystal orientation was rarely strongly marked in APC2 produced by the normal recommended moulding regime (crystallites randomly orientated).

The percentage crystallinity of PEEK in APC2 is plotted as a function of cooling rate and annealing temperature in figures 4.4a and 4.4b respectively. The cooling rate determines the temperature range over which crystallization occurs (between 180°C and 320°C) and this in turn influences the level of crystallinity attained. For a wide range of cooling rates (between 10°C/min and 600°C/min) the crystallinity appears to be confined to a narrow band of 25%-30%, increasing slowly with decreasing cooling rate.

Annealing within the temperature range of 200°C - 300 °C will also produce a similar narrow band of crystallinities. Total crystallinity greater than 40% can be achieved at very slow cooling rates, below 0.5°C/min, or annealing at high temperatures of around 320°C.

As the cooling rate approaches 1000°C/min the spherulites are unable to complete their growth process before the APC cools below the T_g of the PEEK. This leaves amorphous regions in between the spherulites. Blundell et al (107,108,109) suggest that this situation should be avoided if the full solvent resistance typically associated with properly crystallised APC2 is to be achieved. At cooling rates beyond 2000°C/min very little crystallisation will be able to occur and the PEEK matrix will be essentially amorphous. In order to attain the minimum satisfactory level of crystallisation, APC2 should be fabricated so that cooling rates from the melt do not exceed 700°C/min. If they do, post annealing at between 200°C and 300°C for around 30 minutes will give the required degree of crystallinity, the optimum isothermal crystallisation temperature being 230°C.

4.1.5 Mechanical Properties

Basic tensile, compressive and shear static mechanical properties of PEEK/carbon fibre composites produced by film stacking and from APC have been determined for various lay-up/orientations mainly by ICI and some associated workers (78,84,88,89,96,100,102,105,117,118,119). The basic mechanical properties of APC2 quoted by ICI as preliminary data (42,85,100) are summarised in table 4.1. The mechanical properties of APC1 and APC2 are claimed to compare favourably with state of the art epoxy composites (42,85,90,91).

The fibre dominated properties such as strength and modulus measured in axial tensile tests on UD lay-ups, are on a par with those of epoxy based composites of similar fibre volume fraction (42,85,102).

In shear dominated tests, APC shows extensions of greater than 20% (104), as is demonstrated by the stress/strain curves of $[\pm 45]_{4s}$ APC1 at different temperatures in figure 4.5. Substantial local yielding in the resin phase is claimed, which should imply good toughness and delamination resistance (91), yet adequate shear strength (88,104). Hartness (91) reports an approximate doubling of the strength of APC1 when tested in this configuration compared to epoxy composites. Short beam flexural strengths, reported by Belbin et al (102) for APC1 of around 80 MN/m², are on a par with those of epoxy composites, but the modes of failure are quite different. The epoxies fail by delamination and interlaminar shear, whilst APC1 showed little interlaminar damage.

The compressive strength of unidirectional APC1 and APC2 has been investigated by Lee (117). Although results were found to be dependent on test and gauge length, thus limiting the absolute value of the data, APC2 yielded a compression strength of around 1400 MN/m². This was 16% greater than that for APC1 and approximately equal to carbon/epoxies of similar fibre volume fractions. This is in spite of the fact that the shear modulus, G, and compressive yield strength of PEEK resin (1.22 GN/m² and 95 MN/m²

respectively) are both less than those of epoxy resins (typically 1.42 GN/m² and around 150 MN/m²) (117). McGrath et al (101) have also determined the compressive strength of APC2, their value being somewhat lower at 1094 MN/m².

The good solvent resistance of the PEEK, the result of its semi-crystalline structure, yields improved retention of properties in aggressive environments (84,88,89), particularly warm, wet atmospheres (95,102). Maximum moisture absorption by long exposure to boiling water from 0.25% (84,91,120) to 0.5% maximum is considered normal (94,95).

Owing to PEEK's high T_g (143°C) and melting point (343°C), retention of the mechanical properties of the composite up to significantly elevated temperatures are claimed (87,92,95,102). Retention of a full property spectrum up to 100-110°C is reported by Hartness (95), although stiffness significantly deteriorates as the T_g is reached. Belbin et al (87,102) claim a continuous use rating up to 200°C and limited use up to 300°C is possible for short periods.

Cogswell and Leach (88) and Belbin (87) have investigated the creep response of APC, concluding that carbon fibre/PEEK compares very favourably with thermosetting composites as demonstrated in figure 4.6.

Hartness and Kim (78,105) and Dickson et al (94) have investigated the fatigue behaviour of PEEK/carbon composites. Hartness and Kim reported improved tension-tension fatigue behaviour over state of the art epoxy/carbon as a result of greater resistance to the initiation and growth of fatigue damage related to the matrix (78,105). Dickson et al concluded that the superior toughness of PEEK and the improved adhesion to the carbon fibres, in addition to resistance to hygrothermal attack, indicate promising fatigue performance of PEEK/carbon for aerospace applications (94).

4.1.6 Toughness

While stiffness and strength are relatively easy to define, the toughness of a composite material is less amenable to analysis (88). Leach and Moore (96) have suggested a variety of techniques for toughness evaluation. These can be placed into two categories. The first group includes comparative measures of toughness, such as drop weight impact tests, compression after impact (96), Izod and Charpy tests. These provide a quantitative measure of toughness under specific conditions which are likely to be geometry dependent. The second category includes intrinsic measures of toughness based on some theoretical basis, for example linear elastic fracture mechanics tests which use SEN or DCB specimens (as recommended by Whitney (121)). These attempt to provide both fundamental and comparative toughness values which are claimed to be geometry independent (96,121).

The fracture toughness of PEEK/carbon composites has been determined by both comparative and intrinsic means. Hartness has used the DCB and SEN tests (96). Impact resistance (90) and notch sensitivity (97) have also been determined. The approximate order of magnitude increase in interlaminar fracture toughness of APC over rival epoxies has generated substantial interest and study (88,96,111,112,122,123,124,125) and appears to be due to a combination of a strong fibre/matrix bond and a tough and ductile matrix. Results presented later illustrate this point.

Leach and Moore investigated the toughness of APC2 in cross-ply, quasi-isotropic and unidirectional lay-ups in both comparative and intrinsic toughness tests (96). An instrumented falling weight impact test, conducted at different temperatures, involved the fracture of 75 mm square panels with a hemispherical nose impactor (diameter 12.5 mm). The impactor, which always fractures the specimens, includes a force transducer enabling force-deflection curves to be determined during impact. Integration of different portions of this curve gave a measure of the energy associated with initiation and propagation fracture processes. Subsequent C-scanning showed that impact energies

below about 10 J produced no detectable damage. However, above this level there was an initial linear increase in the area of damage with increasing applied impact energy, internal delaminations at intermediate energies, and more extensive fibre fracture at higher energies. The relative quantities of energy absorbed by APC1, APC2 and AS4 carbon fibre/epoxy are shown in figure 4.7. A qualitative indication of the toughness of APC2 can be made from the fact that neither longer range cracking nor internal, C-scan identified damage was located outside the immediate visually observed impact damage area. The impact energy absorbed during fracture initiation and propagation was found to be only mildly temperature dependent over the range -50°C to 80°C , with no drop off below -16°C , a ductile-brittle transition temperature of PEEK. This implies therefore that the fibres have a dominant influence on toughness.

Compression-after-impact tests involved the compression of edge supported plates (with anti-buckling guides) which had previously been impacted at their centres. The deformation at failure, at which point the plate showed buckling damage in the area of impact damage, decreased with increasing applied impact energy. Beyond this the test was not found to be of great use owing to its high geometry dependence and the tendency towards plate failure at clamping points in the absence of damage. This prevented determination of a reference strength for undamaged plaques.

Leach and Moore ⁽⁹⁶⁾ determined intrinsic toughness with both single edge notched specimens (SEN) and a double cantilever beam test (DCB). Both of these tests have been used in this thesis and are described later. DCB tests produced 'slip-stick' crack propagation, with G_c around 2.4 kJ/m^2 for slow crack propagation, and 2.1 kJ/m^2 during fast propagation. Similar behaviour was reported in APC1 by Hartness ⁽⁹¹⁾ who determined mean G_{1C} values of 1.4 and 1.8 kJ/m^2 for fast and slow crack propagation respectively.

Another measure of toughness, the plastic zone size, $K_c^2/2\pi(\sigma_{\text{yield}})^2$, or at least a lower limit of it, was determined by Cogswell to be greater than 20 microns ⁽⁸⁹⁾ for PEEK resin. For good toughness in the composite, the plastic zone size should be smaller than the typical thickness of the resin phase. This thickness, set by the constraint of the presence of the fibres, is typically between 1 and 10 microns.

Barlow and Windle used an alternative method to investigate G_{1C} of APC2, namely the razor blade test ^(98,111), in which a crack is propagated by driving in a wedge to split off a thin section. Values of G_{1C} of $1.95 \pm 0.31 \text{ kJ/m}^2$ were reported.

Leach and Moore concluded that APC2 exhibited complex mechanisms of toughening with contributions from fibre fracture and high matrix ductility ⁽⁹⁶⁾.

4.1.7 Moulding

PEEK/carbon fibre composites can be moulded either from APC unidirectional pre-preg or by film stacking. Film stacking was used by a few researchers during the early development of PEEK/carbon fibre composites ^(78,95). Alternate layers of 5 mil amorphous PEEK film and graphite cloth are laid up into a matched die mould and then consolidated in a press at 400°C and 200 psi pressure for at least 2 hours. This is followed by a slow cool under pressure, before removal from the die ⁽⁹⁵⁾. In 1982, the development of APC pre-preg, ready wetted out with PEEK, superseded film stacking, because of the much reduced moulding/consolidation times and reduced pressures needed to achieve suitable fibre wet out. Details of APC2 moulding, carried out at Bath, are given later.

APC is processed at temperatures of around 380°C, pressures of 10^6 N/m^2 and cycle times of 0.5 hours. This compares with 150°C, $5 \times 10^5 \text{ N/m}^2$ and 7 hours respectively for thermosetting based composites ⁽⁹⁰⁾. The higher temperatures and pressures which infer expensive hot presses are an obvious disadvantage. However, fabrication is much

quicker, and conventional automated metal working technologies such as hydro-forming and roll forming (87,88) may be applicable to APC, thereby reducing fabrication costs and speeding mass production (99). Also, the expense of autoclaves and possible vacuum bagging which is used to reduce void content and improve consolidation and cure is of course avoided. One of the most significant assets of APC is its ability to be repeatedly remoulded, thus allowing multistage moulding for the production of complex articles (88).

Various manufacturing processes for APC2 have been suggested (87,100). With pre-consolidated sheet feed-stock, hydro-rubber forming, press forming, roll forming, diaphragm shaping and matched die moulding are possible. With pre-impregnated tape and tow feed-stock, filament winding, tape laying, braiding, pultrusion and autoclave and vacuum bag moulding can be used. Infra-red heating has been proposed (100), and Grove (93) has made a study of flat bed tape laying with the use of a laser as a localised heat source.

The ability of APC to be repeatedly remoulded has considerable importance to the repair of damage. Delaminations can be repaired by simple remoulding (with total recovery of the original properties) (88,90,92), whilst fibre breakage can be repaired by patching and remoulding. Minor repairs could even be possible with a heavy duty soldering iron as a heat source.

Scrap APC material has been reclaimed by diluting with additional resin and processing into a high performance injection moulding compound. Belbin et al report reclaimed injection moulding grade APC (containing 50% by weight carbon fibres) giving moduli of 32 GN/m² and strengths of 250 MN/m² (90,102), which are slightly lower than the figures claimed by ICI (92). McGrath et al (101) have successfully moulded plates from chopped waste APC2 pre-preg without added matrix and reported tensile strengths and

modulii around 215 MN/m² and 40 GN/m² respectively, and flexural strengths and modulii around 430 MN/m² and 33 GN/m²

4.1.8 Conclusions

The increased interest in thermoplastic matrix composites is reflected in the variety of commercial materials on offer by ICI at the time of writing. These include, in addition to glass and carbon fibre reinforced PEEK, polyether sulphone, nylon 66, polyethylene terephthalate and polypropylene resins reinforced with glass fibres. Furthermore, other manufacturers are introducing alternative thermoplastic systems; Ryton (Phillips Chemicals' polyphenylene sulfide), Torlon C (Amoco's poly-amide-imide) and K-Polymer (DuPont's polyimide) (116).

Solution impregnation, powder impregnation and melt coating have been attempted as solutions to the problem of producing thermoplastic composite pre-preg (89). ICI's development of the technology to continuously impregnate high performance carbon fibres with the viscous PEEK matrix and achieve very good wet out and fibre/matrix bonding, has clearly been essential to the development of APC.

In fibre dominated properties, APC appears to equate well to conventional epoxy based composites. This indicates the high utilisation of the fibre properties in APC and confirms the good wetting of the composite and satisfactory bond between resin and fibre. The claims of substantial advantages of APC over epoxy composites in the areas of indefinite shelf life, well defined moulding chemistry, high toughness and damage tolerance, environmental resistance and the possibility of rapid processing appear to be justified by the literature. However, the high moulding temperatures (380°C), high cost and the inability to easily carry out simple hand-lay up and moulding must limit the prospects of this material.

4.2 APC2 Moulding And Specimen Preparation

APC2 composite laminate fabrication involves stacking layers of APC2 pre-preg between presses, heating to 380°C under low pressure, applying a consolidating pressure, and cooling rapidly.

Optimised moulding temperatures and pressures are essential to achieve the best matrix and interface properties (116). Rapid but high crystallisation giving small imperfect crystallites with many tie molecules inter-connecting adjacent crystallites is thought to give optimum properties, hence the need for rapid cooling from the melt to the required annealing temperature (99).

The APC2 specimens used for initial tensile and SEN fracture toughness testing were cut from plates produced and supplied by ICI, Wilton, because moulding facilities at Bath were initially unavailable. Once operational, all APC2 test pieces except those used for DCB tests, were produced from plates moulded in-house with a pair of Bradley and Turton 100 ton presses fitted with heated platens. Unidirectional and 0/90 cross-ply plates up to 40 plies thick were moulded using either matched metal moulds (for unidirectional lay-ups) or with simple picture frame surrounds to prevent seepage of the matrix. The moulding operation, run by Dr. J. Nixon, produced plates up to 450 mm x 450 mm from APC2 pre-preg tape of the highest quality. Full details of APC2 moulding are given in the literature (100,126). The important stages are outlined more briefly below.

1. Lay-up of pre-preg was carried out cold. Successive layers were tacked together in a symmetrical and balanced lay-up (to avoid differential thermal contraction on cooling) with a heavy duty soldering iron (400-500°C).
2. To prevent excessive flow of material at plate edges and to help control fibre direction and plate thickness, a stainless steel 'picture frame' was normally used. It was 0.254 mm - 0.380 mm thinner than the finished plaques and left a gap of approximately 3 mm around the edge of the pre-preg to aid eventual disassembly.

3. The pre-preg/picture frame was placed between two layers of high temper aluminium foil, pre-treated with Freekote FRP mould release agent. This whole sandwich was then placed between the heated platens of the Bradley and Turton hot press at 380°C ($\pm 10^\circ\text{C}$). A small contact pressure of 0.5 MN/m² (70 psi) was applied to aid heat transfer without stressing the fibres before the PEEK matrix was soft enough to be compliant. This stage melted the PEEK matrix.
4. Heating times used depended on laminate thickness but approximately five minutes per eight plies was usually sufficient to achieve thermal equilibrium, after which a consolidation pressure of 1.4 MN/m² (200 psi) was applied for five minutes.
5. Post consolidation cooling to 200°C must be rapid to ensure optimum crystallinity. This was achieved by transfer to the 'cold' press (200°C) within 20 seconds, with the immediate application of 2.8 MN/m² (400 psi) pressure for 2 minutes to ensure consolidation. The laminate was removed from the mould after 5 mins.
6. Unidirectional lay-ups had to be moulded in a matched metal mould (8" x 6" nominal) in place of the picture frame to prevent excessive fibre movement during pressing. The pre-preg was laid up into one half of the cold mould between aluminium foil sheets treated with Freekote, hot tacking not being required. The pressing was then carried out as described above, with the exception that the heating and cooling times were approximately doubled to account for the thermal inertia of the mould. Improved surface finish of plaques was achieved by small increases of the consolidation time.
7. One of the main difficulties associated with the moulding of APC2 was achieving the required flatness of the press platens to ensure good surface finish across large plaques. Depressions as small as 0.7 microns could cause defects in the finished plates.

The outer edges of moulded plaques are typically under thickness and defective as a result of fibre movement and some matrix flow during pressing. These 'rough' edges

were removed and specimens cut to shape with a water cooled diamond impregnated circular saw. The cut edges were then abraded with 500 grade silicon carbide paper to remove any burring. All specimens used for acoustic emission testing were either plates or strips of 8 to 40 plies in thickness. Laminates correspond to approximately 0.125 mm in thickness per ply. Plaques were C-scanned at ICI, Wilton before being cut into specimens, defective areas being discarded.

4.3 Mechanical Testing of APC2

The initial objectives of the mechanical testing carried out at Bath were to obtain a base line of properties (to compare with those in the literature) and an understanding of the microstructural behaviour of the material when stressed, by studying fracture surfaces. In addition, it was necessary to standardise a mechanical test from which to analyse the acoustic emission of APC2 when other factors are varied.

Initial testing was performed on APC2 specimens cut from unidirectional laminates moulded by ICI. This involved tensile testing unidirectional APC2 specimens cut at 0°, 10° and 90° to the fibres and SEN fracture toughness flexural testing. Later, the production of laminates in-house, which improved material supply, and the need for a standard test for AE monitoring, led to long beam three and then four point flexural tests comprising much of the remaining programme. A section of work using the double cantilever beam fracture toughness test was also carried out, although this work is covered in a separate chapter (see later). Smaller numbers of double torsion and tensile tests have also been conducted. More than 300 separate APC2 specimens have been mechanically tested throughout the project, largely for the purposes of monitoring acoustic emission. A brief overview of the mechanical property measurements made during this mechanical testing will now be given.

4.3.1 Tensile Testing

Tensile specimens with aluminium end tabs were cut from 20-ply UD APC2 laminates moulded by ICI and from 10 and 20-ply UD APC2 moulded at Bath. The results of these tests are included as table 4.2 and represent a total of 46 specimens tested.

4.3.2 SEN Fracture Toughness Testing

Fracture toughness values (K_{1C}) were determined from 40-ply UD APC2, moulded by ICI, using 5 mm x 5 mm x 25 mm single edge notched (SEN) three point bend test specimens (notch to depth ratio of 0.5). The K_{1C} values (17 samples tested) are shown in table 4.3, in addition to those determined by Leach and Moore ⁽⁹⁶⁾, and relate to the different crack propagation directions explained in figure 4.8. The Bath results, though slightly higher than those of ICI, show good agreement. The fact that they are slightly higher may be the result of using different methods of calculation. The Bath results are mean values for a series of results at a fixed notch depth to specimen ratio ($a/w = 0.5$), while the ICI values were arrived at graphically from a series of tests at differing a/w ratios.

4.3.3 Flexural Testing

More than 100 UD and 0/90 cross-ply APC2 specimens, with and without deliberately introduced defects, have been tested to failure in long beam 3 point flexure. The load deflection curves of all laminates were characterised by a near linear elastic load up, and a small and gradual deviation from linearity towards eventual failure which was catastrophic (see figure 4.9). The deformation to failure was almost exclusively elastic, hence the large and sudden release of stored energy when final failure occurred. APC2 was found to be remarkably unaffected by a variety of deliberately introduced defects.

The grand average and standard deviation of basic mechanical properties determined in 3 point flexure, using 15.5 mm diameter rollers, 100 mm span and crosshead speed 0.5 mm/min for all laminates without deliberate defects are included in table 4.4.

A further 60 16-ply UD specimens have been tested in the 0° orientation in 4 point flexure using 15.5 mm diameter rollers, 0.5 mm/min crosshead speed and 36 mm inner span, 108 mm outer span. The grand averages and standard deviations of these results are also presented in table 4.4.

4.4 Microstructural Investigations Of APC2

4.4.1 SEM of Fracture Surfaces

To determine the microstructural deformation and fracture processes in APC2 and to relate them to the acoustic emission activity, sections from fracture surfaces of specimens tested by the various methods already outlined were sputtered with gold and viewed using scanning electron microscopes, predominantly a JEOL 35C.

Unidirectional 0° tensile specimens fractured catastrophically (as did most) with multiple cracking parallel to fibres as well as perpendicular, leaving the samples in many long thin shards. Fibres were fractured and some pull-out occurred, but the fibres remained matrix covered as demonstrated by figure 4.10. 90° tensile specimens showed similar fracture to the tensile region of orientation 2 SEN fracture toughness specimens. Figure 4.11 shows a fracture surface of an orientation 2 SEN specimen demonstrating the extensive plastic deformation of the PEEK matrix. Fibres again remain largely covered in matrix. This appears to demonstrate the very good adhesion between PEEK and carbon fibres in APC2 since the fracture path usually found a short distance from the interface within the matrix. Failure is thus cohesive within the PEEK and not adhesive along the fibre/matrix interface.

The gross plastic deformation of the matrix helps to explain the high fracture toughness. The matrix plastically deforms (so blunting a crack) and 'tears' rather than undergoing brittle fracture as more commonly found in thermosetting resins. Crack propagation is thought to involve coalescence of microcracks and local yielding of the PEEK (termed

'microyielding' by Hine et al ⁽¹¹²⁾ ahead of the crack front. What would appear to be pores can sometimes be seen along the length of fibre/matrix interfaces on some fracture surfaces (figure 4.12).

In three and four point loaded specimens there is a sharp division between tensile and compressive failure (figure 4.13), the former being characterised by fibre and fibre bundle pull-out with matrix still adhering, and the latter by no fibre pull-out and shear failed fibre ends in deformed pockets of matrix (see figures 4.14 and 4.15).

Microbuckling is also present, a phenomenon aggravated by the fibre waviness seen in APC2 caused by movement of fibres in the melt during moulding. The division line between compressive and tensile failure regions did not lie on the mid plane of the beam, but lay approximately 30-40% of the through thickness distance from the compressive surface. Thus, the compressive region was considerably smaller in area than the tensile. Because of the sudden and catastrophic nature of plate failure it was not possible to check by observation whether failure initiation occurred at the tensile or compressive faces. Purslow ⁽¹²⁷⁾ has considered this point and reports that failure in flexure of most CFRPs will initiate at the compressive surface. This is because the tensile strength is greater than the compressive strength. Furthermore, he suggests that as the crack propagates from the compressive face towards the neutral axis, the increased flexural strain allowed by the compressive failure and the ability of these surfaces to react to loads will cause a tensile failure to propagate from the tensile surface to meet the arrested compression failure. If failure were to initiate at the tensile surface, perhaps because of a flaw, the neutral axis would be expected to move towards the compressive surface as the crack propagates. The presence of residual compressive strains in the carbon fibres near to the surface, caused by thermal contraction from the melt, and reported by Galiotis ⁽¹²⁸⁾ will further complicate the explanation of failure. It should be noted that the compressive and tensile failure stresses of APC2 are similar to those of typical aerospace epoxy/carbon fibre composites (see table 4.1).

Double torsion tests on slow cooled and normal cooled APC2 specimens exhibited different failure behaviour, namely 'slip-stick' crack propagation in the slow cooled specimens but not in the standard specimens. Some differences were evident from the fracture surfaces. Figures 4.16 and 4.17 show normal cooled specimens. A point to note is the broken fibres which have been pulled partly out of the matrix (fibre bridging during crack propagation). The fibres have irregular and quite highly deformed matrix still adhering to them. There is considerable evidence that the PEEK shows greater deformation in areas of stable (slow) crack propagation compared to areas of rapid crack propagation. Figure 4.18, for comparison, shows a slow cooled specimen. In general, there seems to be little matrix deformation and there are few broken fibre ends. This may be a result of better fibre alignment as a result of the greater time that the PEEK resin is molten during moulding, thus allowing the fibres to align themselves better. This would enable the crack to follow an inter-fibre path more easily. In addition, from the literature (107,108) slow cooling produces larger crystallites, which will confer a more brittle matrix behaviour.

Figure 4.19 shows a portion of a slow cooled fracture and plate surface. The defects seen on the plate surface are widespread on slow cooled specimens and appear to be sites of local resin deficiency. These may help to explain the higher acoustic emission event counts recorded from such material (see later).

4.4.2 Fibre/Plies/Matrix Distribution

Sections of 16 and 40-ply UD APC2 were cut in three orthogonal directions (the three principal axes), mounted in room temperature curing resin, and ground and polished to determine the basic microstructure of the composite, in particular the fibre distribution.

Interlaminar fibre deficient regions can be seen in figures 4.20a-c, however, in general the interlaminar region is not clearly defined because of the movement of fibres when the matrix is molten during moulding. Sections taken perpendicular to the fibre direction

show the imperfect alignment of fibres (cross sections not circular), the result of fibre movement in the melt. In local regions of high fibre volume fraction, the fibre packing approximates to a simple hexagonal packing, although basically random elsewhere. The $0.62 V_f$ in APC2 approaches the maximum practical fibre fraction of 0.65⁽⁸⁷⁾. Although not quantified here, the void content in APC2 appears to be very low, as mention in the literature^(92,103).

4.4.3 Fibre Damage Monitoring in APC

At the outset of the project it was hoped to be able to deconvolute the acoustic emission amplitude distributions into areas associated with particular failure processes within the composite (fibre failure, matrix cracking, fibre debonding). The particular nature of the micromechanical deformation which produced a stress wave (AE event) will contribute largely to the characteristics of the event: the frequency, amplitude, ringdown count and duration. The extent to which the output signal from an acoustic emission receiving transducer will relate to the source event after the stress wave has been altered in frequency content and amplitude by the highly attenuating, anisotropic composite material, is a point of considerable interest. In order to correlate source events with the received signals, the source events must be studied and monitored.

SEM studies of fracture surfaces, particularly for DCB and double torsion tests, help elucidate ultimate failure (fracture) processes. However, many events are recorded prior to gross fracture and alternative methods are needed to investigate these. Sectioning and polishing prestressed specimens is one alternative. However, since APC2's ductile matrix and strong fibre/matrix bond are not particularly susceptible to brittle fracture, and fibre debonding and pull-out are uncommon processes, fibre failure is most likely to be the main contributor to the AE output of UD APC2 when tested in the fibre direction.

Two methods of monitoring and locating fibre damage in APC have undergone limited investigation.

Broken fibres may be identified by complete removal of the matrix and separation and counting of the fibres under a microscope. Because PEEK is highly resistant to most solvents, concentrated hot sulphuric acid is needed to dissolve it. However, the small size of the fibres and their tendency to agglomerate/tangle makes them difficult to separate and count. As a result, the following method of separation was developed.

15 100 mm long by 10 mm wide strips of APC2 pre-preg were cut and end tabbed. 5 were loaded to failure in uniaxial tension, 5 loaded to around 60% of failure (2000 N) and 5 not loaded. The latter two groups were then subjected to acid dissolution of the matrix. One end of each specimen (at the edge of the end tab) was removed and the specimens suspended in a boiling tube such that the 40 mm gauge length was submerged in concentrated H_2SO_4 , warmed to $60^\circ C$ with a water bath. The vessel containing the acid and pre-preg was placed into an ultrasonic bath to agitate the pre-preg and so cause the broken fibres to drop under gravity from the pre-preg as the matrix was dissolved. The acid was then neutralised and the broken fibres spread out on a watch glass for counting.

Broken fibres may also be identified by an electrolytic etching process similar to that used by Manders for observing the carbon fibre structure ⁽¹²⁹⁾. Both ends of a UD APC2 specimen were ground flat and square. One end was gold sputtered and silver dagged to produce an electrical contact with the fibre ends. The other end of the APC2 was connected as the anode in an electrolytic bath of 2 molar sulphuric acid, with a carbon cathode. A current density of 14 mA/m^2 was passed through the cell for between 10 and 60 seconds. After this treatment, non broken fibres which have passed current show concentric coloured zones across their section as a result of the anodic oxidation of the carbon. Theoretically, broken fibres should not show this etching pattern, not having passed any current. Unfortunately, with the high fibre volume fraction in APC2, there was found to be too much inter-fibre contact to make this technique valuable for monitoring fibre fracture.

A potentiometric technique which measures the change in resistance of APC2 due to fibre fracture may be of use. Unfortunately, there was insufficient time to carry out full investigations of failure processes in APC2, although the methods of monitoring fibre fracture outlined above may provide a basis for further work.

4.5 Discussion/Conclusions

The basic mechanical properties of APC2 have been determined. Unidirectional APC2 has a failure strength of approximately 1800 MN/m², elastic modulus of 140 GN/m², and strain to failure of 1.4% in the principal fibre direction. It is a strong, high modulus and tough composite material. Similar property values were determined from tensile, three and four point bend tests and compare quite closely with those reported elsewhere (42,85,91,96,102). Some discrepancies do exist. For example flexural strength and modulus of 0°/90° APC2 were both significantly higher than those reported by McGrath et al (101).

The measured elastic modulus of APC2 appears to agree well with that predicted by a simple rule of mixtures which predicts a value of approximately 145 GN/m². Ultrasonic modulus measurements determined by both a time of flight technique using the relation: wave speed = (E/density)^{1/2} and by the ultrasonic resonance technique covered by ASTM C747 also gave very close agreement with the elastic moduli determined mechanically.

Observation of fracture surfaces under an SEM have demonstrated the good adhesion of the PEEK matrix to the fibres with failure typically occurring a short distance from the fibre/matrix interface, so leaving pulled out fibres matrix covered. The ductility of the PEEK has also been demonstrated, with plastically drawn out matrix apparent between the reinforcing fibres. These findings are useful when considering two points. Firstly, the relatively insignificant effect of deliberately introduced defects on both mechanical and

AE behaviour of APC2 (see later). Secondly, the apparent dominance of fibre related failure mechanisms in the acoustic emission output from APC2.

Chapter 5

ACOUSTIC EMISSION

5.1 Introduction

When a material is stressed, discontinuous deformation processes, such as reinforcing fibre breakage, spalling of a coating or the twinning of metals, can cause elastic energy to be dissipated as elastic stress waves which spread in all directions from the source. These AE pulses or events convey information (in coded form) concerning the deformation processes which produce them. The monitoring and analysis of these emissions is the basis of acoustic emission non-destructive testing.

The genesis of today's technology of acoustic emission stems from the work carried out by the German scientist Josef Kaiser and published in his PhD thesis in 1950 ⁽¹³⁰⁾. The first application of acoustic emission to composite materials was carried out by Green et al in 1961 on the hydrostatic testing of filament wound GRP Polaris rocket motor cases ⁽⁶⁴⁾. Today, there are more than a dozen companies producing AE equipment for commercial sale ⁽¹¹⁾, in addition to various books on the subject ^(11,131,132,133) and many papers. In addition, there are several ASTM standards which relate to AE testing of composite structures (E1067, E1118 and E1211). Drouillard ⁽¹³⁴⁾ has published a bibliography of 1996 references on acoustic emission in general, and a comprehensive guide to the literature on acoustic emission of composites ⁽¹³⁵⁾, listing 314 references. By 1987 there were more than 5,000 publications on acoustic emission ⁽¹¹⁾. At least three papers have reviewed the acoustic emission from fibre reinforced composites ^(136,137,138). In the light of the aforementioned literature reviews, there seems little point in going over ground already adequately covered by others. Therefore this introduction to acoustic emission on composite materials will be brief and will concentrate on amplitude distribution analysis.

5.1.1 A Brief Review of the Literature

Bailey et al ⁽¹³⁹⁾ have reported being able to distinguish between matrix cracking and fibre fracture by means of amplitude distribution in epoxy/carbon composites. Becht et al ⁽¹⁴⁰⁾ found, by amplitude distribution analysis, that fibre failures generated higher amplitude, higher energy events compared to inter-fibre failure in glass and carbon fibre reinforced plastics. Wood and Harris ⁽¹⁴¹⁾, on the other hand, found three peaks in the amplitude distribution of GRP pipes associating the mid range and high amplitude peaks with matrix and fibre fracture respectively. Apparently in direct contradiction, Valentin et al ⁽¹⁴²⁾ reported that high amplitude AE events resulted from cracking of the matrix parallel to fibres in UD carbon fibre epoxy composites. Low amplitude events were generated by fibre fracture, a similar conclusion made by Jamison and Reifsnider ⁽¹⁴³⁾. Favre and Laizet ⁽¹⁴⁴⁾ reported their use of high amplitude event counts to monitor fracture parallel to fibres with transverse plies in cross-ply CFRP.

Crosbie et al ⁽⁷²⁾ applied amplitude distribution AE testing to glass reinforced polyesters with and without rubber toughening of the matrix. Fibre/matrix debonding was reportedly associated with low amplitude AE, whilst matrix cracking was associated with a fairly narrow mid amplitude range. AE was clearly able to distinguish between rubber toughened and non toughened matrices, by virtue of a cumulative event count and a significant change in strain required for AE to commence from matrix cracking in the rubber modified composites. Guild et al ⁽⁷⁰⁾ have also demonstrated that AE amplitude distribution analysis can clearly distinguish between different glass fibre reinforcement patterns in a polyester matrix composite at very modest strain levels (0.16%).

Scarpellini et al ⁽¹⁴⁵⁾ have reviewed work conducted into classification of defect signatures by acoustic emission. They have suggested that various defects in reinforced plastics can be detected by AE based on amplitude distributions (b slopes), Felicity ratios (see later), and stress and strain levels at the onset of AE activity.

Selden and Gustafson ⁽¹⁴⁶⁾ found that AE could detect initiation and growth of transverse cracking and delamination during fatigue testing of (0/45/90)_s CFRP. They noted a correlation between the size of a delamination and higher amplitude, longer duration friction generated events.

The different methods of AE analysis may be applied to monitoring different deformation processes. Root-mean-square voltage is considered useful for following matrix failures in composites and ringdown counting for following filament failures or delaminations ^(16,147).

The amplitude distribution analysis systems used for the work on APC are described in the following section.

5.2 Acoustic Emission Systems Used

Two different AE amplitude distribution data collection and analysis systems have been used for the study of AE behaviour of APC2. The older system was based around the 51 channel AETC 203 amplitude sorter, Minc-11 data collection computer and data collection software named DCOL. Data analysis was originally conducted on Prime 750 and Prime 2250 computers, but later on IBM compatible PCs. It was used for much of the work on APC2, but more recently it has been replaced by the improved Marandy MR1004 system which is now widely used by a variety of research groups within the School of Materials Science, and has been referred to in various publications ^(148,149,150).

Since no detailed description of the configuration, capabilities and limitations of the more recent Marandy system has been published elsewhere, this system will be described in more depth. Details of the AETC 203 system can be found in the literature ⁽⁷¹⁾.

Acoustic emission analysis software packages, RFPLOTS and RFGRAPH, have been developed and written by the author for use with either of the AE systems. This was in response to certain limitations of the previous packages which prevented or rendered data analysis difficult, beyond basic graphical representation.

Each of the AE systems may be divided into three main areas:

1. Event detection
2. Signal processing and data storage
3. Data decoding and analysis.

The process of event detection is identical in all cases.

5.2.1 Acoustic Emission Detection

5.2.1.1 Transducers

Acoustic emission events are detected with an ultrasonic sensor (termed an acoustic emission transducer) which produces a low amplitude oscillating voltage in response to dynamic displacement of the piezo - electric crystal within the body of the transducer. This voltage is amplified and filtered, after which it is passed on to the amplitude sorter for signal processing.

Most commercial sensors are designed to be predominantly sensitive to displacements normal to the plane of the wear plate of the sensor. At Bath, the most commonly used AE transducers are differential PZT wideband or broadband sensors with nominal resonant frequencies within the range 300-500 kHz. These include the AETC FAC 500, PAC U30D and AETC MAC300 sensors, the latter two of which have been used throughout most of the AE monitoring of APC2. They are particularly suitable for event counting because the ringing of the transducer dies down in a short time allowing higher event rates to be achieved.

Earlier AE work on APC2 was conducted with an AETC MAC 300, a small (10 mm diameter) broadband (essentially damped resonant) transducer. This gives a broad sensitivity to a range of frequencies either side of the nominal resonance at 300 kHz, as demonstrated by the spectral frequency plot included as figure 5.1b. Since APC2 was found to be a quiet AE source and relatively few emissions were recorded with this transducer, later work was conducted with more sensitive resonant wideband PAC U30Ds. In these, damping is reduced, thereby increasing sensitivity, but at the expense of a narrower frequency response, as demonstrated by the spectral frequency included as figure 5.1a. This transducer has a PZT crystal with a 'near ceramic' wear plate and stainless steel case and is nominally resonant at 300 kHz. Its small size (10 mm diameter), low mass and high sensitivity make it particularly convenient.

5.2.1.2 Preamplifiers

The output from AE transducers is in the form of a very low amplitude alternating voltage of the order of 10 microvolts and above. The signal must be carefully screened from air born and electrical noise and must be amplified before signal processing is carried out. This was achieved by mounting a fixed gain (60 dB) preamplifier (AECL 2100/PA or AETC 160) close to the transducer. Plug in band pass filters (typically 125-2000 kHz) within the preamplifier were incorporated to help exclude noise from the signal (particularly low frequency machine and audible noise).

5.2.1.3 Coupling

An essential part of the acoustic emission system is the coupling medium used to transfer the ultrasonic stress waves from specimen to transducer. Low attenuation and reproducibility are the two main requirements of the couplant. Reproducibility of coupling is, in the author's opinion, a problem too often neglected in acoustic emission.

The most commonly used method of coupling, as in acousto-ultrasonics, is by contact coupling with a viscous fluid and fixed coupling force. Such couplants as oil, water and

glycerine, in addition to adhesives such as epoxy resin, RTV thermoplastic resins and Dow Corning RTV silicone rubber have been used at Bath for AE sensor coupling, although the most common has been petroleum jelly. Since this was deemed most suitable for acousto-ultrasonics, it was retained for all AE testing of APC2. In all cases, it was combined with a spring loaded attachment device which applied a reproducible pressure between the transducer and specimen of magnitude greater than the minimum pressure (0.2 MN/m^2) required for reproducibility (determined in chapter 3).

5.3 Signal Processing And Data Storage

5.3.1 Marandy MR1004 System

The Marandy MR1004 is the current AE amplitude sorter in use at the University of Bath. Two sets of inputs are made to this system; the preamplified signal from the transducer (acoustic emission data) and analogue data (DC voltages) such as load or strain. The number of received events, their amplitude and the number of ringdown counts of each event are recorded on hard disc. Analysis of the data is performed by RFPLOTS and RFGGRAPH. A diagrammatic representation of the system is given in figure 5.2.

Signal processing and data storage is carried out by the Marandy MR1004 25 channel amplitude sorter and ringdown counter. It is interfaced to an IBM compatible PC with hard disc via a Metrabyte PI012 parallel interface board (plugged into one of the 8 bit expansion slots in the PC) for data transfer, and via the RS-232C for all other communications.

It has a sorting range of 60 dB with 26 channels. Each channel is 2.4 dB (± 0.2 dB) wide. Channel 0 has a threshold of 10 mV and channel 25, 7586 mV. Events greater than 10 volts are termed over range and are placed into channel 26. The ringdown count per event can be in the range 1 to 256 (8 bits).

When the acoustic emission signal exceeds the instrument threshold (minimum 10 mV), an event is deemed to have occurred. The following event is only detected if the signal drops below threshold for longer than the 100 microsecond dead time. For the duration of an event, one memory in the Marandy accumulates the ringdown count for that event, whilst a second records the magnitude of the highest amplitude ringdown within the event envelope. The event amplitude is sorted into 1 of the 26 channels. The instrument threshold is adjustable in 2.4 dB increments (a push index switch) from 10 mV to a maximum 69.18 millivolts, corresponding to channels 1 to 7 respectively.

Each time an event is detected, a 16 bit number in two bytes is written chronologically to one of the 8 kilobyte buffers in the IBM PC. The low byte records the number of ringdowns, hence 256 is the maximum number of ringdowns per events which the system can handle. The first 5 bits of the high byte record the channel number (amplitude) of the event. The remaining 3 most significant bits are used to distinguish the module number of the AE event (only one AE module is installed in the system at Bath) and to distinguish AE data words from analogue data words. Two buffers are used so that one will be filling as the contents of the other is written to disc. The two functions of real time data display and recording of data onto disc are performed by the data acquisition software (DAS). This produces a binary sequential file on hard disc in which samples of the analogue channels at regular time intervals are sequentially stored. Acoustic emission events are located in chronological order within this framework of time/analogue data.

The first 256 bytes at the beginning of the AE binary file are termed file header space and contain, in ASCII format, the time interval and number of analogue channels (1-4) used. The time interval determines how often the analogue channels are sampled and recorded. It can be set at any value from 10 milliseconds to 600 seconds, but typically 1000 milliseconds. This information is input by the operator at program start-up.

During a test, at every multiple of the time interval, the magnitude of the DC voltage on each of the active analogue channels is recorded by way of 12 bit A/D converters as two 8 bit bytes of data (an analogue data word). The A/D converters have a pre-calibrated operating range of -10 to +10 volts, thus giving a sensitivity resolution of 2.441 millivolts

Subsequent analysis of the binary file can be carried out on the same PC as that used for data acquisition, or transferred to another IBM compatible using a floppy disc, tape streamer or direct hardware linkage.

The Marandy MR1004 system shows various improvements over the older AETC system. It is based around smaller, cheaper and simpler computing hardware with improved software. The Marandy MR1004 determines the ringdown count of each event in addition to the amplitude. Higher continuous event rates can be sustained without losing data, although the maximum short term event rate is controlled by the 100 microsecond dead time, the damping of the transducer and the amplitude/duration of the events. In addition, much greater numbers of events can be recorded on disc (up to 10 million on a 20 MB hard disk); the accuracy of definition of channel limits is improved; the same PC can carry out data acquisition and analysis, hence no special file transfer facilities are required; the computing hardware required is much smaller and cheaper.

5.3.2 AETC 203 System

Figure 5.3 shows a schematic representation of the AETC 203 system. Full details of the system, in its earliest configuration, have been given by Guild et al ⁽⁷¹⁾. Signal processing is carried out by the AETC 203 51 channel amplitude sorter interfaced to a Digital Equipment Corporation Minc-11/03 mini computer, containing three modules to perform timing, analogue to digital conversions and data transfer. Data was stored onto 8" floppy discs which had a capacity of approximately 400 kilobytes. Post-test, AE data files were transferred using a second Minc-11/03 to a more powerful computer for data

analysis. Originally, this was accomplished using the SERC Prime FTP transfer software to a Prime 750 (R.A.L.) or Prime 2250 (Bath). Later, Kermit transfer software was used to transfer data files to IBM compatible PCs for analysis.

The AETC 203 operates over a 60 dB dynamic range with 50 channels each 1.2 dB wide. Channel 1 has a threshold of 10 mV and channel 50, 8.710V. Events greater than 10 V are placed in channel 51, over range. Apart from using twice the number of channels of half the width, and not counting ringdowns, the AETC 203 amplitude sorter performs the same data processing as the Marandy MR1004.

5.4 RFPLOTS And RFGGRAPH AE Analysis Software

Two software packages, RFPLOTS and RFGGRAPH, have been developed and written by the author for use on any IBM compatible EGA display PC. The former is mainly concerned with decoding acoustic emission binary files into ASCII, with some numerical analysis and only limited graphics. The latter is a more extensive graph plotting and statistical analysis package working on either binary or ASCII AE files. Both operate with either AETC 203 or Marandy MR1004 acoustic emission files.

Figure 5.4 shows a simplified flow diagram of the RFGGRAPH data decoding, analysis and graph plotting software and a listing of the program is included in the appendices. RFPLOTS and RFGGRAPH are written mainly in a compiled basic with some assembler (where maximum speed is required). The former performs the primary function of decoding binary AE data files into comma separated ASCII files (.CSV) which can then be read directly into any spreadsheet package. The latter has more limited decoding facilities but enhanced graph plotting and statistical analysis.

The CSV format is a computer industry standard, in which data are recorded in ASCII, separated by commas, with a carriage return at the end of each line. A portion of a typical decoded .CSV AE file is included as figure 5.5. The file is a large grid or matrix

of numbers. The first row of data identifies the contents of each of the columns. Column 1 is the time during the test. The next eight columns include cumulative event and ringdown counts and rates and the magnitudes of the four analogue (parametric input) channels. The remaining columns are the cumulative event counts in each of the amplitude channels (26 for the Marandy system, 51 for the AETC system). Thus, moving down the file, each row of data is an instantaneous picture of the AE and analogue data at that time during the test.

RFPLOTS also performs basic statistical analysis of the data, gives a summary report of the file and can, by means of the AUTO facility, carry out various functions on a long list of binary files without the need for continual operator interaction. Various additional routines are included to allow control of the way in which data are decoded and thus control of the exact nature of the ASCII file produced.

RFGRAPH allows a variety of parameters to be plotted against each other as X/Y graphs from acoustic emission binary or CSV format files. The parameters are selected by single key strokes from a main menu shown in figure 5.6. The parameters include obvious ones such as time, cumulative events, event and ringdown rate and analogue data (load, strain), in addition to the more unusual, such as percentage share mean amplitude, skewness and kurtosis of the amplitude distribution. Amplitude distribution histograms can also be produced with events selected according to a range of time, analogue channel or event count.

Examples of the type of graphical presentation are given in figure 5.7. Graphs can be recorded by printing or storing to file. When producing histograms, the program also determines a large variety of parameters which both summarise and represent the data in a selected part of the acoustic emission file in simple numerical form. These data are presented to the operator in information pages on screen, examples of which are included in figure 5.8. The data include maxima and minima of all analogue and AE data in

addition to moments of the amplitude distribution, event counts in all channels and percentage shares. All decoded and manipulated data can also be written to file in CSV format for further manipulation in a spreadsheet.

For further information on these software packages, the reader is directed to the operating manual for both RFGGRAPH and RFPLOTS which is included as appendix 3.

The main spreadsheet package used in association with the acoustic emission analysis software has been Microsoft Excel. Other spreadsheet packages such as Lotus 123, Borland's Quattro or SuperCalc 5.0 may also be used in place of Excel.

5.5 Factors Affecting AE Testing

The characteristics of detected acoustic emission events depend on many factors in addition to the micromechanical deformation processes which release stress waves in a material. The structure of the material through which the stress waves propagate will modulate them as a result of attenuation in the form of scattering, absorption, dispersion, and geometric spreading. Further modulation will occur across the material to transducer interface (the coupling layer). Finally, the characteristics of the transducer itself and subsequent signal processing will further contribute to the characteristics of the received and processed AE events. The specificity of AE data to particular structure/AE equipment/test condition combinations and the need for a greater understanding of the effects of variations of AE monitoring parameters has been noted in the literature (138,151,152)

5.5.1 The Effect of Coupling Variation On AE

The quality and, perhaps more importantly, the reproducibility of the coupling between AE transducers and specimens is a subject often not considered in acoustic emission testing. In fact, for much of the earlier work in this thesis, only a cursory interest was

given to coupling reproducibility. The simple pencil lead break test (the Hsu-Nielsen source) has been used as one method for coupling calibration, but is unsatisfactory because of the high amplitude of events recorded.

A simple experiment was conducted to determine the range of variation of the peak amplitude of AE events.

A PAC U30D transducer was coupled centrally to a 16-ply UD APC2 plate, and by means of the pulser unit of the AU206, excited at 500 Hz with a 'pulse mode' electrical spike. Repeated stress pulses which have been shown to mimic real AE events (14,51) were therefore injected into the specimen. A second U30D transducer was then coupled at one end of the plate with a petroleum jelly couplant/spring clip arrangement. This transducer acted as a conventional AE receiver, the signal passing to an oscilloscope via a conventional 60 dB preamplifier and filters. After the peak amplitude of the repeated received events had been determined, the transducer was removed, the specimen surface cleaned, couplant and transducer replaced and peak amplitude re-measured. This process was repeated 50 times, whilst leaving the source transducer coupling undisturbed and thus constant.

Figure 5.9 is a frequency histogram of peak amplitude of the events. As can be seen, there is a variation in voltage from approximately 4 to 9 volts, 7.2 dB, which may be translated into a variation of 6 channels on the AETC 203 amplitude distribution system. Typical amplitude distributions of APC2 show a peak of events in the lowest channels with an exponential type decrease in numbers of events towards higher channels. A shift in the effective threshold by virtue of coupling variation would therefore be expected to have a large effect on the numbers of events recorded at low amplitude.

This may be illustrated hypothetically by taking the amplitude distribution histogram of figure 5.10a and assuming that it arose with optimum quality of coupling. If the same

test had been conducted with the worse case of coupling then a histogram shifted by 6 channels (figure 5.10b) would result. This would amount to a decrease in total events recorded to this load level of 70%. This is clearly an over-simplification of the problem since the effect of coupling quality will probably be dependent on specimen dimensions, amplitude and frequency. However, the fact that the vast majority of AE events recorded from APC2 lie below channel 10 (AETC 203) will obviously magnify the effects of any channel shift on total numbers of events.

5.5.2 AE Transducers

A cursory glance at the literature will rapidly demonstrate that there are a wide variety of different AE transducers. It has become increasingly apparent during the AE testing on APC that there is a large variation in the output (or sensitivity) from nominally identical piezo-electric transducers. These discrepancies exist between transducers of the same type/construction (from the same manufacturer), as well as between transducers of nominally the same specification from different manufacturers.

This variation is significant because it renders comparisons of AE (and AU) data recorded with anything but exactly the same transducer, largely meaningless. Added to this is the unavoidable deterioration and damage which occurs to transducers when subject to the release of large amounts of stored elastic energy when APC2 flexural samples fail. This has meant that a variety of transducers have had to be used during this research program, and comparisons have only been possible from tests using the same transducer.

Some rapid method of checking the calibration of transducers is clearly required. CARP (153) and ASTM (E1106-86) standards do exist for such calibration but they require the use of very large metal reference plates which were not available at Bath. In addition, a variety of quasi acoustic emission sources have been suggested for calibration purposes including the fracture of a pencil lead or capillary tube, helium gas jet and impact of

steel balls (45). A simple comparison of the approximate response to nominally identical artificial AE events was performed by using the AU206 acousto-ultrasonic system. The test was performed on a regular basis to check for deterioration/change in the response of transducers.

A piezo-electric AETC AC175 transducer (the emitter) was coupled/bonded at one end of a 16-ply UD APC2 strip specimen (typical of the specimen used in current AE tests), with a silicone adhesive. The coupling of this transducer was left undisturbed. This emitter transducer was pulsed with a -50 volt, 6 microsecond duration voltage spike by using the pulser module of the AU206. The resultant output was a repeated, constant artificial AE event. At a point 180 mm from this event source, the transducers to be tested for calibration were in turn coupled to the specimen and the output from them analysed on an oscilloscope. The effects of non-reproducible coupling between transducer and APC2 were allowed for in this calibration technique by repeated removal and re-coupling of the receiver transducers, a minimum of 25 times with mean and standard deviations calculated. The same AETC 40 dB preamplifier with 0.125-2.0 MHz bandpass filter was used to preamplify the outputs from the transducers. Three parameters were monitored:

1. Peak (maximum) amplitude of each event determined from a Gould OS250B oscilloscope.
2. Number of ringdowns per pulse above a 1.0 volt threshold.
3. RMS of the repeated events.

The results of this calibration procedure for 6 piezoelectric transducers are given in table 5.1. Clearly there is considerable variation in the response from nominally identical transducers.

5.5.3 The Effect of Distance From Event Source on the Received Event Characteristics

The positioning of the AE transducers on specimens is usually determined purely by the logistics of fitting the transducer in a position where it will not be fouled by grips and supports. Little consideration is given to the effect of displacement of transducers with respect to specimen edges and the attenuation per unit length of the composite.

The AC175 emitter transducer was coupled 20 mm from one end of a 16-ply UD APC2 strip specimen (220 mm long), left undisturbed and repeatedly pulsed with a -50 volts 6 microsecond electrical excitation signal. A PAC U30D was repeatedly coupled at various distances from this artificial AE source. Graphs of peak amplitude, ringdowns per pulse and RMS were plotted against distance and are presented in figures 5.11a-c.

The effect of increasing the distance between event source and receiver results in a decrease in peak voltage of the event, which over short distances appears linear with distance. Over longer distances the rate of decline in peak voltage appears to decrease. Extrapolation to zero distance gives an actual source event of approximately 2.5 mV amplitude.

RMS and the number of ringdowns per pulse show similar decays in magnitude with distance from the event source, but the scatter in the data (caused by variation in coupling) precludes the absolute relationships with distance from being determined.

However linear regression gives the following rates of decrease with distance:

Peak amplitude	0.20 V/cm
Ringdowns per pulse	2.3 Ringdowns/cm
RMS	19 mV/cm.

5.5.4 Attenuation

The attenuation and predominant wave speed of ultrasonic pulses in 16-ply unidirectional APC2 and XAS carbon fibre/epoxy (Ciba Geigy 914) was determined with a commercial instrument, the PUNDIT, operating at 150 kHz. The results are included in table 5.2. The type of matrix, whether thermoplastic or thermoset, appears to have little effect on the ultrasonic wave propagation and attenuation. An attenuation of 1.8 dB/cm measured parallel to fibres in APC2 and 2.2 dB/cm for a similar epoxy/carbon composite agrees with data published in the literature, for example, at 500 kHz attenuation of 3 mm thick T300/5208 UD graphite/epoxy was 30-40 nepers/m (2.6-3.5 dB/cm) (50).

It is perhaps worth considering the possible attenuating effects in APC2 which will affect both true AE events and artificial events used in acousto-ultrasonics.

Defect free APC2 contains structural inhomogeneities on several different length scales.

Obvious dimensions include

1. Reinforcing fibre diameter (8-10 microns)
2. Mean fibre spacing
3. Fibre tow diameter
4. Ply thickness (0.125 mm)
5. Random non uniformity in fibre spacing and fibre alignment (fibre or resin rich areas).

Typical microstructures of APC2 laminates have been presented earlier. Defects in APC2 which may arguably also include point 5. from above include:

1. Voids/porosity (0.1-0.5% in APC2 (100,113))
2. Microcracks/cracks
3. Delaminations
4. Fibre breakage

5. Incorrect PEEK crystallinity (slow cooled from the melt) and transcrystalline regions.

The relative sizes of these inhomogeneities relative to the AE wavelengths will affect the degree of scattering. Scattering is generally at a maximum when the predominant inhomogeneities are commensurate in size with the ultrasonic wavelength.

Geometric factors will also affect the attenuation. In broad terms, AE event sources are point sources, that is spherical wave fronts propagating out in all directions. For Lamb waves in large plates, attenuation caused by spreading out of the front varies with $r^{-1/2}$, where r is the distance from the source. In smaller plates, and in particular strip type test specimens, this relation cannot occur as the plate edges reflect the AE energy and thus the specimen can act as a wave guide. Hence, specimen dimensions are further variables likely to affect AE and AU testing. The frequency spectrum of AE events is another factor affected by specimen dimension, in particular, resonance with respect to plate thickness (4,154).

As a typical acoustic emission test involves the gradual increase of stress in a specimen which will cause the attenuation experienced by events to vary. Attenuation has been reported to be affected by tensile stress, increasing the attenuation at some frequencies, decreasing it at others (65). Furthermore, at higher stresses the material is likely to be more defective, for example as progressively stronger fibres fail. More defects imply greater attenuation due to scattering.

According to Roberts et al (62), it is viable to use an 'effective modulus' theory when contemplating ultrasonic wavelengths which are long compared to the characteristic fibre diameters and spacings. This theory replaces the two-constituent composite with an 'effective' homogeneous material with elastic properties that approximate those of the composite in an average form. Since the 'effective' modulus can vary due to local fibre

deficiencies, breakage or misalignment, it becomes apparent how these variations or 'inhomogeneities' can contribute to scattering if their dimensions are commensurate with the wavelength.

The viscoelastic nature of the material also contributes considerably to attenuation in composites ⁽⁵⁰⁾ for example the thermoplastic PEEK matrix in APC2. The frequency dependence of wave speed causes dispersion in composites ⁽⁶⁵⁾, so reducing the peak amplitude of stress pulses over distance.

Some of the numerous factors which can affect acoustic emission results have been considered, however the complexity and interaction of these factors leads to the requirement that valid comparisons of AE data can only be made when all experimental conditions are kept constant. This has been the case, as far as is possible, in the AE testing of APC2 covered in the next three chapters.

Chapter 6

ACOUSTIC EMISSION TESTING OF APC2

The primary aim of the acoustic emission testing was to assess and develop AE as a means of non-destructive examination of APC2. In the pursuit of this aim, several narrower objectives had to be addressed, namely:

1. determination of standard test conditions for acoustic emission testing,
2. determination of a base line of acoustic emission activity from different APC2 laminates,
3. comparison of non-defective plates with plates containing moulded-in defects using various acoustic emission parameters,
4. investigation of the cause of acoustic emission activity in APC2,

6.1 Preliminary Investigations/Standardisation Of Test Conditions

Preliminary AE testing of APC2 and subsequent three point flexural defective and non-defective specimen testing was conducted in an Instron 1195 screw driven testing machine, the AETC 203 amplitude distribution system and AETC MAC 300 transducers.

The initial characterisation of mechanical properties of APC2 by tensile, SEN and flexural tests was used to establish standard test conditions for subsequent comparative AE testing. This included the method and rate of loading/gripping and specimen dimensions.

Tensile testing of UD APC2 material in tension highlighted an important problem.

Without end tabbing, the testing machine grips were found to dig into the specimens, causing considerable fibre and matrix damage resulting in many thousands of spurious acoustic emission events, and premature failure at the grips. For example, 0° 20-ply UD specimens produced more than 500,000 events to failure as opposed to 7,000 with end tabs.

Unfortunately, with 0° tensile specimens significantly thicker than 10-ply, the strength of the specimen to end tab bond was found to be inadequate. Although various adhesives were tried end tabs often pulled off (the failure of the epoxy adhesive being an additional source of AE emissions). Use of PEEK's good hot melt adhesive qualities by way of bonding shot blasted aluminium end tabs directly on during moulding, failed to solve the problem. As a consequence, it proved necessary to limit acoustic emission tensile testing to 8-ply laminates with aluminium end tabs bonded with Araldite 2007. Alternative loading methods were investigated.

Buckling type compressive tests (after Leach and Moore ⁽⁹⁶⁾) and long beam four point bend tests were carried out. These were unsuccessful because it proved very difficult to build up sufficient stress in cross-ply and thin UD APC2 specimens to break them without much spurious acoustic activity. A long beam three point bend test was therefore chosen as a standard test configuration.

A major consideration for the adoption of this test was that it allowed the use of wide (150 mm) specimens (plates). As previously stated, one of the key aims of the work was to develop AE as a non-destructive proof test for APC components. By testing a 150 mm plate, the full width of the pre-preg could be utilised and the test piece could be treated more as a moulding rather than a small strip test piece. Furthermore, with a large specimen, defects could easily be introduced into specimens. A disadvantage was that a large amount of material was used, causing shortages towards the end of the project. A standard 16-ply thickness was retained for all subsequent 3 point flexural testing.

6.2 Three Point Bend Testing

An Instron three point loading rig with 15.5 mm diameter support rollers (greased to prevent noise generated from friction of the test laminate on the rollers) was used in an Instron 1195 testing machine. Tests were conducted initially on some 10-ply UD APC2

plates moulded at Bath and then 16-ply UD and 16-ply 0°/90° cross-ply plates, nominally 150 mm x 150 mm. UD plates were tested in two orientations:

1. fibres parallel to rollers (90°),
2. fibres perpendicular to rollers (0°).

Cross-ply plates were tested with the outer plies in the 0° orientation. Acoustic emission data (with event amplitude sorting) were collected with the AETC 203 system. The transducer was always located at the middle of one outer edge of the plates. Crosshead speed was investigated and found to have little effect on the number of events recorded to failure, hence a rate of 5 mm/min was adopted for all tests.

Various narrower test pieces, some as small as 20 mm width, were also tested to determine what effects (if any) specimen size had on the results.

Having characterised mechanical and acoustic emission behaviour of non-defective (standard) plates in three point flexure, interest was directed towards the effect (if any) of known defects on the recorded AE. In other words, whether AE could detect deliberately introduced flaws. For this purpose, four different types of defects were introduced into 16-ply APC2 plates prior to moulding. These plates were then tested under identical conditions to the standard plates and the results compared. The four types of defective plates are as follows:

1. **Non-standard moulding (slow cooled):** since the rate of cooling from the melt has a major effect on the crystallite size and degree of crystallinity within the PEEK matrix, plates were moulded by very slow cooling from the melt (cooling rate <1°C/min).
2. **Broken fibres ('cut plies'):** a 50 mm cut was made across the fibres of the two central plies prior to moulding.

3. **Delamination ('Aluminium insert')**: a piece of folded aluminium foil (measuring 30 mm x 30 mm after folding) was introduced between the central plies to induce a delamination.
4. **Missing plies ('plies removed')**: a 30 mm x 30 mm section was removed from the central two plies prior to moulding.

The positions of the moulded-in defects through the thickness of a beam tested in flexure would be expected to have a significant effect on the response of the specimen to that defect. As a consequence, further 'plies missing' UD plates were produced, with the two 30 mm square sections removed from adjacent plies positioned at various depths through the beam. Plates were tested in the 0° configuration such that the defect was located as follows:

1. 1 ply down from the tensile surface.
2. 4 plies down from the tensile surface.
3. 4 plies up from the compressive surface.
4. 1 ply up from the compressive surface.

For comparison with the characteristics of APC2, a small number of 16-ply UD carbon fibre reinforced epoxy (CG 914 with 60% by volume XAS carbon fibre reinforcement) and unreinforced PEEK (3 mm thick) 150 mm x 150 mm plates were tested under the same conditions as APC2.

6.2.1 0° Plates

6.2.1.1 Standard plates

The typical mechanical and acoustic emission behaviour of UD 0° plates is summarised in the compilation of graphs presented as figures 6.1a-d. Figure 6.1a is a stress/strain plot showing a near linear elastic load up to failure which was catastrophic. This released considerable elastic energy in the form of audible sound, high frequency (ultrasonic

energy) and kinetic energy of fractured plate halves. The plates fractured in an erratic line opposite the central loading support with some splitting parallel to fibres.

On first inspection, the acoustic emission behaviour from nominally identical standard 0° plates varied considerably, as demonstrated by figure 6.2 in which event counts in four channel ranges are all plotted against time. In some cases there were very few emissions until just prior to failure, whilst in others there was a low level of emission throughout the tests. The most typical behaviour was an exponential type build up of events from approximately 0.7% strain to failure, and in all cases a rush of events at failure.

The events recorded from APC2 were predominantly low amplitude (up to channel 10-12). This is demonstrated by figures 6.1c and 6.1d which are amplitude distribution histograms of all events recorded to maximum stress and to failure of a three point bend test. There is an exponential type decay in numbers of events towards higher channel numbers. Some higher amplitude events occur near to failure but few occur above channel 20. The event amplitude always increased towards failure, probably indicating that more energetic event sources were becoming active. Similar results have been reported by Yamaguchi et al for thermosetting resin matrix composites (155). In general there were very few emissions in a test run to failure compared to many other composites (118,121) and as a rule, of the 100-200 events recorded during a test, over 50% were produced at failure.

6.2.1.2 Comparison of defective 0° laminates with non-defective

6.2.1.2.1 Numeric AE parameters

For each category of defect introduced into APC2 laminates, between 4 and 8 repeat specimens were prepared and tested. The results recorded from these different groups were compared with the data from the group of non-defective laminates, the outcome of which will now be discussed for 0° laminates. It was essential to take into account the scatter when comparing grouped data. This was achieved for all numerical parameters by

quoting and comparing data ranges; non-overlap being used as evidence of a possibly useful distinction.

The mechanical properties flexural strength, strain to failure and elastic modulus of the different groups of non-defective and defective UD 0° plates are presented in tables 6.1a and table 6.1b. Only the 'plies removed' defect positioned away from the neutral axis (centre of the plate) made any detectable reduction in the strength (25% reduction) and modulus (20%). The other defects had no statistically significant effect on the measured properties.

The first and simplest stage in comparing the AE behaviour of defective with non-defective laminates was based on cumulative event counts to failure (see column 5 in tables 6.1a and b). At a 95% confidence interval the slow cooled plates and some of the 'cavity' plates produced significantly more events than standard plates. Otherwise total events to failure did not prove to be a very useful parameter for distinguishing good from defective plates, being subject to very large variability between nominally identical specimens. This appeared to be due to the rush of events at failure being complicated by spurious noise as the transducer and specimen sometimes parted company when the fractured specimen halves were catapulted across the laboratory.

A better comparison would be to compare events until the instant before failure (maximum load). Such a comparison is provided in column 6 of table 6.1a. The coefficients of variation for events prior to failure are either similar to or markedly less than those including failure. Even so, coefficients of variation exceeding 0.5 are common; event counts being subject to large intrinsic variability from nominally identical specimens. The scatter was not reduced by selecting specific amplitude channel ranges over which to sum events.

As a result of the above, alternative acoustic emission parameters not based on event counts were therefore investigated. These included characteristics of the amplitude distribution; the mean (centre of mass), variance (width or spread) skewness and kurtosis (peakedness), termed the four moments of an amplitude distribution histogram (see appendix for definitions). These parameters are included for standard (non-defective) and slow cooled laminates in table 6.2. Unfortunately, these parameters were also subject to large scatter. This was partly because insufficient numbers of events were recorded to build and establish the characteristics of a distribution.

The main problems involved in carrying out the comparisons between these defective and non-defective groups of specimens were the relatively small number of events, the variability of the data and the relatively small number of specimens available. There were, however, some clear differences between some, but not all, of the 'plies removed' defects and the slow cooled plates. These differences included greater numbers of events, a tendency towards higher amplitude (higher mean amplitude) and a slightly broader distribution (greater variance). The 'Aluminium insert' and 'cut plies' defects showed no apparent difference from standard.

It was expected that the most significant effects on the AE behaviour would be seen when the 'plies removed' defects were positioned closest to the surface (compressive and tensile), since the stresses seen across the defect would be enhanced. In practice, it was the '1 down, tensile' and the '4 down, compressive' plates which produced more events at lower strains, showing a greater event rate throughout the test and many more events to failure. The '1 down, compressive' and the '4 down tension' plates did not exhibit much difference to standard based on event or event rate counts. There was some indication that they produced more events at lower strains but the overlap of the data was too great to prove anything conclusively and differences were not statistically significant.

6.2.1.2.2 Graphical methods of comparison

Having investigated many numerical acoustic emission parameters, attention switched to graphical presentation/comparison of the data, for example, by shapes of event versus time graphs.

It was noted that in some tests there was an initial period of emission associated with the application of the first 200-400 MN/m² stress after which the emission rate reduced almost to zero (see figure 6.2). This was considered to be caused by plates 'settling down' on the supports and the slight buckle left over from moulding being flattened out. As a consequence, event/time graphs from nominally identical specimens were shifted to remove the events produced during the first fifty five seconds of the test and plotted on one graph. Figures 6.3a-d show these plots for the standard and defective 0° plates. By comparison, differences can be seen between plots for the 'plies removed', 'Aluminium insert' and standard plates but not for 'cut plies'. Standard plates show a definite 'elbow' (sharp change in event emission rate) in the graphs close to failure, whilst the 'cavity' plates do not, having a more gradual increase in events to failure. 'Cavity' plates generally start to emit at lower strains and produce more events before failure. The 'Aluminium insert' plates show an intermediate behaviour between the two.

Even after the removal of the AE activity during 'settling in' there still appeared to be considerable residual variation in the AE activity from nominally identical specimens. This was reducing the significance of any differences between defective and non-defective samples. In light of this, it is interesting to note figure 6.4. In this figure, the aforementioned events/time graphs have been shifted to a common failure time. On this basis, within group variability is considerably reduced. All samples tend to show a similar AE build up as they approach eventual failure, but their failure deflections (times) may be quite different.

Comparison of amplitude distribution histograms for events produced up to 2000 N and failure and included as figures 6.5a-f and 6.6a-f indicated possible differences between standard and all 'plies removed' defects. The shaded regions in these graphs demonstrate the ranges of the data. As is typical of APC2, all specimens show peak numbers of events around channels 5-10 but at pre-failure stresses and at failure, all defective plates show an increased minimum number of events in lower channel ranges (note the unshaded regions in figures 6.5a-f and 6.6a-f).

6.2.2 90° Plates

The basic mechanical and AE behaviour of 90° plates is demonstrated by the graphs in figure 6.7a-d. These plates showed a near linear load up to failure which is catastrophic, with a well defined fracture surface parallel to and opposite the central loading line. In general, 90° plates produce very little or no emission (perhaps 10 events) until the rush of events at failure. Total events per plate were still 100-200 and most were low amplitude. No higher amplitude events are seen until final failure when AE energy output is at a maximum. This is demonstrated by figures 6.7c and d, which are amplitude distributions of events until just prior and just after failure respectively.

Standard and small numbers of defective plates were tested in the 90° orientation. The very low level of emissions prior to failure made comparison of AE data from defective and non-defective samples inappropriate. None of the mechanical properties measured and included as table 6.3, were significantly affected by the presence of the moulded-in defects.

As with 0° orientation plates, 'slow cooled' produced considerably more AE events than standard. This may be due to the higher PEEK crystallinity and larger spherulite size, the presence of surface defects or simply greater fibre misalignment due to fibre movement in the melt.

In this configuration the PEEK matrix and carbon fibre/PEEK interface should play a dominant role in the AE activity. Since almost all events are generated during failure, a test which produces a slow, stable interlaminar or intralaminar crack propagation was needed. For this reason, interest was directed towards double torsion and double cantilever beam tests.

6.2.3 0°/90° Cross-ply

As with unidirectional laminates, 0°/90° laminates showed a near linear elastic load up to failure which again was catastrophic (figure 6.8a). The cross-ply specimens underwent greater strains to failure than UD 0° specimens and sustained lower stresses prior to failure, yet the acoustic emission behaviour was very similar. This is demonstrated by figure 6.8b which shows an exponential increase in events from a starting point around 1.1% strain with again a rush of events at failure. Once again total event counts were typically around 100-200. These were almost exclusively low amplitude, being below channel 20, prior to failure, as shown by figure 6.8c, with a few high amplitude events associated with failure (see figure 6.8d). The average values of the moments of the distribution were almost identical with those determined for UD 0° specimens.

No statistically significant differences were evident between the mechanical properties of the standard and defective plates, which are presented in table 6.4.

As with the 16-ply 0° UD specimens, the AE activity of groups of defective and non-defective specimens were compared by a variety of methods including graphs of cumulative events with time shifted to remove the first 55 seconds of AE activity (settling in of plates) as shown in figure 6.9. As seen for 16-ply 0° UD specimens, the 'plies removed' and 'Aluminium insert' defective samples tended to show a more rapid yet smoother increase in events with time than standard. They produced more events at lower specimen deflections, whilst the 'cut plies' samples showed no difference from standard.

The 'plies removed' defective specimens produced greater numbers of events to failure than standard, but any other differences that may exist are almost certainly masked by the apparently inherent variability in the data.

6.2.4 Narrow Plates

In order to determine the effect of specimen width on mechanical and acoustic emission results, 16-ply (nominally 2 mm thick) plates ranging in width from 18 mm to 150 mm were tested under standardised conditions. Three graphs of failure stress, elastic modulus and total event count plotted against cross-sectional area for 0° plates are included as figures 6.10a-c. Failure stress seems to be insensitive to specimen size but elastic flexural modulus increases slightly with specimen size (also seen in cross-ply and 90° plates). This is possibly a result of edge effects; a greater proportion of the material being subject to reduced elastic constraint. For 0° plates, total numbers of acoustic emission events increase with specimen size as would be expected. Smaller plates usually started to emit at higher deflections. As the specimen size increases, in particular the width, there will be two competing factors affecting the numbers of events recorded by a single AE transducer. A greater stressed volume of material should generate more events (more AE sources active), but these events will on average emanate at greater distances from the receiving transducer. They will consequently be attenuated more, and therefore be less likely to exceed threshold and be detected. Clearly, specimen size must be held constant for the comparison of AE data.

6.3 Carbon Fibre Epoxy And Unreinforced PEEK

For comparison with APC2, a small number of 16-ply UD XAS carbon fibre/epoxy (CG914) plates were tested under standardised conditions in long beam three point flexure. The cumulative events time graphs of the tests are included as figure 6.11, and the mechanical properties determined included in table 6.5. As for APC2, there is only a

very low level of emission prior to the rush of events at failure. In fact, on average, the rate of increase in events is lower and commences at higher strains than for APC2.

Since the reinforcing fibres are identical and the attenuation coefficients (see earlier) and mechanical properties are similar, it must be concluded that the quiet behaviour of APC2 in long beam three point flexure is a common phenomenon of carbon fibre reinforced plastics. It is also partly due to the test configuration (tensile stressing and stable crack propagation generate many more events as is shown later). Observation and comparison of the fracture surfaces of APC2 and the carbon fibre/epoxy samples shown in figure 6.12a and 6.12b further demonstrate the similarity in behaviour in this test configuration. Both materials show the typical 'brush' type debonded fibres, similar fibre pull-out lengths, and both show the pulled out carbon fibres covered in matrix.

Unreinforced PEEK resin plates, supplied by ICI, Wilton were tested in three point flexure, again under standard conditions. The PEEK samples behaved in a ductile manner undergoing gross ductile yielding such that it was not possible to fracture the samples in the long beam three point bend configuration. Almost no emissions were recorded during the tests and therefore no data analysis has been attempted.

6.4 Double Torsion Testing

As a means of recording AE data from a slowly growing crack, both standard and slow cooled 190 mm x 60 mm 16-ply UD APC2 plates were tested in double torsion. Lee (155a) gives a detailed description of this test method (applied to glass/epoxy composites) though it was originally suggested by Outwater and developed by Kies and Clark (155b). A 5 mm starter crack was machined into the end of each specimen. The outer supports for the test (300 mm long 10 mm diameter bars) which were parallel to the longest specimen edge and thus also parallel to the fibres, were greased and set 60 mm apart. The inner set (45 mm long) were placed 10 mm apart and mounted under the Instron 1195 crosshead. Vertical displacement of the inner supports down over the machined

crack caused the machined crack to propagate along the length of the specimen, guided by the fibres (in the intralaminar direction). A crosshead speed of 5 mm/min was used throughout and both standard and slow cooled specimens were tested.

Both slow cooled and standard specimens showed an initial linear load up followed by a break-away from linearity with an associated onset of acoustic emission as the starter crack began to grow. Crack growth took place by two modes, slow progressive propagation and fast fracture (crack jumps), the latter being evident on the load displacement graphs as load drops, as shown in figures 6.13a and 6.13b. Crack propagation always became unstable (fast fracture) over the last 20 mm - 30 mm of the specimen.

Acoustic emission took place throughout the test once the initial break-away from linearity had occurred. This, coupled with the fact that the load time curve is never perfectly linear, even during the load increase after a fast crack jump, may be taken as evidence that crack propagation was a continuous process. The emission rate rose immediately preceding a crack jump and fell immediately afterwards.

Several differences were observed between the mechanical and acoustic emission behaviour of slow cooled and standard plates and these are now summarised. The maximum load recorded during the initial load up, prior to the break-away from linearity, was 175 - 225 N for standard plates and 125 - 150 N for slow cooled. In addition, standard specimens recorded a higher mean maximum load (225 N compared to 158 N) during each test and required greater crosshead displacement to produce complete failure. Slow cooled plates fractured by a series of fast crack jumps (the first at the break-away from linearity) showing little of the slow stable propagation seen in standard specimens. The standard specimens tended to produce more events (17500 compared to 10800 on average per test) and around 70% of these were within channels 0-10 (see figure 6.14a and 6.14b). A greater proportion of the events from slow cooled

specimens lay in channels 11-20 (see figure 6.14b), only 50-60% being in channels 0-10 and, in general, they showed a wider amplitude distribution as shown by figures 6.15a and 6.15b.

6.5 Tensile Tests

As previously stated, tensile tests on UD O° APC2 for the purposes of AE monitoring have been limited to 8-ply laminates due to problems with end tab failure and end tab/grip noise.

Three batches of five 10 mm wide 8-ply unidirectional APC2 strip specimens were cut from specially prepared plaques. The three batches were:

1. 'Standard' - good quality, nominally non-defective.
2. 'Plies removed' - 10 mm square sections removed from the central two laminates.
3. 'Aluminium insert' - a folded piece of aluminium foil, 10 mm square, introduced between the central two plies.

The specimens were end tabbed with shot blasted aluminium sheet by means of Araldite 2007 adhesive, a technique shown earlier to eliminate grip noise. All samples were tested to failure at 0.5 mm/min crosshead speed in an Instron 1195 screw driven testing machine. Associated AE monitoring was conducted using the AETC 203 system and AETC MAC 300 transducer mounted centrally on each specimen.

In order to check that end tab adhesive cracking was not contributing to the AE output of these samples, an extra non-defective specimen was end tabbed and loaded to 12 kN.

The end tabbed portions of the specimen were then cut off and new tabs bonded on to the specimen which was then reloaded to 12 kN. Very few emissions were recorded on this reloading, a significant event rate only commencing close to the previously attained load level. This indicated therefore that very few events were generated by the end tabs. It also indicates that APC2 shows the Kaiser effect.

Unfortunately, accurate strain measurement was not possible, and excessive deflection in the specimen grips and linkages precluded the use of the crosshead displacement as an approximate measure of specimen deflection. Strain gauges were not used in case they generated any spurious noise. Consequently, only failure strength can be quoted for mechanical properties of the three sets of specimens in table 6.6. The mean failure strength of 1590 MN/m^2 was reduced by the presence of the two types of defects, by only 10% for 'Aluminium insert', but by 40% for the 'plies removed' specimens.

The load/time and cumulative event/time graphs for the replicate specimens for 'standard', 'Aluminium insert' and 'plies missing' conditions are presented in figures 6.16a-6.16c and figures 6.17a-6.17c respectively. The non linearity in the initial load up was due to flexing of the Instron grips. Total failure was preceded by small sudden load drops caused, it is thought, by longitudinal cracking. These generated bursts in the acoustic emission rate, a factor also reported by Valentin et al ⁽¹⁴²⁾ in carbon fibre reinforced epoxies. Cumulative event/time graphs show the typical exponential type shape. The total numbers of events recorded to failure are two orders of magnitude larger than those seen in flexural tests using an identical transducer.

Differences between sample batches have been observed in two areas. Firstly, although 'plies missing' specimens gave fewer total events to failure than standard, as a result of the much lower stresses attained prior to failure, they produced more events at lower stresses, particularly in channels 11-30. The converse appears generally to be true for 'Aluminium insert' samples, although there is overlap with standard specimens.

However, the 'Aluminium insert' samples also produced greater event counts than standard in the middle channel ranges prior to failure. These distinctions must be tempered, however, by the large variation in numbers of events seen between nominally identical specimens. Distinctions not based on absolute numbers of events were statistically more significant.

Some of the most significant differences in the AE response of the three batches may be seen from amplitude distributions at pre-failure loads. Figures 6.18a-6.18c show amplitude distribution histograms for events recorded up to 5000 N, with the range of the data for five replicate specimens shaded in. Although the ranges are considerable, marked differences are apparent; defective samples show more events in most channels and a wider spread in amplitude distribution, with peak numbers of events in channel 7 and channel 11 for 'plies removed' and 'Aluminium insert' respectively. Defective specimens show a greater mean event amplitude and a greater percentage share of events in the 11-30 channel range (see table 6.6).

6.6 Four Point Flexure

Much of the earlier analysis of AE from APC2 encountered problems owing to the very low level of emissions (100-200 events) recorded during a test to failure of even quite large plate specimens. In comparison, tensile tests from relatively small samples produced tens of thousands of events. Clearly, having to use a flexural test (3 point bend) which stresses relatively little of a specimen is a major contributor to the low emission counts. Increasing the stressed area should increase the AE activity.

In addition, since APC2 is basically a quiet AE source in which events are normally low amplitude, a second method of increasing events was to use a more sensitive AE transducer. This was accomplished by use of a high sensitivity PAC U30D transducer, in preference to the AETC MAC300 transducer used to this point. Both transducers were similar in size and nominally resonant at 300 kHz, though the PAC U30D exhibited greater sensitivity over a narrower frequency range.

The effect of using AE transducers of nominally similar resonant frequency, but different sensitivity (one highly damped, one not) on the amplitude distribution of APC2 may be seen by reference to figures 6.19a and 6.19b. Both distributions are for nominally similar 16-ply UD APC2 plates tested in 3 point flexure, 5a.25a using the AETC MAC 300

broad band transducer and 5a.25b using a PAC U30D resonant transducer. The U30D records 50 - 100 times as many events as the MAC 300 (and FAC 500) transducers, yet the amplitude distributions are very similar. The cumulative events/time graph of an APC2 0° laminate tested under the standard 3 point bend conditions outlined earlier, using the U30D transducer, is shown in figure 6.20. The same exponential type of increase in events with time exists as before, however, now the typical total of events recorded to failure (approximately 200) is reached at only 10-15% of the strain to failure. The very sharp rush of events at failure is no longer apparent due to the 100 microsecond dead time limitation of the system event rate, saturating the system at failure.

6.6.1 Comparison of Four with Three Point Loading

Although long beam three point flexural loading of APC2 avoided problems with grip noise, the actual volume of material under maximum stress and therefore likely to emit acoustic emissions is small, compared to the size of the specimen. In an effort to increase this volume under stress and thus increase numbers of events, 4-point flexural testing was performed.

Various combinations of inner/outer span combinations were investigated with 16-ply UD APC2 16 mm wide strip specimens. A 108 mm outer span, 36 mm inner span was adopted. This was the largest combination at which 16-ply UD APC2 did not over deflect and slip between the supports and which conformed to standard long beam four point bend test conditions defined by ASTM D790. This gave greater significance to the mechanical properties determined from the tests. 20 mm diameter support rollers were used with a universal joint between the central supports and crosshead of the testing machine (Instron 1195) to ensure alignment of the specimen/supports. A crosshead speed of 5 mm/min was used in all cases.

Two groups of nominally identical 16-ply UD APC2 16 mm wide specimens were cut from a single plaque. One group was tested to failure in 3 point flexure (100 mm span)

using the previously standardised conditions, and the other group was tested in four point flexure (108 mm/36 mm spans) with a PAC U30D AE transducer. Apart from the loading supports, all other test conditions were held constant.

The basic mechanical properties (and total events to failure) measured from both types of test are included as table 4.4 (see earlier). The failure stresses are essentially identical, but strains to failure may be slightly lower and moduli higher in four point flexure. Total events to failure are approximately 2.6 times greater when measured in four point flexure. The large range in total events from nominally identical specimens ($\pm 65\%$ of the mean) is still disappointing, but this is the subject of an investigation described later.

Typical load/time and total events/time graphs for four point flexure are included as figures 6.21a and 6.21b. As seen in three point flexure, there is again an exponential type increase in events to a catastrophic failure, which usually occurs at two positions opposite the central loading points.

There is a linear elastic load up to around 65% of the failure strain after which a gradual deviation from linearity occurs. From the work of Fuwa et al, it may be surmised that this non-linear behaviour is the result of fracturing of significant numbers of fibres, thus reducing the modulus of the sample. This would thus explain the rapid increase in event rate at this stage in the test.

In figures 6.22a and 6.22b typical amplitude distributions of events recorded to $2/3$ of the failure load and to failure are presented for four point flexure. As seen in three point flexure (see figure 6.19b) there is a single low amplitude, positive skewed (tail to the right) peak in the distribution. Apart from the great difference in numbers of events and a small shift in mean amplitude near to failure, the characteristics of the events are largely similar throughout the load up to failure.

6.7 Interrupted Loading Cycles

In order to investigate the Kaiser effect in APC2 and to determine what effect preloading has on the mechanical and AE response, 16-ply UD APC2 specimens were subjected to a pre-load before being taken to failure. The 4 point flexure loading cycle used is shown in figure 6.23a with the corresponding cumulative AE events in channel ranges as a function of time in figure 6.23b.

There was no significant reduction in the strength or strain to failure of specimens subjected to a 600 N pre-load (approximately 60% of failure stress), but a statistically significant 7% reduction in elastic modulus was observed. As the pre-load level is reached and the load is held constant, the AE rate slowly decreases, but does not reduce to zero before unloading. The events during this load are low amplitude and are probably caused by creep associated micromechanisms within the composite. A very low level of emissions, again only low amplitude, are recorded during unload. During reload to failure, emissions only recommence as the previous maximum load level is reached, showing that APC2 displays the Kaiser effect, a Felicity ratio of unity (at least over short periods). This also demonstrates that machine noise is not a problem.

6.8 Discussion/Conclusions

The acoustic emission studies of APC2 (predominantly by three point flexural testing) have shown APC2 to be a very quiet material under flexural stress. The number of AE events is low (100-200) even from tests on 0° unidirectional plates in which hundreds of thousands of carbon fibres are broken, many of which might be expected to produce emissions. A high proportion of the emissions are of low amplitude (within channels 0-10) and at least 50% occur at failure. In 90° plates almost all emissions occur at failure. It is common for unidirectional carbon fibre reinforced composites to emit only a small proportion of their AE events until near to failure whether stressed parallel or perpendicular to the fibres. However other composites with thermosetting matrices often produce total events up to more than two orders of magnitude greater than APC.

AE produced in 0° UD APC2 is likely to be dominated by the fracture of fibres which is in turn governed by the statistical strength of the fibres. A similar conclusion was drawn by Jamison and Reifsnider ⁽¹⁴³⁾ for a UD carbon fibre reinforced epoxy. They found that fibre fracture density obeyed a power law relationship with tensile load, a similar relationship seen in AE emissions in APC2. Lorenzo and Hahn ⁽¹⁵⁶⁾ also reported that AE emissions from model composites (carbon fibres embedded in both a ductile and a brittle epoxies) were dominated by fibre failures.

As stresses increase during a test, more fibres fail until, in a given cross section, there are insufficient unbroken fibres to sustain the stress and the specimen fails ⁽¹⁵⁷⁾. Clearly the number of events at failure should be very large, given the many thousands of fibre fractures. However, since APC2 fails suddenly and catastrophically (the crack should take only around 1 microsecond to propagate through the thickness of a 16-ply laminate), the many thousands of events will be unresolved in the time domain. Short and Summerscales ⁽¹⁵⁸⁾ have also noted that failure in CFRPs normally occurs by catastrophic fibre fracture with little acoustic activity before the event. The dominance of the fibres in AE event production of APC2 is given further credence by the lack of AE activity of pure PEEK.

The variability in AE from nominally identical specimens is high, particularly in the initial load up period. After removing these initial events there would appear to be good indications that AE will be able to distinguish between standard and at least some kinds of defective plates. It should be noted however, that moulded-in defects, except for 'plies removed', did not significantly affect mechanical properties, so AE should perhaps not be expected to detect their presence.

At this stage, acoustic emission would appear to be able to distinguish between three out of the four types of defective plates and the standard 0° UD plates, by looking at events in all channels. Neither graphs of events in selected channels versus time, event

amplitude histograms nor numeric AE parameters gave much improvement or a more easily recorded distinction between types of plate. This was largely due to excessive experimental scatter in the AE data. Prior to acoustic emission testing all plates were ultrasonically C-scanned by ICI. These scans outlined the defects in the plates, thus showing that acoustic emission requires improvement if it is to compete with C-scanning. However, since some of the defects caused little if any reduction of strength, it may be argued what point there is rejecting a plate with a C-scan observed defect that is not damaging.

In tests with double torsion standard and slow cooled plates, in which matrix differences were particularly under scrutiny, two modes of crack propagation, progressive and 'slip-stick' were seen. Slow cooled specimens behaved in a more brittle manner than standard. They showed predominantly fast fracture and very little of the slow stable propagation seen in standard plates. This produced fewer events but a broader amplitude distribution, with more events in the 11-20 channel range compared to standard plates. Slow cooling APC2 is likely to cause the PEEK matrix to form larger spherulites, fewer inter-spherulite tie-molecules, a higher overall crystallinity (around 35% compared to 25-30% for normal cooled) and, according to Blundell et al (107,108), increased alignment of the crystallites. This will confer a higher matrix yield stress and lower matrix toughness. Inter-spherulite weakness may cause a possible reduction in matrix strength, and certainly reduced toughness. This should explain why the slow cooled specimens appeared weaker and more brittle.

It appears that having to use a flexural test (to avoid grip noise) for AE comparisons has not helped in the development of AE as a means of defect detection in APC2. Tensile testing appears, on the evidence so far presented, to be a better means of stressing samples for AE testing although it has been limited by the very good chemical resistance of APC which causes problems when trying to bond to it with adhesives. Many of the traditional aerospace adhesive systems produce an inadequate chemical bond to PEEK.

The adhesives Ciba Geigy "Redux" 319A, Ciba Geigy "Araldite" 2007 and 3M EC 3430 reportedly give the best results (100). An alternative may be to use the good hot melt adhesive properties of PEEK itself to form bonds, localised electric resistance heating being possible by passing a current through the reinforcing fibres. All these methods of joining give lap strengths of the order of 20 MN/m² (92).

The SEM work conducted on fracture surfaces has helped to explain the good mechanical properties of APC2 and to a lesser extent, the AE behaviour. The very good adhesion of the PEEK matrix to the carbon fibres is apparently due to transcrystallinity from the fibres acting as heterogeneous nucleation sites, into the bulk matrix (84,98). This allows good stress transfer, and thus, the properties of the fibres can be well utilised. Hence, the similar flexural properties of PEEK and epoxy carbon fibre reinforced composites.

Upon fracturing, the tough thermoplastic PEEK matrix undergoes gross plastic deformation and fails in a ductile manner, thus helping to blunt an advancing crack and produce a high fracture toughness. No evidence has been found that APC undergoes fibre/matrix interface failure and clean fibre pullout, failure occurring at some distance into the matrix. It may be argued that the fibres fail at the point where the crack meets the fibre and not at some critical flaw along the fibre after debonding has uncovered a longer length of fibre. The probability of finding a major flaw increases (and the effective strength decreases) as fibre length increases. Since debonding of fibres does not generally occur in APC2, the mean length of carbon fibre under maximum stress at the crack tip is very small and thus the fibres appear stronger and higher strength is conferred to the overall composite.

Two important points had arisen from the AE testing of APC2 to this point, which led to the work included in the following two chapters. Firstly, crack propagation, particularly stable, slow propagation in DCB or double torsion specimens of APC2 for example,

generated a large number of events, the characteristics of which appeared to be very sensitive to the condition/type of the material. Secondly, there was considerable scatter of the AE response of nominally identical APC2 specimens which appeared to limit the prospects of AE becoming a useful means of NDT for APC2. The cause of this scatter requires investigation.

Chapter 7

ACOUSTIC EMISSION AND CRACK LENGTH MONITORING OF DCB APC2 AND FIBERITE/CARBON FIBRE COMPOSITES

7.1 Introduction

In late 1987, a joint programme of work was conducted between the University of Bath and ICI, Wilton (M Davies and R Prediger). A series of tests were conducted on crack propagation in double cantilever beam (DCB) epoxy and PEEK matrix carbon fibre laminates, employing electronic crack length measuring equipment from ICI, with the AETC 203 acoustic emission monitoring system at Bath. The programme of work was preceded by preliminary investigations which are detailed below.

7.1.1 Preliminary Investigations

Preliminary tests were conducted on DCB specimens of APC2 moulded at Bath under normal and slow cooling conditions and on an epoxy/carbon fibre composite. Load and AE data only were recorded from 40-ply UD material. The aim was to investigate the interrelationships between crack growth and AE behaviour. Crack growth, however, could only be inferred from the load and AE/time plots.

In figure 7.1 a comparison is made between the load/time and the cumulative events/time plots for a DCB test performed on APC2 moulded under normal conditions at Bath.

Figure 7.1a shows the typical 'saw tooth' shape of the load time graph which is caused by 'slip-stick' crack propagation: the sudden load drops are caused by rapid (unstable) crack propagation, typically accompanied by an audible cracking (low frequency stress wave emission). Following the load drops, the crack appears to arrest until the load builds up sufficiently for further gross crack propagation, usually stable for a time, then followed by another crack jump.

The corresponding AE event count versus time plot in figure 7.1b demonstrates several important points. During fast crack propagation when tens of millimetres of crack extension occurs, essentially no emissions are recorded. This may be caused, either by the emissions lying outside the frequency range of the data acquisition equipment, or because the emissions occur within such a short time period that they are unresolved by the AETC 203, arriving as one.

Comparison of the cumulative events/time plot with the load/time plot indicates that an appreciable build up of load above the arrest value is needed before further gross crack propagation recommences. This is shown by the build up in event rate to an almost constant level during stable propagation. Further to this, it is evident from the period between the first and second load drops, that this linear build up of events is the same whether the load is increasing or decreasing.

The speed of crack propagation would be expected to have a significant effect on the AE behaviour and fracture surface energy. The observations above demonstrate the importance of having direct crack-length measurements, since without them, it is only possible to make inferences as to the speed of crack propagation. It is not possible to determine whether the crack completely arrests and whether there is any crack propagation during load build up.

The use of a double cantilever beam test was initially proposed for the further investigation of the differences in behaviour seen between slow cooled and standard APC2 double torsion specimens. The trends seen in the double torsion configuration were found to be largely repeated in double cantilever beams.

Preliminary investigations were conducted into the differences between normal cooled and slow cooled APC2, representative results of which are given in figure 7.2. The load time plots demonstrate that for a given crosshead speed, slow cooling causes the crack

propagation to occur by a series of short unstable crack jumps with little evidence of much stable propagation. Normal cooled APC2 showed a significant amount of slow, stable propagation with a smaller number of much larger crack jumps. Little distinction was seen in the total acoustic emission counts recorded from each specimen, although, again, there did appear to be peaks and troughs in the event rate associated with crack jumps and possible crack arrests respectively.

For comparison, a small amount of a conventional epoxy/carbon fibre composite was tested under the same conditions as APC2/AS4 PEEK carbon fibre. Pronounced differences existed in the AE amplitude distributions of emissions from interlaminar crack propagation in these two types of material. These differences may be viewed from figures 7.3a and 7.3b, in which amplitude distributions from the two materials are presented (after Nixon ⁽¹⁵⁹⁾). Both distributions exhibit a dominant peak in the mid to high amplitude ranges (channels 30 - 40), however the peak is wider for APC2 material. The epoxy also shows a secondary peak at low amplitudes (channels 0 - 10), not present for APC2.

These preliminary results were based on a small number of tests. In addition, there were uncertainties regarding the possible influence of coupling variation between AE transducer and specimen, and the relative positions of crack front and transducer.

The absence of the low amplitude peak in the APC2 distribution may have been the result of poor coupling quality which would have raised the effective threshold of the AE instrument, thereby eliminating low amplitude events. Monitoring the coupling quality and ensuring consistency between tests was, as a consequence, one of the aims of the programme.

Use of ICI crack gauges was proposed to facilitate precise measurement of the position of the crack front, and thus to enable comparison of numbers and types of events over

identical crack propagation distances. The relative distance between transducer and crack front (the source of AE emissions) would be expected from attenuation measurements (approximately 1.8 dB/cm or 1.5 channels width per centimetre) to affect the amplitude distribution as the crack propagates down the beam.

7.1.2 Objectives

The objectives of this programme of tests may be summarised as follows:

1. to compare and contrast the AE behaviour of epoxy/carbon laminates with PEEK/carbon laminates and to determine whether AE can distinguish between the two,
2. to compare the mechanical and AE behaviour between interlaminar and intralaminar crack propagation modes,
3. to investigate whether genuine crack arrest occurs after a crack jump and determine how the AE is associated with this phenomenon,
4. to study the variation of amplitude distribution as the crack progresses along the sample, towards the transducer,
5. to investigate whether any relationships exist between the AE and fracture toughness/crack propagation parameters, for example G_c .

7.2 Experimental

7.2.1 Specimen preparation

Both materials investigated were 40-ply UD. The epoxy laminates used a Fiberite matrix with 62% by volume reinforcement of AS4 carbon fibre, moulded according to the manufacturers specification by ICI. These were nominally 7.5 mm thick. The APC2, PEEK reinforced with 62% by volume AS4 carbon fibres was nominally 5 mm thick. Previous work has shown that at room temperature and intermediate crosshead speeds, the Fiberite/carbon exhibited stable crack propagation, but unstable 'slip-stick' propagation in APC2. For the purposes of comparison, the APC2 laminates had been

specially prepared by ICI (by non standard cooling during moulding) to obtain stable crack propagation at room temperature.

Photographs of the four types of DCB specimen tested are included in figures 7.4a-d. The interlaminar specimens were nominally 25 mm wide and included a starter crack by incorporation of a piece of PTFE sheet between the central plies at one end. The intralaminar specimens (crack propagated parallel to fibres but perpendicular to the plies) were 25 mm wide strips, turned on their sides giving a narrow but deep DCB. A starter crack was produced by milling a central slot in the loading end. Metal hinges were bonded to the appropriate faces at one end of each specimen with Araldite 2007 adhesive and gripped in the jaws of an Instron 1195 testing machine.

7.2.2 Testing procedure

An aluminium foil crack-length gauge was bonded to the edge of each interlaminar DCB sample or the face of each intralaminar sample before mounting into the testing machine. The gauge works on the principle of increased electrical resistance, as the thin aluminium sheet bonded to the DCB splits as the crack in the beam passes along its length. The position of the gauge with respect to the end of the sample was recorded and the gauge calibrated such that 50 mm of crack movement gave a 0 to 10 volt linear output (this being 100% on the instrument scale).

The ICI crack length system utilises a Hewlett Packard PC with dedicated software for data acquisition and analysis and is described in full elsewhere (160).

The output from the crack gauge and the load signal from the Instron load cell were simultaneously fed into both the ICI H-P system, and into two of the A/D input analogue voltage channels on the Bath AETC 203 AE system. The ICI crack length monitoring system is capable of recording, analysing and presenting crack length and load data. Plots of load and crack length are produced as a function of time (crosshead

displacement) in addition to automatic calculation of fracture surface energy, G_c and crack speed.

Having mounted the sample into the Instron, two PAC U30D transducers were coupled to opposite faces, 10 mm from the free end of the DCB. Petroleum jelly was used as couplant and a sprung loaded mounting jig gave constant contact load. Transducer 1 was connected via an AETC model 160 (60 dB) preamplifier with integral 0.125-2.0 MHz band pass filters to the AETC amplitude distribution amplifier. Transducer 2 had two functions. Before the start of the test, this transducer was connected to the pulse transmitter module of the AU206 acousto-ultrasonic instrument and used to transmit an AU pulse between the two transducers for the purpose of monitoring coupling quality. During the crack growth test, transducer 2 was used as a second AE receiver. The signal from transducer 2 was passed via an AETC model 140 (40 dB) preamplifier with integral 0.125-2.0 MHz bandpass filters to the AU206 unit where a further 30 dB of gain was used. Both cumulative ringdown counts above a 0.24 V threshold and signal RMS were monitored and recorded onto a chart recorder via the AU206.

To support the weight of the beam and transducers, the free end of the beam was supported with twine. Actual testing was performed at two crosshead speeds to investigate the effect of loading on the type of fracture. These speeds were 0.5 mm/min (low) and 5 mm/min (high).

Post-test, sections were cut from the DCB fracture surfaces, gold sputtered and viewed in a Jeol T330 SEM to assess the type of fracture behaviour, including quantification of fibre breakage.

7.3 Results

7.3.1 *Ensuring Reproducibility of Coupling*

Once the two transducers had been coupled to a DCB, but prior to loading, the quality of the coupling was checked by directing the preamplifier output from transducer 1 to an oscilloscope, while exciting transducer 2 with a -250 volt pulse at a rate of 1 kHz. The peak amplitude of the received pulse was recorded from the oscilloscope and is presented in table 7.1 for each of the DCB samples tested.

It is not strictly possible to compare the coupling test parameters for APC2 and Fiberite/carbon because of the differing degrees of attenuation and thickness of the two types of specimens. However, the results do compare quite closely. There is a high level of consistency with only three samples showing marked deviation from the norm. For samples FRL07 and ARL10, the transducers were attached to the edges rather than the faces of the DCB. This caused a reduced transducer/specimen contact area and an increased wave path length by a factor of between 3 and 5. As a consequence, the transmitted pulse amplitude was reduced. It is interesting to note that sample FRL03 was found to contain a PTFE 'crack starter' strip between the central plies, thereby explaining its reduced pulse amplitude. For the remainder of the specimens the variation in pulse amplitudes was no more than 3 dB which is just over 2 channels on the AETC 203. The contribution of coupling variability to any differences in amplitude distributions between specimens can thus be considered insignificantly small and ignored.

7.3.2 *Acoustic Emission and Crack Growth Behaviour*

Three different variables were investigated for their effect on crack propagation and AE behaviour of DCB specimens. These were:

1. type of matrix (APC2 PEEK/CARBON and Fiberite/carbon, symbols A and F),
2. orientation of crack propagation (interlaminar or intralaminar, symbols E and R),
3. rate of loading (either low, 0.5 mm/min, or high, 5 mm/min, symbols L and H).

DCB specimens fitted with crack gauges were selected and tested to cover all the available combinations of these variables. However, it was found that at the high crosshead speed the rapidity of crack propagation down the full length of the beam, particularly for Fiberite/carbon, precluded the recording of much useful information.

7.3.2.1 Acoustic emission with simultaneous crack length monitoring

Combined load and crack length versus crosshead displacement curves, generated by the ICI Hewlett Packard system, are presented in figures 7.5a-d for APC2 and Fiberite/carbon in the interlaminar and intralaminar crack configurations at the lower crosshead speed.

In each case there occurs an initial near linear elastic load up of the DCB until initiation of crack propagation at the PTFE or folded aluminium insert, which results in a subsequent drop in load.

In the interlaminar configuration, the load decreases smoothly as the crack front moves along the beam. In the intralaminar configuration however, some unstable rapid crack propagation is evident. Once the crack front reaches the start of the crack gauge, crack length data appear on the graphs, continuing for the 50 mm of the gauge length after which the ICI data collection was terminated. The figures above the load line indicate locations at which crack speed and fracture toughness values were determined automatically by the ICI software. These data are summarised later. In spite of the slightly greater beam dimensions of the Fiberite/carbon specimens, significantly higher loads are required to cause crack propagation in APC2 than in the epoxy based composite.

The propagation of a crack along the full length of a DCB generated a very large number of AE emission (hundreds of thousands of events), generating very large AE data files. Unfortunately, the only data analysis system available at the time (AEANAL on Prime

2250) was incapable of handling such large files (there was no such limit with the later RFGGRAPH and RFPLOTS). Consequently, the data collection with the AETC 203 had to be interrupted at several stages during the continuous propagation of the crack down the DCB. AE data for each specimen therefore appear in several files, with the sixth digit of the filename indicating the sequential order with respect to crack propagation. The first three digits identify the test type according to matrix (A - APC2 or F - Fiberite/carbon), crack orientation (E - interlaminar or R- intralaminar) and crosshead speed (L- low speed or H - high speed) in that order, and digits 4 and 5 the sample number.

In figures 7.6 and 7.7 a synopsis of the graphical representation of data gathered by the Bath system is included for an APC2 interlaminar and a Fiberite/carbon intralaminar DCB at low crosshead speed. Four parameters, crack length, load, cumulative events and total event rate are plotted as a function of time, which at a constant crosshead speed of 0.5 mm/min is equivalent to load point deflection. These plots are a magnification in the time domain of the load and crack length data displayed by the ICI plots in figure 7.5.

With reference to figure 7.5a, for APC2 interlaminar crack (AEL04), the crack propagation is stable throughout at a slowly decreasing load. On a finer scale (figure 7.6a) the crack propagation appears less constant. Although the cumulative events/time plot (figure 7.6b) shows a reasonably constant increase in events with time, a plot of event rate (figure 7.6d) shows considerable variation; the AE appears to be generated in bursts, with lulls in between, suggesting that crack growth is in fact discontinuous, or at least varying in speed. The crack gauge plot appears to confirm this observation; short periods of little or no crack propagation corresponding with periods of low emission rate. This phenomenon appears to be common to Fiberite/carbon during 'stable' crack propagation as well (see figures 7.7). Hine ⁽¹¹²⁾ has suggested that crack jumps are caused by crack blunting which causes stored strain energy to build up until there is sufficient for unstable propagation. The mechanisms for the blunting may be local resin

rich regions (in APC2) or local fibre bridging. It should also be noted that crack propagation does not necessarily imply a load drop.

Figure 7.7 includes a crack jump from 18 mm - 38 mm through the crack gauge for Fiberite/carbon intralaminar specimen FRL03 which corresponds to a 11% drop in the load. Examination of the event rate plot demonstrates that there is a peak in emission rate as the crack jumps, followed by a short dwell. It should be noted however, that only approximately 1500 events are associated with a crack jump of 10 mm, compared to typically 13,000 from the subsequent 10 mm of stable crack propagation. It will be shown later that very few events are recorded during much larger crack jumps in APC2.

7.3.2.2 Tabulation of crack growth and AE data

A summary of the parameters derived from AE, crack growth data and scanning electron microscopy of fracture surfaces is given in table 7.2.

For each material/crack orientation/crosshead speed combination there were repeat specimens with multiple measurements recorded at various locations on each sample. Within each major group there was a high level of consistency in AE, SEM and mechanical data, and so mean values have been determined and included in table 7.2. An estimate of the variability of the data is given in each case by a data range (in brackets). Comparisons were consequently made between these means of grouped data.

Columns 2 and 3 in the table are crack speed and fracture toughness (G_c), both determined from the ICI Hewlett Packard system. Good agreement was found by determining time and distances from stable propagation from the AE data files and calculating speed independently. Columns 4 and 5 require some further explanation. The parameter 'fibre breaks per mm² of new crack area' was determined from the SEM study of fracture surfaces of the DCB samples. Various fields of equal area were surveyed and

the numbers of visible fibre breaks were counted. These fibre ends were either individual or part of fibre bundles.

The parameter 'Quasi-energy per mm² of new crack area' (column 5) is defined as:

$$E_{\text{quasi}} = \sum N_i V_i^2 / A \quad \dots 7.1$$

where N_i = number of events with peak voltage V_i
 A = new crack surface area.

This parameter is essentially an event count per unit crack area but with each event's contribution to the total weighted according to the square of its peak amplitude which is reported to be generally proportional to its energy content (161).

Acoustic emission event counts were recorded over various sections of each DCB and were normalised with respect to area of new crack surface produced in generating the events. This was accomplished by determination of crack front position at the start and end of each section of the beam over which AE events were recorded. Multiplication of crack front movement by beam width gave the measurement of the new crack surface area produced. This will not be the true new surface area, because, as is shown later, the crack surfaces are not planar. Crick et al (114) has investigated this point. This value did, however, allow event counts per mm² of gross crack surface to be quoted, removing the effect of different specimen dimensions from the analysis. Event counts in various channel ranges have been included because different event amplitudes appeared to be associated with different fracture processes. AE was more capable of distinguishing between material and crack orientations by selected event amplitude ranges.

One point should be noted. As stated previously, fast fracture produced negligible AE in APC2. Therefore, event counts are only quoted for regions of predominantly stable crack propagation. Regions of the beam containing large crack jumps were excluded, though these are dealt with separately later.

There is considerable scatter in the acoustic emission data, ranges of ± 30 being about the norm. However, with the exception of crack speed, which appears to show little correlation with any other parameter, there are major and significant differences between the different material/crack type groups. Furthermore, good agreement is seen between the trends in AE, broken fibres per unit area and G_c .

Clearly, the PEEK/AS4 carbon fibre composite is considerably tougher than the Fiberite/AS4 carbon fibre composite by a factor of approximately 10. For example PEEK/carbon intralaminar has a fracture toughness of 3.3 KJ/m^2 and interlaminar 1.7 KJ/m^2 . This compares to 0.35 KJ/m^2 and 0.12 KJ/m^2 for Fiberite/carbon. Interlaminar fracture in Fiberite/carbon produces very low AE output (44 per mm^2) whereas intralaminar fracture produces 217 per mm^2 . The corresponding values for APC2/PEEK are 259 and 538 for interlaminar and intralaminar fracture respectively, clearly much greater. The mean broken fibre end count per unit area is also much higher for each material in the intralaminar direction, which agrees with the trend in fracture toughness values.

7.3.2.3 Correlation of G_c /fibre breaks and AE events

The correlations between G_c , fibre breaks and AE events were remarkably good, clearly demonstrating a close relationship between them. These can best be displayed by the scatter graphs in figure 7.8a-d. Fibre breaks per mm^2 has been plotted against events in channels 21-40 and fracture toughness has been plotted against fibre breaks per mm^2 , E_{quasi} and events in channels 31-50 per mm^2 .

The correlation between G_c and fibre breaks would appear to infer that fibre fracture is a major contributor to energy absorption during both interlaminar and intralaminar fracture. The relationship is clearly non linear, and other mechanisms must exist which contribute to energy absorption, for example fibre bridging and matrix cracking. The

parameter breaks/area does not take into account the fibres which had bridged the cracking zone within the tied zone and had been partly debonded prior to fracture.

Hine et al (124) have calculated that actual fibre breakage absorbs insignificant amounts of energy compared to fibre peeling (bridging). This is apparently in contradiction to Champaneria (162) who reported that 0.5 KJ/m² are absorbed by fibre fracture. However, Hine et al (124) suggest that energy absorption resulting from fibre peeling/bridging effects is directly proportional to the number of fibre breaks, contributing approximately 30% of the total energy absorbed in the interlaminar orientation and 55% in the intralaminar orientation. This bridging zone was more extensive in the intralaminar crack orientation than in the interlaminar, and greater in APC2 compared to Fiberite/carbon.

The lower G_c for interlaminar specimens compared to intralaminar should be the result of the well defined resin-rich layer through which the crack can propagate in the former case, this being absent in the latter. This gives a macroscopically planar fracture surface. For APC2 the ratio of the fracture toughness measured in the intralaminar compared to the interlaminar directions is approximately 2, compared to 3 for Fiberite/carbon. This is explained by the fibre distributions shown in figure 7.9a and 7.9b which are metallographic ground and polished sections through 40-ply PEEK/carbon and Fiberite/carbon. During the fabrication of APC2, the higher pressures and flow of the melted PEEK matrix helps to smear the resin rich interlaminar regions, by allowing fibre movement. Fibre misalignment by as little as 2° will reportedly double the fracture toughness (124).

It has been suggested elsewhere in the literature that different event amplitudes may be associated with different micromechanical source events and that the more energetic of these tend to generate more energetic acoustic emission events (72,139,140,141,142,144,146). From an energetic viewpoint, a simple event count per unit area of new crack surface in all channel ranges will not necessarily correlate well with a measure of strain energy

release rate (G_c). The higher amplitude events would clearly be expected to contain more energy than the low amplitude events. Hence the calculation of E_{quasi} which rates events according to the square of their amplitude and which shows a very good correlation with G_c , being able to correctly rate the different material/orientation/speed combinations according to fracture toughness.

It may be argued that the correlation of events in the higher channel ranges with G_c and fibre fractures, and the lack of correlation of events in lower channel ranges, may indicate that there are two main groups of acoustic emission event sources active in these DCB specimens. The higher amplitude, and therefore more energetic, events are generated by the fracture processes which absorb most energy. These should therefore be most closely correlated with G_c . It is also interesting to note that the closest correlation between fibre breaks and AE activity occurs between events per unit area of new crack surface in channel ranges 21-40. This is generally the upper main peak in the amplitude distributions (see later) and infers that the upper peak is caused by fibre fracture/fibre debonding. Furthermore, the absolute numbers of these AE events and fibre breaks are broadly similar.

7.3.2.4 AE amplitude distribution and crack growth

The three main experimental variables of material type, crack orientation and crosshead speed all produced significant variations in fracture behaviour which resulted in differences in the acoustic emission output. These differences, in particular of amplitude distributions, and their possible causes will now be considered.

Figure 7.10 displays the main features of the distributions at comparable positions of the crack front for all categories of DCB. The amplitude distributions, perhaps with the exception of those from APC2 intralaminar specimens, appeared to be composed of two peaks; a mid to high amplitude, near symmetrical peak centred around channels 20-30 and a low amplitude peak around channels 5-12, skewed towards higher channel

numbers. The more obvious differences which exist between the different categories of DCBs may be summarised as follows:

1. The low-amplitude peak is associated with, or at least more dominant in, interlaminar rather than intralaminar propagation.
2. The main (high amplitude) peak for APC2 is broader than for Fiberite/carbon.
3. The main peak for APC2 occurs at a higher amplitude than for Fiberite/carbon.
4. Crack growth in Fiberite/carbon intralaminar DCBs produces a broader high amplitude peak than in Fiberite/carbon interlaminar. The distributions might be confused with that from APC2, however the latter exhibits a much reduced low amplitude peak, allowing them to be distinguished.

These comparisons of amplitude distribution histograms show subjective differences. A more rigorous method of comparison is to calculate numerical parameters which quantify the distributions, and to compare these. Such parameters include the mean (centre of mass), variance (width of the distribution), skewness and kurtosis (how peaked the distribution is) and percentage share of events in selected channel ranges relative to events in all channels (1-50). Average values (with ranges in brackets) of these parameters are presented in tables 7.3-7.5. It should be noted that the ranges of the data are relatively large. This is because the data has been averaged over a variety of different locations relative to the transducer, although the mean distances are similar. In spite of this, obvious differences exist which reinforce the conclusion that AE can clearly distinguish between the various material/crack orientation/loading rate combinations, and that it is closely related to the fracture processes present.

7.3.2.4.1 Effect of crosshead speed

The effect of increasing the crosshead speed from 0.5 mm/min to 5 mm/min in tests on interlaminar specimens produced a very small increase in the fracture toughness (measured over stable propagation) and number of fibre breaks recorded. However, a near order of magnitude increase in stable crack propagation speed resulted, along with

promotion of unstable crack jumps and considerable changes in the acoustic emission characteristics.

The effect of crosshead speed on key AE parameters is demonstrated by table 7.3. The high crosshead speed reduces the total event count in all channels by around 30%, but closer inspection shows that this decrease in events is only in channels 1-30, while a marked increase occurs in channels above 30 (see table 7.2). Percentage share further demonstrates the shift in events towards higher channels. The share of events in channels 30 and above increases on average by at least a factor of 2. The mean event rate of APC2 high crosshead speed DCBs is less than 300 events per second, so saturation of the data acquisition system would not explain the decreased event count. However, superposition of events arriving in close succession may cause the event with the highest amplitude to dominate.

The effect on the amplitude distribution of events is demonstrated subjectively by comparison of the two graphs in figure 7.11 for low and high crosshead speed interlaminar PEEK/carbon. This shows how the main peak in the distributions becomes more clearly defined, more peaked and narrower and moves up the amplitude range.

These changes can be quantitatively demonstrated by the four moments of the distribution shown in table 7.3. The mean amplitude migrates upwards by approximately 7 channels (24-32 for PEEK/carbon and 22-29 for Fiberite/carbon). The relative kurtosis increases by approximately 40%, proving that the distribution is more peaked and the relative skewness becomes more negative demonstrating a greater skewness to the left.

Clearly, the rate of crosshead movement has a profound effect on the AE output from DCBs and must be considered when investigating the effects of material and crack orientation. Smiley and Pipes have also investigated the effect of crosshead speed on G_c in APC2, but over a much greater range (122). They report that the interlaminar strain

energy release rate decreases from 1.5 to 0.35 kJ/m² as the crosshead speed increases from 4.2 x 10⁻⁶ m/s to 6.7 x 10⁻¹ m/s. The behaviour was characterised by a near constant G_c until a critical strain rate was reached beyond which a very rapid decrease was seen. Mall et al (125) report similar behaviour for PEEK/woven carbon fibre produced by film stacking. Gillespie et al (123) have suggested that the explanation of this behaviour lies in plastic and viscoelastic effects in the process zone ahead of the crack tip.

7.3.2.4.2 Comparison of PEEK/carbon with Fiberite/carbon DCBs

The differences between the AE output from the two materials investigated are considerable. These are summarised for intralaminar low crosshead speed fracture in table 7.4. These differences must stem from the approximate order of magnitude increase in G_c of APC2 over Fiberite/carbon. The fracture processes are occurring at higher loads and absorbing considerably more energy. Increased fibre bridging and fibre failure implies that greater numbers of event sources are in operation. This should explain the much greater event count, particularly in the higher channel ranges (31-51) where a factor of between 6 and 10 can differentiate APC2 from Fiberite/carbon.

The amplitude distributions also show some differences. The mean amplitude lies between 2 and 5 channels higher for APC2, demonstrating that, on average, events are of greater energy as a result of more energetic micromechanical fracture processes.

Comparison of figure 7.12a, percentage share versus crack length for Fiberite/carbon interlaminar cracking, with figure 7.12b (APC2 interlaminar) reveals a distinct difference between the two materials. For Fiberite/carbon, the fraction of high amplitude events (40-50) is negligible at all stages. Ranges 21-30 predominate, as before, but the proportion of events in ranges 31-40 is less than in the lower ranges (0-20), whereas in APC2 the 31-40 range is ranked second largest.

7.3.2.4.3 Comparison of interlaminar with intralaminar crack propagation

A comparison of key AE parameters between interlaminar and intralaminar PEEK/carbon fibre DCBs at low crosshead speeds is presented in table 7.5. Intralaminar crack propagation generates significantly more events in all channel ranges, particularly in the highest channels where a factor of 3 for PEEK/carbon and 10 for Fiberite/carbon differentiates intralaminar from interlaminar orientations.

In addition, intralaminar crack growth shows a greater percentage share of events in channels above 30, and a smaller share of events in the lower amplitude channels (<10). This is the result of the relatively smaller (near non-existent in APC2) low amplitude peak in the intralaminar orientation. The lack of this peak helps explain the greater skewness of the distribution to the left, greater kurtosis and lower variance of intralaminar DCBs.

7.3.2.5 The effect of crack front to transducer distance

As mentioned earlier, one of the aims of this work was to determine what effect the distance between transducer and crack front had on the AE recorded.

Firstly, it should be noted that as the crack front moves down the specimen the two beams which make up the DCB become longer, yet the rate of displacement of their ends remains constant. Hence, as shown in figure 7.13, the mean crack speed decreases as the crack front moves towards the transducer.

There was no statistically significant increase in the number of events per unit area of new crack surface as the crack front moved along the beam (towards the transducer). If anything the trend was a decrease. This is somewhat surprising considering the 1.8 dB/cm attenuation determined earlier. E_{quasi} also showed little systematic change. However, the tendency was in this case for an increase with decreasing distance from the transducer, a trend particularly evident in the intralaminar specimens.

The amplitude distributions of all DCB samples with the exception of APC2 intralaminar specimens, appeared to be composed of two peaks which clearly overlapped. In order to trace the effect of experimental conditions on these two peaks, they had to be deconvoluted. This was achieved by assuming that the higher amplitude peak was symmetrical about its peak, the lower amplitude peak consequently being determined by subtraction.

This process has been conducted for three distributions of APC2 interlaminar specimen AEL04 and Fiberite/carbon interlaminar specimen FEL05 at three different progressive locations along the DCB. The distributions are included in figure 7.14. Both materials show similar trends. The higher amplitude peak moves steadily towards higher channels whilst its width narrows. At the same time, the height and number of events (area) associated with the lower amplitude peak relative to the higher amplitude peak increases. The increased significance of the lower peak is particularly evident in Fiberite/carbon.

For the single peak distributions seen in APC2 intralaminar specimens (see figure 7.10c), deconvolution is unnecessary and the changes of the peak may be followed best by plots of the four moments of the distributions against mean distance of the crack front from the transducer. Four such plots are presented for sample ARL10 in figure 7.15a-d. Each moment shows a systematic change with distance of the crack front from the transducer.

The mean amplitude moves from channel 27 to channel 30 as the crack front distance from the transducer decreases by 7 cm (see figure 7.15a), giving an approximate 0.5 dB/cm shift in the peak. This compares with approximately 0.37 dB/cm for the upper peak in interlaminar APC2. The kurtosis of the peak increases (see figure 7.15d) as the crack front moves towards the transducer. The peak becomes progressively more skewed towards lower amplitudes (figure 7.15c).

Further evidence of the shift in the amplitude of events is given by percentage share. The share of events in the highest amplitude ranges (channels 31-40 and 41-50) exhibit an increase as the crack front moves along the DCB, as does the lowest amplitude range 1-10. Events in the range 11-20, corresponding to the region of channel numbers between the two peaks, show a marked decrease.

7.3.2.6 Unstable crack propagation

One of the objectives of the DCB testing was to investigate whether AE emissions occurred only during crack propagation or during crack arrest as well.

As noted elsewhere, the crack propagation in APC2 at the higher crosshead speed in the interlaminar orientation, and at either speed in the intralaminar orientation, showed mixed stable (slow) and unstable (rapid) propagation, the latter being termed crack jumps. This behaviour has also been reported by Smiley and Pipes ⁽¹²²⁾, Hartness ⁽⁹¹⁾ and Leach and Moore ⁽⁹⁶⁾. A good example of this behaviour is shown in figure 7.16. In figure 7.16a, the load and crack position in the crack gauge are plotted against time and in figure 7.16b, the cumulative acoustic emission count and total event rate are also plotted against time. During the first three seconds of the test, the crack is propagating in a stable manner and the event rate is correspondingly high at around 1000 events/second. At 3 seconds into the test the crack jumps 25 mm. There is essentially no peak in the event rate associated with this, in spite of the obviously large drop in load and release of energy. After the jump, the load gradually increases again and crack propagation recommences. One should note that crack propagation recommences and continues during load increase, demonstrating that it is not possible to follow crack propagation by the load trace.

Although the acoustic emission event rate is very low after the crack jump, it does not become zero. Subsequently, the event rate gradually increases in line with the load trace

regaining its approximate 1000 events/second rate as stable propagation resumes towards the end of the test.

Significant numbers of acoustic emissions are thus recorded when there is no gross crack propagation. The amplitude distributions of the events recorded during crack arrest and crack propagation are however quite different. This is demonstrated in figures 7.17a-c, where amplitude distribution histograms are presented over three stages of the test: initial stable propagation, crack arrest (load build up) and final stable propagation. During crack propagation, the distribution may be characterised as a mid to high amplitude, near symmetrical peak with a very small low amplitude peak. Without crack propagation, the mean amplitude is much lower with no clear mid/high amplitude peak and with the mode of the distribution at very low amplitudes.

The shift in the distribution can be further demonstrated by figure 7.18, a plot of percentage share versus time. The share of events in the 31-40 channel range shows a dip during the crack arrest, rising as crack propagation commences, whilst the share of lower amplitude events (below channel 20) shows the converse.

7.3.3 SEM of DCB Fracture Surfaces

Various sections of the DCB fracture surfaces were removed, mounted and sputtered with gold before being viewed in a Jeol T330 scanning electron microscope. Unless otherwise stated, the crack has propagated from left to right in the following micrographs.

Differences exist between the fracture surfaces of Fiberite and PEEK matrix composites, between the two crack orientations and between fast (unstable) and slow (stable crack propagation). The SEM analysis of fracture surfaces further helped to explain the trends seen in mechanical properties and acoustic emission.

7.3.3.1 APC2 interlaminar

Figure 7.19 shows typical areas of stable crack growth in ICI supplied APC2 interlaminar specimens at the low crosshead speed. The PEEK matrix is highly deformed and drawn out. Some carbon fibres are debonded and fractured, although on the whole, the crack has propagated through the matrix, and is consequently fairly planar on a macroscopic scale. Occasional fibre bundles have also been partially debonded and fractured, although these appear few in number. Note that when the crack grows in a stable manner, the fibres on the fracture surface show areas which appear to be almost clean of matrix, the PEEK only being left adhering in a few places, although highly drawn from between the fibres.

There are some areas (small and few in number) where the matrix is largely undeformed and the surface appears relatively featureless as shown in figure 7.20. These areas seem to be local sites of rapid crack propagation (see later) within a specimen which, on a macroscopic level, undergoes only stable crack growth. This would appear to explain the fine peaks and troughs in the acoustic emission event rate during macroscopically stable crack growth. Further credence to this is given by figure 7.21 which shows an interlaminar specimen of APC2 moulded at Bath under standard conditions. This sample showed almost exclusively 'slip-stick' behaviour with propagation by large unstable crack jumps. The PEEK matrix shows little plastic deformation and most fibres remain covered in matrix.

7.3.3.2 APC2 interlaminar high crosshead speed

The difference in fracture surfaces between slow and fast crack propagation is demonstrated very clearly by the photograph (figure 7.22) of an APC2 interlaminar specimen tested at the high crosshead speed, showing two major crack jumps which correspond to the two darker regions. A higher magnification shot (SEM) of the region near to the end of the second crack jump is shown in Figure 7.23a. Three regions can be seen. On the left are two regions of fast crack propagation. Note the undeformed PEEK.

The interface between these two regions of fast fracture is well defined (see figure 7.23b) and is repeated at regular intervals along the unstable region of fracture at intervals of 0.5 mm - 1.0 mm, appearing as 'tide lines' throughout the crack jump region in figure 7.22. The third region (furthest right) is stable, slow fracture. Note the ductile behaviour of the matrix in this region (the right hand portion of figure 7.23c) and again the very clear definition of the interface. This definition is not seen at the start of the fast fracture region indicating that the acceleration of the crack into fast fracture is slower than the deceleration into stable, slow fracture. At this interface the crack will have arrested and subsequently not started to propagate for some time as the load (and thus stored elastic energy) built up again. There appears to be no obvious difference between stable fracture surfaces as seen in APC2 specimens tested at the different crosshead speeds.

7.3.3.3 APC2 intralaminar

In many respects, the fracture surfaces of APC2 intralaminar specimens were very similar to those of the high crosshead speed interlaminar specimens. This is demonstrated by figures 7.24 and 7.25 which show typical areas of stable and unstable crack growth respectively. In the former, the matrix is highly plastically deformed and drawn out from between the closely packed fibres. Note the featureless areas of what appears to be clean (free of matrix) fibre surface. Long lengths of debonded fibres, fractured fibre ends and fibre bundles are evident. In the latter, the matrix appears to have fractured in a brittle fashion and most fibres remain matrix covered. As shown in figure 7.25, small groups of fibres have debonded prior to fracture (even in regions of unstable crack growth).

In spite of the similarities between interlaminar and intralaminar fracture surfaces, certain differences were evident. The fracture surfaces of intralaminar specimens were much less planar, the crack not having a well defined plane (such as between laminates in interlaminar specimens). Comparing regions of stable crack growth, intralaminar fracture exhibits a greater proportion of debonded (peeled) and broken fibres and fibre

bundles than interlaminar. The peel length of fibres/fibre bundles varied considerably, reaching 30 mm - 40 mm in some instances.

7.3.3.4 Fiberite/carbon interlaminar

The presence of an epoxy matrix in place of the thermoplastic PEEK matrix results in quite different fracture surfaces. Figure 7.26 is a typical region of an interlaminar specimen. There were no regions which could be designated as areas of either fast or slow crack propagation. All areas appeared similar. Note the featureless areas which appear to be the Fiberite matrix which has undergone a brittle cleavage type of fracture. There appears to be almost no deformation of the matrix prior to fracture. Few carbon fibres can be seen indicating that the crack has run through a matrix rich zone (interlaminar zone). Some fibres have partly debonded, however the long lengths of debonded fibres seen in APC2 are not present in these specimens. As is seen in APC2, the carbon fibres usually remain covered in matrix.

A fractured fibre bundle is shown in figure 7.27. This is not a common occurrence in Fiberite/carbon interlaminar specimens, but bundle failure obviously does occur and may thus be another contributor to the various failure processes seen in the fracture of these specimens.

7.3.3.5 Fiberite/carbon intralaminar

Intralaminar Fiberite/carbon specimens show (according to the ICI crack length versus time graphs) regions of stable/slow crack growth and regions of fairly rapid crack growth. There was no obvious difference between regions of faster or slower crack propagation, all appearing similar to that shown in figure 7.28. Debris, presumably fractured matrix, is scattered over the surface.

Fiberite/carbon intralaminar DCB specimens show a greater proportion of fractured fibre bundles and individual fibres than do interlaminar samples, though the brittle cleavage

type fracture of the epoxy matrix is common to both. The fracture surface in the intralaminar specimens is far more uneven on a macroscopic scale, as found with APC2.

7.4 Discussion/Conclusions

The combination and interfacing of the Bath AE system and the ICI crack length/fracture toughness system has been accomplished successfully and this has yielded some very interesting results.

The fracture propagation studies of cracks and AE in DCB specimens have demonstrated that APC2 shows an approximate order of magnitude improvement in interlaminar and intralaminar fracture toughness, G_c over an epoxy/carbon fibre. This difference has been demonstrated by SEM which has shown the far greater ductility of the PEEK matrix, increased fibre and fibre bundle fracture and fibre pull out in APC2. The much greater AE event count and the greater proportion of high energy, high amplitude events further reinforces this point.

For comparison, the values of interlaminar fracture toughness, G_{1C} determined by Leach and Moore⁽⁸⁶⁾ for various thermosetting composites are included in table 7.6.

Crack propagation in APC2 in the interlaminar and intralaminar orientations, particularly at higher crosshead speeds, shows a combination of fast, unstable (crack jumps) and slow, stable propagation. The former is characterised by relatively brittle fracture of the PEEK matrix and the latter with highly ductile deformation and tearing of the PEEK matrix. Hartness⁽⁹¹⁾ has also observed such behaviour and termed slow crack growth as ductile fracture and fast crack growth as cleavage. Smiley and Pipes⁽¹²²⁾ suggest that APC2 shows three modes of crack propagation, depending in part on the loading rate. These are ductile stable, brittle unstable and brittle stable. Leach and Moore⁽⁹⁶⁾ have determined a G_c for interlaminar crack growth to be 2.4 KJ/m² and 2.1 KJ/m² for slow and fast crack growth respectively, slightly greater than the values recorded at Bath.

According to Barlow and Windle ⁽⁹⁸⁾, when cracks propagate rapidly, during unstable crack growth or in impact tests, fracture surfaces of all materials tend to look the same. Fast cracks usually run within the resin, rather than following the fibre-matrix interface even if it is weaker, and little resin ductility is apparent. During slow crack propagation, the crack should run along the lowest energy path. If the fibre-matrix interface is weak, then this path will be largely at this interface, giving a fracture surface characterised by clean fibres. A strong interfacial bond will tend to give fibres still covered in matrix.

The acoustic emission event rate was found to be at a maximum during stable propagation and a minimum during major crack jumps, during which essentially no events were recorded in APC2.

The amplitude distributions recorded from both Fiberite and PEEK matrix composites and in both interlaminar and intralaminar orientation were composed of two peaks; a narrow, lower amplitude positively skewed peak centred around channel 5-12 and a mid to high amplitude near symmetrical peak centred around channels 20-30. The low amplitude peak is insignificant in intralaminar APC2 DCBs. Analysis of these distributions would indicate that the higher amplitude peak was probably associated with fibre fracture processes (fibre fracture and fibre debonding/bridging), processes which absorb most energy.

Acoustic emission has been capable of distinguishing between PEEK and Fiberite matrices, interlaminar and intralaminar crack propagation directions and low and high crosshead speeds. These distinctions have been achieved by the shapes of amplitude distribution histograms, the share of events in selected ranges and by simple event counts per unit area of crack growth and energy content of the acoustic emission recorded. Good correlation has been found between G_c and fibre breaks per unit area of new crack surface with both normalised event counts in selected channel ranges and AE energy content.

It has also been demonstrated that crack front arrest after a rapid crack jump does not cause a cessation of acoustic emission activity, only a reduction in event rate. However, amplitude distribution analysis can clearly indicate gross crack propagation, differentiating it from crack arrest.

CHAPTER 8

CORRELATION OF ACOUSTIC EMISSION, ACOUSTO-ULTRASONICS AND MECHANICAL PROPERTIES OF APC2

8.1 Introduction

Both the acoustic emission output and acousto-ultrasonic parameters determined from nominally identical APC2 can vary considerably. The question may be asked whether all or part of these variations are totally random or whether they are the result of the intrinsic variation in material structure or properties. It may be hypothesized that part of the variation in AE and AU output is the result of, and will therefore correlate with, some variation in the mechanical properties of nominally identical specimens. Further, if acoustic emission and acousto-ultrasonics are valid and useful means of NDT, then they should be sensitive to the material's response to stress or strain. Consequently they should also be sensitive to changes in measured mechanical properties.

This chapter covers a body of work that seeks to cross-correlate AE and AU with measured mechanical properties from replicate, nominally identical APC2 specimens tested in four point flexure.

8.1.1 The problem

It has been shown above that standardised test conditions are essential to achieve even moderately consistent results. The effect of altering specimen dimensions, modes of stressing (for AE), specific piezoelectric transducers used and instrument settings is to produce changes in results which can far outweigh the more subtle effects of the APC2 under investigation. Even when test parameters are kept constant, there remains a considerable variation from nominally identical specimens in both AE output and AU SWF and RMS.

From an extensive investigation of the test equipment used, it has been established (though results are not included) that these apparently uncontrolled variations were not a result of fluctuations in the mechanics or electronics of the apparatus. Therefore it must be concluded that they arise from two sources:

1. intrinsic variation of the material,
2. coupling of AE/AU transducers to specimens.

With reference to the specific case of acoustic emission and point (1) above, this problem of uncontrolled/unexplained variation can be illustrated with reference to figure 8.1. In figure 8.1a are the load/time plots for four nominally identical APC2 specimens tested in four point flexure. In figure 8.1b, the corresponding events in channels/time plots are included, and in figure 8.1c the amplitude distribution histograms for events recorded to failure (shaded region indicate the range of the data). Clearly, the failure load and deflection, which translates into variation of strength and strain, vary considerably, as do the number and rate of events. The question of whether these are related remains to be addressed.

Uncertain quality of coupling is the other probable source of AE variation. For AE events to be received, they must pass across the specimen to transducer interface, a process which involves incomplete transmission of stress wave energy. The interface effectively attenuates the signal. It has been shown earlier that the variation in the quality of the coupling can cause the received amplitude of an event to vary by up to 7.2 dB, corresponding to 6 channels on the AETC amplitude distribution system. This will profoundly affect total event counts because of the large skew of the distribution towards higher channels; lower amplitude events may fall below threshold and not be detected.

The program of investigation has been to determine, and if possible quantify, the effect of these two sources of variation: the effect of material variation on AE, AU and measured mechanical properties and the effect of variation in coupling quality on the AE

output from stressed APC2. The interactions of these factors have subsequently been investigated by cross-correlation studies, with a statistical rank correlation test.

8.1.2 Aims

There were four principal aims of this investigation:

1. To quantify the spread or scatter in the four point flexural mechanical properties of APC2.
2. To monitor AE on tests with two similar amplitude distribution systems:
 - a) to correlate the AE events and their amplitudes from the two systems,
 - b) to determine whether some part or characteristic of the amplitude distribution is sensitive to basic mechanical properties such as failure stress or elastic modulus.
3. To determine whether AU type testing can be used to monitor the quality of coupling of AE transducers to specimens.
4. To test whether optimised AU testing with SWF and RMS parameters correlates with flexural properties of APC2.

8.2 Experimental

A flow diagram of the methodology for this testing is included as figure 8.2. The previously adopted standard lay-up of 16-ply UD APC2 was retained for this investigation. Strip specimens, nominally 16 mm x 2 mm x 220 mm, were cut with a water cooled diamond impregnated saw from 16-ply UD APC2 plates moulded with the in-house facilities at the University of Bath. These plates were C-scanned at ICI, Wilton prior to cutting and any possibly defective areas were set aside as scrap/defective material. The width and thickness of each specimen were measured to an accuracy of ± 0.005 mm at five positions over the portion of the specimen which would comprise the stressed span.

8.2.1 Acousto-Ultrasonic Measurements SWF and RMS Voltage Measurements

Acousto-ultrasonic measurements of both SWF and quasi-RMS parameters, with both the pulse and burst mode of pulse excitation, were made at two positions encompassing the specimen beam span prior to mechanical stressing. An FC500 broadband emitter transducer and AC375 resonant receiver transducer were used. A mounting jig held the transducers 85 mm apart and coupling was with petroleum jelly and 10 N per transducer coupling force.

A variety of instrument setting combinations were used, spanning the available ranges. This included optimised test conditions determined earlier. The mean value of the six repeat measurements was used as the representative AU SWF or RMS voltage value for each sample. Full details of AU measurements have been given in chapter 3 which includes determination of the sensitivity of AU to the introduction of defects into these APC2 strip specimens.

8.2.2 Monitoring the Quality of the Coupling

After AU testing, the sample was transferred to the four point loading rig in an Instron 1195 testing machine.

Three AE transducers were coupled to the upper surface of the specimen with petroleum jelly couplant and a spring clip constant load device (isolated from transducer and specimen by layers of a compliant rubber). The arrangement of strip specimen, supports and AE transducers is shown in figure 8.3. The disposition of transducers on all repeat specimens was the same. All three transducers were PAC U30D wideband piezo-electric transducers nominally resonant at 300 kHz. At this stage no load was applied to the specimen.

From results presented earlier on acousto-ultrasonics, it is evident that variation resulting from coupling is considerable and is largely associated with the receiver transducer,

whenever thin film coupling techniques must be used. Thus, an acousto-ultrasonic approach may be used as a test of the coupling. The obvious signal parameter to monitor is pulse amplitude, though amplitude, ringdown count and RMS voltage all show broad proportionality.

Firstly, transducer III (middle transducer in figure 8.3) was connected to the pulser module of the AU206 and repeatedly pulsed (2000 per second) with a 6 microsecond duration, -50 volt spike. This repeated stress pulse was received by the other two transducers (I and II) and amplified through their respective preamplifiers. The received pulse amplitude and the RMS of the repeated pulsed signal were monitored with an oscilloscope and digital RMS meter respectively. This was repeated for a second excitation signal (10 microsecond duration square wave signal pulse of 300 kHz frequency) termed the 'burst' mode. In an identical manner, pulses were propagated from transducer II to I so that each transducer had values of received pulse amplitude and RMS associated with them, which should rank specimen/transducer coupling according to quality.

8.2.3 Flexural Testing and AE Monitoring

After completion of pre-test coupling checks, the specimen was loaded to failure in four point flexure with associated acoustic emission monitoring. This testing configuration, 36 mm inner/108 mm outer span, (long beam four point flexure) was retained for this investigation since it gave a good combination of large stressed volume and no grip noise. 15.5 mm diameter steel roller beam supports were used and greased to prevent frictional noise. A constant crosshead speed of 5 mm/min was used.

Transducers I and II were used for simultaneous monitoring of AE during loading with two separate amplitude distribution systems, termed the AETC and the Marandy systems. Transducer I was connected to the AETC 203 amplitude distribution unit, whilst transducer II was connected to a Marandy 25 channel amplitude sorter. Both

instruments operated under the same software and computer hardware (DCOL and Minc PDP 11 computers), the main difference being that the Marandy had 25 channels, 2.4 dB wide whilst the AETC 203 had 50 channels, 1.2 dB wide. The main elements of the respective systems are listed below:

	Transducer I	Transducer II
Distance from centre of specimen	105 mm	105 mm
Transducer type	PAC U30D (300 kHz, ceramic shoe)	PAC U30D (300 kHz, ceramic shoe)
Preamplifier	AETC 60 dB	AECL 60 dB
Bandpass filter	0.125 - 2.0 MHz	0.125 - 2.0 MHz
Amplitude sorter	AETC 203	MARANDY
no. of channels	50	25
channel width	1.2 dB	2.4 dB
minimum instrument threshold	10 mV	10 mV

23 nominally non-defective specimens were tested to failure in flexure, together with a further 7 samples cut from the scrap/defective areas of the original large moulded APC2 plates. Various hardware faults prevented the completion of the full population (50 samples) of tests originally envisaged, however results are presented for all tests completed.

For each specimen various parameters characterising mechanical response were determined, the most important of which are listed below.

1. Flexural failure stress
2. Failure load
3. Flexural failure strain
4. Failure deflection

5. Flexural elastic modulus
6. Compliance
7. Secant modulus at failure
8. (Failure load)/(failure deflection)
9. Total area under load-time graph (stored elastic energy)
10. Deviation of area under load-time graph from linear elastic
11. Specimen width (width of beam)
12. Specimen depth (depth of beam)
13. Specimen cross-sectional area

These, in addition to mean values of specimen dimensions, were termed mechanical property parameters. Various acoustic emission parameters were also calculated for each specimen. These AE parameters were defined arbitrarily, but based on theories and trends observed from previous acoustic emission work on APC2 at Bath and from the literature. They were, for example, event counts in chosen channel (amplitude) ranges, moments of the amplitude distribution histogram produced within chosen load, deflection or stress levels and AE delay parameters after Williams and Lee ⁽¹⁶³⁾. The AE parameters may be grouped into sets in the following manner.

1. Numbers of events in chosen channel ranges within chosen load and time levels.
2. Numbers of events in chosen channel ranges within chosen stress and strain levels.
3. Events just prior to failure and including failure.
4. Percentage share of events in chosen channel ranges within chosen load and time levels.
5. Percentage share of events in chosen channel ranges within chosen stress and strain levels.
6. AE delay parameters.
7. Moments of amplitude distributions for selected load and time intervals

In addition to these acoustic emission parameters, parameters involving pre-test coupling values (to equate for variations in coupling) were also used in the cross correlation procedure. All acoustic emission parameters and acousto-ultrasonic SWF and RMS voltage values were tested for their possible correlation with all mechanical property parameters. The correlation test deemed most suitable for such testing was Spearman's rank correlation test.

This test method is performed on paired values contained in two columns. The values in each column are ranked according to magnitude and assigned a rank according to position in the column. The difference between ranks for each half of a pair is determined, squared and the sum of all squared differences substituted into the equation

$$r = 1 - \frac{6 \cdot \sum d^2}{n^3 - n} \quad \dots 8.1$$

where r is the Spearman's rank correlation coefficient and n the number of pairs. A correction factor was used to adjust r for tied ranks. The rank correlation coefficient lies between -1 and +1 (and is subject to the sample population magnitude for significance at confidence limits), -1 being a perfect inverse correlation (negative slope), +1 being a perfect positive rank correlation (positive slope). For any monotonic correlation, Spearman's test will give a large value of r .

Any mechanical property/acoustic emission correlation significant well above the 99% confidence level was plotted out as a scatter diagram and further regression analysis for best line fitment conducted if deemed useful to do so.

There were many hundreds of possible paired combinations of mechanical properties and acoustic emission parameters which may have correlated, involving hundreds of thousands of calculations. Software was therefore developed, named RFSPEAR, which would allow input of the appropriate data onto disc, then conduct multiple rank

correlation and linear correlation tests and the subsequent graphical presentation of data. Originally written in BBC Basic, the software was later transferred and converted to run on the IBM MSDOS system, with a compiled basic (TBASIC).

8.3 Results

Of the 23 'non-defective' samples which have been tested to failure, one sample delaminated, failing close to the neutral axis. All other samples fractured in 1 or 2 locations close to the central loading supports. Failure was thought to be initiated by compressive fibre buckling near to the central supports which apparently cause some stress concentration.

8.3.1 Correlating AU parameters with Four Point Flexural Properties

Correlation of acousto-ultrasonic SWF and RMS voltage values with flexural mechanical properties was generally disappointing. The only parameter to show any indication of sensitivity to the APC2 samples was pulse RMS at high gains (80 dB), energy E1. This AU-RMS parameter showed good correlation with specimen thickness, failure load and elastic modulus (measured in flexure).

Figures 8.4a and 8.4b are scatter diagrams of AU RMS plotted against specimen thickness and failure load (respectively) for 16-ply UD APC2 strip specimens. It is probable that the major contribution to the variation in failure load is caused by the variation in specimen thickness, and that the AU RMS parameter is predominantly sensitive to specimen thickness; a decrease in plate thickness producing a lower received RMS voltage. This may be the result of changes in the main resonant frequency associated with plate thickness. The degree of sensitivity of this parameter to small variations in specimen thickness (and hence to failure load) is quite remarkable in comparison with the insensitivity of any SWF parameter.

Some indication of AU RMS showing sensitivity to flexural elastic modulus is shown in figure 8.4c. There is considerable scatter in the data, but the trend of increased elastic modulus with decreased stress wave attenuation is plausible, if not expected.

8.3.2 Monitoring Coupling Quality

Both the maximum amplitude and the RMS voltage of the two types (burst and pulse mode of excitation) of repeated 'pre-test coupling pulses' were recorded. With reference to figure 8.5, in which RMS voltage reading is plotted against peak amplitude, it may be observed that these two parameters are proportional. There was a similar proportionality between pulse and burst mode. It is therefore sufficient to choose one characteristic of the 'pre-test coupling pulse' as a proposed measure of coupling quality, the most obvious being peak amplitude, which has most relevance to the AE testing. Data for pulse mode, peak amplitude are included in columns 2 to 4 in table 8.1, for propagation between the three pairs of transducers. Columns 5 and 6 give cumulative event counts until just prior to failure for each AE system used.

Systematic differences exist between the peak amplitudes of the pre-test pulses from different transducer combinations because of the differences in sensitivities, inter-transducer separations and preamplifiers.

The 23 specimens are separated into two groups. Specimens 1 to 14 show generally consistent coupling pre-test pulse amplitudes and cumulative event counts in the range 4 to 350. Specimens 15 to 23 show pre-test pulse amplitudes significantly higher, in some instances an order of magnitude greater, with a corresponding increase in cumulative event count by a similar proportion. The magnitude of the variation of both pre-test pulse amplitudes and event counts was greater than expected from previous experimentation. Hence a second factor, possibly specimen attenuation may be involved in addition to coupling quality. However, it is clear that in order to be justified in assuming generally

consistent coupling, only specimens 1 to 14 must be selected for inclusion in subsequent AE and mechanical property correlation investigation.

8.3.3 Comparison of the Acoustic Emissions from Two Systems on the Same Specimen

It would be assumed that all other factors being constant, the acoustic emissions recorded from the same specimen, with two similar AE systems simultaneously, should yield similar results. The data collected from the AETC and Marandy AE systems were therefore compared at various load increments during the tests in order to determine the extent of systematic differences caused by transducers/preamplifiers, and the extent to which pre-test coupling monitoring can reduce residual differences.

Before direct comparison, consideration should be given to any systematic differences between the two AE systems. The frequency response of both transducers was very similar, though transducer I showed a 6% increased peak voltage output for an artificially produced standard AE pulse in the mid amplitude range. The AECL preamplifier (Marandy system) produced a slightly larger amplification than the AETC preamplifier, in spite of both being rated as 60 dB. It was confirmed by testing that apart from relatively minor inaccuracies in channel widths in the AETC unit, both amplitude distribution systems correctly sort received events into the appropriate channels. In short, AE system II (Marandy) showed an overall greater sensitivity, and therefore in all cases, a greater number of events for a fixed instrument threshold (22.9 mV).

A comparison of the event counts recorded from the two systems may be made from figures 8.6a through 8.6e which are plots of cumulative events recorded by the AETC system against those by the Marandy system up to successively higher load levels. It is evident that there is a linear relationship between the two event counts, but the scatter in the data decreases as the load range (and hence the numbers of events) increases. The goodness of fit of the data to a straight line was quantified by determining the linear regression coefficient, R , at each load level. Results are presented in table 8.2, along

with mean cumulative event counts. R increases from 0.58 at low loads up to 0.95 just prior to failure. Whether this increase in R is simply the result of the greater event counts at higher loads, or whether the few events recorded at low loads are more often the result of noise, rather than genuine micromechanical deformation within the specimen remains unresolved. Clearly a significant number of events and/or a sufficiently high load level must be attained before good agreement is achieved between the two AE systems.

8.3.4 Correlation of AE with Mechanical Properties

The amount of variation of mechanical property parameters from nominally identical APC2 strip specimens may be seen from table 8.3 in which the mean, standard deviations, maxima and minima are presented. The coefficients of variation can range from as little as 0.04 for specimen thickness up to 0.15 for deflections to failure, clearly quite large variations. The distribution of the results varied, some showing an essentially normal distribution, for example failure stress shown in figure 8.7. Others showed a marked skew, for example specimen compliance shown in figure 8.7b. The variations of acoustic emission parameters was generally much larger, with coefficients of variation up to 1.2.

The most statistically significant correlation found by Spearman's rank correlation test was between a measure of specimen compliance (the deflection at a load of 1000 N) and the number of events recorded in low amplitude ranges (channels 1 - 6) in an intermediate load range (200-800 N), and is shown in figure 8.8a. Curve fit regression gave a regression coefficient of 0.942, clearly a very good fit.

Having discovered this correlation, it was then necessary to attempt to determine its cause. As expected, it was found that the compliance showed a very high inverse linear correlation with the cube of the specimen depth, demonstrated by figure 8.8b. A scatter plot of specimen depth cubed against the previously mentioned AE parameter (see figure 8.8c) demonstrated that the correlation with compliance appeared to be the result of

specimen depth variation. This effect was magnified by the cube relationship between depth and compliance. For such small variation in specimen dimensions to cause such a large variation in numbers of events was unexpected and could not be easily explained. The question of exactly what caused the variation of the AE parameter remains unsolved).

Two other highly statistically significant correlations determined between the AE and mechanical response of APC2 are shown in figures 8.9a and 8.9b. These figures are scatter plots of failure stress and failure strain against cumulative event counts in all channel ranges to failure. The greater the stress or strain sustained prior to failure, the greater the number of events recorded. Correlations of this sort are of limited use in the application of AE to NDT, where AE parameters associated with a specific proof load or proof stress are required.

An example of a 'pre-failure' AE parameter which showed good correlation with failure stress and strain, and could thus be used as a predictor of such parameters is shown in figures 8.10a and 8.10b. The AE parameter is the number of events in the low to mid channel range (channels 7 - 10) recorded within an intermediate time range, 40 - 140 seconds, which relates to crosshead displacement range. The apparent correlation appears good, although the actual numbers of events involved is very small, varying from 0 to only 17 events. However, the trend is similar to that seen between cumulative event count to failure and failure stress or strain, namely more events for stronger specimens.

These AE/mechanical property correlations appear to be in antithesis to the results of defective/non-defective specimen comparisons with AE presented earlier. These indicated that grossly defective specimens, which were weaker, were found to produce generally more events. A model for the AE behaviour of APC2 must be based on two factors. The first is that of intrinsic strength: the stronger the specimen, the greater the

stresses achieved in the specimen prior to failure. As a rule, the event rate in APC2 always broadly increases with increasing load (stress) during the typical test using constant crosshead speed and monotonically increasing load. In broad terms, higher stresses in the composite cause more events. To what extent this is the result of the greater overall energy content in a more highly stressed material, or the statistical probability of increasing numbers of fibre failures, is unclear. The second factor is the increase in events caused by overt defects. The defects will cause local stress concentrations and misalignment of fibres which will generate acoustic emissions as the material locally begins to fail at lower stresses than the bulk, non-defective material.

It is apparent from this model that considerable problems may be associated with detection of subtle defects in APC2 by a proof test with AE monitoring. This is because a relatively larger event count in a particular specimen may be the result of either an intrinsically stronger specimen or the presence of a weakening overt defect.

8.4 Discussion/Conclusions

In chapter 3 it has been shown that no statistically significant difference exists between mean SWF or RMS voltage measurements made before and then after introduction of 3 types of defect (drop weight impact, 3.0 mm drilled hole and indentation/crush damage) into the 16-ply UD APC2 strip specimens. The SWF was also found to be insensitive to any mechanical property or specimen thickness variation for these specimens. However, the positive correlation of RMS voltage with small variations in thickness (and hence failure load), in addition to elastic modulus, is encouraging considering the otherwise negative results presented earlier. An increased RMS voltage in a sample, which is stiffer and can sustain a higher load before failure, may be explained by improved stress wave transmission associated with improved fibre alignment and fewer defects; essentially a more perfect structure. An increased RMS voltage with increased specimen thickness has also been demonstrated on a larger scale by measurements on UD APC2 of different numbers of plies (range 1 to 40 plies).

The literature states that a reduced quality of material (resulting from the presence of defects such as porosity, poor fibre/matrix adhesion or low fibre volume fraction) will cause an increased attenuation of the AU pulse. Conversely a decreased ability to transmit stress pulses would also imply a decreased ability to sustain stress. RMS voltage, which gives an integrated measure of the contribution of waves propagated throughout the thickness of the thin APC2 plates, is not directly affected by the shape of the received pulse envelope as is SWF. However it has been stated to be generally proportional to the SWF. In this case the proportionality is not so good.

It has been demonstrated that the AU system can be used as a simple means of reducing the scatter in AE results by identifying those results which arise from large variations of the coupling of AE transducers to specimens from the norm. The test is clearly not only a coarse check of coupling quality, but will be affected by variations in specimen attenuation.

Comparison of the AE recorded from two similar systems connected to the same specimen has been carried out. The comparison has demonstrated that a significant number of events and/or a sufficiently high load level must be achieved before good agreement is achieved between the two AE systems.

The correlation of mechanical properties with the AE response of nominally identical APC2 specimens has produced some interesting results. The AE response is very sensitive to small changes in specimen thickness. There is good correlation between the failure strain and stress and numbers of events. AE parameters based on events in selected channel ranges, recorded within selected pre-failure displacement ranges, show good correlation with failure stress and strain. This is particularly important since it provides evidence that the proof testing of APC2 components with associated AE monitoring may be a valid method of strength estimation, essentially NDT. This conclusion must be tempered by the fact that the results are based on small absolute

numbers of events, and quite high deflections at which permanent, significant damage to the material may be occurring.

In conclusion, the results presented have demonstrated that the intrinsic variability of mechanical properties, acoustic emission and acousto-ultrasonic parameters from nominally identical APC2 are not completely random and do show statistically significant interrelationships.

Chapter 9

FINAL DISCUSSION

Two non-destructive testing techniques, acoustic emission and acousto-ultrasonics, have been applied to a new fibre reinforced thermoplastic (APC2). Both techniques have shown some value as a means of NDT of APC2.

At this point, it is perhaps worth contemplating the similarities and differences of the two NDT techniques. In both techniques, ultrasonic waves (stress wave pulses) are propagated through a material and are detected with acoustic emission transducers (high sensitivity sensors) and with acoustic emission types of signal processing. In AE however, the events or emission pulses are produced spontaneously by micromechanical deformation processes resulting from the external application of stress (the response of a material or structure to stressing). This compares with AU where a standard, controlled, artificial event or pulse is injected into the material.

In AE the source events are of varying type and the technique seeks to characterise the processes which produce the stress wave pulses. On the other hand, AU seeks to characterise the response of the material to the propagation of a fixed type of stress wave. AU characterises the modulation effects of the material on a standard repeated pulse. The same modulation effects must exist for true AE events, however they are usually ignored in AE because it is so difficult to account for them. This is particularly the case for composite materials.

In acousto-ultrasonics each event is nominally the same as the previous one, whilst in acoustic emission each event is different. Thus in AE statistical analysis of the variation in event characteristics may be undertaken as part of the NDT process. Since AU uses a standard source event, somewhat more involved and sophisticated methods of signal processing such as digitisation and fast fourier transform analysis can be utilised to

distinguish frequency ranges. In AE on the other hand, the normally large population of received events has tended to preclude this, although the recent development of very fast and inexpensive microprocessors is beginning to reverse this trend.

Although AE is termed NDT, it may be argued that the technique can not be truly non-destructive and benign, since material must be stressed to produce non-elastic micromechanical deformations which release stress waves. Since these deformations are typically non-reversible, some permanent change must have been made to the test article. However, AE can be no less non-destructive than any pre-service proof test. In AU, the pulses are benign, and generate only elastic deformation, assuming the stress wave amplitudes do not exceed the yield or fracture strength of bonds within the test material.

Both AU and AE are capable of yielding parameters sensitive to the overall integrated damage state, thereby evaluating the integrity of a structure, including its response to flaws. This is in contrast to other techniques which simply detect the presence of such flaws, the effect of which on service life is often uncertain. In practice, both techniques suffer from considerable experimental scatter and this is one of the major factors limiting the success of their application to NDT of APC2.

The investigation of both techniques has involved studying system hardware, instrumentation and experimental variables with a view to optimising the technique towards NDT of APC2. Subsequently, both techniques have been applied to defective/non-defective material comparisons.

A base line of AE data has been established for APC2 stressed in various methods including long beam flexure, tension and torsion. The acoustic emission testing has shown that APC2 is a quiet material when stressed in flexure, although this appears to be a common feature of high quality carbon fibre reinforced epoxies. Glass/polyesters for example are generally much noisier prior to failure. Failure in normal flexural tests on

APC2 is sudden and catastrophic. It is probable that many true AE events are recorded as one at failure, because of the dead time limitation of event counting rate. The double torsion and DCB tests tend to reinforce this view. When gross crack propagation is slow, many thousands of events are recorded.

Acoustic emission has shown mixed results when applied to the detection of various moulded-in defects, some being detectable, some not. However, since these defects made little difference to the flexural properties, perhaps this should not be seen as a failure of AE. Rather it is a good indication that APC2 has a high resistance to the weakening effects of flaws, particularly those introduced prior to moulding. It should be noted that Nixon et al have demonstrated that AE can detect impact damage above a critical level in APC2 (77).

This ability of APC2 to resist the effects of flaws and its high interlaminar and intralaminar fracture toughness are significant in the consideration of the quiet AE behaviour of APC2 prior to gross crack propagation (failure).

The initial stages of composite failure (which will generate AE events) involve three main modes and usually complicated interactions of the three. These modes are:

1. tensile/shear/compressive failure of the matrix,
2. fibre/matrix interface failure,
3. tensile or compressive failure of fibres.

Failure of a composite, particularly those including the less tough thermosetting matrices, may not necessarily mean gross fracture, but property degradation, for example reduced flexural modulus resulting from delaminations and inter-ply matrix cracking.

The tough and ductile PEEK matrix and the good fibre/matrix bond strength would point to modes 1 and 2 above being of considerably less importance in APC2 than in many other noisier composites. Pure PEEK samples tested in tension and flexure produced almost no events. DCB specimens of APC2 produced significantly higher event counts

than an epoxy based composite, probably because APC2 exhibited much higher fibre bridging and fibre fracture.

During a three point flexural test with monotonically increasing load/displacement, there is typically a small amount of activity during initial application of load. This is followed by a gradual increase in event rate to a maximum at failure. Since the matrix is a tough and ductile thermoplastic which is well bonded to the fibres, AE activity from matrix cracking and fibre debonding prior to total failure will be very limited. The source of these events must therefore be fibre failure.

The strength of carbon fibres depends upon the distribution and magnitude of flaws (caused either during fabrication or as a result of poor alignment of the graphite layers along the fibre length). Assuming little AE activity originates from matrix cracking and fibre debonding prior to final failure in APC2, it would follow that AE events produced at the early part of a bend test were caused by the failure of weak or badly aligned fibres. The build up of events close to failure is a result of the stress reaching the critical strength (failure strength) of more fibres, which thus fail until the remaining fibres can no longer sustain the stress and the whole composite fails.

Energy absorption theories developed to explain toughness in conventional thermoplastic matrix composites, for example the Cook-Gordon mechanism ⁽¹⁶⁴⁾, appear to be contradicted in APC2. A relatively weak fibre/matrix bond is needed in thermoplastic composites for high toughness, yet APC2 exhibits a very strong fibre/matrix bond.

The Cook-Gordon mechanism ⁽¹⁶⁴⁾ suggests that when a crack propagating through the resin phase meets a fibre, it is deflected along the interface, debonding the fibre, and energy is absorbed by the creation of new surface area. When a site of weakness in the fibre is exposed, the fibre breaks and is pulled out of the tube, with friction absorbing more fracture energy. Hence a weaker interface would infer a tougher composite. This

mechanism appears to work well for thermosetting composites ⁽¹⁶⁵⁾, but does not apply to APC which exhibits a large improvement in toughness over epoxies, yet has a strong fibre to matrix bond. The bond is so strong in fact that fracture surfaces are characterised by fibres or bundles of fibres broken together and still coated with resin. An alternative mechanism of toughness would have to be based on the following factors. Firstly the plastic zone size of the PEEK, which is large relative to the typical thickness of the matrix between fibres in APC2. And secondly, the good fibre/resin adhesion which would suggest that a crack propagating through the composite would have to break fibres where the crack meets the fibres. Statistically, fibres will be inherently stronger over short gauge length. The effective gauge length becomes longer in the case of debonded fibres.

Although acoustic emission had difficulty in detecting some specific moulded-in defects, correlations have been demonstrated between acoustic emission parameters and the intrinsic variation of failure stress and strain in laminates containing no overt defects. In addition, AE has clearly been able to distinguish between two types of material containing different matrices, between two crack orientations, and between stable and unstable crack growth in DCBs. Slow and normal cooled laminates were also differentiated by AE in double torsion tests. In view of the considerable scatter in AE data recorded from nominally identical specimens, it has been essential to justify these claims of differences by some simple statistical method. This has been done by ensuring that the ranges of two sets of compared data do not overlap.

In order to conduct such comparisons, many numerical acoustic emission parameters have been used. These include event count, mean amplitude, percentage share, skewness and kurtosis of the amplitude distribution histogram. The parameters seek to summarise acoustic emission characteristics thereby simplifying them and allowing ease of comparison. Development of AE analysis software to calculate such parameters has been essential in this.

Relatively little time has been devoted to determining which deformation processes produce which type of events. One reason for this is that the characteristics of received AE events will be strongly affected by the hardware used for their detection and the material through which they propagate. The greater the distance and the more contorted the path between source and receiver, the greater this modification.

These modulation effects or alteration of event characteristics, form the basis of acousto-ultrasonics, although for acoustic emission they are a considerable problem. The factors which cause these modulation effects must be considered. Attenuation caused by, for example, internal friction and deformation hysteresis will reduce the magnitude of the stress waves, particularly the higher frequency components. Scattering from internal inhomogeneities, such as fibre/matrix interfaces or interlaminar boundaries will generate reflected waves (and probably some mode conversions. Dispersion will cause a broadening of the pulse envelope and separation of frequencies. Compressional and shear mode transformations will occur at any specimen boundaries, thereby altering the wave modes of the events.

Further complications will be caused by the reception and conversion of the stress waves into an electrical signal by the transducer. Not all the energy incident on a transducer will be detected. In general, transducers are most sensitive to one mode of ultrasonic wave. The resonant frequency and mechanical damping of the transducer will effect the sensitivity to specific frequencies and the degree to which the transducer 'rings'.

The method of coupling transducer to specimen and the disposition of transducer relative to reflecting boundaries will further affect the received event, because superposition of incident and reflected waves causes distortion of the signal.

Given this multitude of factors altering the characteristics of events, in these highly anisotropic, inhomogeneous composite materials, standardisation of test conditions

become essential for any comparison of AE or AU data. Consequently, AE analysis tends to be largely confined to searching for general relationships between trends in received AE activity and material properties/behaviour.

In conclusion, it is perhaps unfortunate that such a damage resistant composite as APC2 was chosen as the subject of the extensive non-destructive testing in this thesis. A more brittle, more easily damaged composite would probably have shown considerably greater sensitivity to the defects investigated, giving more positive and fewer negative results. A simple qualitative measure of the toughness may be taken by the fact that APC can be machined, drilled and tapped without excessive interlaminar damage ⁽¹⁰²⁾. AE has shown itself to be very sensitive to factors affecting gross fracture processes. For example amplitude distribution analysis could distinguish between slow and standard cooled APC2 in double torsion tests, and close correlations have been demonstrated between AE parameters and fracture toughness and fibre fractures.

Acoustic emission testing is still very dependent on relatively sophisticated data reduction and analysis. The author hopes that the AE data analysis software, developed as part of this thesis, has gone some way towards overcoming the limitations of previous systems at Bath. It should allow other researchers to make further progress in the development of the acoustic emission technique.

Chapter 10

FINAL CONCLUSIONS

The broad conclusions drawn from this project may be summarised as follows.

10.1 Aromatic Polymer Composite 2

1. Mechanical testing of APC2 at Bath has yielded results which agree with those of ICI with respect to tensile, flexural and fracture toughness mechanical properties.
2. Strength and elastic modulus agree well with that predicted by a rule of mixtures, putting APC2 on a par with other CFRP.
3. In interlaminar fracture toughness, the PEEK matrix has given APC2 up to an order of magnitude improvement over conventional carbon/epoxies.
4. SEM observation of fracture surfaces has demonstrated that the PEEK matrix fractures generally in a highly ductile manner, being drawn from around the reinforcing fibres. However, this behaviour is rate dependent; high fracture speeds in DCB specimens causing a more brittle behaviour of the PEEK.
5. In general, the bond between PEEK and fibres is very good, broken and/or debonded fibres being usually covered in a layer of matrix.

10.2 Acousto-Ultrasonics

Acousto-ultrasonics has been investigated and applied to the NDT of APC2 carbon fibre/PEEK composites. Two AU parameters, Vary's Stress Wave Factor and the root-mean-square voltage, have been used.

1. Without optimisation of instrument settings, AU is likely to be insensitive to most material variables in APC2.
2. Coupling variability appears to be the limiting factor with respect to the sensitivity of AU to defects in APC2.
3. AU is sensitive to variations in fibre orientation.

4. AU appears to be of little use as a means of NDT for APC2. This conclusion relates in particular to the Stress Wave Factor recorded with the pulse mode of excitation and employing the AU206 instrument. RMS and burst mode have also been investigated with largely similar conclusions.

10.3 Acoustic Emission

1. APC2 is a quiet material with respect to the production of acoustic emission events. This appears to be the result of its thermoplastic ductile matrix and good fibre/matrix bond strength.
2. The acoustic emission output from APC2 is dominated by fibre related processes (ie fibre fracture), in contrast to other fibre reinforced plastics.
3. Attenuation of ultrasonic pulses (ie AE events) in APC2 is comparable to other fibre reinforced plastic. At 150 kHz, attenuation in UD APC2 is 1.8 dB/cm parallel to fibres and wave speed 8300 m/s. The respective figures perpendicular to fibres are 2.5 dB/cm and 2500 m/s
4. APC2 produces largely low amplitude events with an amplitude distribution following an exponential type decay towards higher amplitudes from a peak in channel 1. Only in some interlaminar DCB tests was different behaviour observed.
5. APC2 usually shows the Kaiser effect.
6. Standardised test conditions are required for AE testing. Variations in the method of stressing samples, specimen dimensions and AE hardware can all produce very large variations in the acoustic emission output from APC2. These variations are much larger than those caused by material parameters.
7. AE was incapable of conclusively detecting many moulded-in defects in APC2 when tested in three point bend, but was able to with tensile loading. These defects caused no statistically significant deterioration in flexural mechanical properties.
8. Making use of double torsion testing, slow cooled and standard APC2 plates could be distinguished by differences in the amplitude distributions. Differences in the type of crack propagation (stable and slip-stick) were apparent from the fracture surfaces.

Greater deformation of the PEEK matrix was seen in slow crack propagation regions and generally less deformation in slow cooled specimens.

9. The large amount of uncontrolled variation in AE output from APC2 tests is attributable to the following factors:
- a) Nominally identical transducers showed significant differences in sensitivity.
 - b) Numbers of events produced are a function of cross sectional area of specimens, following a broadly linear relationship.
 - c) Variation in the coupling between specimen and transducer can cause variation greater than 6 channels (7.2 dB) in the amplitude of received events.

10.4 Cross-Correlation Of AU, AE And Mechanical Properties

Acoustic emission, acousto-ultrasonics and mechanical properties were cross correlated. A simple coupling quality test was carried out with the AU206 and the comparability of two different amplitude sorting AE systems was investigated. The following main conclusions apply:

1. Acousto-ultrasonic RMS measurements showed some sensitivity to plate thickness, but otherwise AU exhibited little sensitivity to the variations in mechanical properties or AE output from a population of nominally identical APC2 specimens.
2. Calibration of coupling quality with the AU equipment was able to reduce the scatter in the AE data down to a level which appears to be inherent within the technique.
3. The numbers of events recorded from two separate AE systems operating on the same specimen are similar only when a significant number of events have been recorded.
4. Acoustic emission parameters correlate very closely with small changes in specimen thickness.
5. Acoustic emission parameters appear to be sensitive to failure stress and failure strain. This conclusion is based on small numbers of events. More tests are therefore required to prove this.

10.5 AE Study Of Fracture In The Fibre Direction Of UD Composites

- 1. The amplitude distribution of events from carbon fibre/PEEK DCB specimens had two peaks namely the typical low amplitude peak and a second much broader peak around channel 28-34.**
- 2. APC2 laminates exhibited both slow/stable and fast/unstable crack propagation. Very few events were recorded during crack jumps.**
- 3. AE was capable of distinguishing between interlaminar and intralaminar crack propagation, between carbon fibre/PEEK and carbon fibre/Epoxy and between 0.5 mm/min and 5 mm/min crosshead speed. These distinctions have been based on the shapes of amplitude distribution histograms, on event counts in selected channel ranges per unit area of crack growth and on energy content of the acoustic emission recorded. For example, APC2 produces more events, a greater proportion of which are high amplitude, than does epoxy CFRP. Interlaminar crack propagation shows a greater low amplitude peak than intralaminar propagation.**
- 4. The PEEK matrix confers an approximate order of magnitude increase in fracture toughness over the Epoxy matrix.**
- 5. AE parameters have been correlated closely with fibre fractures per unit area and with fracture toughness, G_c .**

Chapter 11

SUGGESTIONS FOR FURTHER WORK

1. Application of AU to conventional thermosetting matrix composites, using alternative AU parameters from Vary's SWF and possibly with higher frequency transducer and frequency spectrum analysis. These may help to improve AU, so making it a more promising method of NDT of composites.
2. Application of AE to other defects. APC2 appeared remarkably resistant to defects introduced prior to moulding. Impact damage, fatigue, delamination and environmental degradation may be more easily detected.
3. Correlation of AE events with actual fracture processes in APC2, for example, fibre fractures with the electrolytic etching or matrix acid dissolution methods outlined in chapter 4. Determination of what level of PEEK matrix cracking occurs prior to gross failure in APC2 UD material tested in flexure and tension, and whether this contributes to the AE recorded.
4. Investigation of the interrelationship between peak amplitude, ringdowns, event duration and RMS of true events from APC2 and other materials. With the new AE system it may be possible to gain a better approximation of event energy and duration from event amplitude and ringdown count.
5. Use of the software developed by the author to calculate numeric AE parameters which can then be systematically cross correlated with mechanical properties in other composite materials as a means of further developing AE as a method of NDT. Correlation of AE parameters with failure stress and strain in chapter 8 were promising, but based on small number of events and specimens. Further investigation in this area may lead to AE becoming a practical method of NDE.
6. AE testing of more complex APC2 components which have much more complex fibre lay-ups and stress states.

REFERENCES

1. Vary, A. and Bowles, K.J. Use of an ultrasonic-acoustic technique for non-destructive evaluation of fibre composite strength. In: Proceedings of the 33rd Annual Conference; Society of the Plastics Industry, New York, 1978, 24A, pp. 1-5.
2. Vary, A. and Bowles, K.J. Ultrasonic evaluation of the strength of unidirectional graphite-polyamide composites. In: Proceedings of the Eleventh Symposium on Non-destructive Testing. American Society for Non-destructive Testing, San Antonio, Texas, 1977, pp. 242-258.
3. Vary, A. and Bowles, K.J. An ultrasonic-acoustic technique for Non-destructive Evaluation of Fiber Composite Quality. Polymer Engineering and Science, April 1979, Vol. 19, No. 5, pp. 373-376.
4. Vary, A. and Lark, R.F. Correlation of Fiber Composite Tensile Strength with the Ultrasonic Stress Wave Factor. Journal of Testing and Evaluation, July 1979, Vol. 7, No. 4, pp. 185-191.
5. Vary, A. A Review of Issues and Strategies in Non-destructive Evaluation of Fiber Reinforced Structural Composites. In: National SAMPE Technical Conference Series, Vol. II, November 1979, pp. 166-177.
6. Duke, J.C. Jr. Non-Destructive Evaluation Of Composite Materials: A Philosophy, An Approach, And An Example. In: Browning, C.E. ed. Composite Materials: Quality Assurance And Processing, ASTM, 1983, pp. 75-95.
7. Vary, A. Acousto-Ultrasonic Characterisation of Fiber Reinforced Composites. Materials Evaluation, May 1982, Vol. 40, No. 6, pp. 650-662.
8. Green, J.E. Acousto-Ultrasonic Evaluation of Impact-Damaged Graphite Epoxy Composites. In: 27th National SAMPE Symposium, May 46, 1982, pp. 428-439.
9. Reifsnider, K.L. Non-Destructive Test Methods For Composite Structures. Proceedings of the National SAMPE Symposium and Exhibition, March 19-21, 1985, pp. 1131-1142.

10. Govada, A. and Duke, J.C. Application of Ultrasonics to Damage Development in Metal Matrix Composites. In: ASNT National Conferences, Spring Conference, March 22-25, 1982, Boston, pp. 379-385.
11. McIntire, P. and Miller, R.K. eds. NDT Handbook: Acoustic Emission Testing, Vol. 5. Ohio, USA: ASTM, 1988.
12. Rodgers, J.M. The developing role of acoustic emission in aircraft maintenance and structural integrity. In: The Fifth International Acoustic Emission Symposium, Tokyo, 1980, pp. 537-549.
13. Williams, J.H., Kahn, E.B. and Lee, S.S. Effects of Specimen Resonances on Acousto-Ultrasonic Testing. *Materials Evaluation*, Vol 41, No. 13, pp. 1502-1510, Dec 1983.
14. Egle, D.M. and Brown, A.E. Considerations for the detection of acoustic emission waves in thin plates. *Journal of the Acoustical Society of America*, Vol. 57, No. 3, March 1975, pp. 591-597.
15. Rodgers, J.M. Quality assurance and in-service inspection application of acousto-ultrasonics to bonded and composite structures. Paper supplied by AETC, Sacramento, California, USA. (January 1983).
16. Green, A.T. Evaluation of Composite Structures by Stress Wave Factor and Acoustic Emission. In: *Composite Structures: Proceedings of the 1st International Conference*, Paisley, Scotland, September 16-18, 1981, pp. 450-483. London: Applied Science Publishers.
17. Henneke, E.G. and Lamascon, A. Examination of the stress wave factor technique for NDE of composite laminates. In: *American Society for Non-destructive Testing Conferences, Spring Conference*, March 25, 1981, Las Vegas, pp. 371-376.
18. Vary, A., Moorhead, P.E. and Hull, D.R. Metal Honeycomb to Porous Substrate Diffusion Bond Evaluation. *Materials Evaluation*, Vol. 41, No. 8, July 1983, pp. 942-945.
19. Ono, K. and Despain, R. Characterisation of Carbon Fiber Composites using

- Acousto-Ultrasonic Techniques. In: Proceedings of the 1st Symposium on Acoustic Emission from Reinforced Composites, San Francisco, California, USA, July 19-21, 1983.
20. Williams, J.H., Jr and Lampert, N.R. Ultrasonic Evaluation of Impact Damaged Graphite Fiber Composite. *Materials Evaluation*, Vol. 38, No. 12, December 1980, pp. 68-72.
 21. Vary, A. Recent Advances in Acousto-Ultrasonic Measurements of Composite Mechanical Properties. In: 1979 ASNT Fall Conference, St. Louis, Missouri, October 1979.
 22. Green, A.T. Composites Stress-Wave-Factor and Acoustic Emission. In: Proceedings of the 1982 Joint Conference on Experimental Mechanics, Oahu, Hawaii, May 23-28, 1982, pp. 1102-1111.
 23. Madhav, A. and Nachlas, J.A. Statistical Evaluation of Quality in Composites Using the Stress Wave Factor Technique. In: *Acousto-Ultrasonics: Theory and Application* (Duke, Jr, J.C., ed.), pp. 165-176. New York: Plenum Press, 1988.
 24. Phani, K.K. and Bose, N.R. Hydrothermal ageing of jute-glass fibre hybrid composites - an acousto-ultrasonic study. *Journal of Materials Science*, Vol. 22, 1987, pp. 1929-1933.
 25. Phani, K.K. and Bose, N.R. Hydrothermal ageing of CSM-laminate during water immersion - an acousto-ultrasonic study. *Journal of Materials Science*, Vol. 21, 1986, pp. 3633-3637.
 26. Kautz, H.E. Acousto-Ultrasonic Verification of the Strength of Filament Wound Composite Materials. Pressure Vessel Conference, Chicago, Illinois, July 21-24, 1986.
 27. Kautz, H.E. Ultrasonic Evaluation of Mechanical Properties of Thick, Multilayered, Filament Wound Composites. NASA technical memorandum, report no. TM-87088, Sept 1985.
 28. Dos Reis, H.L.M. and McFarland, D. On The Acousto-Ultrasonic Non-Destructive Evaluation Of Wire Rope Using The Stress Wave Factor Technique. British

Journal of NDT, May 1986, pp. 155-156.

29. Williams, J.H., Hainsworth, J. and Lee, S.S. Acousto-Ultrasonic Non-Destructive Evaluation of Double-Braided Nylon Ropes Using The Stress Wave Factor. *Fibre Science and Technology*, Vol. 21, 1984, pp. 169-180.
30. Srivastava, V.K. and Prakash, R. Fatigue life prediction of glass fiber reinforced plastics using the acousto-ultrasonic technique. *International Journal of Fatigue*, Vol. 9, No. 3, 1987, pp. 175-178.
31. Phani, K.K. Niyogi, S.K., Maitra, A.K. and Roychaudhury, M. Strength and elastic modulus of a porous brittle solid: an acousto-ultrasonic study. *Journal of Materials Science*, Vol. 21, 1986, pp. 4335-4341.
32. Williams, J.H. and Lee, S.S. Promising Quantitative Non-Destructive Evaluation Techniques For Composite Materials. *Materials Evaluation*, Vol 43, April 1985, pp. 561-565.
33. Williams, J.H. Jr and Lee, S.S. Non-Destructive Evaluation of Strength and Separation Modes in Adhesively Bonded Automotive Glass Fiber Composite Single Lap Joints. *Journal of Composite Materials*, Vol. 21, Jan 1987, pp. 14-35.
34. Govada, A., Henneke, E.G. and Talreja, R. Acousto-Ultrasonic Measurements To Monitor Damage During Fatigue of Composites. In: *Proceedings of the Winter Annual Meeting on Advances in Aerospace Sciences and Engineering: Structure, Materials, Dynamics and Space Station Propulsion*, New Orleans, LA, Dec 9-14, 1984, pp. 55-60.
35. Kautz, H.E. Ray Propagation Path Analysis of Acousto-Ultrasonic Signals In Composites. NASA technical memorandum, report no. 100148, July 1987.
36. Duke, J.C., Jr and Kiernan, M.T. Predicting Damage Development in Composite Materials Based on Acousto-Ultrasonic Evaluation. In: *Acousto-Ultrasonics: Theory and Application* (Duke, Jr, J.C., ed.), pp. 191-200. New York: Plenum Press, 1988.
37. Talreja, R. Application of Acousto-Ultrasonics to Quality Control and Damage Assessment of Composites. Unpublished paper. The Technical University of

Denmark, Lyngby, Denmark, 1987.

38. Talreja, R., Govada, A. and Henneke, E.G. Quantitative Assessment Of Damage Growth In Graphite Epoxy Laminates By Acousto-Ultrasonic Measurements. Proceedings of the 10th Annual Review: Review of Progress in Quantitative Non-Destructive Evaluation, Santa Cruz, C.A., Aug 7-12, 1983, pp. 1099-1106.
39. Talreja, R. Application of Acousto-Ultrasonics to Quality Control and Damage Assessment of Composites. In: Acousto-Ultrasonics: Theory and Application (Duke, Jr, J.C., ed.), pp. 177-190. New York: Plenum Press, 1988.
40. Talreja, R., Govada, A. and Henneke, G. II. Quantitative assessment of damage growth in graphite epoxy laminates by acousto-ultrasonic measurements. Proceedings of the Review of Research in Quantitative Non-destructive Evaluation, University of California, Santa Cruz, Aug 1983.
41. Mittelman, A., Roman, I., Bivas, A., Leichter, I., Margulies, J.Y. and Weinreb, A. Acousto-Ultrasonic Characterisation of Physical Properties of Human Bones. In: Acousto-Ultrasonics: Theory and Application (Duke, Jr, J.C., ed.), pp. 305-310. New York: Plenum Press, 1988.
42. Vary, A. Concepts and Techniques for Ultrasonic Evaluation of Material Properties. Mechanics of Non-destructive Testing, Plenum Press, 1980, pp. 123-141.
43. Dos Reis, H.L.M. Acousto-Ultrasonics: Applications to Wire Rope, Wood Fiber Hardboard, and Adhesion. In: Acousto-Ultrasonics: Theory and Application (Duke, Jr, J.C., ed.), pp. 283-300. New York: Plenum Press, 1988.
44. Phani, K.K. and Rose, N.R. Application of Acousto-Ultrasonics for Predicting Hygrothermal Degradation of Unidirectional Glass-Fiber Composites. In: Acousto-Ultrasonics: Theory and Application (Duke, Jr, J.C., ed.), pp. 327-336. New York: Plenum Press, 1988.
45. Sundaresan, M.J. and Henneke, II, E.G. Measurement of the Energy Content in Acousto-Ultrasonic Signals. In: Acousto-Ultrasonics: Theory and Application (Duke, Jr, J.C., ed.), pp. 275-282. New York: Plenum Press, 1988.

46. Williams, J.H., Karagulle, H., Jr and Lee, S.S. Ultrasonic Input-Output for Transmitting and Receiving Longitudinal Transducers Coupled to Same Face of Isotropic Elastic Plate. *Materials Evaluation*, Vol 40, No. 6, Aug 1981, pp. 655-662.
47. Duke, J.C., Henneke, E.G., Stinchcomb, W.W. and Reifsnider, K.L. Characterisation of Composite Materials by Means of the Ultrasonic Stress Wave Factor. In: *Proceedings of the 2nd International Conference, Paisley, Scotland, September 14-16, 1983*, pp. 53-60. London: Applied Science Publishers.
48. Tang, B., Henneke II, E.G. and Stiffler, R.C. Low Frequency Flexural Wave Propagation in Laminated Composite Plates. In: *Acousto-Ultrasonics: Theory and Application* (Duke, Jr, J.C., ed.), pp. 45-66. New York: Plenum Press, 1988.
49. Pilarski, A., Rose, J.L. Balasubramaniam, K. and Da-Le, J. Utilisation of Oblique Incidence in Acousto-Ultrasonics. In: *Acousto-Ultrasonics: Theory and Application* (Duke, Jr, J.C., ed.), pp. 79-92. New York: Plenum Press, 1988.
50. Moon, S.M., Jerina. K.L. and Hahn, H.T. Acousto-Ultrasonic Wave Propagation in Composite Laminates. In: *Acousto-Ultrasonics: Theory and Application* (Duke, Jr, J.C., ed.), pp. 111-126. New York: Plenum Press, 1988.
51. Egle, D.M. and Brown, A.E. A Note on Pseudo-Acoustic Emission Sources. *Journal of Testing and Evaluation*, Vol. 4, No. 3, May 1976, pp. 196-199
52. Brahma, K.K. and Murthy, C.R.L. Bond Quality Evaluation of Bimetallic Strips: Acousto-Ultrasonic Approach. In: *Acousto-Ultrasonics: Theory and Application* (Duke, Jr, J.C., ed.), pp. 337-344. New York: Plenum Press, 1988.
53. Srivastava, V.K. and Prakash, R. Acousto-Ultrasonic Evaluation of the Strength of Composite Material Adhesive Joints. In: *Acousto-Ultrasonics: Theory and Application* (Duke, Jr, J.C., ed.), pp. 345-350. New York: Plenum Press, 1988.
54. Mitchell, J.R. Multi-Parameter, Multi-Frequency Acousto-Ultrasonic for Detecting Impact Damage in Composites. In: *Acousto-Ultrasonics: Theory and Application* (Duke, Jr, J.C., ed.), pp. 311-318. New York: Plenum Press, 1988.
55. Govada, A.K., Duke, J.C., Henneke, E.G. and Stinchcomb, W.W. A Study of the

Stress Wave Factor Technique for the Characterisation of Composite Materials.

NASA Contractor report 174870, Feb 1985.

56. Asok, D.E., Phani, K.K. and Kumar, S. Acousto-ultrasonic study on glass ceramics in the system $\text{MgO-Al}_2\text{O}_3\text{-SiO}_2$. *Journal of Materials Science Letters*, Vol. 6, 1987, pp. 17-19.
57. Dos Reis, H.L.M. and McFarland, D.M. On the Acousto-Ultrasonic Characterisation of Wood Fiber Hardboard. *Journal of Acoustic Emission*, Vol. 5, No. 2, April-June 1986, pp. 67-70.
58. Russell-Floyd, R.S. Hydrothermal degradation of polyester/glass sheet and dough moulding compounds: Final Year Project, School of Materials Science, University of Bath, 1984.
59. Henneke, E.G., Duke, J.C., Stinchcomb, W.W., Govada, A. and Lemascon, A. A Study of the Stress Wave Factor Technique for the Characterisation of Composite Materials. NASA Contractor report 3670, Feb 1983.
60. Hemann, J.H., Cavano, P., Kautz, H. and Bowles, K. Trans-Ply Crack Density Detection by Acousto-Ultrasonics. In: *Acousto-Ultrasonics: Theory and Application* (Duke, Jr, J.C., ed.), pp. 319-326. New York: Plenum Press, 1988.
61. Kinra, V.K. and Dayal, V. Non-destructive evaluation of composite material using ultrasound. In: *Acousto-Ultrasonics: Theory and Application* (Duke, Jr, J.C., ed.), pp. 111-126. New York: Plenum Press, 1988.
62. Roberts, R.A., Qu, J. and Achenbach, J.D. Experimental and Theoretical Analysis of Backscattering Mechanisms in Fiber-Reinforced Composites. In: *Acousto-Ultrasonics: Theory and Application* (Duke, Jr, J.C., ed.), pp. 151-164. New York: Plenum Press, 1988.
63. Freerick, J.R. *Ultrasonic Engineering*. New York: John Wiley & Sons, 1965.
64. Goldman, R. *Ultrasonic Technology*. New York: Chapman & Hall, 1962.
65. Hemann, J.H. and Baaklini, G.Y. The Effect of Stress on Ultrasonic Pulses in Fiber Reinforced Composites. NASA Contractor report 3720, Aug 1983.
66. Karagulle, H., Lee, S.S. and Williams, J.H., Jr. Input-Output Characterisation of an

- Ultrasonic Testing System by Digital Signal Analysis. NASA Contractor report 3756, Jan 1984.
67. Krautkramer, J. and Krautkramer, H. Ultrasonic Testing of Materials. 3rd. ed. New York: Springer-Verlag, 1983.
 68. Weaver, R.L. Diffuse Waves for Materials NDE. In: Acousto-Ultrasonics: Theory and Application (Duke, Jr, J.C., ed.), pp. 35-44. New York: Plenum Press, 1988.
 69. Anon. AET Data Sheet Model 206 AU. Data sheet supplied with the AU 206 by AETC, 1812J Tribute Road, Sacramento, California.
 70. Guild, F.J., Phillips M.G. and Harris, B. Acoustic Emission From Composites: The Influence Of Reinforcement Pattern. In: First International Symposium on Acoustic Emission from Reinforced Composites, The Society of the Plastics Industry, July 19-21, 1983.
 71. Guild, F.J., Ackerman, F.J., Phillips, M.G. and Harris, B. Amplitude distribution analysis of acoustic emission from composites: the development of a data collection and processing system. First International Symposium on Acoustic Emission from Reinforced Composites, San Francisco, California, July 19-21, 1983.
 72. Crosbie, G.A., Guild, F.J. and Phillips, M.G. Acoustic emission studies in glass fibre-polyester composites with rubber toughened matrices. In: Proceedings of the International Conference on: Testing, Evaluation and Quality Control of Composites, Guildford, England, 13-14 Sept 1983, pp. 114-124.
 73. Moroney, M.J. Facts From Figures. London: Pelican Books Ltd. 1978.
 74. Bhatt, M. and Hogg, P.J. Private communication. QMC, University of London, 1987.
 75. Bhatt, M. and Hogg, P.J. Test Conditions in Stress Wave Factor Measurements for Fiber Reinforced Composites and Laminates. In: Acousto-Ultrasonics: Theory and Application (Duke, Jr, J.C., ed.), pp. 259-274. New York: Plenum Press, 1988.
 76. Bhatt, M. and Hogg, P.J. Test Conditions in Stress Wave Factor Measurements for Fiber Reinforced Composites and Laminates. NDT International, Vol. 20, 1988,

pp. 3-10.

77. Nixon, J.A., Phillips, M.G., Moore, D.R. and Prediger, R.S. A study of the development of impact damage in cross-ply carbon-fibre/PEEK laminates using acoustic emission. *Composite Science and Technology*, Vol. 31, No. 1, 1988, pp. 1-14.
78. Hartness, J.T. and Kim, R.Y. A comparative study of fatigue behaviour of polyetheretherketone and epoxy with reinforced graphite cloth. In: 28th National SAMPE Symposium, April 12-14, 1983, pp. 535-544.
79. Leaird, J.D. and Kingdon, M.C. Considerations for Developing Calibration Standards for Acousto-Ultrasonic Inspection. In: *Acousto-Ultrasonics: Theory and Application* (Duke, Jr, J.C., ed.), pp. 247-258. New York: Plenum Press, 1988.
80. Patton-Mallory, M. and Anderson, K. D. An Acousto-Ultrasonic Method for Evaluating Wood Products. In: *Acousto-Ultrasonics: Theory and Application* (Duke, Jr, J.C., ed.), pp. 301-304. New York: Plenum Press, 1988.
81. Noiret, D. and Roget, J. Calculation of Wave Propagation in Composite Materials Using the Lamb wave concept. *Journal of Composite Materials*, Vol 23, Feb 1989, pp. 195-206.
82. Sarrafzadeh, A., Churchill, R.J. and Nilmura, M.G. Laser Generated Ultrasound. In: *Acousto-Ultrasonics: Theory and Application* (Duke, Jr, J.C., ed.), pp. 201-208. New York: Plenum Press, 1988.
83. Brunk, J.A., Valenza, C.J. and Bhardwaj. M.C. Applications and Advantages of Dry Coupling Ultrasonic Transducers for Materials Characterisation and Inspection. In: *Acousto-Ultrasonics: Theory and Application* (Duke, Jr, J.C., ed.), pp. 221-238. New York: Plenum Press, 1988.
84. Cogswell, F.N. and Hopprich, M. Environmental Resistance of Carbon Fibre Reinforced Polyether-etherketone. *Composites*, Vol. 14, No. 3, July 1983.
85. Anon. Data sheets on Aromatic Polymer Composites. Provided by the New Science Group, ICI plc, Wilton, 1985.
86. Anon. Aromatic Polymer Composites APC-1/APC-2 Comparison. Private

- communication. Report supplied by ICI plc, Wilton, 1985.
87. Belbin, G.R. Thermoplastic Structural Composites - A Challenging Opportunity. In: The Institution of Mechanical Engineers: Proceedings 1984, Vol. 198, No. 47, 1984.
 88. Cogswell, F.N. and Leach, D.C. Continuous Fibre Reinforced Thermoplastics: A Change In The Rules For Composite Technology. *Plastics and Rubber Processing and Applications*, Vol. 4, No. 3, 1984, pp. 271-276.
 89. Cogswell, F.N. Microstructure and Properties of Thermoplastic Aromatic Polymer Composites. In: 28th National SAMPE Symposium, April 12-14, 1983, pp. 528-534.
 90. Belbin, G.R., Brewster, I., Cogswell, F.N., Hezzell, Fibre Reinforced Thermoplastics: A Change In The Rules For Composite Technology. *Plastics and Rubber Processing and Applications*, Vol. 4, No. 3, 1984, pp. 271-276.
 91. Hartness, J.T. An Evaluation of Polyetheretherketone Matrix Composites Fabricated from Unidirectional Prepreg Tape. In: 29th National SAMPE Symposium, April 3-5, 1984, pp. 459-474.
 92. Anon. APC1, The Product of High Technology, Technical Literature, ICI plc, Welwyn Garden City.
 93. Grove, S.M. Thermal modelling of tape laying with continuous carbon fibre-reinforced thermoplastic. *Composites*, Vol. 19, No. 5, Sept 1988, pp. 367-375.
 94. Dickson, R.J., Jones, C.J., Harris, B., Leach, D.C. and Moore, D.R. Environmental Fatigue of Carbon Fibre PEEK. *Journal of Materials Science*, Vol. 20, 1985, pp. 60-70.
 95. Hartness, J.T. Polyetheretherketone Matrix Composites. *SAMPE Quarterly*, January 1983, pp. 33-37.
 96. Leach, D.C. and Moore, D.R. Toughness of aromatic polymer composites. Presented at Composites: Materials and Engineering, University of Delaware, September 24-28, 1984.
 97. Carlile, D.R. and Leach, D.C. Damage and Notch Sensitivity of Graphite/PEEK

- Composite. In: 15th National Technical Conference, October 1983.
98. Barlow, C.Y. and Windle, A.H. Structure and Properties of Aromatic Polymer Composites. Presented at the ICI symposium on APC, December 1985, Wilton.
 99. Shukla, J.G. and Sichina, W.J. Thermal Behaviour of Carbon Fibre Reinforced Polyether Etherketone. ANTEC 84, pp. 265-267.
 100. Anon. APC2, Technical Literature, ICI plc, Welwyn Garden City.
 101. McGrath, G.C., Clegg, D.W. and Collyer, A.A. The mechanical properties of compression moulded reconstituted carbon fibre reinforced PEEK (APC-2). Composites, Vol. 19, No. 3, May 1988, pp. 211-216.
 102. Belbin, G.R., Brewster, F.N., Cogswell, D.J., Hezzell, M.S. and Swerdlow, M.S. Carbon Fibre Reinforced Polyether Etherketone: A Thermoplastic Composite For Aerospace Applications. Meeting of the Society for the Advancement of Material and Process Engineering, Stresat, 8-10 June, 1982.
 103. Mock, J.A. ed. Engineering Resins '84 - reaching new heights. Plastics Engineering, Feb 1984, pp. 25-39.
 104. Leach, D.C., Curtis, D.C. and Tamblin, D.R. Delamination Behaviour of Aromatic Polymer Composite. In: ASTM Symposium on Toughened Composites, Houston, Texas, March 13-15, 1985.
 105. Kim, R.Y. and Hartness, J.T. The Evaluation of Fatigue Behaviour of Polyetheretherketone/Graphite Composite Fabricated From Prepreg Tape. In: 29th National SAMPE Symposium, April 3-5, 1984, pp. 765-776.
 106. Blundell, D.J. and Osborn, B.N. The Morphology of Poly(aryl- ether-etherketone). Polymer, 1983, Vol. 24, pp. 953-958.
 107. Blundell, D.J., Chalmers, J.M., Mackenzie, M.W. and Gaskin, W.F. Crystalline Morphology of the Matrix of PEEK - Carbon Fibre Aromatic Polymer Composites I. Assessment of Crystallinity. SAMPE Quarterly, Vol. 16, No. 4, July 1985, pp. 22-30.
 108. Blundell, D.J. and Osborn, B.N. Crystalline Morphology of the Matrix of PEEK - Carbon Fibre Aromatic Polymer Composites II. Crystallization Behaviour. To be

submitted to SAMPE Quarterly.

109. Blundell, D.J. and Willmouth, F.M. Crystalline Morphology of the Matrix of PEEK - Carbon Fibre Aromatic Polymer Composites III. Prediction of Cooling Rates During Fabrication. To be submitted to SAMPE Quarterly.
110. Harris, B. Engineering Composite Materials. London, Institute of Metals, 1986.
111. Barlow, C.Y. and Windle, A.H. The Measurement of Fracture Energy in Aligned Composites. Composites Science and Technology, Vol. 33, 1988, pp. 135-150.
112. Hine, P.J., Brew, B. Duckett, R.A. and Ward, I.M. The Fracture Behaviour of Carbon Fibre Reinforced Poly(Ether Etherketone). Composites Science and Technology, Vol. 33, 1988, pp. 35-71.
113. Berglund, L. and Johannesson, T. Mixed-Mode Fracture Of Carbon Fiber/PEEK composites. In: Proceedings of the First European Conference on Composite Materials, ECCM-1, Bordeaux, France, 1985.
114. Crick, R., Meakion, P., Moore, R. and Leach, D. Fracture And Fracture Morphology Of Aromatic Polymer Composites. In: Proceedings of the First European Conference on Composite Materials, ECCM-1, Bordeaux, France, 1985.
115. Talbott, M.F., Springer, G.S. and Berglund, L.A. The Effects of Crystallinity on the Mechanical Properties of PEEK Polymer and Graphite Fiber Reinforced PEEK. Journal of Composite Materials, Vol. 21, Nov 1987, pp. 1056-1081.
116. Lustiger, A. Considerations in the Utilisation of Semicrystalline Thermoplastic Advanced Composites. SAMPE Journal, September/October 1984, pp. 13-16.
117. Lee, R.J. Compression strength of aligned carbon fibre-reinforced thermoplastic laminates. Composites, Vol. 18, No. 1, January 1987, pp. 35-39.
118. Jones, D.P., Leach, D.C., and Moore, D.R. The application of instrumented falling weight impact techniques to the study of toughness in thermoplastics. Plastics and Rubber Processing and Applications, Vol. 6, 1986, pp. 67-79.
119. Curtis, D.C., Moore, D.R. Slater and Zahlan, N. Fatigue testing of multi-angle laminates of CF/PEEK. Composites, Vol. 19, No. 6, November 1988, pp. 446-452.
120. Wang, Q. and Springer, G.S. Moisture Absorption and Fracture Toughness of

- PEEK Polymer and Graphite Fiber Reinforced PEEK. *Journal of Composite Materials*, Vol. 23, May 1989, pp. 434-447.
121. Whitney, J.M., Browning, C.E. and Hoogsteden, W. A Double Cantilever Beam Test for Characterising Mode I Delamination of Composite Materials. *Journal of Reinforced Plastics and Composites*, Vol. 1, Oct 1982, pp. 297-313.
 122. Smiley, A.J. and Pipes, R.B. Rate Effects on Mode I Interlaminar Fracture Toughness in Composite Materials. *Journal of Composite Materials*, Vol. 21, July 1987.
 123. Gillespie, J.W. Jr, Carlsson, L.A. and Smiley, A.J. Rate-Dependent Mode I Interlaminar Crack Growth Mechanisms in Graphite/Epoxy and Graphite/PEEK. *Composites Science and Technology*, Vol. 28, 1987, pp. 1-15.
 124. Hine, P.J., Brew, B., Duckett, R.A. and Ward, I.M. Failure Mechanisms in Continuous Carbon-Fibre Reinforced PEEK Composites. *Composites Science and Technology*, Vol. 35, 1989, pp. 31-51.
 125. Mall, S., Law, G.E. and Katouzian, M. Loading Rate Effect on Interlaminar Fracture Toughness of a Thermoplastic Composite. *Journal of Composite Materials*, Vol. 21, June 1987, pp. 569-579.
 126. Pratt, J.E. Private communication concerning recommendations for APC2 sheet production, ICI plc, Wilton, 1985.
 127. Purslow, D. Fractography of fibre-reinforced thermoplastics, Part 3. Tensile, compressive and flexural failures. *Composites*, Vol. 19, No. 5, September 1988, pp. 358-366.
 128. Galiotis, C., Melanitis, N., Batchelder, D.N., Robinson, I.M. and Peacock, J.A. Residual strain mapping in carbon fibre/PEEK composites. *Composites*, Vol. 19, No. 4, July 1988, pp. 321-324.
 129. Manders, P.W. (1978). Carbon Fibre Structure By Electrolytic Etching. *Nature*, Vol. 271, No. 5641, pp. 142-143.
 130. Kaiser, J. Untersuchungen uber das auftreten von gerauschen beim zugversuch. Phd Thesis, Technische Hochschule, Munich, FRG, 1950.

131. Symposium on Acoustic Emission, ASTM, Bal Harbour, Florida, December 7-8, 1971.
132. Nichols, R.W. (1976). Acoustic Emission. London: Applied Science Publishers Ltd.
133. Williams, R.V. (1980). Acoustic Emission. Bristol: Adam Hilger Ltd.
134. Drouillard, T.F. Acoustic Emission: A Bibliography with Abstracts. New York: IFI/Plenum, 1979.
135. Drouillard, T.F. and Hamstad, M.A. A Comprehensive Guide to the Literature on Acoustic Emission from Composites. First International Symposium on Acoustic Emission from Reinforced Composites, San Francisco, California, July 19-21, 1983.
136. Guild, F.J., Walton, D., Adams, R.D. and Short, D. The application of acoustic emission to fibre reinforced composite materials. Composites, Vol. 7, No. 3, July 1976, pp. 173-179.
137. Williams, J.H. and Lee, S.S. 'Acoustic emission monitoring of fibre composite materials and structures. Journal of Composite Materials, Vol. 12, No. 4, October 1978, pp. 348-370.
138. Duke, J.C. and Henneke, E.G. Acoustic emission monitoring of advanced fibre reinforced composite materials - a review. 5th Acoustic Emission Symposium, Tokyo, Japan, 18-20 November 1980, pp. 147-162.
139. Bailey, C.D., Freeman, S.M. and Hamilton, Jr., J.M. Acoustic Emission Monitors Damage Progression in Graphite Epoxy Composite Structures. Materials Evaluation, Vol. 38, No. 8, 1980.
140. Becht, J., Schwalbe, H.J. and Eisenblaetter, J. Acoustic Emission as an aid for investigating the Deformation and Fracture of Composite Materials. Composites, Vol. 7, 1976, pp. 245-248.
141. Wood, B.R.A. and Harris, R.W. Evaluation of fibre reinforced plastic materials using acoustic emission techniques. Proceedings of the Pan Pacific Conference on Nondestructive Testing, 4th, Sydney, Australia, November 15-18, 1983.

142. Valentin, D., Bonniau, Ph. and Bunsell, A.R. Failure discrimination in carbon fibre-reinforced epoxy composites. *Composites*, Vol. 14, No. 4, October 1983, pp. 345-351.
143. Jamison, R.D. and Reifsnider, K.L. Assessment of microdamage development during tensile loading of graphite/epoxy laminates.
144. Favre, F.-P. and Laizet, J.-C. Amplitude and Counts per Event Analysis of the Acoustic Emission Generated by the Transverse Cracking of Cross-ply CFRP. *Composites Science and Technology*, Vol. 36, 1989, pp. 27-43.
145. Scarpellini, R.S., Swanson, T.L. and Fowler, T.J. Acoustic Emission Signatures of RP Defects. In: *First International Symposium on Acoustic Emission from Reinforced Composites*, The Society of the Plastics Industry, Inc. July 19-21, 1983.
146. Selden, R.B. and Gustafson, C. Transverse Cracking and Delamination in (0/45/90)_s CFRP Detected Through Acoustic Emission. *Journal of Reinforced Plastics and Composites*, Vol. 4, October 1985, pp. 365-382.
147. Green, A.T. Acoustic Emission NDE For Advanced Composite Structures. In: *The Conference on Advanced Composites - Special Topics*, December 4-6, 1979, El Segundo, California, pp. 228-245.
148. Rahat, K., Russell-Floyd, R. and Reiter, H. The effect of residual stress on the formation of the cracks in plasma sprayed zirconia thermal barrier coatings. *Proceedings of the 12th International Thermal Spraying Conference*, London, June 1989.
149. Habib, F.A., Cooke, R.G. and Harris, B. Cracking in Brittle Matrix Composites. *Br. Ceram. Trans. J.*, Vol. 89, 1990, pp. 115-124.
150. Yang, M. and Scott, V.D. Interface and Fracture of Carbon Fibre Reinforced Al-7 Wt% Si Alloy. *Journal of Materials Science*, Vol. 25, 1991.
151. Cole, P.T. Using Acoustic Emission (AE) to Locate and Identify Defects in Composites. *Composite Structures*, Vol. 3, 1985, pp. 259-267.
152. Wood, B.R.A. and Robert, W.H. Structural Integrity Evaluation Using Acoustic

- Emission Techniques. World Meeting on Acoustic Emission, 1989, pp. S66-S69.
153. Droge, M.A. Recommended Practice for Acoustic Emission Testing of Reinforced Thermosetting Resin Pipe (RTRP). First International Symposium on Acoustic Emission from Reinforced Composites, San Francisco, California, July 19-21, 1983.
 154. Speake, J.H. and Curtis, G.J. Characterisation of the Fracture Processes in CFRP using Spectral Analysis of the Acoustic Emissions Arising from the Application of Stress. Carbon Fibres, 2nd International Conference, Proceedings, London, Feb 18-20, 1974.
 155. Yamaguchi, K., Oyaizu, H. and Nagata, Y. Characteristics of acoustic emission generated from GFRP during tensile test. Journal of Acoustic Emission Supplement, Vol. 4 (April-Sept), 1985, pp. S191-S194.
 - 155a. Lee, S.M. Double torsion fracture toughness test for evaluating transverse cracking in composites. Journal of Materials Science Letters, Vol. 1, 1982, pp. 511-515.
 - 155b. Kies, J.A. and Clark, A.B.J. Proceedings of the Second International Conference on Fracture, Brighton 1969, Pratt, P.L. ed. London: Chapman Hall, 1969, p. 483.
 156. Lorenzo, L. and Hahn, H.T. Acoustic Emission Study of Fracture of Fibers Embedded in Epoxy Matrix. In: First International Symposium on Acoustic Emission from Reinforced Composites, The Society of the Plastics Industry, Inc. July 19-21, 1983.
 157. Fuwa, M., Bunsell, A.R. and Harris, B. Tensile failure mechanisms in carbon fibre reinforced plastics. Journal of Materials Science, Vol. 10, 1975, pp. 2062-2070.
 158. Short, D. and Summerscales, J. Amplitude distribution acoustic emission signatures of unidirectional fibre composite hybrid materials. Composites, Vol. 15, No. 3, July 1984, pp. 200-206.
 159. Nixon, J. Private communication. University of Bath, 1987.
 160. Prediger, R.S. Private communication concerning details of the Fractomat crack length monitoring system. ICI, Wilton, 1987.
 161. Szilard, J. ed. Ultrasonic Testing. Chichester: John Wiley & Sons, 1982.

162. Champaneria, R.K. Presentation at the ICI symposium on APC, December 1985, Wilton.
163. Williams, J.H. and Lee, S.S. Acoustic Emission Characterisation Of Composite Materials Using The AE [Parameter] Delay Concept. First International Symposium on Acoustic Emission from Reinforced Composites, San Francisco, California, July 19-21, 1983.
164. Gordon, J.E. The New Science of Strong Materials, 2nd edition, London: Penguin Books, 1976.
165. Hull, D. An introduction to composite materials. Cambridge: Cambridge University Press, 1981.

FIGURES AND TABLES

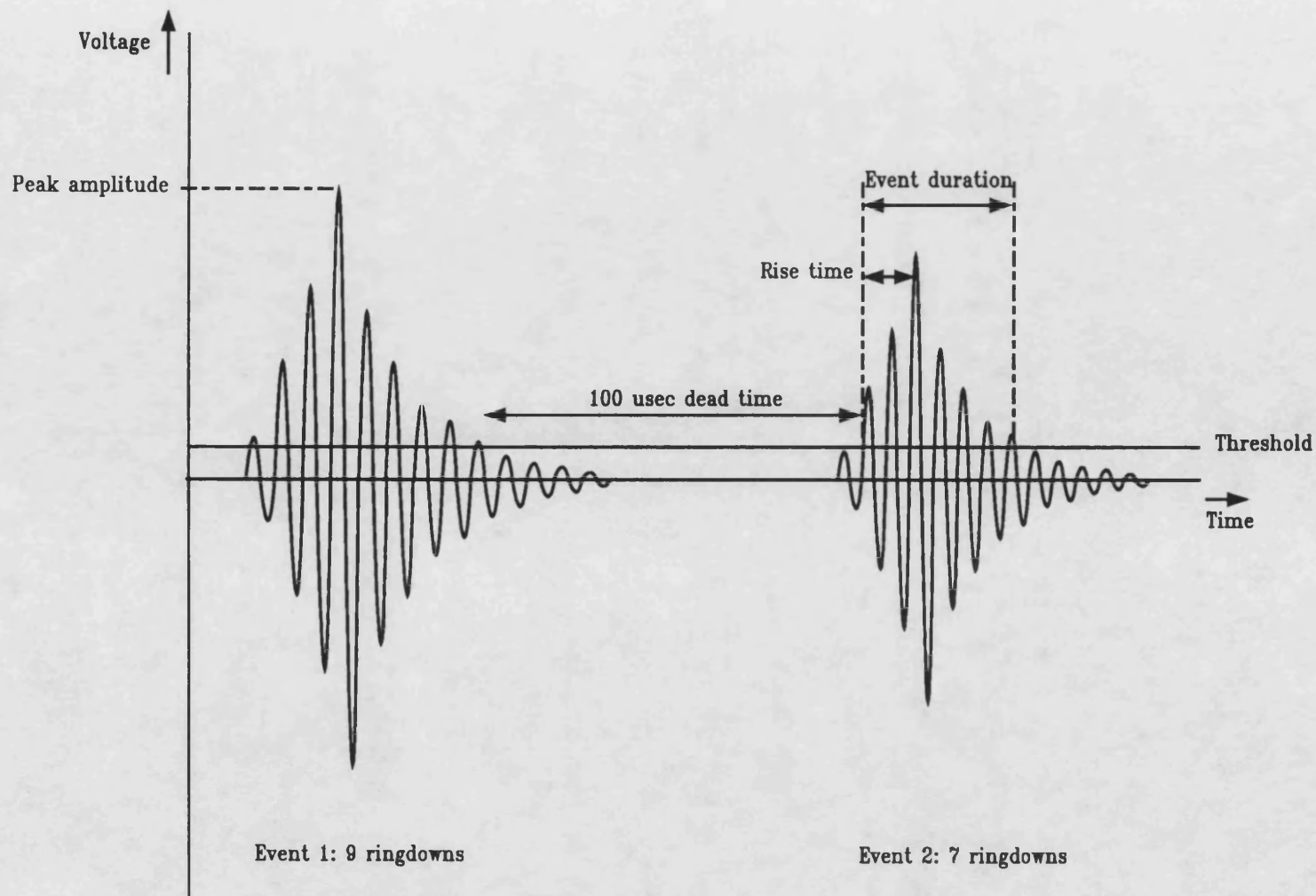


Figure 1.1. The characteristics of acoustic emission events.

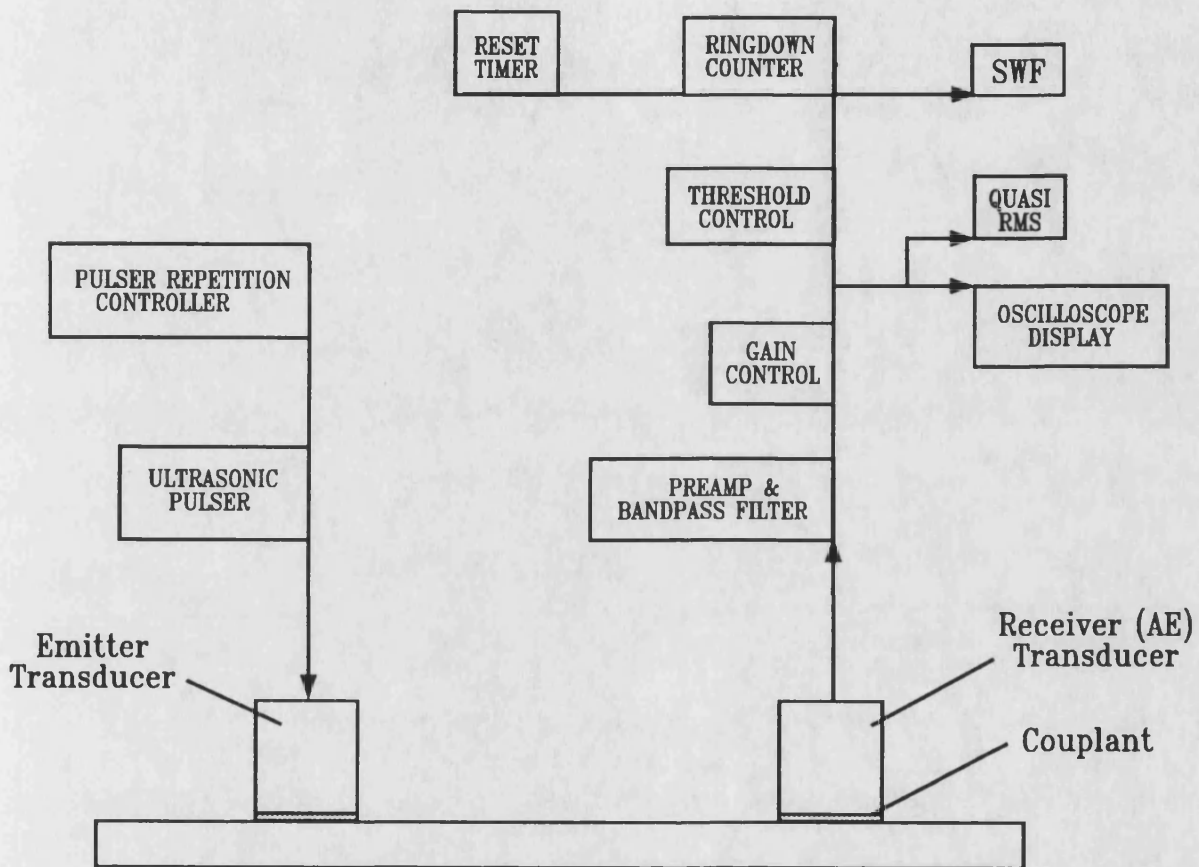
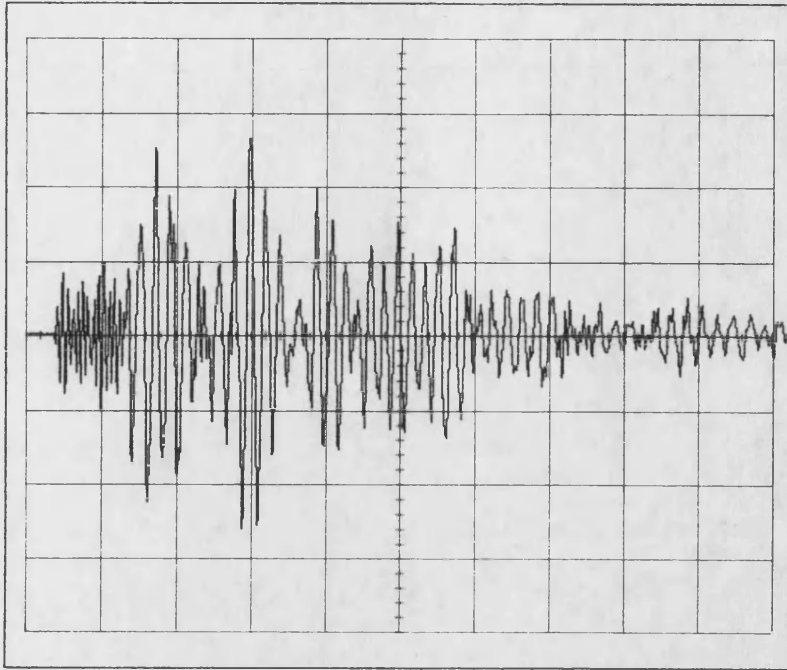


Figure 2.1. Schematic diagram of the AU206 acousto-ultrasonic testing system.

a



b

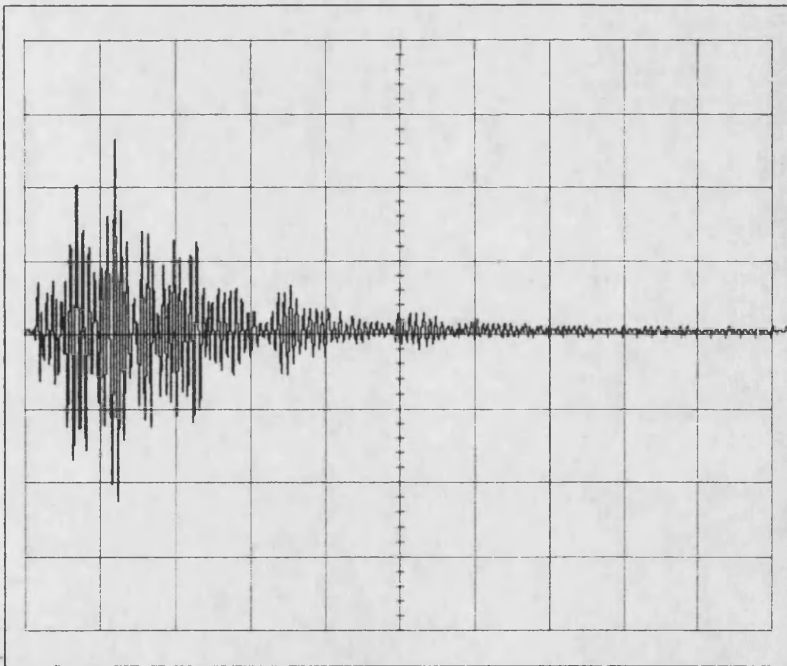
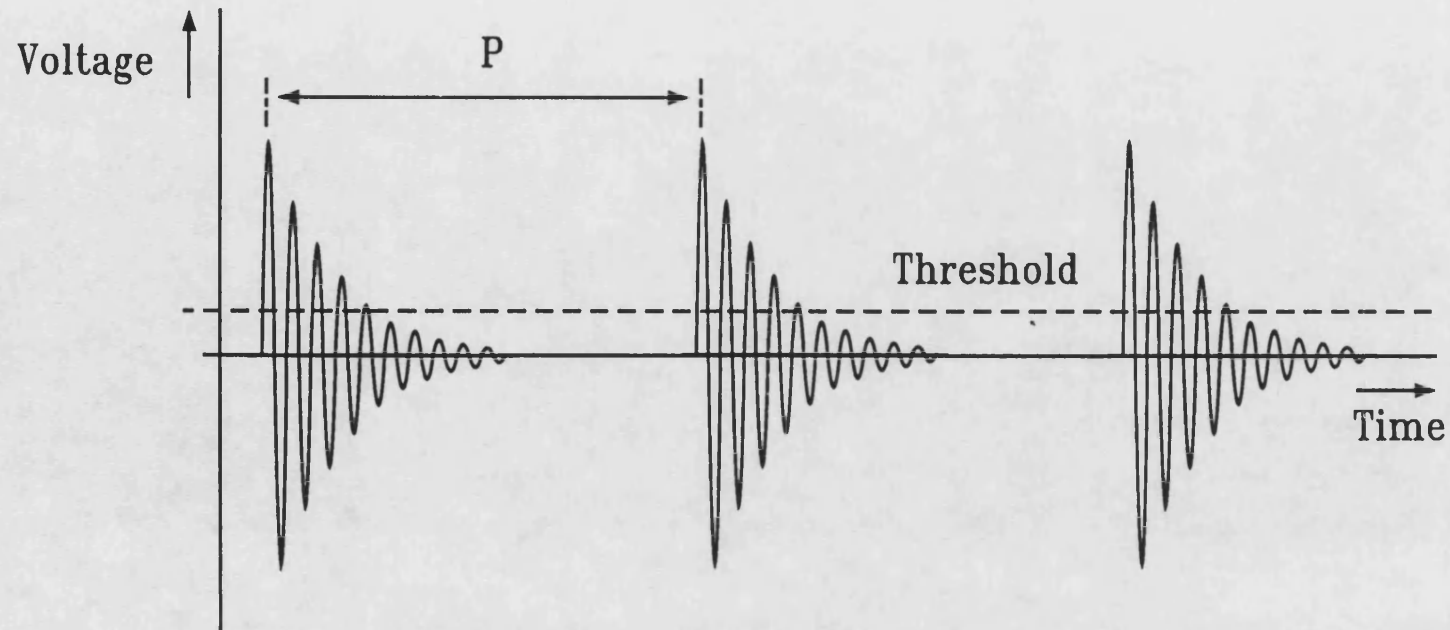


Figure 2.2. Typical received AU pulses recorded using the pulse mode and propagated between transducers 85 mm in separation coupled to 16-ply APC2. a) Vertical scale 2.0V/div, horizontal scale 40 microseconds/div. b) Vertical scale 2.0V/div, horizontal scale 100 microseconds/div.



$$\text{SWF} = C \cdot T \cdot 1/p$$

C = Number of ringdowns

T = Accumulation time period

1/p = Pulse repetition rate

Figure 2.3. Determination of the Stress Wave Factor.

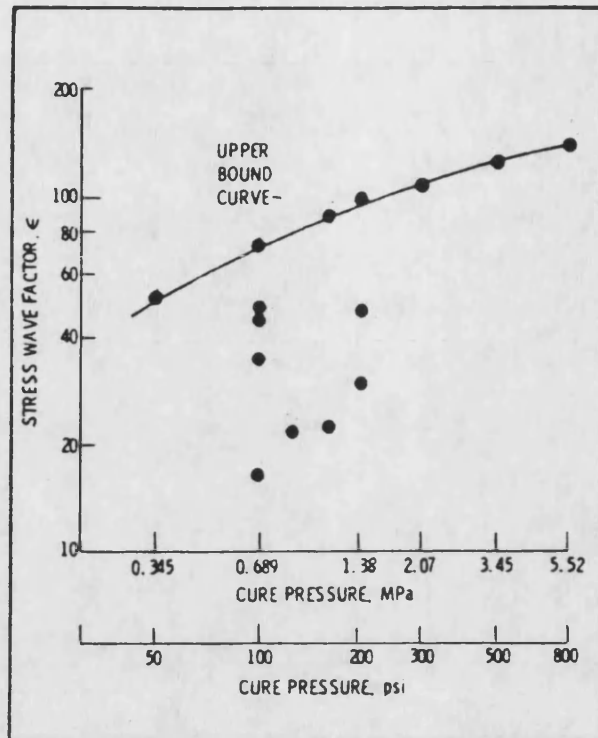


Figure 2.4. SWF as a function of cure pressure for 12-ply unidirectional graphite/polyimide composite panels (after Vary and Bowles (1))

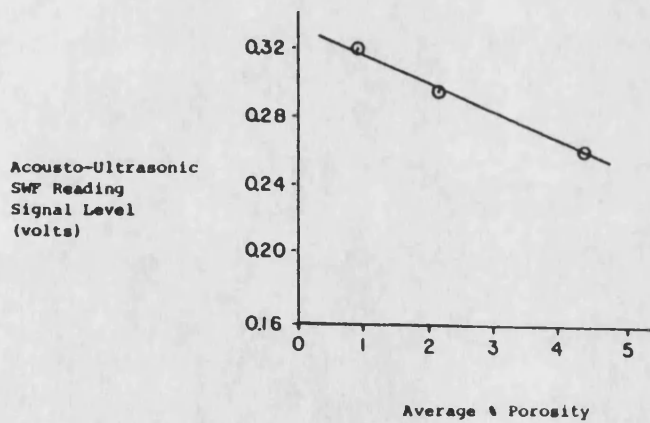


Figure 2.5. Acousto-ultrasonic signal level (RMS voltage) as a function of average porosity in 2 mm thick multi-ply graphite/epoxy panels. Each point represents the average of 30 readings on each panel (after Rodgers (15)).

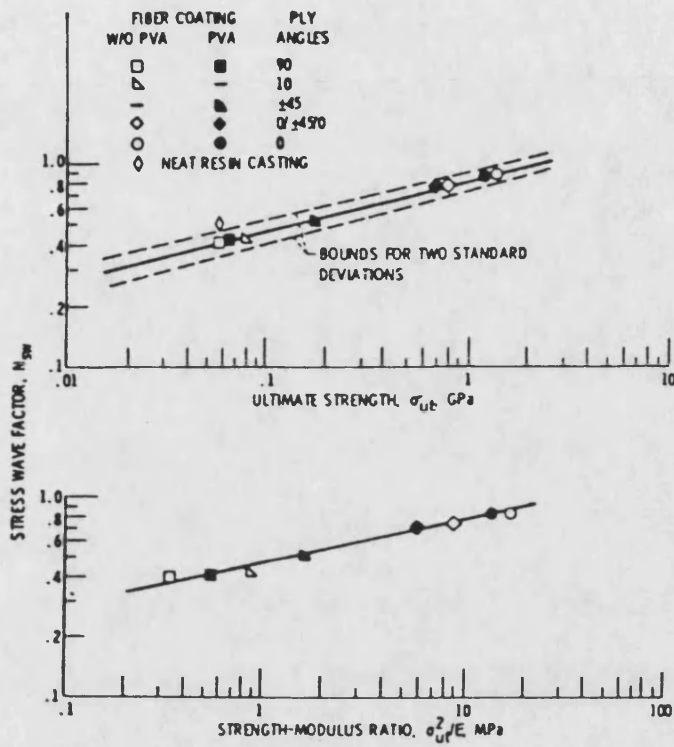


Figure 2.6. Normalised SWF as function of ultimate tensile strength, σ_{UTS} , and strength-modulus ratio, $(\sigma_{UTS})^2/E$ for 8-ply graphite/epoxy composites with and without PVA coated fibres and various reinforcement arrangements. Fibre reinforcements are 0° , 10° , 90° , $0^\circ/\pm 45^\circ/0^\circ$ and $\pm 45^\circ$ (after Vary and Lark ⁽⁴⁾).

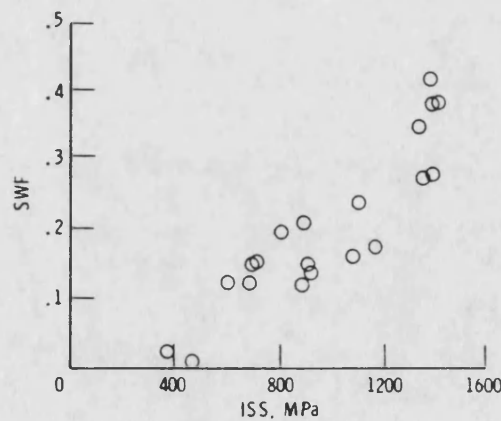


Figure 2.7. Kautz's SWF (RMS voltage of the signal partitioned in the 0.5-0.75 MHz range) as a function of interlaminar shear strength (after Kautz ⁽²⁷⁾).

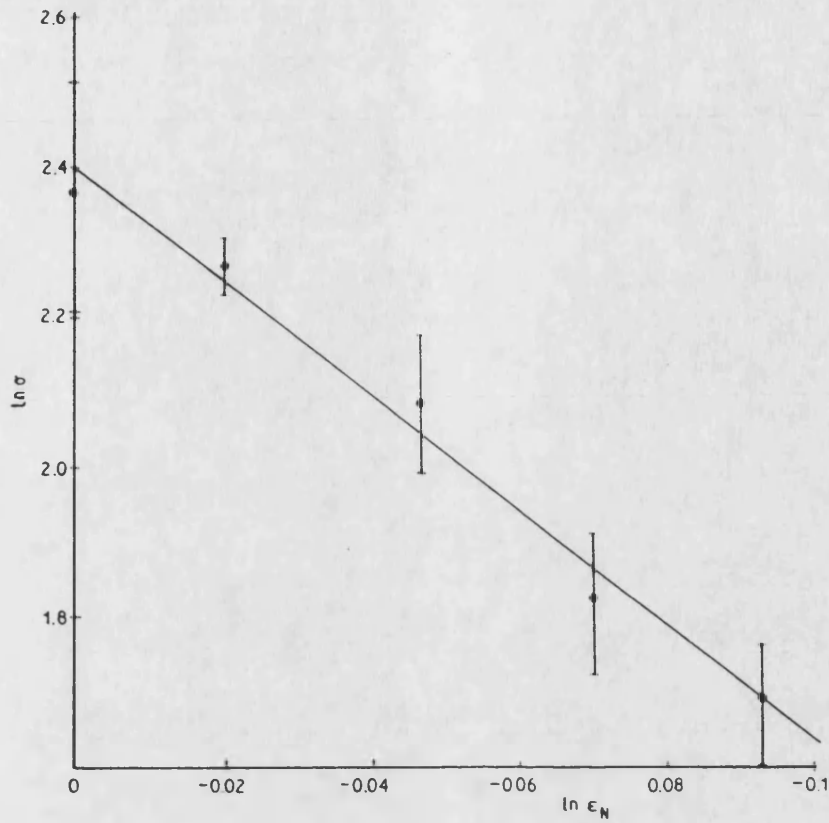


Figure 2.8. Variation of the compressive failure strength of gypsum with normalised SWF (after Phani et al (31)).

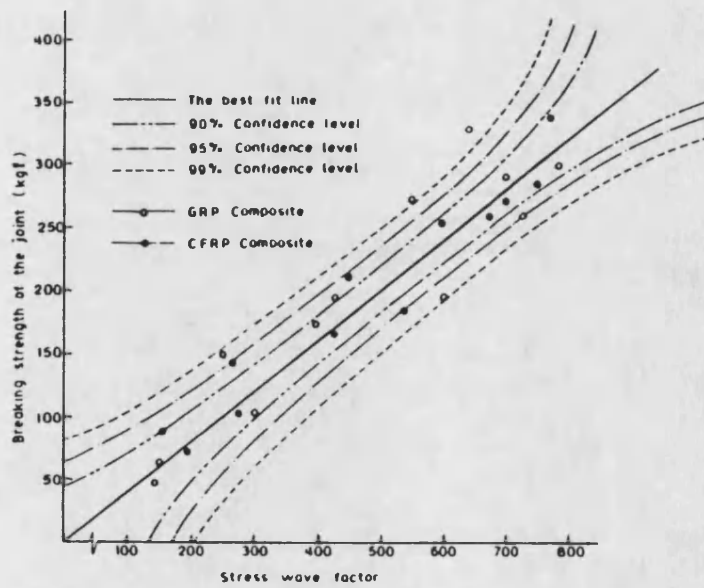


Figure 2.9. Variation of the SWF with breaking strength of Araldite epoxy joints between GRP and CFRP laminates (after Srivastava and Prakash (53)).

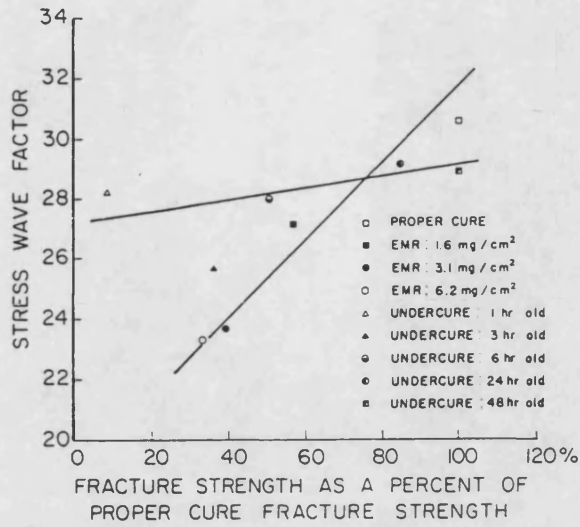


Figure 2.10. SWF as a function of the normalised fracture strength for adhesively bonded single lap-joint specimens (after Williams et al (33)).

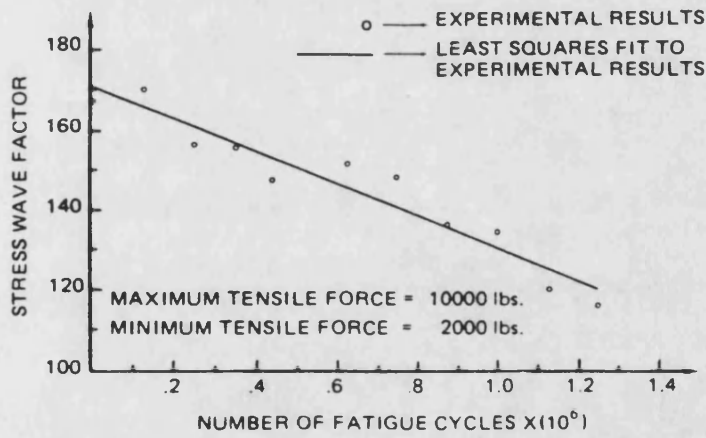


Figure 2.11. Variation of SWF with the number of fatigue cycles of wire rope samples (after dos Reis and McFarland (28))

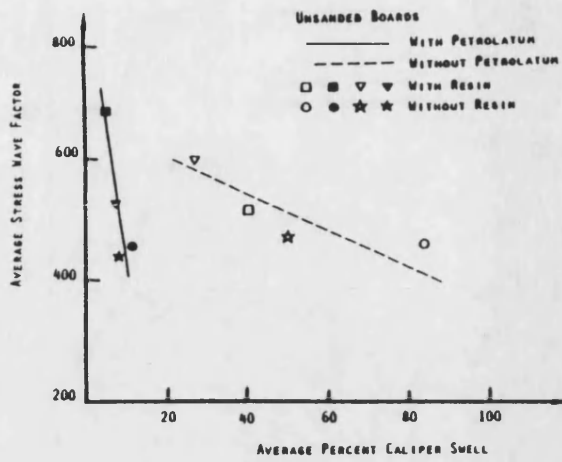


Figure 2.12. Average SWF as a function of average percentage caliper swell of wood fibre hardboards (after dos Reis ⁽⁴³⁾).

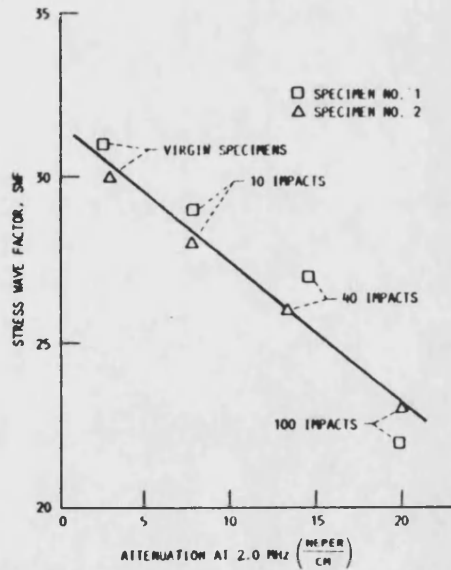


Figure 2.13. SWF versus through thickness attenuation at 2.0 MHz for drop weight impact tests on 10-ply unidirectional graphite/epoxy specimens (after Williams and Lampert ⁽²⁰⁾)

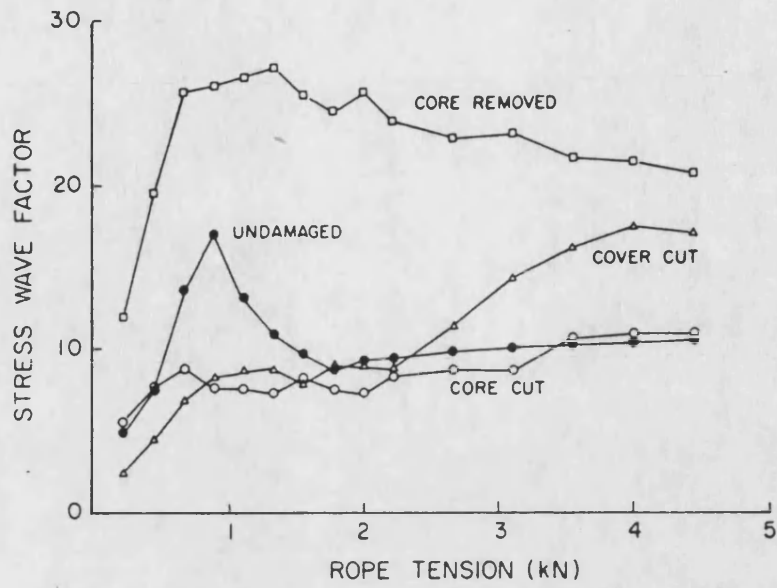


Figure 2.14. SWF versus rope tension for undamaged and various damaged double braided nylon rope samples (after Williams et al (29)).

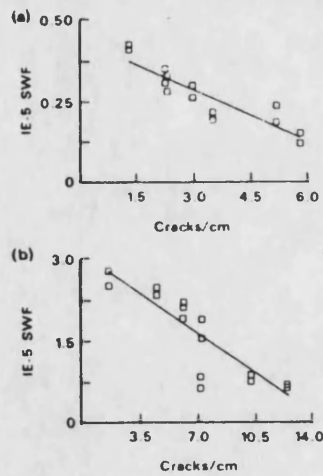
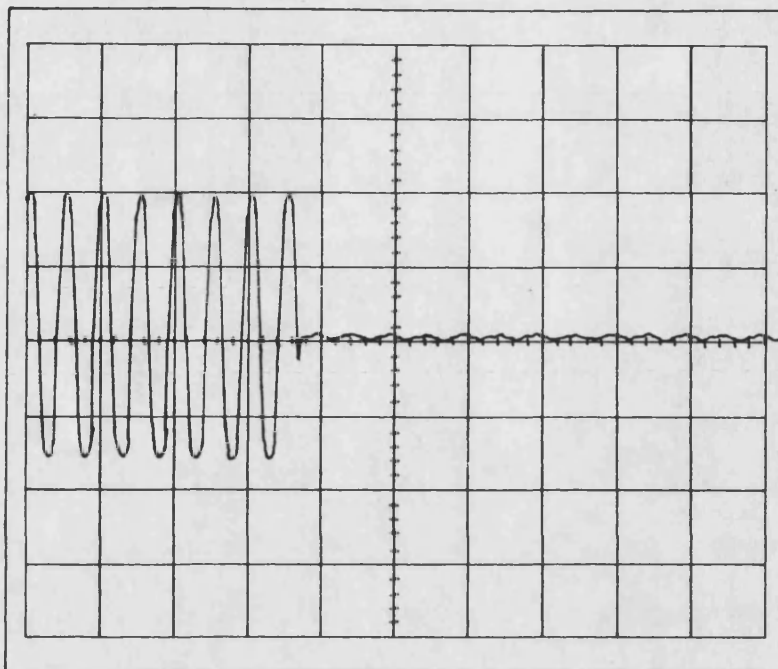


Figure 2.15. Hemann's SWF (RMS voltage of the signal partitioned in the 10-20 microsecond, 0 - 1.285 MHz range) as a function of crack density in carbon fibre/polyimide composites a) cross-ply laminate b) woven fabric laminate (after Hemann et al (60)).

a) BURST MODE



b) PULSE MODE

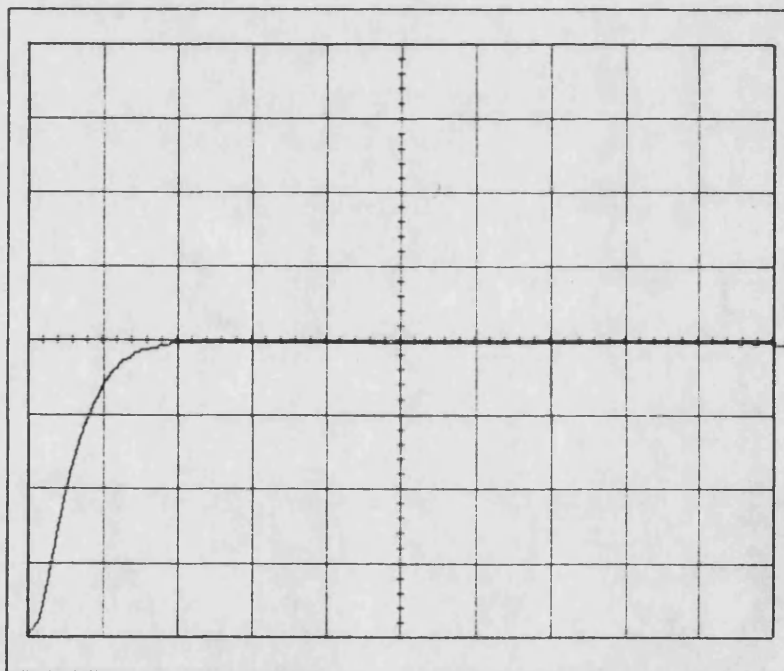
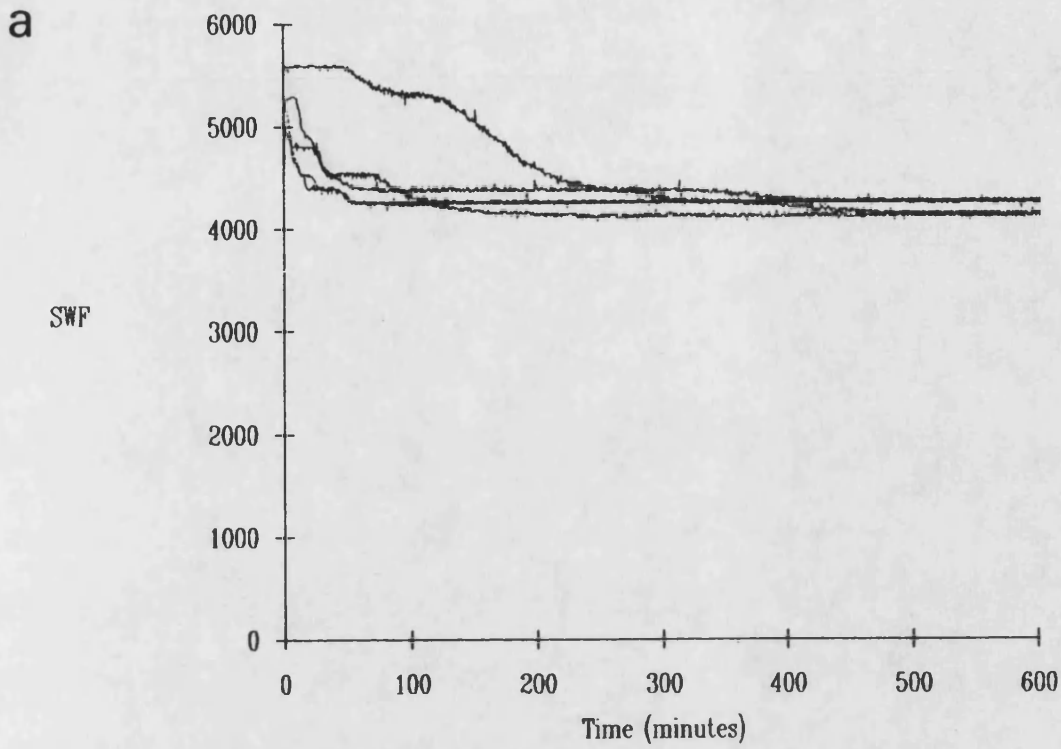


Figure 2.16. Oscilloscope trace of the two types of electrical excitation pulse available with the AU206 acousto-ultrasonic system: a) burst mode (2 V/div vertical scale, 10 μ s/div horizontal scale b) pulse mode (20V/div vertical scale, 10 μ s/div horizontal scale).

Variation of the SWF with time using the AU206



Variation of quasi-RMS voltage with time using the AU206

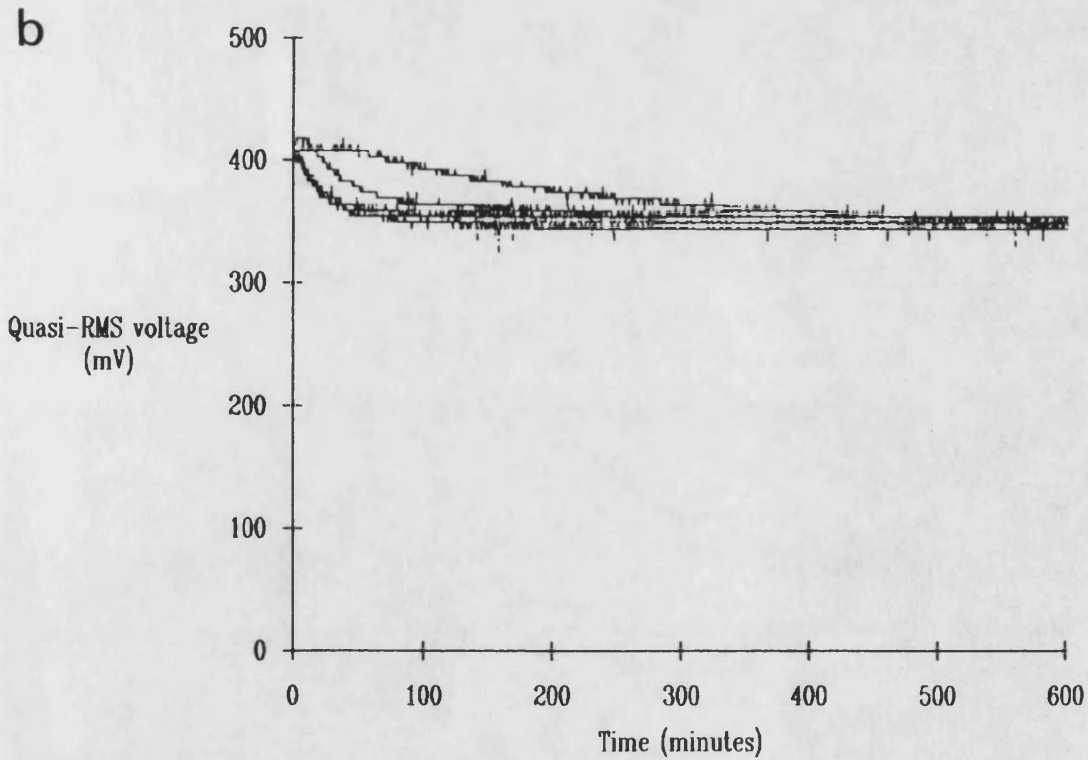


Figure 3.1. Variation of a) SWF and b) Quasi-RMS voltage during warm up from cold of the AU206 acousto-ultrasonic testing system.

SWF as a function of cumulation time for 16-ply 0°/90° APC2 at 4 pulser repetition rates

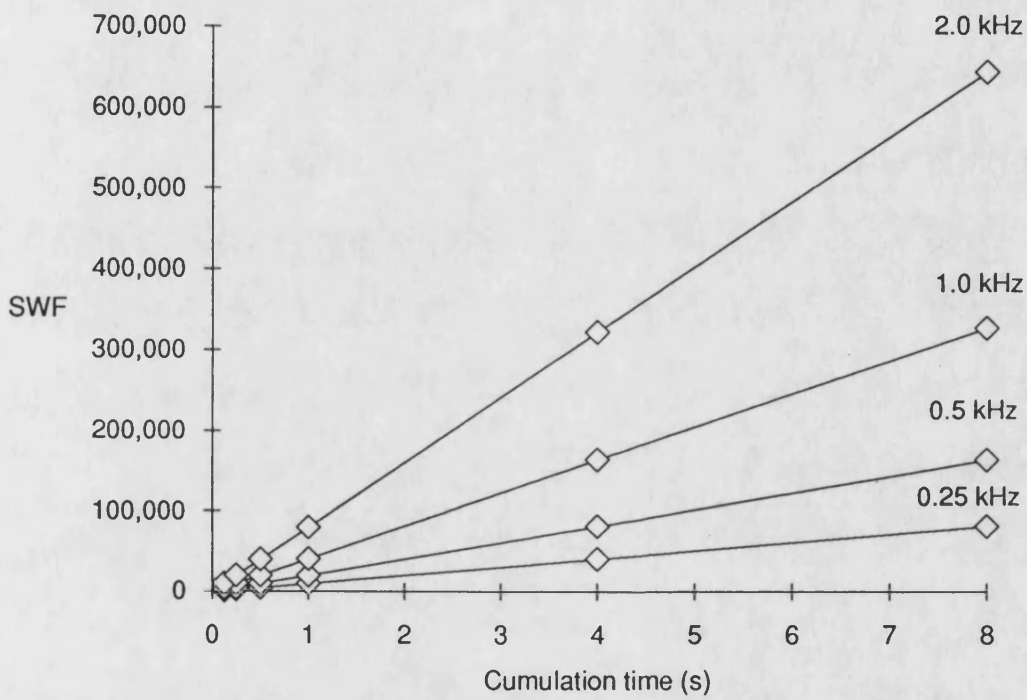


Figure 3.2. Variation of SWF with cumulation time at the four available repetition rates. Transducers are coupled to 16-ply 0°/90° APC2.

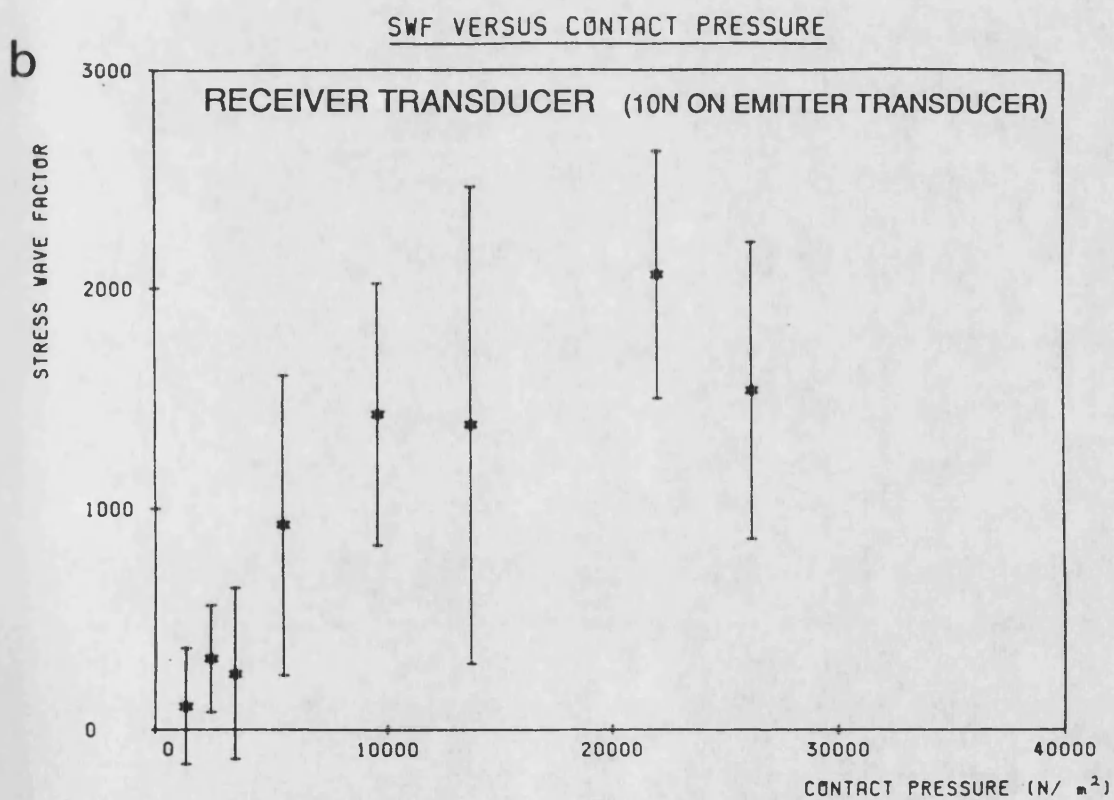
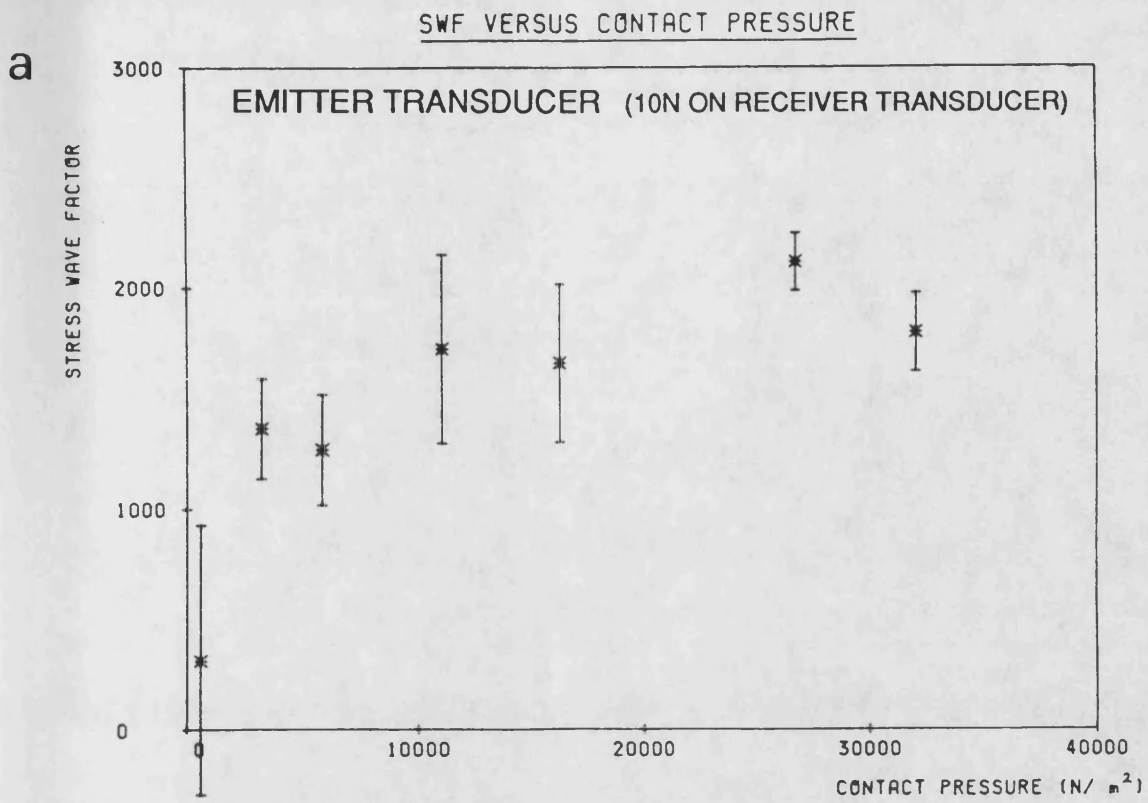


Figure 3.3. Influence of contact pressure on SWF, for fixed transducer position and instrument settings; (a) emitter contact pressure varied; (b) receiver contact pressure varied. (Error bars are ± 2 standard deviations)

COEF' OF VARIATION VERSUS CONTACT PRESSURE

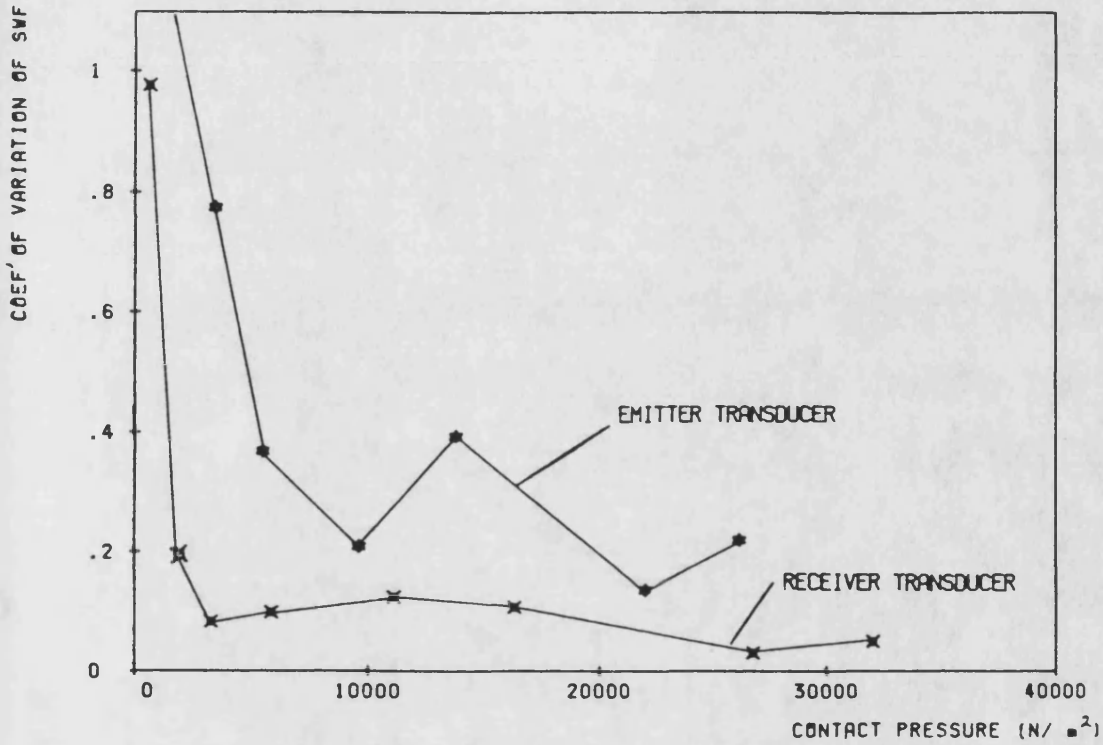


Figure 3.4. Influence of contact pressure on SWF variability, for fixed transducer position and instrument settings. Coefficient of variation = standard deviation/mean.

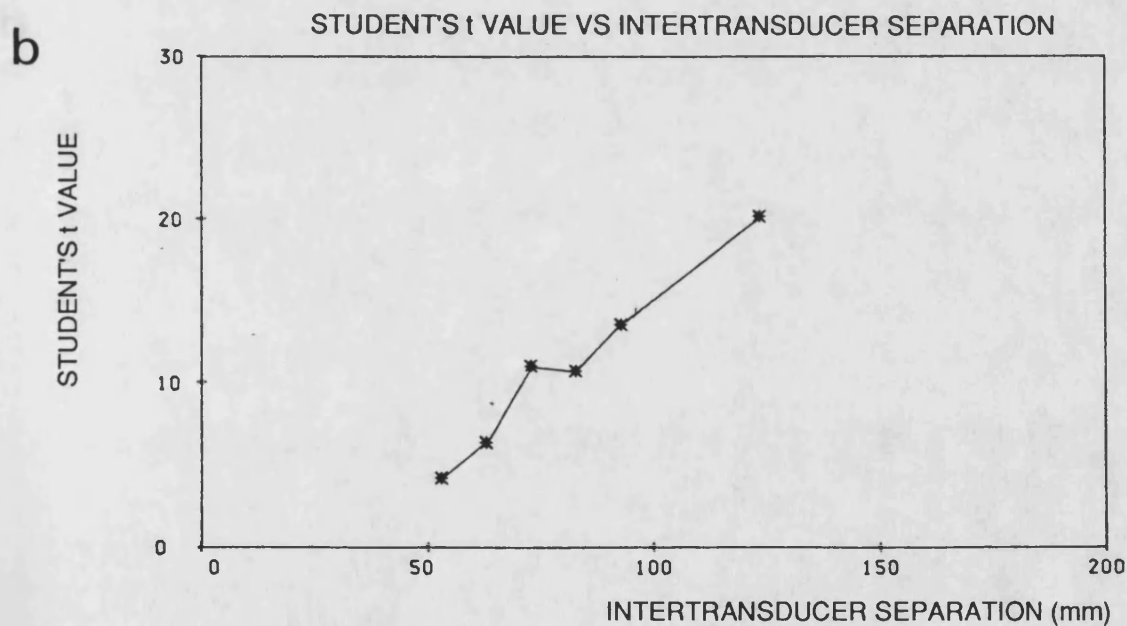
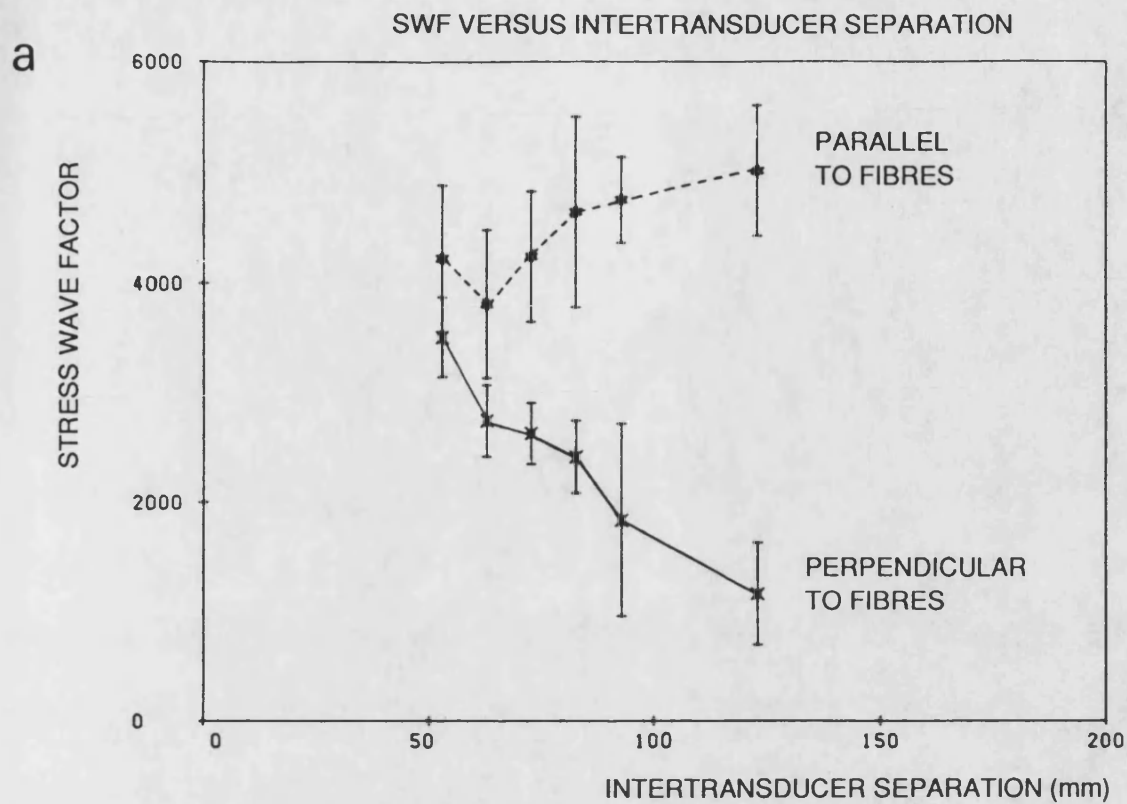


Figure 3.5. Comparison of SWF measurements parallel and perpendicular to fibres of unidirectional APC2, showing the effect of intertransducer separation: (a) SWF values for the two orientations (error bars are ± 2 standard deviations); (b) values of Student's *t* for corresponding mean SWFs in the two orientations.

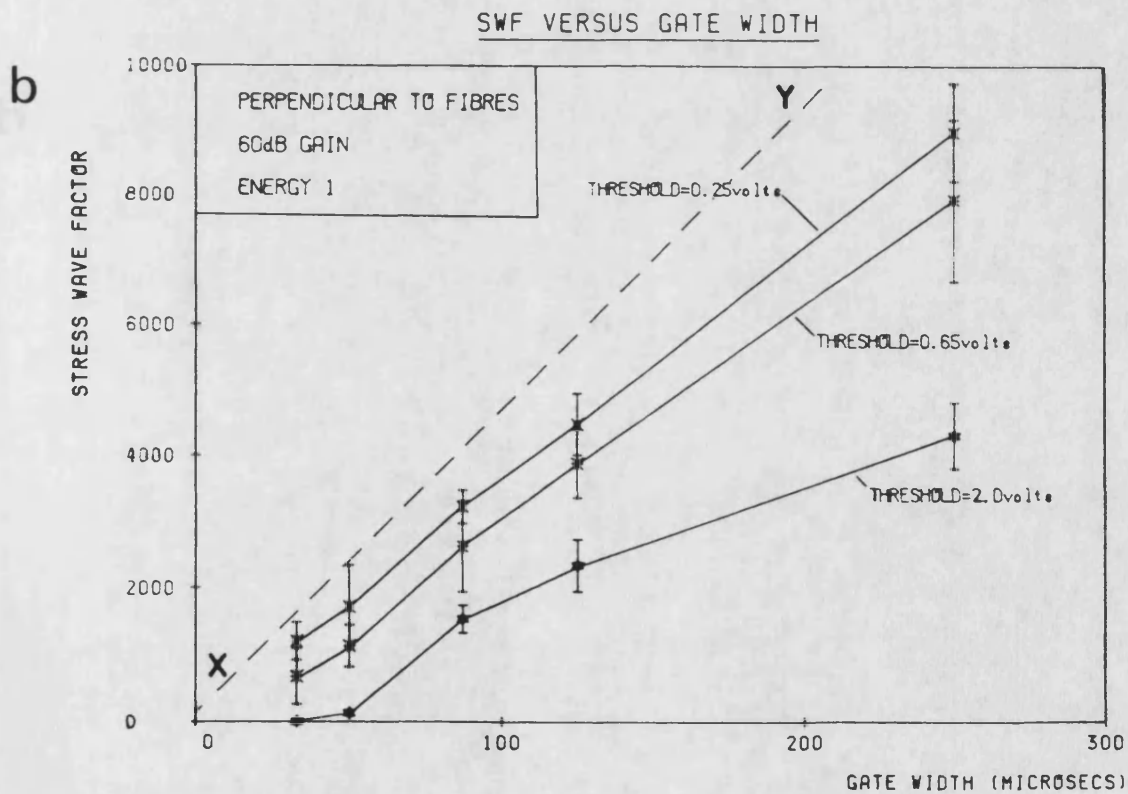
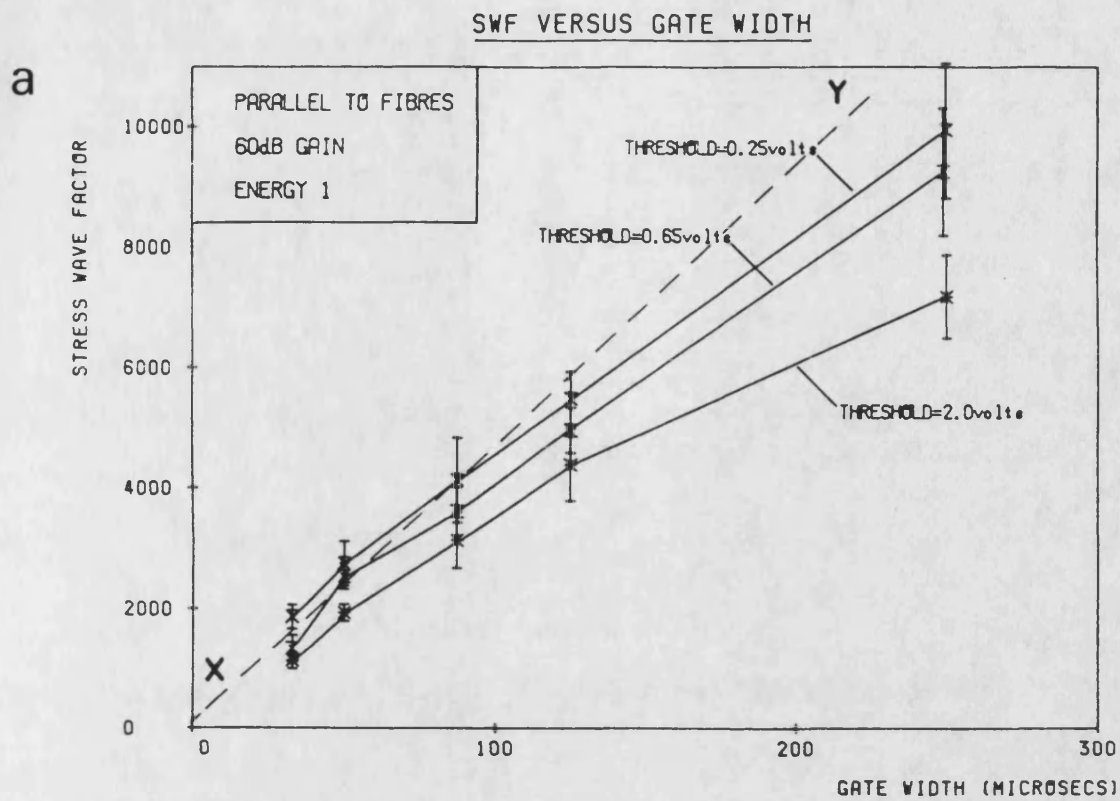
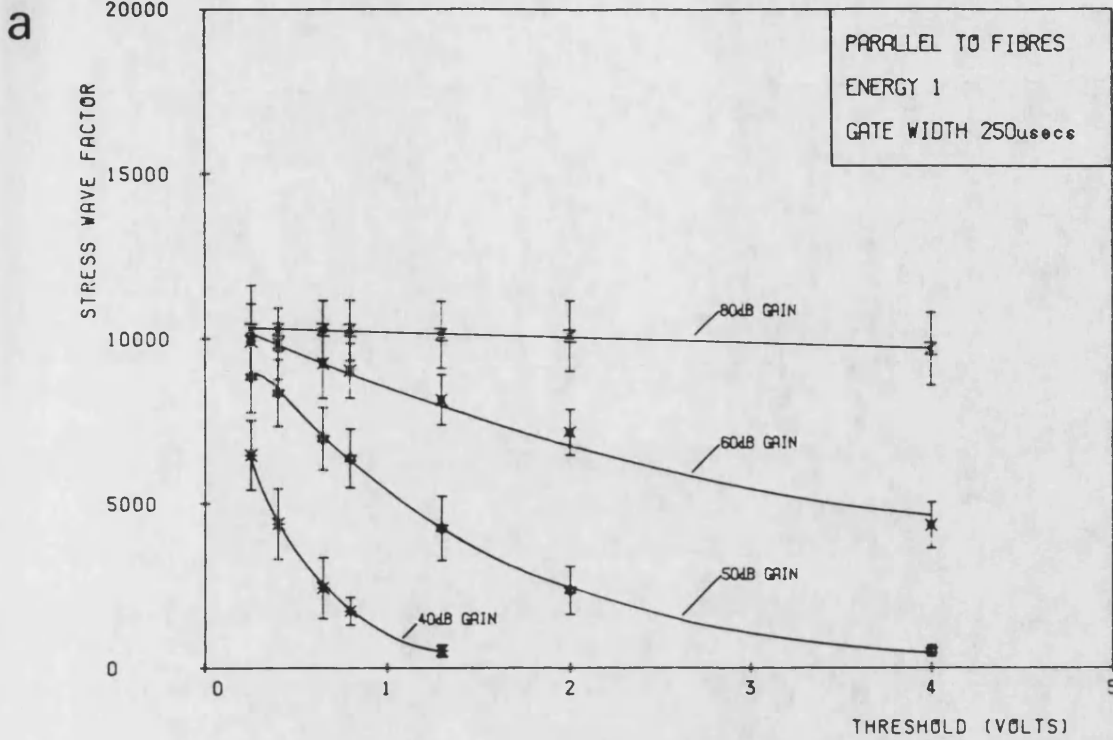


Figure 3.6. Variation of SWF with gate width for three levels of threshold setting: (a) parallel to fibres of unidirectional APC2; (b) perpendicular to fibres. See text for explanation of line XY. Error bars are ± 2 standard deviations.

SWF VERSUS THRESHOLD FOR VARIOUS GAINS



SWF VERSUS THRESHOLD FOR VARIOUS GAINS

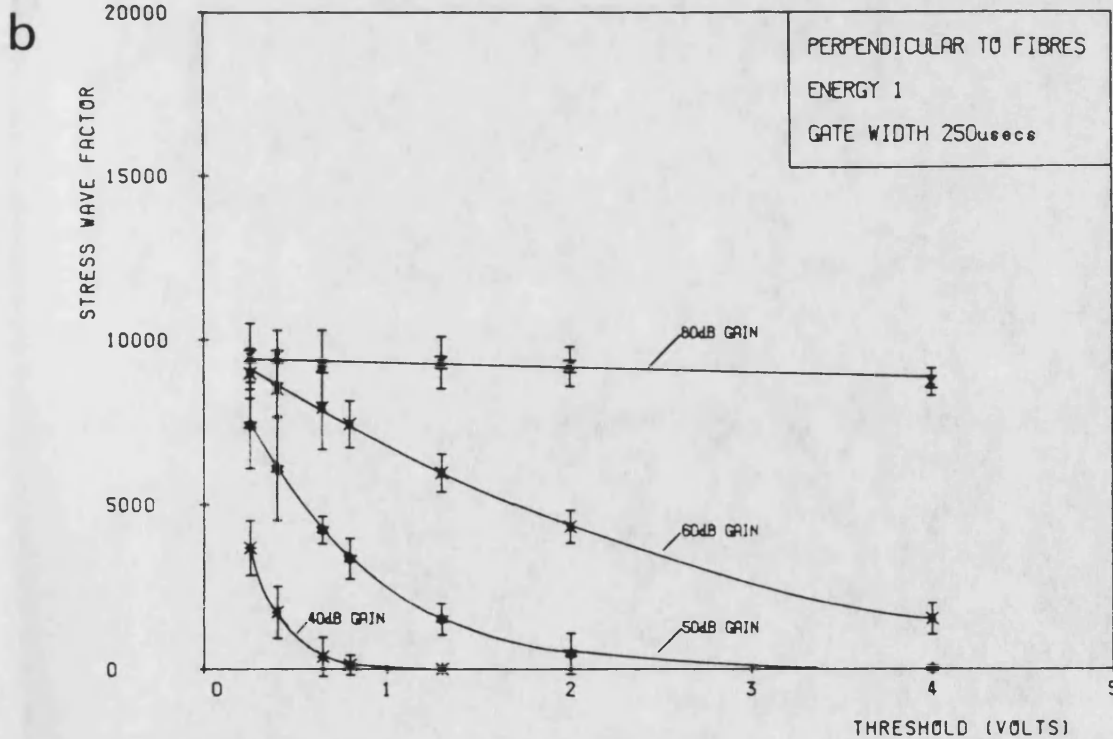
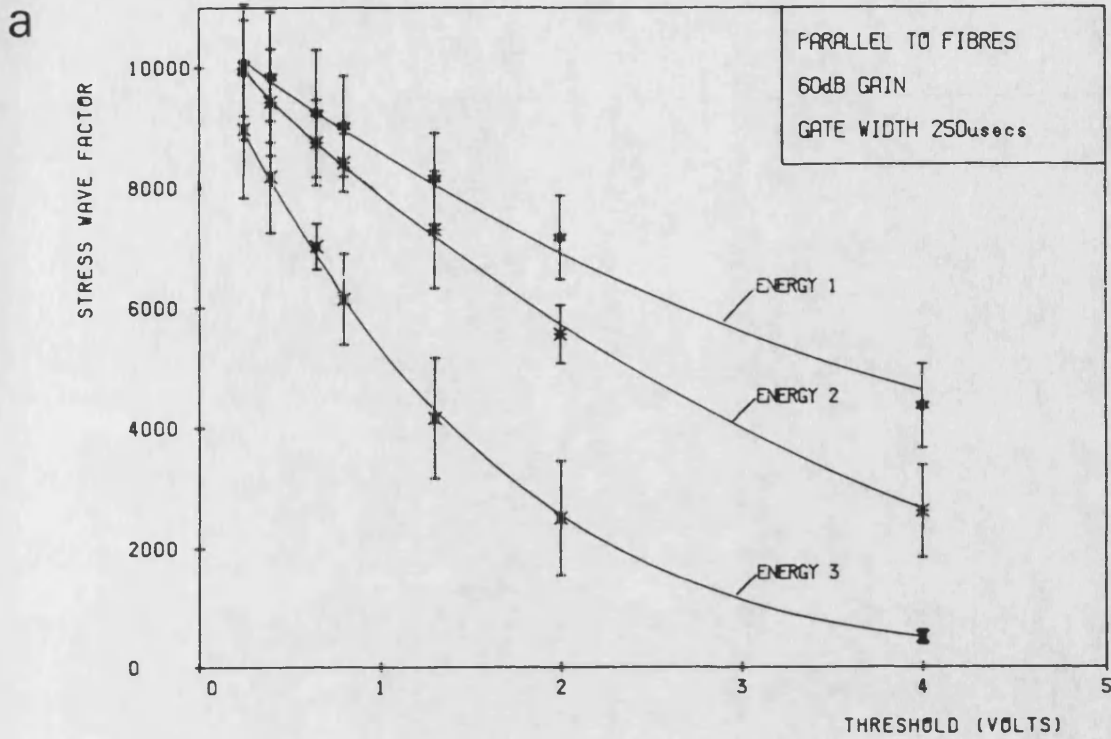


Figure 3.7. Variation of SWF with threshold setting for four gain settings: (a) parallel to fibres of unidirectional APC2; (b) perpendicular to fibres. Error bars are ± 2 standard deviations.

SWF VERSUS THRESHOLD FOR 3 ENERGIES



SWF VERSUS THRESHOLD FOR 3 ENERGIES

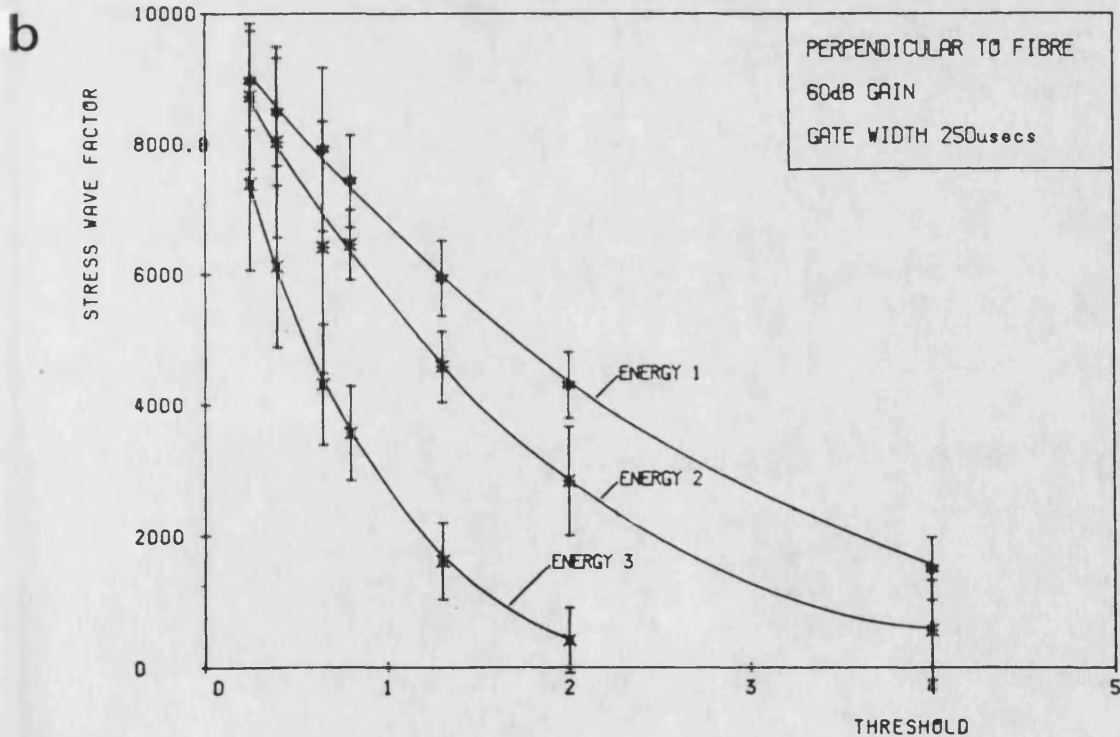


Figure 3.8. Variation of SWF with threshold setting for three levels of excitation pulse energy: (a) parallel to fibres of unidirectional APC2; (b) perpendicular to fibres. Error bars are ± 2 standard deviations.

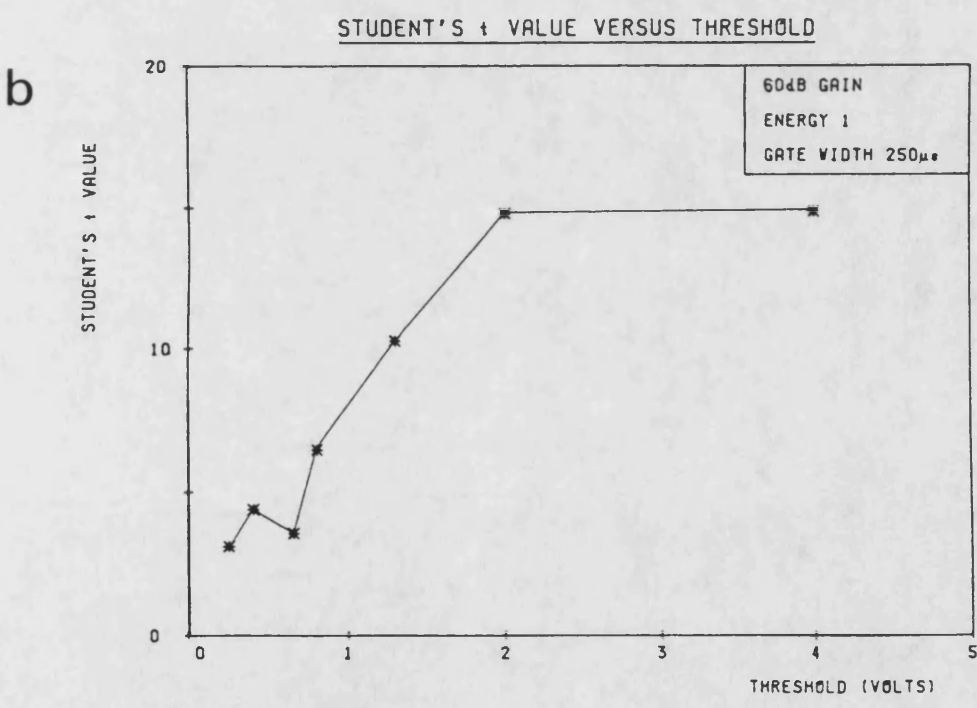
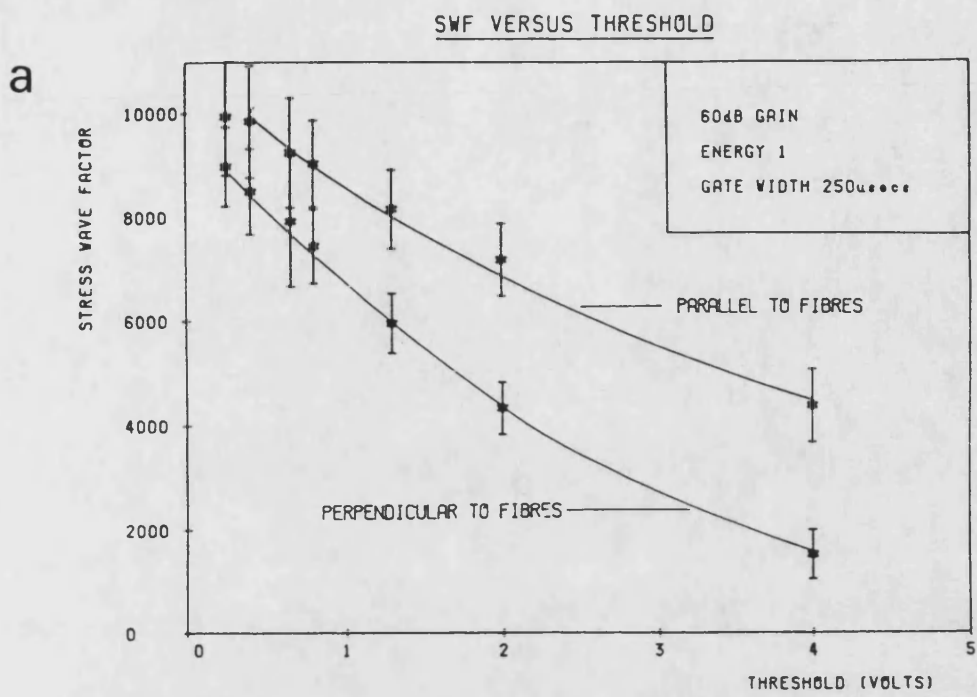
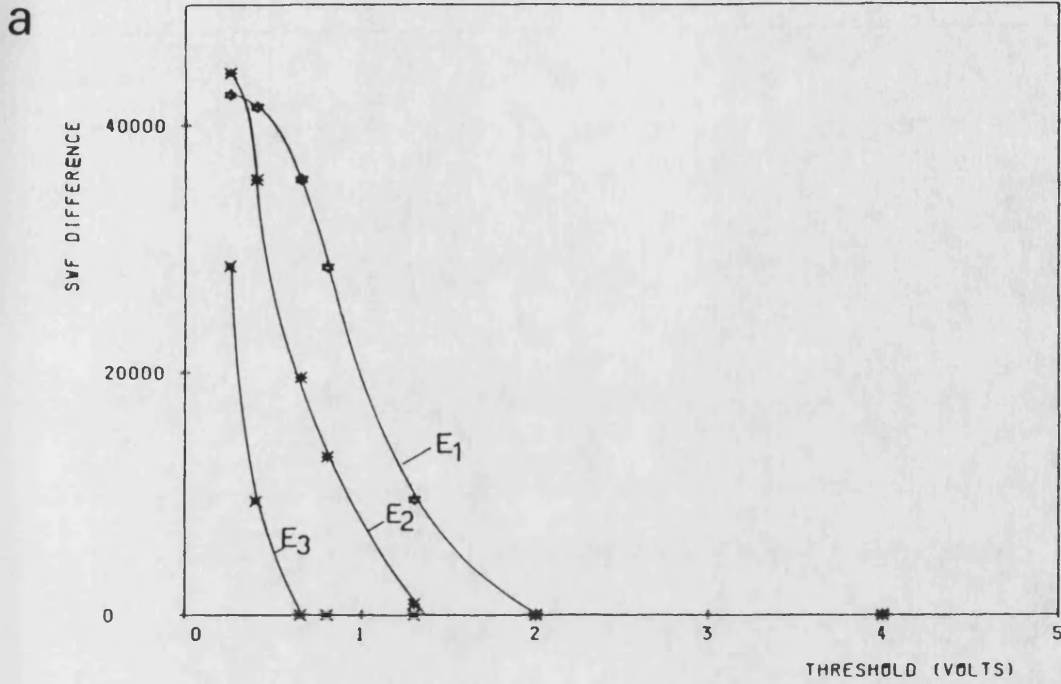


Figure 3.9. Comparison of SWF measurements parallel and perpendicular to fibres of unidirectional APC2, showing effects of threshold setting: (a) SWF values for the two orientations (error bars are ± 2 standard deviations); (b) values of Student's t for corresponding mean SWFs in the two orientations.

SWF DIFFERENCE VERSUS THRESHOLD FOR G=40dB



SWF DIFFERENCE VERSUS THRESHOLD FOR G=50dB

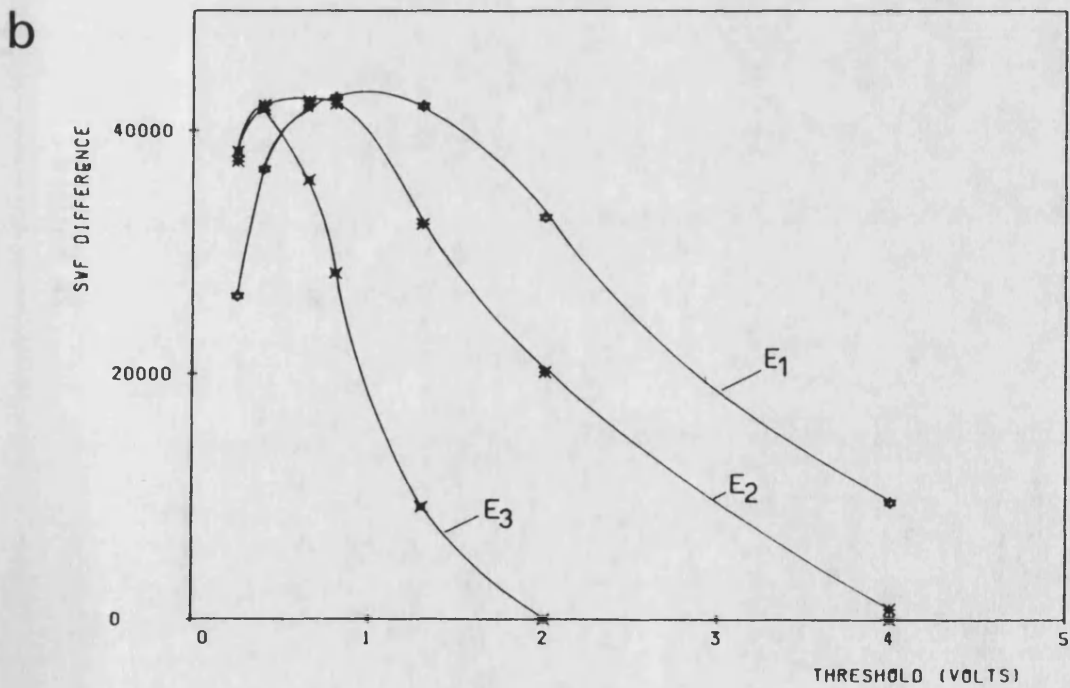
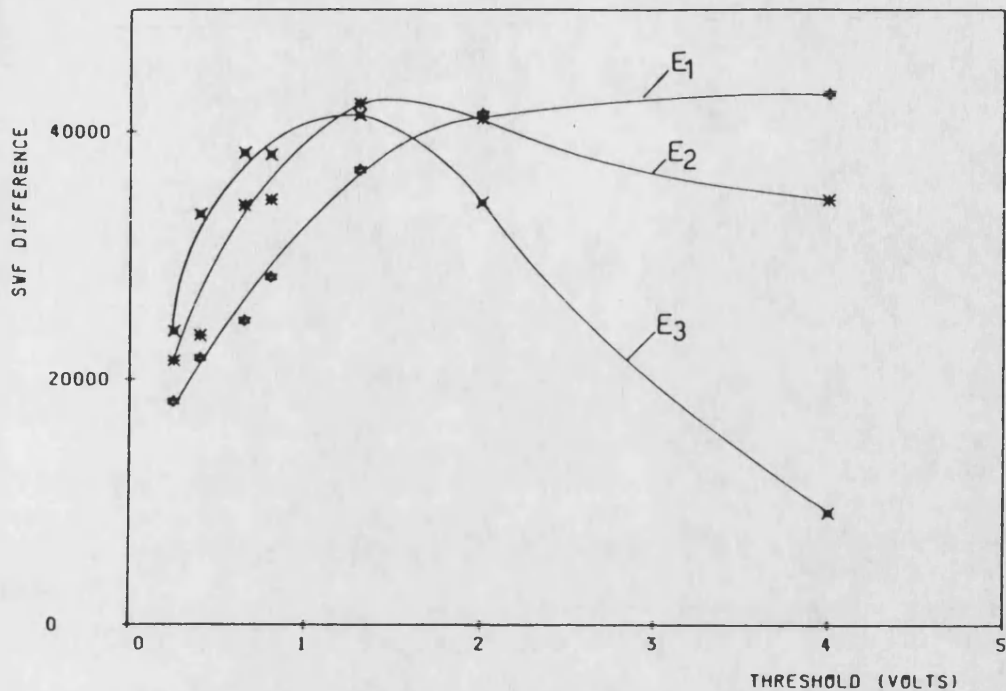


Figure 3.10. Threshold/pulse energy interactions upon DSWF at four levels of gain: (a) 40 dB; (b) 50 dB; (c) 60 dB; (d) 80 dB. See text for definition of DSWF. Each ordinate value is the sum of 20 measurements.

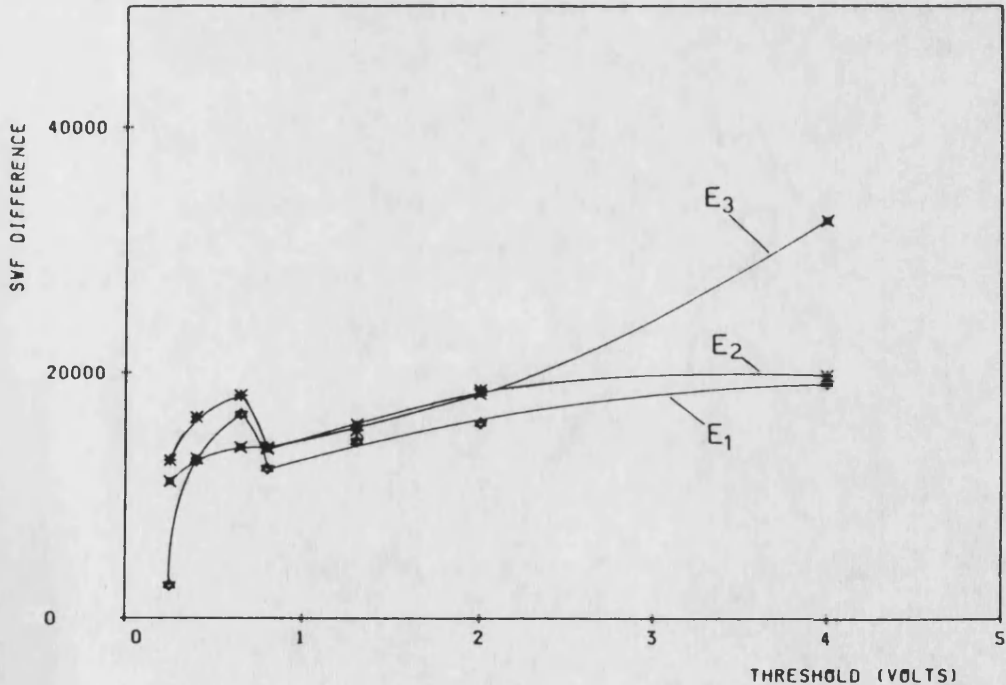
SWF DIFFERENCE VERSUS THRESHOLD FOR G=60dB

C



SWF DIFFERENCE VERSUS THRESHOLD FOR G=80dB

d



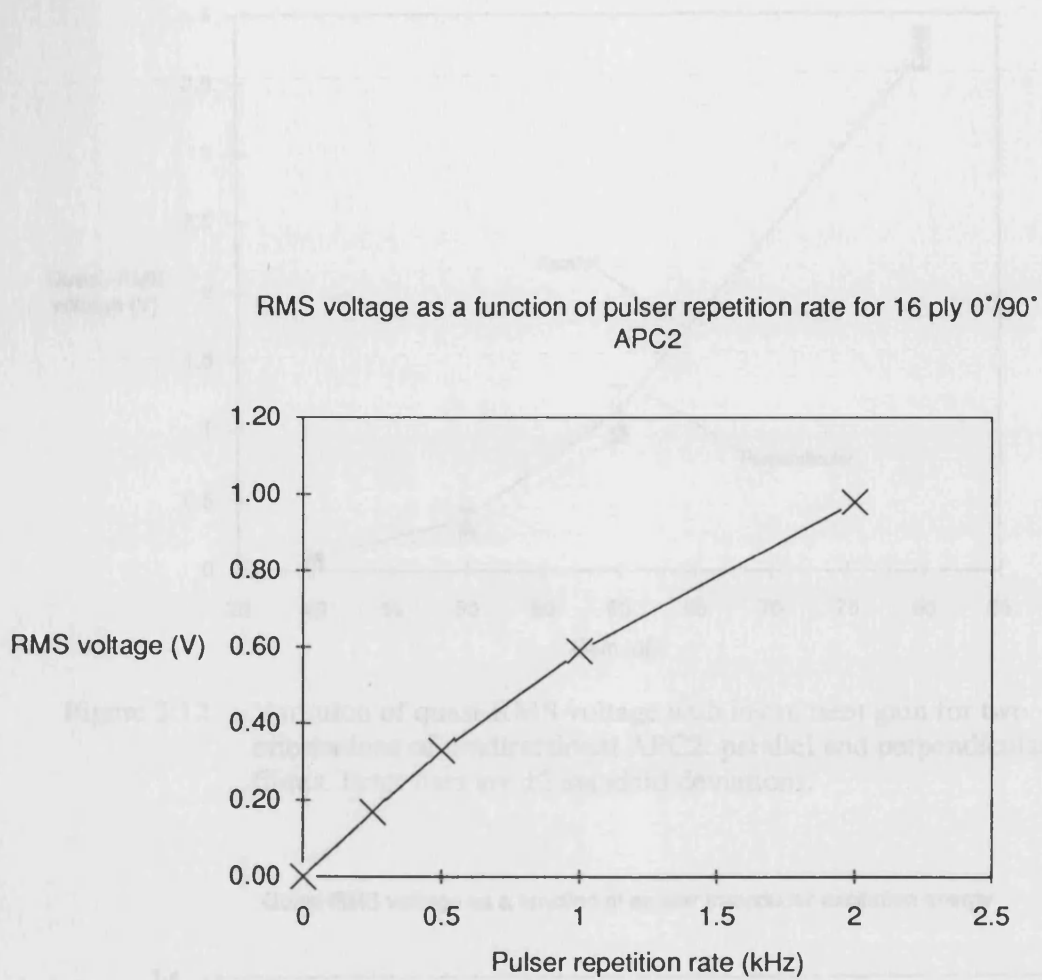


Figure 3.11. Variation of quasi-RMS voltage with pulser repetition rate for 16-ply $0^{\circ}/90^{\circ}$ APC2.

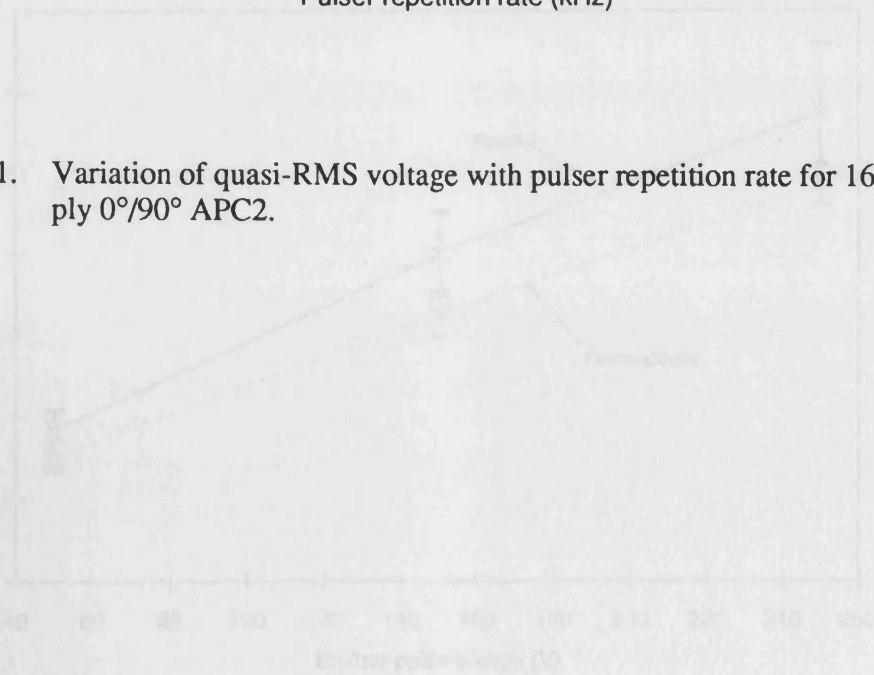


Figure 3.13. Variation of quasi-RMS voltage with excitation pulse energy for two orientations of unidirectional APC2: parallel and perpendicular to fibers. Error bars are ± 2 standard deviations.

Quasi-RMS voltage as a function of gain

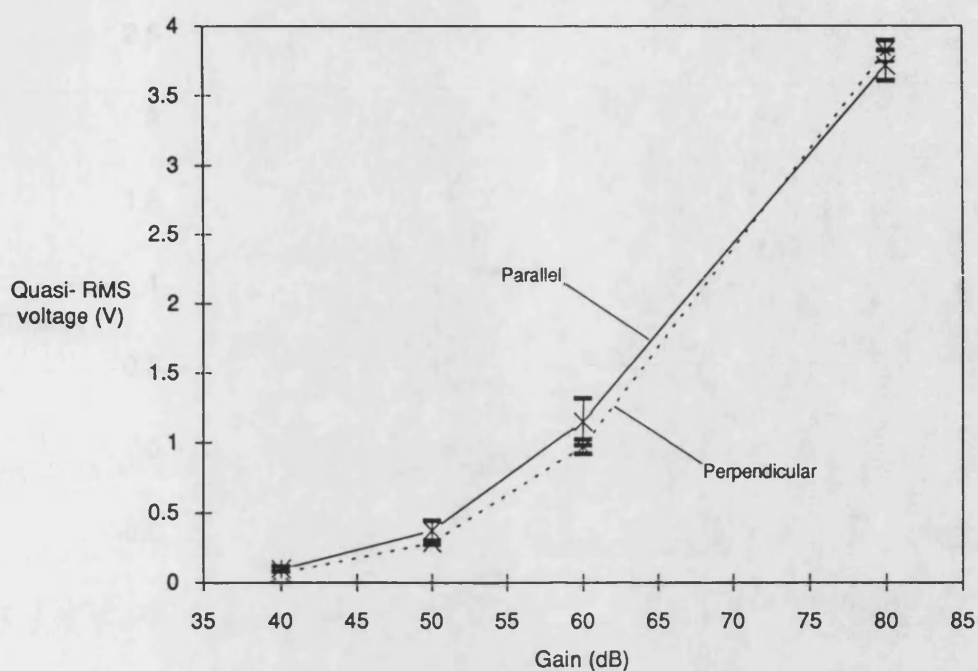


Figure 3.12. Variation of quasi-RMS voltage with instrument gain for two orientations of unidirectional APC2: parallel and perpendicular to fibres. Error bars are ± 2 standard deviations.

Quasi-RMS voltage as a function of emitter transducer excitation energy

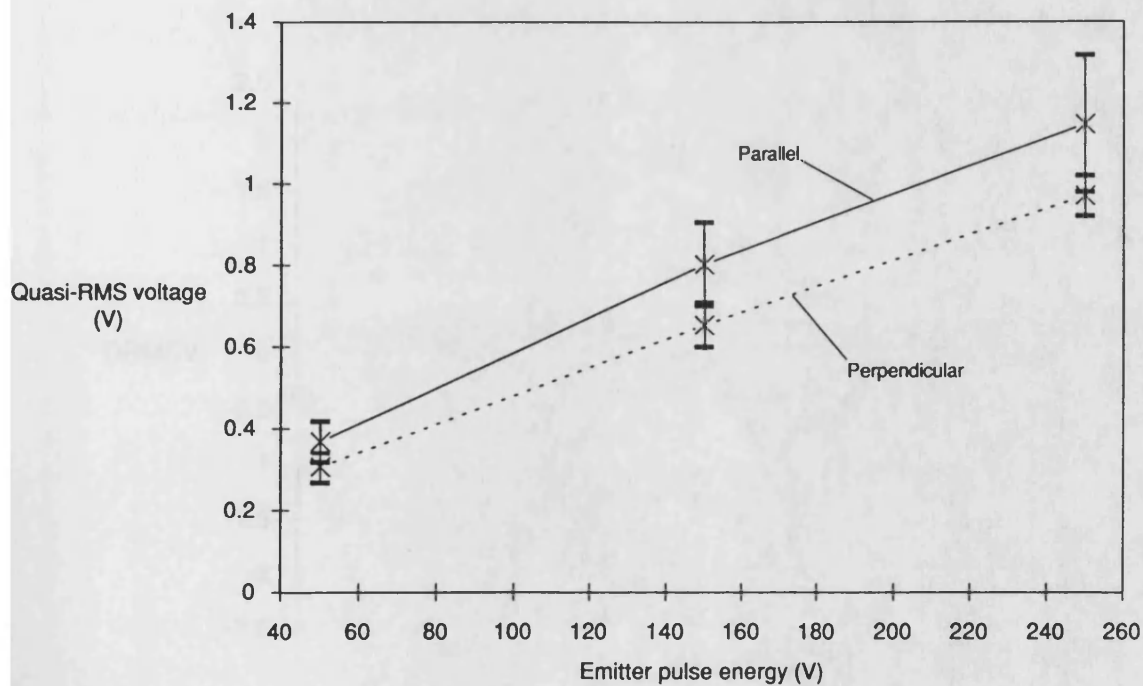


Figure 3.13. Variation of quasi-RMS voltage with excitation pulse energy for two orientations of unidirectional APC2: parallel and perpendicular to fibres. Error bars are ± 2 standard deviations.

DRMSV (arithmetic difference between RMSV parallel and perpendicular to fibres) as a function of pulse energy

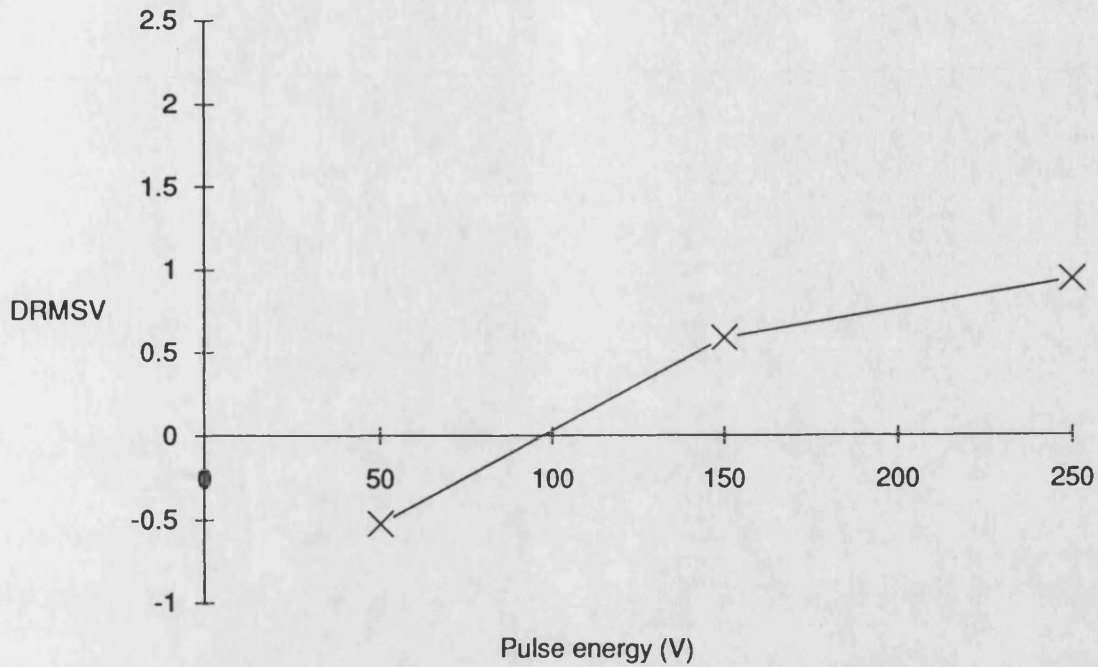


Figure 3.14. The effect of excitation pulse energy on DRMSV. See text for definition of DRMSV. Each ordinate value is the sum of 20 measurements.

DRMSV (arithmetic difference between RMSV parallel and perpendicular to fibres) as a function of gain

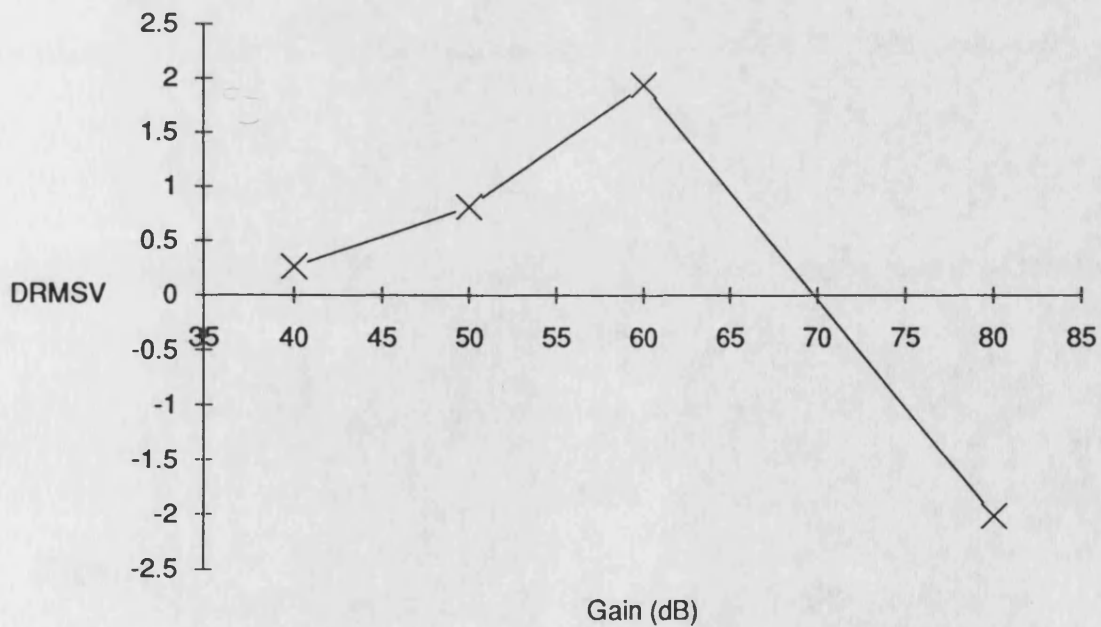


Figure 3.15. The effect of instrument gain on DRMSV. See text for definition of DRMSV. Each ordinate value is the sum of 15 measurements.

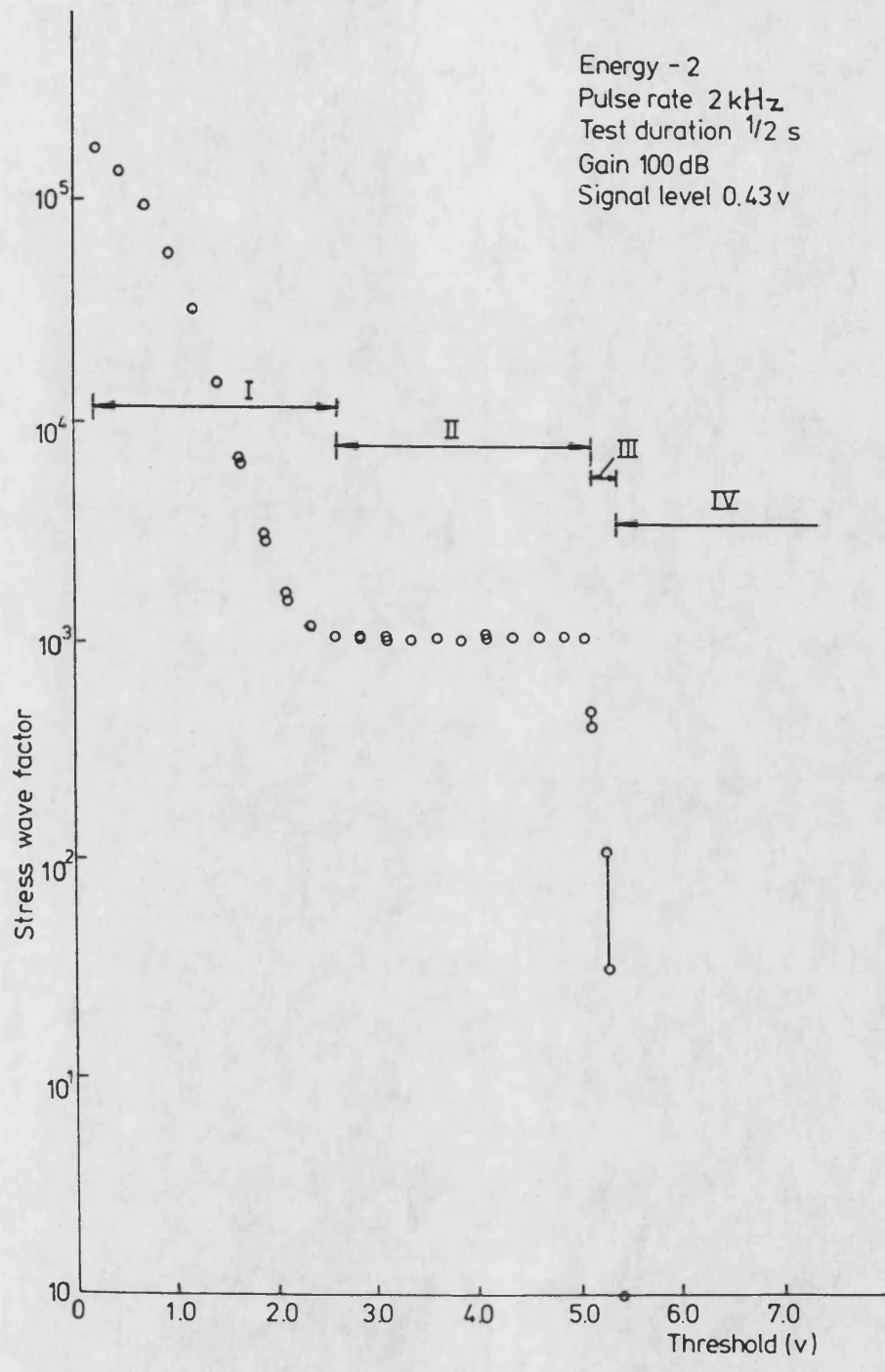
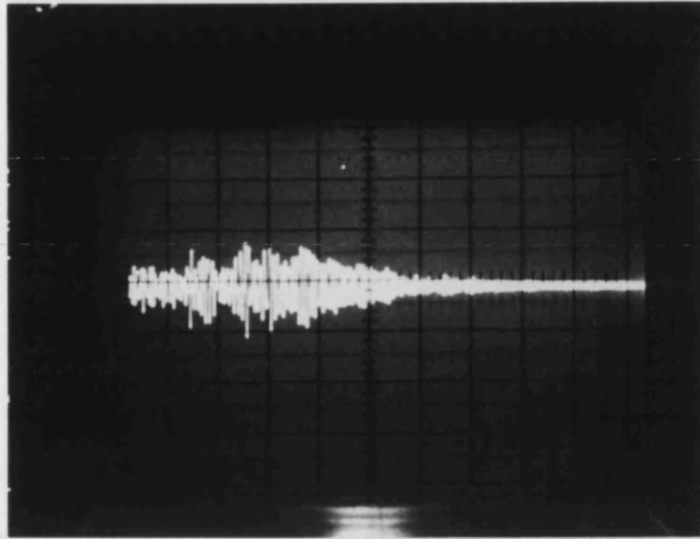


Figure 3.16. Variation of SWF with threshold with a 10 cm air gap between emitter and receiver transducers (after Bhatt and Hogg (74,75,76))

a

LOW GAIN



b

HIGH GAIN

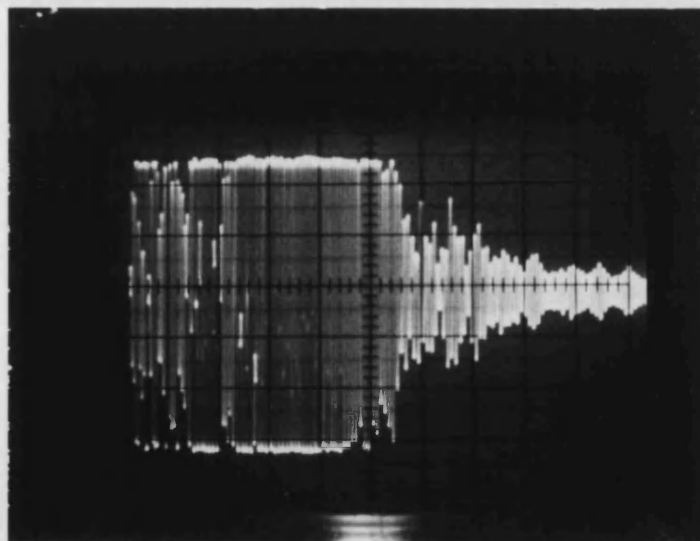


Figure 3.17. Typical received AU pulse shapes: (a) low gain; (b) high gain. 2 V/div vertical scale, 20 microseconds/div horizontal scale.

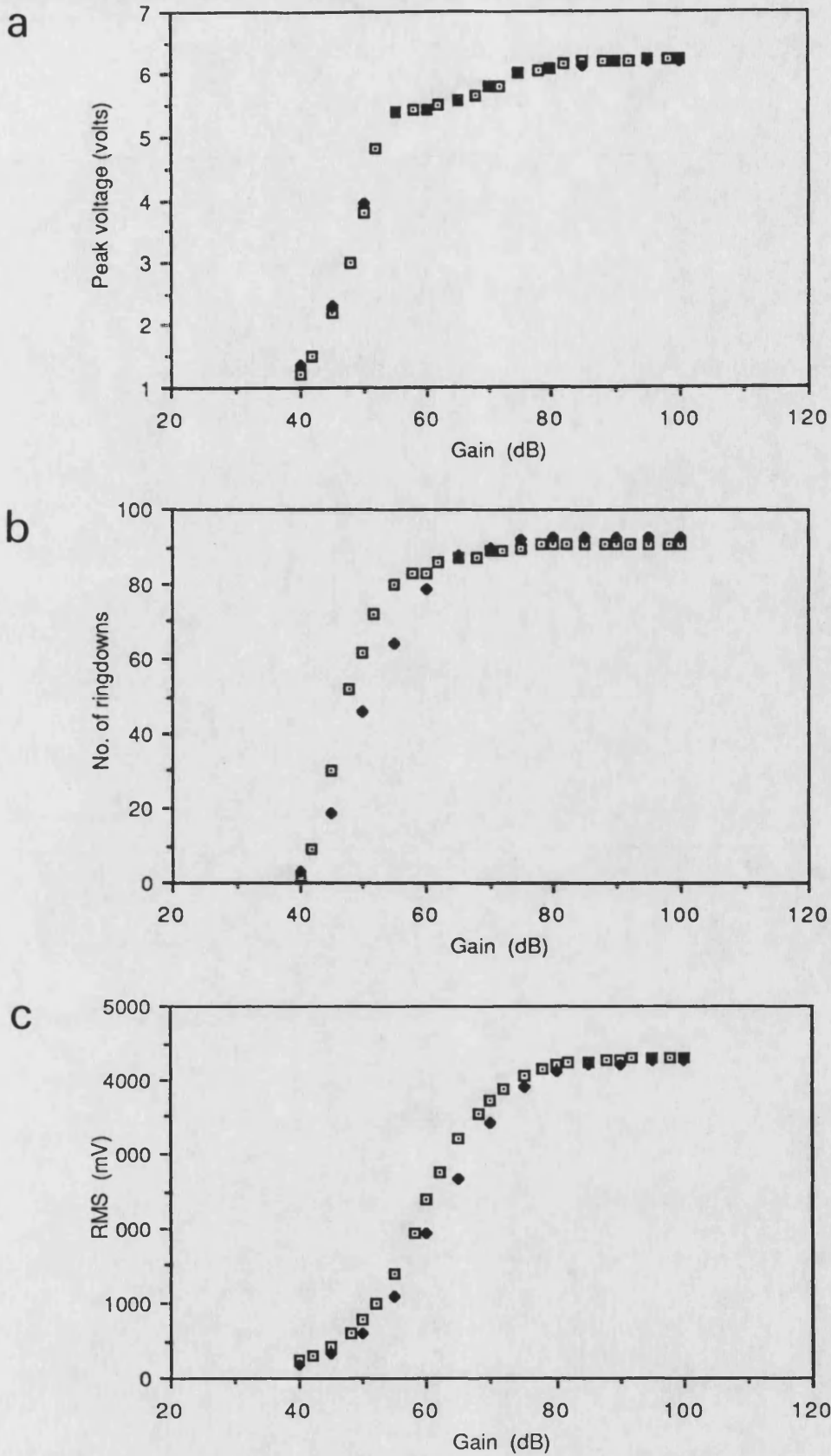


Figure 3.18. The effect of gain (using the AU206) on three characteristics of an AU pulse: a) peak amplitude b) number of ringdowns per pulse ('SWF') c) RMS voltage. Data from two repeat recouplings of the transducers are included in each graph.

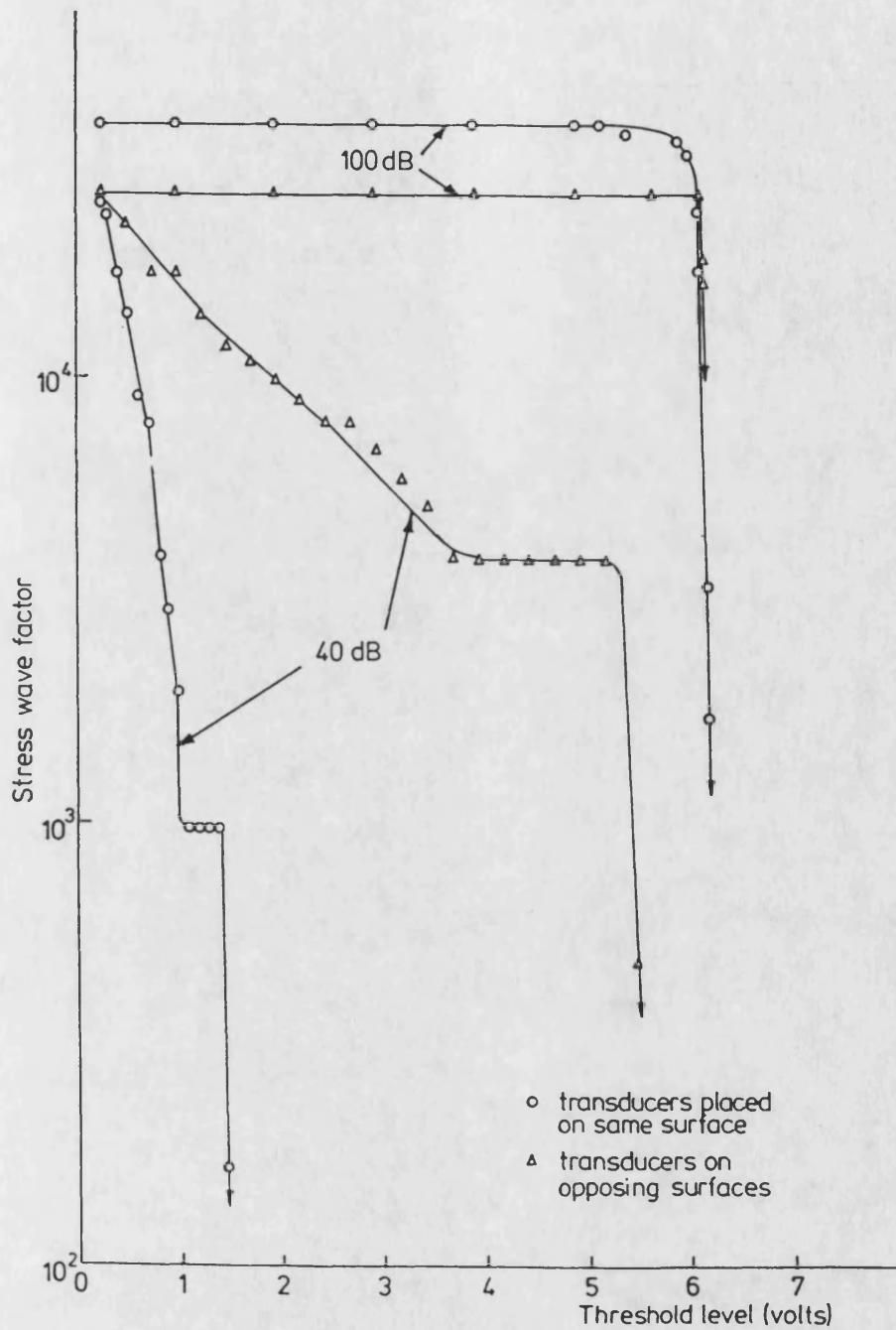


Figure 3.19. Variation of SWF with threshold for through transmission and same surface AU testing of APC2 (after Bhatt and Hogg ^(74,76,75)).

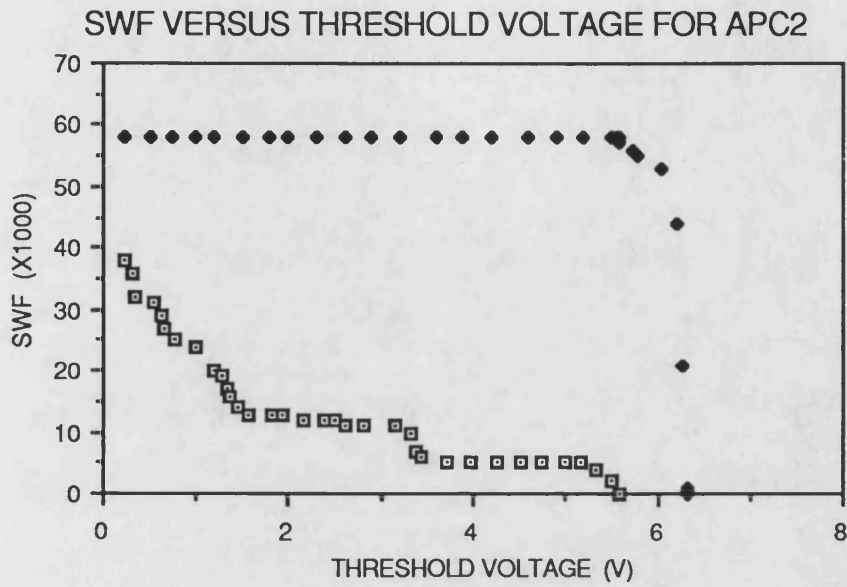
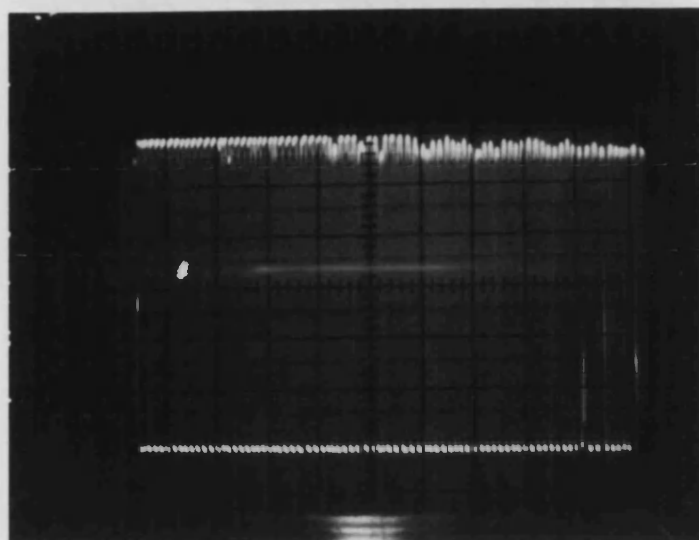


Figure 3.20. Variation of SWF with threshold for through transmission AU testing of 40-ply UD APC2 at 40 dB and 100 dB gain. See text for test conditions.

a

100 dB GAIN



b

40 dB GAIN

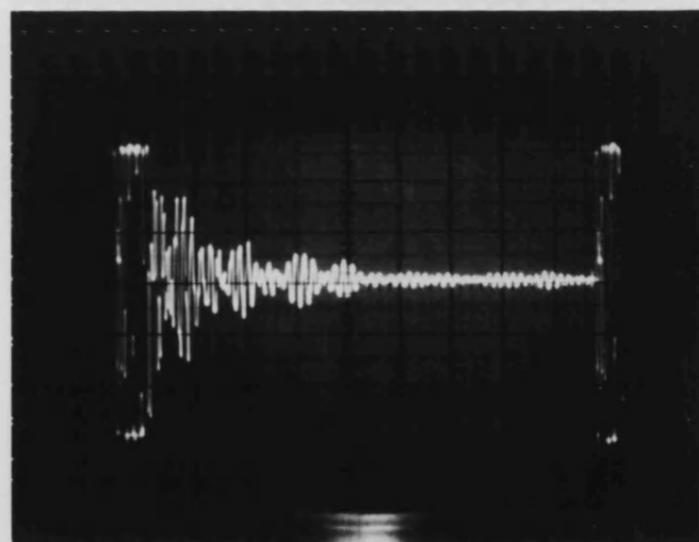


Figure 3.21. AU pulse shapes for the through transmission mode of AU testing of 40-ply UD APC2 using test conditions used by Bhatt and Hogg (74,76,75), 2 V/div vertical scale, 50 microseconds/div horizontal scale.

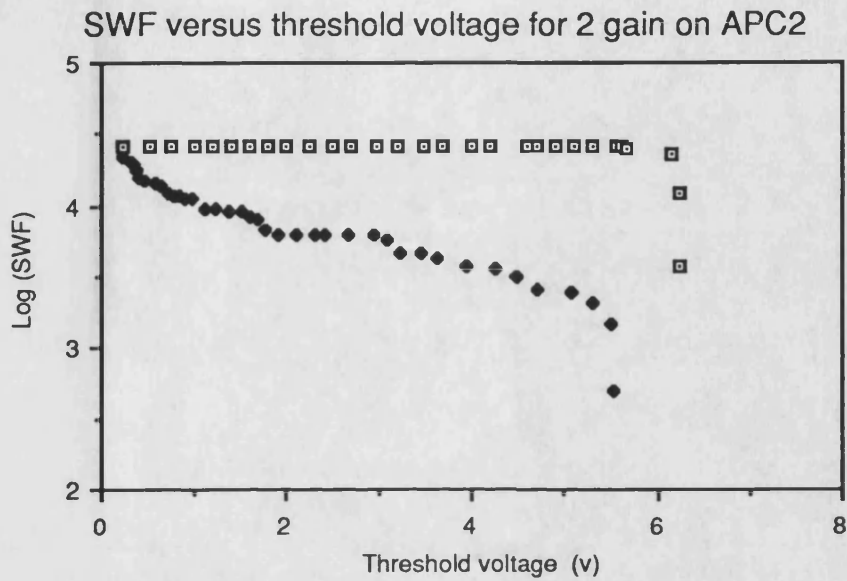
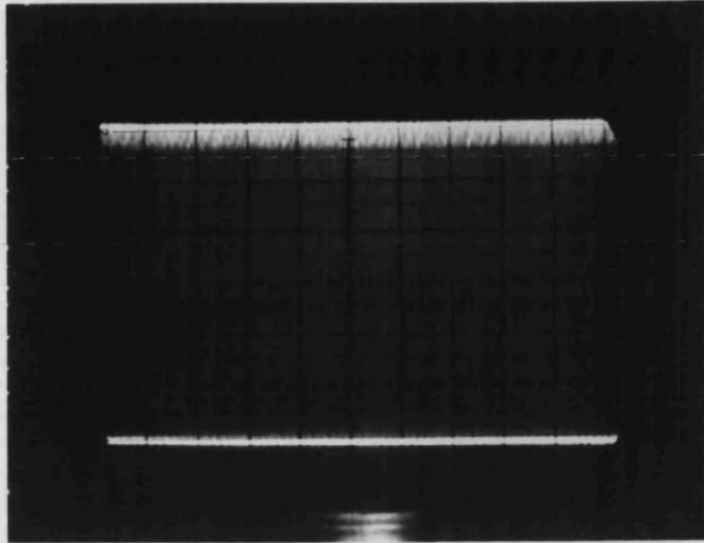


Figure 3.22. Variation of SWF with threshold for through transmission AU testing of 40-ply UD APC2 at 40 dB and 100 dB gain. Test conditions: pulse energy E1, pulse rate 1 KHz, sample time 0.5 seconds and gate width 350 microseconds.

a

100 dB GAIN



b

40 dB GAIN

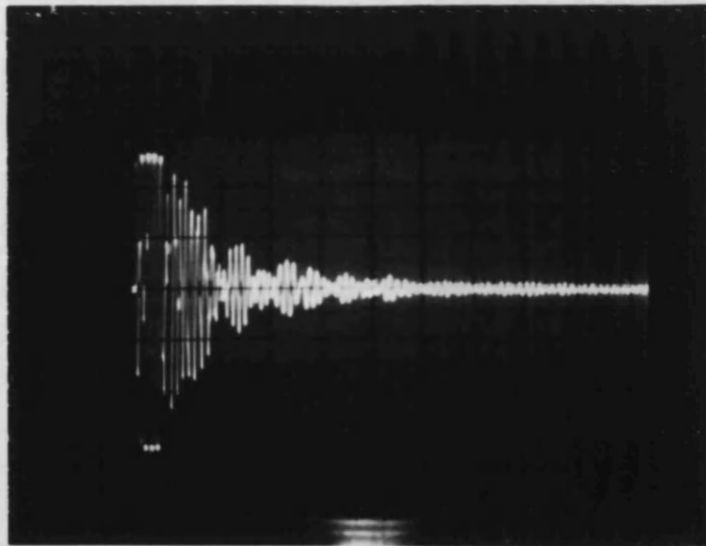


Figure 3.23. AU pulse shapes for the through transmission mode of AU testing of 40-ply UD APC2 at 40 dB and 100 dB gain. Test conditions: pulse energy E1, pulse rate 1 KHz, sample time 0.5 seconds and gate width 350 microseconds. 2 V/div vertical scale, 50 microseconds/div horizontal scale.

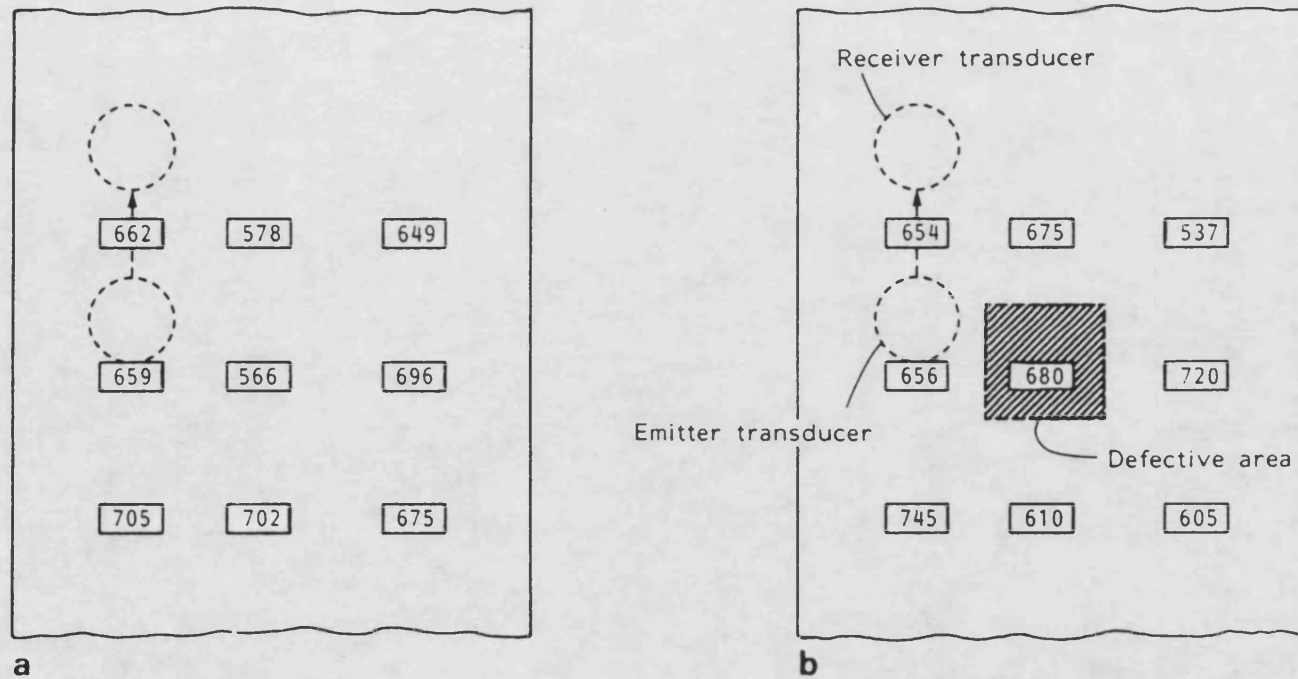


Figure 3.24. Variation of SWF measured PARALLEL to fibres with location in 16-ply unidirectional APC2 plates. Figures are the mean of five measurements. First three of four digits are shown. (a) Standard plate (non defective). (b) Defective plate (30 mm x 30 mm square sections removed from two centre plies prior to moulding).

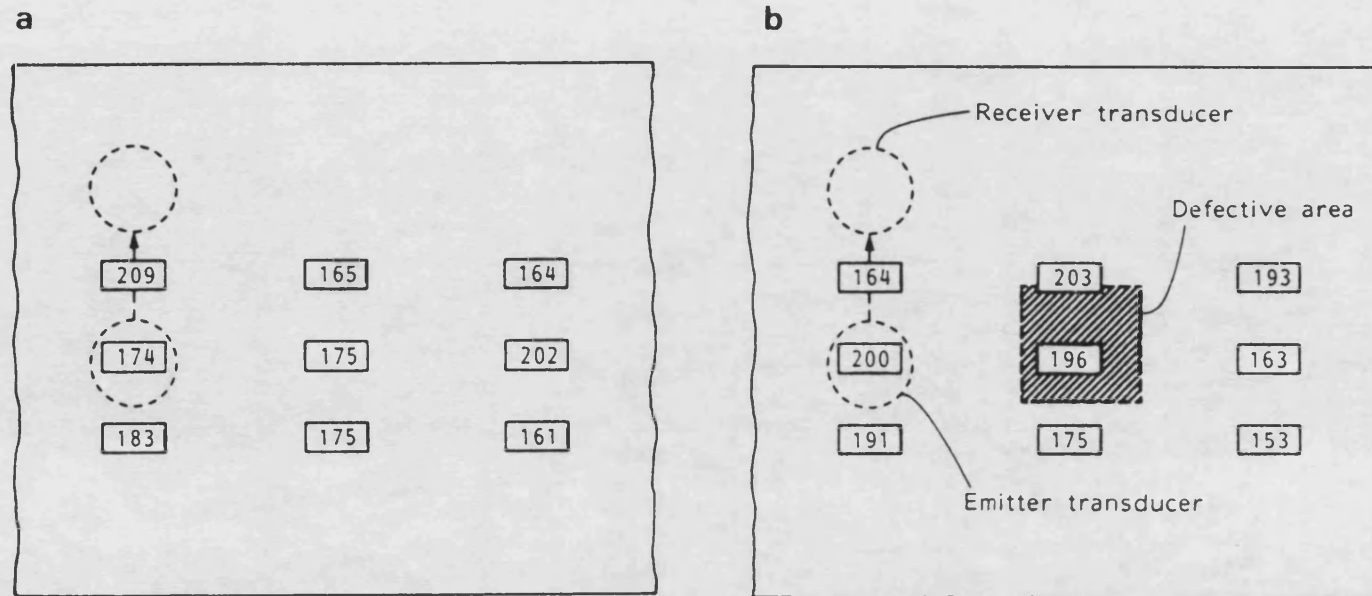


Figure 3.25. Variation of SWF measured PERPENDICULAR to fibres with location in 16-ply unidirectional APC2 plates. Figures are the mean of five measurements. First three of four digits are shown. (a) Standard plate (non defective). (b) Defective plate (30 mm x 30 mm square sections removed from two centre plies prior to moulding).

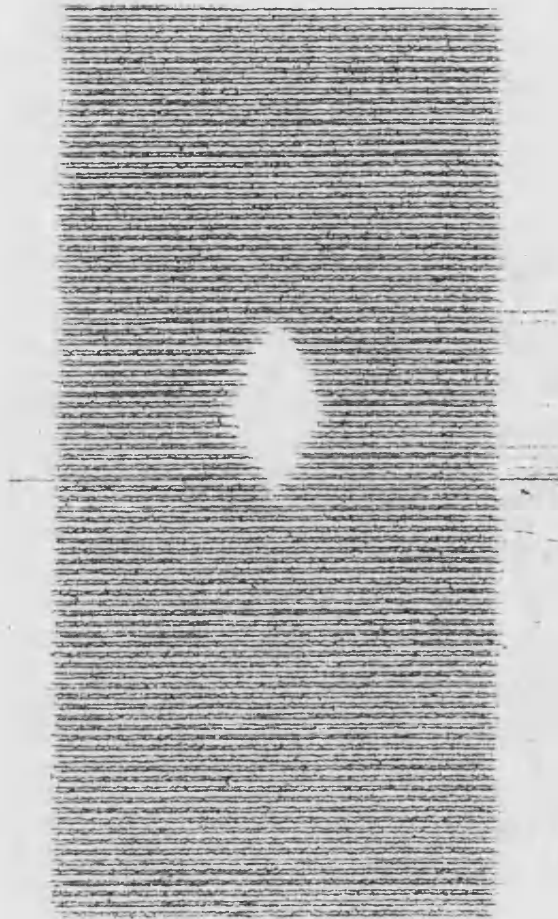
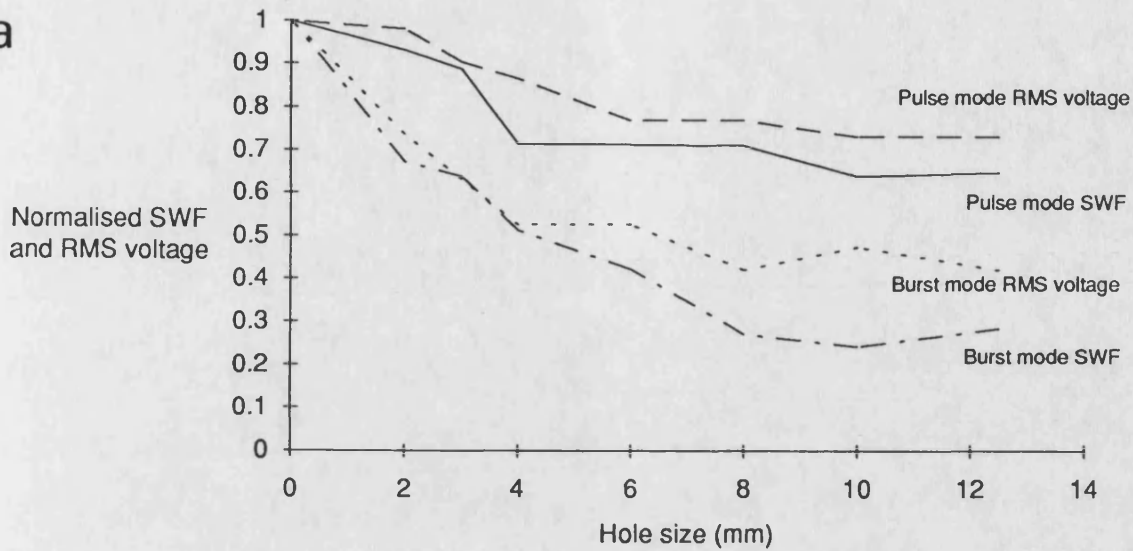


Figure 3.26. A typical C-scan of a 16-ply 0°/90° APC2 plate after a 4 joule drop weight impact.

a

Normalised SWF and RMS voltage (measured parallel to fibres) as a function of hole size in 20 ply UD APC2



b

Normalised SWF and RMS voltage (measured perpendicular to fibres) as a function of hole size in 20 ply UD APC2

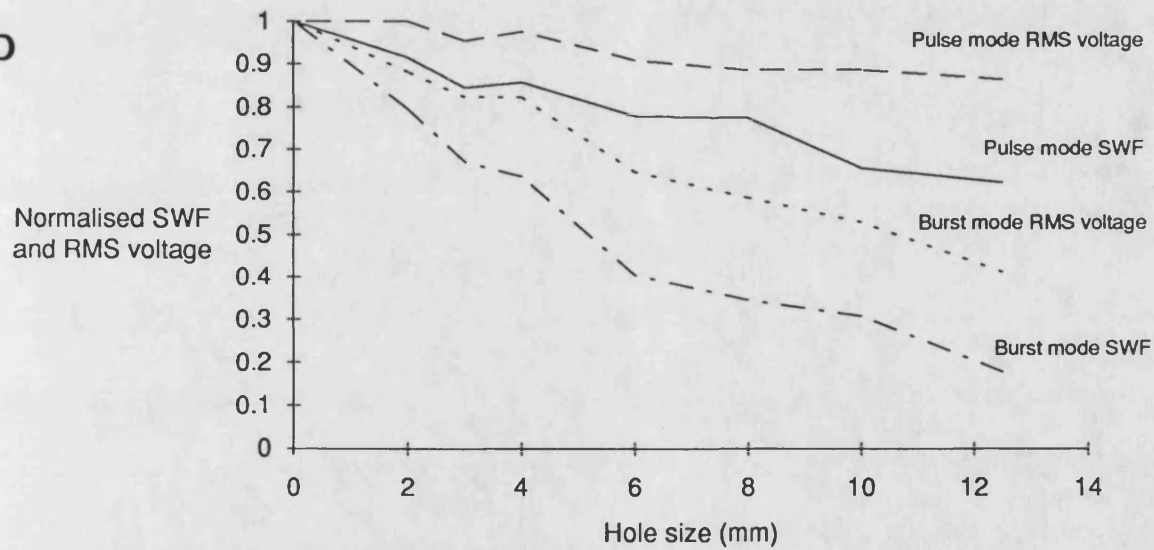


Figure 3.27. Variation of SWF and RMS voltage with through thickness hole size in 20-ply unidirectional APC2. (a) Measurements made parallel to fibres. (b) Measurements made perpendicular to fibres. Ordinate values have been normalised by dividing by their initial values prior to the introduction of a through thickness hole.

FACTOR	SYMBOL	SETTING LEVELS USED	SETTINGS AVAILABLE
Threshold	T	0.25 V 0.40 V 0.65 V 0.80 V 1.30 V 2.00 V 4.00 V	0.25 V min 6.40 V max
Gate width	Q	33.0 microsecs 50.0 microsecs 87.5 microsecs 125.0 microsecs 250.0 microsecs	33 microsecs min 312 microsecs max
Gain	G	40 dB 50 dB 60 dB 80 dB	40 dB min 100 dB max
Energy	E	1 (-250 V) 2 (-150 V) 3 (- 50 V)	1, 2, 3
Orientation w.r.t fibres	O	Parallel (0°) Perpendicular (90°)	Infinite

Table 3.1. The main instrument variables, their ranges and the values selected for experimental measurements.

SOURCE	SUM OF SQUARES (X1000)	DF	ESTIMATE OF VARIANCE (X1000)	F RATIO
T	2102447	6	350407	3691
Q	6399954	3	2133318	22473
G	8913002	3	2971000	31297
E	645110	2	322555	3397
O	1080279	1	1080279	11380
TQ	624945	18	34719	365
TE	15451	12	1287	13
TG	614972	18	34165	359
TO	43232	6	7205	75
QE	179657	6	29942	315
QG	3135411	9	348379	3669
QO	18218	3	6072	63
EG	119611	6	19935	210
EO	15327	2	7663	80
GO	120928	3	40309	424
TQE	11200	36	311	3.27
TQG	411957	54	7628	80
TQO	1798	18	99	1.05
TEG	174044	36	4834	50
TEO	6954	12	579	6.1
TGO	171787	18	9543	100
QEG	74299	18	4127	43
QEO	150	6	25	0.26
QGO	6944	9	771	8.12
EGO	25285	6	4214	44
TQEG	120196	108	1112	11
TQEO	2934	36	81	0.85
TQOG	9540	54	176	1.86
TOEG	62153	36	1726	18
QOEG	2817	18	156	1.64
TQEGO	10035	108	92	0.97
RESIDUAL	255162	2688	94	1

Table 3.2. Table of analysis of variation and covariation of SWF for five variables: threshold (T), gate width (Q), gain (G), excitation pulse energy (E) and orientation (O).

SOURCE	SUM OF SQUARES	DF	ESTIMATE OF VARIANCE	F RATIO
Q	36437247	3	12145749	59.8582706
T	86464474	6	14410745.7	71.0209237
E	30654854	2	15327427	75.5386327
G	241857237	3	80619079	397.317501
GE	50571117	6	8428519.5	41.5385334
QG	13888856	9	1543206.22	7.60543097
QE	300178	6	50029.6667	0.246562754
TG	343574499	18	19087472.2	94.0693796
TE	13908311	12	1159025.92	5.71206328
TQ	3596557	18	199808.722	0.984723508
QGE	5634977	18	313054.278	1.54283508
TGE	124307819	36	3452994.97	17.017502
TQE	5869085	36	163030.139	0.803466477
TQG	19080901	54	353350.019	1.74142583
TQEG	20071143	108	185843.917	0.915900324
RESIDUAL	272708959	1344	202908.452	1

Table 3.3. Table of analysis of variation and covariation of DSWF for four instrument variables: threshold (T), gate width (Q), gain (G) and excitation pulse energy (E). See text for definition of DSWF.

AMPLIFIER GAIN (dB)	AMPLITUDE OF RECEIVED INPUT SPIKE (Volts)
40	0.38
50	0.42
60	0.44
70	0.79
80	2.54
90	5.40
100	5.60

Table 3.4. Magnitude of the received ringdown caused by leakage of the emitter excitation spike from the emitter module of the AU206 to the receiver module.

AU Parameter	Test Conditions	Good Quality	10 x 4.9J Impacts	Student's t value
SWF	50dB,E1	3039 (409)	2787 (452)	1.45
SWF	60dB,E2	3450 (156)	3396 (236)	0.69
RMS V	60dB,E2	0.1027 (0.0171)	0.081 (0.0166)	3.14
RMS V	80dB,E1	0.6067 (0.0981)	0.483 (0.0529)	3.64

Table 3.5. Instrument settings and corresponding mean SWF and RMS voltage values from good quality and impact damaged unidirectional plates of APC2. Values in brackets are standard deviations. Student's t values are for the comparisons of means recorded for good quality and those for impact damaged plates and relate to 23 degrees of freedom.

AU parameter	Gain (dB)	Threshold (V)	Gate (microsecs)	Pulse (V)	Before impact	After impact	Student's 't'
SWF	50	1.31	250	-250	3410 (392)	3946 (242)	2.59
SWF	60	1.31	250	-250	6972 (420)	7102 (500)	0.45
RMSV	60	-	-	-250	0.2 (0.007)	0.228 (0.011)	4.80
SWF	60	1.31 (AUTO)	250	-250	6438 (508)	6724 (742)	0.71
SWF	55	1.31	250	-250	5576 (512)	5856 (380)	0.98
SWF	60	1.31	250	-150	6180 (709)	6606 (645)	0.99
SWF	60	1.31	62	-150	2280 (56)	2300 (74)	0.48

Table 3.6. Instrument settings and corresponding SWF and RMS voltage values before and after infliction of impact damage on cross ply plates of APC2. Standard deviations are included in brackets. See text for explanation of Student's t values.

AU Parameter	Good Quality	Impacted and flexed to top ply failure	Student's t value
SWF	6812 (320)	4598 (640)	6.92
RMS V	0.672 (0.063)	0.322 (0.086)	7.34

Table 3.7. Mean values of SWF and RMS voltage for good quality laminates and defective laminates. Defective laminates have been subjected to a single 5.7 J impact followed by flexing in 3 point bend until top ply failure. Student's t values are for mean comparisons between defective and non-defective plates. Values in brackets are standard deviations.

	Pulse mode SWF 50dB, E1	Pulse mode SWF 60dB, E2	Pulse mode SWF 60dB, E2, Auto	Pulse mode RMS 60dB, E1	Pulse mode RMS 80dB, E1	Burst mode RMS	Burst mode SWF
Mean	3104	3311	3266	0.152	0.488	0.193	3601
Standard deviation	213	154	177	0.016	0.015	0.048	48
Coefficient of variation	0.069	0.046	0.054	0.104	0.031	0.247	0.013
95% confidence limits	426	307	353	0.032	0.030	0.096	97

Table 3.8. The scatter in AU data as a result of coupling, recorded from 16-ply UD strip specimens. Mean, standard deviation, coefficient of variation and 95% confidence limits for corresponding combinations of AU parameter/instrument settings are presented for 30 repeat measurements (recouplings) at a single location on a single unidirectional APC2 strip specimen

Pair comparison	Pulse mode SWF 50dB, E1	Pulse mode SWF 60dB, E2	Pulse mode SWF 60dB, E2, Auto	Pulse mode RMS 60dB, E1	Pulse mode RMS 80dB, E1	Burst mode RMS	Burst mode SWF
Before impact	3275 (235)	3432 (179)	3396 (171)	0.163 (0.014)	0.51 (0.012)	0.498 (0.119)	3887 (212)
After impact	3353 (168)	3524 (152)	3469 (117)	0.183 (0.009)	0.514 (0.011)	0.627 (0.068)	4170 (207)
Before hole	3130 (213)	3470 (43)	3418 (15)	0.132 (0.014)	0.48 (0.013)	0.289 (0.101)	3773 (48)
After hole	2730 (582)	3171 (407)	3088 (426)	0.111 (0.020)	0.448 (0.028)	0.297 (0.150)	3464 (368)
Before indent	3692 (459)	3944 (448)	3911 (432)	0.163 (0.015)	0.513 (0.026)	0.42 (0.256)	4316 (488)
After indent	3312 (310)	3522 (209)	3448 (205)	0.157 (0.018)	0.495 (0.019)	0.648 (0.085)	4232 (186)
All non-defective(48)	3332 (339)	3584 (313)	3549 (303)	0.149 (0.020)	0.49 (0.027)	0.577 (0.249)	4046 (367)
Mean coefficient of variation for all non-defective	0.081	0.068	0.068	0.111	0.04	0.323	0.068

Table 3.9. Mean SWF and RMS voltage values for strip specimens of unidirectional APC2 before and after infliction of damage by three methods. Figures in brackets are standard deviations.

Pair comparison	Pulse mode SWF 50dB, E1	Pulse mode SWF 60dB, E2	Pulse mode SWF 60dB, E2, Auto	Pulse mode RMS 60dB, E1	Pulse mode RMS 80dB, E1	Burst mode RMS	Burst mode SWF
Before/after impact	0.60	0.88	0.79	2.68	0.55	2.11	2.14
Before/after hole	-1.12	-1.23	-1.30	-1.58	-1.82	0.08	-1.40
Before/after indent	-1.53	-1.92	-2.17	-0.57	-1.25	1.89	-0.36
5 IMPACTED/ 48 NON-DEFECTIVE	0.14	-0.42	-0.57	3.64	1.95	0.44	0.74
5 HOLED/ 48 NON-DEFECTIVE	-3.52	-2.73	-3.11	-4.03	-3.37	-2.45	-3.37
5 INDENTED/ 48 NON-DEFECTIVE	-0.13	-0.43	-0.72	0.80	0.37	0.63	1.11

Table 3.10. Tests for detection of damage by AU, based on figures from the previous table. The values of Student's t relate to testing the significance of any difference between two means: in the upper half of the table, between means from batches of 5 samples before and after the introduction of defects and in the lower half of the table, between batches of 5 defective samples and the total population of 48 non-defective samples.

Pair comparison	Pulse mode SWF 50dB, E1	Pulse mode SWF 60dB, E2	Pulse mode SWF 60dB, E2, Auto	Pulse mode RMS 60dB, E1	Pulse mode RMS 80dB, E1	Burst mode RMS	Burst mode SWF
Before/after impact	0.52	0.76	0.69	2.29	0.41	2.49	2.18
Before/after 3mm hole	-1.02	-1.27	-1.29	-1.00	-1.01	0.50	0.42
Before/after indent	-3.87	-3.36	-4.05	-2.84	-3.44	2.23	-0.42

Table 3.11. Values of Student's t, testing the significance of any deviation of the mean difference between AU measurements before and after introduction of defects, from zero. Student's t must exceed 4.6 for significance. A negative value indicates a decrease in the AU parameter after introduction of a defect and a positive value, the converse.

PARALLEL TO FIBRES

a

Hole diameter (mm)	PULSE MODE				BURST MODE			
	SWF 80dB, E2	RMSV 60dB, E2	SWF 50dB, E1	SWF 60dB, E2	SWF 60dB	RMSV 60dB	RMSV 70dB	SWF 50dB
None	10160 (384)	0.715 (0.0375)	4611 (375)	7272 (434)	6551 (676)	0.463 (0.0423)	1.139 (0.0423)	2918 (269)
2	9442 (450)	0.642 (0.0402)	4298 (325)	6610 (422)	5486 (313)	0.398 (0.0328)	1.012 (0.0665)	2602 (235)
4	9724 (390)	0.618 (0.0389)	3964 (444)	6040 (490)	5396 (661)	0.382 (0.0377)	1.010 (0.0539)	2500 (282)
6	9040 (553)	0.578 (0.0390)	3790 (444)	5748 (349)	4770 (508)	0.342 (0.4820)	0.954 (0.0764)	2092 (215)
9	8332 (182)	0.480 (0.0316)	2386 (302)	4918 (169)	3026 (452)	0.228 (0.0192)	0.728 (0.0576)	1188 (319)
12.5	7542 (663)	0.388 (0.0228)	1262 (302)	4648 (276)	2132 (403)	0.142 (0.0130)	0.546 (0.0571)	0 (0)

PERPENDICULAR TO FIBRES

b

Hole diameter (mm)	PULSE MODE				BURST MODE			
	SWF 80dB, E2	RMSV 60dB, E2	SWF 50dB, E1	SWF 60dB, E2	SWF 60dB	RMSV 60dB	RMSV 70dB	SWF 50dB
None	9066 (350)	0.359 (0.0179)	1526 (358)	4639 (351)	3537 (442)	0.239 (0.0321)	0.814 (0.0948)	7886 (357)
2	9036 (428)	0.360 (0.0283)	1132 (90)	4480 (280)	3278 (345)	0.224 (0.0182)	0.784 (0.0733)	7556 (204)
4	8908 (233)	0.322 (0.0216)	672 (214)	4244 (432)	2898 (604)	0.180 (0.0158)	0.658 (0.0593)	7636 (204)
6	8858 (351)	0.310 (0.0292)	422 (182)	4006 (399)	2664 (352)	0.168 (0.0217)	0.610 (0.0632)	7668 (433)
9	8200 (427)	0.278 (0.0110)	312 (71)	3386 (539)	1640 (331)	0.124 (0.0134)	0.480 (0.0308)	7200 (397)
12.5	8034 (274)	0.270 (0.0141)	104 (109)	3096 (365)	1606 (290)	0.128 (0.0130)	0.510 (0.0620)	6844 (326)

Table 3.12. Mean values of SWF and RMS voltage recorded on a 20-ply unidirectional APC2 plate with through thickness holes. (a) Measurements made parallel to fibres. (b) Measurements made perpendicular to fibres. Values in brackets are standard deviations.

PARALLEL TO FIBRES

a

Hole diameter (mm)	PULSE MODE				BURST MODE			
	SWF 80dB, E2	RMSV 60dB, E2	SWF 50dB, E1	SWF 60dB, E2	SWF 60dB	RMSV 60dB	RMSV 70dB	SWF 50dB
2	3.23	3.48	1.59	2.81	3.30	3.95	4.55	2.23
4	2.06	4.46	2.97	4.98	3.14	4.66	5.10	2.80
6	4.62	4.15	4.50	6.79	5.17	6.16	6.13	5.95
9	9.96	11.99	11.47	11.52	10.45	16.41	15.79	11.07
12.5	9.81	17.73	17.27	12.21	13.33	23.49	26.55	23.80

PERPENDICULAR TO FIBRES

b

Hole diameter (mm)	PULSE MODE				BURST MODE			
	SWF 80dB, E2	RMSV 60dB, E2	SWF 50dB, E1	SWF 60dB, E2	SWF 60dB	RMSV 60dB	RMSV 70dB	SWF 50dB
2	0.15	0.08	2.38	0.88	1.14	0.96	0.62	1.73
4	0.91	3.53	4.86	1.91	2.35	3.83	3.33	1.44
6	1.08	4.07	6.41	3.15	3.83	4.43	4.32	1.04
9	4.21	9.19	7.38	5.47	8.43	7.57	7.56	3.39
12.5	5.74	9.66	8.54	7.93	8.78	7.33	6.45	5.47

Table 3.13. Sensitivity of AU to the presence of a through thickness hole in a 20-ply unidirectional APC2. Student's t values are presented for the comparison of mean AU parameter values before and after the introduction of the stated hole diameter. (a) Measurements made parallel to fibres. (b) Measurements made perpendicular to fibres.

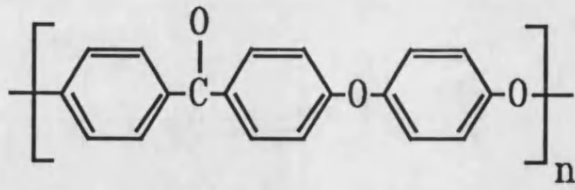


Figure 4.1. The molecular structure of polyetheretherketone.

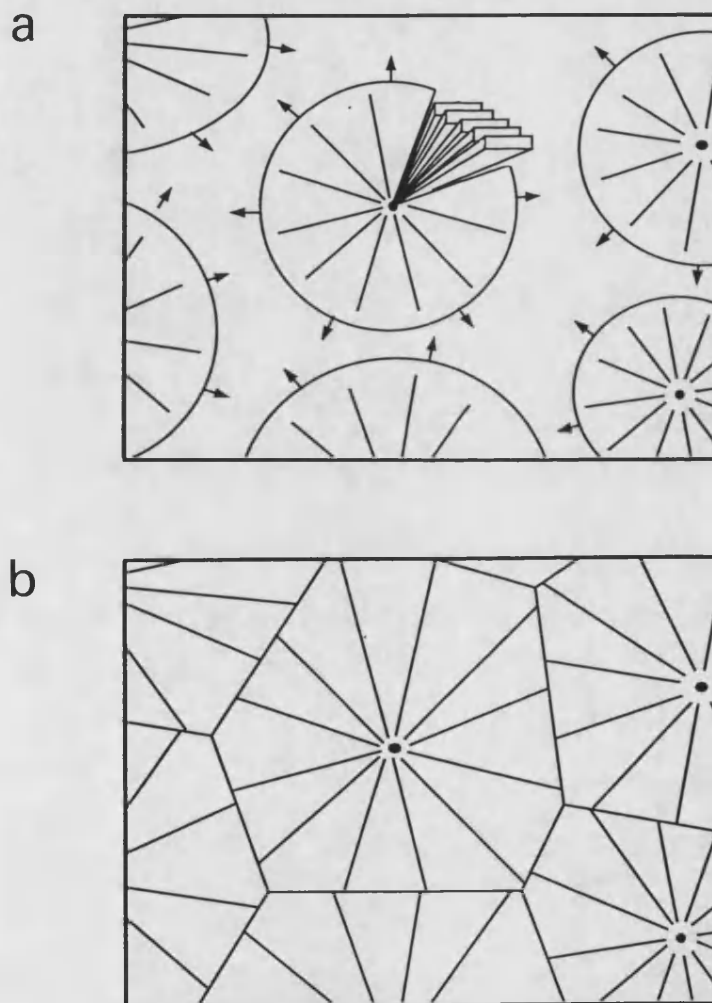


Figure 4.2. Diagrammatic representation of PEEK crystallisation and formation of lamellae and spherulites. a) The early stages of the crystallisation process: spherulites (1 to 10 microns diameter) made up of much smaller lamellar crystals (around 5 microns thick) growing radially. b) Crystallisation complete.

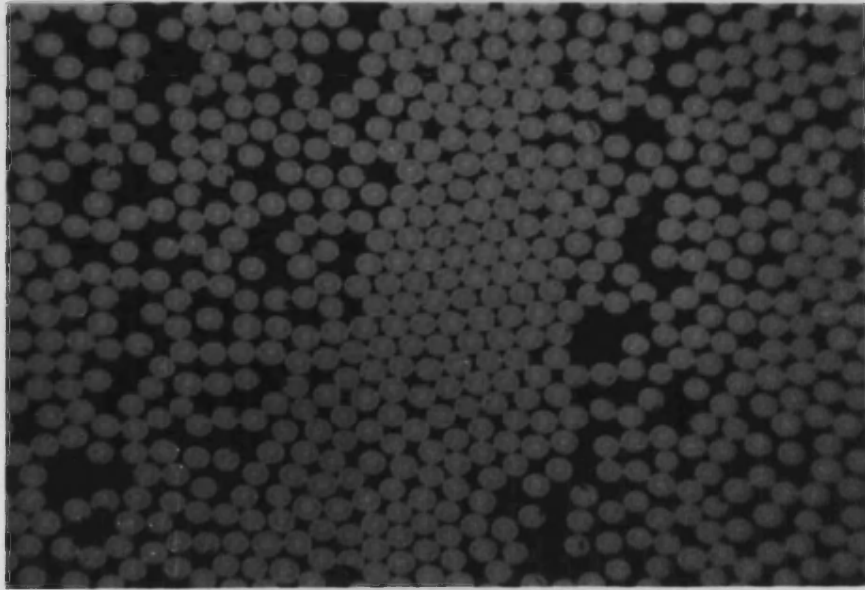


Figure 4.3. Cross section perpendicular to fibres in 16-ply UD APC2. Note approximate hexagonal packing of the carbon fibres in localised areas. Magnification x 350.

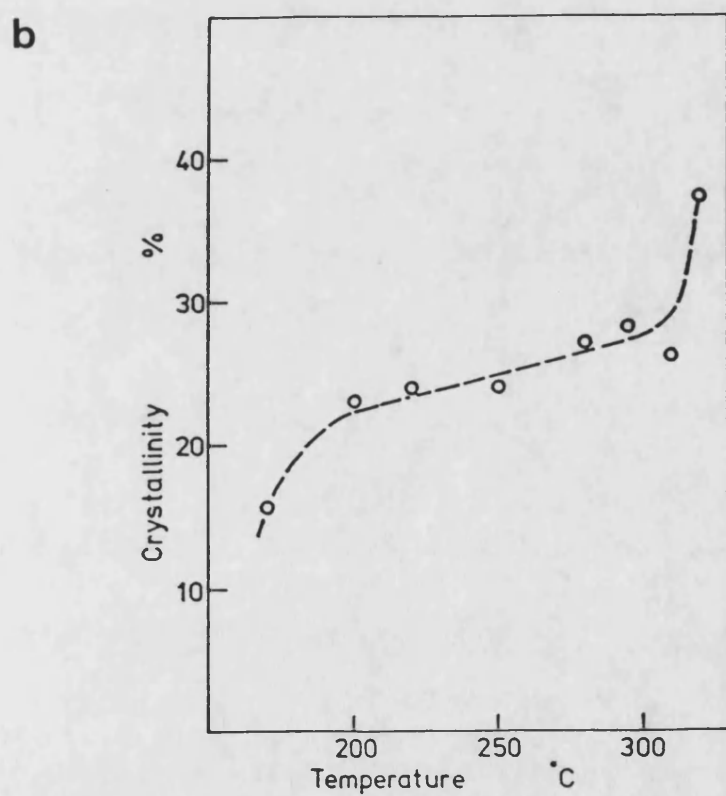
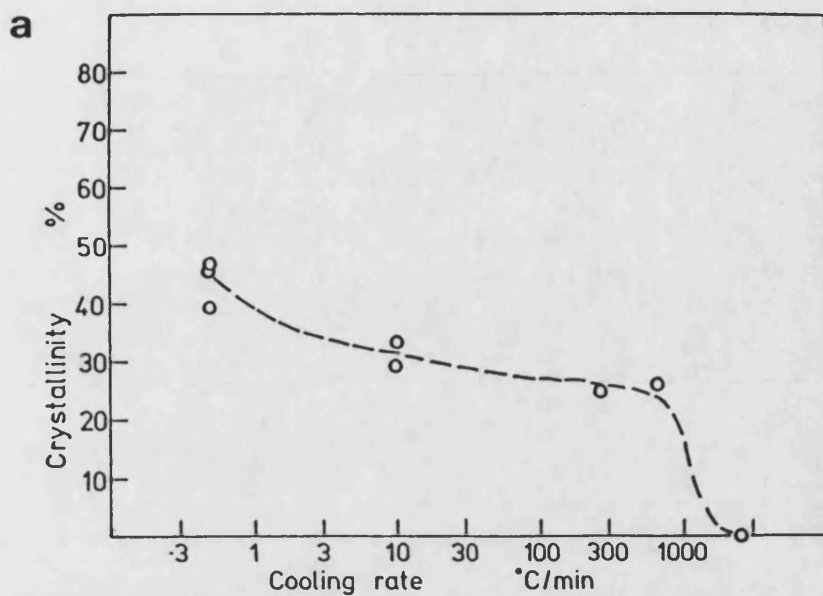


Figure 4.4. Percentage crystallinity of PEEK in APC2 as a function of a) cooling rate and b) annealing temperature (after Blundell et al (107)).

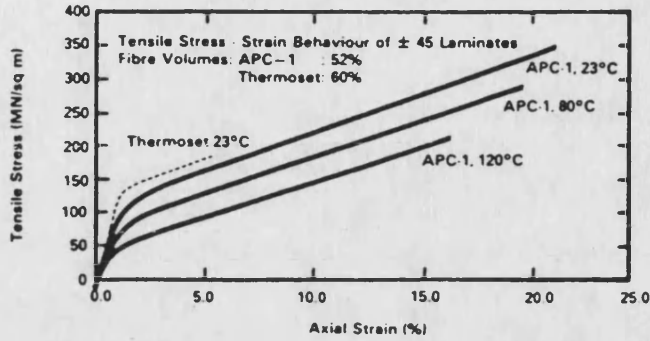


Figure 4.5. Stress/strain curve for $[\pm 45]_{45}$ APC1 at different temperatures (88).

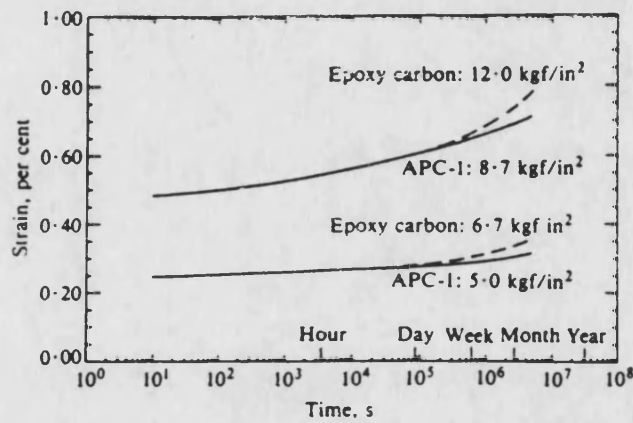


Figure 4.6. Creep behaviour of carbon fibre reinforced PEEK and epoxy ± 45 laminates (after Belbin (87)).

Damage tolerance test.
Compressive deformation at failure vs applied impact energy.

Quasi-isotropic lay-up - 5mm thick

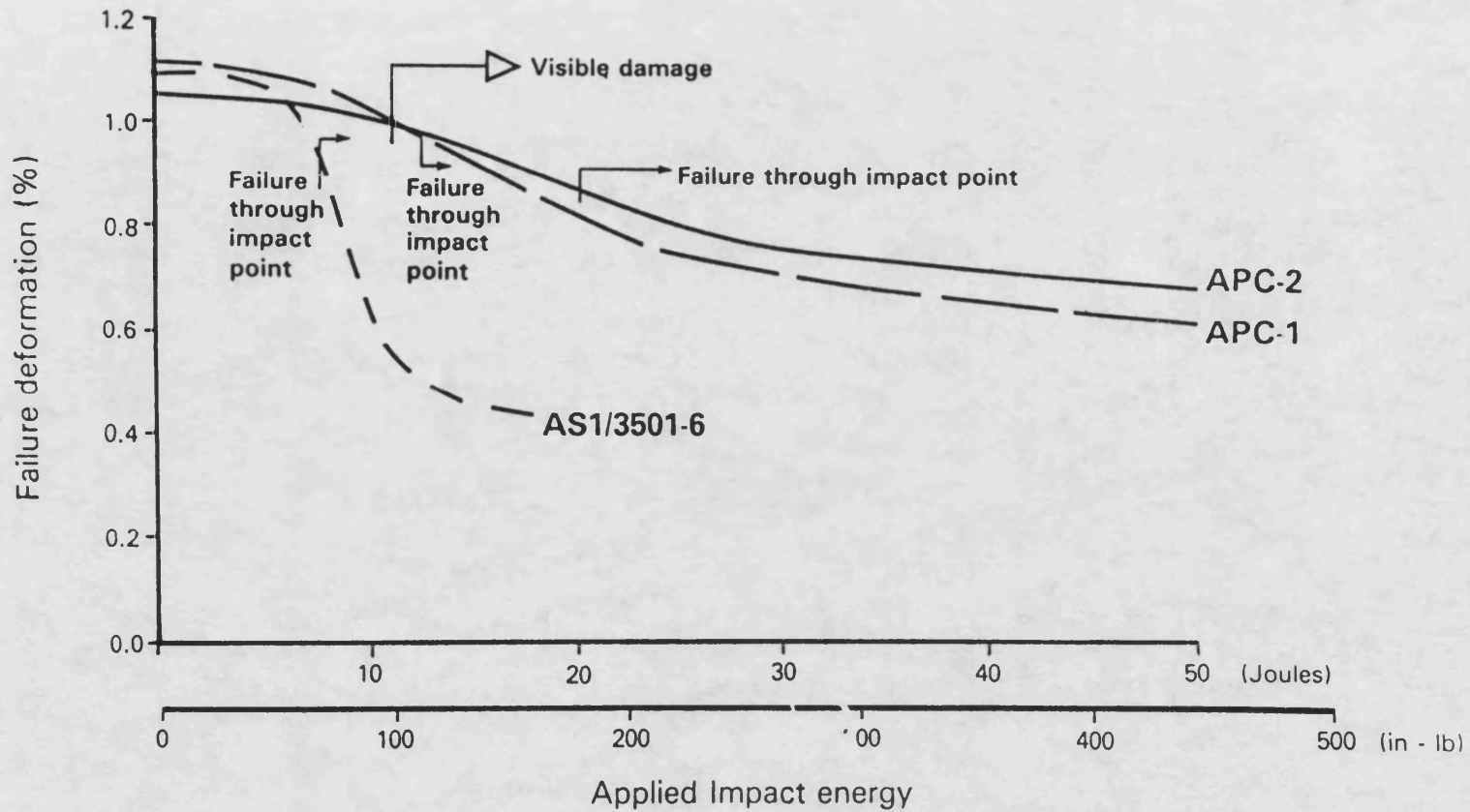


Figure 4.7. Damage tolerance of carbon fibre reinforced PEEK and epoxy composites (86).

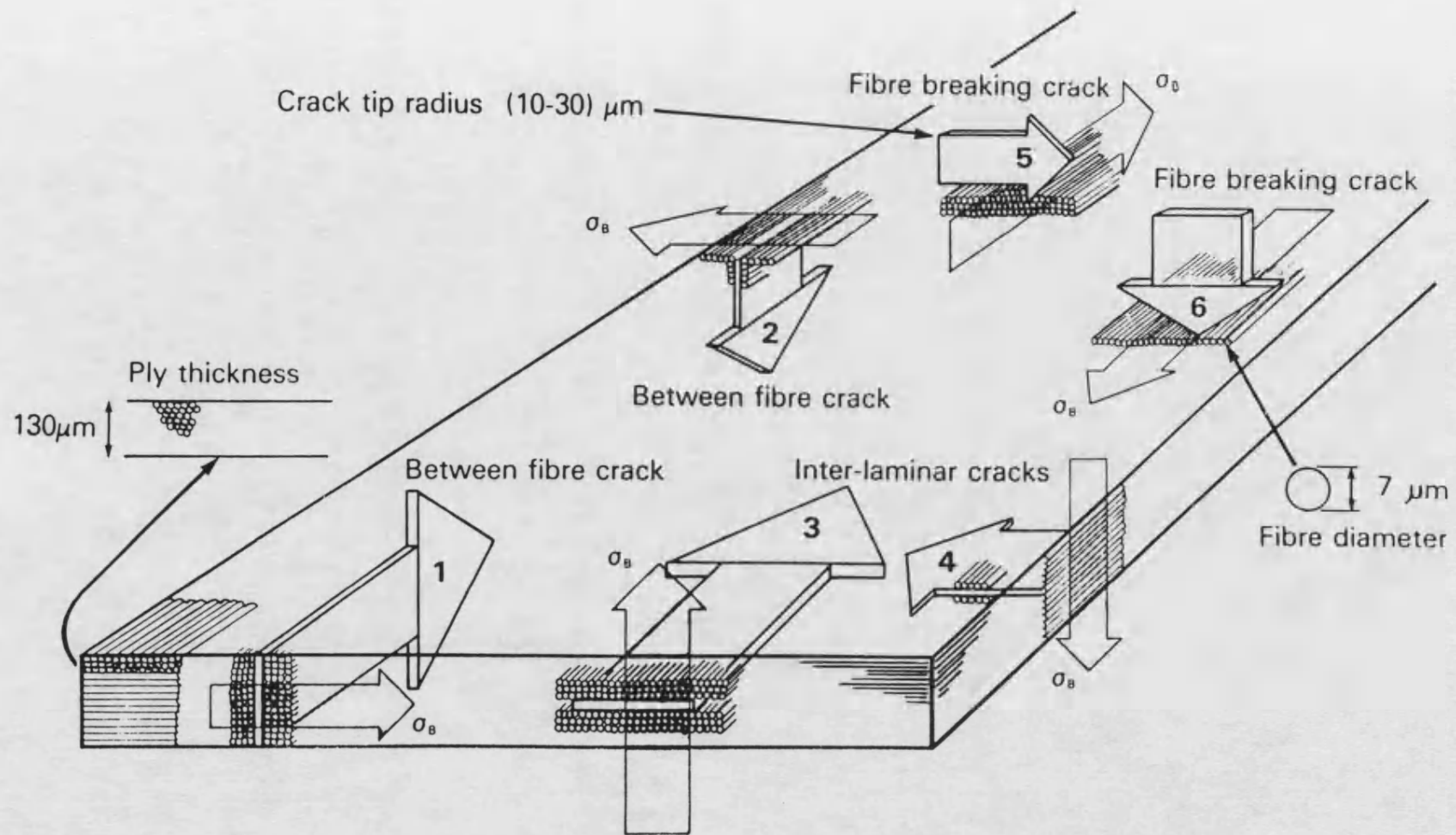


Figure 4.8. Crack propagation in unidirectional composites (96).

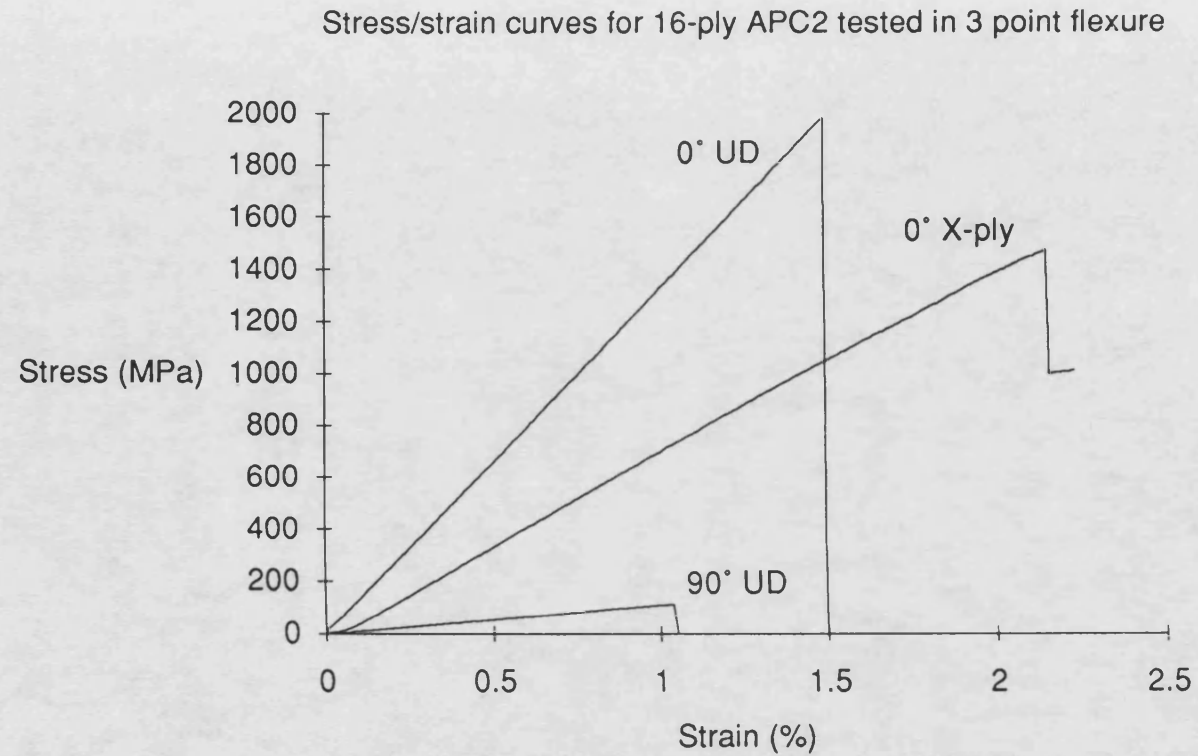


Figure 4.9. Stress/strain curves for 16-ply APC2 plates loaded in long beam three point flexure. 0° indicates fibres parallel to the support span, 90° perpendicular to the support span and 0° Cross-ply indicates outer plies parallel to the span.

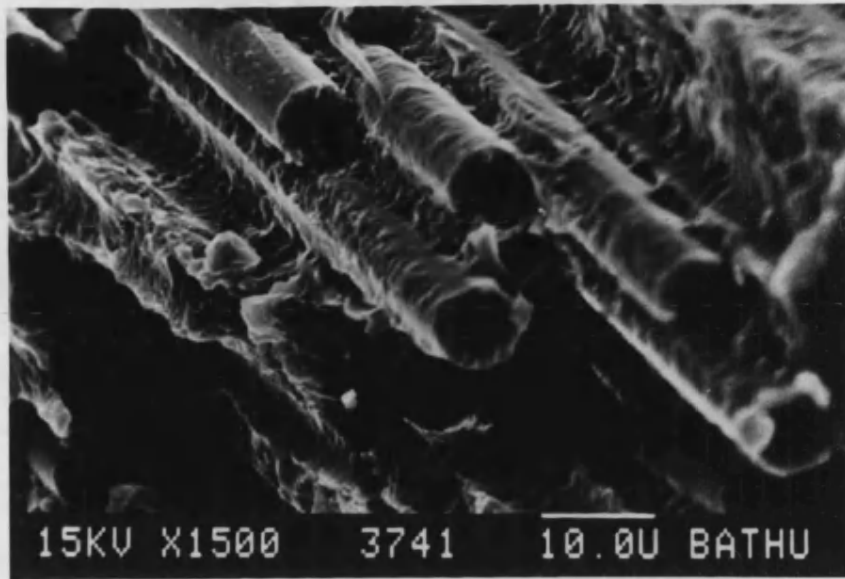


Figure 4.10. A unidirectional APC2 0° tensile specimen. Note that where fibres have been pulled out the failure has occurred within the matrix and not at the fibre/matrix interface.

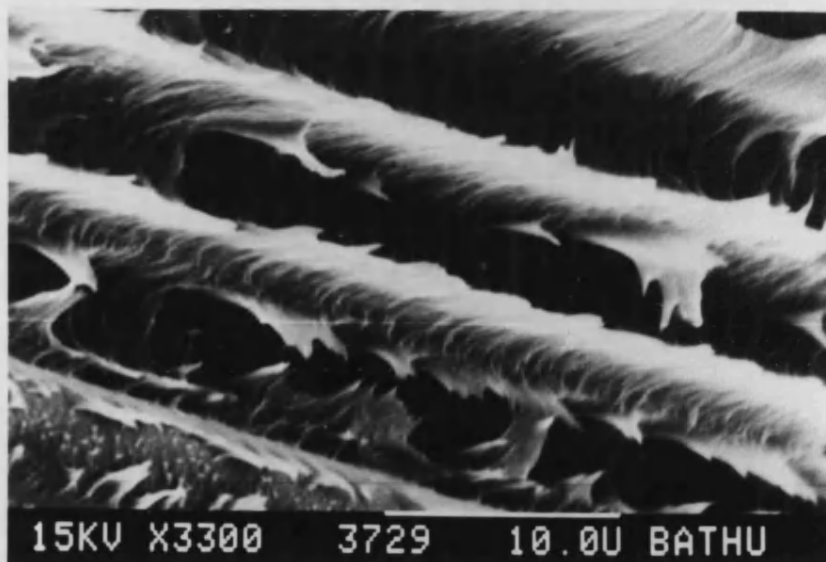


Figure 4.11. Single edge notched fracture toughness specimen of APC2. Crack orientation 2 in figure 4.8. Gross plastic deformation of the matrix is evident within inter-fibre regions.

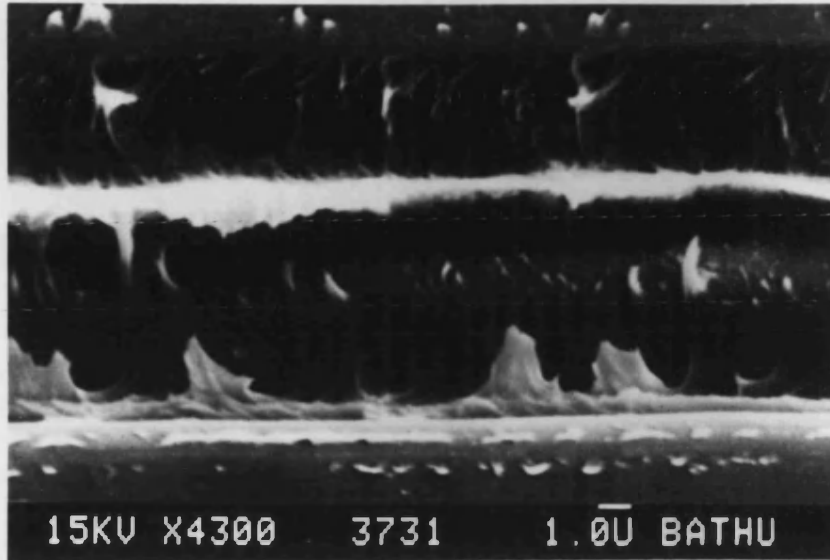


Figure 4.12. APC2 single edge notched fracture toughness specimen. Crack orientation 2 in figure 4.8. What appears to be pores may be seen in the matrix close to fibres and running along the length of the fibres.

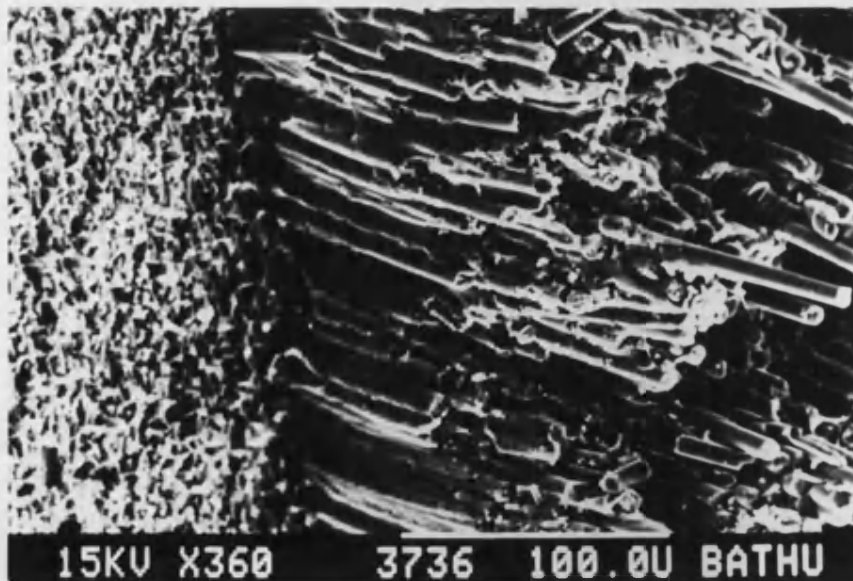


Figure 4.13. APC2 single edge notched fracture toughness specimen. Crack orientation 6 in figure 4.8. The fracture surface shows a sharp division between two modes. To the right, long fibre pull out occurs with a transition to no fibre pull out in the compressive region, on the left.

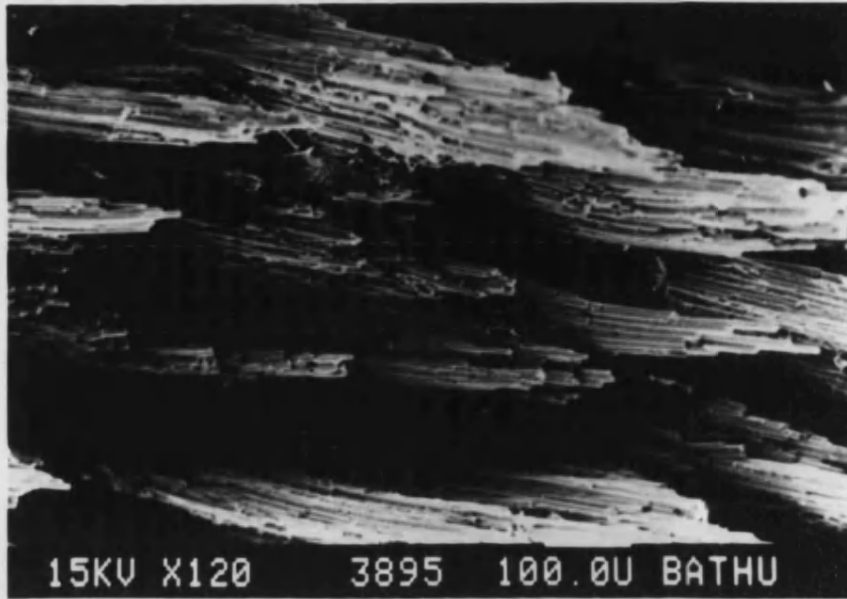


Figure 4.14. Tensile failure region of a 0° UD three point bend specimen. Note that fibre bundles, in addition to individual fibres, have been pulled out of the matrix. However both fibres and bundles are still matrix covered.



Figure 4.15. Compressive failure region of a three point bend specimen. Note how the matrix has been deformed leaving the fibre ends sitting in hollows.

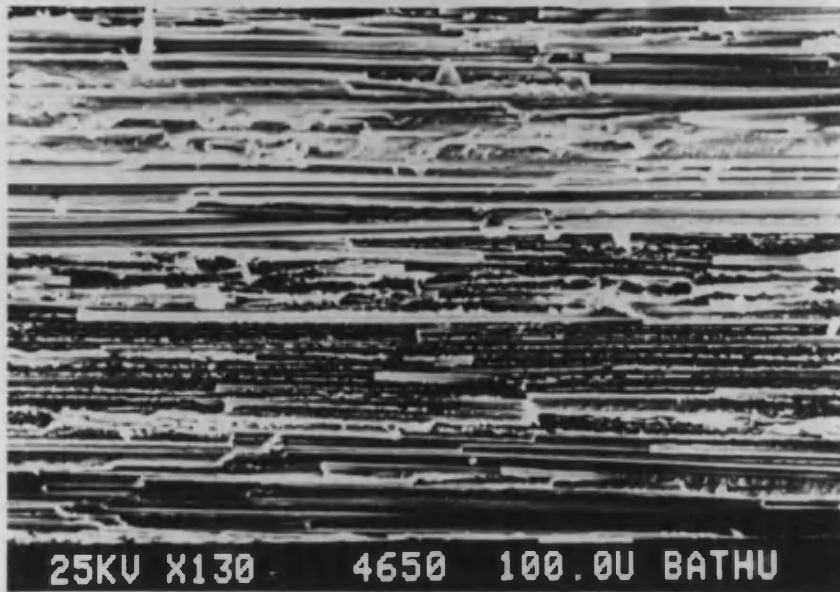


Figure 4.16. Normal cooled double torsion fracture surface. Note the profusion of partly pulled out fibres.

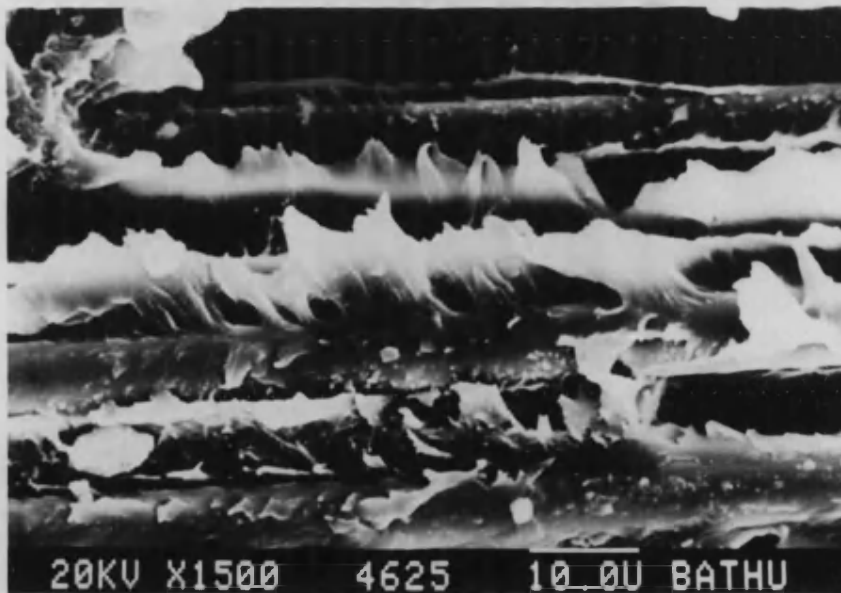


Figure 4.17. Normal cooled double torsion fracture surface. Note the well deformed matrix adhering to the fibres.

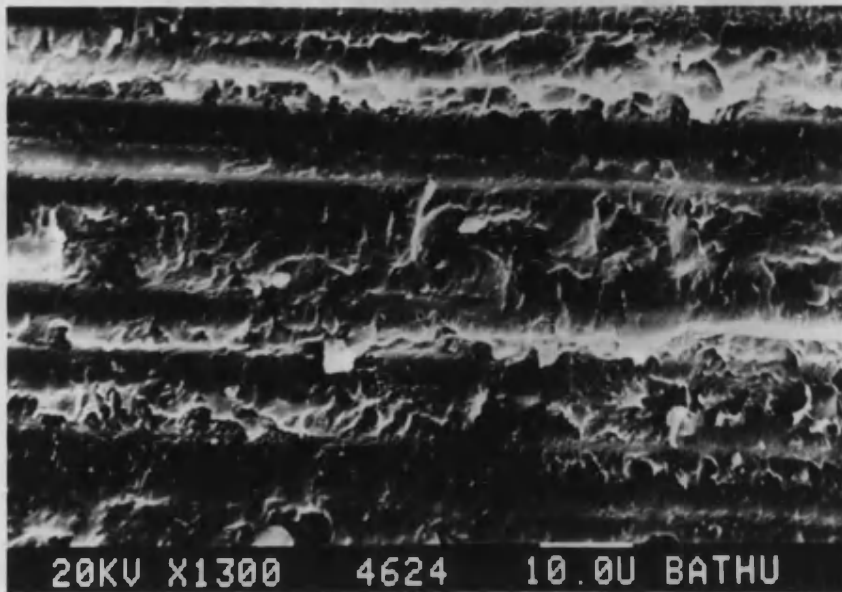


Figure 4.18. Slow cooled double torsion fracture surface. Note the relatively undeformed matrix indicating relatively rapid brittle fracture.

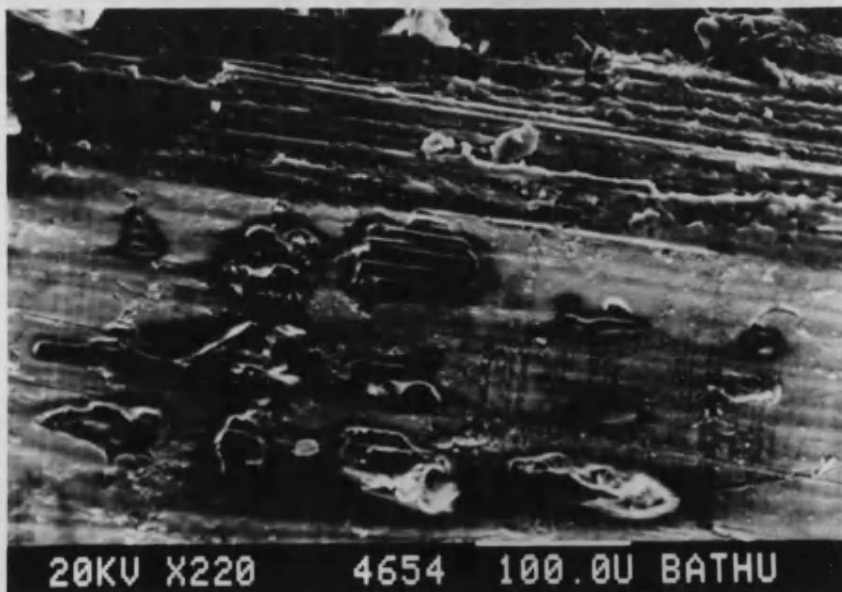


Figure 4.19. Slow cooled specimen. Note the defects on the plate surface in the lower portion of the micrograph.

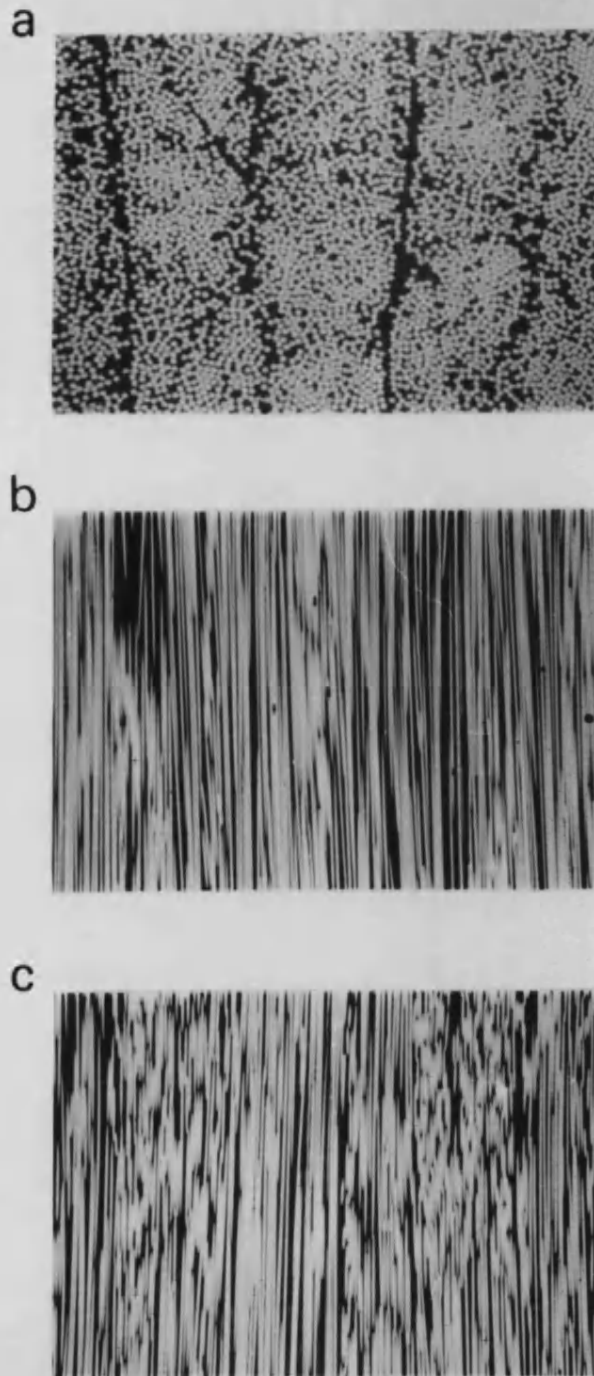


Figure 4.20. Microstructures of APC2 in three orthogonal planes, exhibiting the distribution of carbon fibres. (Magnification x 160)
a) Cross section across fibre direction (orientation 5 in figure 4.8).
b) Section parallel to fibres and plies (orientation 4 in figure 4.8).
c) Section parallel to fibres and perpendicular to plies (orientation 2 in figure 4.8).

PROPERTY / TEST METHOD	UNITS	APC1	APC2	HERCULES AS4/3501-6
0° Tensile (ASTM D-3039)				
Strength	MPa	1828	2130	2130
Modulus (E ₁₁)	GPa	122	134	148
Strain to failure	%	-	1.45	-
Poisson's Ratio		0.31		0.28
90° Tensile (ASTM D-3039)				
Strength	MPa	>62	80	70
Modulus (E ₂₂)	GPa	9.2	8.9	13.1
Strain to failure	%	-	1.0	-
±45° Tensile (ASTM D-3518)				
Strength	MPa		300	221
Modulus	GPa		19.2	17.6
Strain to failure	%		17.2	5.1
0° Compression (IITRI Test)				
Strength	MPa		1100	1350
0° Short Beam Shear				
Apparent ILSS	MPa	105	105	127
Fracture Toughness				
Mode 1 - interlaminar				
-cleavage mode	KJ/m ²		2.1	
-ductile mode	KJ/m ²		2.4	
Volume Fraction	%	52	62	61

Table 4.1. The mechanical properties of APC2 and an equivalent carbon fibre/epoxy determined by ICI (100,85,42).

Property /orientation	Bath value	ICI value
Strength (MPa) 0°	1877	2130
90°	95	80
Modulus (GPa) 0°	145	134
90°	9.5	8.9

Table 4.2. Tensile test results from APC2 tested at ICI, Wilton and at Bath. Material moulded at ICI, Wilton.

Crack orientation	K_C (MNm ^{-3/2})	
	Bath value	ICI value
1	5.2	3.8
2	4.4	3.6
3	45.0	42.0
4	43.0	38.0

Table 4.3. SEN three point bend fracture toughness results from APC2 tested at ICI, Wilton and at Bath. Material moulded at ICI, Wilton..

Orientation & Lay-up	Number of tests	Strength (MPa)	Strain (%)	E (GPa)	Secant (GPa)	Test Method	Statistic
0°,16-ply UD	26	1801	1.41	128.7	127.7	3 pt bend	Mean
		0.105	0.092	0.094	0.086		Coef' of var'
		(1436-2287)	(1.13-1.66)	(107.7-158.2)	(115.4-161.1)		Range
90°,16-ply UD	12	125	1.26	10.6	10.03	3 pt bend	Mean
		0.214	0.238	0.078	0.088		Coef' of var'
		(90.08-175.7)	(0.87-1.76)	(9.23-12.05)	(8.03-10.9)		Range
0°, 16-ply 0°/90°	12	1453	1.74	89.7	85.0	3 pt bend	Mean
		0.093	0.172	0.136	0.117		Coef' of var'
		(1263-1719)	(1.42-2.35)	(71.3-114.5)	(66.06-94.5)		Range
0°,16-ply UD	40	1733	1.23	148.4	129.6	4 pt bend	Mean
		0.097	0.106	0.042	0.096		Coef' of var'
		(1306-2113)	(1.02-1.58)	(133.7-158.3)	(97.6-168)		Range

Table 4.4. A summary of the mechanical properties of APC2 determined from long beam flexural testing.

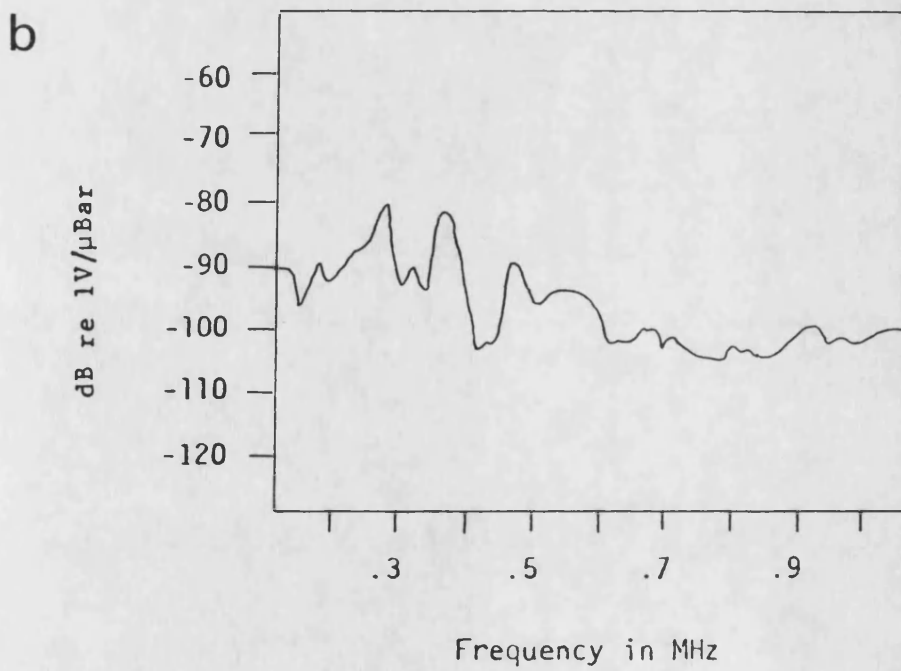
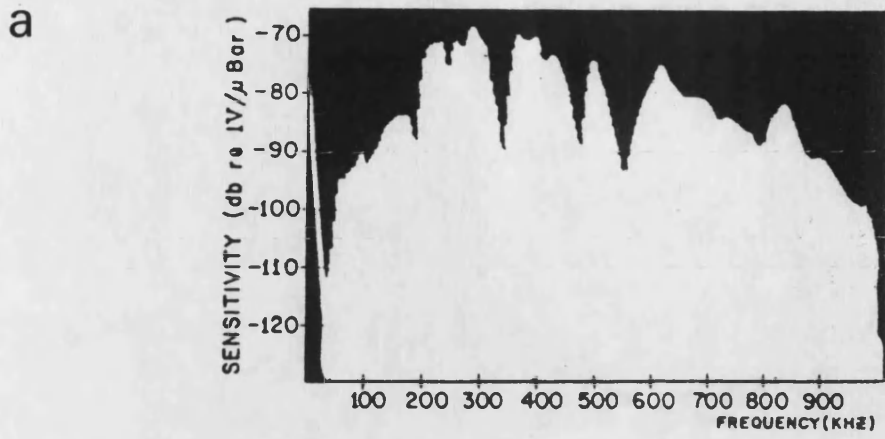


Figure 5.1. The frequency response of acoustic emission transducers a) PAC U30D b) AETC MAC 300.

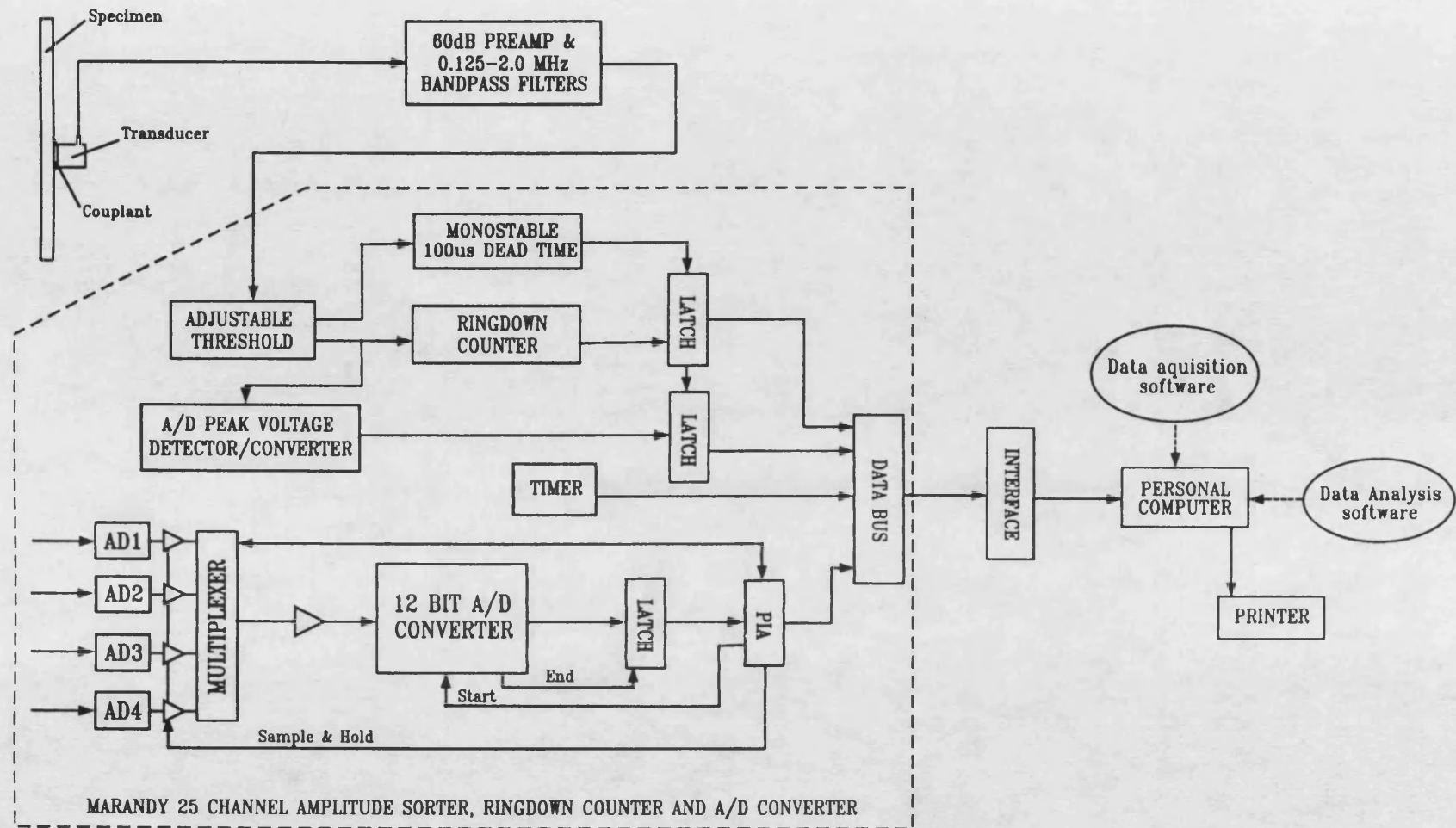


Figure 5.2. Diagrammatic representation of the Marandy MR1004 based AE amplitude distribution system.

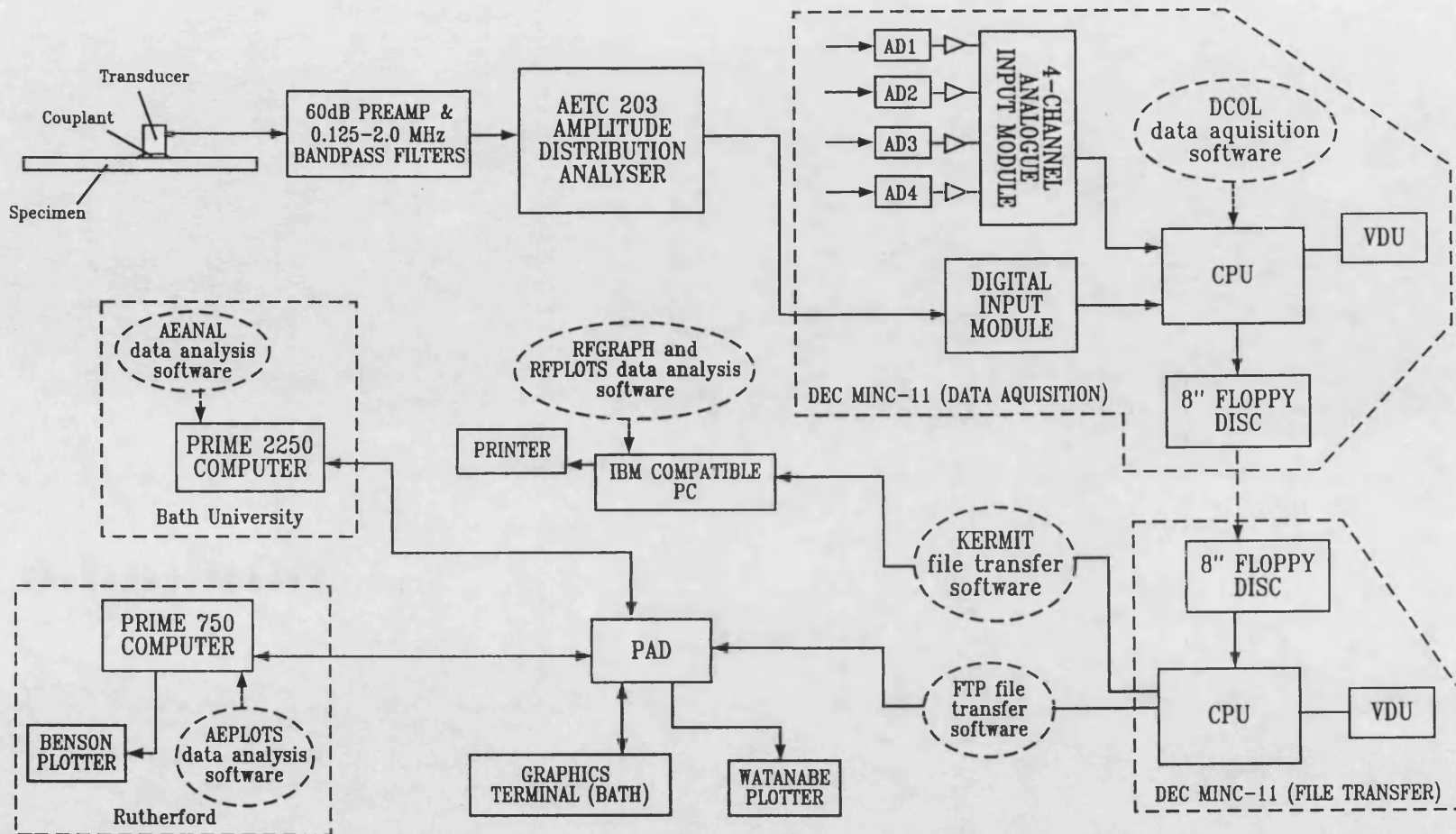


Figure 5.3. Diagrammatic representation of the AETC 203 based AE amplitude distribution system.

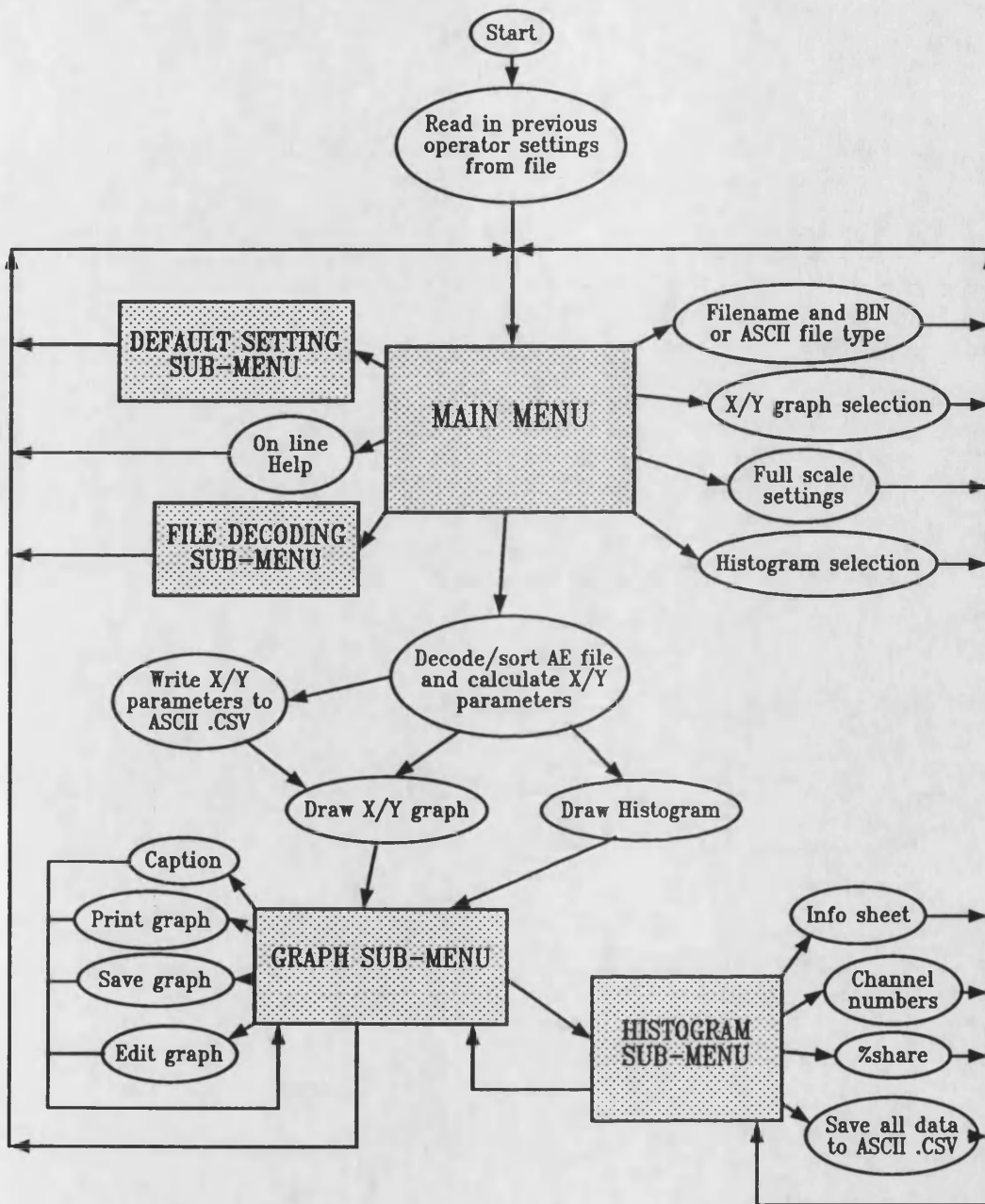


Figure 5.4. A flow diagram of the RFGGRAPH AE data analysis software.

Time	Total AE	AE Rate	AD 1	AD 2	Ch 1	Ch 2	Ch 3	Ch 4	Ch 5	...
1	100	100	122.5	69.8	0	0	4	2	5	...
2	196	96	122.5	69.8	0	0	6	2	10	...
3	345	149	123.0	69.8	0	0	7	12	15	...
4	472	127	123.0	70.5	0	0	7	16	17	...
5	584	112	122.5	70.5	0	0	7	21	21	...
6	677	93	122.5	70.6	0	0	7	21	27	...
7	785	108	122.5	70.6	0	1	9	23	30	...
8	858	73	122.5	70.7	0	1	9	27	31	...
9	957	99	122.5	70.7	1	1	10	29	33	...
10	1084	127	122.5	70.7	1	1	10	30	34	...
11	1185	101	122.5	70.7	1	1	10	32	42	...
12	1312	127	122.5	70.7	1	2	11	35	47	...
13	1421	109	122.5	70.7	1	2	11	37	56	...
14	1524	103	122.5	70.8	1	2	12	38	63	...
15	1641	117	122.0	70.8	1	2	14	38	63	...
16	1728	87	122.0	70.8	1	2	14	43	67	...
17	1800	72	122.5	70.8	1	2	15	43	73	...
18	1897	97	122.5	70.8	1	2	15	46	77	...
19	1968	71	122.5	70.8	1	2	15	51	84	...
20	2088	120	122.5	70.8	1	3	15	52	86	...

Figure 5.5. A portion of a DCOL5 AE file decoded into ASCII .CSV (comma separated values) file format.

BINARY	GRAPH PLOTTING	ARL103.BIA
X	Stress MPa AD 1	Percentage share PS
	Elongation mm AD 2	Mean amplitude MA
	AD3 in mV AD3	Variance VA
	AD4 in mV AD4	Kurtosis KU
	Time in seconds TI	Skewness SK
	Total AE events CE	Relative kurtosis RK
	Total ringdowns CR	Relative Skewness RS
Y	AE in channels EC	Ringdowns/event RE
	Total event rate TR	Histogram wrt A/D HL
	Event rate in chs SR	Histogram wrt time ... HT
	Histogram wrt events . HE	Ringdown rate RR

Y axis scale	min: 0	max: 12500	Cumulate : Y
X axis scale	min: 0	max: 2000	A/D ch : 1
Channel no	min: 1	max: 50	
Hist range	min: 50	max: 100	

Figure 5.6. The main menu of the RFGRAPH AE analysis program, showing the various parameters which can be plotted as X/Y graphs and histograms.

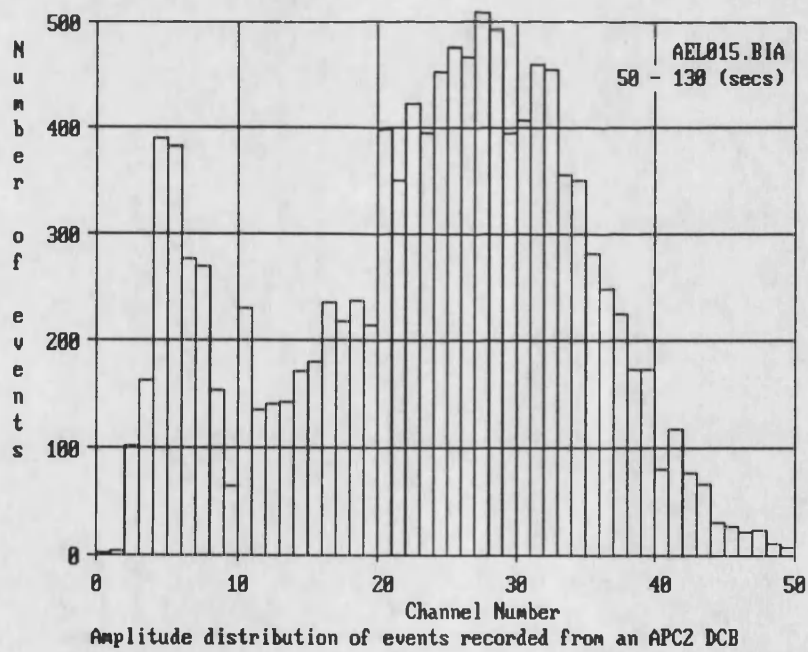
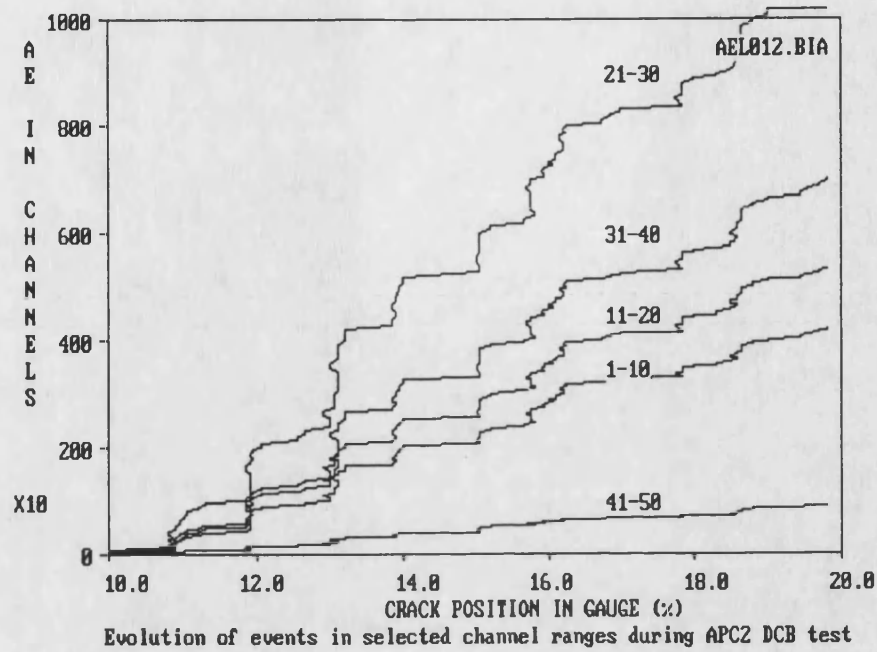


Figure 5.7. Examples of the screen graphical presentation available with RFGGRAPH.

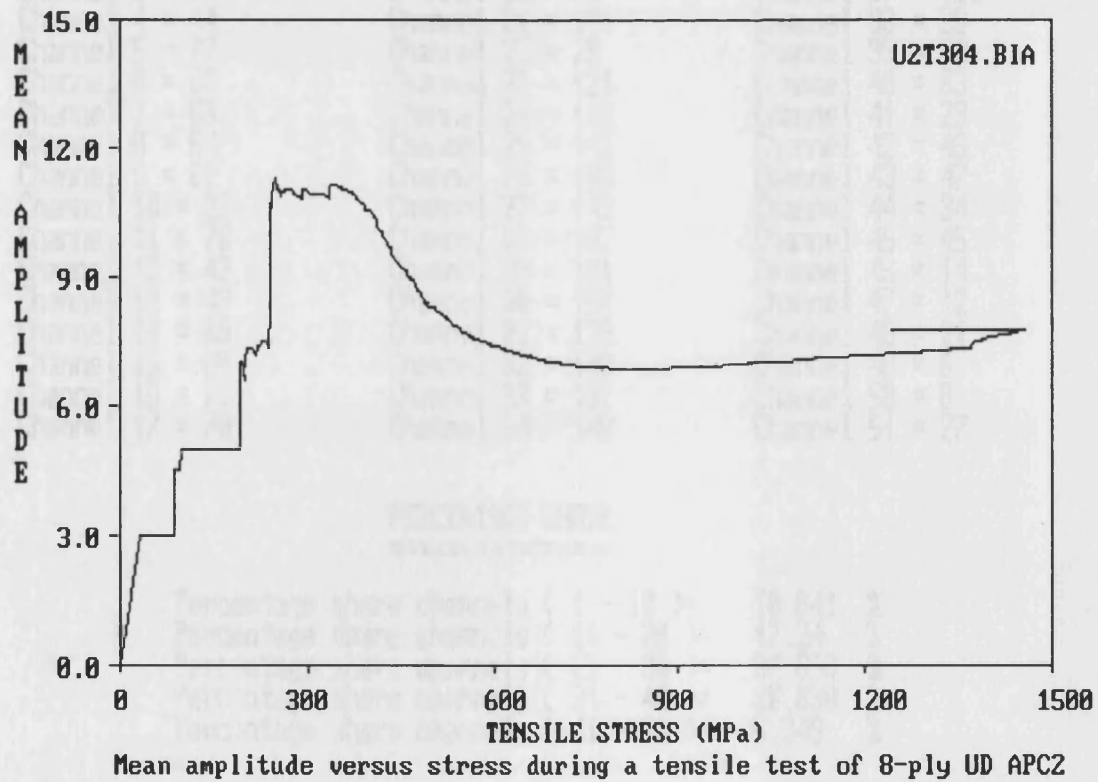
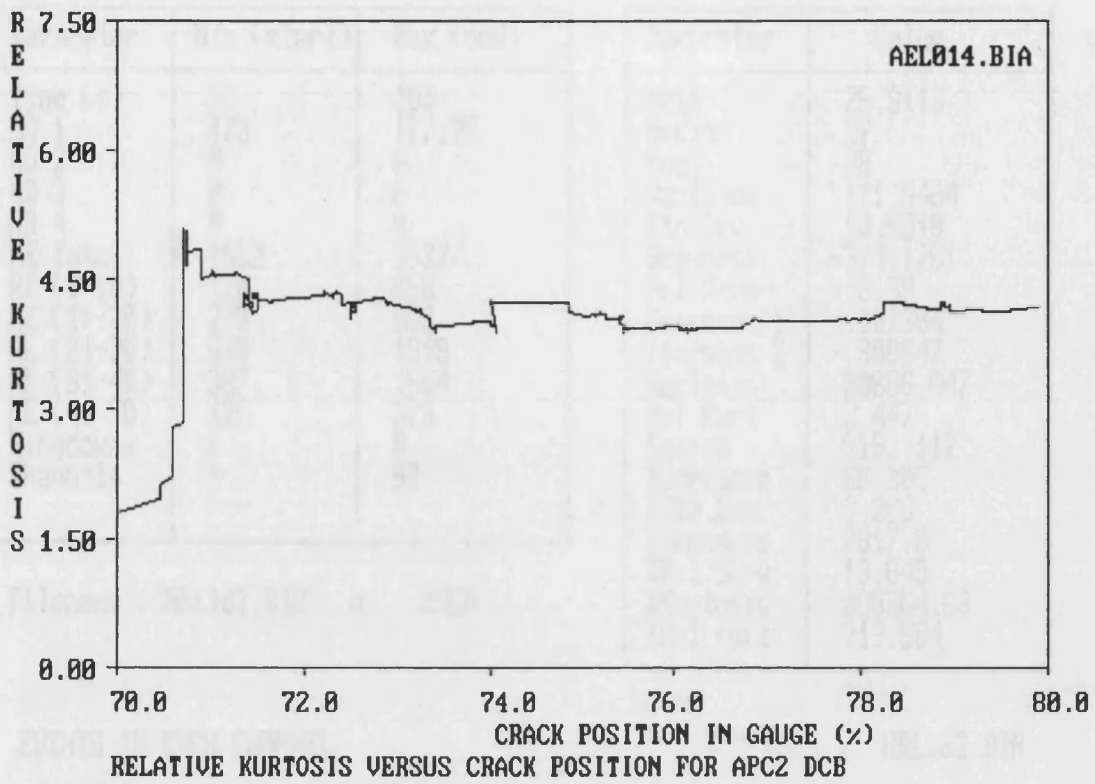


Figure 5.7. Examples of the screen graphical presentation available with RFGGRAPH (continued).

HISTOGRAM INFORMATION (DCOLS)

Parameter	Min (start)	Max (end)
Time (s)	50	100
AD 1	173	177.25
AD 2	0	0
AD 3	0	0
AD 4	0	0
AE Total	1552	5537
AE (1-10)	224	656
AE (11-20)	279	966
AE (21-30)	530	1919
AE (31-40)	387	1584
AE (41-50)	126	379
Ringdowns	0	0
Channels	1	50

Parameter	Value
Mean	25.9113
Median	27
Mode	28
Variance	111.9464
Std Dev	10.5818
Skewness	-374.1261
Rel Skew	-.3159
Pearsons 1	-.197384
Pearsons 2	-.308647
Kurtosis	30666.047
Rel Kurt	2.447
Energy	9192.112
XVariance	68.305
XStd Dev	8.266
XSkewness	7817.8
XRel Skew	13.849
XKurtosis	998364.69
XRel Kurt	213.984

Filename : ARL102.BIA n : 3958

EVENTS IN EACH CHANNEL:

ARL102.BIA

Channel 1 = 0	Channel 18 = 91	Channel 35 = 92
Channel 2 = 9	Channel 19 = 74	Channel 36 = 135
Channel 3 = 29	Channel 20 = 69	Channel 37 = 121
Channel 4 = 44	Channel 21 = 121	Channel 38 = 99
Channel 5 = 77	Channel 22 = 79	Channel 39 = 70
Channel 6 = 62	Channel 23 = 121	Channel 40 = 63
Channel 7 = 63	Channel 24 = 118	Channel 41 = 23
Channel 8 = 64	Channel 25 = 141	Channel 42 = 43
Channel 9 = 62	Channel 26 = 160	Channel 43 = 47
Channel 10 = 22	Channel 27 = 142	Channel 44 = 34
Channel 11 = 78	Channel 28 = 192	Channel 45 = 45
Channel 12 = 42	Channel 29 = 161	Channel 46 = 14
Channel 13 = 43	Channel 30 = 154	Channel 47 = 12
Channel 14 = 69	Channel 31 = 129	Channel 48 = 21
Channel 15 = 80	Channel 32 = 148	Channel 49 = 6
Channel 16 = 71	Channel 33 = 192	Channel 50 = 8
Channel 17 = 70	Channel 34 = 148	Channel 51 = 27

PERCENTAGE SHARE

=====

Percentage share channels (1 - 10)=	10.841	%
Percentage share channels (11 - 20)=	17.24	%
Percentage share channels (21 - 30)=	34.856	%
Percentage share channels (31 - 40)=	30.038	%
Percentage share channels (41 - 50)=	6.349	%

Figure 5.8. An example of the data presentation of the information screens available in RFGRAPH.

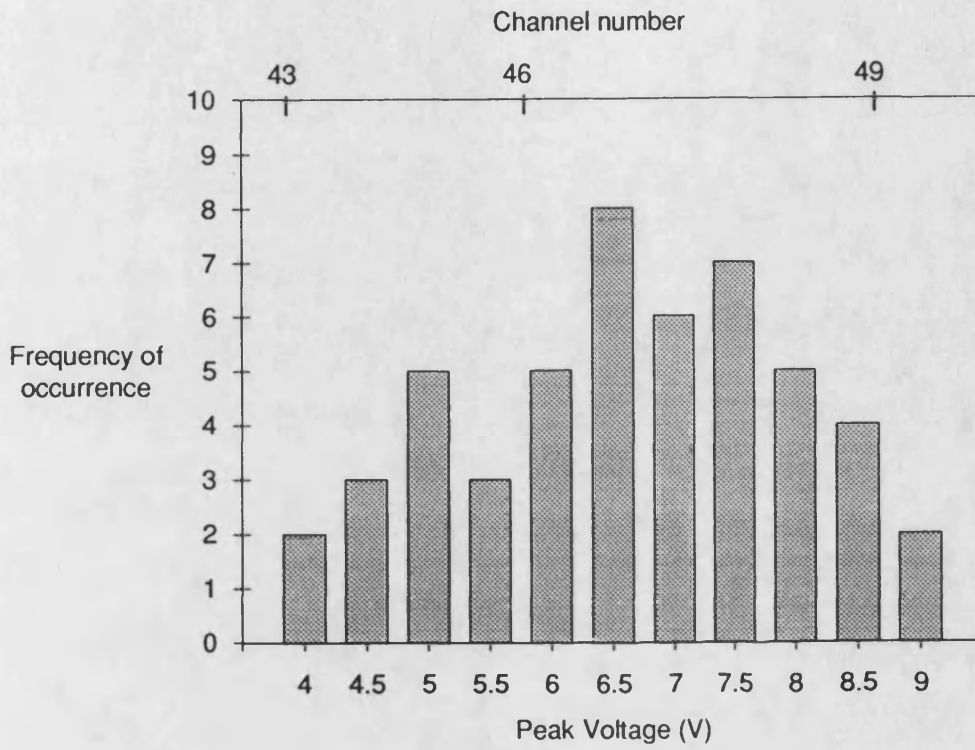


Figure 5.9. Frequency histogram of the peak amplitude of a standard artificial AE event after 50 re-couplings of the AE transducer. The scatter in the data is the result of variation of coupling quality.

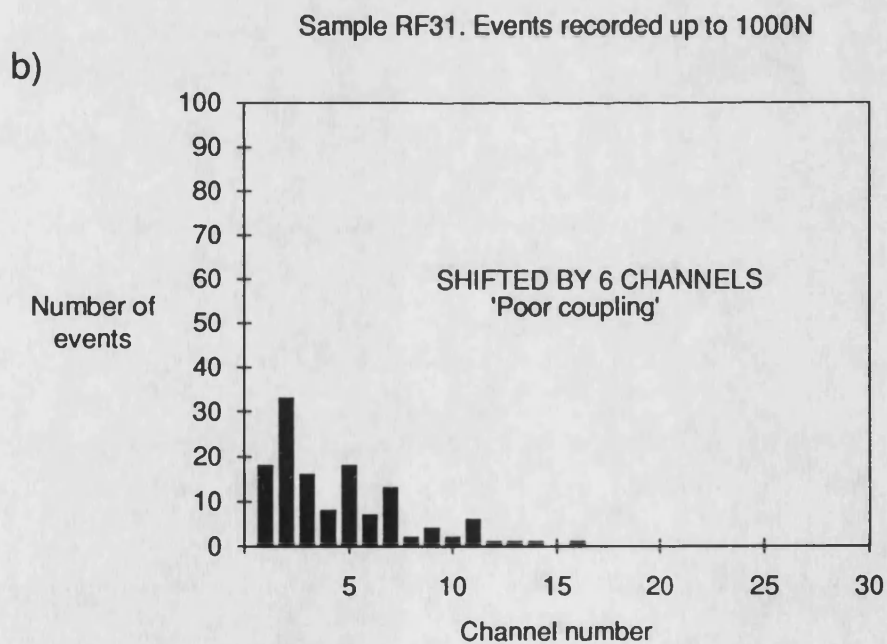
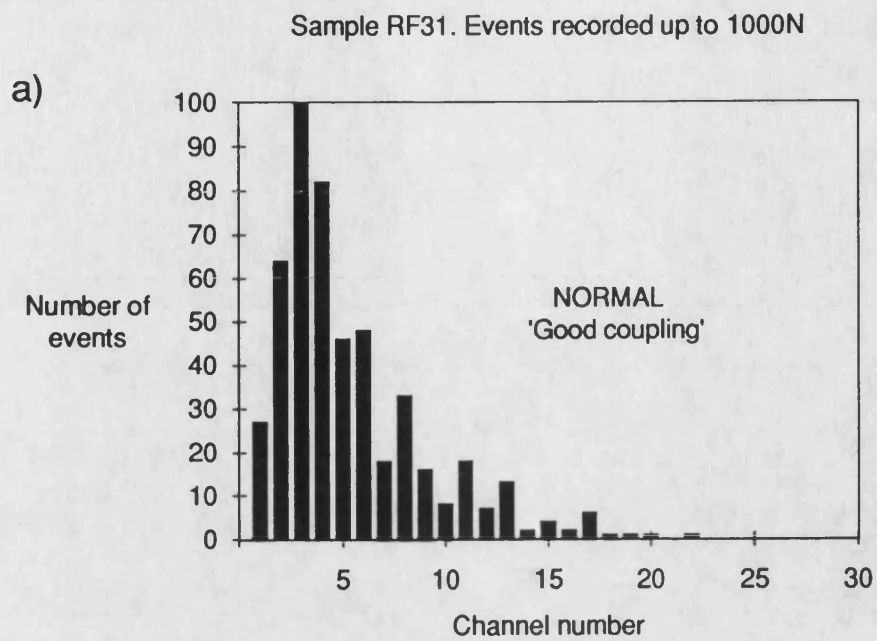


Figure 5.10. An illustration of the hypothetical effect of coupling variation on the recorded acoustic emissions: a) an amplitude distribution with optimum coupling b) the same distribution shifted by 6 channels as a result of poor coupling.

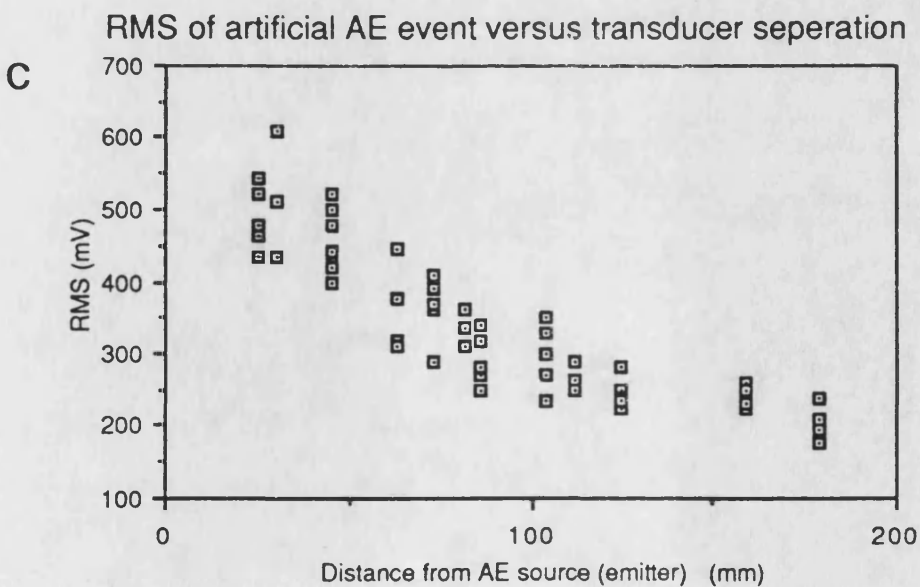
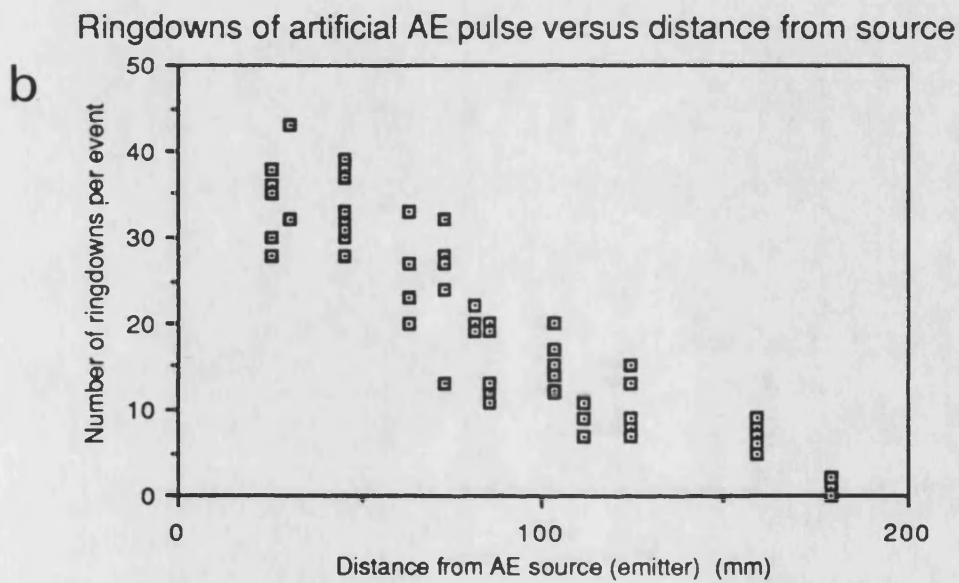
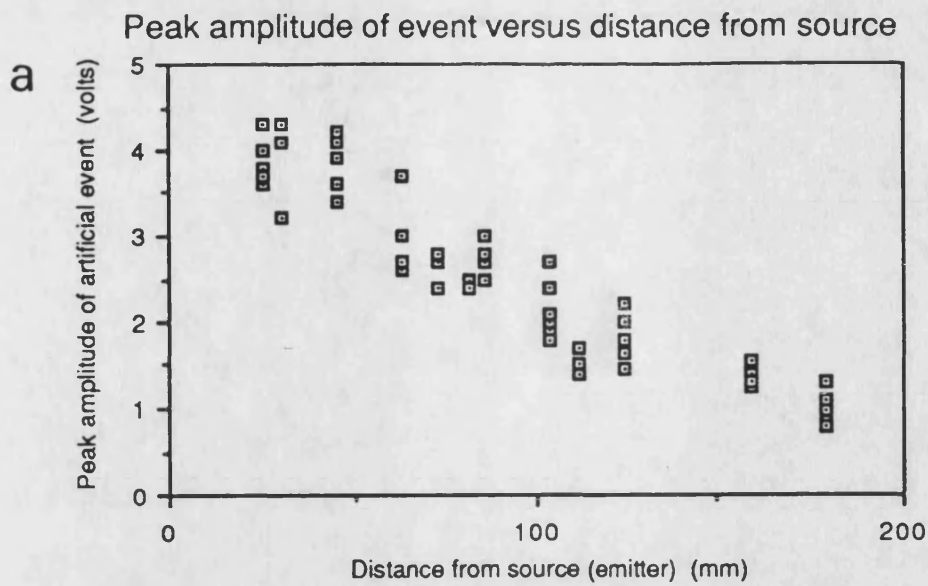


Figure 5.11. The effect of distance on simulated acoustic emission events. a) Peak amplitude. b) Ringdowns per event. c) RMS voltage.

Transducer	Peak Voltage (V)	Ringdowns	RMS Voltage (V)
PAC U30D (No 118)	3.44 (0.375)	55.6 (5.75)	0.674 (0.043)
PAC U30D (No 117)	4.62 (0.539)	53.3 (3.53)	0.832 (0.095)
PAC U30D (No 107)	2.38 (0.371)	16.8 (6.84)	0.309 (0.072)
PAC U30D (No 123)	3.11 (0.439)	37.8 (9.03)	0.550 (0.104)
PAC U30D (No 108)	2.43 (0.412)	16.9 (7.12)	0.336 (0.069)

Table 5.1. Comparison of the outputs of various acoustic emission transducers with respect to ringdown count, RMS voltage and peak amplitude of a reference/simulated AE event.

Material	Longitudinal Wave Speed (m/s)	
	Parallel	Perpendicular
APC2	8290	2508
CG 914/XAS	8602	2676

Material	Attenuation (dB/cm)	
	Parallel	Perpendicular
APC2	1.8	2.5
CG 914/XAS	2.2	2.6

Table 5.2. Ultrasonic wave speed and attenuation at 150 kHz for 16-ply UD APC2 and XAS carbon fibre/epoxy (Ciba-Geigy 914).

16-PLY UD 0° APC2 (3 POINT FLEXURE)

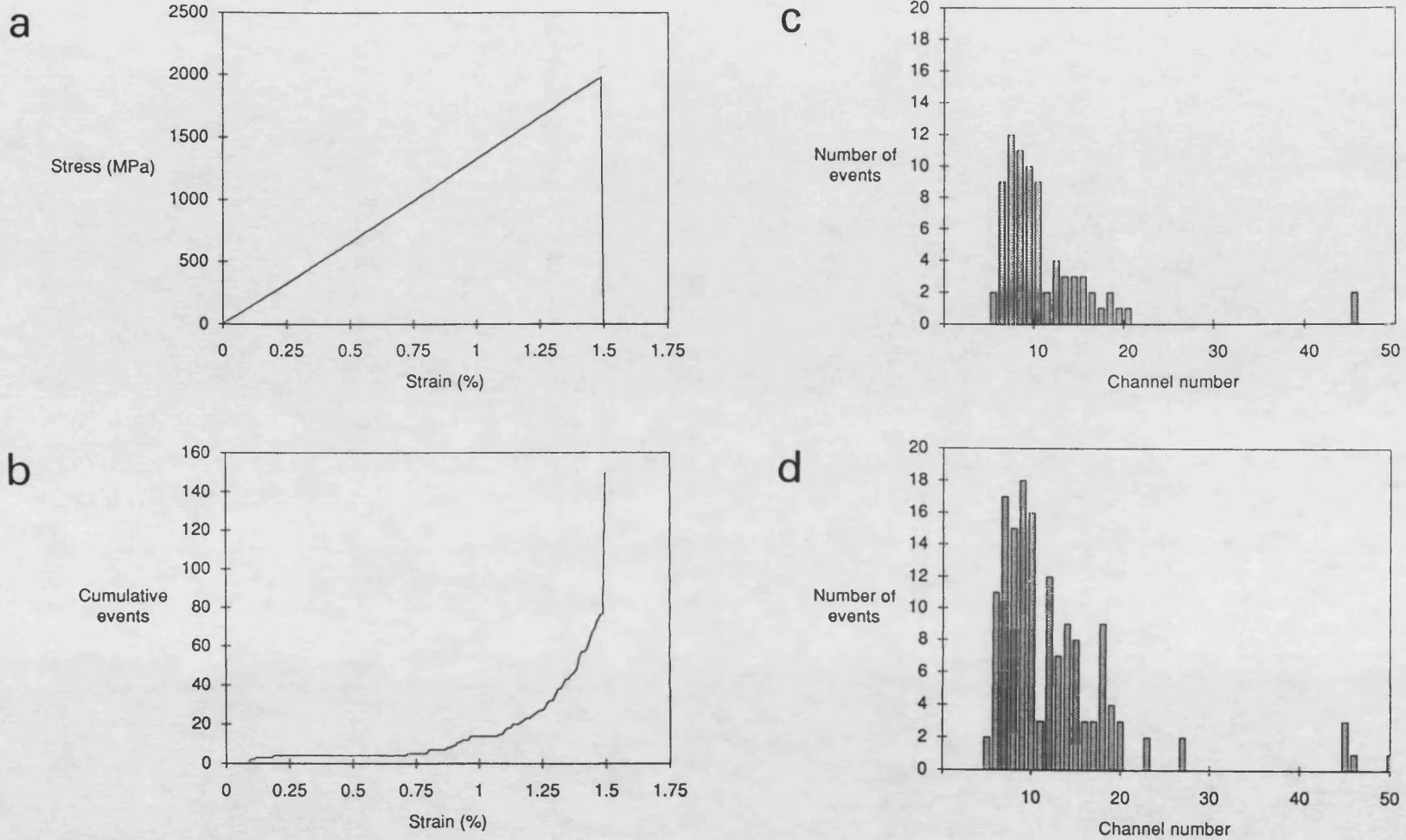


Figure 6.1. A summary of the mechanical and acoustic emission behaviour of 16-ply UD 0° APC2 tested in three point flexure. a) Stress/strain graph. b) Cumulative acoustic emission events as a function of strain. c) Amplitude distribution of events recorded up to maximum stress (prior to failure). d) Amplitude distribution of events recorded until and including failure.

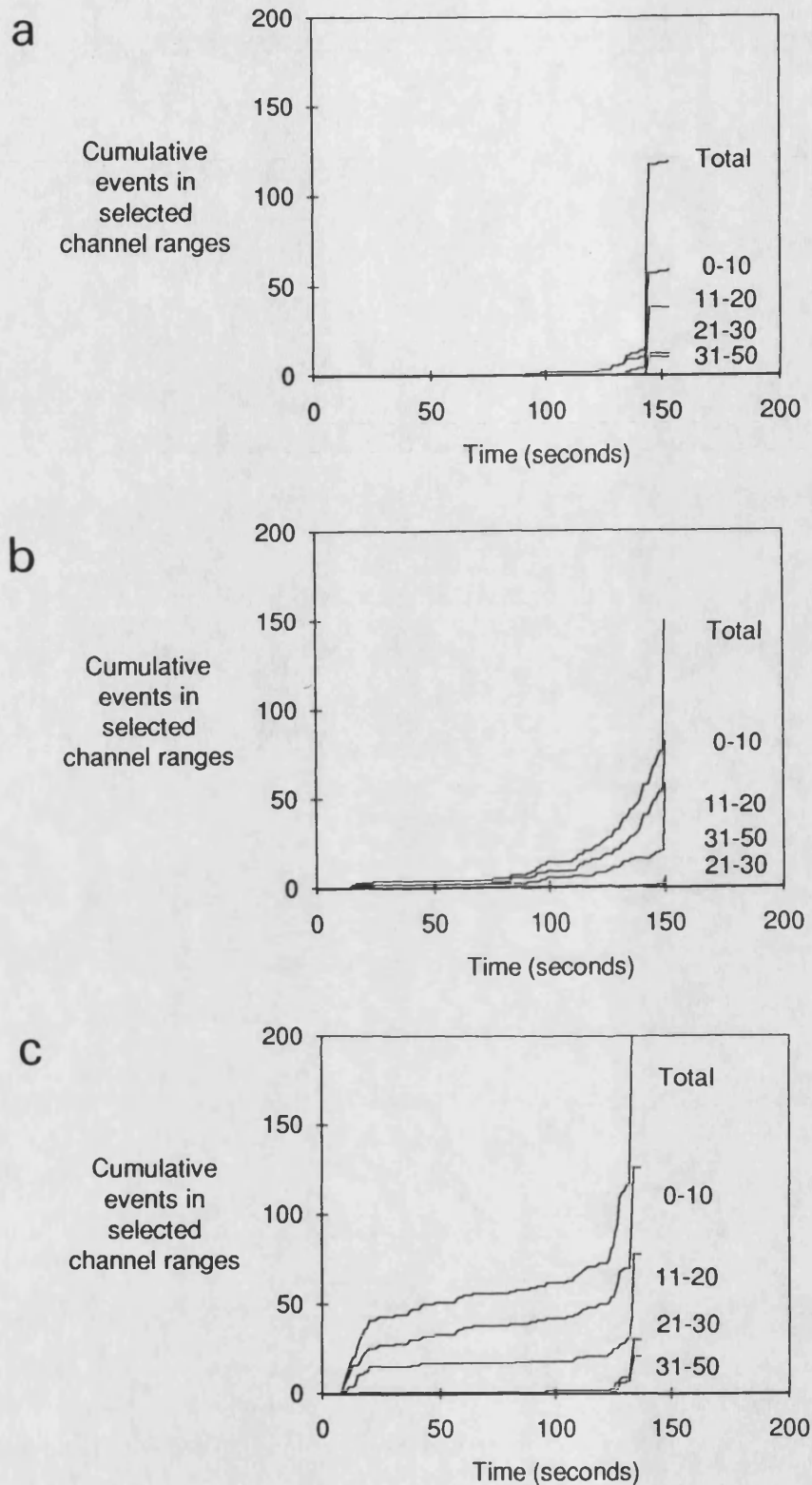


Figure 6.2. Variation of AE behaviour from nominally identical specimens: events in selected channel ranges versus time for 16-ply UD 0° APC2 plates tested in three point flexure. a) Almost no emissions until failure. b) Gradual build-up of events. c) Rush of events during initial load up.

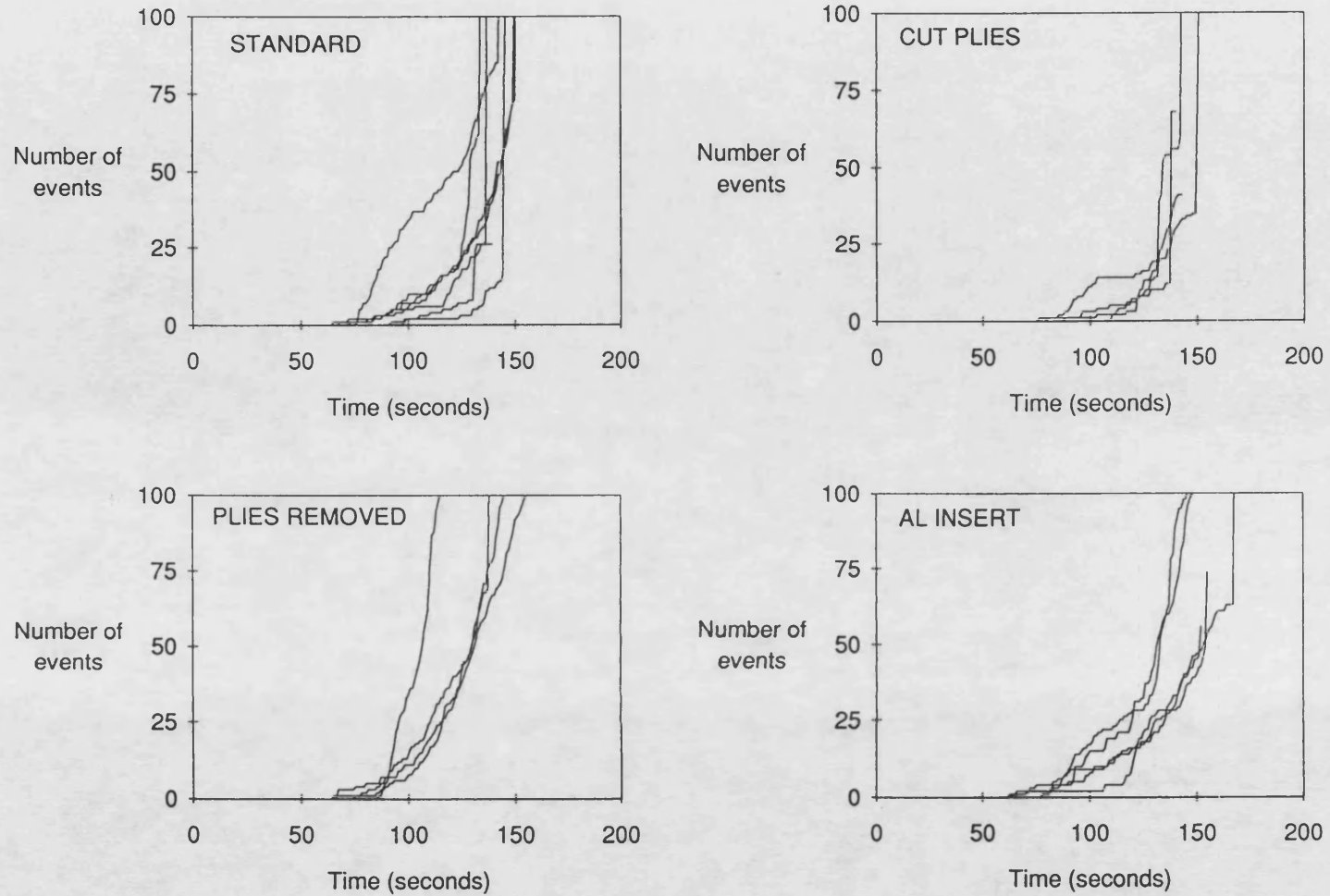


Figure 6.3. Total events/time plots for groups of defective and non-defective 16-ply UD 0° APC2 plates tested in three point flexure. Each graph line, which relates to a different specimen, has been shifted to remove the events produced during the first fifty five seconds of the test and plotted on one graph.

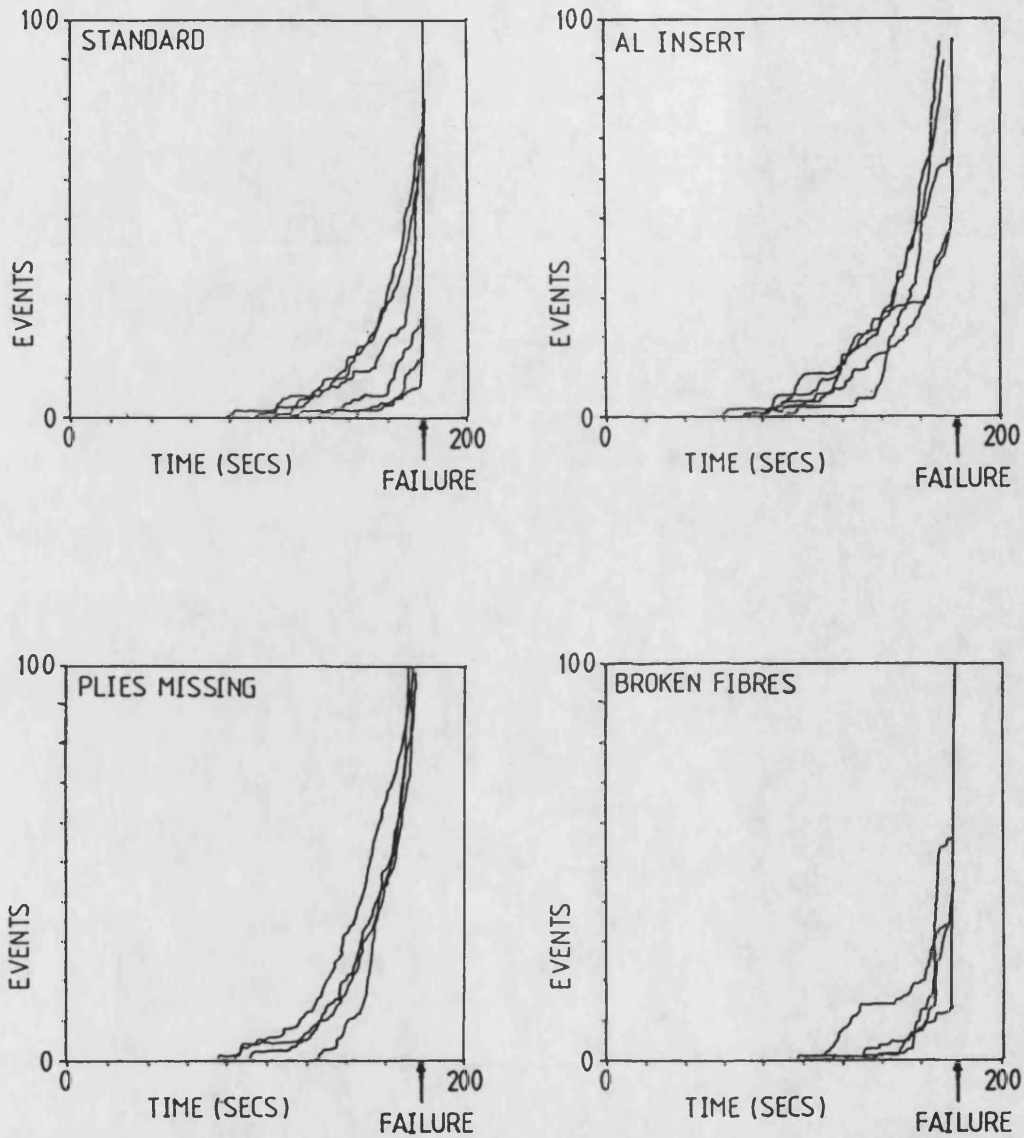


Figure 6.4. Total events/time plots for groups of defective and non-defective 16-ply UD 0° APC2 plates tested in three point flexure. Each graph line, which relates to a different specimen, has had the events produced during the first fifty five seconds of the test removed and has then been shifted to a common failure point on the time axis.

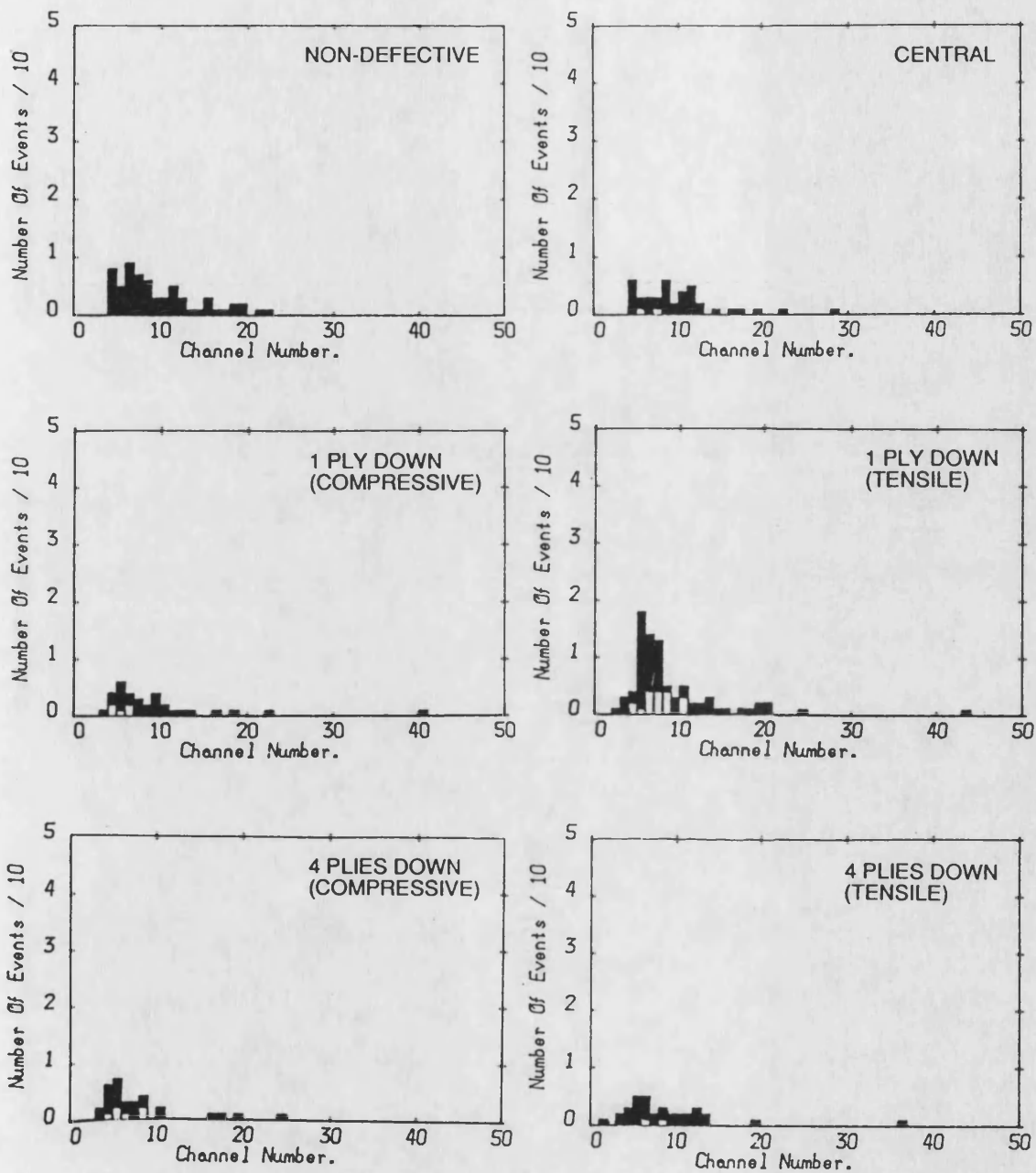


Figure 6.5. Amplitude distribution histograms of events recorded up to 2000N for standard and 'plies removed at different depths' defective 0° 16-ply UD APC2 plates tested in three point flexure. The shaded regions indicate the range of the data.

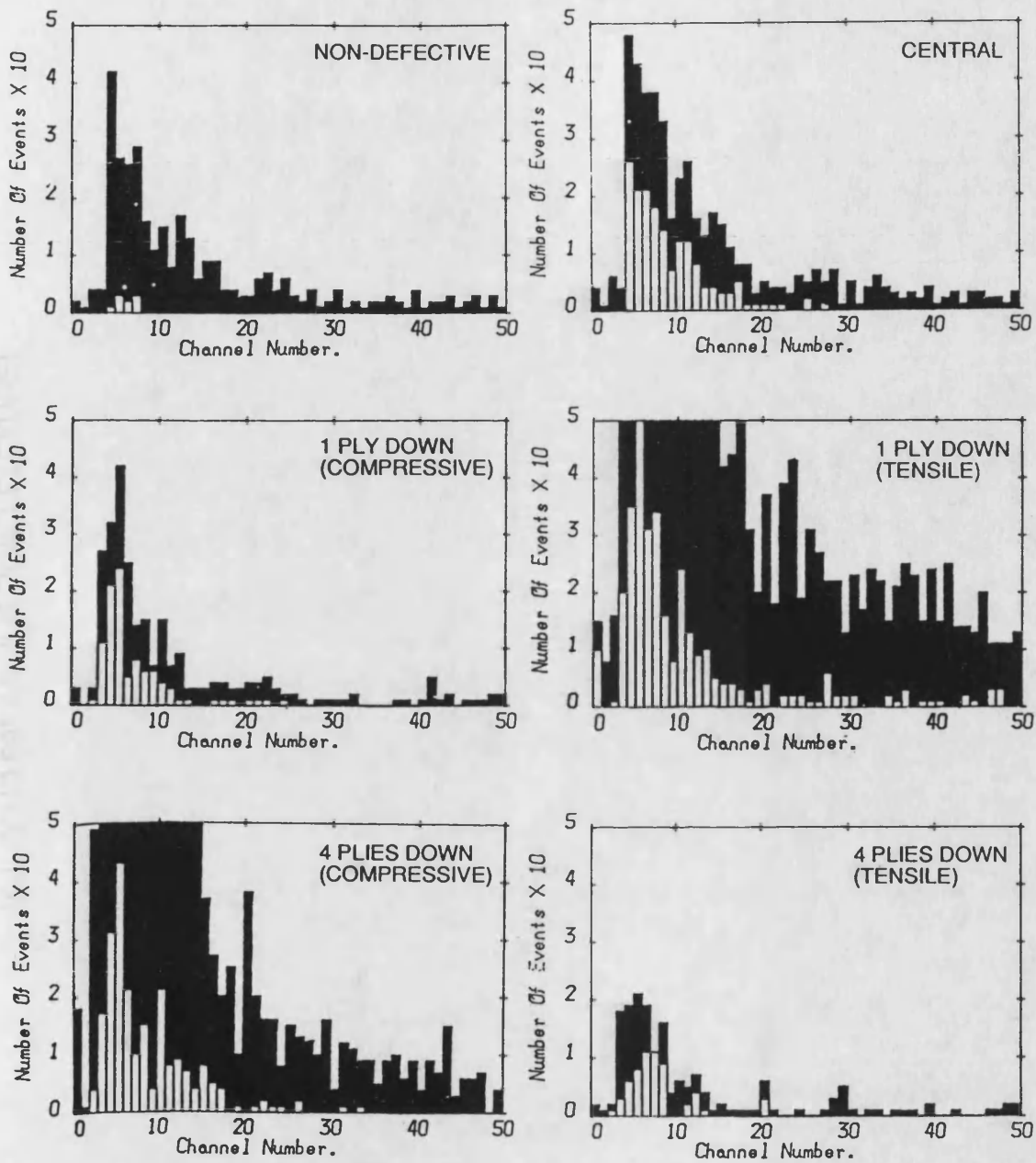


Figure 6.6. Amplitude distribution histograms of events recorded to failure for standard and 'plies removed at different depths' defective 0° 16-ply UD APC2 plates tested in three point flexure. The shaded regions indicate the range of the data.

16-PLY UD 90° APC2 (3 POINT FLEXURE)

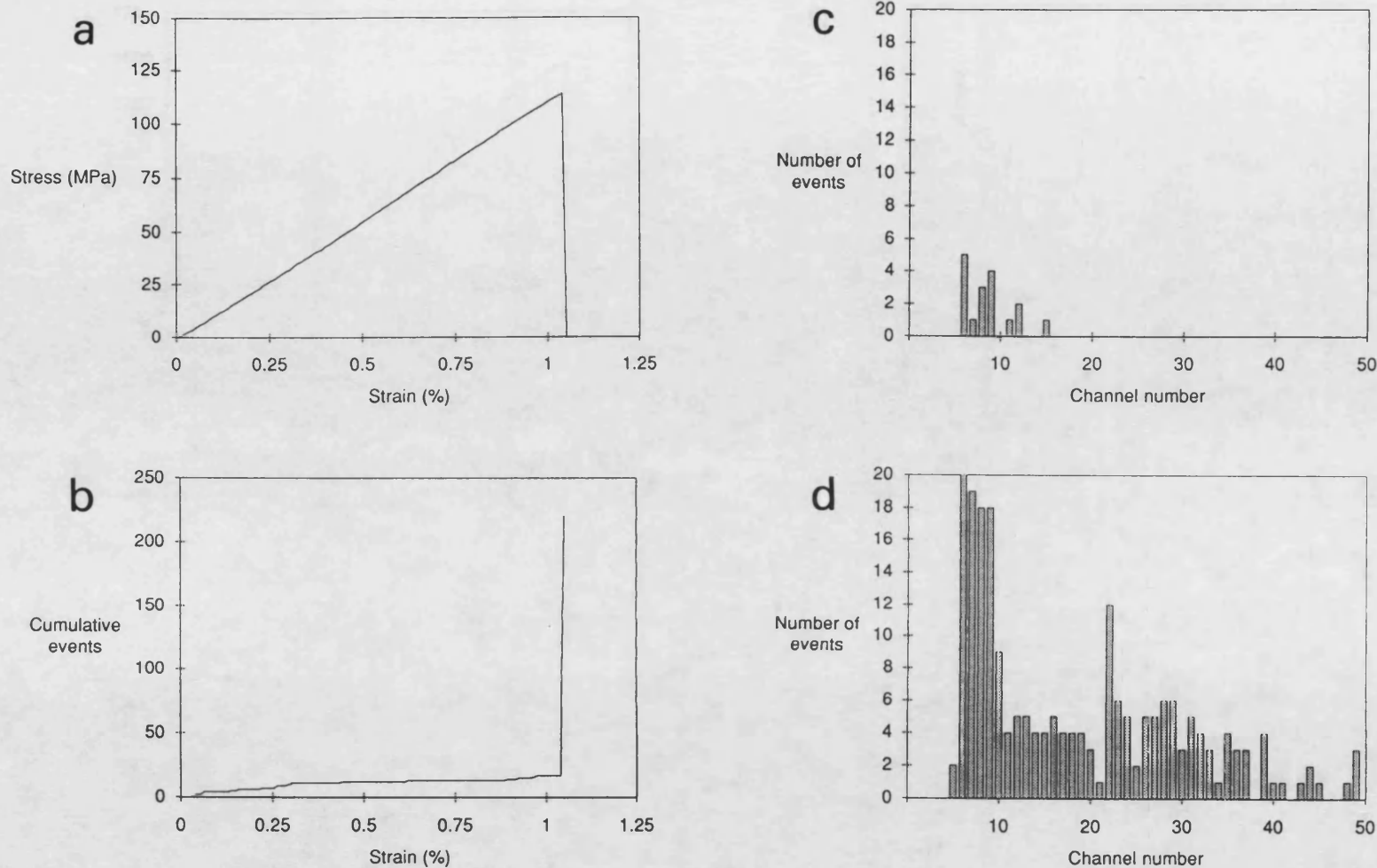


Figure 6.7. A summary of the mechanical and acoustic emission behaviour of 16-ply UD 90° APC2 tested in three point flexure. a) Stress/strain graph. b) Cumulative acoustic emission events as a function of strain. c) Amplitude distribution of events recorded up to maximum stress. d) Amplitude distribution of events recorded until failure.

16-PLY UD 0°/90° APC2 (3 POINT FLEXURE)

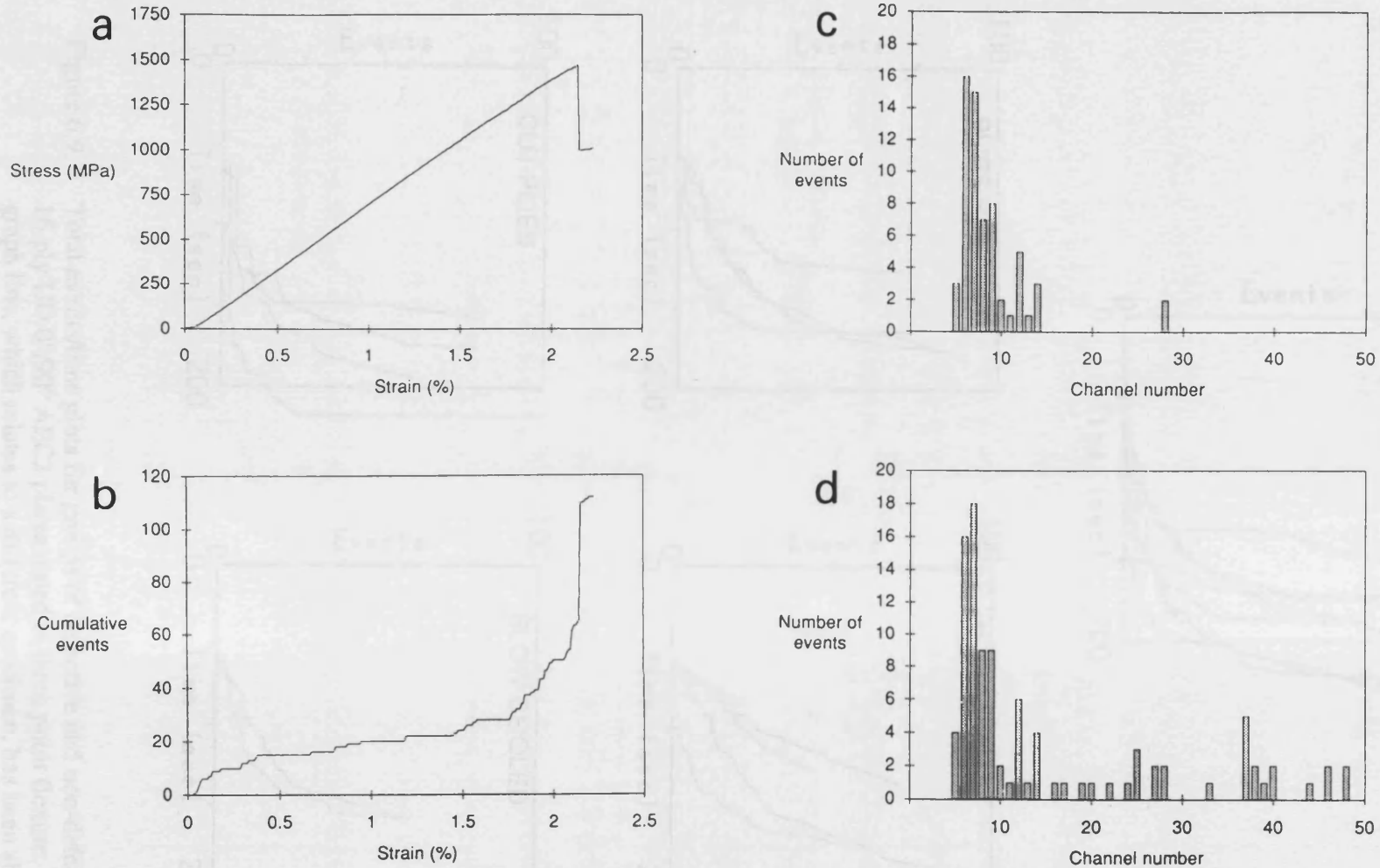


Figure 6.8. A summary of the mechanical and acoustic emission behaviour of 16 cross-ply APC2 tested in three point flexure. a) Stress/strain graph. b) Cumulative acoustic emission events as a function of strain. c) Amplitude distribution of events recorded up to maximum stress. d) Amplitude distribution of events recorded until failure.

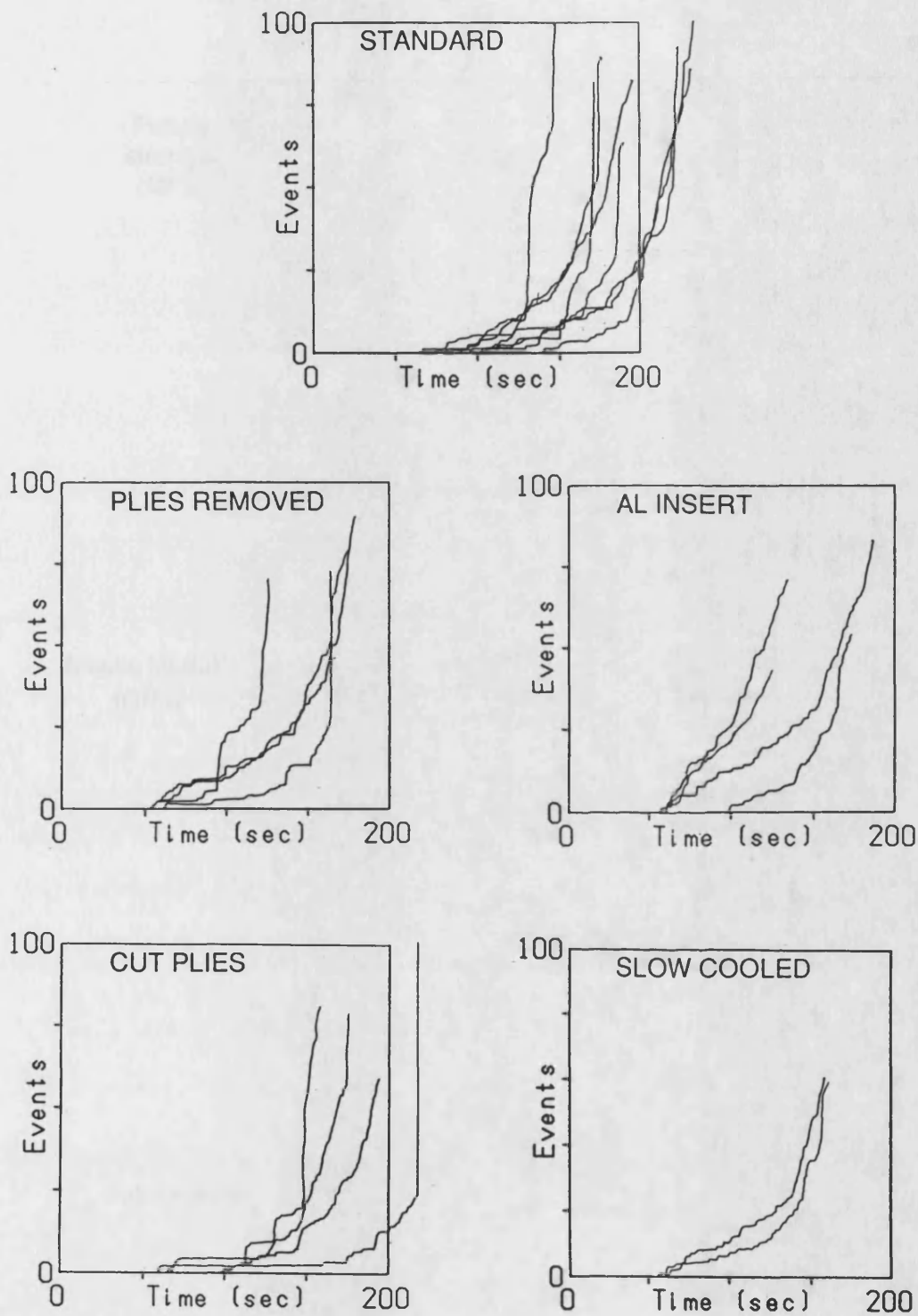


Figure 6.9. Total events/time plots for groups of defective and non-defective 16-ply UD $0^{\circ}/90^{\circ}$ APC2 plates tested in three point flexure. Each graph line, which relates to a different specimen, has been shifted to remove the events produced during the first fifty five seconds of the test and plotted on one graph.

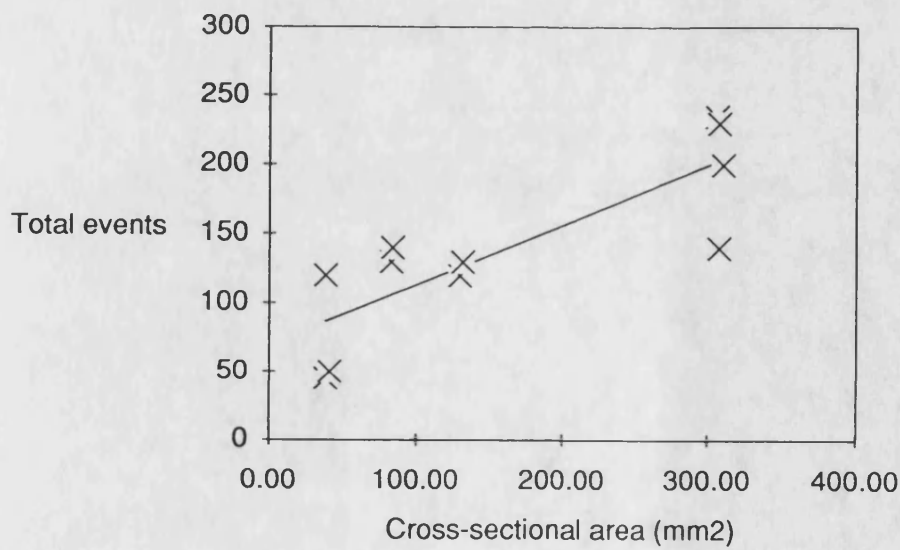
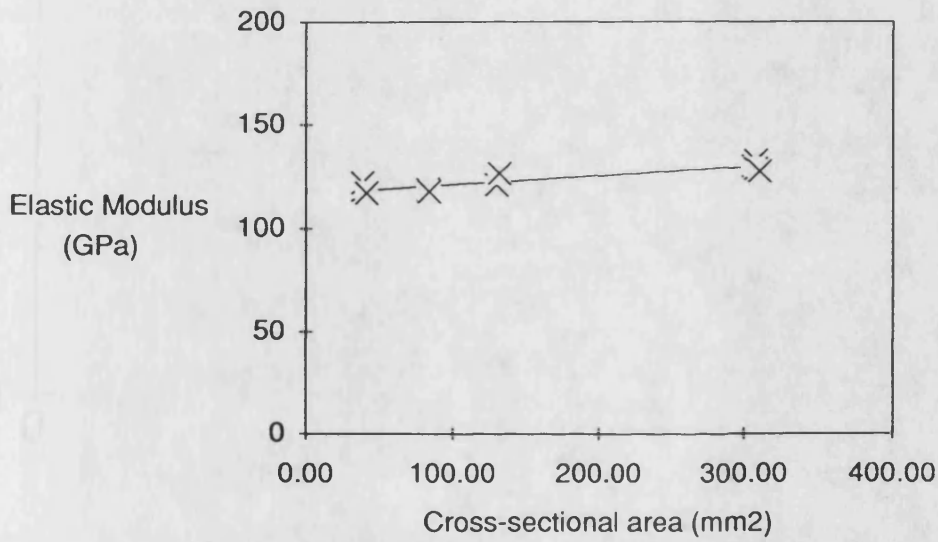
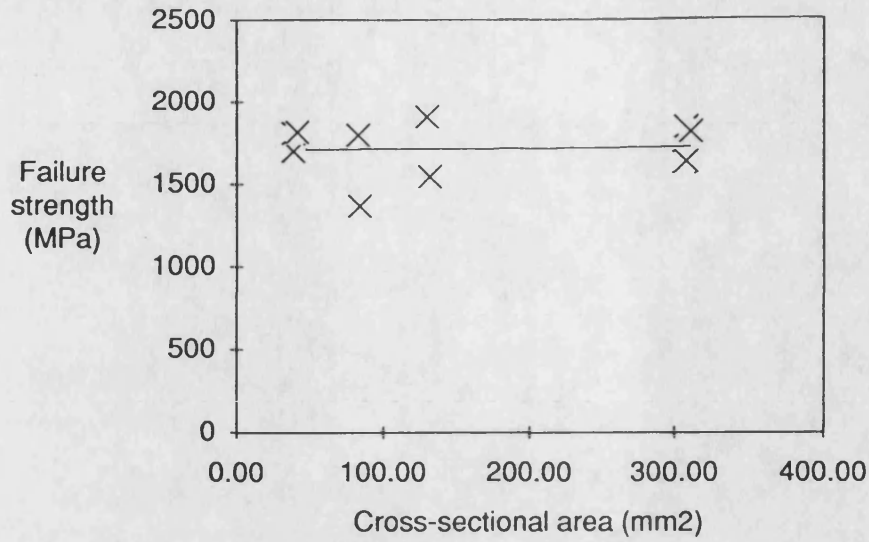


Figure 6.10. Variation of flexural strength, elastic modulus and cumulative events as a function of cross sectional area for 16-ply UD 0° plates tested in three point flexure.

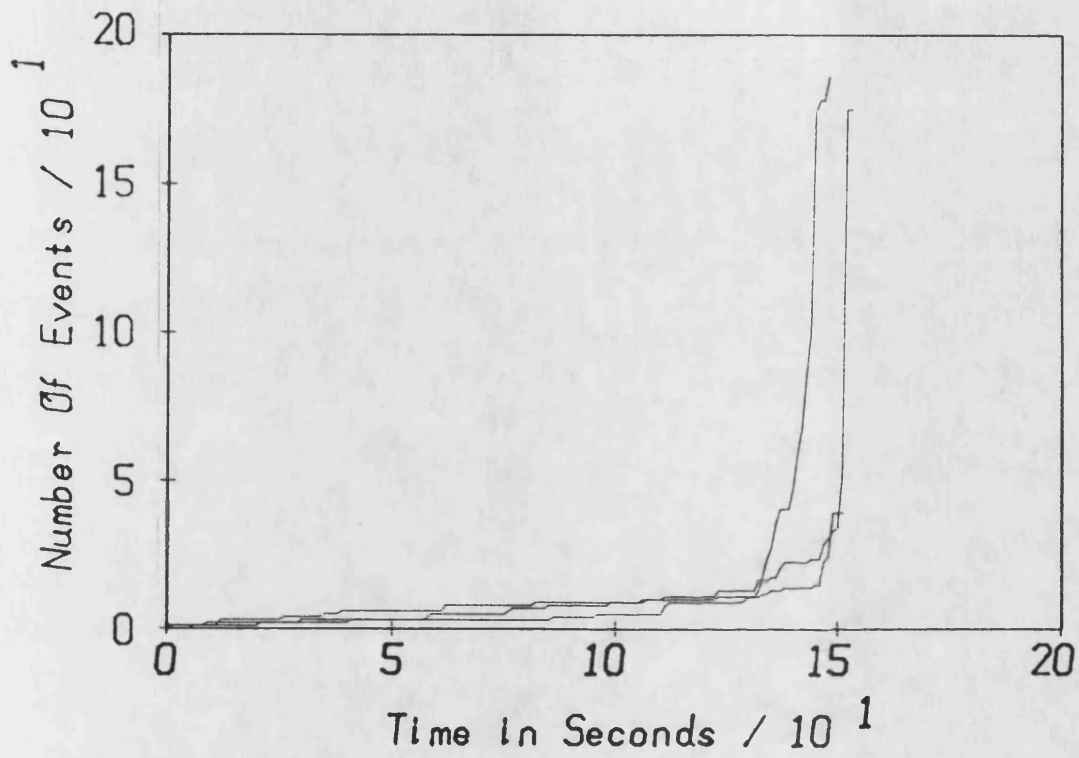


Figure 6.11. Event/time plots for three 16-ply UD 0° carbon fibre reinforced epoxy plates tested in three point flexure.

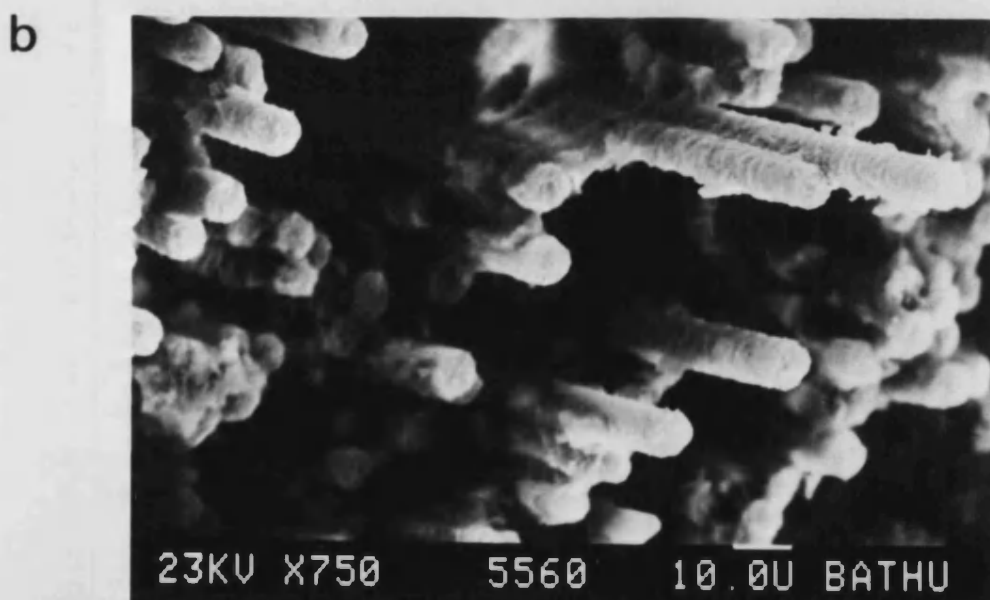
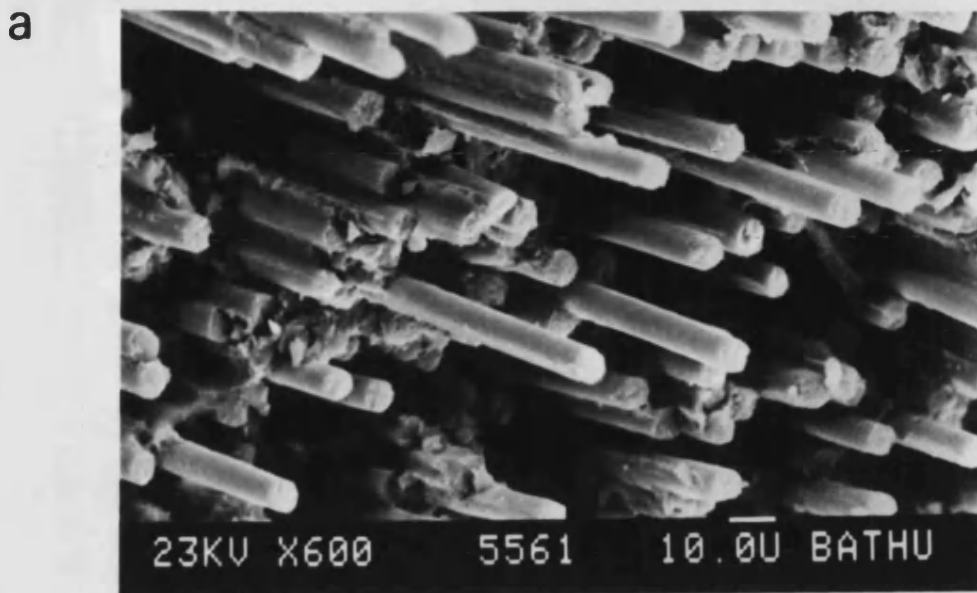


Figure 6.12. SEM micrographs of typical fracture surfaces of laminates tested in three point flexure. a) APC2 b) carbon fibre/epoxy. Note the similarity of the fracture surfaces in spite of the differences in matrices.

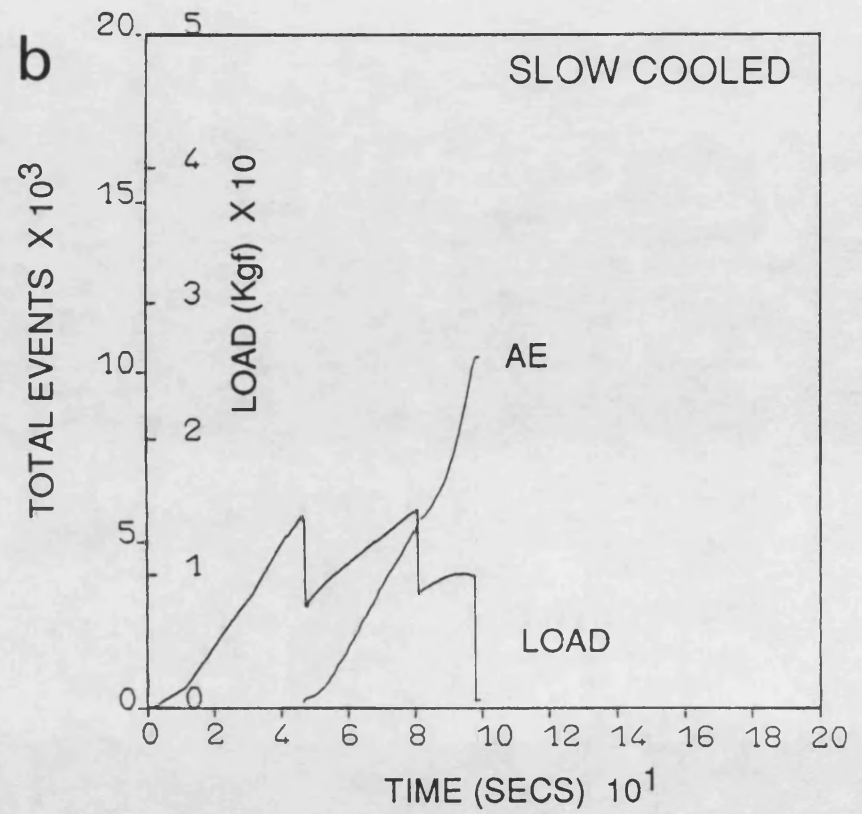
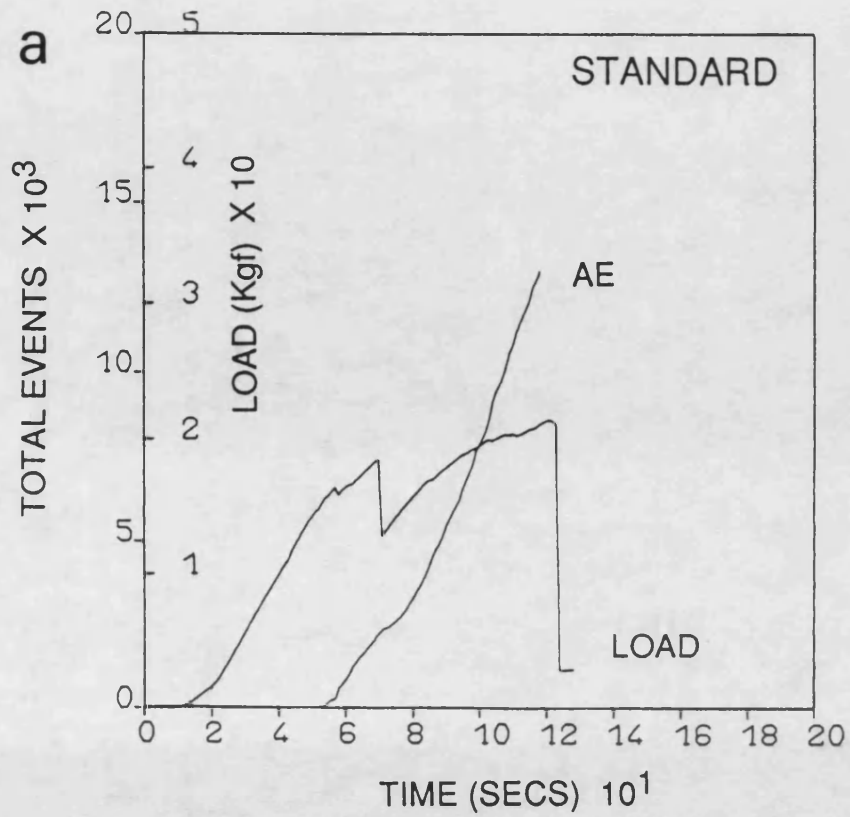


Figure 6.13. Load against time and cumulative events versus time graphs for double torsion 16-ply UD APC2 plates:
a) standard b) slow cooled.

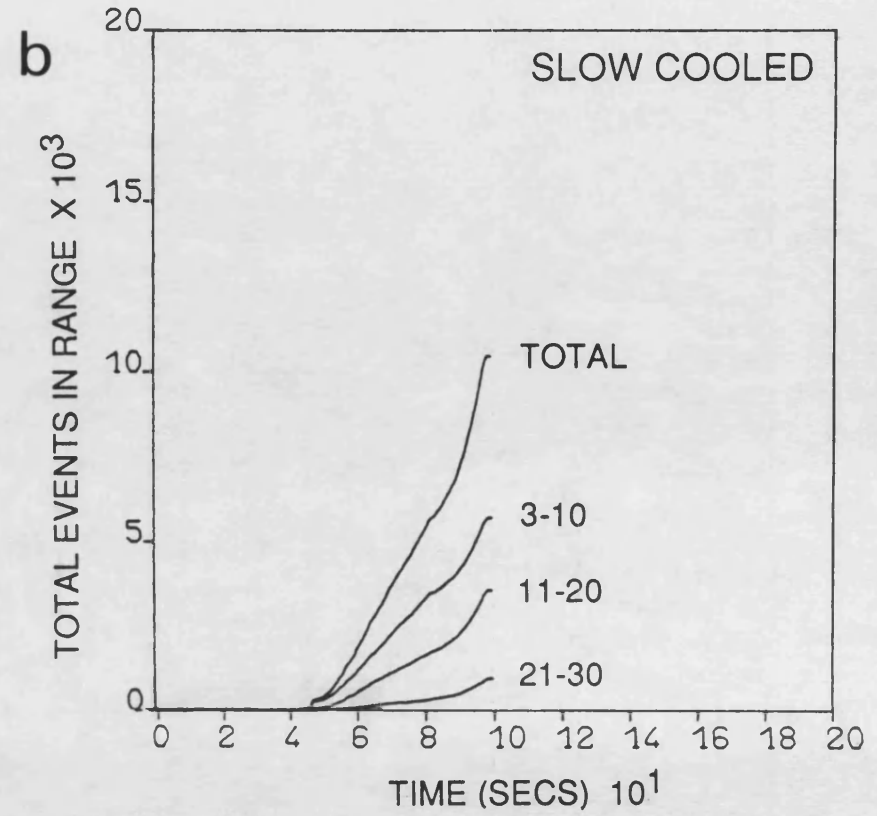
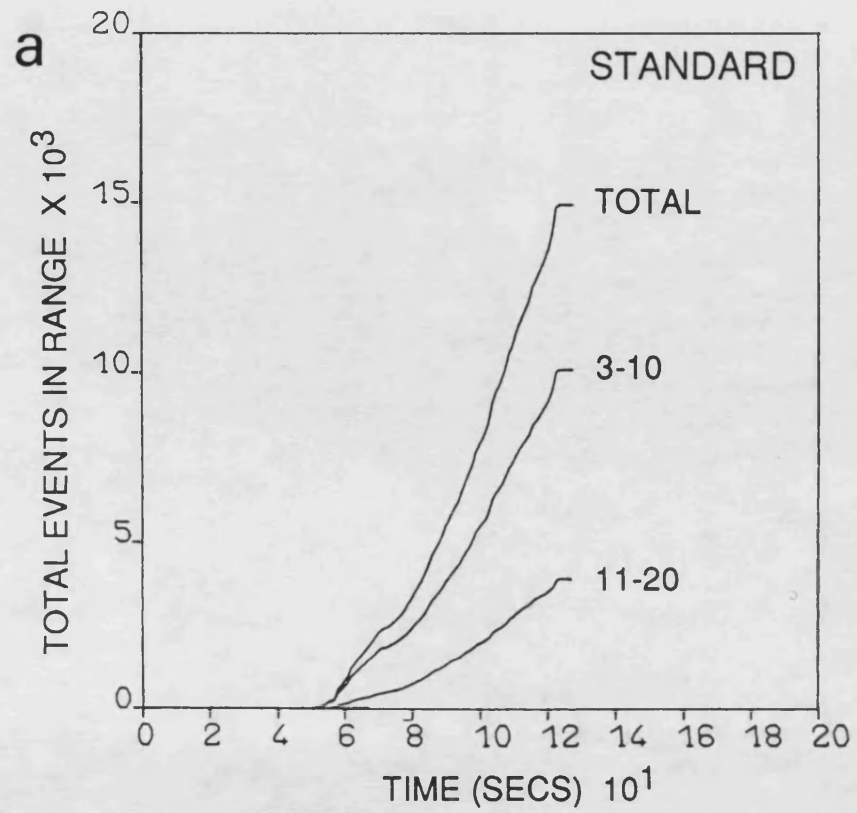


Figure 6.14. Total events in selected channel ranges versus time graphs for double torsion tests: a) standard b) slow cooled.

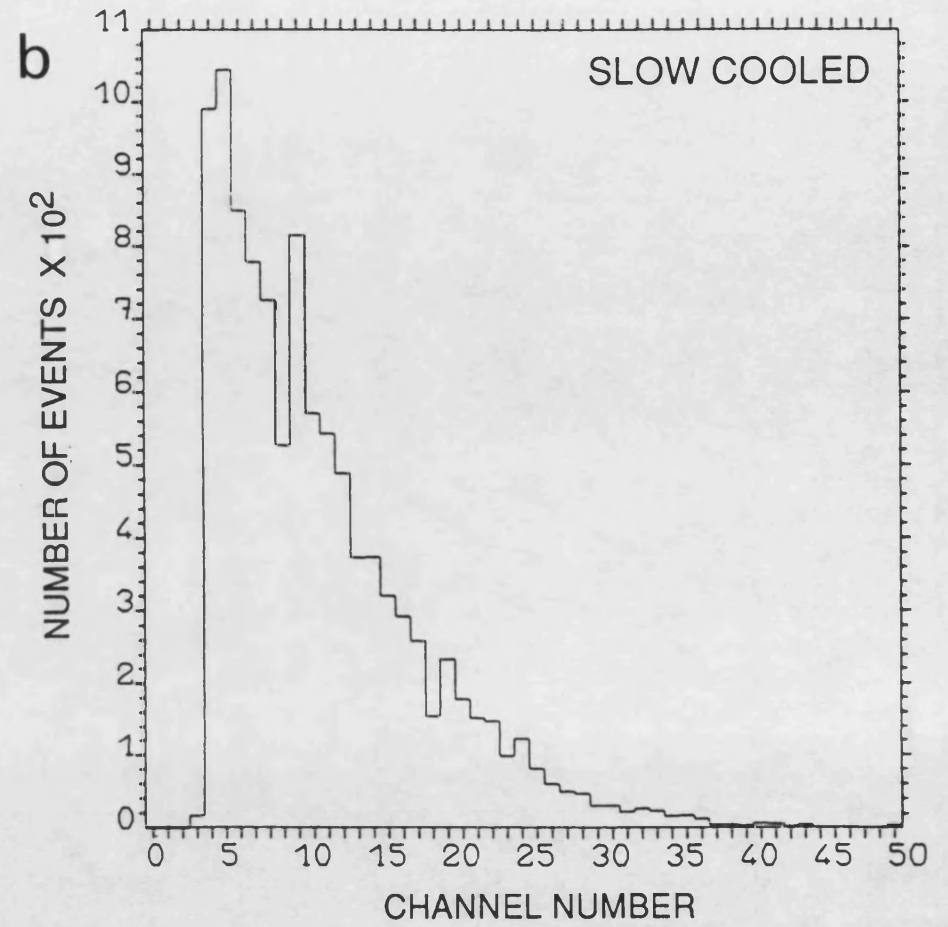
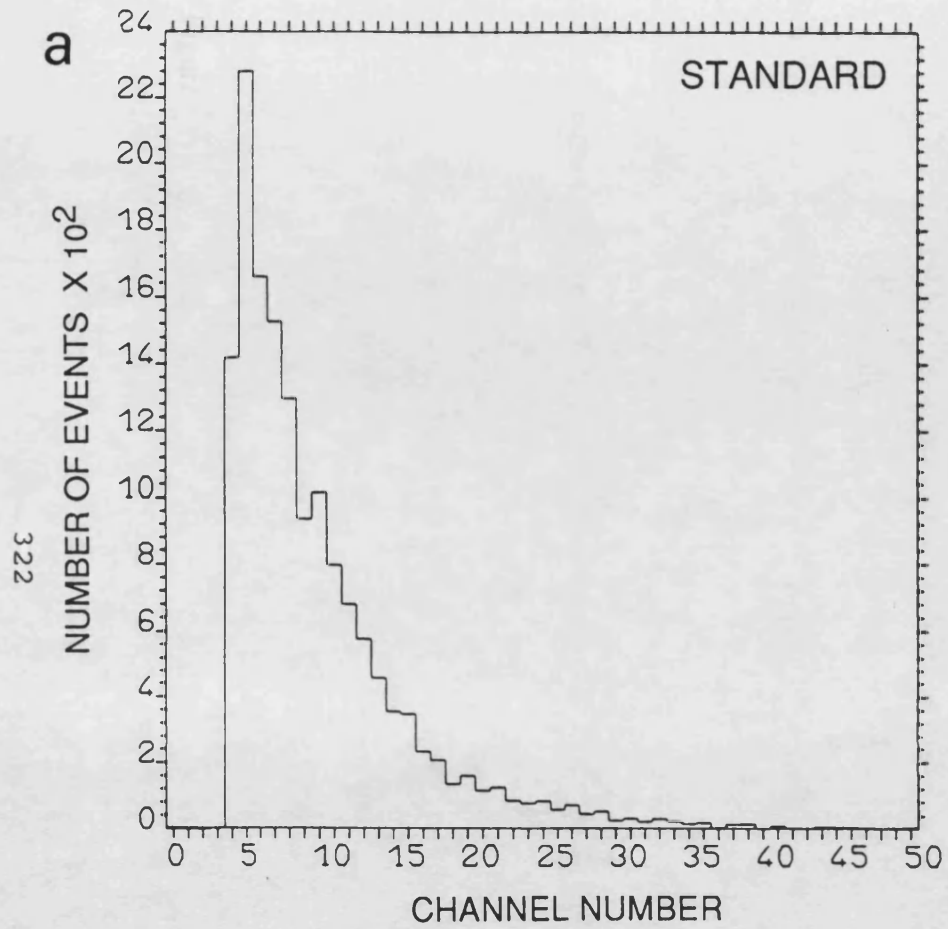


Figure 6.15. Amplitude distribution histograms from double torsion tests: a) standard b) slow cooled.

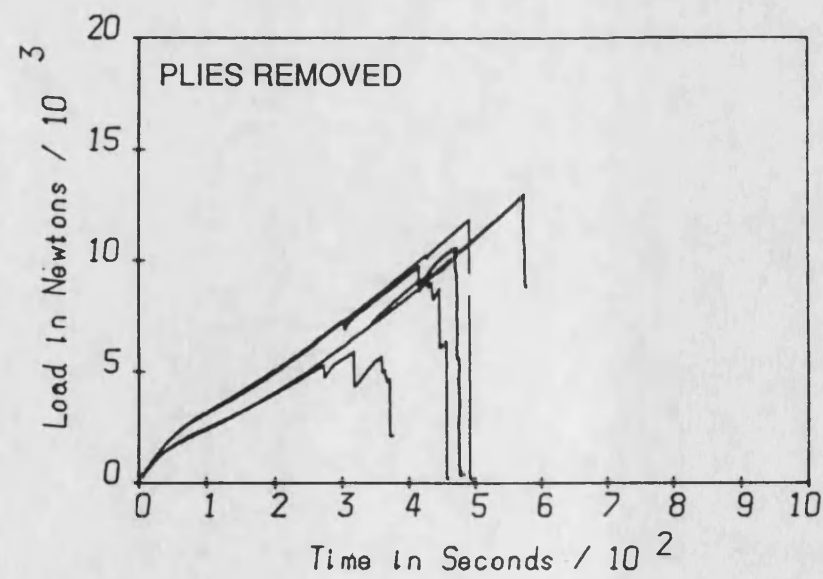
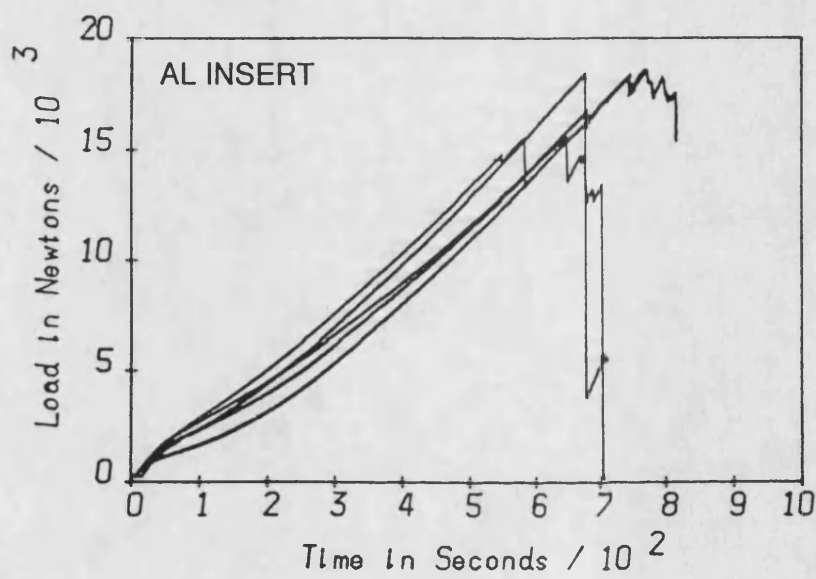
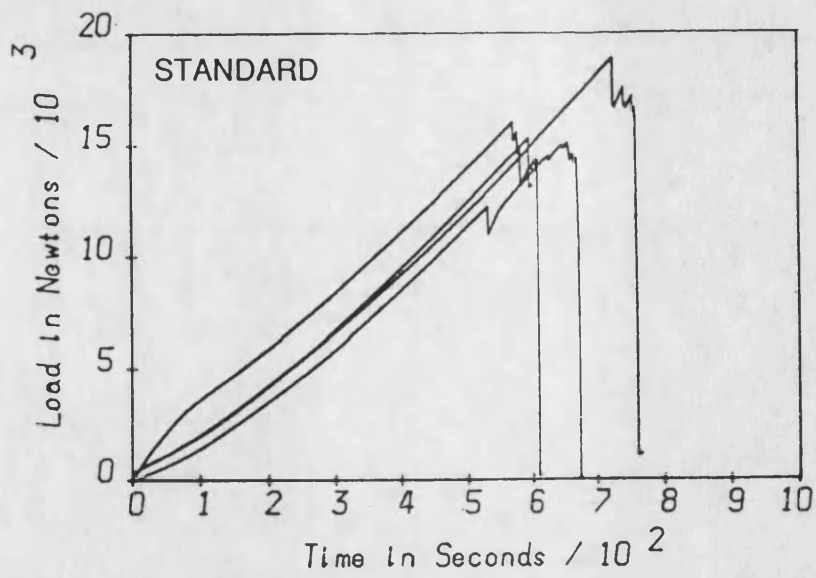


Figure 6.16. Load/time graphs for standard, 'Al insert' and 'plies removed' 8-ply UD 0° APC2 strip specimens tested in tension. Five nominally identical specimens are included in each figure.

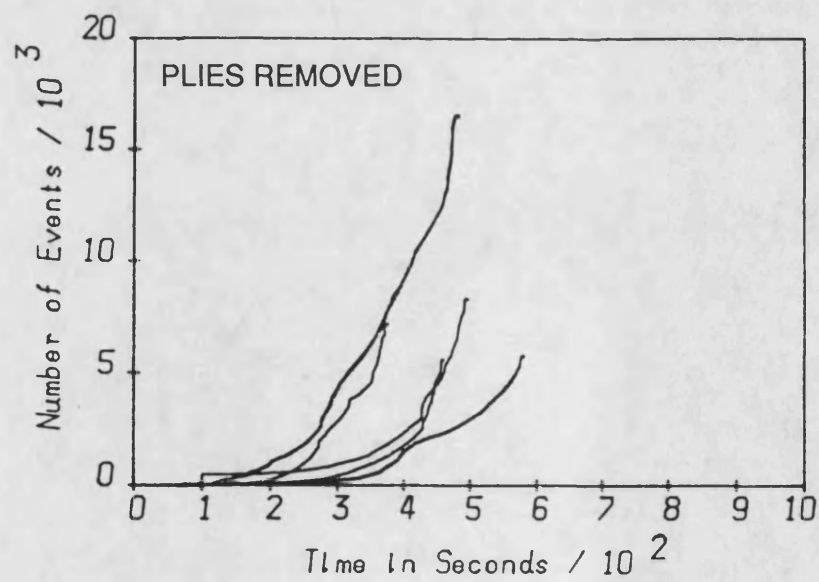
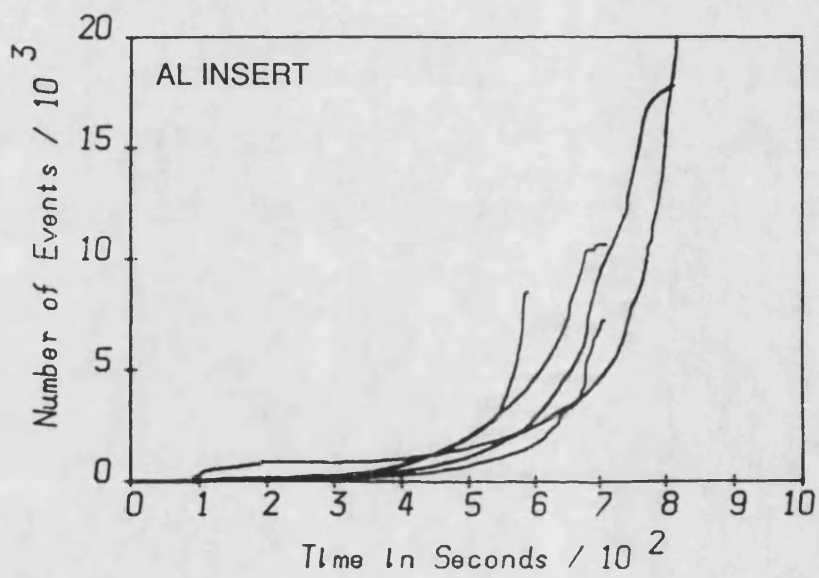
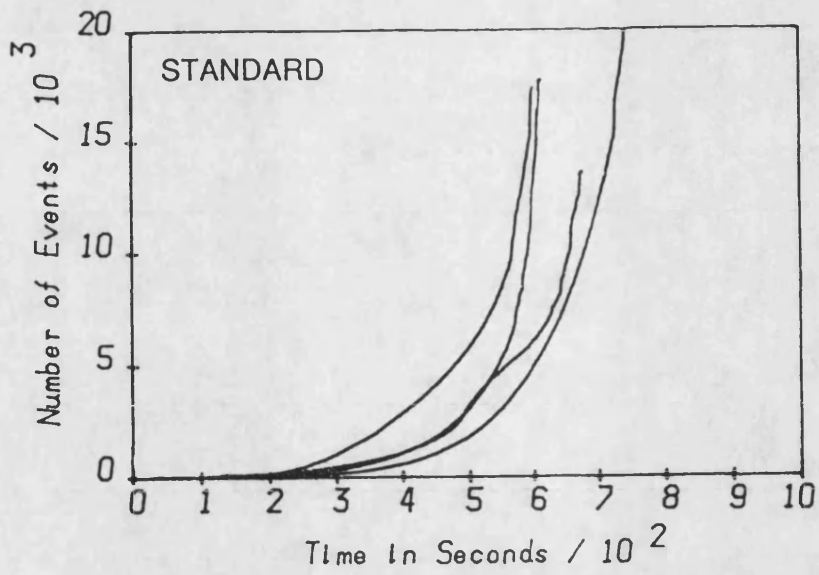


Figure 6.17. Total events in all channels versus time graphs for standard and defective 8-ply UD 0° APC2 strip specimens tested in tension.

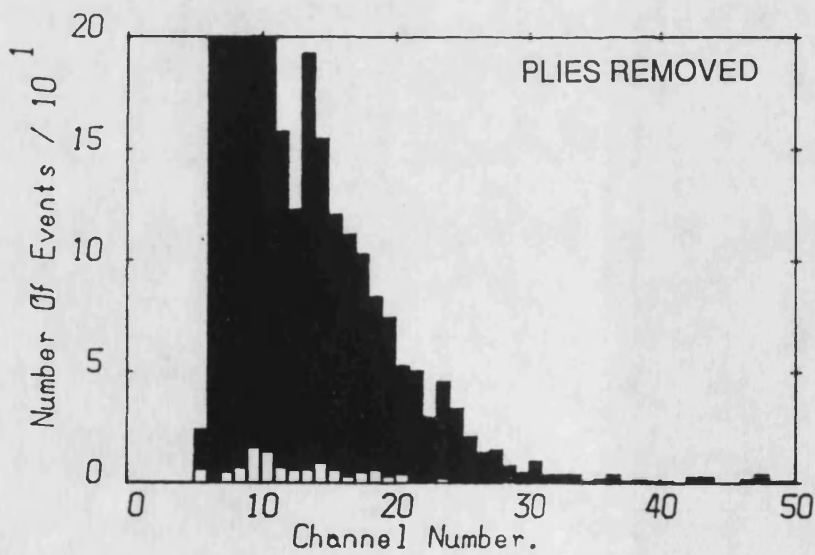
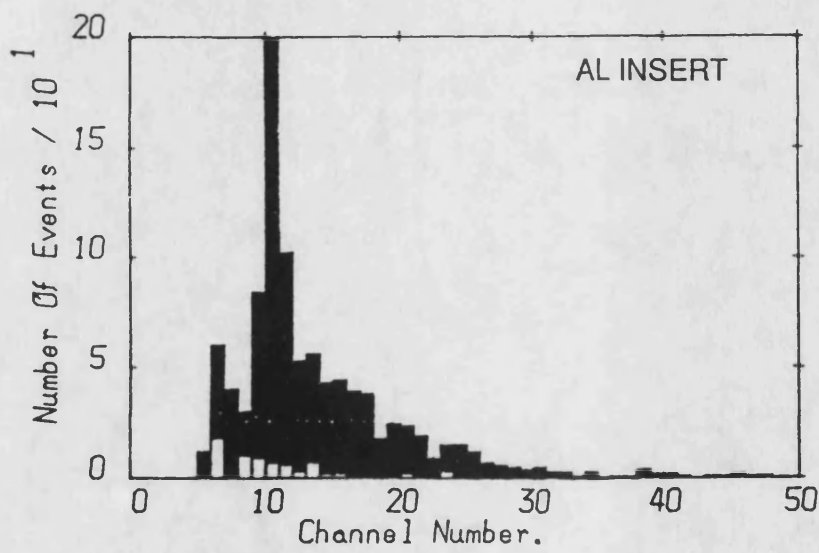
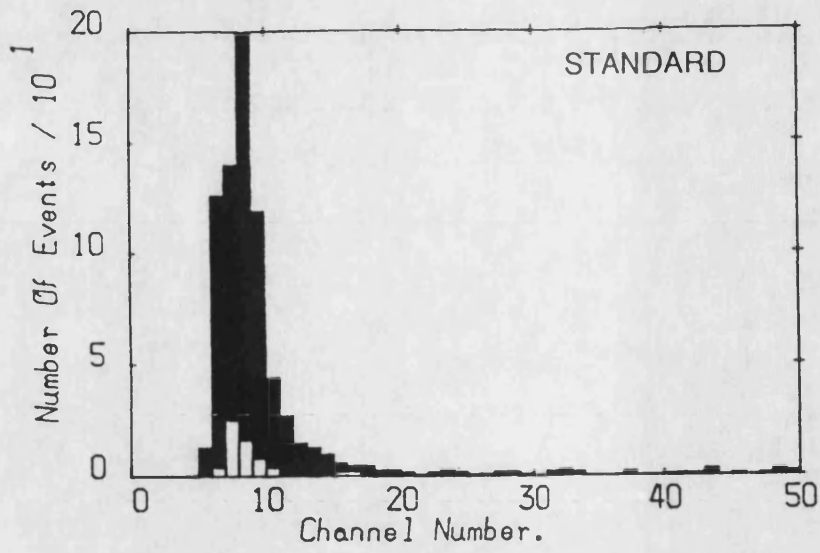


Figure 6.18. Amplitude distribution histograms for events recorded up to 5000N from standard and defective 8-ply UD 0° specimens. The shaded regions represent the range in the data from five nominally identical specimens.

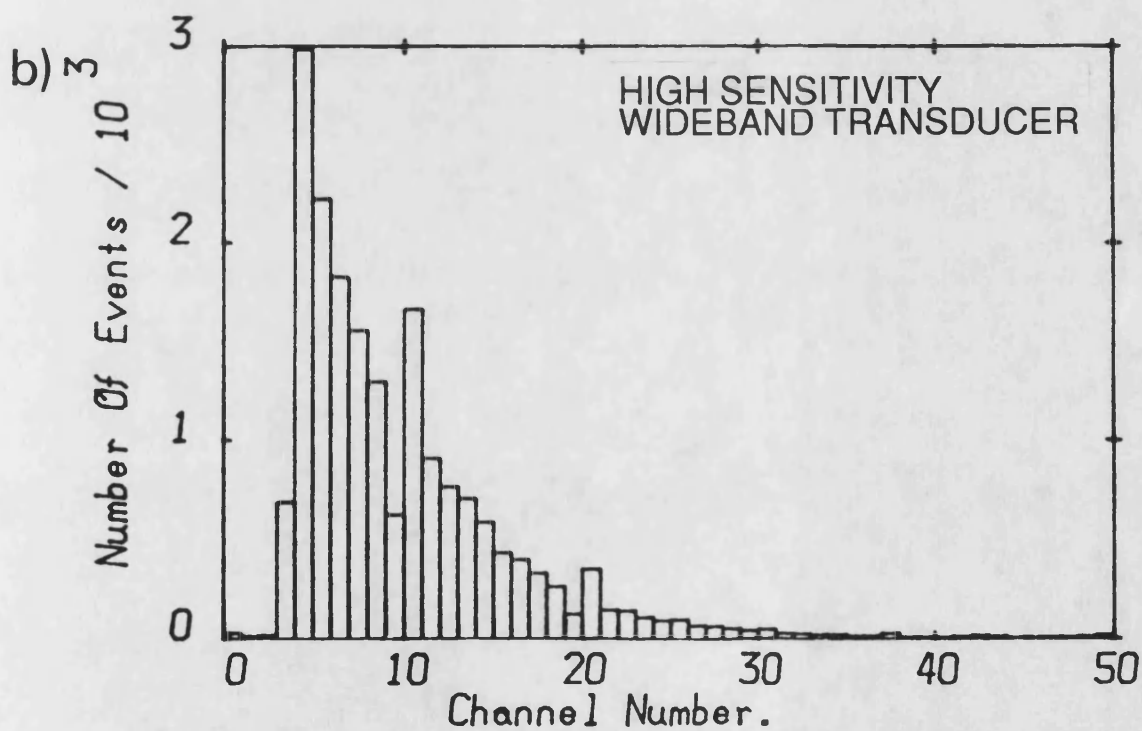
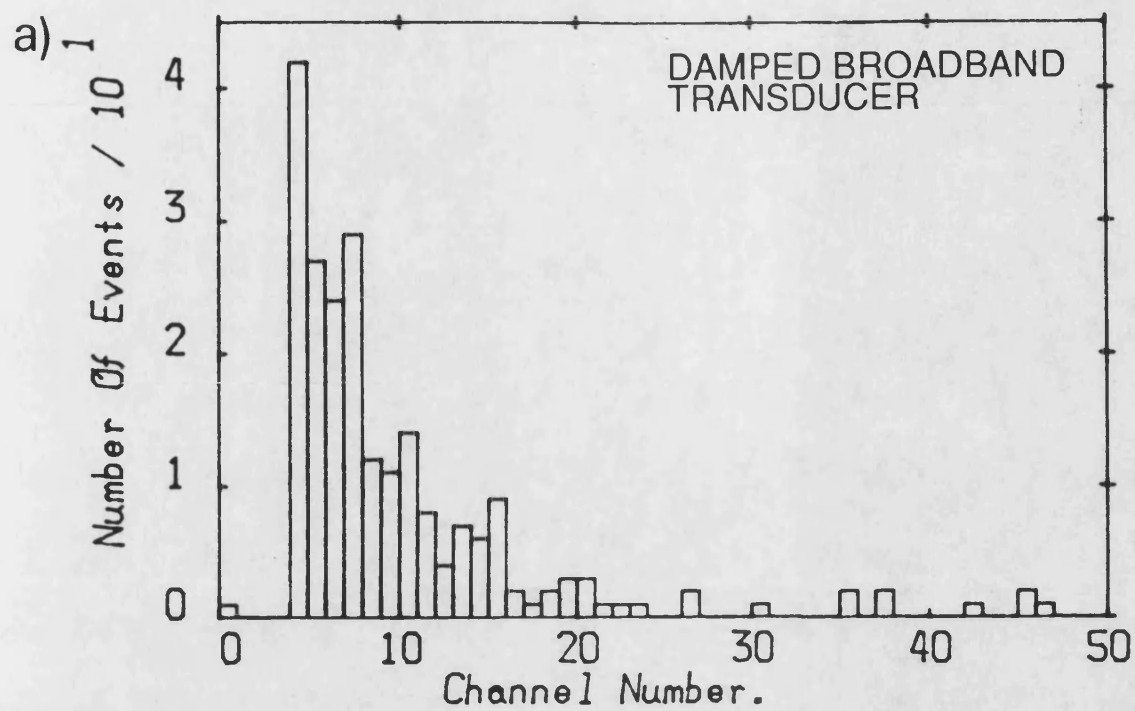


Figure 6.19. Amplitude distribution histograms of events recorded to failure for typical 16-ply UD 0° APC2 plates tested in three point flexure using: a) an AETC MAC 300 transducer b) a PAC U30D transducer.

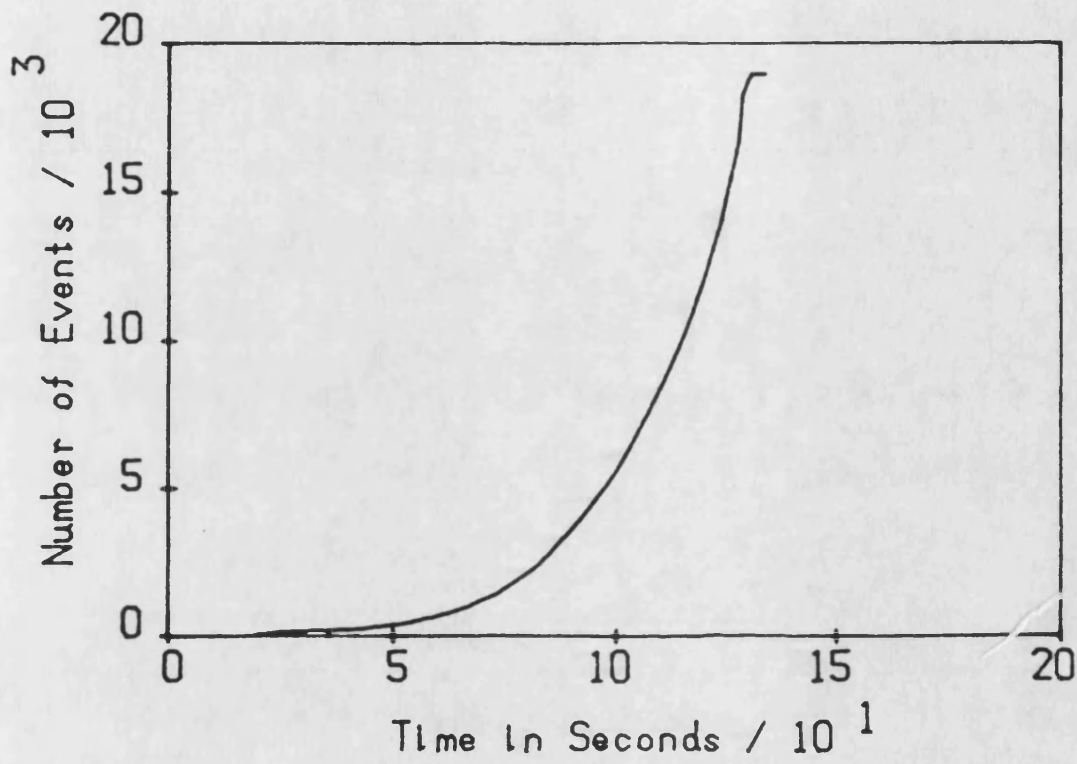


Figure 6.20. Cumulative events/time graph for a 16-ply UD 0° APC2 plate tested in 3 point flexure under standard conditions using a high sensitivity PAC U30D transducer.

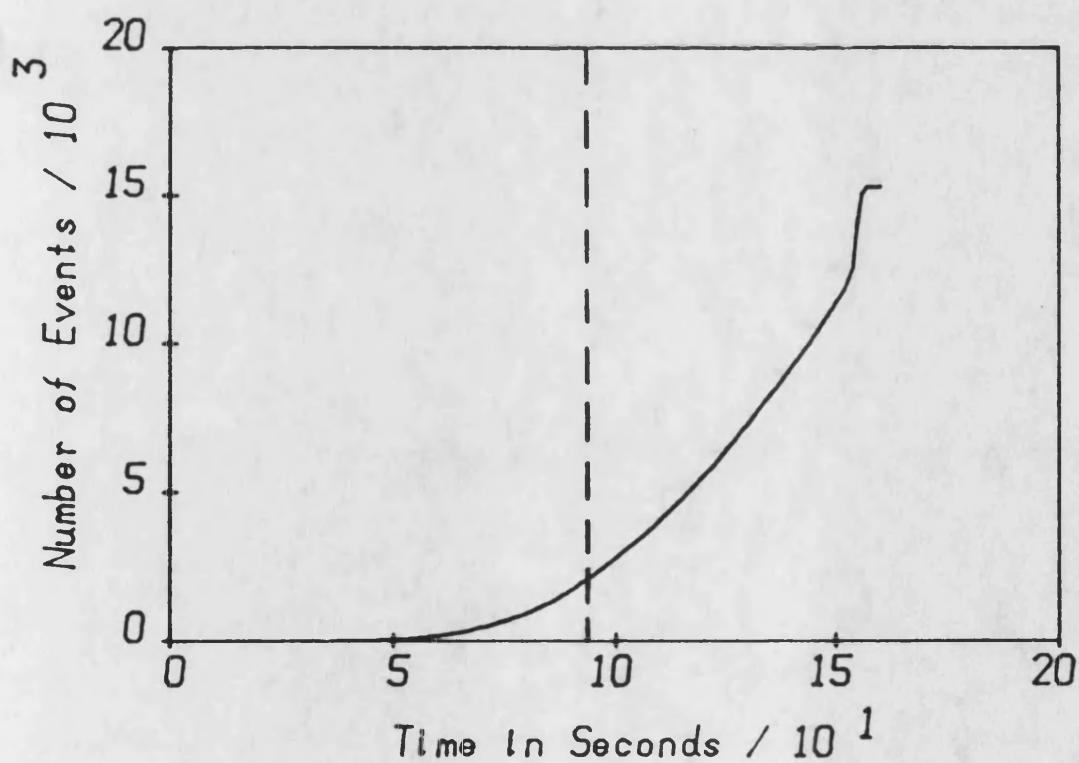
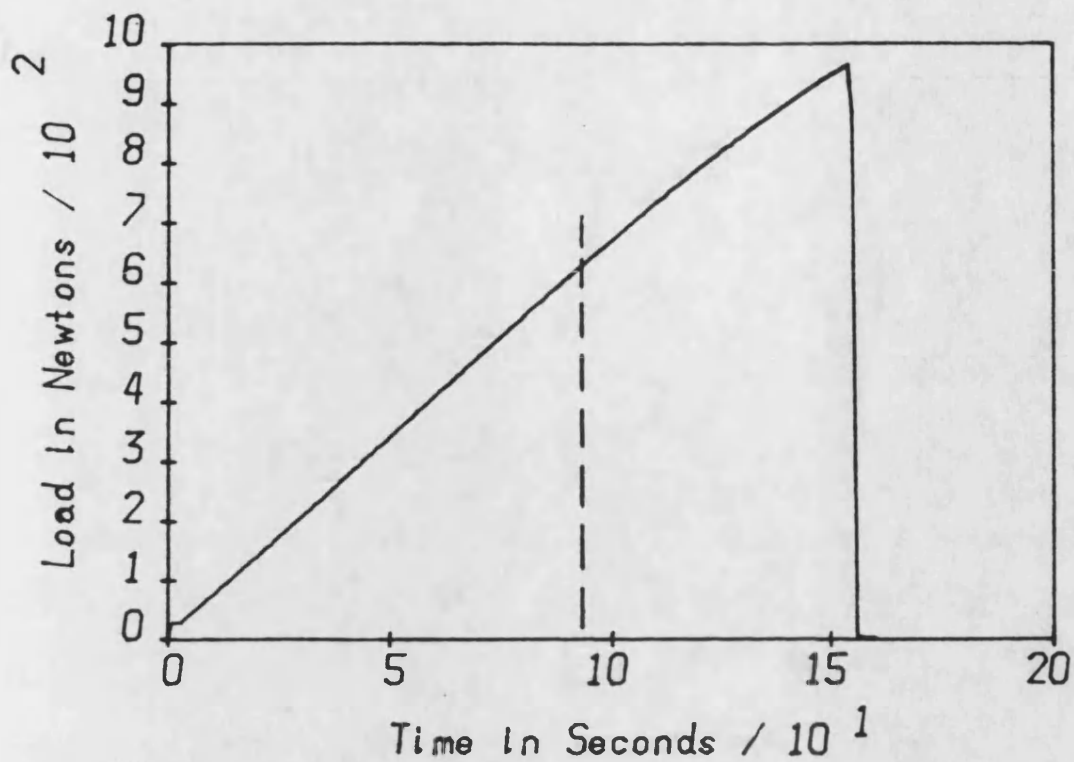


Figure 6.21. A typical 16-ply UD 0° APC2 specimen tested in four point flexure: a) load/time graph b) cumulative events time graph.

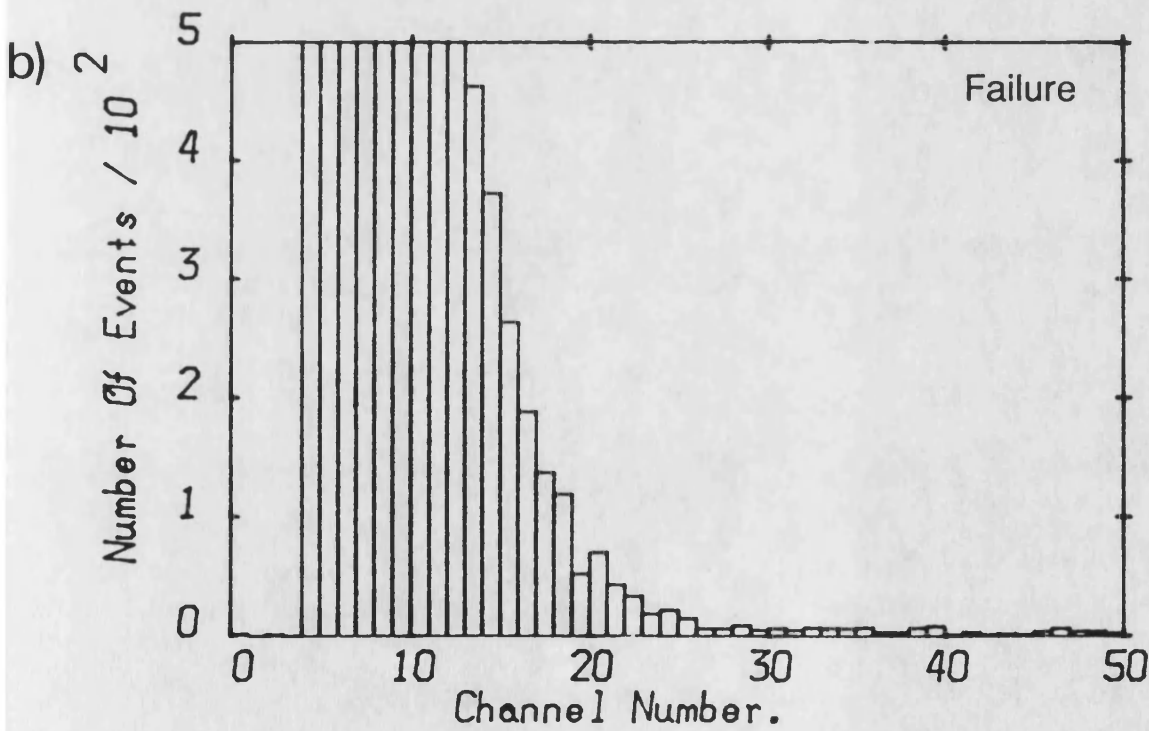
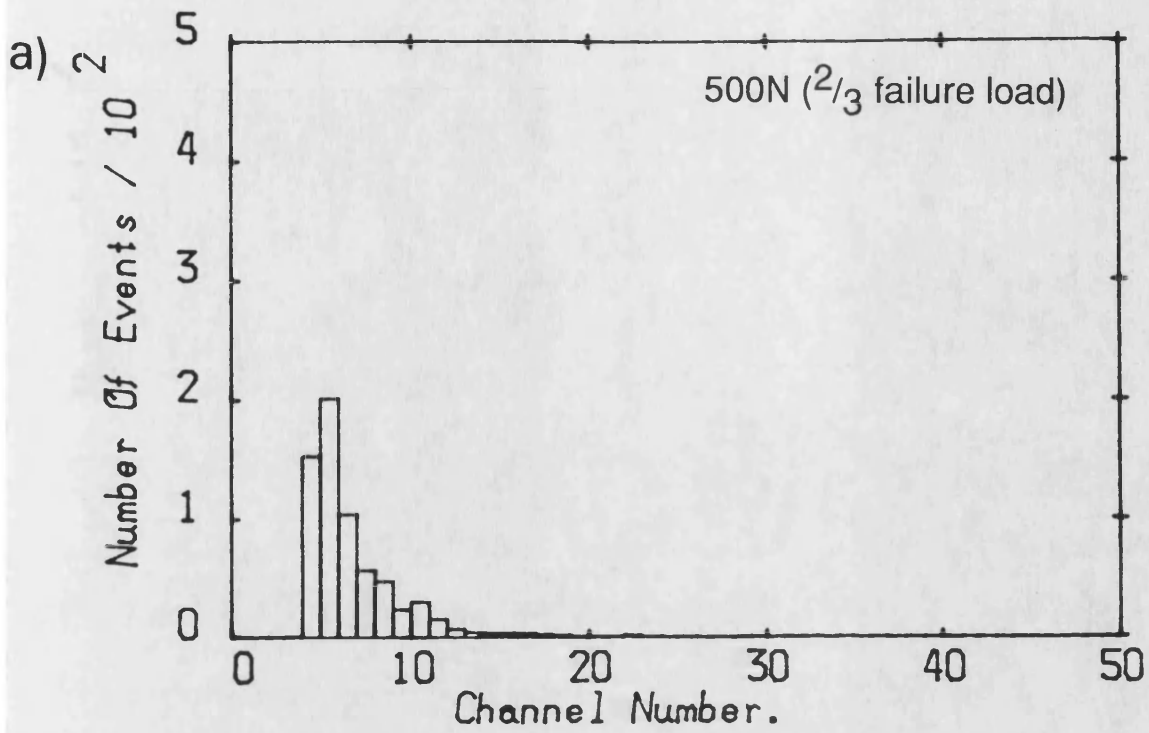


Figure 6.22. Amplitude distribution histograms of events recorded from 16-ply UD 0° APC2 tested in four point flexure and loaded to: a) 500N ($2/3$ failure load) b) failure.

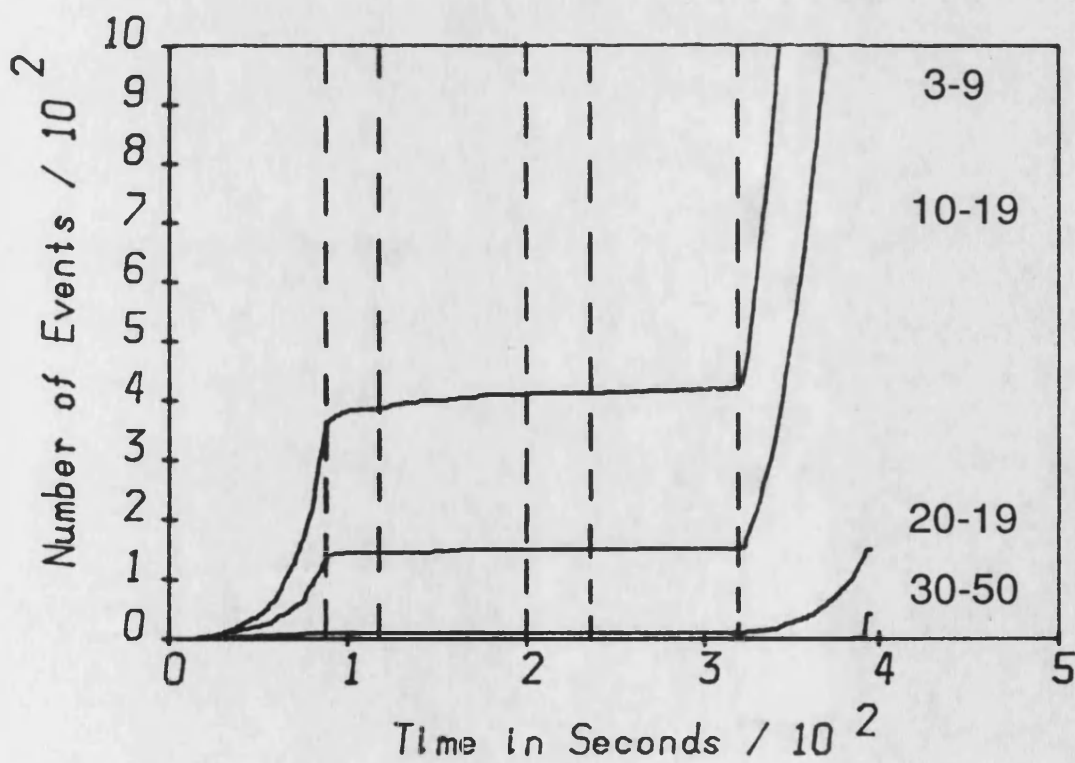
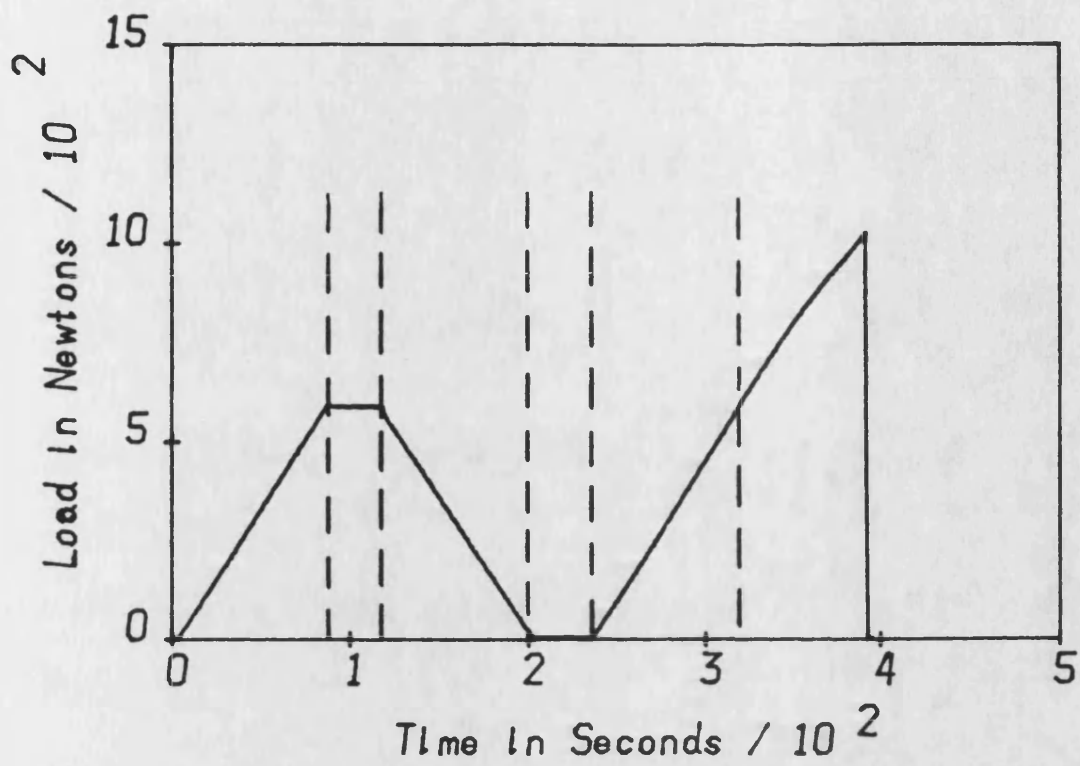


Figure 6.23. Interrupted loading of 16-ply UD 0° APC2 tested in four point flexure: a) load/time graph b) events in selected channels versus time graph.

0° UD Laminate Quality	Strength (MPa)	Strain (%)	E (GPa)	Total events to failure	Total events prior to failure	Statistic
Good Quality	1907	1.390	136.7	159	67.50	Mean
	0.109	0.055	0.104	0.440	0.564	Coef of var'
	(2287-1652)	(1.482-1.304)	(158.2-119.3)	(255-28)	(116 - 8)	Range
Slow cooled	2115	1.523	141.3	1070	271.33	Mean
	0.106	0.133	0.071	1.229	0.403	Coef of var'
	(2305-1831)	(1.716-1.323)	(154.9-131.9)	(3037-275)	(395 - 187)	Range
Broken fibres	1753	1.385	127.1	218	42.00	Mean
	0.067	0.084	0.019	1.248	0.575	Coef of var'
	(1906-1654)	(1.526-1.273)	(128.7-123.6)	(623-46)	(75 - 17)	Range
Al insert	1930	1.531	124.6	152	88.00	Mean
	0.045	0.035	0.018	0.322	0.289	Coef of var'
	(2070-1860)	(1.614-1.479)	(127.4-121.9)	(202-90)	(116 - 60)	Range

Table 6.1a. Mechanical properties and cumulative event counts for groups of non-defective and defective 16-ply UD 0° APC2 plates tested in three point flexure. Means, coefficients of variation and ranges of data from repeat specimens are presented.

0° UD Laminate Quality	Strength (MPa)	Strain (%)	E (GPa)	Total events to failure	Total events prior to failure	Statistic
Good Quality	1907 (2287-1652)	1.390 (1.482-1.304)	136.7 (158.2-119.3)	159 (255-28)	67.5 (116 - 8)	Mean Range
Plies missing (1 ply down, tension)	1309 (1428-1203)	1.197 (1.220-1.160)	112 (126.2-103.2)	1525 (3037-334)	225.0 (251 - 187)	Mean Range
Plies missing (4 ply down, tension)	1426 (1538-1347)	1.373 (1.470-1.270)	103.3 (105.9-100.4)	117 (142-96)	65.7 (91 - 46)	Mean Range
Plies missing (central)	1822 (2048-1652)	1.414 (1.602-1.214)	128.1 (137.3-123.0)	724 (2385-271)	150.6 (283 - 37)	Mean Range
Plies missing (1 ply down, comp)	1432 (1500-1378)	1.373 (1.440-1.340)	101.3 (103.6-97.8)	176 (212-137)	106.0 (136 - 80)	Mean Range
Plies missing (4 ply down, comp)	1318 (1382-1231)	1.317 (1.350-1.290)	100.6 (101.2-99.8)	912 (2031-275)	419.3 (907 - 147)	Mean Range

Table 6.1b. Mechanical properties and cumulative event counts for groups of non-defective (good quality) plates and plates with 'plies removed' defects at various ply positions. Results are from 16-ply UD APC2 plates tested in three point flexure. Means and ranges of the data from repeat specimens are presented.

Events recorded prior to failure

0° UD APC2 specimen description	Number of events	Max no. of events in any channel	Mean amplitude	Variance	Relative skewness	Relative kurtosis	Statistic
STANDARD	67.50	14.75	9.08	29.50	2.24	11.47	Mean
	0.564	0.583	0.144	0.721	0.663	0.741	Coef of var'
	(116 - 8)	(28 - 3)	(11.96 - 7.88)	(66.1 - 3.4)	(3.692 - 0.136)	(22.7 - 1.46)	Range
SLOW COOLED	271.33	47.67	11.56	54.90	1.73	6.60	Mean
	0.403	0.202	0.226	0.723	0.395	0.522	Coef of var'
	(395 - 187)	(58 - 39)	(14.34 - 9.16)	(99.3 - 22.8)	(2.349 - 0.995)	(9.84 - 2.98)	Range

Table 6.2. Various characteristics of the amplitude distribution of events recorded until maximum load (just prior to failure) for groups of defective and non-defective 16-ply UD 0° APC2 plates. Means, coefficients of variation and ranges of data are presented.

90° UD Laminate Quality	Strength (MPa)	Strain (%)	E (GPa)	Total events to failure	Statistic
Good quality	122 (176-90)	1.158 (1.703-0.872)	11.0 (12.1-10.3)	116 (240-30)	Mean Range
Slow cooled	122 (152-69)	1.156 (1.356-0.634)	11.2 (12.3-10.5)	665 (2340-46)	Mean Range
Broken fibres	136 (161-112)	1.376 (1.670-1.081)	10.7 (10.8-10.6)	125 (140-109)	Mean Range
Al insert	143	1.492	10.8	238	
Plies missing (central)	122	1.093	11.0	114	

Table 6.3. Mechanical properties and total event counts to failure for groups of non-defective and defective 16-ply UD 90° APC2 plates tested in three point flexure. Means and ranges of the data from repeat specimens are presented.

0/90 X-ply Laminate Quality	Strength (MPa)	Strain (%)	E (GPa)	Total events to failure	Total events prior to failure	Statistic
Good quality	1453 (1719-1263)	1.737 (2.348-1.420)	89.7 (114.5-71.3)	242 (730-83)	98.1 (204 - 45)	Mean Range
Slow cooled	1411 (1503-1319)	1.670 (1.710-1.630)	88.9 (89.9-87.9)	229 (340-118)	157.0 (224 - 90)	Mean Range
Broken fibres	1580 (1746-1366)	1.660 (1.910-1.420)	102.8 (115.3-89.8)	214 (317-122)	121.0 (184 - 31)	Mean Range
AI insert	1528 (1630-1449)	1.765 (2.000-1.590)	96.7 (111.6-90.2)	304 (463-153)	241.8 (389 - 121)	Mean Range
Plies missing (central)	1402 (1535-1262)	1.54 (1.730-1.470)	92.0 (97.0-87.8)	1459 (4826-226)	194.5 (511 - 44)	Mean Range

Table 6.4. Mechanical properties and cumulative event counts for groups of non-defective and defective 16-ply 0°/90° APC2 plates tested in three point flexure. Means and ranges of the data from repeat specimens are presented.

Material	Strength (MPa)	Strain (%)	E (GPa)	Total events to failure	Statistic
16-Ply UD Carbon Fibre/Epoxy	1488 (1513-1439)	1.378 (1.395-1.370)	109.1 (111.5-104.8)	133 (186-39)	Mean Range
Unreinforced PEEK	-	-	3.7 (4.0-3.1)	5 (12-3)	Mean Range

Table 6.5. Mechanical properties and total event counts to failure of 16-ply UD 0° carbon fibre/epoxy and unreinforced PEEK plates tested in three point flexure. Means and ranges of data from repeat specimens are presented.

8-ply laminate quality	Failure stress (MPa)	At failure		At 5.5 KN			
		Total events	Mean amplitude	Total events	Events in ch's 11-30	Mean amplitude	%share ch's 11-30
STANDARD	1694 (1947-1429)	18301 (24479-13580)	7.75 (7.88-7.64)	295 (511-91)	26.5 (47-13)	8.28 (9.57-6.24)	12.37 (22.14-3.81)
PLIES MISSING (CENTRAL)	928 (1178-587)	8691 (16549-5602)	10.50 (11.94-9.77)	1002 (2708-175)	407 (1194-48)	10.51 (11.52-8.59)	36.33 (48.01-8.2)
AL INSERT	1469 (1564-1330)	16281 (37231-7220)	7.85 (8.87-7.15)	319 (897-118)	114 (384-28)	10.81 (11.71-10.22)	30.06 (42.86-23.93)

Table 6.6. Strength and acoustic emission results from non-defective and defective 8-ply UD 0° APC2 tested in tension. Means with ranges of the data from repeat specimens are presented in brackets.

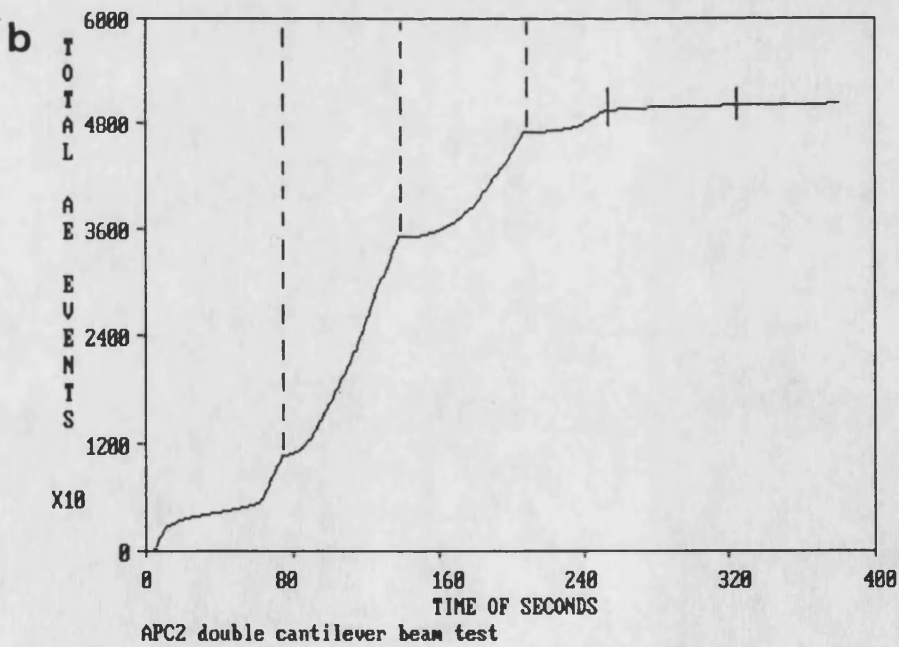
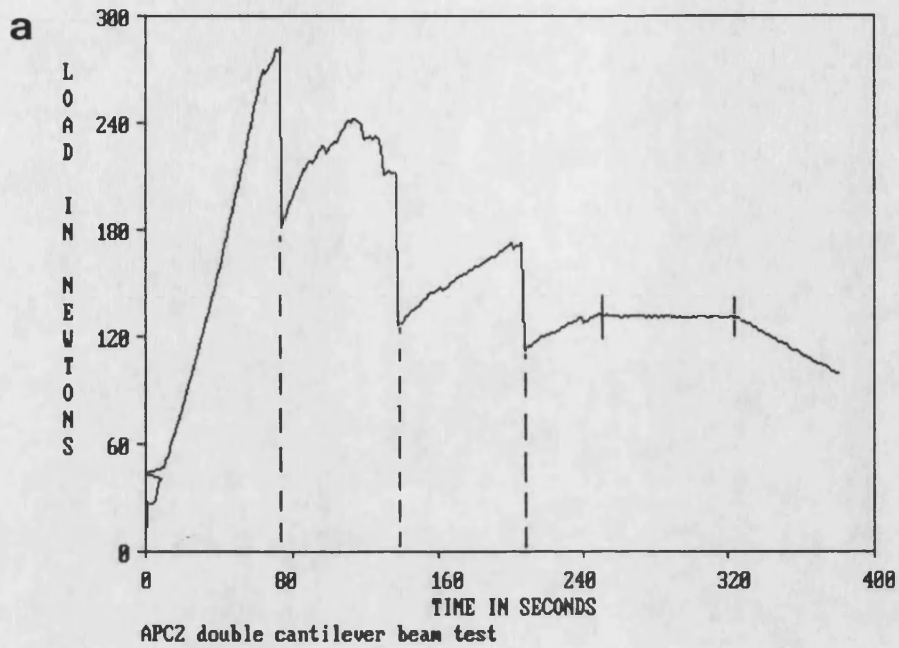


Figure 7.1. DCB specimen of APC2 moulded under standard conditions at Bath showing slip-stick crack propagation. a) Load/time graph. b) AE event/time graph. Note the correspondence between load drops (crack jumps) and subsequent lulls in the evolution of events.

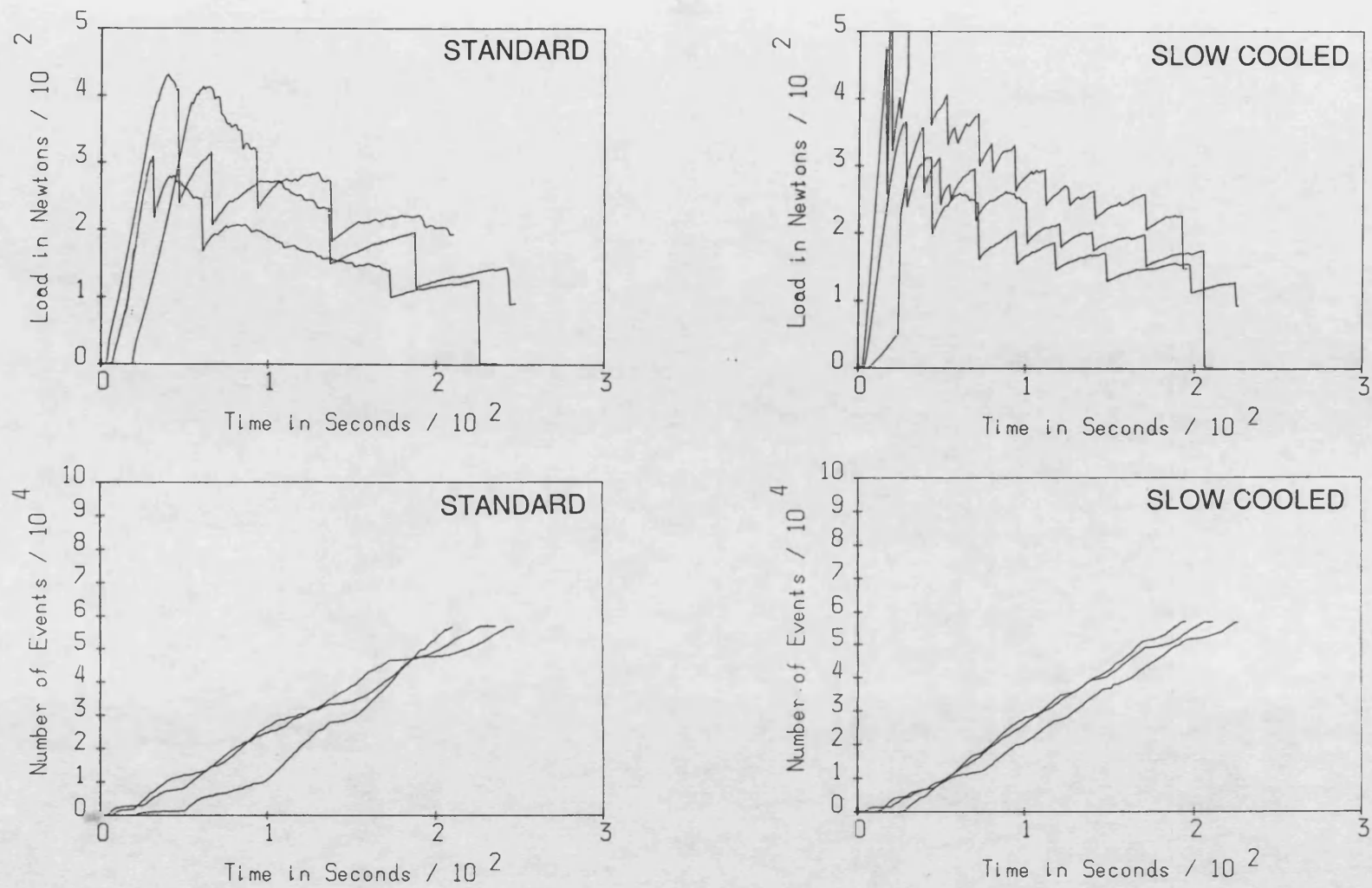


Figure 7.2. Comparison of standard and slow cooled APC2 DCB specimens, moulded at Bath. Results from three repeat normal cooled and three repeat slow cooled specimens are included in each graph.

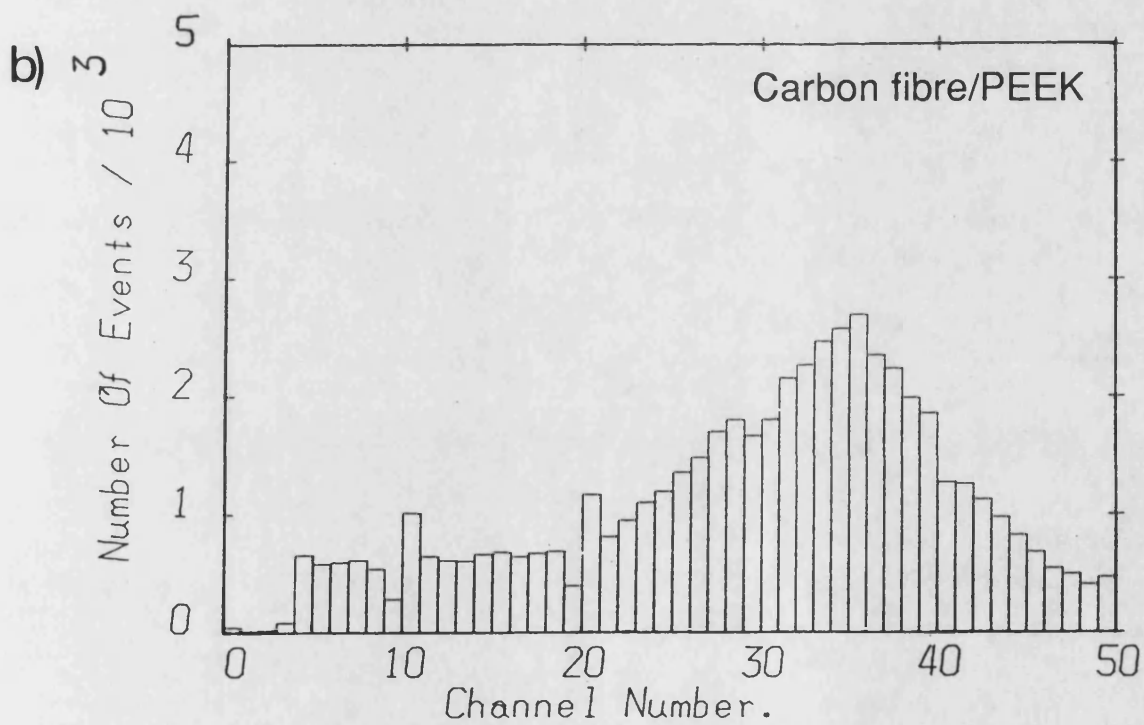
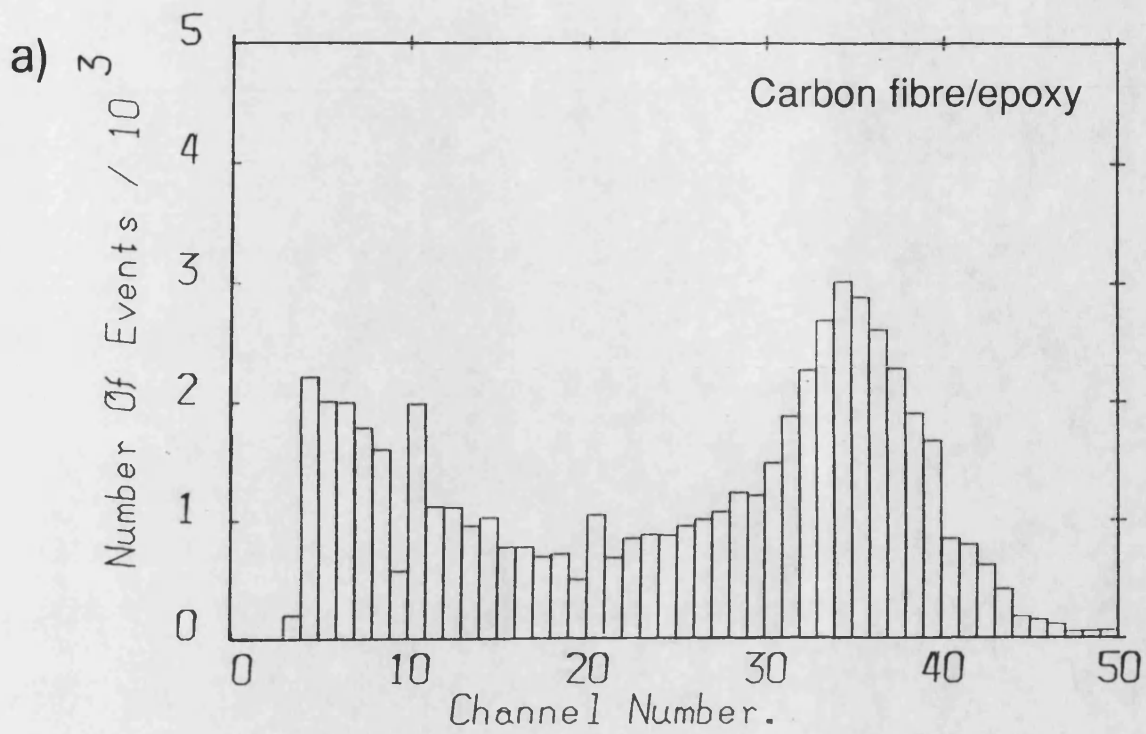


Figure 7.3. Preliminary comparison of amplitude distribution histograms from DCB tests conducted on UD carbon fibre composites. a) Fiberite epoxy matrix b) APC2/PEEK matrix. (after Nixon (159)).

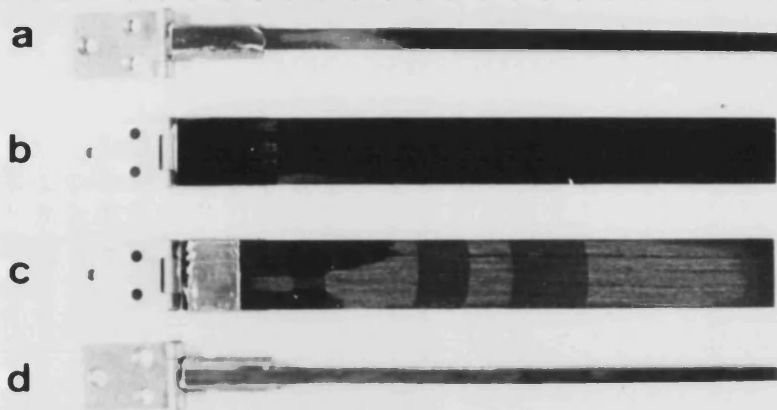


Figure 7.4. The four types of DCB specimen used to determine G_c . From top to bottom:
a) Intralaminar Fiberite/carbon.
b) Interlaminar Fiberite/carbon.
c) Interlaminar APC2.
d) Intralaminar APC2.
The PTFE sheet used as a crack starter is clearly visible on the interlaminar APC2 specimen.

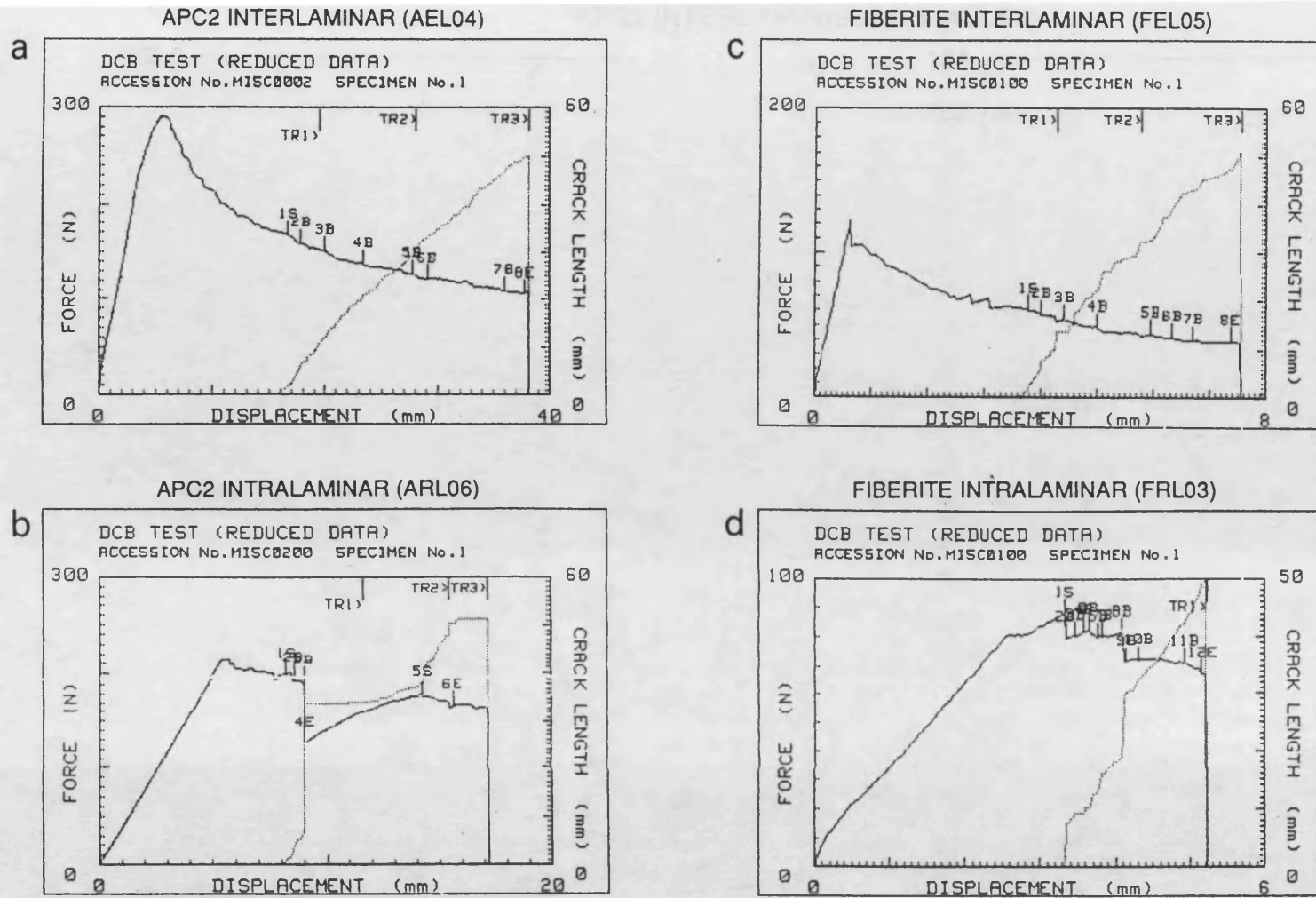
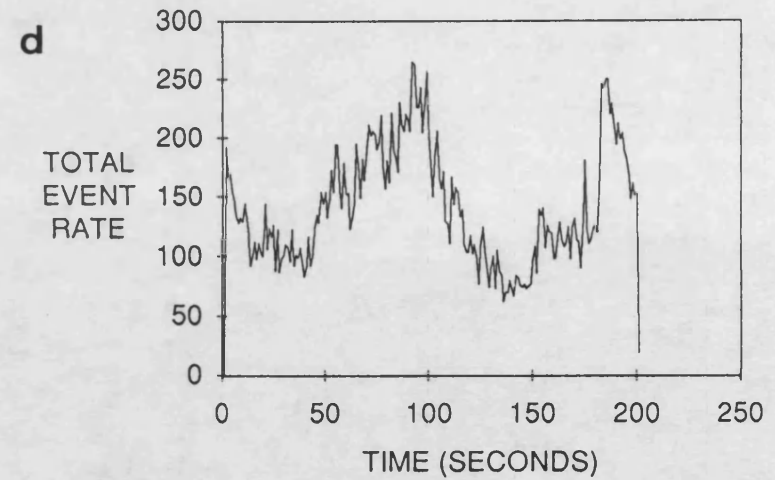
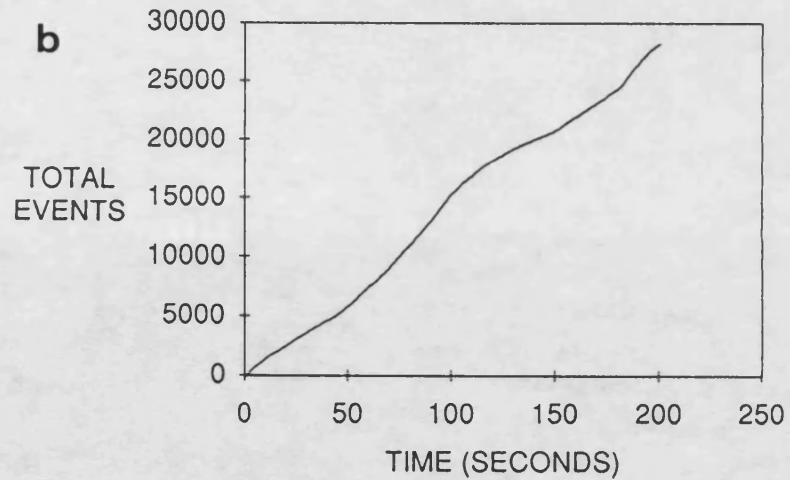
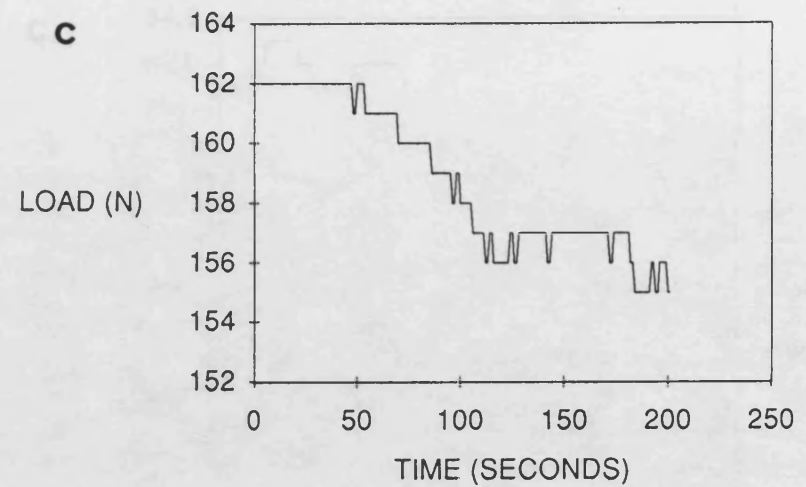
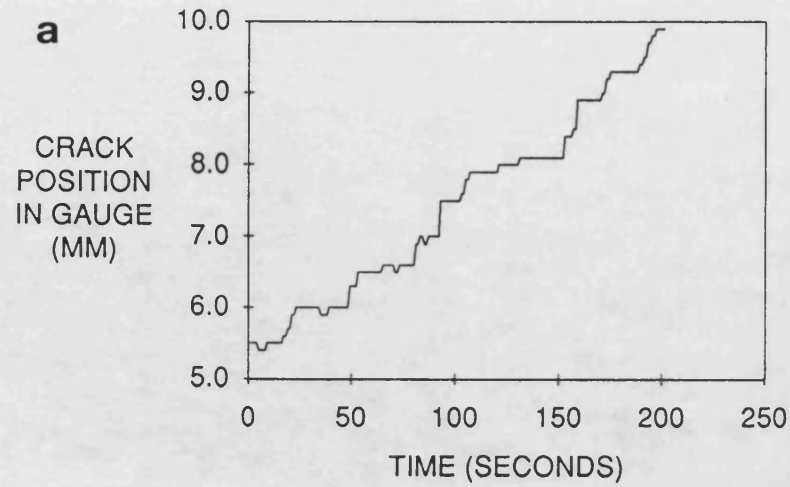


Figure 7.5. Combined load and crack length versus crosshead displacement curves for DCB tests at 0.5 mm/min crosshead speed, generated by the ICI Hewlett Packard system. a) AEL04 interlaminar APC2. b) ARL06 intralaminar APC2. c) FEL05 interlaminar Fiberite/carbon. d) FRL03 intralaminar Fiberite/carbon.

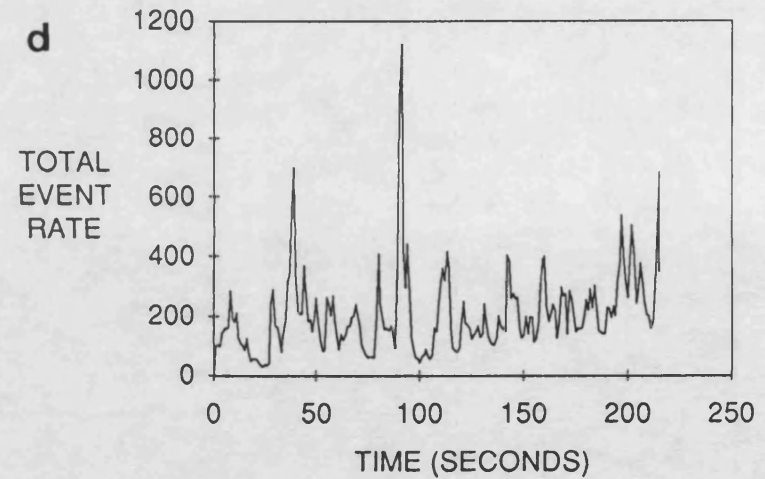
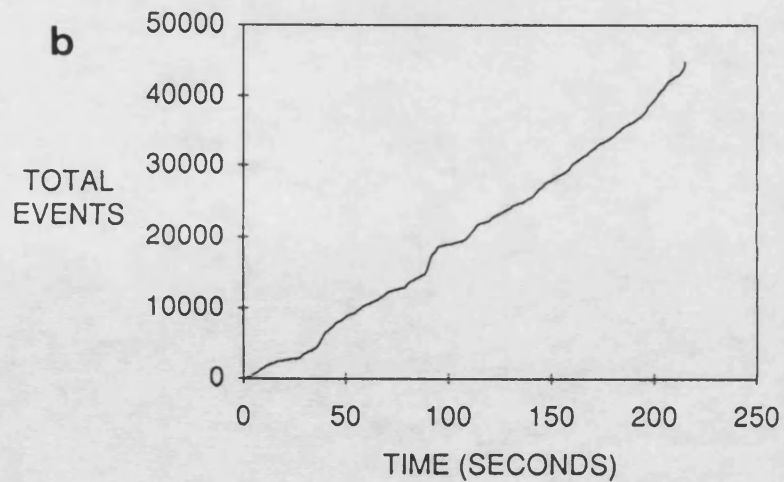
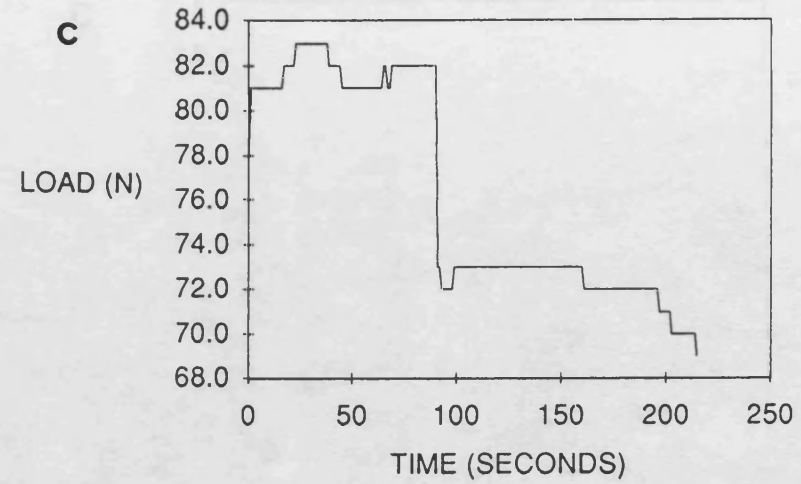
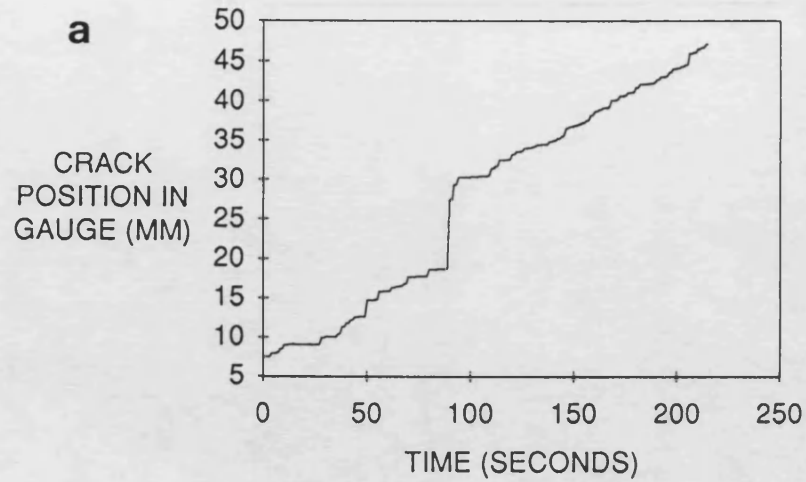
APC2 INTERLAMINAR DCB (AEL04)



343

Figure 7.6. A portion of the test of interlaminar APC2 DCB specimen, AEL04. Four parameters are plotted as a function of time, which at a constant crosshead speed of 0.5 mm/min, is proportional to load point deflection. These are a) crack length, b) load, c) cumulative events and d) total event rate.

FIBERITE INTRALAMINAR DCB (FRL03)



344

Figure 7.7. A portion of the test of intralaminar Fiberite/carbon DCB specimen, FRL03. Four parameters are plotted as a function of time, which at a constant crosshead speed of 0.5 mm/min, is proportional to load point deflection. These are a) crack length, b) load, c) cumulative events and d) total event rate.

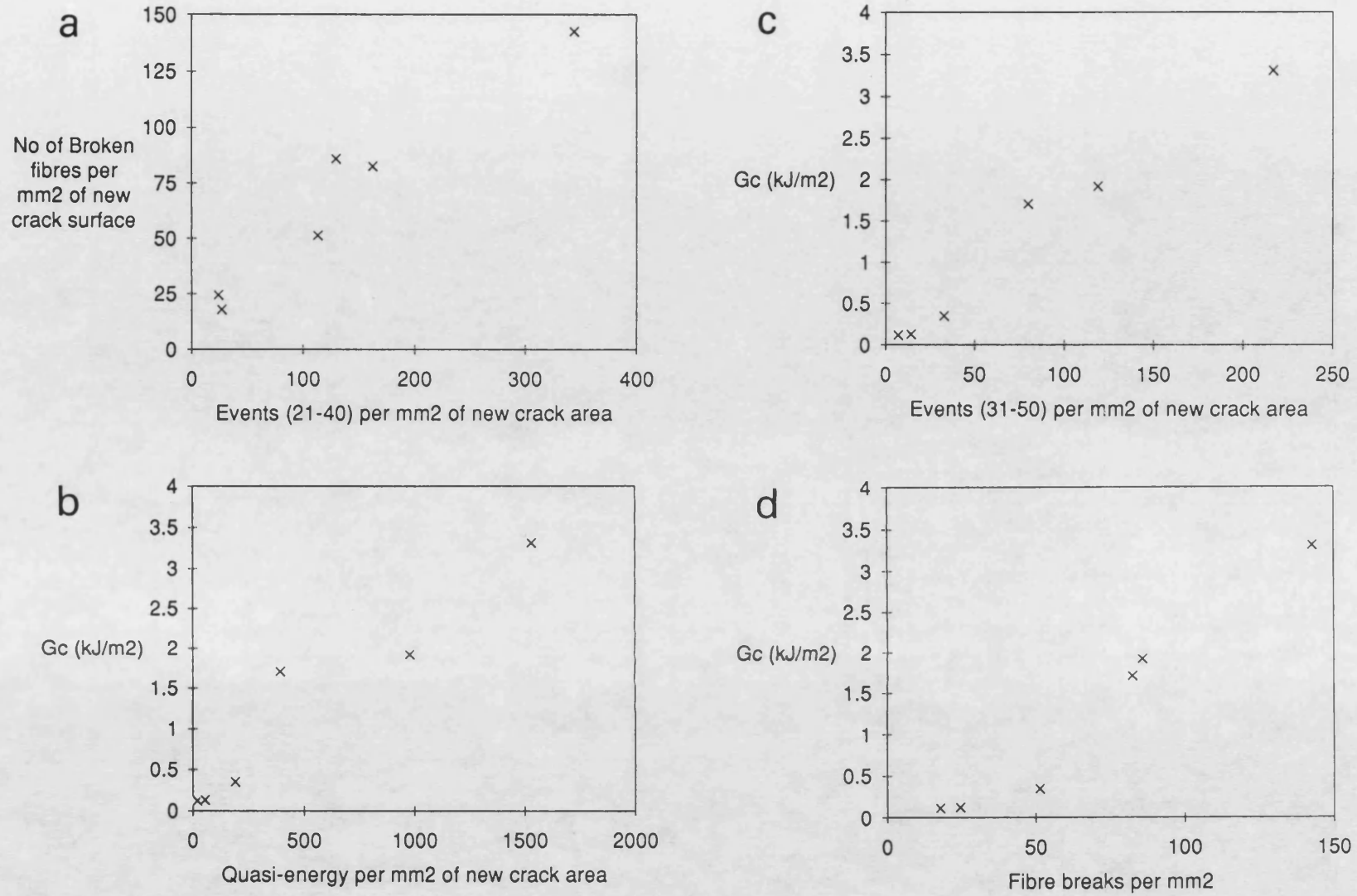
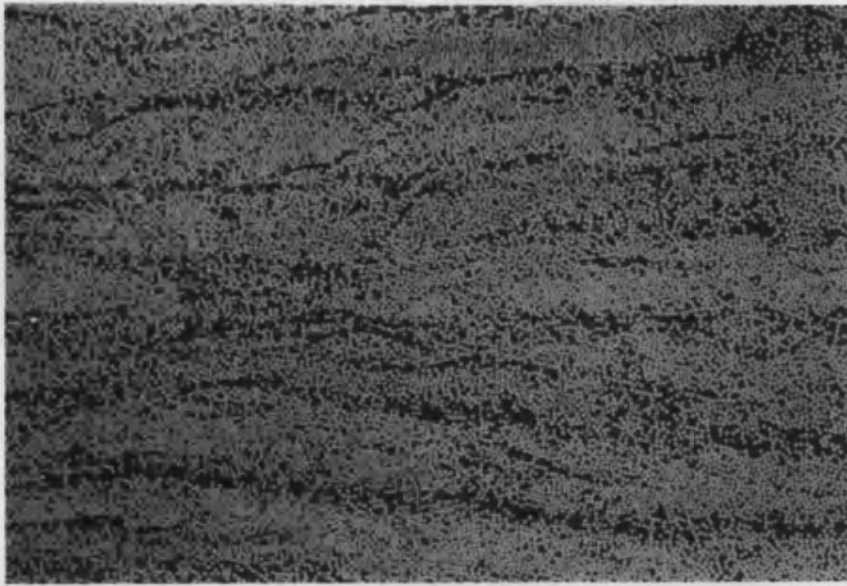


Figure 7.8. Scatter graphs demonstrating the correlations between G_c , fibre breaks, and acoustic emission. a) Fibre breaks per mm² versus events in channels 21-40 per mm². b) G_c versus E_{quasi} . c) G_c versus events in channels 31-50 per mm². d) G_c versus fibre breaks per mm².

APC2 (carbon fibre/PEEK)

a



FIBERITE (carbon fibre/epoxy)

b

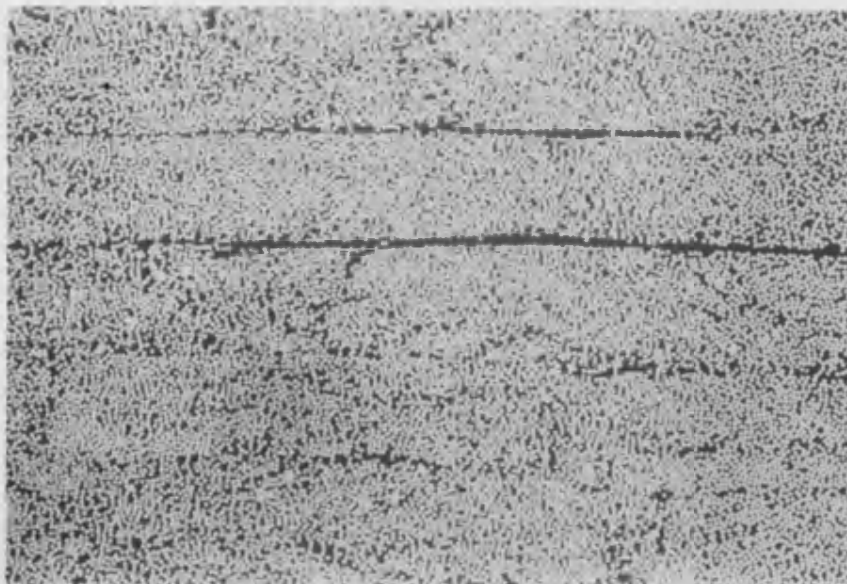


Figure 7.9. Metallographic ground and polished sections through 40-ply Fiberite/carbon fibre and APC2 PEEK/carbon fibre showing the distribution of fibres and matrix rich inter-ply regions. a) APC2. b) Fiberite/carbon fibre. (Magnification x 80)

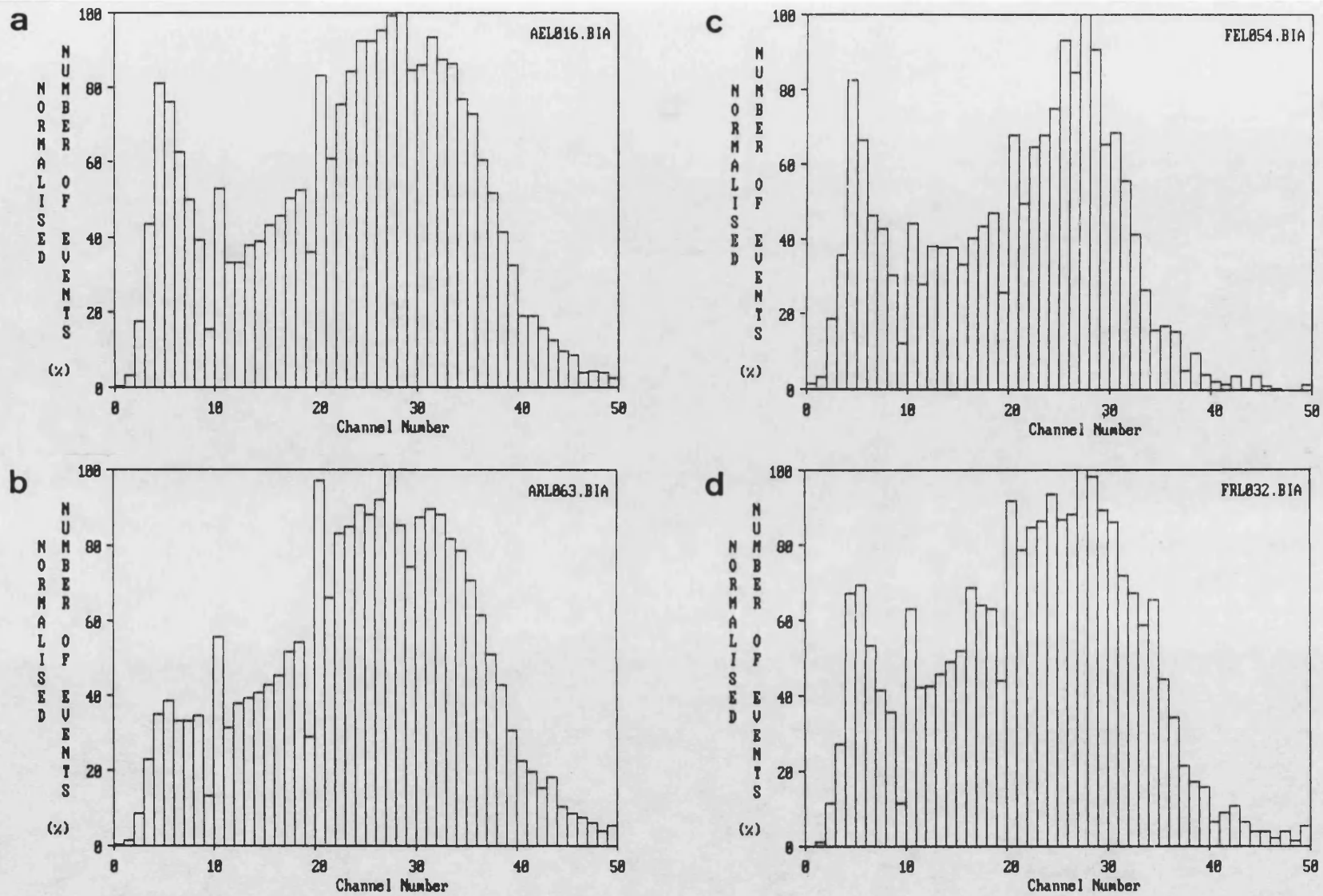


Figure 7.10. Comparison of the typical amplitude distributions from the four types of DCB specimen (crack front at the same distance from the transducer): a) Interlaminar APC2 (AEL04). b) Intralaminar APC2 (ARL063). c) Interlaminar Fiberite (FEL05). d) Interlaminar Fiberite (FRL03).

a 2250

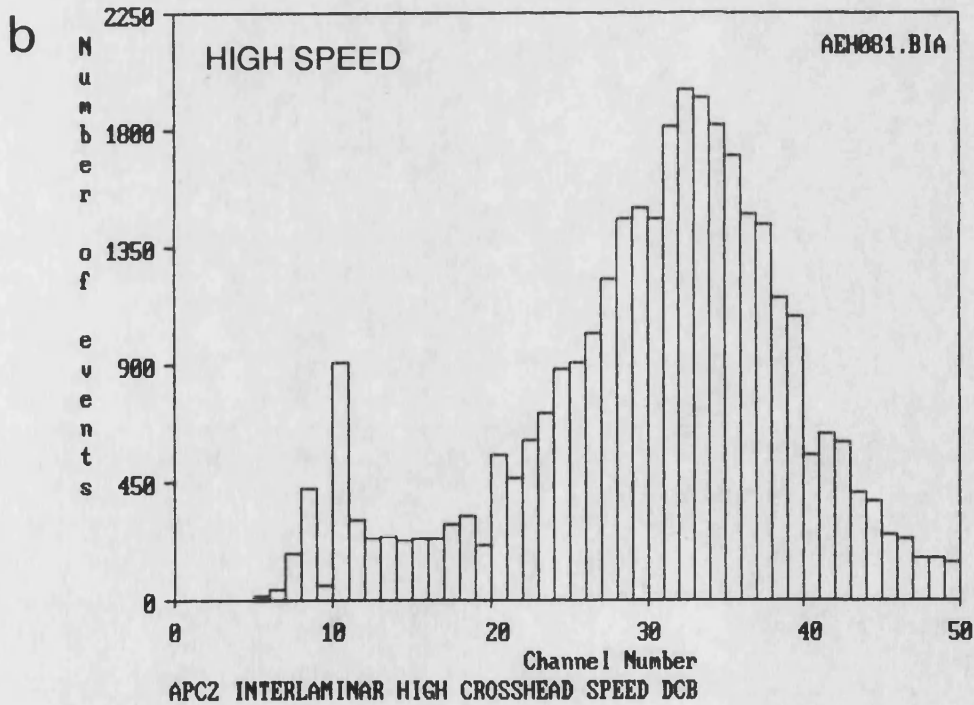
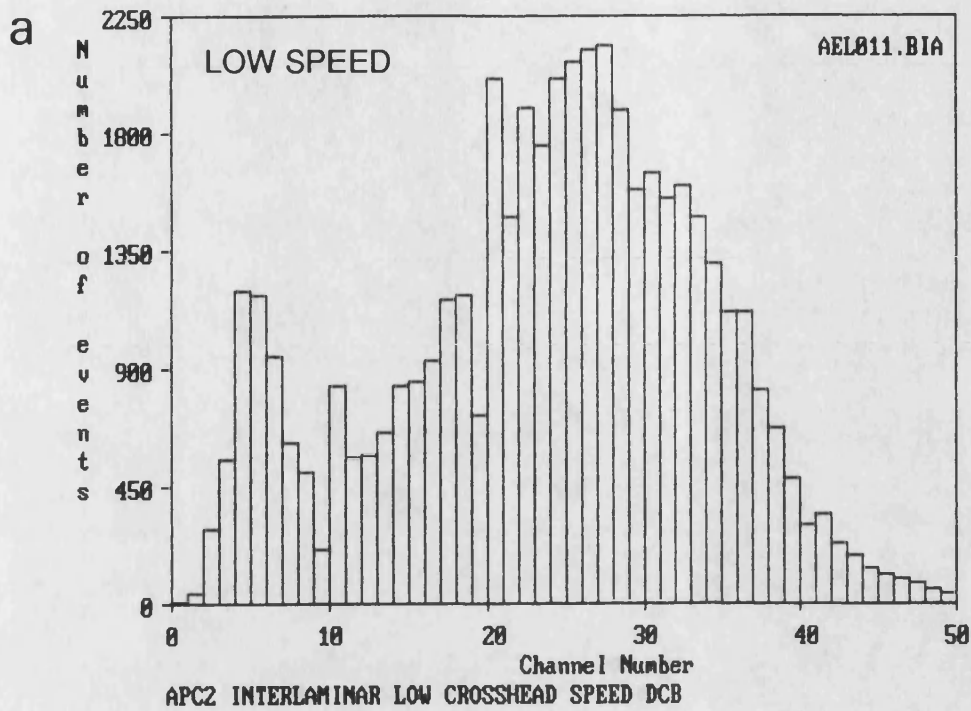


Figure 7.11. Comparison of amplitude distributions recorded from APC2 interlaminar specimens tested at a) low crosshead speed (0.5 mm/min) and b) high crosshead speed (5 mm/min). Note that the mean crack distance from the transducer is 150 mm for both distributions.

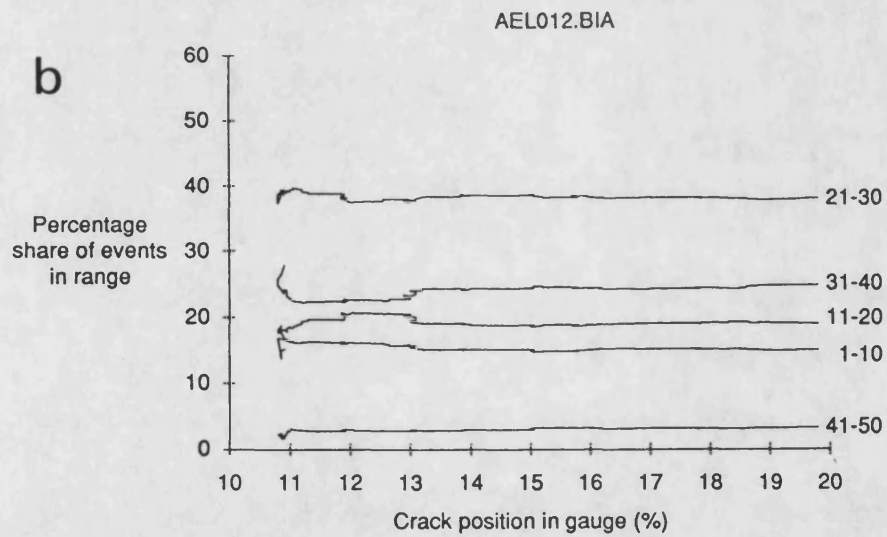
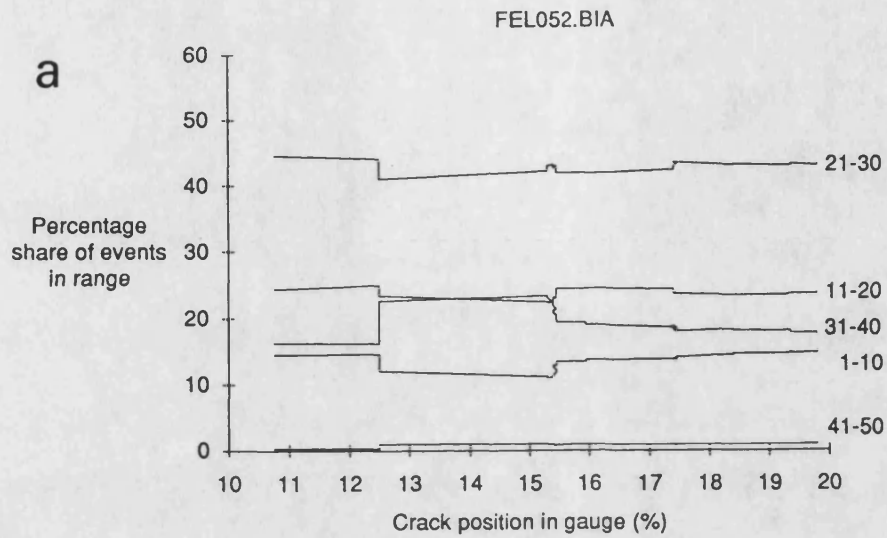


Figure 7.12. Variation of percentage share of events in selected channel ranges during stable crack propagation. a) Fiberite/carbon and b) APC2 PEEK/carbon.

Variation of crack speed with distance from transducer end of DCB

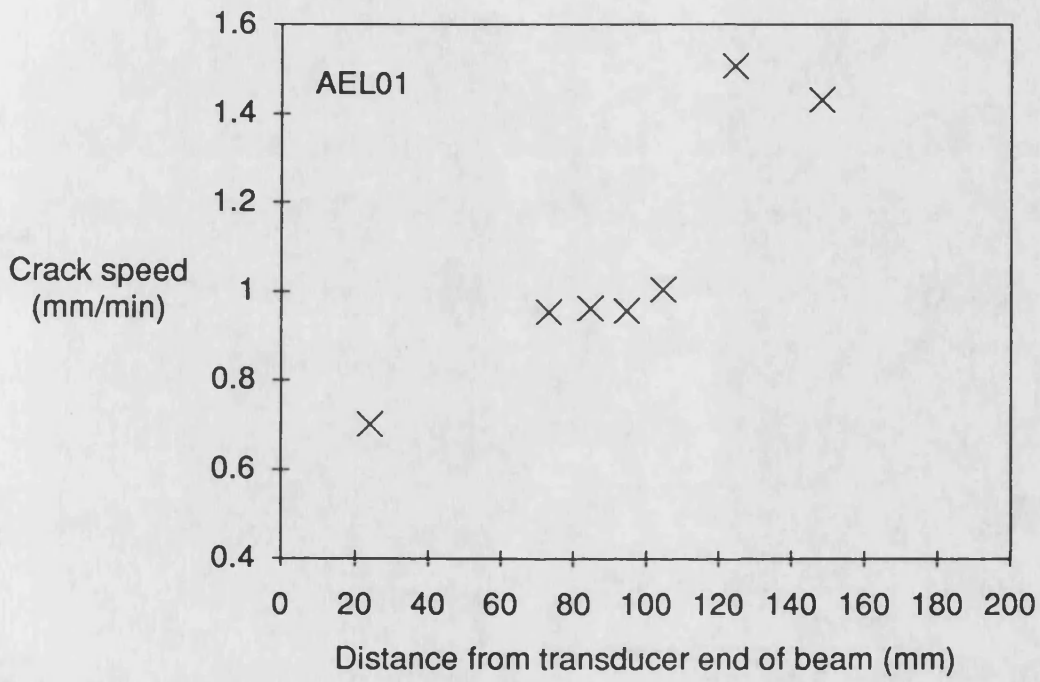


Figure 7.13. Variation of mean crack speed as the crack front propagates down an APC2 interlaminar DCB.

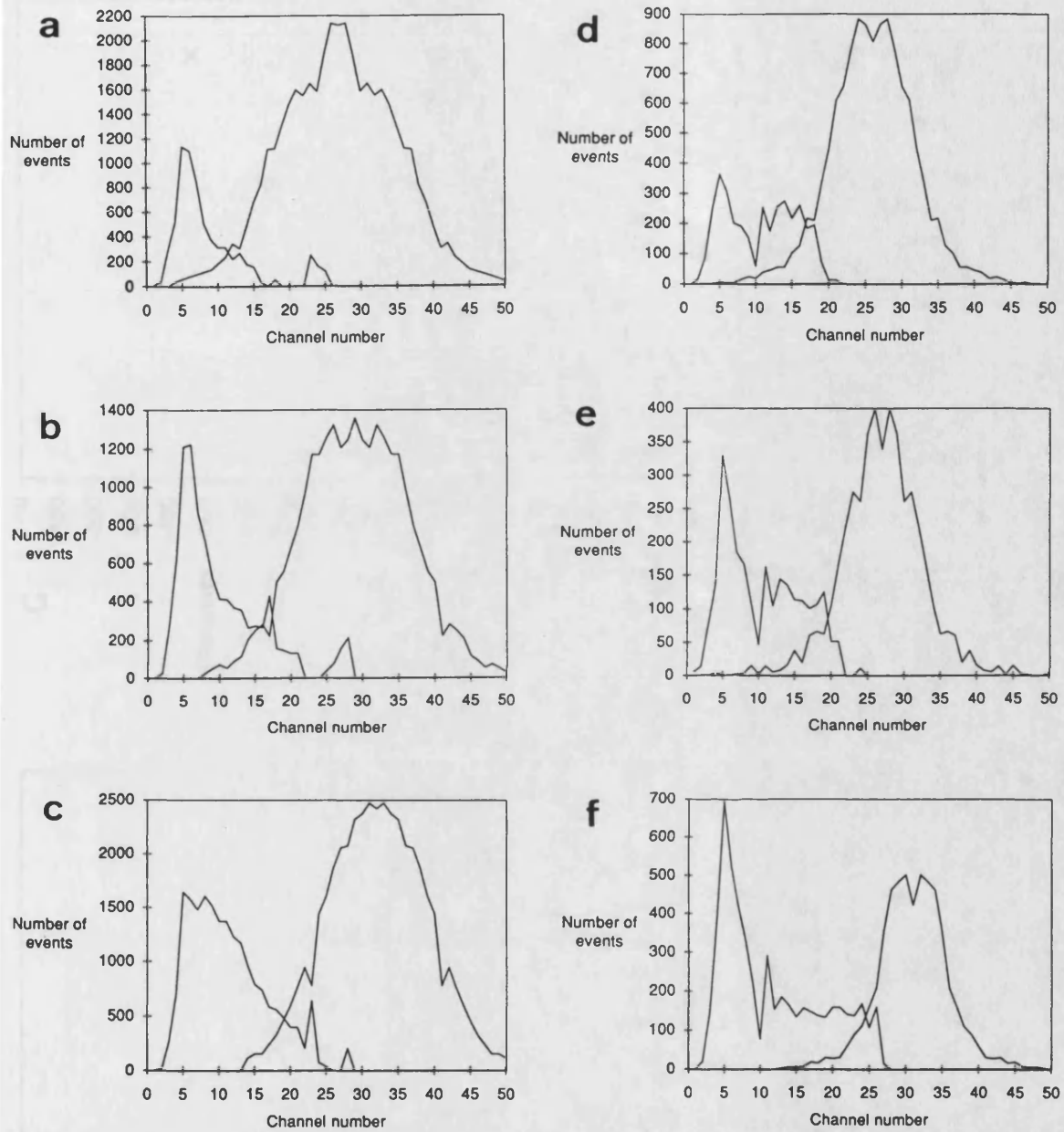


Figure 7.14. Deconvoluted twin peak amplitude distributions for a-c) APC2 interlaminar specimen AEL04 and d-f) Fiberite interlaminar specimen FEL05 at three locations progressively closer to the transducer.

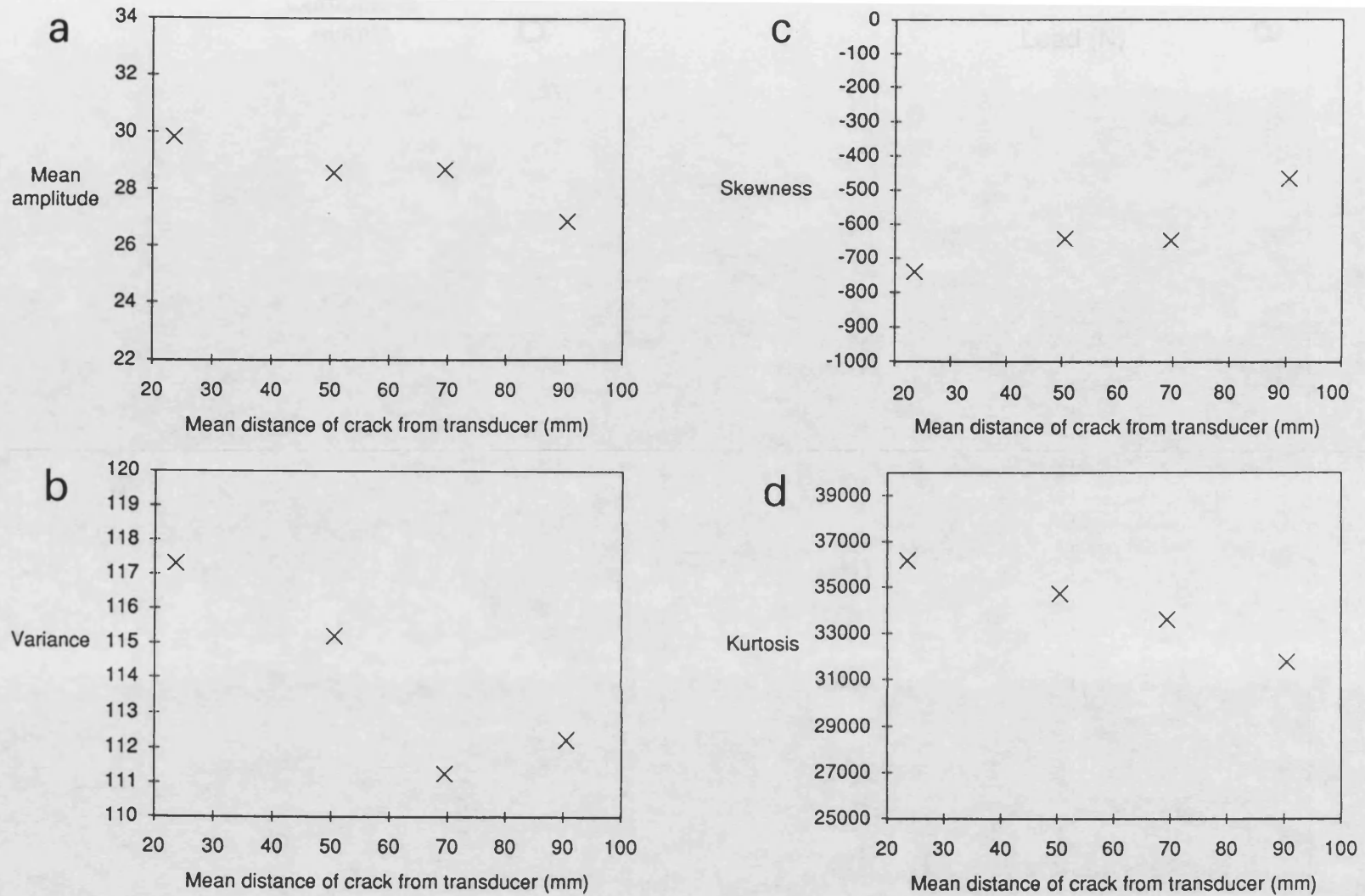
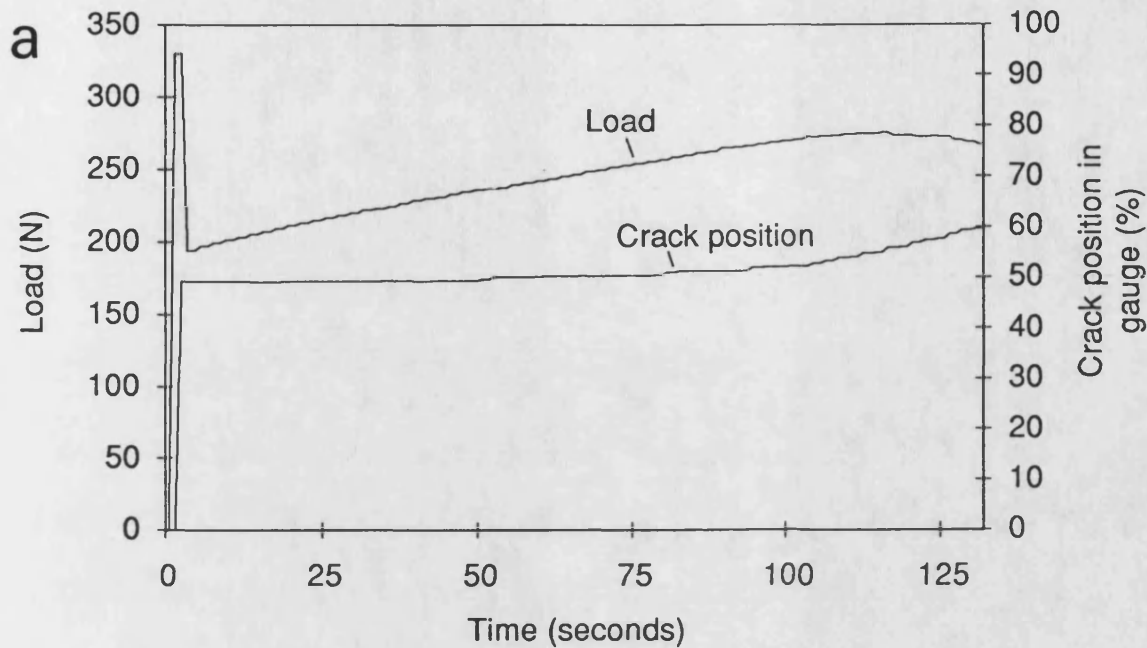


Figure 7.15. Variation of the first four moments of the amplitude distributions of APC2 intralaminar specimen ARL10 with mean distance of the crack front from the transducer. a) Mean amplitude. b) Variance of the amplitude distribution. c) Skewness. d) Kurtosis.

Load and crack front position (in crack gauge) as a function of time for APC2 interlaminar high crosshead speed



Cumulative AE events and event rate as a function of time for APC2 interlaminar high crosshead speed

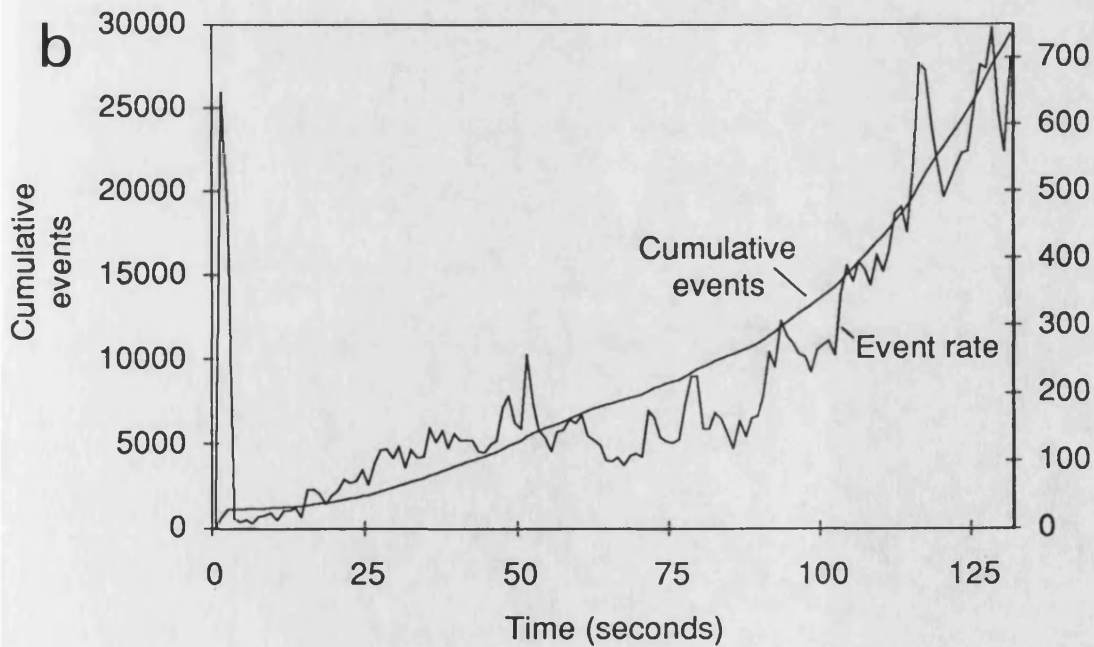


Figure 7.16. Behaviour of APC2 interlaminar high crosshead speed specimen AEH08 showing mixed stable and unstable crack growth. a) Combined Load and crack length plots as a function of time. b) Combined cumulative event and event rate plots as a function of time.

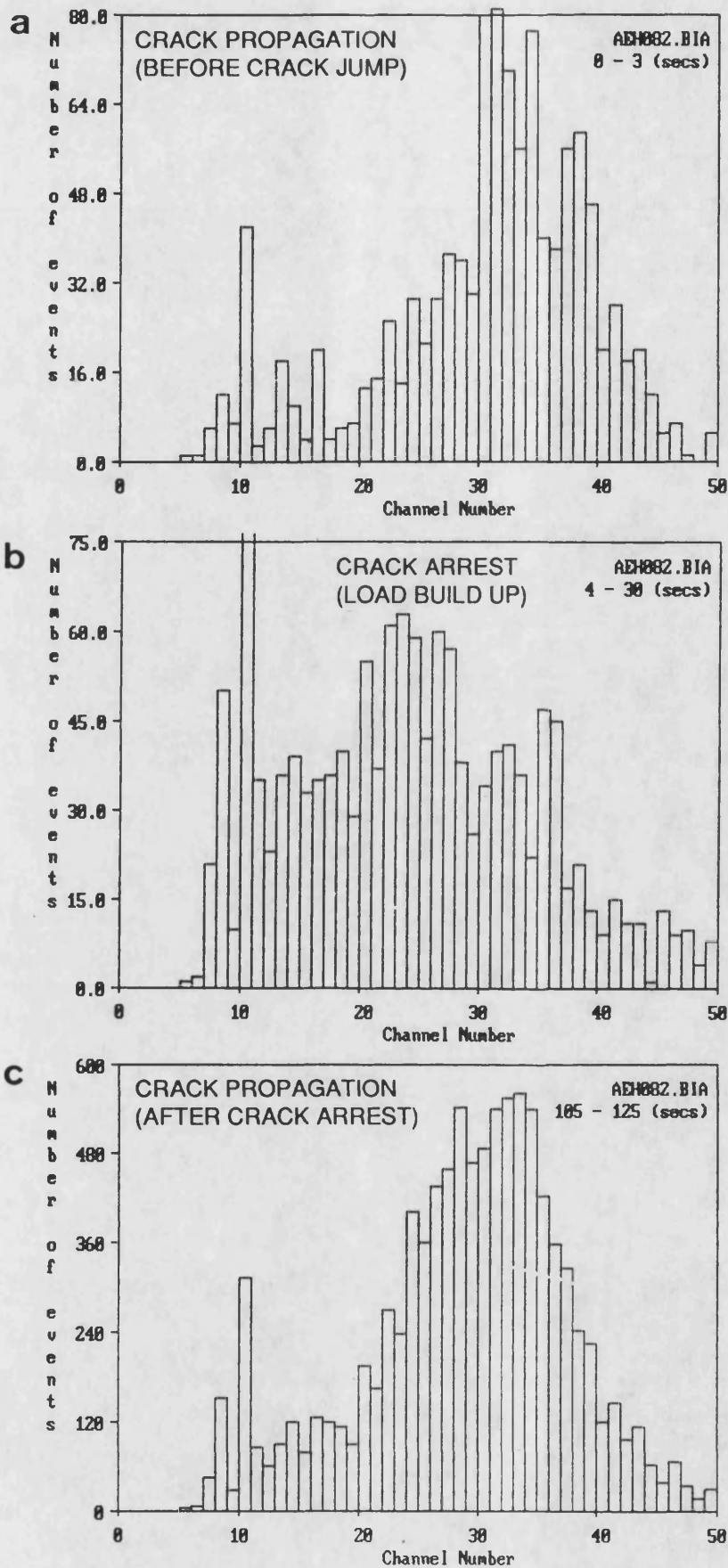


Figure 7.17. Comparison of amplitude distribution histograms from APC2 interlaminar high crosshead speed sample AEH08 for stable crack propagation and load build up without crack movement. a) Initial stable crack propagation. b) Crack arrest and load build up. c) Recommencement of stable crack propagation.

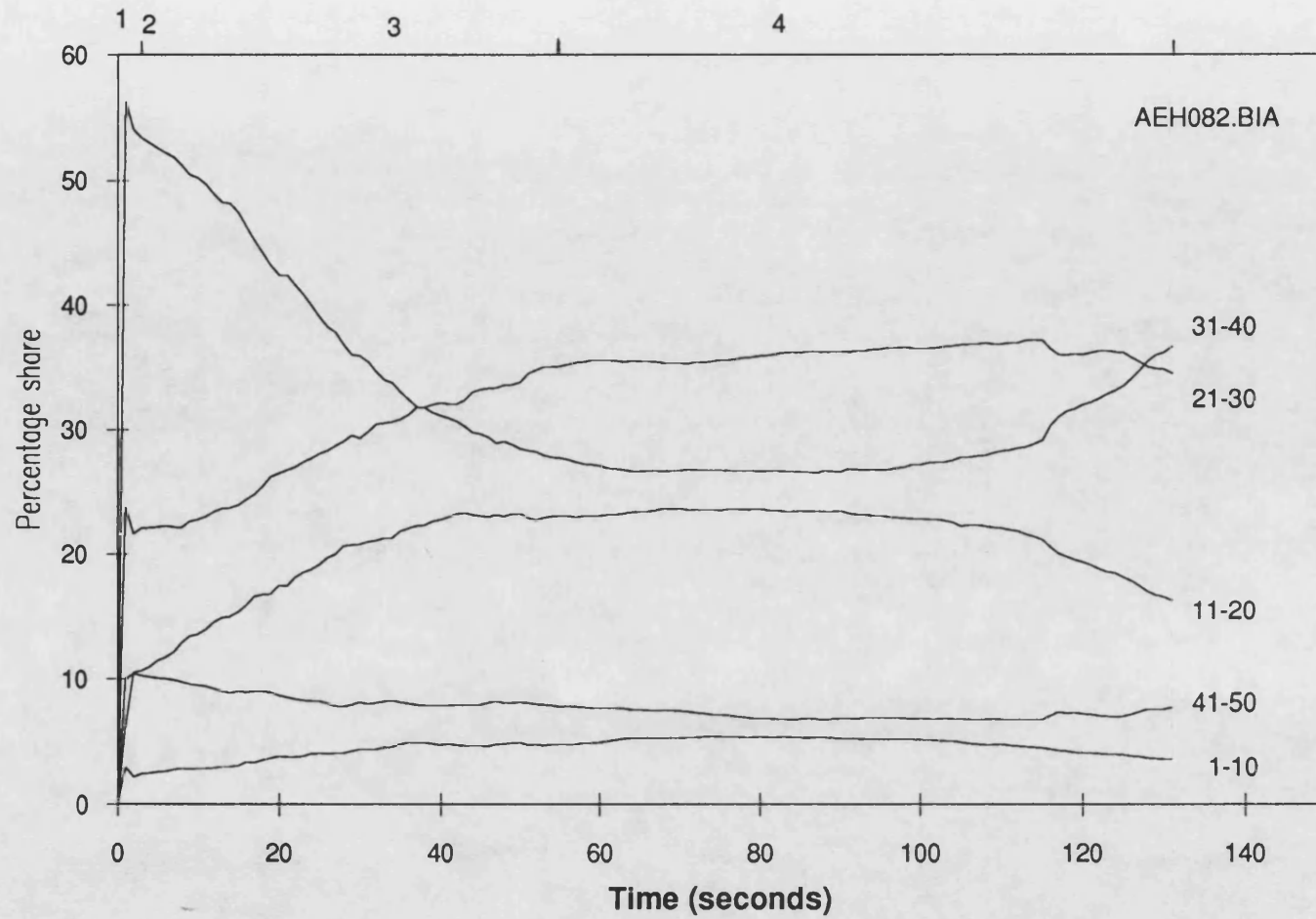


Figure 7.18. Percentage share of events in five channel ranges versus time plot for APC2 interlaminar high crosshead speed DCB test. The graph covers four consecutive periods: 1) Stable crack growth. 2) Crack jump. 3) Crack arrest and load build up. 4) Restart of crack propagation.

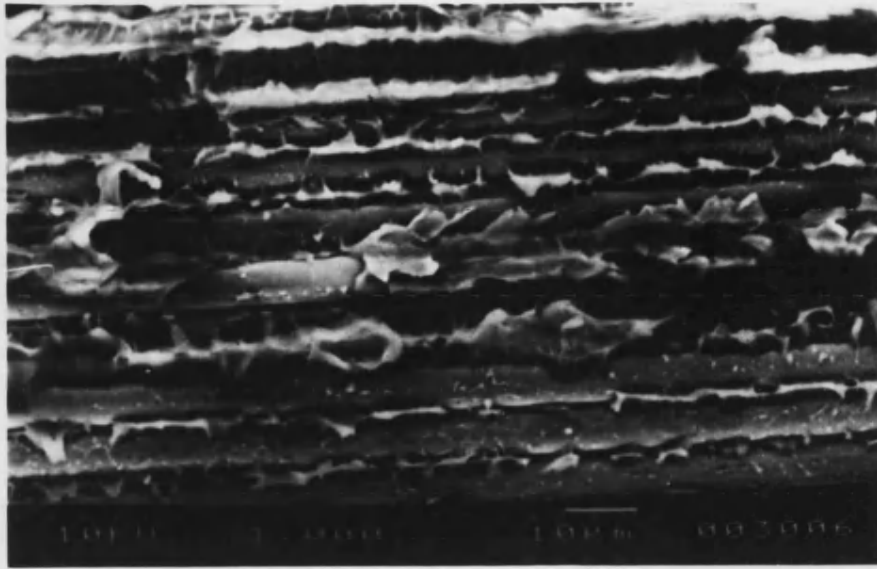


Figure 7.19. A typical area of APC2 interlaminar specimen AEL04 showing stable crack growth within the region of the test piece which fractured during AE test AEL012.BIA. Note the highly deformed and drawn PEEK matrix.

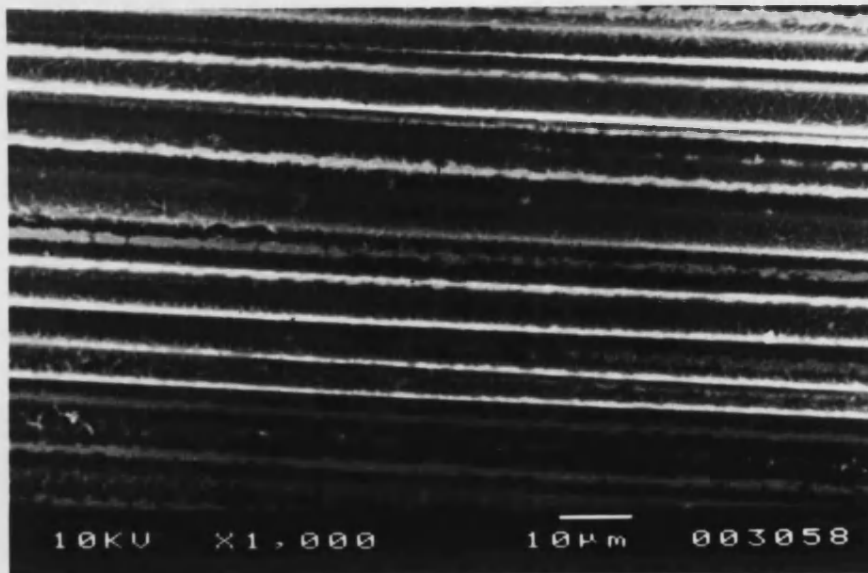


Figure 7.20. An untypical region of an APC2 interlaminar low crosshead speed DCB specimen. A few small areas exhibit largely undeformed matrix. These areas seem to be local sites of rapid (brittle) crack propagation within a specimen which on a macroscopic level has undergone only stable crack growth.

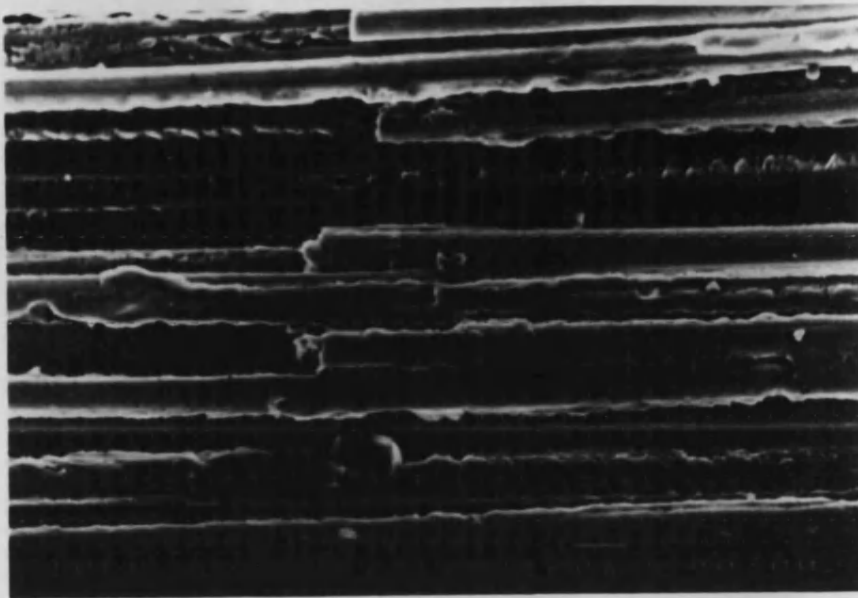
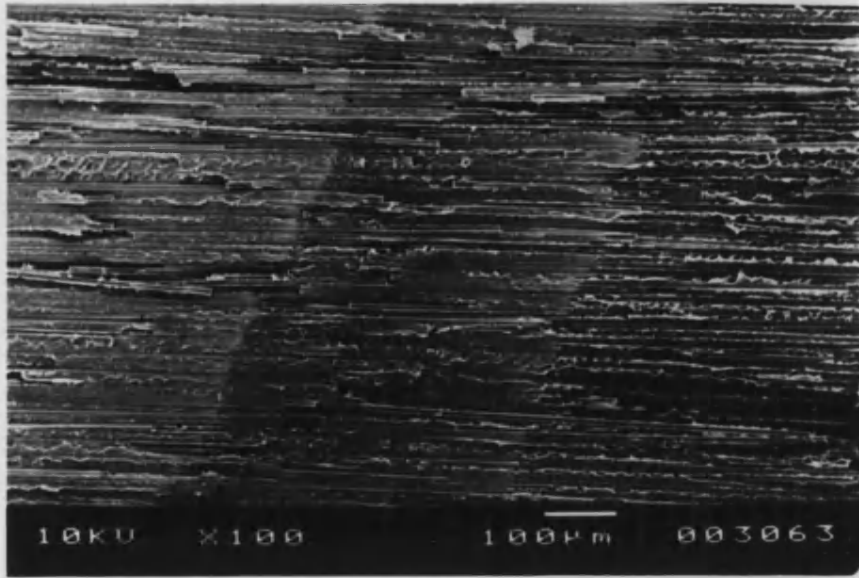


Figure 7.21. A typical region of APC2 interlaminar DCB, moulded at Bath under standard conditions. This is a fast fracture area, typified by the relatively brittle failure of the matrix, and the numerous fractured fibres which are still matrix covered.

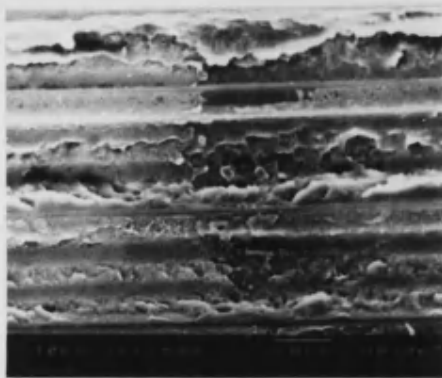


Figure 7.22. A 0.7 magnification photograph of APC2 interlaminar fast crosshead speed DCB specimen (AEH08). Note the two dark regions which are fast, unstable crack propagation regions. Regular lines at approximately 0.5-1.0 mm spacing are evident across the fast fracture regions.

a



b



c

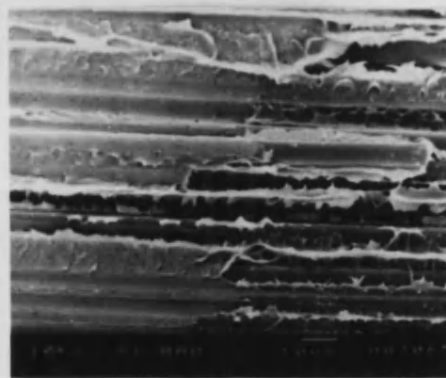


Figure 7.23. APC2 interlaminar high crosshead speed specimen (AEH08). a) Three regions are evident with well defined interfaces between them. On the left are two regions of fast crack propagation. Note the undeformed PEEK. Furthest right is stable, slow fracture. The crack ran left to right. b) Exploded view of the interface between the two regions of fast fracture. c) Exploded view of the interface between fast and slow fracture.

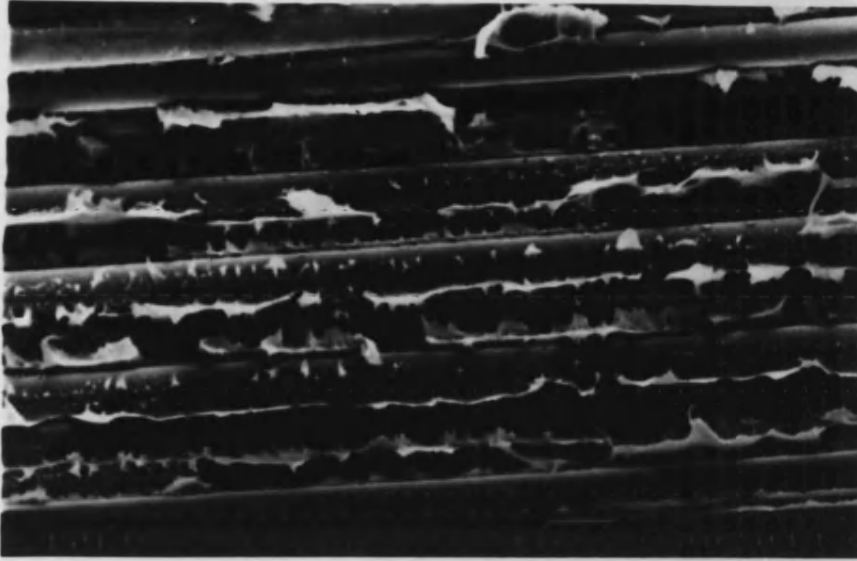


Figure 7.24. APC2 intralaminar DCB sample (ARL06). A typical region of an intralaminar specimen in a region of stable crack growth.

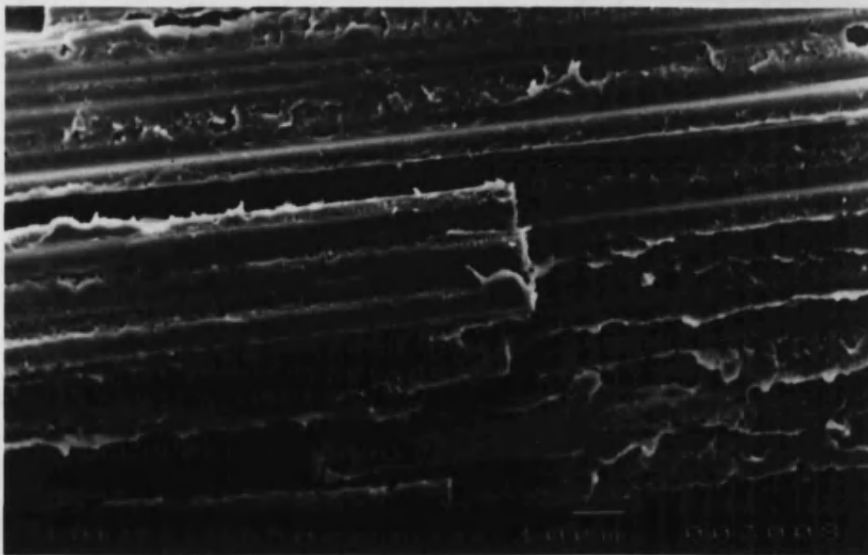


Figure 7.25. APC2 intralaminar DCB sample (ARL06). A fast fracture area. Note the partly debonded fibre bundle of 7 fibres which has been fractured.

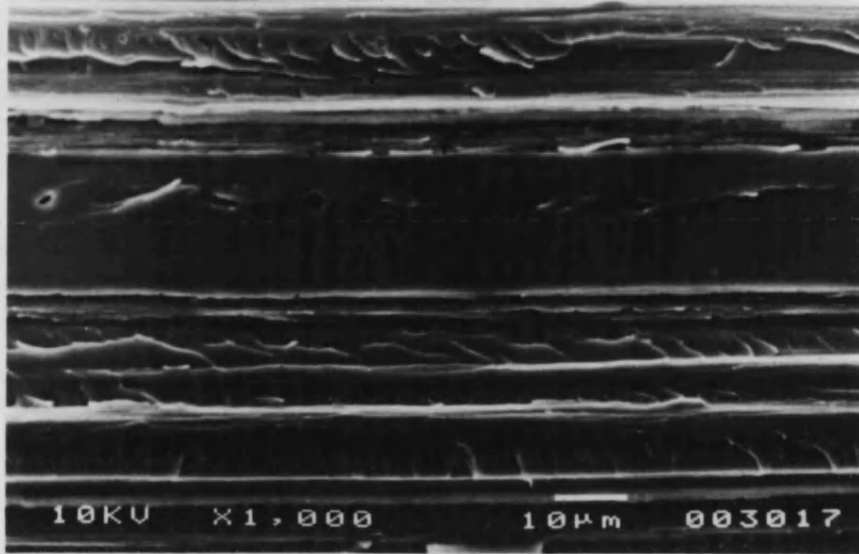


Figure 7.26. A typical area of Fiberite/carbon fibre interlaminar DCB specimen (FEL05). No regions were evident which may be considered to be either fast or slow crack propagation.

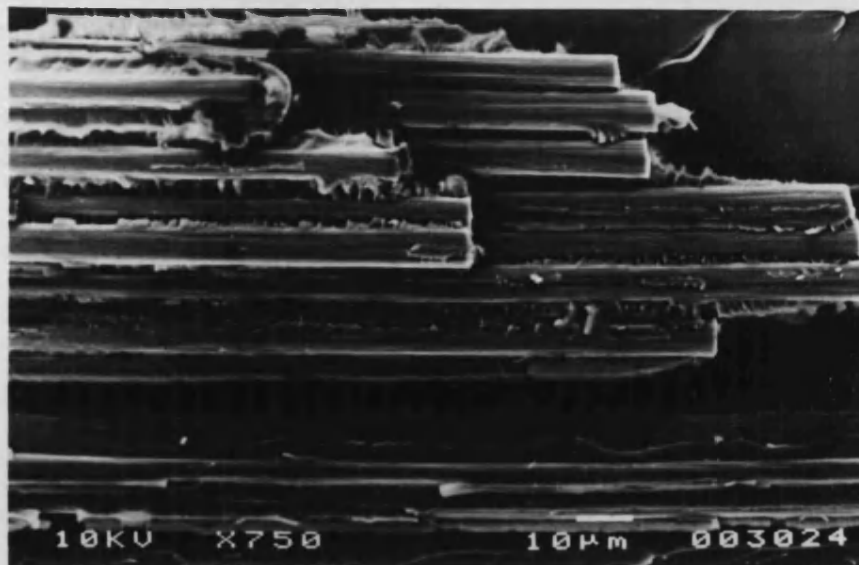


Figure 7.27. Fiberite/carbon fibre interlaminar DCB specimen (FEL05). A fractured fibre bundle (a relatively uncommon occurrence).

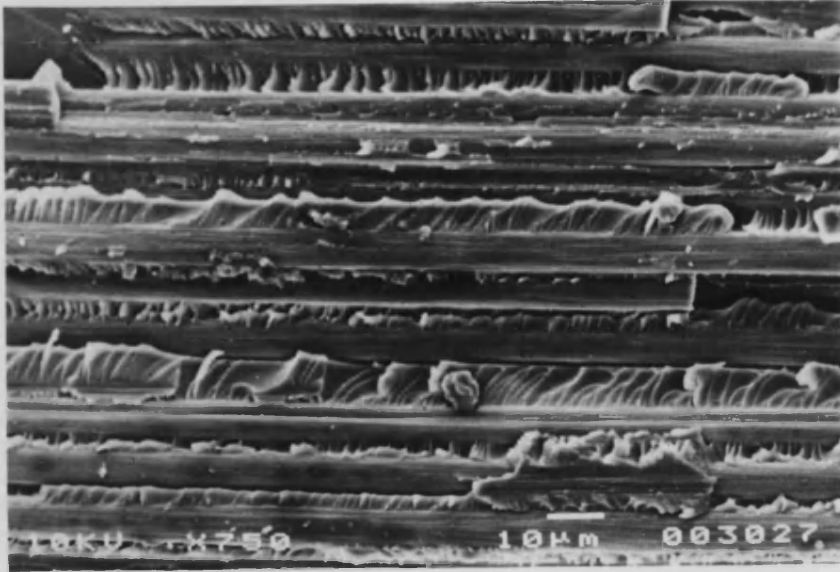


Figure 7.28. Fiberite/carbon fibre intralaminar DCB specimen (FRL03). A typical area which is very similar to that seen in Fiberite interlaminar specimens. Note the two fractured fibre ends and the debris (probably Fiberite matrix).

Sample Identity	Voltage (V)
FEH01	2.92
FEH02	3.08
FRL03 ^a	0.20
AEL04	3.80
FEL05	3.12
ARL06	3.78
FRL07 ^b	1.90
AEH08	4.00
FEH09	3.12
ARL10 ^b	1.30
FEHA9	3.28
FEL11	3.15
AEL12	3.79

a Sample contained PTFE insert

b Measurement through sample width

Table 7.1. Assessment of coupling quality. Pre-test coupling pulse amplitudes (through thickness transmitted pulses with common energising pulse) for DCB tests on APC2 and carbon fibre/epoxy specimens.

Sample description	Crack speed (mm/min)	Gc KJ/m ²	Fibre breaks per mm ² of new crack area	Quasi-energy per mm ² of new crack area	Events per mm ² of new crack area					
					Ch's 1-50	Ch's 1-10	Ch's 11-20	Ch's 21-30	Ch's 31-40	Ch's 41-50
APC2 INTRALAMINAR LOW SPEED	4.2 (4.58-3.59)	3.31 (3.61-3.04)	142.9 (75.9)*	1531.6 (2409-664)	531.5 (750.7-346.4)	48.6 (83.7-31.9)	88.4 (169.7-55.5)	171.4 (255.3-127.0)	172.7 (248.8-101.4)	44.2 (74.0-17.4)
APC2 INTERLAMINAR LOW SPEED	1.21 (1.75-0.9)	1.71 (2.1-1.57)	82.6 (25.7)*	394 (585-284)	257.7 (307.9-217.4)	38.8 (45.5-32.5)	45.4 (55.2-40.1)	92.6 (125.7-66.6)	69.7 (80.1-53.8)	10.4 (17.4-6.92)
APC2 INTERLAMINAR HIGH SPEED	9.61 (10.94-8.51)	1.92 (2.31-1.71)	85.9 (25.6)*	979.4 (1465-494)	183.8 (239.3-128.3)	4.3 (5.85-2.76)	17.7 (22.9-12.4)	40 (43.7-36.2)	89.3 (117.3-61.4)	29.7 (45.9-13.6)
FIBERITE INTRALAMINAR LOW SPEED	8.67 (14.08-5.54)	0.35 (0.47-0.26)	51.3 (34.6)*	192.7 (258-118)	215.8 (275.7-161.9)	28.6 (32.9-22.8)	68.3 (90.4-38.3)	84.7 (110.8-59)	28.7 (37.1-13.2)	4.3 (5.59-2.69)
FIBERITE INTERLAMINAR LOW SPEED	7.42 (13.23-3.23)	0.12 (0.15-0.08)	17.9 (15.6)*	19.5 (31.8-10.9)	43.6 (60.4-26.4)	7.2 (11.4-3.38)	9.4 (13.7-4.52)	19.7 (30.3-13.2)	6.9 (11.6-3.77)	0.3 (0.61-0.18)
FIBERITE INTERLAMINAR HIGH SPEED	56.62 (64.03-41.33)	0.13 (0.14-0.11)	24.6 (16.7)*	55.3 (97.2-32.7)	29.7 (32.9-27.4)	1.5 (2.28-0.95)	2.8 (3.51-2.19)	11.1 (14.6-4.74)	12.9 (15.1-9.95)	1.4 (2.96-0.68)

Table 7.2. Summary of crack growth parameters and AE event counts per unit of new crack surface area from DCB tests. Figures in brackets are ranges of the averaged data.

EFFECT OF CROSSHEAD SPEED IN FIBERITE INTERLAMINAR DCB

Crosshead speed	Gc	Total events per mm ²	Events in Ch's 31-51 per mm ²	%age share in channels 31-51	Moments of amplitude distribution			
	KJ/m ²				Mean	Variance	Relative skewness	Relative kurtosis
LOW	0.12 (0.15-0.08)	43.6 (60.4-26.4)	7.22 (12.13-4.01)	16.82 (27.87-11.49)	21.8 (23.4-20.2)	85.2 (129.4-70.8)	-0.341 (0.07--0.654)	2.322 (2.767-1.692)
HIGH	0.13 (0.14-0.11)	29.7 (32.9-27.4)	14.35 (18.2-10.6)	48.89 (66.3-36.9)	28.8 (30.7-27.4)	73.2 (109.5-53)	-0.919 (-0.667--1.079)	3.735 (4.302-3.389)

Table 7.3. The effect of crosshead speed on acoustic emission characteristics (event counts and parameters describing the amplitude distribution) recorded from DCB specimens (Fiberite/interlaminar). Means with data ranges in brackets are presented.

COMPARISON OF MATERIALS. INTRALAMINAR DCB.
(LOW CROSSHEAD SPEED)

Material	Gc KJ/m ²	Total events per mm ²	Events in Ch's 31-51 per mm ²	%age share in channels 31-51	Moments of amplitude distribution			
					Mean	Variance	Relative skewness	Relative kurtosis
PEEK/ carbon fibre	3.31 (3.61-3.04)	531.5 (750.7-346.4)	223.24 (312.2-122.1)	43.64 (55.8-24.3)	27.1 (29.8-22.9)	109 (117.3-95.8)	-0.391 (-0.044--0.582)	2.55 (2.715-2.356)
FIBERITE/ carbon fibre	0.35 (0.47-0.26)	215.8 (275.7-161.9)	34.25 (44.6-16.5)	16.06 (24.1-10.2)	21.2 (22.8-19.3)	82.6 (97.3-75.8)	0.189 (0.335--0.144)	2.667 (2.908-2.366)

Table 7.4. The effect of matrix material on acoustic emission characteristics (event counts and parameters describing the amplitude distribution) recorded from DCB specimens (intralaminar orientation). Means with data ranges in brackets are presented.

EFFECT OF CRACK ORIENTATION IN PEEK/CARBON FIBRE DCB
(LOW CROSSHEAD SPEED)

Crack orientation	Gc	Total events per mm ²	Events in Ch's 31-51 per mm ²	%age share in channels 31-51	Moments of amplitude distribution			
	KJ/m ²				Mean	Variance	Relative skewness	Relative kurtosis
INTRALAMINAR	3.31 (3.61-3.04)	531.5 (750.7-346.4)	223.24 (312.2-122.1)	43.64 (55.8-24.3)	27.1 (29.8-22.9)	109 (117.3-95.8)	-0.391 (-0.044--0.582)	2.55 (2.715-2.356)
INTERLAMINAR	1.71 (2.1-1.57)	257.7 (307.9-217.4)	80.92 (98.4-61.4)	31.5 (40.6-28.2)	24.1 (25.5-23.6)	114.8 (134-99.6)	-0.263 (-0.221--0.3)	2.231 (2.513-1.995)

Table 7.5. The effect of crack orientation on acoustic emission characteristics (event counts and parameters describing the amplitude distribution) recorded from DCB specimens (PEEK/carbon fibre). Means with data ranges in brackets are presented.

MATERIAL	INTERLAMINAR FRACTURE TOUGHNESS - G_{1C} (KJ/m²)
AROMATIC POLYMER COMPOSITES	
APC2: Fast crack propagation	2.1
APC2: Slow crack propagation	2.4
THERMOSETTING COMPOSITES	
Ciba Geigy 914	0.19
Hercules AS4/3501-6	0.21
Cycom 985	0.25
Hercules AS4/2220-3	0.40
Cycom 907	0.60
OTHER THERMOPLASTIC COMPOSITES	
Amoco Polyamide-imide (Torlon)	1.1
Phillips Polyphenylene sulfide (Ryton)	1.4

Table 7.6. Interlaminar fracture toughness of various carbon fibre composites.

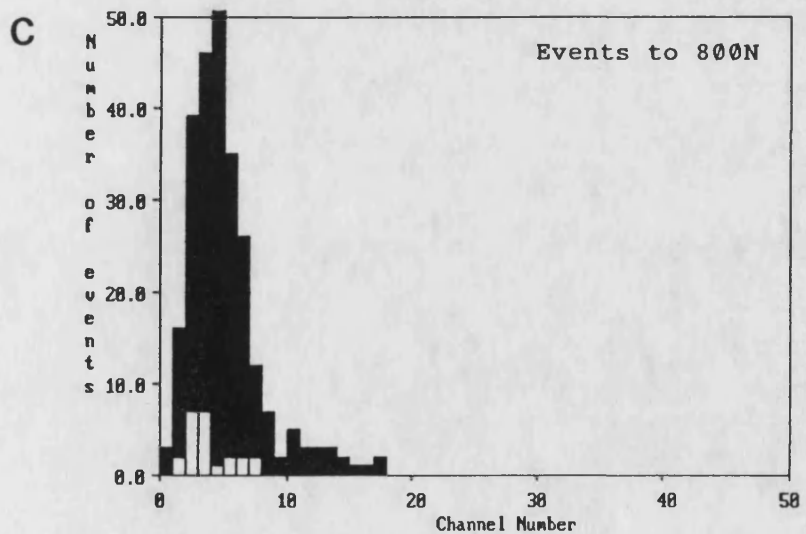
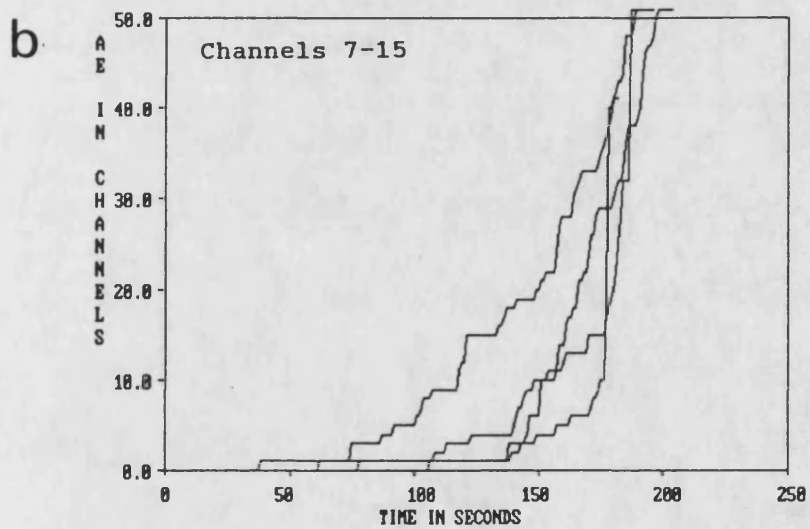
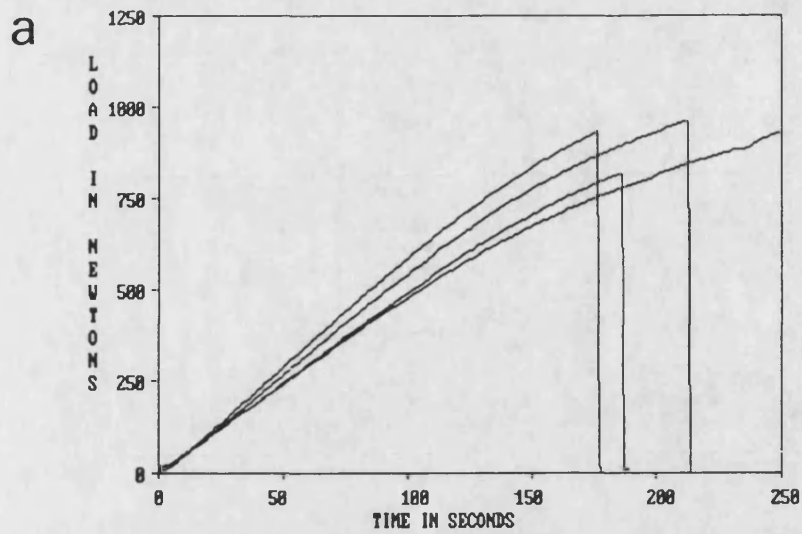


Figure 8.1. Typical variation of mechanical and AE response of nominally identical 16-ply UD 0° APC2 specimens. a) Load/time graphs. b) Cumulative events/time graphs. c) Amplitude distribution histogram (the shaded regions indicate the ranges).

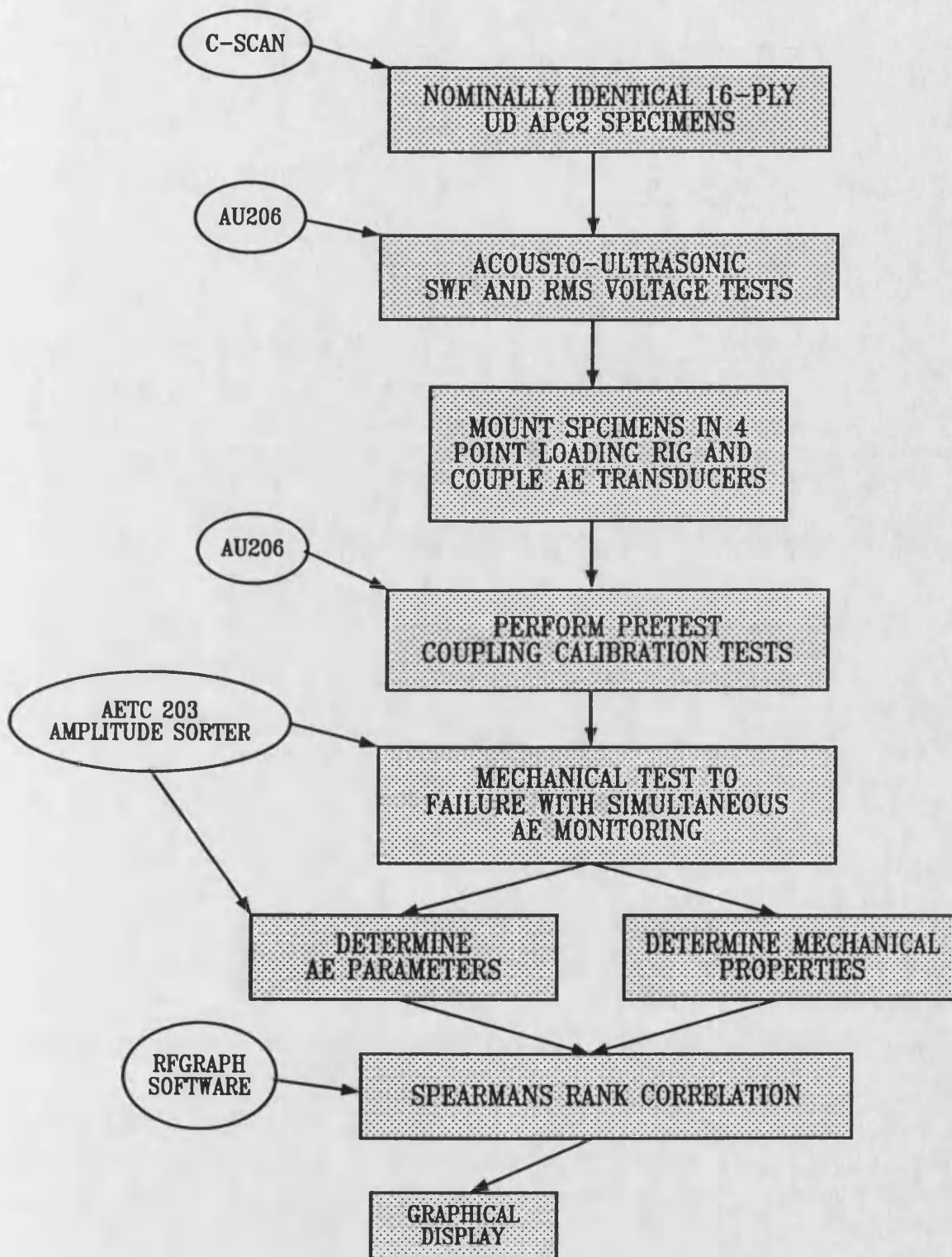


Figure 8.2. A flow diagram to explain the procedure for carrying out the cross correlation of mechanical properties with acousto-ultrasonics and acoustic emission.

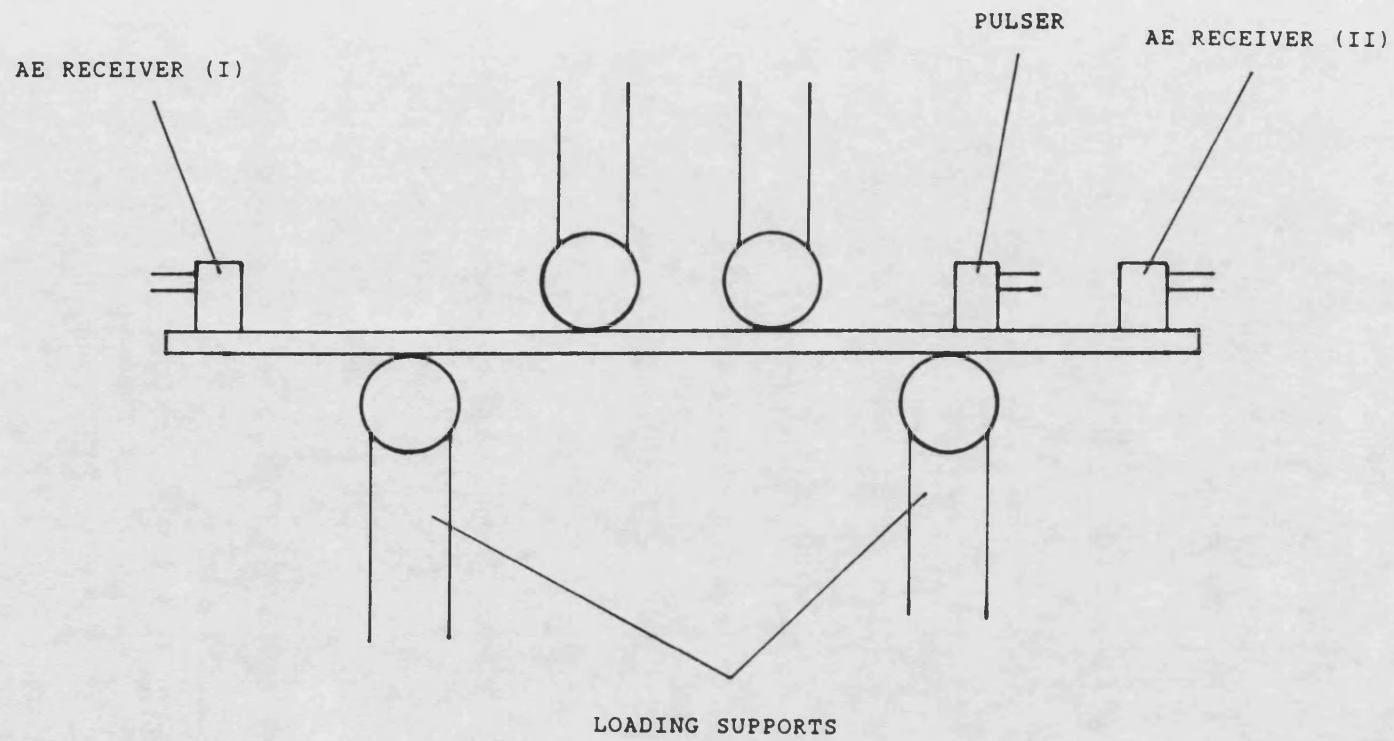
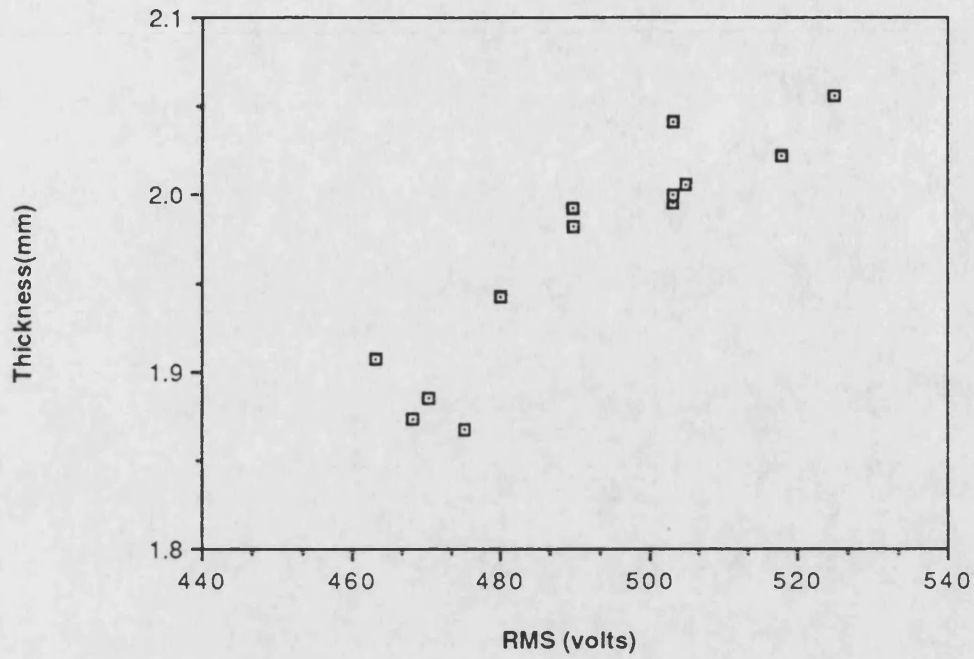


Figure 8.3. The relative disposition of AE transducers and loading supports.

a)

Specimen thickness vs AU RMS



b)

Failure load vs AU RMS

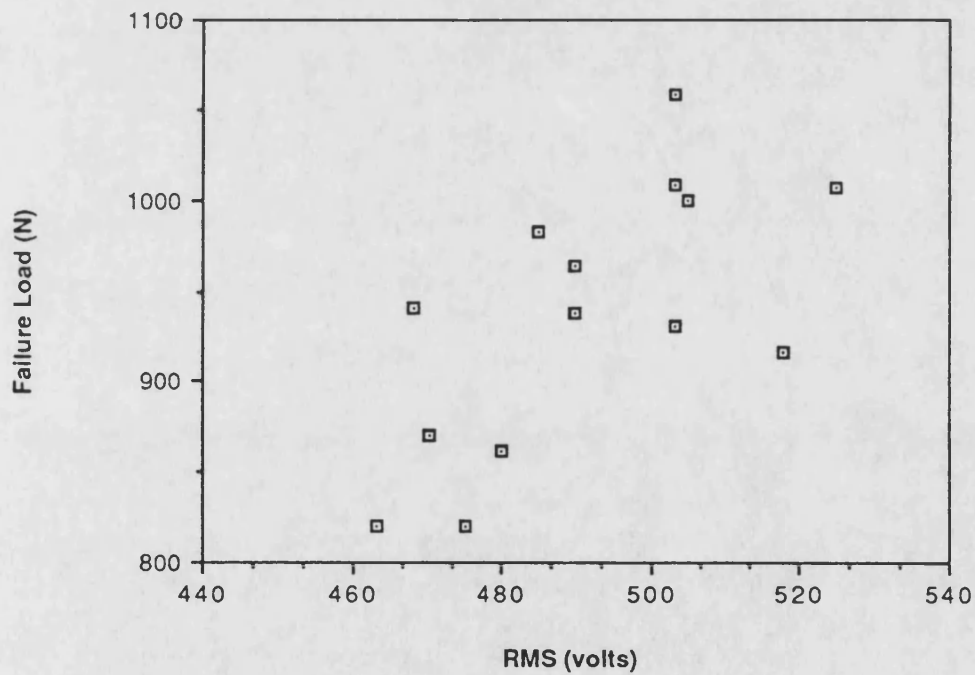
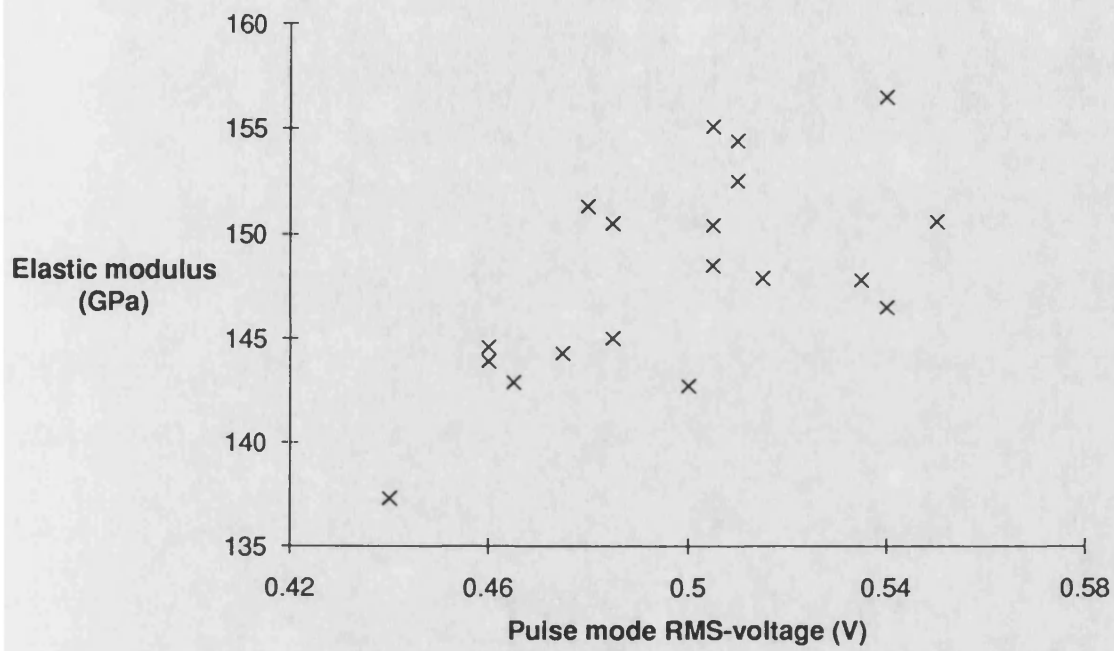


Figure 8.4. Scatter plots of acousto-ultrasonic RMS voltage, determined on nominally identical 16-ply UD 0° APC2 specimens, as a function of: a) specimen thickness b) failure load c) elastic flexural modulus.

C) Correlation of elastic modulus with AU RMS-voltage (pulse mode 80dB, E1)



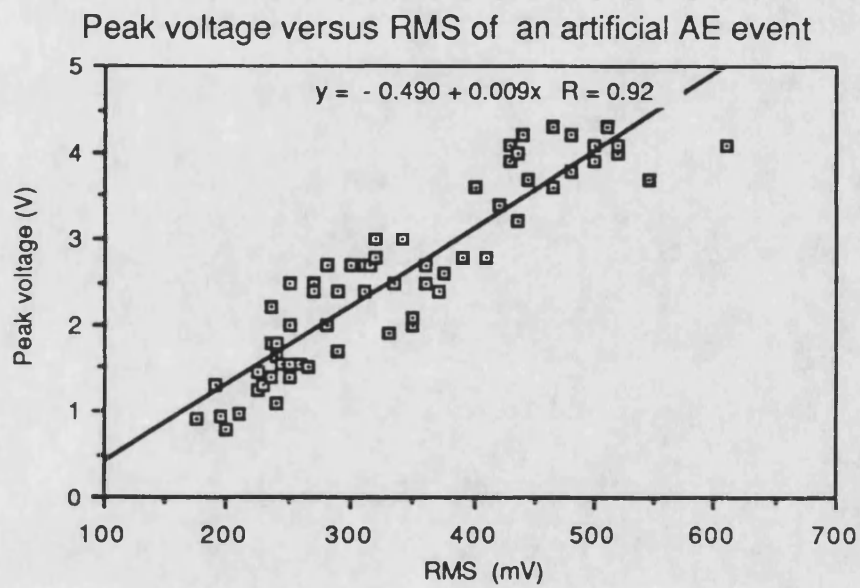


Figure 8.5. Correlation of AU RMS voltage with peak amplitude of an artificial AE event.

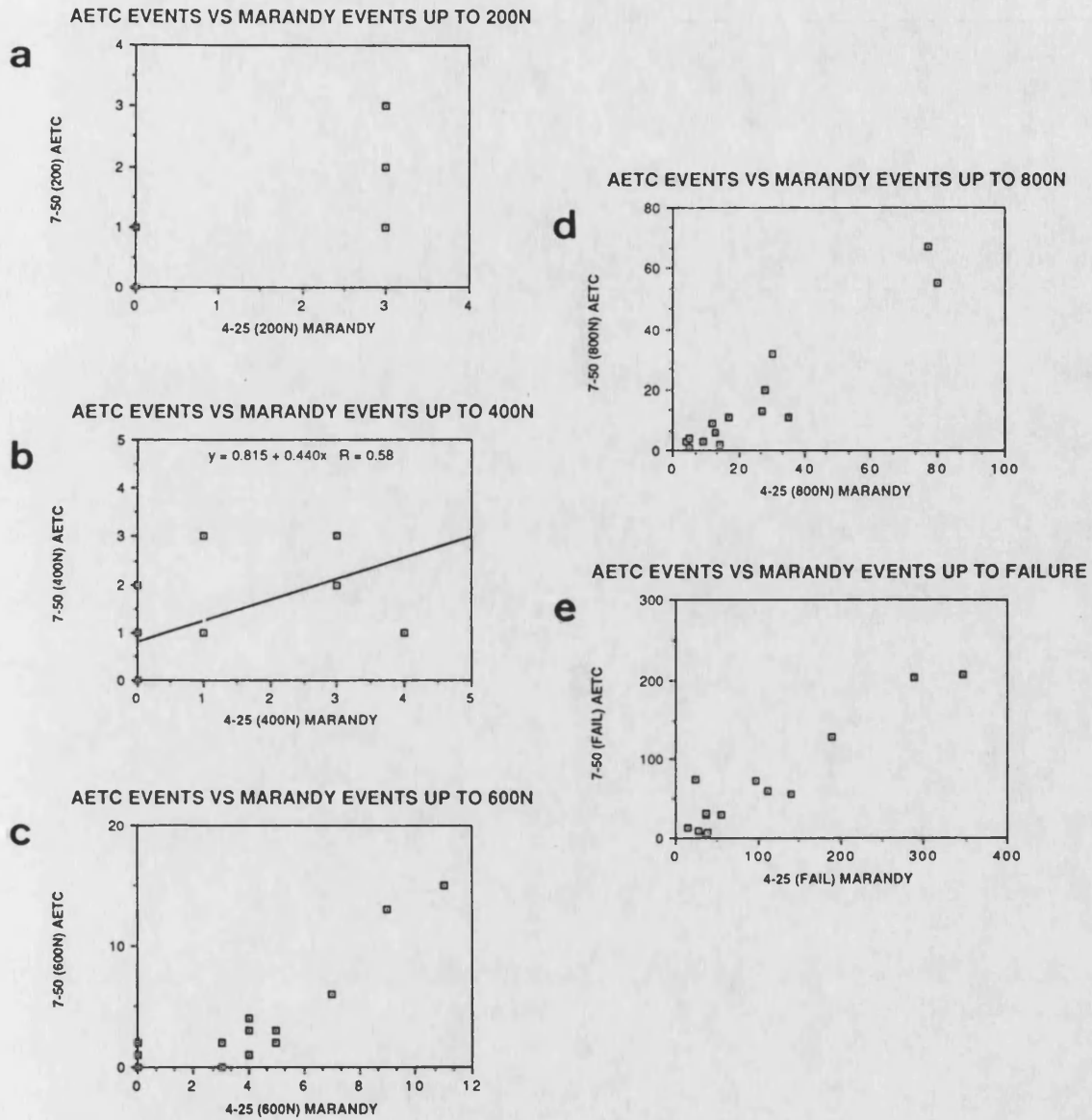
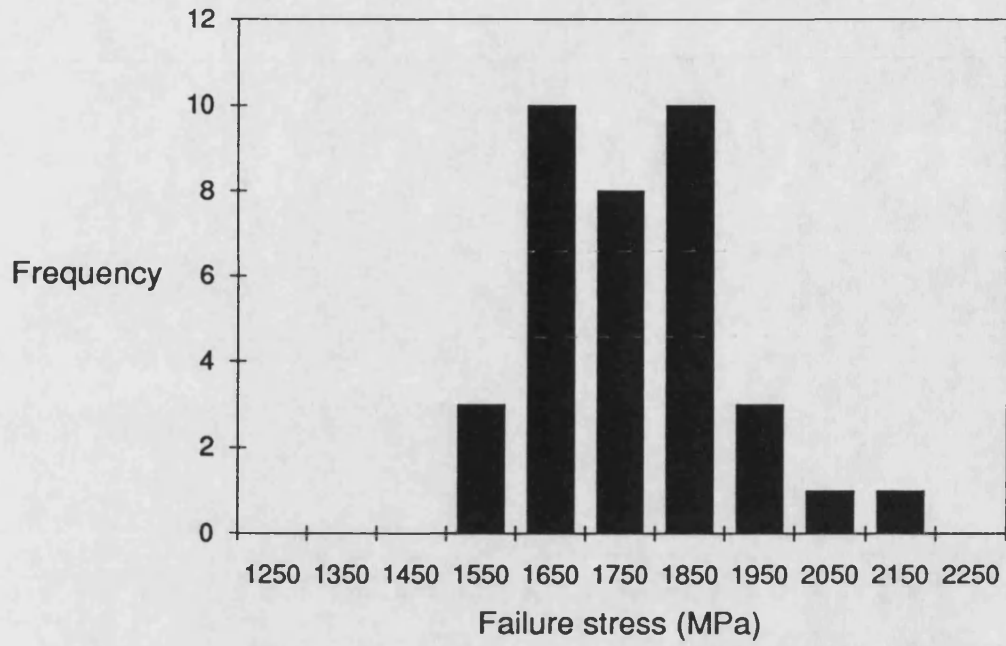


Figure 8.6. Scatter plots of cumulative event counts recorded from two AE systems to specified load levels.
 a) 200N. d) 800N.
 b) 400N. e) Failure.
 c) 600N.

a

Frequency histogram of failure stress



b

Frequency histogram of deflection at 1000 N

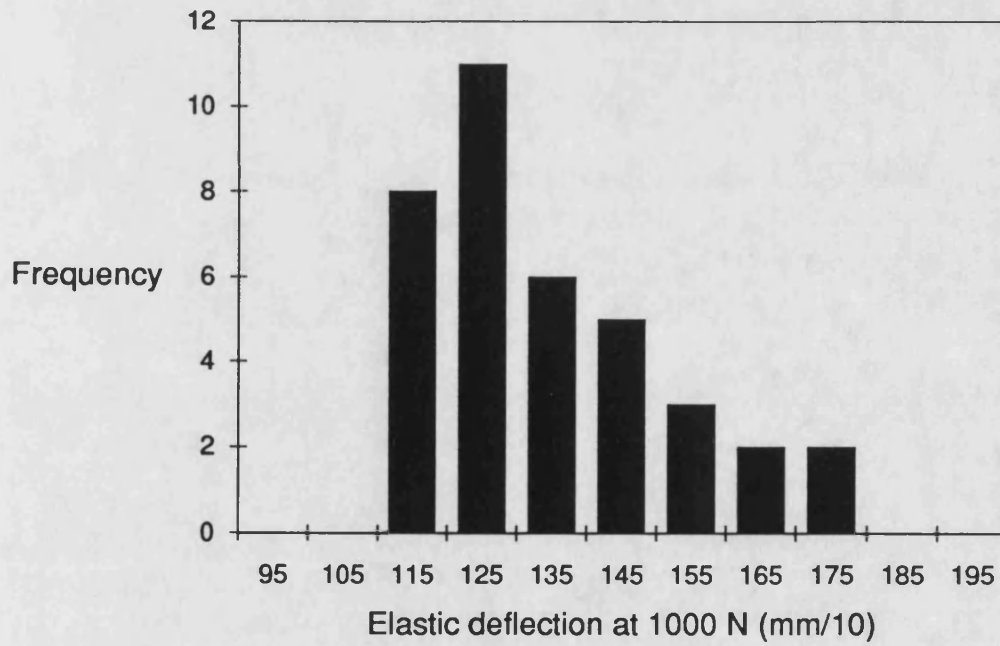


Figure 8.7. Frequency histograms of mechanical properties recorded from nominally identical 16-ply UD 0° APC2. a) Flexural strength. b) Elastic deflection at 1000N.

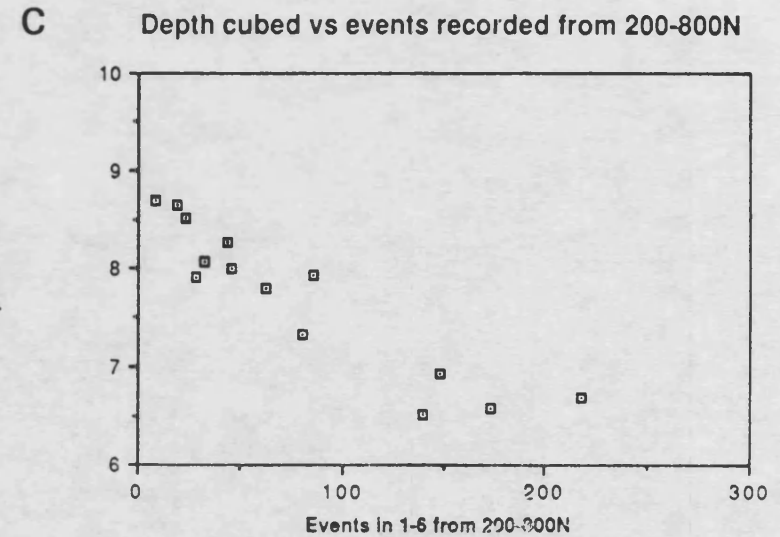
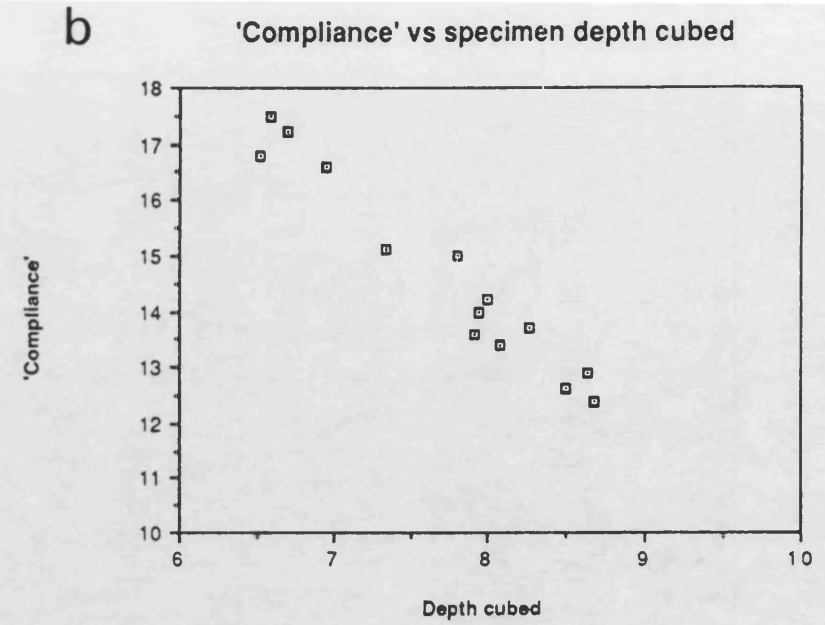
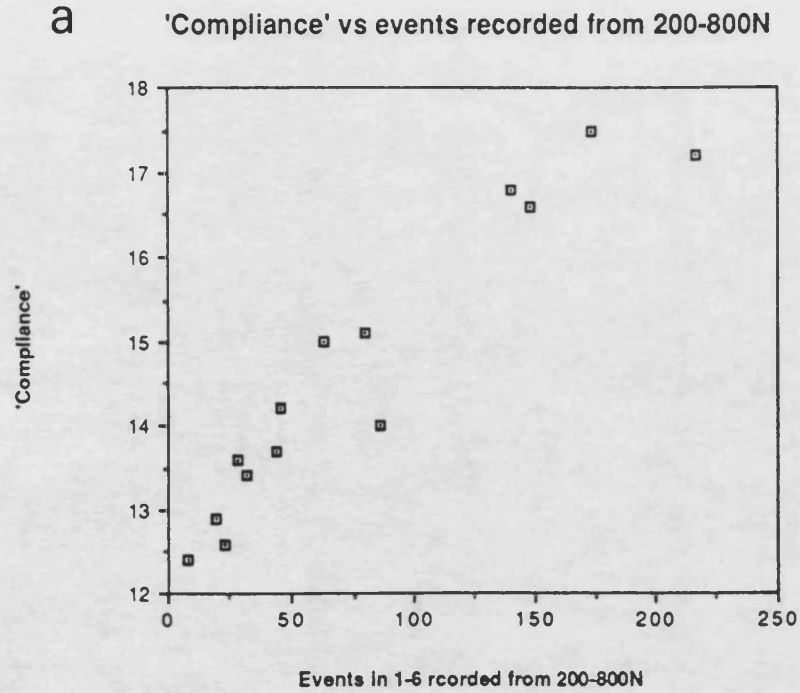


Figure 8.8.

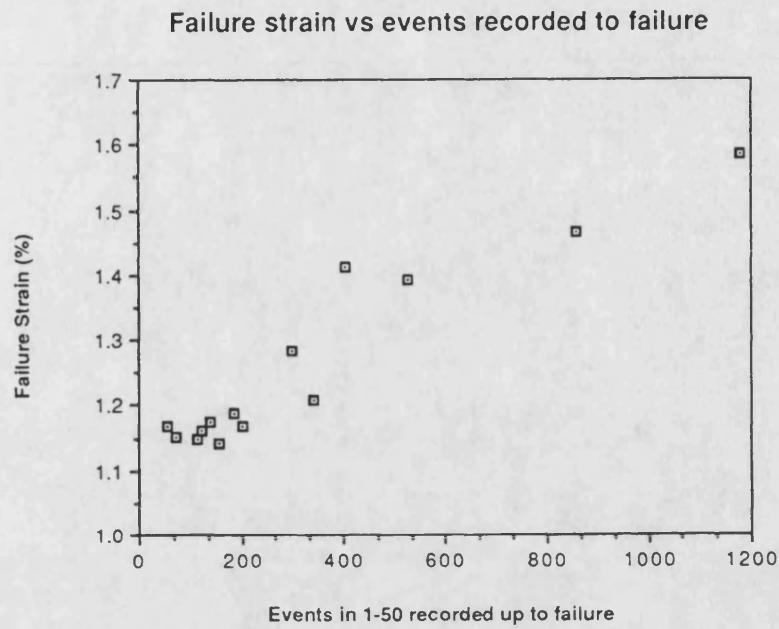
Scatter plots demonstrating correlations between data recorded from nominally identical 0° 16-ply UD APC2.

a) Specimen compliance and number of events recorded in channels 1-6 over the load range 200-800N.

b) Specimen compliance and the cube of specimen depth.

c) The cube of specimen depth and number of events recorded in channels 1-6 recorded over the load range 200-800N.

a



b

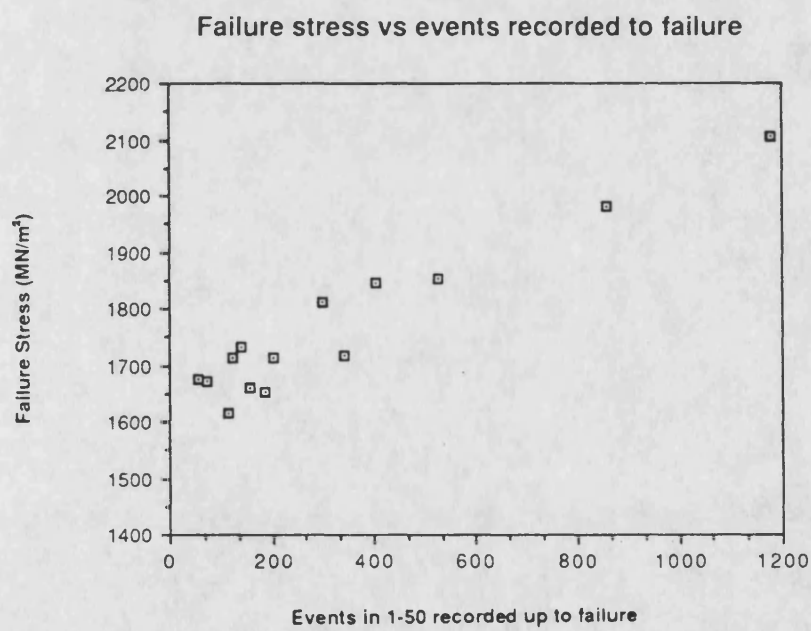
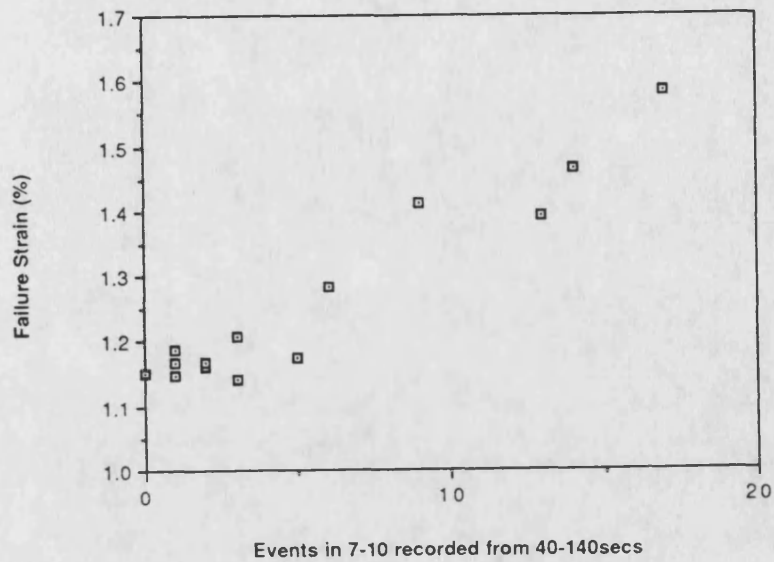


Figure 8.9. Correlation of failure stress and failure strain with the cumulative event count to failure for 0° 16-ply UD APC2.

Failure strain vs events recorded from 40-140secs



Failure stress vs events produced form 40-140secs

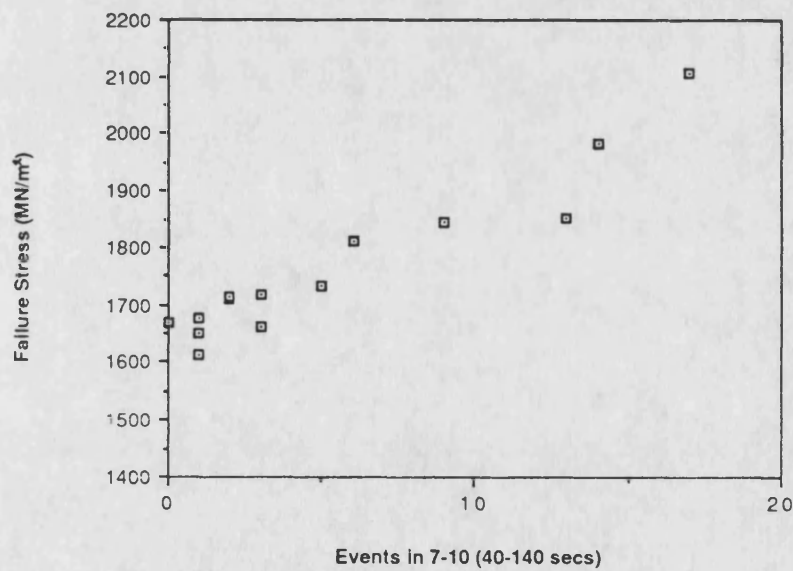


Figure 8.10. Correlation of failure stress and failure strain with the number of events recorded in channels 7-10 over the time range (equivalent to a crosshead displacement range) of 40-140 seconds.

Specimen number	Peak amplitude of pretest coupling pulse (volts)			Total events to just before failure	
	AU1 III > I (x 10)	AU2 III > II (x 1)	AU3 II > I (x 100)	AE System I	AE System II
1	6.0	4.6	9.0	13	15
2	4.4	1.6	12.5	207	347
3	5.0	2.2	13.5	4	37
4	4.8	1.8	9.5	55	141
5	4.8	1.6	8.0	8	39
6	4.2	4.4	10.0	59	111
7	3.4	4.8	12.0	73	97
8	5.6	4.4	9.5	10	27
9	3.8	4.6	6.6	30	54
10	6.4	5.6	10.5	7	23
11	3.2	3.6	9.5	203	289
12	3.2	4.8	10.5	32	37
13	3.6	4.4	10.0	128	190
14	3.6	6.2	9.0	29	36
15	22.0	*0.6	80.0	2956	*0
16	26.0	*1.3	220.0	970	*20
17	21.0	10.5	125.0	108	576
18	17.0	14.0	115.0	784	3585
19	16.5	14.0	95.0	104	7173
20	8.0	8.2	68.5	77	1102
21	7.4	3.8	8.5	63	196
22	5.1	1.7	16.0	51	100
23	7.0	1.5	23.0	311	422

* 40 dB Preamplifier used

Table 8.1. Assessment of coupling quality. Pre-test coupling pulse amplitudes (common energising pulse, propagated between pairs of transducers) for 16-ply UD 0° APC2 strip specimens prior to four point flexural testing. Total event counts with amplitudes above 22.9 mV are also presented.

Load	Linear Regression Coefficient	Mean event count	
		AETC	MARANDY
200 N	0.79	0.6	0.6
400 N	0.58	1.3	1.1
600 N	0.86	3.9	4.3
800 N	0.95	16.9	25.4
Failure	0.95	61.3	103.7

Table 8.2. Linear regression coefficients for the comparison of total numbers of events recorded with amplitudes greater than 22.9 mV at specified load levels from two AE systems. The mean total event counts at each load are also presented (14 samples).

'Mechanical Property Parameter	Mean	Standard Deviation	Maximum	Minimum
Failure Stress (MPa)	1760	131	2106	1507
Failure Strain (%)	1.24	0.14	1.585	1.015
'Compliance' (mm/1000N)	13.4	1.75	17.5	11.1
Deflection to Failure (mm)	15.2	2.14	21.0	12.4
Specimen Thickness (mm)	2.046	0.084	2.180	1.867

Table 8.3. A summary of the ranges of the mechanical properties determined from nominally identical three point bend test 16-ply UD 0° strip specimens.

APPENDICES

Appendix 1: The Fundamentals Of Ultrasonics

The following treatment of the fundamentals of ultrasonics is based upon that given by Krautkramer (67) and Szilard (161).

A1.1 The Physical Principles of Ultrasonics

A solid can be thought of as a collection of particles held in position by elastic restoring forces (the interatomic bonds) which cause them to return to equilibrium positions and oscillate about them when displaced. If an external sinusoidal force is applied to a surface of an elastic solid, an oscillating elastic wave will propagate through the material as subsequent planes of particles transmit the imposed alternating stress via the elastic interatomic bonds. The bond elasticity introduces a time delay into the transmittance of the stress (a phase lag) which increases with distance. The oscillations of the particles obey a sine function (figure A1.1) such that, for example, the particle displacement y is given by:

$$y = a.\sin \omega t \quad \dots \text{A1.1}$$

where a = displacement amplitude

f = frequency

$\omega = 2.\pi.f$

There are a variety of different types of ultrasonic wave which can occur in solids. In an infinite elastic body there are two types of wave propagation: longitudinal (or compression) and shear (or transverse). An instantaneous diagrammatic picture of a longitudinal wave propagating through an elastic body is shown in figure A1.2. Zones of compression and rarefaction travelling at phase velocity v , are regularly spaced at intervals of λ (wavelength) and occur at a frequency f . The relationship linking these three parameters,

$$v = \lambda.f$$

... A1.2

is valid for all waves. For compression waves, particle displacement occurs in the same direction as wave propagation. This compares to shear waves (shown in figure A1.3) in which particle displacement is perpendicular to the direction of propagation and thus involves shear rather than compressive stress regions. For this reason, shear waves can only propagate in materials with shear elasticity (solids), longitudinal waves being the only wave mode possible in bulk liquid or gaseous media. The latter are the most commonly used waves in conventional ultrasonic testing.

Wave velocities depend upon three main parameters, density ρ , elastic modulus E and Poissons ratio μ . The velocity of longitudinal and shear waves are given by the relationships:

$$c_{\text{longitudinal}} = \left(\frac{E}{\rho} \cdot \frac{1-\mu}{(1+\mu)(1-2\mu)} \right)^{1/2} \quad \dots \text{A1.3}$$

$$c_{\text{shear}} = \left(\frac{E}{\rho} \cdot \frac{1}{2(1+\mu)} \right)^{1/2} = \left(\frac{G}{\rho} \right)^{1/2} \quad \dots \text{A1.4}$$

For a given frequency and material, shear waves have a lower velocity and shorter wavelength than longitudinal waves.

In a semi-infinite body with one boundary, shear and longitudinal wave components can combine to produce surface (Rayleigh) waves. These waves, which are not strictly speaking sinusoidal (the particles describing elliptical orbits (see figure A1.4)) are associated with media which have thicknesses significantly larger than the wavelength. The amplitude of Rayleigh waves decreases exponentially with distance from the surface such that, at one wavelength, the particle movement is less than 10% of that at the surface.

In plates or rods where the distances between boundaries are comparable with the wavelength (\leq shear wavelength), plate waves (Lamb waves) can occur, again by the combination of longitudinal and shear wave components. In fact, Lamb waves can be considered to consist of a pair of longitudinal and a pair of shear waves, reflecting (bouncing) backwards and forwards within the plate from surface to surface (see figure A1.5a). Combinations of the effects of the two wave modes yield symmetric and asymmetric Lamb waves (see figure A1.5b and A1.5c). Particle movement at the surface is similar to that found in Rayleigh waves (which cannot exist in these conditions). The velocity of Lamb waves depends on complex relationships involving frequency and longitudinal and shear wave velocity.

In a thin rod where thickness $d \leq 0.1\lambda$, the velocity is simply:

$$c_{\text{rod}} = \left(\frac{E}{\rho} \right)^{1/2} \quad \dots \text{A1.5}$$

Using this relationship and measuring the time of flight of ultrasonic pulses along rod shaped specimens gives a quick and simple method of determining a simple dynamic elastic modulus (ρc_{rod}^2).

A1.1.1 Ultrasonic waves at boundaries

When an ultrasonic wave strikes a boundary between two media of different elasticities joined together, part of the sound pressure is reflected and part is transmitted, the relative proportions of which are governed by the acoustic impedances of the media. The characteristic impedance is defined as:

$$R = \rho c \quad \dots \text{A1.6}$$

At normal incidence at an interface between two media of large proportions in intimate contact, the reflection and transmission coefficients for ultrasonic waves depend on the ratios of the characteristic impedances of the two media:

$$\frac{P_r}{P_i} = \frac{R_2 - R_1}{R_2 + R_1} \quad \text{reflected pressure ratio} \quad \dots \text{A1.7}$$

$$\frac{P_t}{P_i} = \frac{2 R_2}{R_2 + R_1} \quad \text{transmitted pressure ratio} \quad \dots \text{A1.8}$$

where R_1 = specific acoustic impedance of 1st medium
 R_2 = specific acoustic impedance of 2nd medium

The significance of these coefficients becomes apparent when we consider the transmission of ultrasound across the interface between a solid (steel) and a gas (air). $R_{\text{air}} = 4.3 \times 10^2 \text{ kg/m}^2$ and $R_{\text{steel}} = 4.5 \times 10^7 \text{ kg/m}^2$, therefore the transmitted pressure ratio is 1.9×10^{-5} . In other words, only 0.0019% of the incident sound pressure is transmitted. Thus, an air/solid interface is essentially a free boundary at which almost all ultrasonic energy is reflected. This has very obvious consequences for both air filled cracks within solids and for the dry coupling of ultrasonic transducers to material under investigation (a liquid couplant is normally used).

In the case of a thin layer of one material embedded within another the determination of reflection and transmission coefficients is complicated by the interference of waves which undergo multiple reflections, integer multiples of $(2 \times \text{thickness})/\lambda$ causing resonance effects. Examples of this are an air filled crack or to a lesser extent the coupling layer between the epoxy wear plate of a transducer and an epoxy specimen. In this instance the reflection and transmission coefficients are also dependent upon the ratio of layer thickness to wavelength:

$$\frac{P_t}{P_i} = \left(1 + \frac{1}{4} \left(m - \frac{1}{m} \right)^2 \sin^2 \frac{2\pi d}{\lambda} \right)^{-1/2} \quad \text{transmission coef} \quad \dots \text{A1.9}$$

$$\frac{P_r}{P_i} = \left(\frac{\frac{1}{4} \left(m - \frac{1}{m} \right)^2 \sin^2 \frac{2\pi d}{\lambda}}{1 + \frac{1}{4} \left(m - \frac{1}{m} \right)^2 \sin^2 \frac{2\pi d}{\lambda}} \right)^{1/2} \quad \text{reflection coef} \quad \text{A1.10}$$

where $m = R_1/R_2$

The presence of the sine function in these expressions leads to maxima and minima in reflection and transmission. Maxima in reflection and minima of transmission occur at integer multiples of $d/2\lambda$, while minima of reflection and maxima of transmission occur at $d/\lambda = 1/4, 3/4, 5/4 \dots$. This has obvious consequences for the optimisation of coupling layers between transducers and any material under investigation.

If an ultrasonic wave strikes an interface between two materials at an oblique angle, reflected and transmitted waves will result; the transmitted wave (or waves) being refracted. The angles of reflection and refraction are dependent on the velocities of the materials and obey Snell's Law.

Ultrasonic waves, in addition to undergoing reflection and refraction at interfaces, can also undergo mode conversion. This is the change of an incident longitudinal wave into a reflected or refracted shear wave or vice-versa. In general, mode conversion is only partial, and the lower velocity of shear waves infers a smaller angle of reflection or transmission than longitudinal waves. This helps to explain how boundaries can serve to help scatter ultrasonic waves. In addition, it is evident that, in the case of acousto-ultrasonics, where the sending transducer emits largely longitudinal waves into a test specimen, the multiple reflections of the waves at the specimen faces will cause the dissemination of the incident energy into both shear and longitudinal components. The interactions of these within the plate may generate Lamb waves.

A1.1.2 The decibel notation

It is common in the field of ultrasonics to express amplitude and intensity ratios in terms of decibels (dB) defined as

$$\frac{A_2}{A_1} \text{ ratio in decibels} = 20 \log \frac{A_2}{A_1} \text{ dB} . \quad \dots \text{ A1.11}$$

For example, the attenuation of materials and the amplitude of acoustic emission events are usually quoted in terms of dB. In the latter case, the logarithmic decibel scale is particularly useful for dealing with the wide dynamic range of the amplitudes of events. The decibel scale is of course based upon ratios, and therefore values in dB are not absolute, but relative with respect to a reference.

A1.1.3 Resonance

It is the phenomenon of resonance which largely controls the frequency spectra of most oscillating bodies. Resonance is the condition such that the waves of a specific length, corresponding to a specific frequency, are reflected back and forth (or travel round an object) and interfere exactly in phase. The minimum frequency for resonance, and hence longest wavelength, is termed the fundamental frequency, integer multiples of which are the harmonics. At resonance, the effect of a system's elasticity and the effect of its mass cancel each other out, and the only resistance to vibration is given by internal losses. Hence, attenuation is decreased and amplitudes are greater than at non-resonant frequencies. At resonance in a plate:

$$\text{plate thickness} = \lambda_0/2 = c/2f_0 \quad \dots \text{A1.12}$$

where λ_0 is the fundamental wavelength
 f_0 is the fundamental frequency

The frequency spectrum of AE and AU events will largely be governed by the resonance effects caused by the specimen dimensions and by the resonant frequency of the transducers used (13,14).

A1.2 Attenuation

All ultrasonic waves are attenuated to a greater or lesser extent by the media through which they propagate, that is, their incident amplitude or intensities decrease with distance from their source. For a plane wave (no geometric attenuation) the relationship

between the incident sound pressure amplitude A_0 and its value A after travelling a distance r is:

$$A = A_0 e^{-\alpha r} \quad \dots \text{A1.13}$$

where α is the amplitude attenuation coefficient.

In homogeneous media such as gases, liquids or amorphous solids, ultrasonic wave energy is absorbed and turned into heat. However, in polycrystalline solids or homogeneous media containing other particles, additional losses can occur by scattering. Hence, the attenuation coefficient can be made up of more than one component:

$$\alpha = \alpha_a + \alpha_s \quad \dots \text{A1.14}$$

where α_a is the absorption coefficient

α_s is the scattering coefficient

The relative importance of the contributions of these different sources to the total attenuation is dependent on the material, dimensions, frequencies, distribution and size of inhomogeneities etc. The different sources of attenuation will now be considered.

A1.2.1 Geometric attenuation

One contribution to the decrease in amplitude with distance from the source is the geometrical effect of beam spread. Examples of this include beam spread of the ultrasonic beam of a probe in the far field or spherical waves generated from a localised source, such as acoustic emission events. In a perfectly elastic infinite homogeneous medium, where no other attenuation affects exist, the energy in the wavefront of a spherical wave remains constant but spreads out over a larger spherical surface, the radius of which is the distance from the source. For the energy to remain constant, the amplitude of the wave must decrease with distance from the source. In general, the amplitude of both longitudinal and shear waves decrease inversely as the distance from the source increases (proportional to $1/r$), assuming no limitations on the dimensions of the medium. For surface waves, however, the decrease in amplitude is proportional to

$1/r^{1/2}$ owing to the two rather than three dimensional spread of the energy. For Lamb wave propagation over a thin plate, assuming the source is localised to a size small in comparison to the source to receiver distance, then the attenuation is proportional to $1/r^{1/2}$.

The only waves that are not subject to geometric attenuation are one dimensional waves (plane waves in infinite bodies) and waves in one dimensional media such as strings, bars or beams.

A1.2.2 Absorption

Absorption is the result of the acoustic wave performing work as it propagates through a medium, hence losing energy. Kinetic and potential energy are not conserved as the wave of particle displacements propagate through the medium. Absorption is most important in plastics. Szilard ⁽¹⁶¹⁾ states that absorption is mainly caused by four factors which are dependent on either the first or second power of frequency:

1. internal friction (viscosity),
2. elastic hysteresis,
3. heat conduction,
4. other factors such as relaxational phenomena, and molecular structure.

Friction effects are the result of the 'rubbing' or relative movement between particles subjected to different degrees of strain by virtue of the propagation of ultrasonic waves. Hysteresis may be described as the condition, in the interval of frequencies for which damping is appreciable, where the strain is out of phase with the stress. Heat generation occurs by a simple mechanical interaction between the excited particles in the sound wave and the unexcited particles in its path (heat will flow from areas of high strain to areas of low strain). In general, absorption can be visualized as the braking effect of the oscillations of particles. This also helps to explain why higher frequency oscillations lose more energy than low frequency (slow) oscillations. Plastic deformation and crack

extension can also contribute to absorption if the amplitude of oscillations is sufficiently great.

In solids, absorption generally varies linearly with frequency. Internal friction and elastic hysteresis are the most important absorption mechanisms in solids, whilst in liquids and gases, frictional and heat conduction losses predominate and absorption is dependent on the square of the frequency. In fibre reinforced plastics, viscoelasticity of the matrix and friction between surfaces such as debonded fibres, delaminations and from incompletely bonded fibres or inclusions will contribute to attenuation by absorption.

A1.2.3 Scattering

Scattering is the refraction and reflection of the wave out of the path of wave propagation. It is generally important in polycrystalline material, particularly metals and in any inhomogeneous material such as composites. Scattering of ultrasonic waves is caused by the presence of inhomogeneities with acoustic impedances which are different from the surrounding material, and with dimensions commensurate in size with the sound wavelength. Such inhomogeneities may be pores, flaws (cracks), inclusions, fillers or reinforcing fibres in composites, bubbles in liquids and so on. The scattering coefficient varies with, amongst other things, the wavelength λ to mean diameter D ratio. Other factors which affect the degree of scattering are differences in the elastic constants and densities of the inhomogeneities and the surrounding medium and the type of ultrasonic wave. Szilard ⁽¹⁶¹⁾ gives three ranges of λ/D over which the scattering coefficient exhibits different behaviour:

1. Where $\lambda \gg D$ (Rayleigh scattering range), $\alpha_s \propto D^3 f^4$.
2. Where $\lambda \approx D$ (Random phase scattering range), $\alpha_s \propto D f^2$.
3. Where $\lambda \ll D$ (Diffusion scattering range), $\alpha_s \propto 1/D$.

The transitions between these different ranges are not sharply defined. Krautkramer ⁽⁶⁷⁾ states that if D lies in the range $1/100 - 1/1000$ of λ then scattering is essentially negligible, whilst from $1/10 - 1/1$ of λ scattering can become so great that conventional

ultrasonic testing can become impossible. This type of attenuation is of particular significance to the highly inhomogeneous fibre reinforced plastics (18).

A1.2.4 Dispersion

Dispersion is caused by the frequency dependence of the speed of waves in certain systems. A disturbance made up of various frequency components, for example, the AU pulse from a broadband transducer, will change in form as the components propagate along a bar or plate because each component propagates at different speeds. The duration of the disturbance will increase with distance from the source as the energy is dispersed in the time domain, a fact which complicates source location in AE.

In the case of acoustic emission events in fibre reinforced plastic plates, geometric attenuation, dispersion, scattering and diffraction from and around discontinuities and energy loss mechanisms will all contribute to the attenuation of the events.

A1.3 Transducers

The most common method of both generating and receiving ultrasonic waves is by use of the piezoelectric effect, used exclusively during the work for this thesis. If a plate is cut from a crystal of a piezoelectric material (such as quartz) having a certain orientation with respect to the crystallographic axes and deformed in the correct direction, electric charges are produced on opposite surfaces. Conversely, the application of an external electric field over the correct surfaces will cause the plate to contract or expand depending on the polarity of the electric field, as shown in figure A1.6. An alternating electric field will therefore produce sound waves, and an alternating stress on the crystal will produce an alternating electric charge. The piezoelectric transducer is effectively a capacitor, with the piezoelectric plate acting as the dielectric.

The particular orientation of the crystallographic axes within a piezoelectric material plate (the 'cut') will control the predominant type of ultrasonic wave emitted and the type

of wave to which the transducer is most sensitive when acting as a receiver. It should be noted that distortion in one direction will of course cause distortion of the plate in transverse directions, thus pure longitudinal or pure transverse emitters/receivers do not exist.

The most commonly used piezoelectric materials for ultrasonic transducers are the lead zirconate titanate group of ceramics (PZT). Plates for PZT transducers must be produced by pressing and sintering of polycrystalline material above 1000°C, since large enough single crystals are generally not available. The randomly orientated small crystals within the plate are then aligned by polarization in an applied electric field of several thousand volts per centimetre thickness whilst heating above the Curie temperature (the field being maintained during cooling). Subsequent heating of the ceramic to temperatures near the Curie temperature will cause randomisation of the alignment of the crystals. In addition, there is an ageing effect seen in these transducers which slightly decreases the piezoelectric constants with time.

These piezoelectric plates are usually mounted within a stainless steel case for protection and support and the entire assembly is called a probe or transducer (see figure A1.7). Electrical contacts (often silver) are sputtered down or baked onto the appropriate faces, onto which wires are soldered. A wear plate usually protects the front face of the plate from mechanical damage and a layer of low acoustic impedance material, which is chosen to control the frequency spectrum of the transducer, backs the plate to reduce ringing. All transducers will tend to oscillate at their resonant frequency. If they are forced to oscillate at other frequencies the amplitude of oscillation is considerably lower. By varying the method of mounting in the probe and/or the material used as the backing to the plate, the damping of the transducer can be controlled. Hence, broader and flatter frequency spectra (bandwidths) can be achieved over which sensitivity is moderately constant. However, the sensitivity is considerably lower than in the undamped condition. This explains the difference between broad band acoustic emission sensors and resonant

sensors, the latter being required particularly in situations where high sensitivity in a small frequency range is needed (i.e. in a generally noisy environment). The fundamental frequency of oscillation of the piezoelectric plate is controlled by its ultrasonic constants and its thickness (equation A.12).

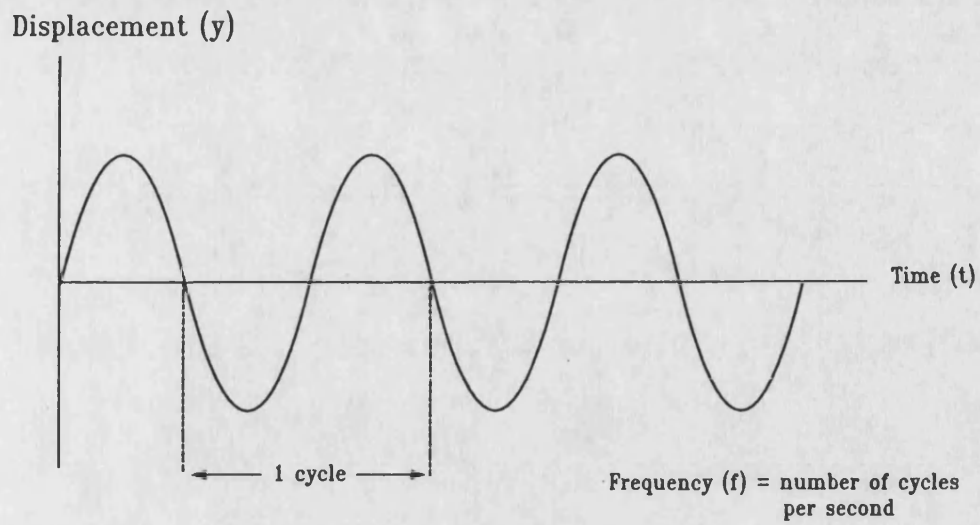


Figure A1.1. Sinusoidal oscillation of an undamped particle undergoing simple harmonic motion.

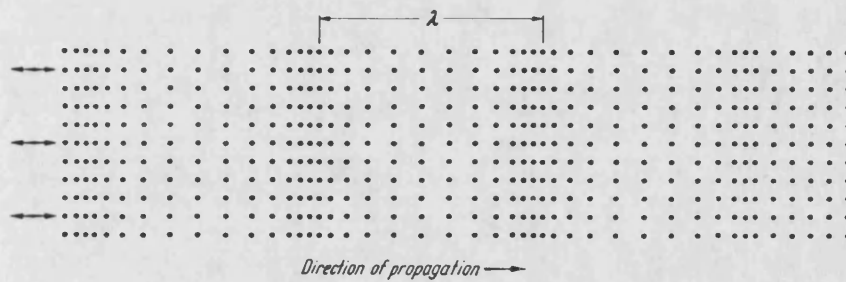


Figure A1.2. Longitudinal (pressure) wave propagation in a homogeneous elastic solid (after Krautkramer ⁽⁶⁷⁾).

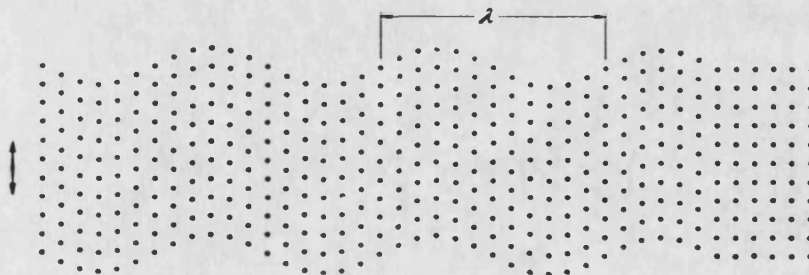


Figure A1.3. Shear (transverse) wave propagation in a homogeneous elastic solid (after Krautkramer ⁽⁶⁷⁾).

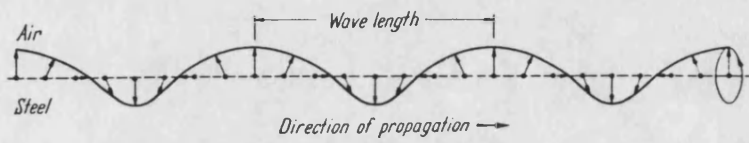


Figure A1.4. Rayleigh (surface) wave propagation (after Krautkramer (67)).

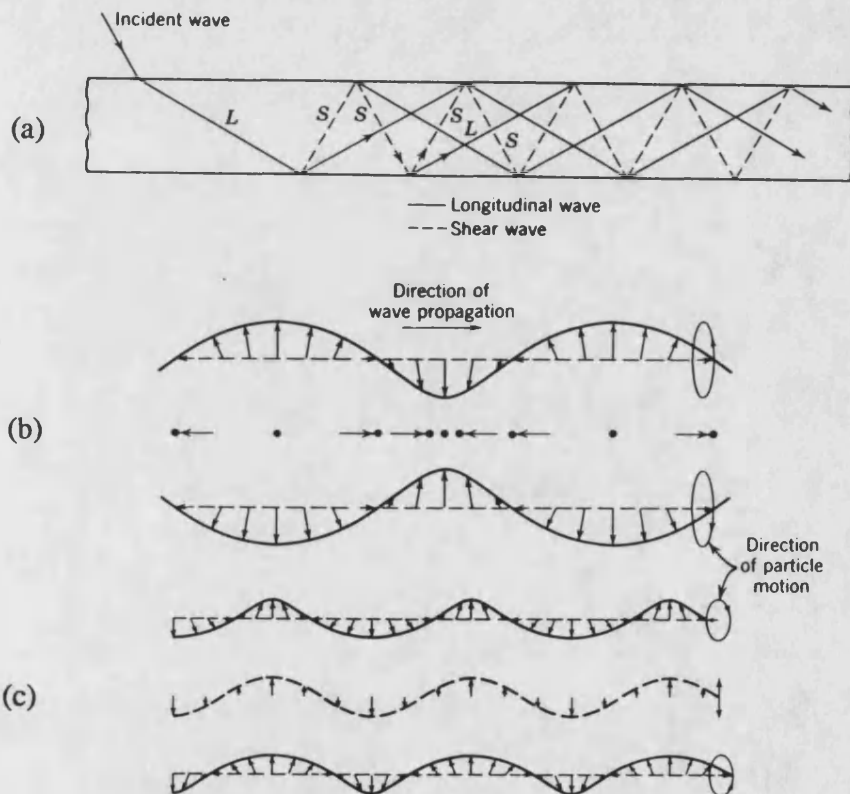


Figure A1.5. Lamb (plate) wave propagation in a thin plate. (a) An incident longitudinal wave generates a shear wave in the plate shown above. Certain angles of incidence are more favourable than others for generating particular modes of propagation. (b) Asymmetrical (bending) waves. (c) Symmetrical (dilatational) waves (after Krautkramer (67)).

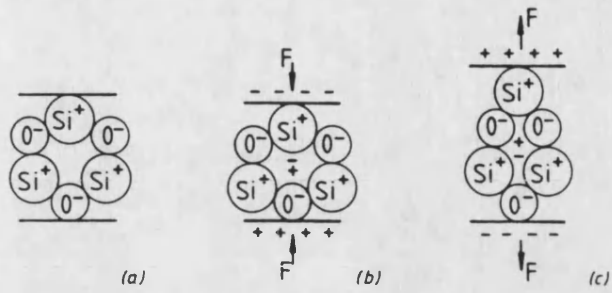


Figure A1.6. Piezoelectric behaviour of an elementary cell in a quartz crystal. (a) Cell unstressed. (b) Cell compressed. (c) Cell extended (after Szilard (161)).

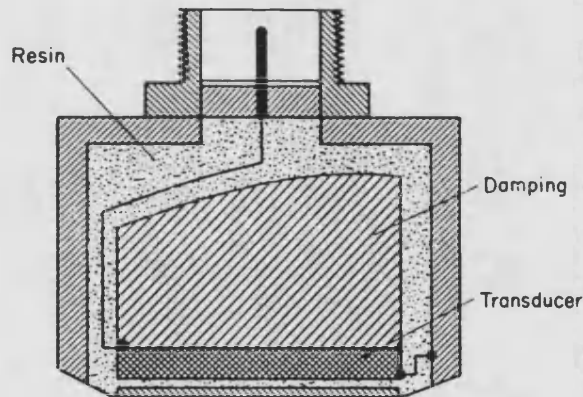


Figure A1.7. A typical ultrasonic probe (transducer) for normal incidence (after Szilard (161)).

Appendix 2: Statistical Techniques

A2.1 Snedecor's F Test

This test determines the significance of the difference between two estimates of variance, and is of particular importance to the analysis of variance. The F test may be defined as

$$F \text{ ratio} = \frac{\text{greater estimate of variance}}{\text{lesser estimate of variance}} \quad \dots \text{A2.1}$$

For two sample sizes of 5, the variance estimates are deemed different at the 1% level if F is 16, and at the 5% level if F=6.39.

A2.2 Descriptive Measures of an Amplitude Distribution Histogram

The amplitude distribution histogram is the standard data presentation format for the peak amplitudes of acoustic emission events. The peak amplitudes of AE events are recorded by sorting into discrete amplitude channel ranges (channel number 1 - 26 or 1 - 51 depending on the amplitude sorter used). Therefore, the fundamental continuous variable, 'AE event amplitude (in volts)', is grouped into a range of discrete values, namely amplitude channel number. Only these grouped data are available for analysis and manipulation. The probability of occurrence of an AE event in a specific channel is the probability function which the acoustic emission amplitude distribution histogram describes.

Although a frequency histogram is very useful in displaying and summarizing the very large amount of acoustic emission data often gathered during a mechanical test, it is limited in its applicability for quantitative comparison. A small number of parameters which can quantify both the size and shape of a distribution, will enhance the ability to quantitatively compare amplitude distributions. Examples of such parameters which have been used in this thesis include the mean, variance, skewness and kurtosis which will now be defined.

A2.2.1 Moments for grouped data

If X_1, X_2, \dots, X_k occur with frequencies f_1, f_2, \dots, f_k , respectively, the r th moment about any origin A is defined as

$$m_r' = \frac{\sum_{j=1}^k f_j (X_j - A)^r}{N} = \frac{\sum f (X - A)^r}{N} = \frac{\sum fd^r}{N} \quad \dots \text{A2.2}$$

where $d = X - A$ are the deviations of X from A .

$$N = \sum_{j=1}^k f_j = \sum f_j$$

If $A = 0$, taking moments about the origin, the first moment with $r = 1$ is the arithmetic mean M . The r th moment about the mean M is thus

$$m_r = \frac{\sum_{j=1}^k f_j (X_j - M)^r}{N} = \frac{\sum f (X - M)^r}{N} \quad \dots \text{A2.3}$$

If $r = 1$, $m_1 = 0$ (the first moment is zero), and if $r = 2$, $m_2 = s^2$ (the second moment is the variance).

In order to avoid particular units, dimensionless moments about the mean can be defined

$$a_r = \frac{m_r}{s^r} = \frac{m_r}{(\sqrt{m_2})^r} = \frac{m_r}{\sqrt{(m_2)^r}} \quad \dots \text{A2.4}$$

where $s = \sqrt{m_2}$ is the standard deviation. Since $m_1 = 0$ and $m_2 = s^2$, $a_1 = 0$ and $a_2 = 1$.

A2.2.2 Skewness

The skewness is the degree of asymmetry of a distribution. If a distribution has a longer 'tail' to the right of the central maximum than to the left, the distribution is said to be

skewed to the right and to have a positive skewness. The converse is true for a left skewed distribution. Many of the typical amplitude distribution histograms seen from APC2 show marked positive skewness.

For distributions, the means tend to lie on the same side of the mode as the longer 'tail', and hence an alternative measure of symmetry is supplied by the difference (Mean - Mode), made dimensionless on division by the standard deviation (a measure of dispersion), thus

$$\text{Skewness} = \frac{\text{mean} - \text{mode}}{\text{standard deviation}} = \text{Pearson's first coefficient} \quad \dots \text{A2.5}$$

To avoid use of the mode, an alternative measure of skewness is defined as

$$\text{Skewness} = \frac{3(\text{mean} - \text{median})}{\text{standard deviation}} = \text{Pearson's second coefficient} \quad \text{A2.6}$$

Another important measure of skewness uses the third moment about the mean, m_3 , or expressed in dimensionless form

$$\text{Relative skewness } (\sqrt{b_1}) = \frac{m_3}{(\sqrt{m_2})^3} \quad \dots \text{A2.7}$$

The relative value of skewness ($\sqrt{b_1}$) may be considered in relation to the normal distribution which has a relative skewness, $\sqrt{b_1}$, of zero (mean, median and mode are all equal), since it is perfectly symmetrical. Negative values of $\sqrt{b_1}$ indicate that the mean and median are less than the mode and thus the distribution is skewed to the left. Positive values of $\sqrt{b_1}$ indicate the converse.

A2.2.3 Kurtosis

The kurtosis is the degree of peakedness of a distribution, and is usually taken relative to a normal distribution. One important measure uses the fourth moment about the mean, m_4 , or expressed in dimensionless form

$$\text{Relative kurtosis } (b_2) = \frac{m_4}{(m_2)^2} \quad \dots \text{ A2.8}$$

The value of the relative kurtosis (b_2) for a normal distribution is 3, thus values less than 3 are less peaked, and values greater than 3 are more peaked than the normal distribution. A very peaked distribution is called leptokurtic, a very flat topped distribution, platykurtic, and the normal distribution which is neither very peaked nor flat topped, is called platykurtic.

**Appendix 3: The Marandy MR1004 Acoustic Emission System (A Manual For
RFPLOTS And RFGGRAPH - Acoustic Emission Analysis Software)**

The following manual describes the operation and use of the Marandy MR1004
amplitude distribution system and the AE analysis software packages RFPLOTS and
RFGGRAPH.

THE MARANDY MR1004 ACOUSTIC
EMISSION SYSTEM

School of Materials Science
University of Bath
Claverton Down
Bath
Avon BA2 7AY

August 1990

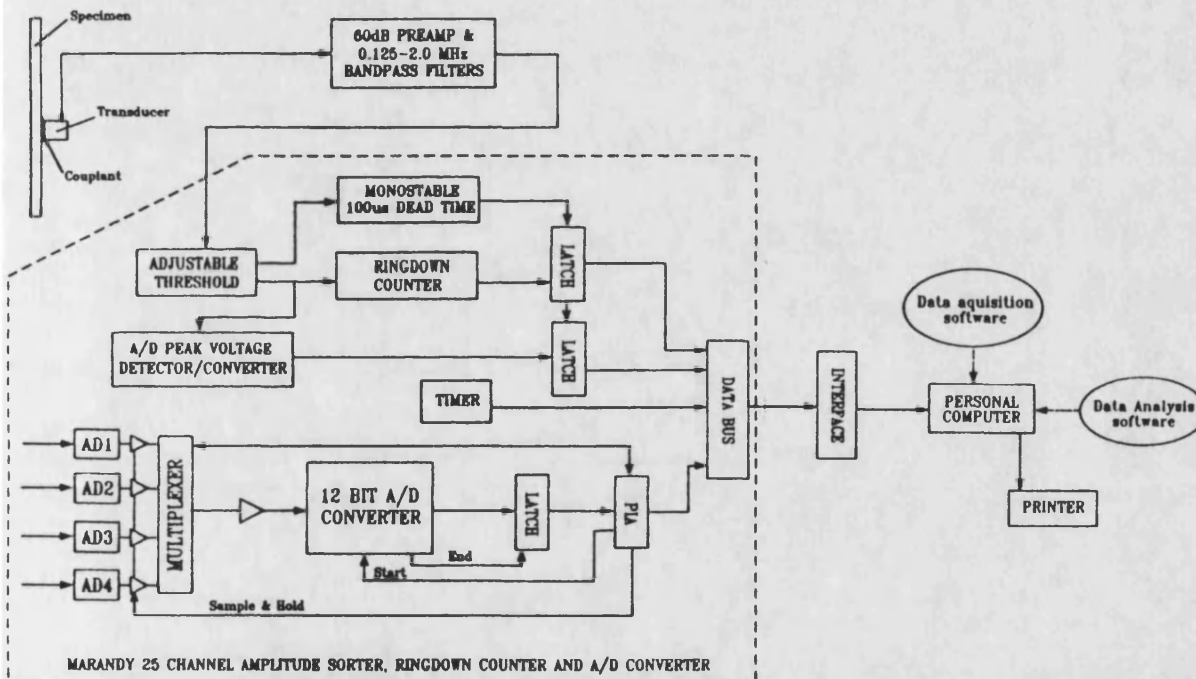
R Russell-Floyd

USING THE MARANDY MR1004 ACOUSTIC EMISSION SYSTEM

This manual covers the operation and use of the acoustic emission system based around the Marandy MR1004 25 channel amplitude sorter and ringdown counter, which is used in association with an IBM compatible PC (OPUS PCV) and printer.

Any problems with the acoustic emission system should be referred to Richard Russell-Floyd (3W 2.6).

The manual comprises two major sections, namely data collection and data analysis, preceded by a short introduction to the technique of acoustic emission amplitude distribution monitoring and followed by an appendix detailing AE binary file structure. A simple diagrammatic representation of the system is included below.



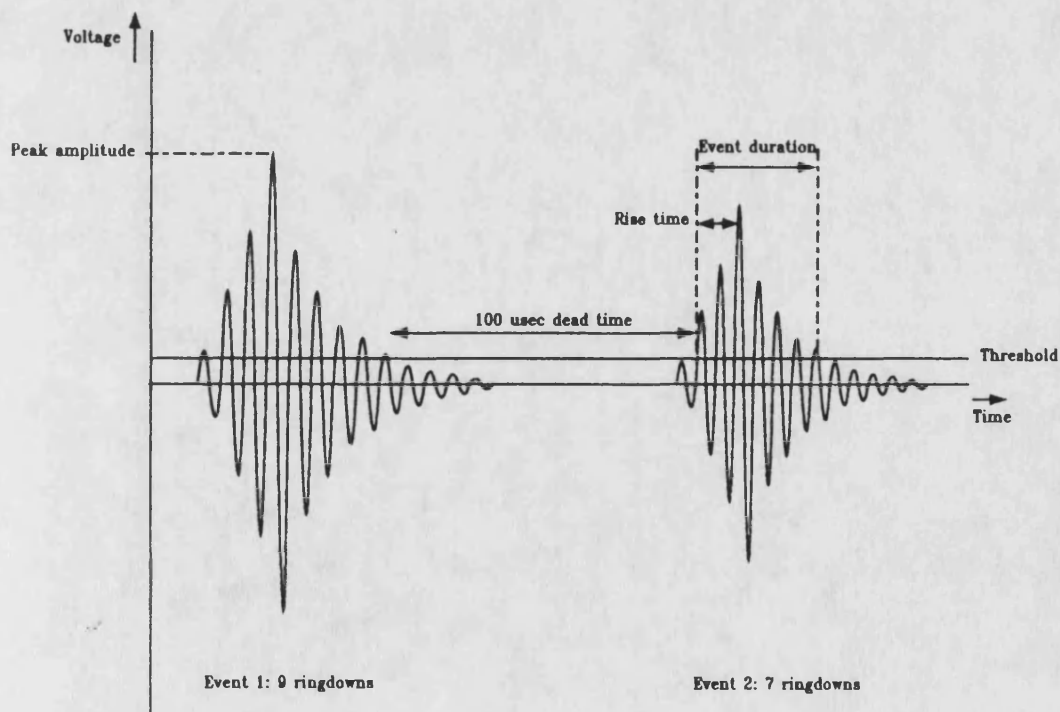
Diagrammatic representation of the Marandy MR1004 based AE amplitude distribution system.

Background

When a material is stressed, discontinuous deformation processes (such as reinforcing fibre breakage or spalling of a coating) can cause elastic energy to be dissipated as elastic stress waves, which spread in all directions from the source. These pulses, typically in the ultrasonic frequency range, are AE events and can convey (in coded form) information concerning the deformation processes which produce them. Analysis of these emissions is the basis of acoustic emission non-destructive testing, a technique started by Joseph Kaiser in the late 1940's. The technique was first applied to composites in the early 1960's, to investigate 'Polaris missile' filament wound glass reinforced plastic rocket motor cases.

Acoustic emission events are usually detected with a piezoelectric transducer coupled to the surface of the item under stress, often using a viscous liquid such as petroleum jelly. The transducer or probe converts the stress waves into a sinusoidal electrical voltage of low amplitude. Before being processed, this signal is passed through a preamplifier (typically 60dB gain) and often a high pass filter to cut off low frequency noise below around 100 kHz. Amplification is necessary because the voltages produced by the transducer are of very low amplitude and thus very susceptible to noise. Preventing the ingress of noise, whether mechanical or electrical, can be a major problem in acoustic emission testing. Various characteristics of AE pulses (which are essentially damped sinusoids) can be recorded and analysed.

The characteristics of the AE events, which are measured using the MARANDY MR1004, are the peak amplitude and the number of ringdowns per event. These characteristics may be explained by reference to the figure below, which shows two idealised acoustic emission events.



The characteristics of acoustic emission events.

An acoustic emission event is detected by virtue of an oscillation of the voltage from the transducer exceeding a minimum value (threshold). This threshold on the MR1004 is variable, but has a minimum value of 10 mV. Each of the excursions of the signal above threshold is called a ringdown. From the start of an event, these ringdowns increase in amplitude up to a maximum, then decay down to the background noise level. This maximum is the peak amplitude, the time taken to reach the peak is the rise time, the time from peak amplitude to the last ringdown of the event is the decay time and the summation of the two is the event duration. The peak amplitude of each event is sorted into one of 25 amplitude channels, each of which is 2.4 dB wide. The decibel scale gives the voltage amplitudes relative to a reference voltage which in this case is the minimum instrument threshold of 10 mV, thus

$$\frac{V}{V_i} \text{ ratio in dB} = 20 \log_{10} \frac{V}{V_i}$$

where V_i is the instrument threshold

Channel 1 will thus include events of peak amplitude from 10 mV (at the Marandy MR1004) to 13.2 mV, channel 2 from 13.2 mV to 17.4 mV and so on. Events of amplitude greater than 10 volts (the upper limit of channel 25) are recorded as "over range" in channel 26. An event is distinguished from the subsequent event by a dead time of 100 microseconds. Consequently, no excursions of the signal may occur for the dead time before a new event is deemed to have occurred. It is thus apparent that two events arriving in very quick succession will not necessarily be resolved into two separate events, a condition which is more likely to occur at very high event rates, such as near or at failure.

When a test is in progress, the MR1004 amplitude sorter/IBM PC system records both analogue data such as load or strain, and AE events with their channel numbers and ringdown counts onto the hard disk of the PC in binary format. This format of data recording is optimised for speed of data acquisition, but is less suitable for direct subsequent (post-test) analysis. The data must either be analysed using dedicated graph plotting and analysis software, or must be decoded into an ASCII format which can then be read into a spreadsheet software package (ie Microsoft EXCEL) for analysis and production of graphs. A real time amplitude distribution histogram, the total event count, test duration and the magnitude of analogue channel 1 are displayed on screen during a test. All other data presentation and graphing must be done post-test.

DATA ACQUISITION

Connections To The Marandy MR1004 Amplitude Sorter

The Marandy MR1004 amplitude sorter is interfaced to an IBM compatible PC via two interface boards:

- (i) A Metrabyte PI012 25 way parallel interface board (which is plugged into an 8 bit expansion slot within the IBM PC).
- (ii) The RS-232C serial port.

The cables facilitating these connections generally need not be disturbed.

On the front panel of the MR1004 are two input modules. The left-hand module is the AE input (misleadingly labelled 'channel 1') and the right-hand module is the analogue data input (labelled '12 bit a/d').

An acoustic emission transducer should be connected via a preamplifier (an AECL 60dB preamp with integral 0.125-2.0 MHz bandpass filters for example) to the AE input socket.

The BNC plug labelled 'monitor' is present for connection of an external oscilloscope to monitor the incoming AE events. Use of this connection is optional.

Up to 4 analogue data lines (such as load or strain) can be fed into the AE system via the 4 analogue input channels (the 4 BNC connectors labelled 'ad1 - ad4'). The MR1004 12 bit A/D sorter can accept voltages from 0 to ± 10 volts and thus has a voltage-measuring resolution of 4.88 mV. Always connect the analogue data lines to the lowest numbered A/D channels and where possible ensure that recorded voltages are positive in polarity. As an example, the load output from the Instron 1195 is typically connected to A/D1 (via an attenuator adjuster box which allows fine adjustment of the full scale output). If a second source of analogue data was to be recorded this would be connected to channel 2.

Pre-test preparations

Once all connections have been made to the MR1004 and PC, turn on both units.

On the PC, change directory to MARANDY (CD C:\MARANDY).

First run MRCAL and adjust the zero and full scale values of the A/D inputs. For ease of post-test analysis, it is important to adjust any analogue input voltages, for example, load, such that zero load corresponds to zero volts. Note that the analogue channels can only accept maxima of +10 V or -10 V and have a resolution of 4.88 mV. It is important to know which A/D channel each analogue data line is connected to, and the calibration conditions for each channel.

Next, check that the AE transducer is operating correctly by tapping the front face of this sensor and watching the green LED on the left front face of the MR1004 amplitude sorter. This light should flash each time an event is detected. The threshold adjustment on this instrument is calibrated to exclude events up to the start of channels 1 to 7. Noise, either electrical or mechanical, may be detected by the transducer. If this noise is of low amplitude it can be excluded with the threshold adjustment.

Running the data acquisition software

To run the data acquisition software (DAS), type MR1004 at the prompt.

Answer the questions which are asked by the program. Any invalid answers will result in an exit from the program. Note the following:

(i) Filenames in MS DOS (the PC's operating system) can have a maximum length of 8 characters followed by a full stop and a 3 letter extension. Always give the AE binary files, which MR1004 produces, the extension ".AEB" (standing for Acoustic Emission Binary).

(ii) The time interval, which can range from 10 ms to 600 seconds, governs how often the magnitude of the analogue A/D channels are recorded and thus the time resolution within the file. 1000 ms is a very commonly used time interval which causes the magnitudes of the A/D channels to be recorded every second.

To start data collection press 'B', and to stop type 'CTR S'. The real time amplitude distribution and total event count on screen will give the operator an indication of the AE activity which is occurring. Duration of test and the magnitude in mV of analogue channel 1 (ad1) are also displayed. Data analysis is carried out post-test.

It is important that the operator copies all acoustic emission binary files onto floppies for safe storage and erases the original files from the hard disk to leave space for subsequent use.

DATA ANALYSIS

As previously mentioned, the acoustic emission files produced by the MR1004 amplitude sorter are a compact binary format, and unsuitable for direct analysis (they are totally illegible). There are two methods of data analysis.

1. The files can be analysed using a dedicated graph plotting and analysis package using the original binary file format or via a second file format (ASCII). A software package called RFGGRAPH has been developed, which is dedicated to Marandy MR1004 and DCOL file analysis and graph plotting.

2. The files can be converted into the ASCII format mentioned earlier, which is then read into any commercial spreadsheet package such as MS Excel for graph plotting and manipulation/analysis. The program RFPLOTS.EXE has been developed to carry out the production of ASCII files from the source binary files and, in addition, can be used to analyse some of the AE data i.e. some statistical analysis and production of amplitude distributions histograms. The following two sections deal with the use of these two programs - RFPLOTS.EXE and RFGGRAPH.EXE.

Five main programs are resident in the directory 'C:\RRFTMP';

MR1004.EXE,	the data acquisition program,
MRCAL.EXE,	a program which displays the voltages on each of the 4 A/D channels for calibration purposes,
RFPLOTS.EXE,	the file decoding and analysis program
RFGGRAPH.EXE,	the AE data graph plotting, decoding and analysis program.
RFSPPOOL.EXE,	a graph spooling utility.

RFPLOTS

RFPLOTS (Acoustic Emission Decoding and Analysis Program)

To run, type 'RFPLOTS'. The program will ask whether you wish to analyse Marandy or DCOL5 files. Answer 'M' for Marandy. DCOL5 files are now an out-of-date format produced by the AETC 203/MINC 23 acoustic emission system.

MAIN MENU

MENU	MR1004
------	--------

File input menu	1
OS Shell	2
AUTO decoding	3
Set defaults	4
Information	5
Histograms	6
Directory	7
Statistics	8
Graph plotting	9

CURRENT BINARY FILE IS PE010002.AEB
CURRENT ASCII FILE IS PE010002.CSV

The main menu shown above gives the different functions and options available. It is essential that the operator always selects the directory within which the AE binary files (.AEB files) are located, before attempting to select files for decoding. Use option 7 to set the directory path name.

The Different Menu Options

The different menu options shown above will be described in numerical order.

DECODING SELECTION	MR1004
---------------------------	---------------

Binary filename	PE010002.AEB	ASCII filename	PE010002.CSV
Start time (secs)	25	A/D channel	none
Stop time (secs)	150	*Start point (mV)	0
A/D 1 f'scale	20000	*Stop point (mV)	max
A/D 2 f'scale	10000	Threshold	0
A/D 3 f'scale	10000	*Start event	0
A/D 4 f'scale	10000	*Stop event	Max
BINARY decode	decode	ASCII (Y/N)	Y

Current directory : C:\MARANDY	* not in use
A/D inputs used : 1	
Time interval (ms) : 1000	
File length (bytes): 466944	

This sub menu controls the normal decoding of binary files and the production of 'comma separated value' (.CSV) files for subsequent reading into a spreadsheet for further manipulation and graph plotting of the data. The menu allows the operator to input the binary file name, the ASCII file name (the name of the .CSV file to be generated), full scale values for the A/D channels and the time portion of the test which is analysed (decoded). The cursor is used via the cursor keys to move between the different input positions on the menu. When a binary filename is input, the file header information is read and displayed at the bottom of the menu. The time interval between each A/D channel sampling is displayed, as are the A/D inputs used in the file, the file length and the current directory.

'Start time' and 'stop time' inputs allow the operator to select the portion of the file (with respect to time) which is decoded. If 'stop time' is given as zero or 'END', decoding will proceed to the end of the file.

The full scale input values are simple scaling factors for the voltages recorded on the A/D channels. The default scaling factor of 10,000 will yield A/D data in terms of millivolts.

The 'threshold' value allows the operator to exclude all events from below the 'threshold' value set before decoding.

To produce an ASCII .CSV file, the operator must select 'Y' at the ASCII (Y/N) input position. Use the carriage return key to toggle between 'Y' and 'N'.

When all decoding selection parameters are correct, move the cursor to the 'BINARY decode' position and press carriage return. The binary file will now be decoded. The progress of the decoding is shown by a percentage of file completed in the top left of the menu screen. When decoding is complete you will automatically be returned to the main menu. The decoding process, in particular the .CSV file generation, is not a particularly

COMMAND FILE PRODUCTION

```

ENTER COMMAND FILE NAME      COMFILE1.CSU
AE FILENAME                  PE010002.AEB
FULL SCALE (a/d 1)          20000
FULL SCALE (a/d 2)          10000
FULL SCALE (a/d 3)          10000
FULL SCALE (a/d 4)          10000
Start time (ms)             25000
End time (ms)               150000
Full scale on histograms    5000

```

```

APPEND TO COMMAND FILE (Y/N)  Y

```

Use this section of the program to write a command file. The input parameters have the same definition as for the main input menu.

Options 2 - 4 will append one line of the specified data to the end of the specified file. This is performed for each AE file, or section thereof, which is specified in the command file. A truncated form of the sort of file produced from option 2 ('GENERATE LOAD/GENERAL AE DATA') is shown below:

Filename,	Total events,	Channels(1-5),	Channels(5-10),....
AEL011.AEB,	46399,	5551,	8324,.....
AEL012.AEB,	28242,	4222,	5339,.....
AEL013.AEB,	37723,	5912,	6847,.....
AEL014.AEB,	31279,	5158,	5573,.....
AEL015.AEB,	35216,	5756,	5755,.....

GENERATE LOAD/GENERAL AE DATA 2

This function calculates all the data normally viewed in the INFO display sheet (see later) but records the data in ASCII file CSV format into one file with data from each .AEB file recorded on subsequent lines. The file can then be read into a spreadsheet package.

GENERATE MOMENTS DATA 3

This function determines all the statistical parameters viewed in the MOMENTS review sheet. These parameters are then recorded in one ASCII .CSV file, with data for each file listed row by row for transfer into a spreadsheet package.

GENERATE CHANNEL NUMBER DATA 4

This function records the total number of events in each of the 26 channels for each file and time period combination given in the command file and records this data in an ASCII CSV file for reading into a spreadsheet.

GENERATE FULL ASCII FILES

5

This function produces a full ASCII file (35 columns) for each of the files in the command file. This is the auto version of the ASCII file generation function in the main input menu. Note that the .CSV files produced are automatically named by taking the main filename of the binary file and adding the .CSV extension. It is therefore essential that the original binary files have a different extension (namely '.AEB').

AUTO HISTOGRAMS

6

This function automatically produces the amplitude distribution histogram for the prescribed time periods and the prescribed full scale values in the command file and prints them on an attached Epsom compatible dot matrix printer.

AUTO PRINTOUTS

7

This function automatically produces the information sheets found in INFO and produces a hard copy on the printer.

GENERATE SINGLE THERMAL CYCLE FILE

8

This function is for the generation of ASCII files from CARE project thermal shock tests and will therefore not be described.

DEFAULT SETTINGS

4

DEFAULT SETTINGS

Decode display active (Y/N)	N
Cycle counter channel number (1-4)	3
Printer scrolling active (Y/N)	N
Time factor	1
Include AE in ASCII files (Y/N)	Y
Threshold level (inclusive)	0
Thermal cycle temp conversion (Y/N)	N
Thermal cycle ascii file (Y/N)	N
Front face a/d channel (0,1,2,3)	0
Max cycle duration (s)	105
AD1 zero point (mV)	0
AD2 zero point (mV)	0
AD3 zero point (mV)	0
AD4 zero point (mV)	0
CHANGE DEFAULTS (Y/N)	N

This menu allows the control of various default settings used by the program. Most of these parameters are used for special CARE project thermal shock test analysis. The few of these defaults which are generally applicable will be explained.

1. IF 'Decode display' is active, the magnitude of the A/D channels , the event rate and time are displayed on screen as the binary file is being decoded.
2. If the 'Printer scrolling active' option is set to 'Y' then the scrolling of the printer can be controlled by the operator via the program.
3. The option 'Include AE in ASCII file' controls whether full sized or truncated ASCII .CSV files are produced when binary files are decoded. The normal ASCII .CSV file format contains the following columns of data: time, cumulative event count, cumulative ringdown count, total event rate, ringdown rate, the A/D channels 1 to 4 and the

cumulative event count in each of the 26 amplitude channels. Thus, the full sized ASCII file contains one row of 35 columns of data for each 'sampling time interval' increment, which will be every second if a sampling time interval of 1000 ms has been used. A truncated ASCII file does not contain the last 26 columns of AE cumulative event count in each amplitude channel and is therefore considerably smaller in size.

INFORMATION

5

FILE ANALYSIS INFORMATION

=====

AE BINARY FILENAME	= PE010002.AEB	Total AE events (1-26) = 37275
Default directory	= C:\MARANDY	total AE events (1- 5) = 15469
ASCII filename	= PE010002.CSV	total AE events (6-10) = 5192
		total AE events (11-15) = 2130
A/D channels used	= 1	total AE events (16-20) = 4228
Time interval (ms)	= 1000	total AE events (21-25) = 7417
Start time (s)	= 25	
Endtime (s)	= 150	MEAN event amplitude = 11.656
Duration of test (s)	= 125	Max number of events = 7494
		in channel = 2
A/D 1 fscale	= 20000	Total ringdowns = 1484063
A/D 1 max wrt fs	= 4410	Events missed = 0
		Events above 25 = 2839
		Events with no ringdowns = 78

EVENTS IN EACH CHANNEL:

PE010002.AEB

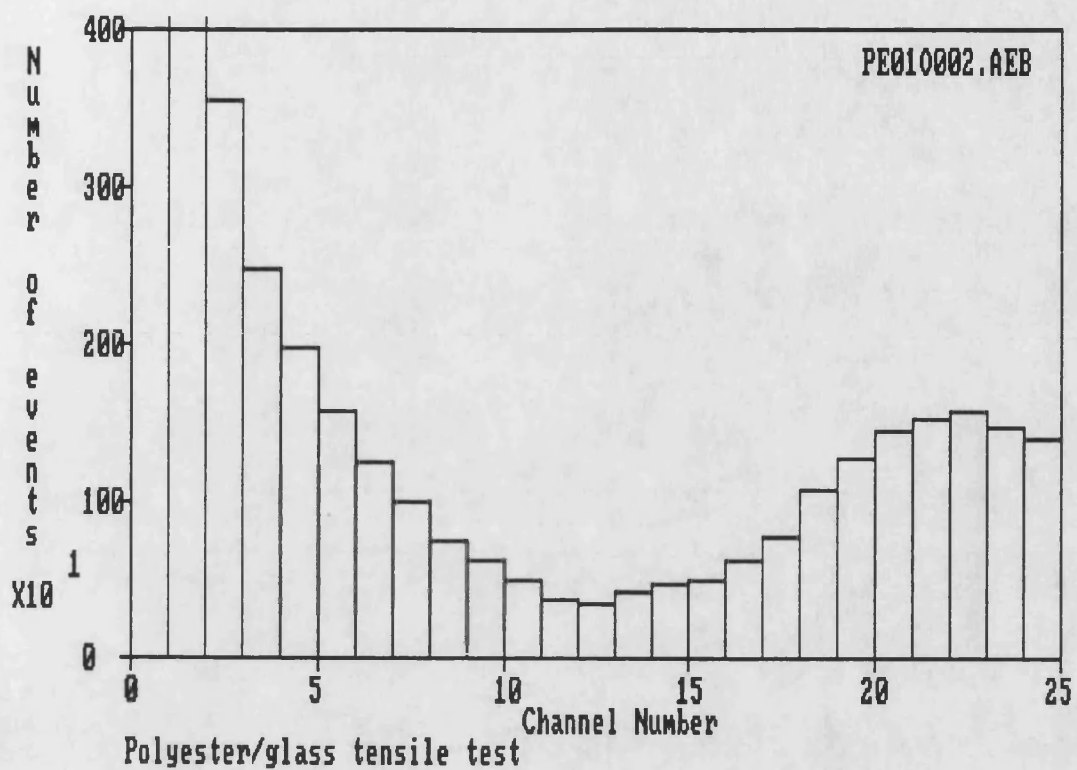
Channel 1 = 0	Channel 14 = 420
Channel 2 = 7494	Channel 15 = 466
Channel 3 = 3538	Channel 16 = 493
Channel 4 = 2464	Channel 17 = 616
Channel 5 = 1973	Channel 18 = 787
Channel 6 = 1578	Channel 19 = 1065
Channel 7 = 1240	Channel 20 = 1267
Channel 8 = 991	Channel 21 = 1444
Channel 9 = 749	Channel 22 = 1536
Channel 10 = 634	Channel 23 = 1577
Channel 11 = 498	Channel 24 = 1469
Channel 12 = 387	Channel 25 = 1391
Channel 13 = 359	Channel 26 = 2839

Above is a typical example of the information displayed by this option.

This option displays a variety of useful review data about the last file or section of a file decoded. The description of the data produced on screen is self evident, but includes such parameters as maximum values recorded on each of the A/D channels, cumulative event counts in five channel ranges, cumulative event counts in all 26 channels and duration of test.

HISTOGRAM

6



This option produces an amplitude distribution histogram of all events recorded in the last decoded file or section of file. A full scale value for the vertical axis must be given. Histograms on screen can be printed out using the 'Print Screen' key on the key board.

DIRECTORY

7

This option is used to type in the directory in which the binary (.AEB) files are located. The full path name must be typed in when changing the directory, for example 'C:\MARANDY\DATA'.

MOMENTS OF THE HISTOGRAM

=====

Mean	= 10.473	Filename	= PE010002.AEB
Median	= 7	Start time (s)	= 25
Mode	= 2	End time (s)	= 150
Variance	= 70.352		
Standard Deviation	= 8.388		
		Jon's Parameters	
Skewness	= 296.579	Variance	= 2898.753
Pearsons coef 1	= 1.0102	Standard Deviation	= 53.8409
Pearsons coef 2	= 1.24227	Skewness	= 14898095
		Kurtosis	= 98159640576
Kurtosis	= 7894.76	Relative Skewness	= 95.4583
		Relative Kurtosis	= 11681.8193
Relative Skewness	= .5026	Quasi energy	= 360658
Relative Kurtosis	= 1.5951	Norm' Energy	= 48.1262
n	= 34436	Channels 1 - 25	

This menu option produces a variety of statistical parameters about the current amplitude distribution. Above is a typical example. The statistical parameters are determined for the probability function $p(x_i)$ being the probability of an event occurring in amplitude channel $i = 1, 2, \dots, 26$. The moments of the distribution are defined in appendix 1 of this manual.

GRAPH PLOTTING

9

Graph plotting within this package is limited to the production of histograms already mentioned.

To escape from RFLOTS press CTRL and BREAK together.

READING THE DECODED .CSV FILES INTO A SPREADSHEET

Once the appropriate binary files or section of binary files have been decoded into ASCII CSV format the data can be read into a spreadsheet. The most widely used spreadsheet package currently available at Bath, and the one recommended for AE graph plotting, is Microsoft EXCEL. In EXCEL, the .CSV files can be read directly in without any further manipulation. This is because the '.CSV' file extension tells EXCEL what format to expect. EXCEL has been installed on most of the PCV computers within the department, including the AE data acquisition PCV (next to the 1195 INSTRON) and the AE data analysis PCV in the Computer Room. The latter machine has an expanded memory board fitted and can therefore handle much larger AE files than the standard machines. To run EXCEL just type 'EXCEL' at the prompt. Manuals for this package are retained in 3W2.6.

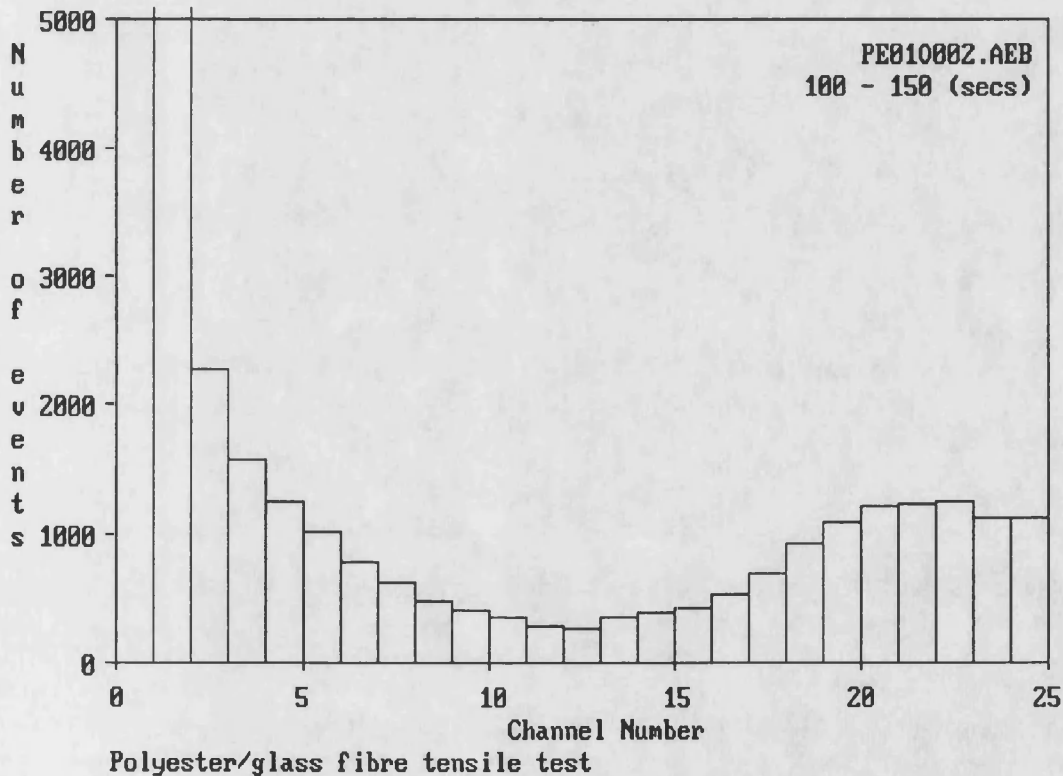
RFGRAPH

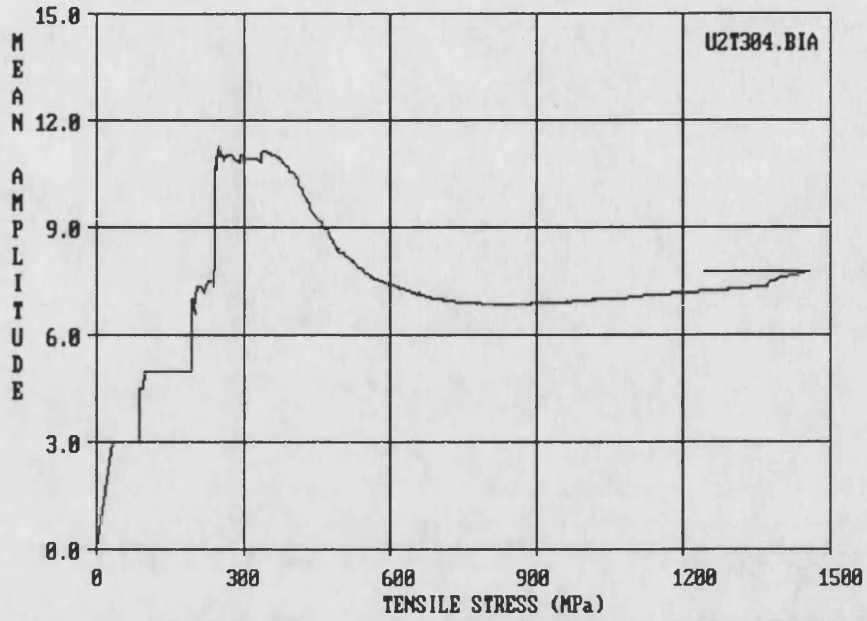
RFGRAPH (Acoustic Emission Decoding, Graph plotting and Analysis Program)

RFGRAPH will run on any IBM compatible PC with hard disc and EGA or VGA monitor. The program requires various files in addition to the main program file to run correctly. All such files are contained in the sub-directory 'C:\RRFTMP'. The AUTOEXEC.BAT file in the root directory of the boot disc must contain the statement 'PATH C:\RRFTMP'.

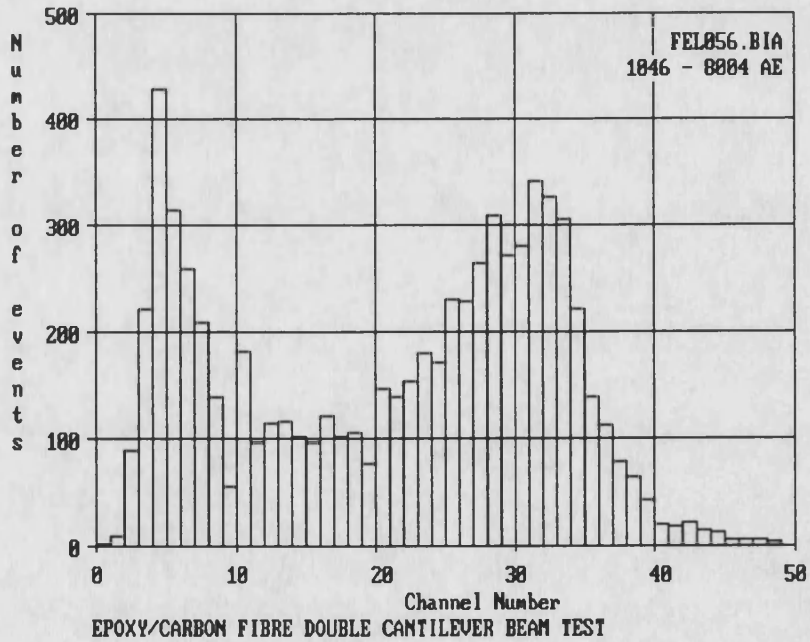
The program is based around a main menu which allows quick selection and adjustment of the X/Y graph parameters, full scale readings on graphs, default and decoding sub menus. From the main menu, graphs are plotted on screen, after which a sub menu allows editing, saving and printing of the graph and, in the case of histogram plots, access to information/statistical data screens. The program will now be described and explained in more detail. Note that capitals should always be used on the main menu.

Some examples of the types of graphs produced by RFGRAPH are shown below:





Mean amplitude versus stress during a tensile test of 8-ply UD APC2



EPOXY/CARBON FIBRE DOUBLE CANTILEVER BEAM TEST

To run, RFGRAPH, just type 'RFGRAPH' at the prompt and the main menu will then be displayed.

MAIN MENU

BINARY		GRAPH PLOTTING		PE010002.AEB	
Load N	AD 1	Percentage share	PS		
AD2 in mV	AD2	Mean amplitude	MA		
AD3 in mV	AD3	Variance	VA		
AD4 in mV	AD4	Kurtosis	KU		
Time in seconds	TI	Skewness	SK		
X Total AE events	CE	Relative kurtosis	RK		
Total ringdowns	CR	Relative Skewness	RS		
AE in channels	EC	Ringdowns/event	RE		
Total event rate	TR	Histogram wrt A/D	HL		
Event rate in chs	SR	Y Histogram wrt time	HT		
Histogram wrt events	HE	Ringdown rate	RR		

Y axis scale	min: 0	max: 5000	Cumulate : Y
X axis scale	min: 0	max: 20000	A/D ch : 1
Channel no	min: 1	max: 50	
Hist range	min: 100	max: 150	

The main menu is shown above. The operator is always returned to this menu after any operation. The menu is cursor controlled. A blue cursor is moved around the screen with the keyboard cursor keys. Selections and adjustments are made by placing the cursor at the appropriate location and giving the relevant information/commands as described below.

BINARY or ASCII: RFGRAPH can operate on either the binary acoustic emission files (.AEB) produced via data acquisition or from ASCII files (.CSV) produced by decoding binary files into comma-separated value 35 column files. The correct file type should be selected by placing the cursor at the top left position and pressing B - binary or A - ASCII. The same graphs can be produced from either binary AE files or from decoded ASCII .CSV files. In general terms, graph plotting is fastest from binary AE files when the data in the files is predominantly analogue (A/D), and from ASCII files when there are many AE events.

Filename.AEB: The acoustic emission data file name is input top right in the menu. When the filename is input, the program checks that the file exists in the current directory. If it does not, an error message is given. The directory must be changed accordingly, using the F3 function key to temporarily escape to DOS, and typing in the appropriate change directory command (for example 'CD c:\marandy\DATA'), before returning to RFGRAPH by typing 'exit'. Do not attempt to give path names preceding the filename on the menu.

Selecting variables for plotting: Any one of a total of 19 different parameters can be plotted as either the X axis or Y axis on an X/Y line graph. The description of these parameters is self evident from the menu. Three further parameters are available as histograms. The X and Y axis variables are selected by moving the cursor to the

appropriate position on the screen and pressing 'X' or 'Y' respectively (ensure that capitals are used). Histogram options are selected as the Y axis, in which case the X axis is automatically set as amplitude channel number.

X and Y axis scales: The X and Y axis scale are set by the operator. There is no auto scaling.

Channel number: Channel number min and max give the range of channels which are summed and plotted with the 'AE in channels' and 'Event rate in chs' variables. In addition, this channel range is used for the determination of the information screens (see later), most importantly, determination of moments of the amplitude distribution histogram. This allows statistical analysis of the AE data to be directed at specific amplitude ranges. The range between maxima and minima inputted values are inclusive (for example min = 1, max = 5 gives channels 1,2,3,4 and 5).

Hist range: Hist range is the range over which events are cumulated to produce an amplitude distribution histogram (and information sheets). The units of this range depend on which of the three histogram options have been selected:

Histogram wrt events: Hist range gives the range of cumulative events in all channels, for example min = 500, max = 1000 will produce a histogram of 500 events starting with event 500 and finishing with event 1000.

Histogram wrt A/D: Hist range will cause the program to search through the sequential A/D values in the A/D channel selected (see *A/D ch* below) until it finds the first value exceeding hist range min within the specified time period of the AE data file. It will then cumulate all events from this point in the data file until it finds an A/D value in the selected A/D channel which is smaller than or equal to hist range max. The specified time period of the file, over which this search is conducted, is given by the X axis scale (otherwise redundant for histogram graph plotting) with units in seconds. For example, if X axis min is 50 and X axis max is 100, then the search will be conducted starting from time 50 seconds and finishing at time 100 seconds

Histogram wrt time: Hist range will cause the program to cumulate all events recorded between the start time of hist range min and finish time of hist range max, units in seconds.

A/D ch: This is the analogue input channel number which is used for the selection of events for production of histograms with respect to A/D. Allowable values are 1,2,3 or 4 (A/D channel 1,2,3 and 4 respectively).

Cumulate: This option determines whether the variables, such as mean amplitude and variance are determined from the cumulated amplitude distributions, or from distributions of events over each time increment (effectively the equivalent of a rate). Enter 'Y' for events cumulated from time zero (start of file) and 'N' for events cumulated only over each individual time increment.

Function keys

Whilst the operator is using the main menu, there are further functions available through use of the function keys.

F1 Help Screen

FUNCTION KEYS	
F1	Shows this help screen.
F2	Amend full scale settings for binary file decoding.
F3	Escape temporarily to DOS. Type 'EXIT' to return.
F4	Display a graph.
F5	Change graph caption.
F6	Save Current graph to a file. The graph file name must have the extension .PIC.
F7	Print current graph direct to printer.
F8	Set defaults.
F9	Call information menu (after plotting a histogram).
F10	Save current default settings.
F11	Plot a new graph
F12	Plot a graph line over the previous graph

The F1 function key displays the help screen shown above, giving a short explanation of the operation of each of the function keys.

F2 Binary File Decoding Menu

FILE DECODING PARAMETERS	
=====	
Binary file name	: FEL056.BIA
ASCII file name	: none
Time interval (ms)	: 1000
AD1 full scale	: 5000
AD2 full scale	: 100
AD3 full scale	: 10000
AD4 full scale	: 10000
Change zero points (Y/N)	: N
Decode BIN to ASCII (Y/N)	: N

The F2 function key gives access to a sub menu for decoding AE binary files and production of ASCII .CSV files. It is recommended that any ASCII files are given the .CSV extension to differentiate them from binary files (.AEB). The A/D full scale readings are used by the program whenever a binary file is either decoded into ASCII or for graph plotting. A full scale reading of 10000 will caused the analogue data to be given in mV (the original form in which it was recorded), since all the A/D channels operate with respect to a full scale reading of + 10 volts or -10 volts. If for example, the

load from the Instron 1195 was recorded on analogue channel 1 and the Instron load cell was set to 2000 N giving a 5 Volt output to the Marandy, then 4000 should be entered in the menu shown above. This assumes that zero load gives zero voltage. If it does not, then the zero points for each analogue channel can be set to the appropriate non-zero value. To decode a binary file and produce a .CSV file, just answer 'Y' at the bottom location in the menu. A 35 column .CSV file will then be produced. Depending on the size of the data file, this will take from a few seconds to some minutes. Once decoding is complete, you will be returned to the main menu. Note that if you do not wish to alter an entry in this menu, just hit the carriage return (enter) key and the cursor will move down one line. Continue doing this to the bottom of the menu and you will be returned to the main menu.

F3 Escape temporarily to DOS

This function key exits the user temporarily to the MSDOS operating system, where all DOS commands can be used. The most important of these is the 'CD directory' - change directory command. To return to RFGGRAPH simply type 'EXIT' followed by a carriage return.

F4 Display a graph

This function allows the user to display, on screen, any previously produced and recorded graph, by entering its filename. If no filename is given, then the graph which was last shown on screen is displayed.

F8 Default Settings

DEFAULTS			
Marandy (M) or DCOLS	(D)	D	
Filename on graph	(Y/N)	Y	
Gridlines on graph	(Y/N)	Y	
Time factor	(secs)	1	
Info sheet	(Y/N)	Y	
Graph axes color	(0-63)	15	
Graph gridline color	(0-63)	7	
Time conversion factor		1	
Write graph to file	(Y/N)	N	
Special functions	(Y/N)	N	

The F8 function key accesses a sub menu of default settings. These will be explained in sequential order.

Marandy (M) or DCOLS: Always leave this option as shown above, namely 'M' for Marandy. The older DCOLS system/file type is no longer in use.

Filename on graph: If 'Y' is entered, then the file name of the data file used to produce the current graph will be plotted at the top right-hand corner of all graphs.

Gridlines on graph: This will draw grid lines (bright purple) on all graphs which will be recorded and printed. These lines should not be confused with the light grey grid lines which appear on all graphs, but which are not recorded with the graph and are not printed.

Info sheet: If 'N' is selected, then the program will not determine the information required for the information sheets. This accelerates the running of the program.

Graph axes colour: This sets the colour of the graph axes on screen. Colours from 0-64 are available.

Graph grid lines colour: This sets the colour of the grid lines printed on graphs. Colours from 0-64 are available.

Write graph to file: If 'Y' is selected, then whenever an X/Y graph is plotted, the program will ask for a file name. Both X and Y values are recorded in two columns in the ASCII .CSV file. This therefore allows any graph produced on screen to be reproduced using an spreadsheet/graph plotting package in whatever format is required.

Special functions: Leave this option as 'N'. Special functions have been included within the program for specific research applications.

Note: If you do not wish to alter an entry in this menu, just hit the carriage return (enter) key and the cursor will move down one line. Continue doing this to the bottom of the menu and you will be returned to the main menu.

F10 Save current default settings

Pressing F10 records all operator-controlled settings so that they will automatically be loaded in with the program when next run.

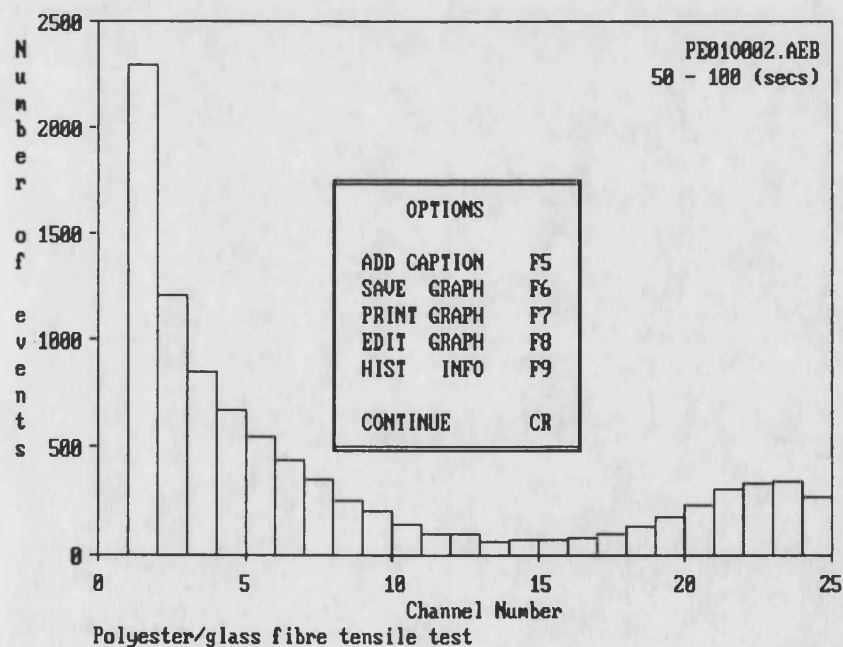
F11 Plot a new graph

A graph will be plotted on screen using all the current settings.

F12 Plot a graph line over the previous graph

A graph line will be plotted on screen using all current settings. This graph line is superimposed upon the graph which was last displayed on screen. Only the graph line itself will be plotted (no new axes, labels, etc).

MENU/OPTIONS AFTER PLOTTING A GRAPH



Once the graph has been plotted, the post-graph options menu shown above will be displayed on screen by hitting any key.

ADD CAPTION F5

A single line of text may be input. This text will be automatically printed underneath the graph as a caption each time a graph is plotted.

SAVE GRAPH F6

After hitting F6, the program will ask the operator for a file name to which an image of the screen will be saved. The filename should always have the .PIC extension. Each graph file will be approximately 33 kbytes long.

PRINT GRAPH F7

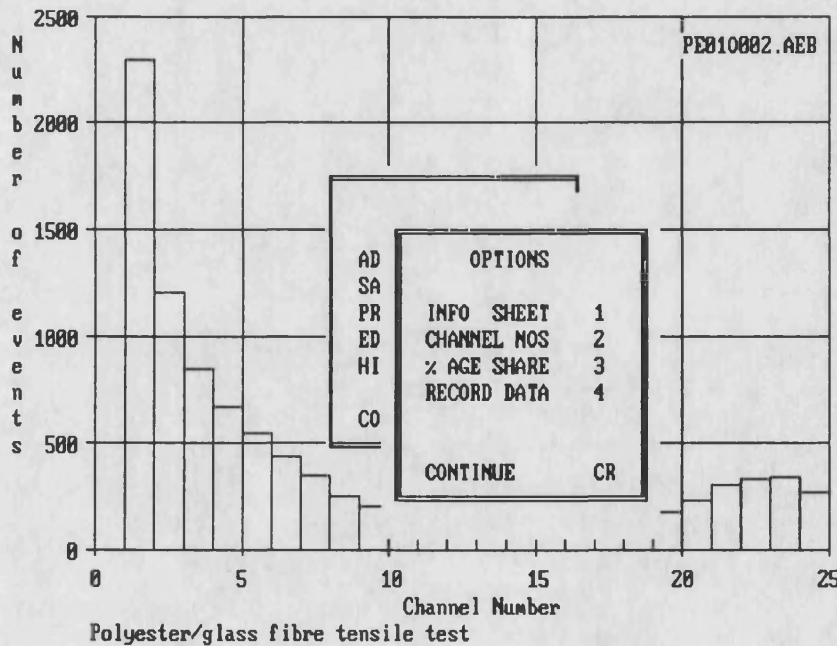
Hitting F7 will print the current graph directly via the parallel printer port to a 24-pin Epsom compatible dot matrix printer. The printer driver will operate correctly with the NEC P2, P6 and P7 and printers available around the department. Graphs are printed half-page size in the portrait orientation. Instead of printing graphs individually, the operator can save multiple graphs to disc and then spool them (print out a list of files). This can be performed by quitting RFGGRAPH (quitting RFGGRAPH is carried out by either hitting 'ctrl break' or 'esc'), then running 'RFSPPOOL'. This utility will display all files with the .PIC extension (all graph picture files). The files can be selected with the cursor and the enter key, de-selected with the F1 key, viewed by hitting 'V' or spooled by hitting 'S'.

A memory resident utility program named 'EGA2EPS.ZOO' is available on the hard disc which will capture and convert the graphs into postscript files for laser printing.

EDIT GRAPH F8

Hitting F7 will place the program into edit mode, in which a small cursor is displayed on screen. This cursor can be moved around the screen with the cursor keys, and text can be typed onto the screen at the required locations. Hitting the escape key will return the operator from the edit mode to the post-graph menu.

HIST INFO F9



This post-graph option is only available after plotting a histogram. A variety of numerical information is tabulated in information screens. A sub menu, shown above, gives the different options available.

INFO SHEET

1

HISTOGRAM INFORMATION (MARBANDY)

Parameter	Min (start)	Max (end)
Time (s)	50	100
AD 1	675	919.5
AD 2	0	0
AD 3	0	0
AD 4	0	0
AE Total	505	10107
AE (1-5)	352	5372
AE (6-10)	132	1918
AE (11-15)	21	493
AE (16-20)	0	551
AE (21-25)	0	1477
Ringdowns	3638	272898
Channels	1	50

Parameter	Value
Mean	8.9888
Median	5
Mode	2
Variance	65.9532
Std Dev	8.1216
Skewness	522.8138
Rel Skew	.9761
Pearsons 1	.860516
Pearsons 2	1.47339
Kurtosis	10306.439
Rel Kurt	2.3694
Energy	145.825
XVariance	944.814
XStd Dev	30.739
XSkewness	1555891.375
XRel Skew	53.575
XKurtosis	3129459712
XRel Kurt	3505.715

Filename : PE010002.AEB n : 9602

The meaning of the information given in the information sheet should largely be self-evident. Each time a histogram is plotted, the program searches through the current AE file and accumulates the appropriate acoustic emission events recorded over a specified time period, cumulative event count interval or range of analogue input (for example load range). Over this interval of the file, the program records the maximum and minimum values of time, A/D values (scaled according to the scaling factors given in the F2 sub menu). The cumulative events in the specified channel ranges at the start and end of the appropriate interval of file are also displayed. In addition, having determined the number of events in each channel for the specified portion of the file, various statistical parameters are determined from the amplitude distribution histogram. These parameters are displayed in the right hand column of the screen and include the first four moments of the distribution (mean, variance, skewness and kurtosis), in addition to other parameters such as energy and some experimental AE parameters (first character 'X'). The definition of these parameters is given in Appendix 2. These AE parameters are determined over the channel range specified in the main menu (for example channels 0 to 25 inclusively in the information screen shown above). This allows selected portions of the amplitude distribution histogram to be analysed.

CHANNEL NOS 2

EVENTS IN EACH CHANNEL:

PE010002.AEB

Channel 1 = 0	Channel 14 = 65
Channel 2 = 2291	Channel 15 = 72
Channel 3 = 1207	Channel 16 = 67
Channel 4 = 848	Channel 17 = 82
Channel 5 = 674	Channel 18 = 96
Channel 6 = 543	Channel 19 = 131
Channel 7 = 439	Channel 20 = 175
Channel 8 = 346	Channel 21 = 231
Channel 9 = 253	Channel 22 = 307
Channel 10 = 205	Channel 23 = 334
Channel 11 = 142	Channel 24 = 336
Channel 12 = 97	Channel 25 = 269
Channel 13 = 96	Channel 26 = 296

This screen gives a listing of the numbers of events in each channel range over the selected portion of the AE file.

% AGE SHARE 3

PERCENTAGE SHARE
=====

Percentage share channels (1 - 5)=	52.281	%
Percentage share channels (6 - 10)=	18.6	%
Percentage share channels (11 - 15)=	4.916	%
Percentage share channels (16 - 20)=	5.738	%
Percentage share channels (21 - 25)=	15.382	%

This option displays the percentage share of events in each of five channel ranges. The percentage share is defined as:

$$\frac{\text{Number of events in selected channel range}}{\text{Number of events in all channels}} \times 100\%$$

RECORD DATA 4

This option allows the operator to record all the data displayed in the three histogram information screens to an ASCII .CSV file. The program asks for a file name to which to write the data. The first row of the file gives a description of the contents of each column of data. If the file already exists, then the data is appended to the end of the file. This will allow the results of analysis of different AE files (tests) to be recorded in the same file, for subsequent correlation studies for example.

PLOTTING A GRAPH

To plot a graph, enter the appropriate file name and file type in the main menu, select the X and Y variables by hitting 'X' and 'Y' with the cursor over the appropriate variables and then hitting the F11 function key (histograms are selected with a 'Y' only, the 'X' selection then being ignored). The graph axes, labels, scales etc will then be drawn on

screen. The graph line will be drawn at the rate at which the program decodes/analyses the file. Pressing the escape key will halt graph plotting. Once the end of the file has been reached, the filename is plotted in the top right corner of the graph and caption underneath. Hitting any key will produce the post-graph menu on screen, which will then allow the operator to alter the caption, save, print or edit the graph. If the graph produced is a histogram, then the post-graph menu will give access to the information screens.

Control of the graphs produced on screen is achieved through the main menu. The annotated graph shown below gives a review of how to alter/control the graph plotting.

Graphs can be printed directly on an Epsom compatible 24-pin dot matrix printer. Graphs can also be printed as postscript files on a laser printer by typing 'EGA2EPS' followed by a carriage return before running RFGGRAPH. When the appropriate graph is on screen, press the ctrl shift and Z keys together. This will produce a postscript file of the current graph with the extension .EPS.

Graphs can also be linked to a word processing document using a screen capture program. For example, if using Microsoft WORD5, run 'CAPTURE' before running RFGGRAPH. Pressing the shift and print screen keys when a graph is on screen will cause an image of the graph to be recorded as a .SCR file. This file can be linked into a document with the Library Link Graphics command.

Grid lines can be plotted by setting the appropriate default (F8 in the main menu) to 'Y'

If the graph line goes off scale, then re-plot the graph with larger full scale settings

The filename will be plotted in the top right hand of the axes box unless the appropriate default (F8 in the main menu) is set to 'N'

With the exception of A/D channels 1 to 4, the labels on the axes can only be changed by overtyping in the graph edit mode

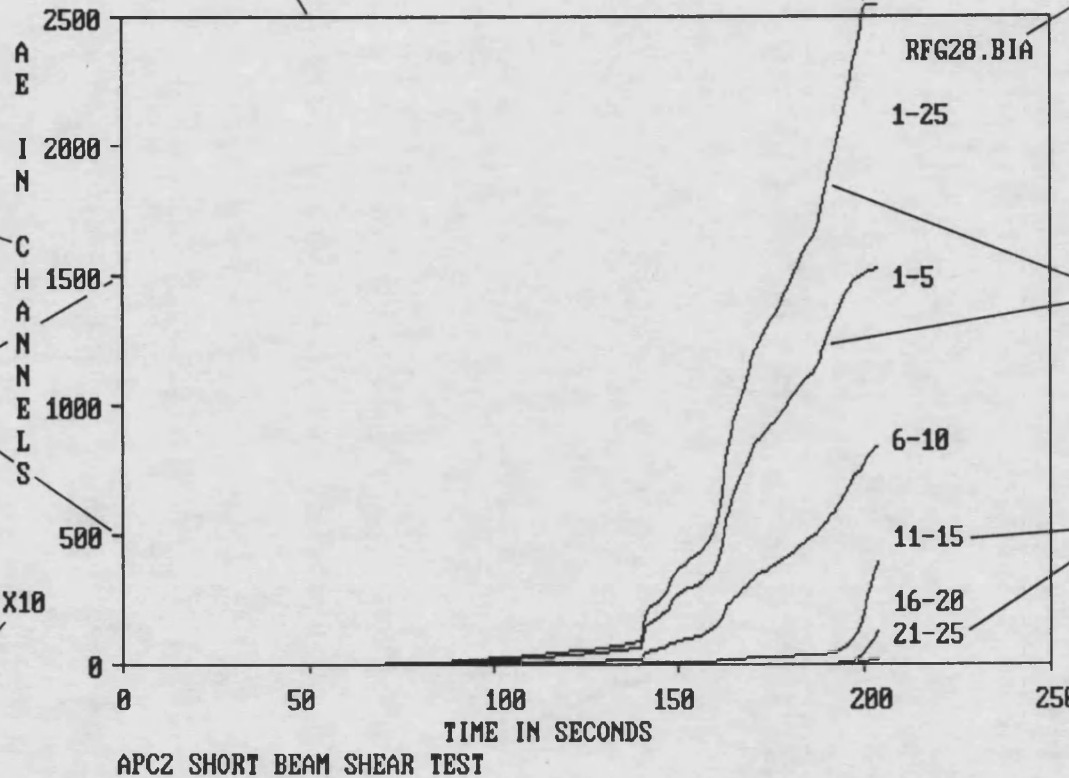
Tick marks are automatically positioned at 5 locations on each axis

Multiple graph lines can be plotted on the same graph by using F12 (over plot graph) to plot a graph rather than F11 (plot new graph)

Extra text can be placed onto the graph using the graph edit mode (see post-graph menu)

The axes scales are subject to a scaling factor of 10 or powers of 10 if their magnitude exceeds 9999

X10



APC2 SHORT BEAM SHEAR TEST

Appendices

Appendix I: Descriptive Measures of an Amplitude Distribution Histogram

The amplitude distribution histogram is the standard data presentation format for the peak amplitudes of acoustic emission events. The peak amplitudes of AE events are recorded by sorting into discrete amplitude channel ranges (channel number 1 - 26 or 1 - 51 depending on the amplitude sorter used). Therefore, the fundamental continuous variable, 'AE event amplitude (in volts)', is grouped into a range of discrete values, namely amplitude channel number. Only this grouped data is available for analysis and manipulation. The probability of occurrence of an AE event in a specific channel is the probability function which the acoustic emission amplitude distribution histogram describes.

Although a frequency histogram is very useful in displaying and summarizing the very large amount of acoustic emission data often gathered during a mechanical test, it is limited in its applicability for quantitative comparison. A small number of parameters which can quantify both the size and shape of a distribution, will enhance the ability to quantitatively compare amplitude distributions. Examples of such parameters which have been used in this thesis include the mean, variance, skewness and kurtosis which will now be defined.

Moments for grouped data

If X_1, X_2, \dots, X_k occur with frequencies f_1, f_2, \dots, f_k , respectively, the r th moment about any origin A is defined as

$$m_r' = \frac{\sum_{j=1}^k f_j (X_j - A)^r}{N} = \frac{\sum f (X - A)^r}{N} = \frac{\sum fd^r}{N}$$

where $d = X - A$ are the deviations of X from A .

$$N = \sum_{j=1}^k f_j = \sum f_j$$

If $A = 0$, taking moments about the origin, the first moment with $r = 1$ is the arithmetic mean M . The r th moment about the mean M is thus

$$m_r = \frac{\sum_{j=1}^k f_j (X_j - M)^r}{N} = \frac{\sum f (X - M)^r}{N}$$

If $r = 1$, $m_1 = 0$ (the first moment is zero), and if $r = 2$, $m_2 = s^2$ (the second moment is the variance).

In order to avoid particular units, dimensionless moments about the mean can be defined

$$a_r = \frac{m_r}{s^r} = \frac{m_r}{(\sqrt{m_2})^r} = \frac{m_r}{\sqrt{(m_2)^r}}$$

where $s = \sqrt{m_2}$ is the standard deviation. Since $m_1 = 0$ and $m_2 = s^2$, $a_1 = 0$ and $a_2 = 1$.

Skewness

The skewness is the degree of asymmetry of a distribution. If a distribution has a longer 'tail' to the right of the central maximum than to the left, the distribution is said to be skewed to the right and to have a positive skewness. The converse is true for a left skewed distribution. Many of the typical amplitude distribution histograms seen from APC2 show marked positive skewness.

For distributions, the means tend to lie on the same side of the mode as the longer 'tail', and hence an alternative measure of symmetry is supplied by the difference (Mean - Mode), made dimensionless on division by the standard deviation (a measure of dispersion), thus

$$\text{Skewness} = \frac{\text{mean} - \text{mode}}{\text{standard deviation}} = \text{Pearson's first coefficient}$$

To avoid use of the mode, an alternative measure of skewness is defined as

$$\text{Skewness} = \frac{3(\text{mean} - \text{median})}{\text{standard deviation}} = \text{Pearson's second coefficient}$$

Another important measure of skewness uses the third moment about the mean, m_3 , or expressed in dimensionless form

$$\text{Relative skewness } (\sqrt{b_1}) = \frac{m_3}{(\sqrt{m_2})^3}$$

The relative value of skewness ($\sqrt{b_1}$) may be considered in relation to the normal distribution which has a relative skewness, $\sqrt{b_1}$, of zero (mean, median and mode are all equal), since it is perfectly symmetrical. Negative values of $\sqrt{b_1}$ indicate that the mean and median are less than the mode and thus the distribution is skewed to the left. Positive values of $\sqrt{b_1}$ indicate the converse.

Kurtosis

The kurtosis is the degree of peakedness of a distribution, and is usually taken relative to a normal distribution. One important measure uses the fourth moment about the mean, m_4 , or expressed in dimensionless form

$$\text{Relative kurtosis } (b_2) = \frac{m_4}{(m_2)^2}$$

The value of the relative kurtosis (b_2) for a normal distribution is 3, thus values less than 3 are less peaked, and values greater than 3 are more peaked than the normal distribution. A very peaked distribution is called leptokurtic, a very flat topped distribution, platykurtic, and the normal distribution which is neither very peaked nor flat topped, is called platykurtic.

Appendix 2: The Structure Of MR1004 Binary Files

The first 255 bytes of each AE file are reserved for file header information in ASCII. This includes sampling time, number of analogue inputs used, events missed, file length and duration of the test.

AE data word

The structure of a typical AE event word is shown below in its hexadecimal, binary and decimal forms.

	LOW BYTE								HIGH BYTE							
HEX	F1								FA							
DECIMAL	241								250							
BIT NO.	8	7	6	5	4	3	2	1	16	15	14	13	12	11	10	9
BINARY	1	1	1	1	0	0	0	1	1	1	1	1	1	0	1	0
Ringdowns	14								-							
Amplitude	-								channel 5							

The low byte (bits 1 to 8) gives the number of ringdowns for the AE event in complementary binary. Bits 9 to 13 give the amplitude channel (1 to 25) of the event, again in complimentary binary. Bits 14 to 15 are the compliment of the channel module number used for AE data collection. The single module AE system uses channel 1 which is 11 in complimentary binary. The 16th bit is always set to 1 for an AE event word.

Analogue data word

A typical analogue input data word in hexadecimal, decimal and binary is shown below.

	LOW BYTE								HIGH BYTE							
HEX	70								0F							
DECIMAL	112								15							
BIT NO.	8	7	6	5	4	3	2	1	16	15	14	13	12	11	10	9
BINARY	0	1	1	1	0	0	0	0	0	0	0	0	1	1	1	1
Input channel									channel 1							

Bits 1 to 12 give the 12 bit representation of the magnitude of the analogue channel sampled (in this case channel 1 - see later) in complementary offset binary. The four analogue input channels can accept a range of -10 volts to +10 volts. FFF hex (4095 in decimal) is calibrated to -10 volts. 7FF hex (2047 decimal) is 0 volts and 000 hex (0 decimal) is thus +10 volts.

Bits 13 and 14 give the analogue channel of the word (00,01,10,11 in binary corresponding to channels 1,2,3,4 respectively). Bit 15 has no function and is thus always 0 and bit 16 is always set to 0 for an analogue word (set to 1 for an AE word).

At each sampling time interval, each of the active parametric input channels is sampled. Thus if 3 A/D channels are in use there will always be 3 analogue words at every time interval.

The last two words in the file are E0E0 (end of file marker) followed by a 16 bit number (in straight binary) which gives the total number of events missed during the data collection.